BASAL MECHANICS AND GEOLOGIC RECORD OF ICE STREAMING, WEST ANTARCTICA

Thesis by

Slawek M. Tulaczyk

In Partial Fulfillment of the Requirements

for the Degree of

Doctor of Philosophy

California Institute of Technology

Pasadena, California

1999

(Submitted July 15, 1998)

This work is dedicated to my parents,

Jadwiga and Stanisław Tulaczyk,

for you have taught me the curiosity that made it possible;

and to my wife, Mica,

for your support.

Ta praca jest zadedykowana moim rodzicom,

Jadwidze and Stanisławowi Tulaczyk,

gdyz Wy nauczyliscie mnie tej ciekawosci, ktora ja umozliwila;

oraz mojej zonie, Majce,

za Twoja pomoc.

ACKNOWLEDGMENTS

First of all I would like to express gratitude to my advisor Barclay Kamb who not only permitted me to stumble into his research program and to choose an exciting research project but also had generously given me the academic freedom I wanted and the academic guidance I needed. Much the same applies to Hermann Engelhardt who must also be recognized for the energy he puts into keeping neatly tied up together the drilling program in West Antarctica, undoubtedly one of the most imaginative field projects in modern Antarctic science. Robin Bosley has to be appreciated here together with Hermann for his skillful ways in improving how things run at home and in the field. I send my heartfelt thanks also to all the numerous members of field parties who have over the last ten years worked hard to help Barclay, Hermann, and Robin recover the samples of subglacial mud with which I played in the lab.

My work and education in the Caltech's Division of Geological and Planetary Sciences was greatly facilitated by many of the fine professors and students that this institution has. Among the students I want to acknowledge especially are: Jim Spotila, Miriam Jackson, Mihai Ducea, Rob Brady and Rowena Lohmann, who have helped with my labwork or writing at different stages of Ph.D. research. They, and many others, have also provided a collegial atmosphere over the years.

From outside the GPS Division, I would like to recognize the contribution of Prof. Ronald F. Scott to this project. He has shared with me some of his broad knowledge of soil mechanics, a subject that plays a crucial part in my research. Prof. Scott permitted access to his soil mechanics laboratory and testing equipment, and facilitated my cooperation with Dr. Less Fruth who made it possible for me to use the excellent triaxial testing setup which he supervises at the Earth Technology Inc. in Irvine, California.

Away from Caltech, interactions with a number of scientists and students in the field of glaciology and glacial geology have steered me through the uncharted world of sub-ice-stream processes. Among these kind people are: Dr. Reed Scherer, Dr. Neal Iverson, Dr. Douglas MacAyeal, Dr. David Mickelson, Dr. Richard Alley, Dr. Ian Whillans, Dr. Robert Bindschadler, Dr. Christina Hulbe, Dr. Jan Piotrowski, Tom Hooyer, and Martin Truffer. I thank also Dr. Ian Joughin of the Jet Propulsion Laboratory for inviting me to cooperate with him in an exciting project involving use of the SAR-interferometry to monitor velocity changes on an outlet glacier in Greenland. Drs. W.D. Harrison and K. Echelmeyer from the University of Alaska-Fairbanks have been so generous to invite me for a short visit to their drilling site on the Black Rapids Glacier; this was an exciting adventure.

Last, but definitely not least, come thanks to my family. My wife, Mica, has been instrumental in making sure that the pace of my work is maintained at a minimum cost to the quality of life. My parents and brother, Jadwiga, Stanislaw, and Jaroslaw Tulaczyk, have lent a long-distance but crucial emotional support over the last several years.

This research was supported by the NSF grant OPP-9219279 to Barclay Kamb and Hermann Engelhardt. Additional support was provided to me by the Henry and Grazyna Bauer Fellowship.

ABSTRACT

Piston coring in boreholes drilled at the UpB camp through Ice Stream B, West Antarctica, provided the first samples of sediments ever recovered from beneath an active ice stream. Sedimentological analyses indicate that the samples come from the layer of weak, subglacial till underlying this ice stream (the UpB till). Textural properties of the till and the Tertiary diatoms found in it suggest that the UpB till is recycled from the sediments of the inferred eastern subglacial extension of the Ross Sea sedimentary basin. Geotechnical tests show that the UpB till can be modeled as a compressible, Coulomb-plastic material whose strength is practically independent of deformation rate but is determined by effective stress which also determines the water content. Simulations of the subglacial behavior of such till have successfully reproduced fundamental features of the observed subglacial till kinematics, e.g., viscous-like vertical distribution of strain and oscillations in tilt rates. The compressible-Coulomb-plastic till model offers a framework for understanding and modeling of ice stream motion and ice-till interactions. The high porosity of the UpB till (≈ 0.4) suggests that effective stress is consistently very low, *ca.* 0.1 to 30 kPa, in the subglacial zone of Ice Stream B. These conditions are explained by the 'undrained-bed' model of sub-ice-stream hydrology that includes only local exchange of water between the water stored in the till pore space and the water stored as basal ice. In this model, there is a negative feedback effect between the basal melting rate and till strength which forces a steady-state in which the basal melting rate is zero and the till is water-rich and weak. Coupling of the undrained-bed model with an equation for the velocity of ice stream sliding yields the undrained-plastic-bed model of ice streaming (the UPB model). In accordance with the existing observations, the physics of the UPB model produces two stable modes: an active 'ice-stream' mode and an 'ice-sheet' mode. The

model may experience thermally-triggered switches between the two modes and it can be used to test the hypothesis that the West Antarctic Ice Sheet will become unstable in the near-future.

TABLE OF CONTENTS

CHAPTER 1

General Introduction

1.1. Purpose and Structure

Modern mountain glaciers and polar ice sheets provide excellent laboratories for studying the glaciological and glacial geological processes which help determine behavior of the terrestrial cryosphere and the geologic record of its changes. However, much of what determines the behavior of ice masses takes place beneath hundreds to thousands of meters of ice, a fact that makes it difficult to understand glacier mechanics as well as the fundamental processes of glacial erosion, transport, and sedimentation. Yet there is a clear need for such understanding because ice masses play an important role in the dynamics of the surficial environment of our planet. This need is nowhere as apparent as in West Antarctica, where the only present-day marine ice sheet is located. Marine ice sheets may be prone to instability, and there is heated debate as to whether the West Antarctic Ice Sheet may collapse in the near future and accelerate the global sea-level rise [Bentley, 1997; Bindschadler, 1997, 1998]. Since ice streams carry the majority of ice draining out of the West Antarctic Ice Sheet, any near-future ice-sheet instability would have to involve changes in their velocity or geometry. Thus, there is a great scientific interest in understanding the mechanism of ice stream motion and the physical controls which determine the stability and evolution of ice streams [Bentley, 1987].

In this context, a long-term research project focused on the West Antarctic ice streams has been developed by the glaciological community. One of the most important recent breakthroughs in ice stream mechanics came slightly more than a decade ago when seismic data collected on Ice Stream B suggested that this ice stream moves over a meters-

thick-layer of weak till rather than over a rigid bedrock as had been previously assumed [Alley *et al.*, 1986; Blankenship *et al.*, 1986]. This discovery brought into sharp focus the potential importance of subglacial sediments to ice stream mechanics and dynamics. The mechanical behavior of subglacial till as well as its relation to subglacial hydrology became the key issues that must be understood before a reliable model of ice-stream and ice-sheet stability can be developed.

Given this increased awareness of the role of subglacial till in ice stream motion, a drilling project designed to open a direct access to the sub-ice-stream environment was initiated ten years ago [Engelhardt *et al.*, 1990]. One of the main goals of the project was sampling of sub-ice-stream till. The coring effort succeeded in providing several cores of the till from a number of locations near the UpB camp on Ice Stream B. Since 1993, the author of this thesis had the opportunity to study sedimentological, hydrological, and mechanical properties of these unique samples. The overarching goal of this research was to provide the answers to two basic questions: 1) what is the origin of the weak, sub-ice-stream till? 2) what is the role of ice-till interactions in determining the stability and evolution of the ice stream?

The following five chapters (2 through 6) present the results of this research. In the first of the five chapters, sedimentological properties of the till are analyzed and compared to the properties of other glacial deposits. Much of this chapter has been included in a paper published in *Journal of Sedimentary Research* [Tulaczyk *et al.*, 1998]. The next chapter, Chapter 3, represents a purely theoretical analysis of ice-till interactions and their dependence on till properties. This chapter has been accepted for publication and throughout this thesis I refer to it as Tulaczyk [in press]. The next three chapters are being prepared for concurrent submission to *Journal of Geophysical Research.* Chapter 4 contains a model of till mechanics based on laboratory geotechnical tests performed on samples of the UpB till [referred to as Tulaczyk *et al.*, in preparation I]. Chapter 5

[referred to as Tulaczyk *et al.*, in preparation II] gives new constraints on *in situ* effective stress beneath Ice Stream B based on the high water content of the till. In this chapter, a new model of sub-ice-stream hydrology is developed. This model provides a plausible explanation for the observed high till water content and the inferred low subglacial effective stress. Chapter 6 merges the new views of till mechanics and hydrology into a self-consistent analytical ice-stream model [referred to as Tulaczyk *et al.*, in preparation III]. The properties of the ice-stream model are analyzed in this chapter to infer what physical controls play the most important role in determining ice stream stability and evolution.

Because each chapter is prepared as a self-contained manuscript, some redundancy occurs in the information and references provided. Each chapter has its own abstract, introduction, acknowledgments, and conclusions. In addition, the style of citations is different for Chapters 2 and 3 than for Chapters 4 through 6. The layout of each chapter is also designed in a way similar to the layout of a submittable manuscript. The body of the text is followed by references, tables, and figures, respectively. Two types of appendices are used. The first type (designated always with an Arabic numeral, e.g., Appendix 1) is intended to be included in the submittable manuscript and contains crucial derivations of equations or necessary data which are better presented separately from the flow of the main text. This type of an appendix is placed in the thesis chapters between conclusions and acknowledgments. The second type of the appendix contains additional data or explanations that are needed in the thesis but are not intended to be included in the submittable manuscripts. It is used only in Chapters 2 and 4 (Appendix 2.A and Appendix 4.A).

1.2. Individual Contributions to the Thesis

The research described in this thesis represents an intrinsic part of the long-term Caltech glaciological research program focused on borehole investigations of West Antarctic ice streams [e.g., Engelhardt et al., 1990]. The work underlying the thesis involved a significant collaboration with the two leaders of this research program: Dr. Barclay Kamb and Dr. Hermann Engelhardt. These two scientists are responsible for developing the West Antarctic field program and, in particular, for collecting the subglacial sediment samples as well as making borehole observations which have been used either in a direct or indirect way to develop the concepts contained herein. The thesis author was not involved in any of the field campaigns which yielded these unique samples and data. Nevertheless, the majority of the laboratory data collection, processing, and interpretation, as well as all of the modeling work represent his original contribution. The writing was also performed independently by the thesis author with subsequent inclusion of editorial comments provided by Dr. Barclay Kamb, Dr. Hermann Engelhardt, and Dr. Reed Scherer in Chapter 2. The following paragraphs provide a more detailed discussion of the individual contributions by the thesis author and the collaborating scientists.

Chapter 2 represents a collaboration between the thesis author, Kamb, Engelhardt, and Scherer. Dr. Reed Scherer contributed data on diatom abundance and ages. He also provided a short description of the methods involved in his work on diatoms as well as a part of the discussion of the geological setting of Ice Stream B. Drs. Kamb and Engelhardt provided the five subglacial sediment cores along with information on the procedures of their acquisition and on the physical conditions at the base of the ice stream in the area of sediment sampling. They have also made the x-ray radiographs of the first four sediment cores: 89-4, 89-6, 89-8, and 89-9. The remaining laboratory analysis of the sediment cores were performed by Tulaczyk: 1) grain-size distribution, 2) sand mineralogy, 3) sand

SEM micromorphology, 4) clay mineralogy, 5) pebble lithology, and 6) pebble roundness, sphericity, and surface markings. Rowena Lohmann provided laboratory assistance with the analysis of grain-size distribution .

The theoretical study of ice-till interactions described in Chapter 3 is entirely due to the thesis author. This chapter is also only indirectly related to the mechanics of West Antarctic ice streams. Chapter 4 is a result of collaboration between Tulaczyk, Kamb, and Engelhardt. The two latter researchers collected the subglacial till samples used in geotechnical laboratory analysis and provided the tethered stake record obtained in a borehole drilled in the UpB area of Ice Stream B. In addition, Engelhardt performed sixteen shear box tests and determined the Atterberg limits on samples of the subglacial till. The author of this thesis conducted the triaxial, ring shear, and consolidation tests as well as the modeling of subglacial till behavior. His work was greatly aided by the advise and geotechnical equipment provided by Dr. Ronald Scott (Division of Engineering and Applied Sciences, California Institute of Technology). Chapter 5 is also a result of collaboration between the same three scientists. Engelhardt and Kamb supplied the subglacial till cores used for water content measurements and in oedometer tests. They provided also the measured basal temperature gradient in the UpB area of Ice Stream B, borehole data constraining subglacial effective stresses in the same area, and other information on the nature of the sub-ice-stream hydrologic system. Engelhardt made the water content measurements on till samples from core 89-4 and performed four oedometer tests on till samples from the same core. Tulaczyk made the remaining water content measurements and oedometer tests. He used these data to derive new estimates of subglacial effective stresses and to model the subglacial and basal water flow. His finite-element model of groundwater flow beneath Ice Stream B utilized a modified version of a FORTRAN code provided by Dr. John Hall (Division of Engineering and Applied Sciences, California Institute of Technology). Chapter 6 represents a modeling effort built

upon the collaborative work described in Chapters 4 and 5. The ice-stream model discussed in this chapter was developed by the author of this thesis. Kamb and Engelhardt provided the expertise necessary to assure that the assumptions which underlie the model are consistent with the existing observations of the physical conditions at the base of Ice Stream B.

References

Alley, R.B., D.D. Blankenship, C.R. Bentley, and S.T. Rooney, Deformation of till beneath Ice Stream B, West Antarctica, *Nature*, 322, 57-59, 1986.

Bentley, C.R., Antarctic ice streams - a review, *J. Geophys. Res.*, 92, 8,843-8,858, 1987.

Bentley, C.R., Rapid sea-level rise soon from West Antarctic Ice Sheet collapse, *Science*, 275, 1,077-1,078, 1997.

Bindschadler, R., Monitoring ice sheet behavior from space, *Rev. Geophys.*, 36, 79-104, 1998.

Bindschadler, R., West Antarctic Ice Sheet collapse, *Science*, 276, 242-246, 1997.

Engelhardt, H., N. Humphrey, B. Kamb, and M. Fahnestock, Physical conditions at the base of a fast moving Antarctic ice stream, *Science*, 248, 57-59, 1990.

Tulaczyk, S., Ice sliding over weak, fine-grained tills: dependence of ice-till interactions on till granulometry, in *Glacial Processes, Past and Modern*, edited by D.M. Mickelson and J. Attig, in press.

Tulaczyk, S., B. Kamb, H. Engelhardt, and R.P. Scherer, Sedimentary processes beneath a West Antarctic ice stream; constraints from textural and compositional properties of subglacial debris, *J. Sediment. Res.*, 68, 487-496, 1998.

Tulaczyk, S., B. Kamb, and H. Engelhardt, Basal mechanics of Ice Stream B, West Antarctica. I. Till mechanics, in preparation I.

Tulaczyk, S., B. Kamb, and H. Engelhardt, Basal mechanics of Ice Stream B, West Antarctica. II. Till hydrology, in preparation II.

Tulaczyk, S., B. Kamb, and H. Engelhardt, Basal mechanics of Ice Stream B, West Antarctica. III. Undrained-plastic-bed model, in preparation III.

CHAPTER 2

Sedimentary Processes at the Base of an Ice Stream and an Adjacent Ice Sheet, West Antarctica: Constraints From Textural and Compositional Properties of Subglacial and Basal Debris

Slawek Tulaczyk, Barclay Kamb, Hermann F. Engelhardt,
Division of Geological and Planetary Sciences, California Institute of Technology,
Pasadena, CA 91125

Reed P. Scherer
Uppsala University, Insitute of Earth Sciences, 752 36 Uppsala, Sweden

Abstract

Samples of subglacial till from beneath Ice Stream B (at camp UpB) and basal debris from the neighboring slow-moving ice of an inter-stream ridge (the "Unicorn") provide insights into the sedimentary environments associated with glaciologically very different conditions beneath the West Antarctic Ice Sheet (WAIS). Piston coring in holes bored by hot water drilling yielded five 1- to 3-meter-long undisturbed subglacial sediment cores from the ice stream and two 0.3-meter-long cores with winnowed sediments from the Unicorn. We analyze granulometry, composition, and particle morphology in these cores.

The UpB till is a clay-rich, unsorted, fossil-bearing diamicton whose components bear no evidence of subglacial crushing, abrasion, or comminution. Morphology of its quartz sands indicates a prolonged (~10^6 years) influence of chemical weathering. The till

consists of material recycled from subjacent Tertiary glacimarine sediments of the Ross Sea sedimentary basin which extends beneath this part of the WAIS. The till appears to provide an analog for some of the Quaternary Ross Sea diamictons which have been interpreted by numerous workers as marine tills. The Ice Stream B and Ross Sea deposits are texturally similar to their inferred glacimarine source and both contain reworked marine diatoms which provide evidence for glacial transport and mixing. The lack of crushing, abrasion, and comminution beneath Ice Stream B is due to low subglacial effective pressure and a 'cushioning' effect of the fine till matrix. The UpB till is not a close sedimentological analog of the Late Pleistocene continental tills that were significantly affected by mechanical processes. The pervasive subglacial deformation that has been proposed as a process of till formation and transport as well as rapid ice-stream motion may be unable to produce such common characteristics of glacial debris as striations, facets, broken particles, and glacial flour. Our results question the proposition that subglacial deformation under low driving stresses is a ubiquitous primary till-forming process. It is rather a secondary process that takes place only if preexisting tills or other unlithified and unconsolidated sediments are present beneath overriding ice.

The sediments in the Unicorn cores come from debris-laden basal ice; they were roiled and winnowed by the jet action of the hot water drill, removing much of the clay and producing a well-graded core by particle settling in the borehole. The winnowed sediments of the first Unicorn core (93-10), from a borehole close to the ice stream, are compositionally and morphologically similar to the UpB till. The till was likely frozen on to the base of the ice since the latter stopped moving at ice stream speeds about a century ago. The second Unicorn core (93-14), from a borehole 7 km distant from the ice stream, has a different mineralogical composition and contains particles with clear breakage features, indicating a different provenance and different mechanical history associated with

ice-sheet (instead of ice-stream) erosion and transport. This Unicorn sample may represent a frozen-on subglacial till or a glacimarine diamicton. The freeze-on is, or was, possible beneath the slow-moving ice (1-4 m/a) because of low basal frictional heating. The high velocity of the ice stream (*ca.* 440 m/a) results in basal melting, which melts out basal debris, leaving relatively clean ice in contact with subglacial till.

2.1. Introduction

Direct observations of basal and subglacial debris from the currently existing ice sheets were up to the present limited either to ice sheet margins (e.g., Sugden *et al.* 1987) or ice domes and divides drilled for climatic record (Gow *et al.* 1968; Herron and Langway 1979). These parts of ice sheets are characterized by special glaciological conditions that are not representative of many of the present-day and past subglacial environments. The drilling project developed by the Caltech glaciological group to study basal mechanics of ice streaming in West Antarctica offered the first opportunity to sample glacial debris and measure physical conditions at the bed of a fast moving ice stream (Engelhardt *et al.* 1990). This project is a part of a larger effort to understand the dynamics and history of the possibly unstable West Antarctic Ice Sheet (WAIS) (Alley *et al.* 1986, 1987a; Alley and MacAyeal 1993; Bentley 1987; Bindschadler *et al.* 1988, 1990; Blankenship *et al.* 1986, 1987; Engelhardt and Kamb 1993; Hughes 1977; Kamb 1991; Scherer 1991; Whillans and van der Veen 1993; and many others).

There is a considerable scientific interest in mechanical and sedimentary processes operating beneath ice streams due to the need to understand the phenomenon of ice streaming and its geologic consequences (Alley *et al.* 1986, 1987a, 1987b; Bentley 1987; Blankenship *et al.* 1986, 1987; Clark 1992; Engelhardt *et al.* 1990; MacAyeal 1992;

Punkari 1994). Ice streams control the mass balance of the WAIS, and significant portions of the Late Pleistocene Antarctic and northern-hemisphere ice sheets may have been drained by ice streams as well (Clark 1992; Hughes 1977; Punkari 1994).

Based on interpretation of seismic data, Alley *et al.* (1986, 1987a) inferred that a pervasively deforming, several-meter-thick subglacial till layer exists beneath Ice Stream B. Furthermore, they proposed that such deforming till controls motion and stability of the Ross ice streams draining the western part of the WAIS. Subsequently, Alley *et al.* (1987b), Alley (1991), Clark (1991), Clark and Walder (1994) and others suggested that many of the Pleistocene paleo-tills in North America and Europe may have been also generated by similar pervasive deformation of glacial beds. It has been proposed that pervasive till deformation represents a new, distinct, and perhaps even predominant genetic mechanism for formation of subglacial tills (Alley *et al.* 1987b; Alley 1991; Boulton 1996). This proposition needs to be tested because it has far-reaching implications for the understanding of ice sheet dynamics and of the geologic record of glaciations (Clark 1992; Clark and Walder 1994).

We cored an unfrozen subglacial diamicton at the base of Ice Stream B. This material provides a sample of the extensive unconsolidated sediments present beneath the ice stream (Blankenship *et al.* 1986, 1987; Rooney *et al.* 1991). We also retrieved basal debris from the slow moving ice sheet bordering Ice Stream B on the south. Our sediment samples and borehole observations provide new insights into the environment of till formation beneath an ice stream and constrain the poorly known sub-ice geology. In this study, we analyze and interpret texture and composition of the basal and subglacial sediments. The data are used to constrain the processes that contributed to the formation of the sediments and to infer the source of their material. We discuss the implications of our findings for models of till genesis, especially for the proposed deforming-bed model.

For terminological clarity, we follow Ronnert's (1992) use of 'basal' and 'subglacial' to refer to the position or the material in the lowermost several meters of the glacier and in the topmost several meters below the glacier, respectively. We refer to Dreimanis (1989) and Drewry (1986) for the definitions of other glacial geologic terms.

2.2. Glaciological Setting

Ice Stream B is one of the Ross ice streams flowing into the Ross Ice Shelf (Figure 1A). At the UpB camp, the ice stream is 30 km wide, 1 km thick and has an average surface slope of about 0.0013. The ice base is roughly 600 m below sea level. The gravitational driving stress is low, 13-20 kPa, but the ice stream moves with a velocity of 440 m/y (Echelmeyer *et al.* 1994; Whillans and van der Veen 1993). The motion is plug flow over a bed lubricated by water and weak deformable sediments (Alley *et al.* 1986; Kamb 1991). Shear margins, about 5 km wide, separate the ice stream from the adjacent ice sheet that moves approximately a hundred times slower (Echelmeyer *et al.* 1994).

Borehole measurements show that the base of the ice stream is at the pressure melting point, -0.8°C (Engelhardt and Kamb 1993). Meltwater is likely produced at the base and feeds into a widespread, but not completely pervasive, basal water system. The effective ice pressure on the bed is low, -40 kPa to 160 kPa (Kamb and Engelhardt 1991). Borehole experiments indicate that most of the motion of the ice stream is accommodated at or near the ice-till interface, probably by basal sliding (Engelhardt and Kamb 1996, submitted).

The Unicorn is slow moving ice, 1-4 m/y (Whillans and van der Veen 1993), wedged between two branches of Ice Stream B (Figure 1B). It contains a faint feature, the "Fishhook" (Figure 1B), that is believed to be associated with a former shear margin of the

B2 branch. This shear margin appears to have moved to its current position about a century ago (Bentley *et al.* 1994). Before then, the northeastern portion of the Unicorn was a part of the ice stream.

2.3. Geological Setting

The subglacial geology of the West Antarctic interior basins is deduced mostly from geophysical data. Blankenship *et al.* (1986, 1987) and Rooney *et al.* (1991) inferred from seismic studies in the UpB area that a several-meter-thick till layer unconformably overlies a bedded sedimentary sequence of at least 600 m thickness. The layer and the underlying sequence are both poorly consolidated. According to Rooney *et al.* (1991), the sediments beneath the ice stream may belong to the sedimentary sequence described from the Ross Sea basin (Hayes and Frakes 1975). Other geophysical studies also suggest that the Ross Sea basin extends beneath part of the WAIS (Jankowski and Drewry 1981). This view is supported by the few geological samples available from West Antarctic interior basins (Scherer 1994a). Glacigenic sediments have been recovered from beneath Ice Stream B (Engelhardt *et al.* 1990; this paper), Crary Ice Rise (Bindschadler *et al.* 1988), Byrd Station (Gow *et al.*, 1968), and the southern Ross Ice Shelf (Webb 1979).

Deep drilling in the Ross Sea (locations in Figure 1A) shows several hundred meters of Tertiary glacimarine deposits lying unconformably beneath several meters of widespread Pleistocene diamictons, which are generally interpreted as marine tills deposited by ice grounded below sea level (Anderson *et al.* 1980, 1984; Kellogg *et al.* 1979). The underlying glacimarine successions are dominantly Miocene in age (Savage and Ciesielski 1983) and consist of pebbly muds and diatomaceous muds (Barrett 1975a) with seismic characteristics indistinguishable from those beneath UpB (Rooney *et al.* 1991).

2.4. Core Sampling

A hot-water drill is used to melt a c. 10 cm diameter hole through roughly 1000 m of ice to the bottom where drill penetration ceases. A piston corer of 6 m length and internal diameter of 5 cm is lowered through this hole to sample the subglacial sediments (if unfrozen) and any basal sediments melted out from the ice by the hot water drilling. During the field season 1989-90, we acquired four cores, 89-4, 89-6, 89-7, 89-8, from a closely (<200 m) spaced cluster of boreholes near the UpB camp (Figure 1B). A single core, 92-1, was recovered during the austral summer 1992-93. This core came from a bed location roughly 600 m downstream from the 1989 sampling sites. Henceforth we will refer to these five cores as the UpB cores. They are between 1 and 3 m in length. We believe that the hot-water drill did not disturb the sediments in these cores because they show no grading or sorting.

We acquired two short (*ca.* 0.3 m) cores, 93-10 and 93-14, from holes drilled in the Unicorn (henceforth the Unicorn cores) (Figure 1B). Core 93-10 came from the transition between the slow moving ice and the ice stream shear margin. Core 93-14 was sampled on the southern side of the Unicorn. The sediment in both cores is graded and sorted, probably due to winnowing caused by hot-water drilling through debris-rich ice.

2.5. Laboratory Methods

Cores and their x-ray radiographs were examined for macroscopic sedimentary structures. The radiographs were used to estimate downcore changes in abundance of pebbles coarser than -2ϕ (>4 mm). Sediment samples (*ca.* 40 gram each) were taken from the UpB cores at a spacing of 0.3 m. Material coarser than 5ϕ (>32μm), was sieved at 1ϕ

intervals. Additional subsamples of 20 gram weight were used for pipetting analyses of grain size distribution (Galehouse 1971b, p. 71 and 81-88) of the fractions finer than 5ϕ.

Composition of thin-sectioned clasts and grain mounts was determined with the petrographic microscope. We prepared grain mounts of the size fraction 1ϕ-2ϕ from all sediment samples. This fraction was selected to represent the sandy mode in the grain-size distribution (henceforth 'the matrix index fraction'). In addition, mineralogical composition of all size fractions (1ϕ interval) smaller than -2ϕ was determined for four selected samples (89-4-20, 92-1-50, 93-10, 93-14). We counted 300 grains in each grain mount (Galehouse 1971a, p. 391-392). X-ray diffraction (XRD) analyses gave a semiquantitative estimate of mineralogy for the fraction finer than 5ϕ. In the size range 5ϕ to 8ϕ, we approximated the content of quartz, plagioclase, potassium feldspar, chlorite+kaolinite, and illite+smectite using XRD intensities at spacings of 4.25, 3.19, 3.24, 7, and 10 Å respectively (Griffin 1971; Haldorsen 1977). The intensities were recalculated into relative mineral abundance by applying calibration factors estimated by us from analysis of synthetic mixtures. For grains smaller than 8ϕ (the clay-size fraction) clay mineral assemblage was determined with the procedure of Griffin (1971, p. 554-558).

Abundance of whole diatoms and diatom fragments was determined on sediment samples of *ca.* 50 g. The samples were dried (50°C), weighed, and disaggregated in 100 ml of hot water (90°C). A 2.5 µL aliquot from a sample suspension homogenized by vigorous shaking was used to prepare a glass slide. The pipette method does not produce a true random distribution of particles (Laws 1983) but clumping or other obvious distributional bias is minimized. Vertical edge-to-edge transects were counted on an Olympus interference contrast microscope with a 60× oil objective. The abundances obtained with this analytical method should be considered as relative figures, since accuracy of this method has not been rigorously tested. As diatom abundance is very low

in our samples, application of more standard methods (e.g., Scherer 1994b) is not practical.

We determined sphericity and roundness of clasts following the procedures of Krumbein (1941). Clasts were also examined for glacial facets and striations.

Scanning Electron Microscopy (SEM) was used to analyze micromorphology of quartz and feldspar grains in the size range 2ϕ to 3ϕ (Krinsley and Doornkamp 1973). We checked for the presence of selected microfeatures on 30 grains of each mineral in each sample studied. Quartz and feldspar were distinguished with an energy disperive x-ray analyzer. The different quartz microfeatures were defined based on the work of Darmody (1985), Douglas and Platt (1977), Krinsley and Doornkamp (1973), Margolis and Kennett (1971), and Mazzullo and Ritter (1991). Out of the 32 selected quartz microfeatures, the following 27 were found on the analyzed grains: 1. cleavage-parallel lines, 2. conchoidal fractures, 3. arcuate steps, 4. low relief, 5. meandering ridges, 6. parallel steps, 7. smooth planes, 8. sharp edges, 9. fracture-propagation cracks, 10. large breakage blocks, 11. adhering particles, 12. small breakage blocks, 13. high relief, 14. scaling or irregular roughness, 15. straight grooves, 16. dull solution surfaces, 17. medium relief, 18. crystallographic overgrowth, 19. irregularly pitted surfaces, 20. oriented pits, 21. anastomozing etching, 22. smooth coating, 23. etch pits, 24. hairline cracks, 25. crevasses, 26. rounded edges, and 27. any evidence of precipitation or solution of silica. The five remaining microfeatures were never found: 28. striations, 29. curved grooves, 30. v-pits, 31. silica flowers, and 32. silica globules.

The feldspar microfeatures were defined mainly by analogy with the quartz microfeatures during our initial SEM investigations. In addition, we used work by Berner and Holdren (1977, 1979) and Holdren and Berner (1979) to define the microfeatures produced by chemical alteration of feldspar grains. We recognized a total of 15 feldspar

microfeatures: 1. cleavage planes, 2. fracture steps, 3. sharp edges, 4. fracture-propagation cracks, 5. breakage blocks, 6. cleavage-parallel lines, 7. adhering particles, 8. scaling, 9. smooth coating, 10. irregular roughness, 11. random crevasses, 12. karst, 13. oriented crevasses, 14. etch pits, and 15. rounded edges.

For calibration of the results, we prepared and identified the microfeatures in five artificially treated grain samples. One of the samples was created by crushing of -1ϕ to 0ϕ diameter grains from the UpB sediments with a pestle and mortar. In three other samples the crushed grains were treated for 24 hrs. with 1% HF, 10% HF and 5% NaOH, respectively. A fifth sample consisted of the crushed grains that were subsequently tumbled in a till slurry at 40 r.p.m. for 28.5 hrs.

We use factor analysis as an aid in extracting the dominant interrelationships between individual samples (Q-mode) and individual microfeatures (R-mode) from the multivariate data sets consisting of the abundances of each microfeature on 30 quartz and 30 feldspar grains from each sample. The factor analysis is performed with a FORTRAN program written by S.T., based on the procedures of Davis (1986, p. 527-574). The raw data on abundance of the various microfeatures in selected samples is given in Appendix 1.

In addition, we apply the weathering scoring method of Darmody (1985). In this method, each grain is checked for five selected breakage microfeatures (quartz features 2, 3, 7, 8, 13, and feldspar features 1, 2, 3, 4, 6) and five chemical weathering microfeatures (quartz features 14, 23, 24, 26, 27 and feldspar features 8, 12, 13, 14, 15); +1 is assigned for the presence of each of the former and -1 for the presence of each of the latter. Zero is assigned when any of the microfeatures is absent. The sum of the points is the weathering score for a grain and the scores for 30 grains are averaged to get the score for a sample.

2.6. Sediment Description

Individual sediment samples to which we refer in the paper are identified with a sample number (e.g., 89-4-20) made up of the core number (e.g., 89-4) and the depth of the sample below the top of the core, in cm (e.g., 20 cm). The core numbers appear at the corresponding locations in Figure 1B. When it was not practical to analyze certain sediment characteristics (e.g., microfeatures on sand grains) in many samples from the UpB cores, we selected samples from near the core tops. This is motivated by our belief that the sediments from the vicinity of the ice base should be affected the most by the modern subglacial processes operating beneath Ice Stream B.

2.6.1. Structure

The five UpB cores are macroscopically structureless (example in Figure 2). They consist of very dark gray (5Y 3/1, when wet) sand-silt-clay matrix with scattered pebbles. The microscopic structure of this sediment (Figure 3) is similar to its macroscopic structure. Sand and coarse silt grains appear randomly dispersed in a matrix of clay and fine silt. The abundance of clasts is spatially highly variable, from 0 to 11 pebbles per 5 cm length of core (Figure 4). The pebble distribution shows no discernible grading or bedding.

The Unicorn cores display strong gradation from pebbles at the bottom to clayey silty sand at the top. All of the clasts occur in the lowermost 10 cm and their abundance reaches *ca.* 40 pebbles per 5 cm length of core (Figure 4).

2.6.2. Texture and Composition

The UpB diamicton.--- The UpB cores consist of an extremely poorly sorted diamicton with 0 to 16 weight percent pebbles (Figure 5A). Particle size ranges from less than 10ϕ to almost -6ϕ. In the 35 analyzed samples mean grain size varies between 4ϕ and 6ϕ and sorting between 3.8ϕ and 5.0ϕ. The sediments have a bimodal grain-size distribution. One mode is in the fine sand fraction, 2ϕ-4ϕ, and the second one in the clay fraction finer than 10ϕ (Figure 5B). As suggested by Pettijohn (1975, p. 48-50), in Figure 5C we decompose the average grain-size distribution into two log-normal subpopulations assuming a mixing model of the form:

$$F(\phi) = A \cdot F_1(\phi) + (1 - A) \cdot F_2(\phi) \qquad (1)$$

where: ϕ = logarithmic grain size = $-\log_2 d$ where d is grain diameter in mm

A = fraction of coarse subpopulation,

$F(\phi)$ = total grain-size distribution,

$F_1(\phi)$, $F_2(\phi)$ = subpopulations with normal frequency distributions given by:

$$F_i(\phi) = \frac{1}{\sqrt{2\pi}\sigma_i} \cdot e^{-(\phi - m_i)^2 / 2\sigma_i^2} \qquad (2)$$

where: m_i = mean and σ_i = standard deviation of each subpopulation (see Ross 1987, p. 96). Numerical least-squares fitting of equation (1) to the average grain-size distribution of the UpB sediments (Figure 5B) shows that the latter may be treated as a 65%-35% mixture of a sandy subpopulation (m_1 = 3ϕ, σ_1 = 3.2ϕ, A = 0.65) and a clayey subpopulation (m_2 = 12ϕ, σ_2 = 2.7ϕ).

The inventory and abundance of different microfeatures on sand grains is determined by the sedimentary processes that shaped the grains (Krinsley and Doornkamp 1973). The micromorphology of the sand fraction (2ϕ to 3ϕ) from the UpB till (89-4-20, 92-1-0) is dominated by chemical weathering microfeatures and physical breakage

microfeatures. Microfeatures associated with abrasion (15, 28, 29), high energy aqueous environments (30), and severe diagenesis (31, 32) are rare or absent. The chemical alteration microfeatures, e.g., etch pits, silica coating, appear to be younger than the physical breakage microfeatures over which they formed (Figure 6AB). The micromorphology of the grains in samples 89-4-20 and 92-1-0 is similar to that of the grains that were artificially crushed and subsequently treated with strong acid, 10% HF (Figure 7). On the other hand, the UpB samples show little affinity to the sample of freshly crushed grains. In the weathering assessment scheme of Darmody (1985), the UpB samples clearly plot towards the negative scores indicating predominance of chemical alteration microfeatures over physical breakage microfeatures (Figure 7B).

Clasts (230) recovered from the UpB cores are mainly subangular and subrounded in shape (Figure 8) with facets present on 50% of them. However, on 25% of the facetted clasts the facet planes have macroscopic etch pits. These pits are frequently developed in mafic minerals or plagioclase and are sometimes still lined with weathering products. Striations are practically absent; only two clasts (0.9%) have any suggestion of striations, and these are questionable.

A number of different lithologies comprises the sample of 230 clasts extracted from the UpB diamicton (Table 1). Figure 9 shows that the mineralogical composition of 100 thin-sectioned clasts is highly variable. Crystallinic rock fragments clearly predominate over sedimentary rock fragments in the UpB cores. The sedimentary fragments are mainly diamictites that have composition and appearance similar to the UpB matrix (Figure 3) with an average estimated clay content of 30%. These diamictite clasts survived the sieving procedure but at least some of them can be easily scratched with a fingernail.

The matrix index fraction, 1ϕ-2ϕ, from the UpB samples is significantly higher in quartz and lower in plagioclase than the mean composition of the UpB clasts (Figure 9).

When we take lithics into consideration, the index fraction has on average *ca.* 15% polymineralogic grains with quartz and feldspar grains comprising approximately 60% and 25%. Subsidiary minerals -- muscovite, biotite, amphibole, pyroxene, chlorite and opaques -- constitute <5% of the total grain count.

Changes in the mineralogical composition with grain size are dominated by decrease in the abundance of lithics in the size range -1ϕ to 5ϕ and increase in clay content in grain sizes finer than 5ϕ (Figure 10). Relative proportions of other constituents do not vary significantly with grain size. The clay-size fraction is a mixture of illite, smectite, kaolinite, and chlorite (Table 2).

The UpB sediments contain also diatoms, sponge spicules, foraminifera, radiolaria, mollusc fragments, marine and terrestrial palynomorphs, and coal fragments. Miocene marine diatoms constitute a majority of the microfossils (Scherer 1989, 1991). Our data from the core 92-1 suggest that abundance of diatoms is significantly higher near the ice base than in the deeper parts of the cores (Table 3). The data are consistent with qualitative observations from other UpB sampling locations where whole or nearly whole diatoms were also found mainly in the material from near the ice base (Scherer 1994a).

Sediments from the Unicorn.--- The Unicorn cores consist of sediment that is coarser and better sorted than the UpB diamicton (Figure 5AB). The two bottom samples from the cores 93-10 and 93-14 have a mean grain size of 0.4ϕ and 0.2ϕ whereas the two top samples have 4.0ϕ and 4.2ϕ. Sorting varies between 2.2ϕ and 3.9ϕ compared to 3.8ϕ to 5.0ϕ in the UpB diamicton. The largest clasts recovered from the two Unicorn cores are *ca.* -4.7ϕ (26 mm) in length.

The micromorphology of the Unicorn sand fractions, 93-10-20 and 93-14-20, is less influenced by chemical alteration features than is the micromorphology of the UpB

sand samples, 89-4-20, 92-1-0 (Figure 6C and 7). Of all analyzed grain samples from UpB and Unicorn, the 93-14-20 sand grains show the greatest morphological affinity to the freshly crushed and relatively unaltered samples (crushed, tumbled, 1%HF, 5%NaOH) (Figure 7). The sample 93-10-20 is more similar to the two UpB samples and to the strongly etched sample 10%HF. The lack of v-pits, microfeatures typical for high energy aqueous environments (Krinsley and Doornkamp 1973, p. 26), suggests that the micromorphology of grains from the Unicorn cores was not influenced significantly by the action of our hot-water drill.

We recovered 27 pebbles from core 93-10 and 82 pebbles from core 93-14. In terms of average sphericity and roundness the 93-10 clasts are indistinguishable from the UpB clasts (Figure 8). Fifty-two percent of them are facetted and three percent striated. The pebbles from core 93-14 are slightly less spherical than the UpB clasts (Figure 8). Sixty-one percent of the 93-14 clasts had facets with 24% of these showing macroscopic signs of subsequent chemical weathering. Striations occur on 4% of the 93-14 clasts (Figure 11).

Lithological composition of the clasts from core 93-10 appears to be similar to that of the UpB clasts whereas the 93-14 clasts are distinguished by a higher abundance of schists and lower abundance of plutonic rocks (Table 1). The matrix index fraction from Unicorn core 93-10 contains 47% quartz, 34% feldspar, and 19% lithics. It is more nearly similar to the UpB samples than to the 93-14 sands comprised of 32% quartz, 35% feldspar, and 33% lithics. In a quartz/plagioclase/potassium-feldspar plot (Figure 9), the sand fraction from core 93-10 falls within the range of the UpB sediments. Compared to the latter, the 93-14 sample is enriched in plagioclase by 10-20% and depleted in quartz by about the same amount. The greater abundance of lithics and plagioclase at the expense of quartz characterizes all analyzed size fractions of the 93-14 sediments larger than 5ϕ (Figure

10). Material from core 93-10 has a composition-size spectrum very similar to that of the UpB samples (Figure 10) and has nearly identical clay mineral assemblage (Table 2). On the other hand, sample 93-14-20 is the only one that contains almost no smectite and kaolinite and has a detectable amount, *ca.* 25%, of quartz and feldspar in its clay-size fraction (Figure 10).

A very low concentration of diatom fragments was found in both Unicorn cores (Table 3). The diatom fragments are too small to permit identification.

2.7. Sediment Interpretation

2.7.1. The UpB Diamicton

Our sedimentological data indicate that none of the textural properties discussed in this paper are highly variable between and within the UpB cores. Therefore, we feel justified to treat these cores as representing one deposit, to which we refer as the UpB till. The diamicton contained in the UpB cores fits the definition of a till (Dreimanis 1989, p. 34). It exists in a close spatial relationship to a glacier, no evidence for sorting of the sediment by water is present, and its debris was presumably transported and deposited by ice. Sediment mixing is indicated by the occurrence of marine microfossils of various ages, Eocene through Quaternary with dominant Upper Miocene age (Scherer 1991), plus older terrestrial palynomorphs (R. Askin, written comm. to Scherer). We conclude that our cores did not directly sample Tertiary glacimarine sediments inferred to be present only several meters beneath the ice base (Rooney *et al.* 1991), but instead our samples are limited to glacial till lying between in situ glacimarine sediments and glacial ice.

Lack of Mechanical Generation and Modification of Rock Debris.--- Lithologically, the UpB till is similar to typical structureless and poorly sorted subglacial tills (Dreimanis 1989; Karrow 1976). However, unlike common tills, the UpB till bears no evidence of crushing, comminution, and abrasion. These important processes that frequently shape lithology of tills (Dreimanis and Vagners 1969, 1971; Haldorsen 1977, 1981, 1983) do not operate beneath Ice Stream B.

Striations, which usually represent the most dependable indicator of subglacial debris generation and reworking, are not clearly recognizable on the pebble-sized clasts from the UpB cores. In contrast, striations occur on 6 to 57% of the clasts from Late Cenozoic glacial and glacimarine sediments in West Antarctica (Barrett 1975b; Domack *et al.* 1980; Hall 1989) and on 3% to 84% of the clasts in several North American Pleistocene tills (Anderson 1955; Drake 1972; Holmes 1970). Because the UpB clasts are lithologically similar to the clasts studied in the West Antarctic sediments, the lack of striations on the UpB clasts cannot simply result from a lesser susceptibility to production of striations.

Facetted clasts also provide evidence of subglacial mechanical abrasion (Drewry 1986, p. 120). Though they are abundant in the UpB till, the presence of pitted facets suggests that chemical alteration followed an earlier stage of facet generation. This fact, especially combined with the lack of striations, indicates an insignificant amount of recent clast wear beneath Ice Stream B.

Subglacial crushing of larger rock fragments is a major source for sand-sized particles in tills (Dreimanis and Vagners 1969, 1971; Haldorsen 1983). Sand grains produced by crushing should have sharp edges and other breakage microfeatures (Holt 1981; Sharp and Gomez 1986). Sand-sized particles in the UpB till show little such evidence of fresh crushing. They have predominantly rounded edges. Mazzullo and

Anderson (1987) proposed that rounded grain edges may result from subglacial abrasion. However, in the UpB till rounded grain edges are strongly associated with those microfeatures (such as etch pits and crevasses) that are produced by chemical alteration rather than by abrasion (Appendix 1, Figure 14CD). Cross-cutting relationships between different microfeatures suggest that chemical alteration dominated the most recent episode of grain surface evolution.

Development of chemical alteration microfeatures on quartz grains takes place over a long time. Douglas and Platt (1977) analyzed weathering of quartz grains in a soil chronoseqence on Midwestern tills. Weathering microfeatures become significant on grains older than ~10^5 years. Most likely, chemical alteration in Midwestern soils proceeds much faster than in the subglacial zone beneath Ice Stream B (higher temperature and availability of CO_2 and water in the former environment). Kanaori *et al.* (1985) observed relatively freshly looking crushed quartz grains from fault gouges ~10^6 years in age. We hypothesize that the minimum age of the mechanical breakage features seen on grains from the UpB till is of that order. Stresses that acted on the debris since ~10^6 years BP were insufficient to cause significant breakage.

A few lines of evidence show that the UpB till fines (silt and clay) were also not generated by recent mechanical processes. Silt in subglacial deposits frequently represents a prominent mode produced by abrasion (Dreimanis and Vagners 1969, 1971; Haldorsen 1977, 1981, 1983). However, the matrix of the UpB till is depleted in silt as compared to typical tills (Figure 12). Granulometrically and compositionally, the UpB silt is a mixture of the sandy and clayey subpopulations rather than an independent mode (Figure 5C and 10). In addition, the high clay content (38%) and lack of clay-size quartz and feldspar is inconsistent with a subglacial origin of the clay-size material from abrasion of the predominantly crystallinic UpB clasts.

Thus the paradigm of potent mechanical generation and reworking of rock debris beneath ice sheets and glaciers does not apply to the subglacial zone of Ice Stream B. The UpB till did not experience stresses high enough to induce significant crushing and abrasion throughout the whole history of its derivation, transport, and possible deposition. Past subglacial effective pressures may have been as low as the modern ones (average *ca.* 60 kPa). Under such conditions, average inter-particle stresses are low because almost all of the ice overburden weight (~9 MPa) is born by the pore water and little is partitioned onto the solid skeleton of the till. The abundance of fines (~65% of clay and silt) in the till inhibits local stress concentrations between larger grains. This important 'cushioning' effect of fines in the process of crushing and comminution is documented by ball mill (Austin and Bagga 1979) and ring shear experiments (Iverson *et al.* 1995).

In Appendix 2 we develop a simple physical model that illustrates how difficult it is to induce breakage in a grain surrounded by a weak matrix of plastic rheology. Only the situation that maximizes loading on a single grain in contact with one other grain is considered. The condition for grain failure from Appendix 2 is $T \approx 3.6k$, where T is the tensile strength of the grain and k is the yield strength of the till matrix. Only grains made up of relatively weak materials may be broken in the UpB till by the considered mechanism. If we assume 10 kPa for the maximum yield strength of the till matrix (Kamb 1991), T must be less than or equal to 36 kPa. Common minerals and rocks have tensile strengths of the order of 1-100 MPa (Hobbs 1964, Savanick and Johnson 1974).

Hooke and Iverson (1995) and Iverson *et al.* (1995) proposed that build-up and failure of grain bridges may produce crushed sand grains in tills. This mechanism is not likely to be applicable to the UpB till because of its high content of clay and silt. In the present work, we examined *ca.* 200 cm^2 of thin-sectioned UpB till under an optical microscope and found no grain bridges; even contacts of just two sand grains are rare.

Sediment Recycling.--- Since the granular constituents of the UpB till were not created under the present-day subglacial conditions, an alternative model must explain their characteristics. Comparison of our results with the published descriptions of Ross Sea glacigenic sediments shows a strong sedimentological similarity between these deposits (e.g., Figure 13). We infer that the constituents of the UpB till are recycled from an underlying Tertiary basin containing poorly consolidated glacimarine sediments.

The occurrence of fossils in till provides compelling evidence for recycling of preexisting sediments (Collini 1954; Gillberg 1977; Harwood *et al.* 1989). The UpB till contains reworked marine microfossils of multiple ages, indicating incorporation of particles from different marine strata into the deposit. Diatoms and other fossils are found in most marine tills from West Antarctica, including Ross Sea diamictons (RSD) (Kellogg *et al.* 1979), Site J-9 of the Ross Ice Shelf Project (RISP) (Harwood *et al.* 1989) and Crary Ice Rise (CIR) (Scherer 1994b). The UpB samples are, however, distinguishable from RISP, CIR, and RSD sediments by a relative paucity of diatoms, up to 10^4 whole individuals per gram (Table 3). For instance, the RISP material contained an average of 3.85×10^7 whole diatoms per gram in three matrix samples. This disparity is likely caused by significant diatom attrition in the UpB sediments. Diatoms have porous siliceous walls that are only 1 to 2 μm thick.

Composition and morphology of mineral particles from the UpB till also indicate a preexisting unconsolidated sediment as a source for the material. Mineralogically, sands from the UpB till are similar to the basement petrofacies of George (1989) from the glacimarine deposits in the core CIROS-1 (Figure 13A). We do not think, however, that the UpB sand was derived directly from crystalline basement. Enrichment of quartz in the UpB till matrix as compared to the UpB clasts (Figure 9) suggests incorporation of

chemically weathered material (Gillberg 1977). The mineralogy of the UpB sands is, therefore, more consistent with recycling of the Ross Sea sediments into the UpB till than with direct derivation from basement rocks by mechanical processes.

Micromorphology of quartz and feldspar sand grains from the UpB till provides compelling evidence for recycling of chemically weathered debris. If the sands are recycled from the Tertiary Ross Sea sediments, the age of this source material matches the ~10^6 years timescale that is likely needed to create the observed chemical alteration on the UpB quartz grains. Bridle and Robinson (1989) observed chemical alteration microfeatures on sand grains from the Ross Sea glacigenic sequence in the CIROS-1 core.

The grain-size distribution of the UpB till resembles that of tills and glacimarine sediments from the Ross Sea basin. In terms of sand-silt-clay composition the UpB till is indistinguishable from the Ross Sea till (unit 1B from the DSDP site 272, Figure 13B) and very similar to the Miocene glacimarine sediments (unit 2A). Just like the UpB till, the Ross Sea sediments are poorly sorted, clay-rich and, frequently, bimodal (Barrett 1975a, 1989, Hayes and Frakes 1975). Piper and Brisco (1989) suggest that the bimodality results from mixing of sandy and clayey components. The former may represent an ice-rafting and the latter a marine deposition (Barrett 1975a). Similarly, the sandy subpopulation of the UpB till (Figure 5C) lies in the sand-silt-clay plot near the coarse glacial debris from calving glaciers (Mackay and Taylor glaciers, Figure 13B). The clayey subpopulation has the most affinity to fine marine diatomaceous muds.

Preexisting fine-grained sediments provide the most common source of clays in tills (Collini 1954; Karrow 1976). Subglacial chemical weathering does not produce a significant amount of clays (Rosenqvist 1962, 1975). The simplest explanation for the clay minerals in the UpB till is that they are detrital and come ultimately from continental weathering environments. Other students of Antarctic clay-rich sediments reached a similar

conclusion (Anderson *et al.* 1980; Claridge and Campbell 1989; Jacobs 1974). The clay assemblage in the UpB till is very similar to that of the sediments from the Ross Sea and from beneath the Ross Ice Shelf (Figure 13C).

The available evidence strongly suggests that the textural and compositional characteristics of the debris in the UpB till are inherited from the Cenozoic glacigenic sediments of the Ross Sea basin that extends beneath the study area (Rooney *et al.* 1991; Scherer 1994a). The source material itself is likely comparable in strength and the degree of consolidation to the weak UpB till. The Ross Sea sediments of Miocene age drilled during the DSDP Leg 28 were qualitatively classified as soft to stiff (Hayes and Frakes *et al.* 1975). Samples of Miocene sediments selected from the top several hundred meters of the cored Ross Sea sequence had porosity of 34.6% to 43.5% and compressional wave velocity of 1670 to 2090 m/s (Barrett and Froggatt 1978, Table 3). The UpB till has similar porosity, *ca.* 40% (Engelhardt *et al.* 1990), and compressional wave velocity, <1700 m/s (Blankenship *et al.* 1987). Therefore, incorporation of the debris from the poorly consolidated Ross Sea sequence into the UpB till may easily take place without high stresses, thus permitting preservation of the original textural properties. The diamictite clasts and diatomite clasts (Scherer 1991) found in the UpB till likely provide samples of the source material.

The textural properties of the UpB till do not provide a conclusive constraint on the exact genetic mechanism responsible for the recycling of glacimarine deposits and the resulting generation of this till. A key question is whether the UpB till represents "an active till," undergoing continuously pervasive deformation throughout its thickness, as hypothesized by Alley *et al.* (1986, 1987a) or a relict glacial deposit formed under a glacial regime quite different from the current ice stream setting. It is possible that the till unit unconformably overlying (inferred) in-situ Miocene glacimarine sediments at UpB

represents analogy with, if not direct temporal correlation with, the Pleistocene tills overlying the Tertiary glacimarine sequence in the Ross Sea basin. This possibility implies that the debris-poor base of the ice stream moves at present over a relict till layer deforming only in its part adjacent to the ice base and not inducing obvious changes in its sedimentological or physical properties. Borehole observations of basal sliding are consistent with such an inference (Engelhardt and Kamb 1996, submitted).

2.7.2. Sediments From the Unicorn

Both cores from the Unicorn drillholes (93-10 and 93-14) contain graded and sorted debris. We believe that this material was melted out from basal debris-laden ice during hot-water drilling and settled to the bottom of the boreholes before being cored. This interpretation is strongly supported by our measurements showing that the borehole bottom temperatures, -3.4°C in 93-14 and -1.4°C in 93-10 (measured one year after the hole was allowed to refreeze) were below the pressure-melting point of -0.8°C. The thickness of the basal debris-laden ice can be estimated from the drill-hose-tension records. These records show a *ca.* 1-m-thick resistant layer at the bottom of borehole 93-14. In borehole 93-10 the drill encountered a resistant basal layer of 2.9 ± 0.8 m thickness and then broke into a less resistive layer that was penetrated for another 3 ± 0.4 m.

At the time of recovery of the Unicorn cores a significant quantity of clay and fine silt was suspended in the turbid water in the core tube above the cores. We infer that the basal debris sampled by these cores contained originally a wide range of sizes and may have been granulometrically similar to a glacial or a glacimarine diamicton.

We propose that core 93-10 sampled basal debris that represents a frozen-on equivalent of the UpB till. This proposition is strongly supported by the compositional

similarity of all the size fractions in core 93-10 to the corresponding fractions in the UpB till (Table 1 and 2; Figure 9 and 10). In contrast, these fractions are compositionally different than the sediments from the other Unicorn core, 93-14 (Table 1 and 2; Figure 9 and 10).

Our proposition is also consistent with an inferred glaciological history of the area where hole 93-10 was drilled. According to Bentley *et al.* (1994), this area was a part of Ice Stream B perhaps as recently as a century ago. The debris that is now entrained in the base of the slow-moving ice was then probably a southward continuation of the till sheet underlying Ice Stream B. The stoppage of this part of the ice stream decreased the sliding velocity by two orders of magnitude and probably decreased the basal frictional heating by a factor of ~10. In this situation, cooling by upward heat conduction in the basal ice may freeze on several meters of debris-laden ice in a time period of a few centuries (Bindschadler *et al.* 1990; Alley and MacAyeal 1994).

The micromorphology of sand from core 93-10 is similar to that of the UpB sand fraction but has somewhat more predominant mechanical breakage features (Figure 6C and 7). Particle breakage and abrasion may take place beneath the slow-moving Unicorn if subglacial water pressure decreases and effective pressure increases sufficiently. The basal shear stress likely increased from a few kPa (Kamb 1991) to *ca.* 20 kPa (regional average) after the northern part of the Unicorn stopped moving with the ice stream. When grains are incorporated into basal ice by freeze-on, they may undergo some breakage due to the pressure of ice growing into small pre-existing cracks (Moss *et al.* 1991). Deformation of basal debris-laden ice may also lead to particle breakage and abrasion.

The debris from core 93-14 experienced even more significant mechanical breakage and abrasion than the 93-10 material. This fact is documented by: 1. the micromorphologic evidence (Figure 7), 2. the probable comminution debris (quartz and feldspar) in the clay-

size fraction (Figure 10), and 3. clasts with clear striations (Figure 11). These characteristics make the sediments from core 93-14 similar to typical, mechanically generated glacial debris (Dreimanis and Vagners 1969, 1971; Drewry 1986, p. 91-145). Just as in the case of the material from core 93-10, the greater influence of mechanical breakage and abrasion may have been caused here by freeze-on and/or subglacial or basal processes.

The sediments recovered in core 93-14 are from a different source rock than the UpB and 93-10 sediments. Clast lithology (Table 1) and abundance of lithics (Figure 10) suggest that much of the material was originally derived from schists. The high content of plagioclase (Figure 9), the low content of quartz, and near absence of smectite and kaolinite (Table 2) indicate that there is little of pre-glacial chemically weathered debris in the 93-14 sediments. Only the presence of diatom fragments provides evidence for incorporation of marine sediments into the basal debris sampled at this location. Borehole 93-14 was drilled farthest to the south, near the B1 branch of Ice Stream B (Figure 1B). The 93-14 basal debris may represent an entrained, old till layer of the B1 branch. Alternatively, it may have tapped a different part of the Tertiary Ross Sea glacimarine sequence than the one providing the source for the UpB till.

2.8. Implications for Models of Till Genesis

An important question is to what degree the UpB till provides a sedimentological analog for other tills. Alley *et al.* (1987) and Alley (1991) suggested that their deforming-bed model for till formation beneath Ice Stream B may explain also tills deposited beneath other ice sheets such as the Late Pleistocene southern Laurentide ice sheet. A number of authors stated or implied that the deforming-bed mechanism can account for all the

observed sedimentological features of paleo-tills, including those features formed by crushing, abrasion, and comminution (Alley 1991; Boulton 1996; Clark 1991; Cuffey and Alley 1996). However, our observations challenge the idea that till deformation alone is necessarily capable of producing the common mechanically generated characteristics of glacial debris such as striations, facets, broken particles and glacial flour.

Borehole investigations indicate that Ice Stream B moves at present mainly by basal sliding and/or till deformation concentrated in the vicinity of the ice base (Engelhardt and Kamb 1996, submitted). Concentration of till deformation within less than a few decimeters from the base is consistent with the nearly plastic rheology of this material (Boulton 1996, Figure 4). Our sedimentological data do not show any signs of crushing and abrasion near the tops of UpB cores. The presence of fragile diatom shells at the top of the till provides convincing evidence for the weakness of mechanical breakage and abrasion in the very zone where subglacial deformation is the largest.

Low 'aggressiveness' of the mechanical processes is likely to be a general problem for the proposed pervasively deforming subglacial beds. Theory indicates that the pervasive bed deformation is most likely to occur in fine-grained tills subjected to a low effective pressure (Boulton and Hindmarsh 1987). Exactly the same two factors, low effective pressure and fine character of the UpB till, are responsible for the lack of crushing, abrasion, and comminution beneath Ice Stream B. Mineral grains undergoing loading in such till will experience translation rather than breakage or abrasion.

Our observation of insignificant crushing and abrasion in the UpB till is in a general agreement with the theoretical analysis of Cuffey and Alley (1996) suggesting that pervasively deforming subglacial beds are not capable of producing a significant amount of debris by mechanical erosion of lithified bedrock. These results question whether subglacial till deformation can be a widespread primary till-forming process. More likely it

is just a secondary process that occurs only if ice overrides preexisting tills or other relatively fine-grained and weak sediments. It has been proposed that the pervasive subglacial deformation was responsible for creation of tills beneath large parts of past ice sheets (Alley *et al.* 1987b, 1991; Clark and Walder 1994). From the point of view of our findings, the underlying assumption that this process can mechanically produce and shape significant quantities of glacial debris from a variety of substrata is called into question.

The UpB till is not a close sedimentological analog of the typical continental Late Pleistocene tills. Unlike the UpB till, these subglacial deposits have abundant evidence of mechanical crushing, abrasion, and comminution (Anderson 1955; Douglas and Platt 1977; Drake 1972; Dreimanis and Vagners 1971, 1972; Haldorsen 1977, 1981, 1983; Holmes 1952 and many others). They had to be formed under conditions that permitted high inter-particle stresses. This may require considerable effective subglacial pressure and/or proximity of the ice base to hard bedrock or coarse sediments, which would permit local stress concentrations. A large body of research shows that subglacial mechanical generation and reworking of debris does take place beneath ice in contact with hard beds (summary in Drewry 1986). Similar effort is needed to further elucidate the extent to which soft glacial beds are qualitatively or quantitatively different in that respect.

The till from beneath Ice Stream B may be a good sedimentological analog for tills deposited by ice overriding marine or lacustrine basins. The UpB till has general sedimentological affinity to clayey, fossil-bearing Pleistocene tills that incorporated a significant amount of soft marine sediments (e.g., Krinsley and Funnell 1965) and to the marine tills found in the Ross Sea and elsewhere on the Antarctic continental shelf (Anderson *et al.* 1980, 1984; Barrett 1975ab; Domack *et al.* 1980; Kellogg *et al.* 1979). The example of the UpB till shows that grounded ice is capable of producing deposits similar to the Ross Sea tills just as has been inferred by Kellogg *et al.* (1979) and Anderson

et al. (1980).

Does sedimentological similarity of the Ross Sea, or any other, tills to the UpB till imply that they were deposited beneath an ice stream comparable to Ice Stream B? Such similarity provides a permissive but not conclusive evidence. The only characteristic of the UpB till that reflects the sub-ice stream conditions is the lack of mechanical generation and reworking of rock debris and (partial?) preservation of diatoms. Low effective subglacial pressure is consistent with lack of crushing/abrasion in till and with fast ice streaming, but we cannot determine that it is a necessary and sufficient condition for the two.

A comparison between Ice Stream B and the Unicorn illustrates an important role of ice dynamics in controlling the patterns of subglacial debris entrainment and deposition. Our data from the Unicorn support the proposition of Alley and MacAyeal (1994) that stopped ice streams (or, in this case, stopped parts of ice streams) experience freeze-on of basal debris-laden ice. On the other hand, basal velocity and frictional heat production within Ice Stream B are high enough to result in melting and the basal ice is debris-poor. Any basal debris-laden ice that enters Ice Stream B at its head or through the margins (e.g., from the Unicorn) will deposit sediments unto the substratum due to the basal melting that may be as fast as 2 cm/year (Kamb and Engelhardt 1991). Spatial and temporal changes in the extent of the ice-sheet and ice-stream type motion may have a significant impact on the character of the glacial record left by ice (Punkari 1994).

2.9. Conclusions

The paradigm of strong subglacial debris generation and reworking developed for glaciers overriding hard beds does not apply to the till from beneath Ice Stream B. Subglacial crushing, abrasion, and comminution did not influence its textural properties.

This makes the deposit sedimentologically distinct from common continental subglacial tills for which this till was proposed as a potential analog (Alley 1991). The low mechanical 'aggressiveness' of the sub-ice-stream environment is due to small effective subglacial pressure, average of *ca.* 60 kPa, and a fine-grained character of the till matrix. Similar conditions are thought to favor pervasive till deformation (Boulton and Hindmarsh 1987). Our observations suggest that such till deformation alone is unable to account for basic properties of subglacial debris such as striations, facets, broken particles, and glacial flour. Till deformation may be a secondary process occurring only beneath ice overriding preexisting weak sediments rather than a primary process that is by itself capable of forming tills over different substrata.

The till beneath Ice Stream B is composed of material recycled, without much change, from older tills or glacimarine deposits of the Cenozoic Ross Sea basin which extends beneath this part of the WAIS. Only reworked microfossils provide indication of glacial transport and mixing. The UpB till is quite similar to the Ross Sea diamictons that are found near the top of the Ross Sea sequence and have been interpreted by most researchers as subglacial tills (Anderson *et al.* 1980; Kellogg *et al.* 1979). The UpB till illustrates that such deposits may originate beneath grounded ice. Sedimentological similarity of any other till to the UpB till is consistent with its deposition beneath an ice stream analogous to Ice Stream B, but we do not demonstrate here that such similarity provides a conclusive proof regarding genesis.

The basal debris recovered from the northern edge of the slow-moving Unicorn (site 93-10) came from a basal layer of debris-laden ice that was created by freeze-on of the UpB till. The freeze-on occurred probably after this part of the Unicorn stopped moving at ice stream speeds about a century ago (Bentley *et al.* 1994). The other Unicorn core, 93-14, also contains basal debris that may have been frozen-on. This material is

compositionally different than the UpB till and may represent an old till of the B1 branch of the ice stream or a glacimarine diamicton. Perhaps surprisingly, the slow-moving ice appears to be a more efficient agent for production of mechanically-shaped glacial debris than is the fast ice stream. Our data are insufficient to constrain unequivocally the physical processes that are responsible for this situation. The problem calls for experimental investigation.

The presence of basal debris within the slow-moving Unicorn contrasts with scarcity or absence of sediments in the basal ice of the ice stream. High velocity results in significant frictional heat production and melting at the base of the ice stream. Low frictional heating beneath the Unicorn permits, or has permitted in the past, basal freezing. This example shows that ice dynamics has a principal control over spatial patterns of glacial erosion and deposition.

2.10. Appendix 1 - Microfeature Data

Raw microfeature abundance data is difficult to interpret (Figure 14AB). To aid our interpretation, we use factor analyses on quartz and feldspar data separately. In R-mode factor analysis, the relationship within a set of variables is presumed to reflect the correlations of each of the variables with mutually uncorrelated underlying "common" factors (Davis 1986, p. 547). In our case these common factors can be thought of as mutually exclusive virtual microfeatures created by the statistical analysis of variance of the real microfeatures.

Factor analysis makes no prior assumption regarding the underlying cause of the observed feature variance. The meaning of each common factor has to be interpreted based on the loadings from the real microfeatures (Figure 14CD). A first factor accounts for most

of the variance in the data. Examination of the Figure 14CD shows that in both data sets the first factor is dominated by competition between two groups of microfeatures. The first group has positive loadings and comprises mainly features associated with physical breakage of grains (Figure 14CD). The second group has negative factor loadings and consists predominantly of the features generated by chemical alteration. The lower R-mode factors were difficult to interpret and contained significant contributions only from a few microfeatures.

2.11. Appendix 2 - Grain Crushing

Failure of grains is frequently interpreted in terms of build-up of elastic tensile stresses in the interior of a grain loaded on its boundaries (Hiramatsu and Oka 1966). For a grain in a perfectly plastic matrix, the maximum force that may be applied to any point on the grain surface is equal to the force that will result in plastic yielding around the hemisphere of the grain that lies opposite to the point of loading (Figure 15). When such yielding develops, the grain starts to move through the matrix. The maximum point load, P, is equal to the resistive force offered by the matrix, F, which may be estimated for a spherical particle based on plasticity theory (Johnson, 1970, p. 481):

$$P = F = (2 + \pi) \cdot k \cdot \pi \cdot R^2 \qquad (3)$$

where: k = plastic yield strength of the matrix,

R = radius of the grain,

We have not been able to find or derive an explicit solution for the distribution of elastic stresses in a grain under such asymmetric load. We make a heuristic assumption that the loading is analogous to the Brazilian test. In that test two point loads of equal magnitude and opposite direction are applied to a grain. Since an increase in an area over

which a load is distributed causes a decrease in the magnitude of tensile stresses inside the grain (Hiramatsu and Oka 1966, Figure 5), this assumption is consistent with our intention to consider a build-up of maximum stresses for a given magnitude of the load P. Tensile stresses within a sphere loaded in the Brazilian test can be calculated analytically (Hiramatsu and Oka 1966, p. 97). At the center of the spherical grain the tensile stress is:

$$\sigma_t \approx \frac{0.7 \cdot P}{\pi \cdot R^2} \tag{4}$$

Substituting for applied load P (eq. 3):

$$\sigma_t \approx 3.6 \cdot k \tag{5}$$

A failure of the loaded grain will occur only if the tensile stress reaches the tensile strength of the grain, i.e., $T \approx \sigma_t \approx 3.6k$.

In our treatment we omitted the possibility of grain failure due to high tensile stresses building-up on the grain surface around the Hertzian contact between grains. Experimental and theoretical results of Zhang *et al.* (1990) suggest that the Hertzian-contact mechanism produces significant breakage of natural materials at similar loads (of the order of MPa) as the Brazilian test (Hobbs 1964).

2.12. Acknowledgments

This project was funded by grant OPP-9219279 from the National Science Foundation. Partial support was provided to R. Scherer by NSF grant OPP-9496169 and the Swedish Natural Science Research Council. S. Tulaczyk acknowledges support from the Henry and Grazyna Bauer Fellowship. We thank Rowena Lohman for her help with laboratory analyses.

2.13. References

Alley, R.B., 1991, Deforming-bed origin for southern Laurentide till sheets: Journal of Glaciology, v. 37, p. 67-76.

Alley, R.B., Blankenship, D.D., Bentley, C.R., and Rooney, S.T., 1986, Deformation of till beneath Ice Stream B, West Antarctica: Nature, v. 322, p. 57-59.

Alley, R.B., Blankenship, D.D., Bentley, C.R., and Rooney, S.T., 1987a, Till beneath Ice Stream B, 3. Till deformation: evidence and implications: Journal of Geophysical Research, v. 92, p. 8921-8929.

Alley, R.B., Blankenship, D.D., Rooney, S.T., and Bentley, C.R., 1987b, Continuous till deformation beneath ice sheets: Publication of the International Association of Hydrological Sciences, no. 170, p. 81-90.

Alley, R.B., and MacAyeal, D.R., 1993, West antarctic ice sheet collapse: Chimera or clear danger? Antarctic Journal of the United States, v. 28, p. 59-60.

Alley, R.B., and MacAyeal, D.R., 1994, Ice-rafted debris associated with binge/purge oscillations of the Laurentide Ice Sheet: Paleoceanography, v. 9, p. 503-511.

Anderson, J.B., Brake, C.F., and Myers, N.C., 1984, Sedimentation on the Ross Sea continental shelf, Antarctica: Marine Geology, v. 57, p. 295-333.

Anderson, J.B., Kurtz, D.D., Domack, E.W., and Balshaw, K.K., 1980, Glacial and glacial marine sediments of the Antarctic continental shelf: Journal of Geology, v. 88, p. 399-414.

Anderson, R.C., 1955, Pebble lithology of the Marseilles till sheet in northeastern Illinois: Journal of Geology, v. 63, p. 228-243.

Austin, L.G., and Bagga, P., 1981, An analysis of fine dry grinding in ball mills: Powder Technology, v. 28, p. 83-90.

Barrett, P.J., 1975a, Textural characteristics of Cenozoic preglacial and glacial sediments at site 270, Ross Sea, Antarctica: in Hayes, D.E., and Frakes, L.A., eds., Initial Reports of the Deep Sea Drilling Project, v. 28, US Government Printing Office, Washington D.C., p. 757-767.

Barrett, P.J., 1975b, Characteristics of pebbles from Cenozoic marine glacial sediments in the Ross Sea (DSDP sites 270-274) and the South Indian Ocean (site 268): in Hayes, D.E., and Frakes, L.A., eds., Initial Reports of the Deep Sea Drilling Project, v. 28, US Government Printing Office, Washington D.C., p. 769-773.

Barrett, P.J., 1989, Sediment texture: in Barrett P.J., ed., Antarctic Cenozoic history from the CIROS-1 drillhole, McMurdo Sound: Department of Scientific and Industrial Research Bulletin, v. 245, p. 49-58.

Barrett, P.J., and Froggatt, P.C., 1978, Densities, porosities, and seismic velocities of some rocks from Victoria Land, Antarctica: New Zealand Journal of Geology and Geophysics, v. 21, p. 175-187.

Bentley, C.R., 1982, Crustal structure of Antarctica from geophysical evidence - a review: in Oliver, R.L., James, P.R., and Jago, J.B., eds., Antarctic earth science, Cambridge, Cambridge University Press, p. 491-497.

Bentley, C.R., 1987, Antarctic ice streams: a review: Journal of Geophysical Research, v. 92, p. 8843-8858.

Bentley, C.R., Burkholder, P.D., Clarke, T.S., Liu, C., and Lord, N., 1994, Geophysical experiments on ridge B1/B2, Siple Coast: Antarctic Journal of the United States, v. 29, p. 57-59.

Berner, R.A., and Holdren, G.R., 1977, Mechanism of feldspar weathering: Some observational evidence: Geology, v. 5, p. 369-372.

Berner, R.A., and Holdren, G.R., 1979, Mechanism of feldspar weathering-II.

Observations of feldspars from soils: Geochimica et Cosmochimica Acta, v. 43, p. 1173-1186.

Bindschadler, R.A., Koci, B., and Iken, A., 1988, Drilling on Crary Ice Rise, Antarctica: Antarctic Journal of the United States, v. 23, p. 60-61.

Bindschadler, R.A., Roberts, E.P., and Iken, A., 1990, Age of Crary Ice Rise, Antarctica, determined from temperature-depth profiles: Annals of Glaciology, v. 14, p. 13-16.

Blankenship, D.D., Bentley, C.R., Rooney, S.T., and Alley, R.B., 1986, Seismic measurements reveal a saturated porous layer beneath an active Antarctic ice stream: Nature, v. 322, p. 54-57.

Blankenship, D.D., Bentley, C.R., Rooney, S.T., and Alley, R.B., 1987, Till beneath Ice Stream B, 1. Properties derived from seismic travel times: Journal of Geophysical Research, v. 92, p. 8903-8911.

Boulton, G.S., 1996, Theory of glacial erosion, transport and deposition as a consequence of subglacial sediment deformation: Journal of Glaciology, v. 42, p. 43-62.

Boulton, G.S., and Hindmarsh, R.C.A., 1987, Sediment deformation beneath glaciers - rheology and geological consequences: Journal of Geophysical Research, v. 92, p. 9059-9082.

Bridle, I.M., and Robinson, P.H., 1989, Diagenesis: in P.J. Barrett, ed., Antarctic Cenozoic history from the CIROS-1 drillhole: McMurdo Sound, Department of Scientific and Industrial Research Bulletin, v. 245, p. 201-207.

Claridge, G.G.C., and Campbell, I.B., 1989, Clay mineralogy: in Barrett, P.J., ed., Antarctic Cenozoic history from the CIROS-1 drillhole: McMurdo Sound, Department of Scientific and Industrial Research Bulletin, v. 245, p. 185-193.

Clark, P.U., 1991, Striated clast pavements: Products of deforming bed? Geology, v. 19,

p. 530-533.

Clark, P.U., 1992, Surface form of the southern Laurentide Ice Sheet and its implications to ice-sheet dynamics: Geological Society of America Bulletin, v. 104, p. 595-605.

Clark, P.U., and Walder, J.S., 1994, Subglacial drainage, eskers, and deforming beds beneath the Laurentide and Eurasian ice sheets: Geological Society of America Bulletin, v. 106, p. 304-314.

Collini, B., 1954, On the origin and formation of the Fennoscandian Quaternary clays: Geologiska Foereningens i Stockholm Foerhandlingar, v. 78, p. 528-535.

Cuffey, K., and Alley, R.B., 1996, Is erosion by deforming subglacial sediments significant? (Toward till continuity): Annals of Glaciology, in press.

Darmody, R.G., 1985, Weathering assessment of quartz grains: a semiquantitative approach: Soil Science Society of America Journal, v. 49, p. 1322-1324.

Davis, J.C., 1986, Statistics and data analysis in geology: New York, John Wiley & Sons, p. 645.

Domack, E.W., Anderson, J.B., and Kurtz, D.D., 1980, Clast shapes as indicator of transport and depositional mechanisms in glacial marine sediments: Journal of Sedimentary Petrology, v. 50, p. 813-820.

Douglas L.A., and Platt, D.W., 1977, Surface morphology of quartz and age of soils: Soil Science Society of America Journal, v. 41, p. 641-645.

Drake, L.D., 1972, Mechanisms of clast attrition in basal till: Geological Society of America Bulletin, v. 83, p. 2159-2166.

Dreimanis, A., 1989, Tills: their genetic terminology and classification: in Goldthwait, R.P., and Matsch, C.L., eds., Genetic classification of glacigenic deposits: A.A. Balkema, Rotterdam, p. 17-83.

Dreimanis, A., and Vagners, U.J., 1969, Lithologic relation of till to bedrock: in Wright,

H.E., ed., Quaternary geology and climate, Washington D.C., National Academy of Sciences, p. 93-98.

Dreimanis, A., and Vagners, U.J., 1971, Bimodal distribution of rock and mineral fragments in basal tills: in Goldthwait, R.P., ed., Till; a symposium: Columbus, Ohio State University Press, p. 237-250.

Drewry, D., 1986, Glacial geologic processes: London, Edward Arnold, p. 276.

Echelmeyer, K.A., Harrison, W.D., Larsen, C., and Mitchell, J.E., 1994, The role of the margins in the dynamics of an active ice stream: Journal of Glaciology, v. 40, p. 527-538.

Engelhardt, H.F., Humphrey, N., Kamb, B., and Fahnestock, M., 1990, Physical conditions at the base of a fast moving Antarctic ice stream: Science, v. 248, p. 57-59.

Engelhardt, H.F., and Kamb, B., 1993, Vertical temperature profile of ice stream B: Antarctic Journal of the United States, v. 28, p. 63-66.

Engelhardt, H.F., and Kamb, B., 1996, Sliding velocity of Ice Stream B: submitted to Journal of Glaciology.

Galehouse, J.S., 1971a, Point counting: in Carver, R.E., ed., Procedures in sedimentary petrology, New York, Wiley-Interscience, p. 385-407.

Galehouse, J.S., 1971b, Sedimentation analysis: in Carver, R.E., ed., Procedures in sedimentary petrology: New York, Wiley-Interscience, p. 69-94.

George, A., 1989, Sand provenance: in Barrett, P.J., ed., Antarctic Cenozoic history from the CIROS-1 drillhole, McMurdo Sound: Department of Scientific and Industrial Research Bulletin, v. 245, p. 159-163.

Gillberg, G., 1977, Redeposition: a process in till formation: Geologiska Foereningens i Stockholm Foerhandlingar, v. 99, p. 246-253.

Gow, A., Ueda, H., and Garfield, D., 1968, Antarctic ice sheet: preliminary results of first core hole to bedrock: Science, v. 161, p. 1011-1013.

Griffin, G.M., 1971, Interpretation of x-ray diffraction data: in Carver, R.E., Procedures in sedimentary petrology: New York, Wiley-Interscience, p. 541-569.

Haldorsen, S., 1977, The petrography of tills - a study from Ringsaker, south-eastern Norway: Norges Geologiske Undersoekelse, v. 336, p. 1-36.

Haldorsen, S., 1981, The enrichment of quartz in tills: in Evenson, E.B., Schluchter, C., and Rabassa, J., Tills and related deposits: Rotterdam, A.A. Balkema, p. 141-150.

Haldorsen, S., 1983, Mineralogy and geochemistry of basal till and their relationship to till-forming processes: Norsk Geologisk Tidsskrift, v. 63, p. 15-25.

Hall, K.J., 1989, Clast shape: in Barrett, P.J., ed., Antarctic Cenozoic history from the CIROS-1 drillhole, McMurdo Sound: Department of Scientific and Industrial Research Bulletin, v. 245, p. 63-67.

Harwood, D.M., Scherer, R.P., and Webb, P.-N., 1989, Multiple Miocene productivity events in West Antarctica as recorded in Upper Miocene sediments beneath the Ross Ice Shelf (Site J-9): Marine Micropaleontology, v. 15, p. 91-115.

Hayes, D.E., and Frakes, L.A., 1975, General synthesis: in Hayes, D.E., and Frakes, L.A., eds., Initial Reports of the Deep Sea Drilling Project, v. 28, US Government Printing Office, Washington D.C., p. 919-942.

Hayes, D.E., Frakes, L.A., *et al.*, 1975, Sites 270, 271, 272: in Hayes, D.E., and Frakes, L.A., eds., Initial Reports of the Deep Sea Drilling Project, v. 28, US Government Printing Office, Washington D.C., p. 211-334.

Herron, S., and Langway, C.C., 1979, The debris-laden ice at the bottom of the Greenland ice sheet: Journal of Glaciology, v. 23, p. 193-207.

Hiramatsu, Y., and Oka, Y., 1966, Determination of the tensile strength of rock by a

compression test of an irregular test piece: International Journal of Rock Mechanics and Mining Sciences, v. 3, p. 89-99.

Hobbs, D.W., 1974, The tensile strength of rocks: International Journal of Rock Mechanics and Mining Sciences, v. 1, p. 385-396.

Holdren, G.R., and Berner, R.A., 1979, Mechanism of feldspar weathering-I. Experimental studies: Geochimica et Cosmochimica Acta, v. 43, p. 1161-1171.

Holmes, C.D., 1952, Drift dispersion in west-central New York: Geological Society of America Bulletin, v. 63, p. 993-1010.

Holt, C.B., 1981, The shape of particles produced by comminution, a review: Powder Technology, v. 28, p. 59-63.

Hooke, R.L., and Iverson, N.R., 1995, Grain-size distribution in deforming subglacial tills: role of grain fracture: Geology, v. 23, p. 57-60.

Hughes, T., 1977, West Antarctic ice streams: Reviews of Geophysics and Space Physics, v. 15, p. 1-46.

Iverson, N.R., Hooyer, T., and Hooke, R.L., 1995, A laboratory study of sediment deformation, stress heterogeneity and grain-size evolution: Annals of Glaciology, in print.

Jacobs, M.B., 1974, Clay mineral changes in Antarctic deep-sea sediments and Cenozoic climatic events: Journal of Sedimentary Petrology, v. 44, p. 1079-1086.

Jankowski, E.J., and Drewry, D.J., 1981, The structure of West Antarctica from geophysical studies: Nature, v. 291, p. 17-21.

Johnson, A.M., 1970, Physical processes in geology: Freeman, Cooper & Co., San Francisco, p. 577.

Kamb, B., 1991, Rheological nonlinearity and flow instability in the deforming-bed mechanism of ice stream motion: Journal of Geophysical Research, v. 96, p.

16,585-16,595.

Kamb, B., and Engelhardt, H.F., 1991, Antarctic ice stream B: conditions controlling its motion and interactions with the climate system: Publication of the International Association of Hydrological Sciences, no. 208, p. 145-154.

Kanaori, Y., Tanaka, K., and Miyakoshi, K., 1985, Further studies on the use of quartz grains from fault gouges to establish the age of faulting: Engineering Geology, v. 21, p. 175-194.

Karrow, P.F., 1976, The texture, mineralogy, and petrography of North American tills: in Legget, R.F., ed., Glacial till, an inter-disciplinary study: Royal Sociey of Canada Special Publication No.12, Ottawa, Royal Society of Canada, p. 83-98.

Kellogg, T.B., Truesdale, R.S., and Osterman, L.E., 1979, Late Quaternary extent of the West Antarctic ice sheet: new evidence from Ross Sea cores: Geology, v. 7, p. 249-253.

Krinsley, D.H., and Doornkamp, J.C., 1973, Atlas of quartz sand surface textures: Cambridge, The Cambridge University Press, p. 96.

Krinsley, D.H., and Funnell, B.M., 1965, Environmental history of quartz sand grains from the Lower and Middle Pleistocene of Norfolk, England: Quarterly Journal of the Geological Society of London, v. 121, p. 435-461.

Krumbein, W.C., 1941, Measurement and geological significance of shape and roundness of sedimentary particles: Journal of Sedimentary Petrology, v. 11, p. 64-72.

Laws, R.A., 1983, Preparing strewn slides for quantitative microfossil analysis: A test using calibrated microspheres: Micropaleontology, v. 29, p. 60-65.

MacAyeal, D.R., 1992, Irregular oscillations of the West Antarctic ice sheet: Nature, v. 359, p. 29-32.

Margolis, S.V., and Kennett, J.P., 1971, Cenozoic glacial history of Antarctica recorded

in subantarctic deep-sea cores: American Journal of Science, v. 271, p. 1-36.

Mazzullo, J., and Anderson, J.B., 1987, Grain shape and surface texture analysis of till and glaci-marine sand grains from the Weddell and Ross Seas, Antarctica: in Marshall, J.R., ed., Clastic particles: New York, Van Nostrand Reinhold, p. 314-327.

Mazzullo, J., and Ritter, C., 1991, Influence of sediment source on the shapes and surface textures of glacial quartz sand grains: Geology, v. 19, p. 384-388.

Moss, A.J., Green, P., and Hutka, J., 1981, Static breakage of granitic detritus by ice and water in comparison with breakage by flowing water: Sedimentology, v. 28, p. 261-272.

Pettijohn, F.J., 1975, Sedimentary rocks: New York, Harper & Row, p. 628.

Piper, D.J.W., and Brisco, C.D., 1975, Deep-water continental margin sedimentation, DSDP Leg 28, Antarctica: in Hayes, D.E., and Frakes, L.A., eds., Initial Reports of the Deep Sea Drilling Project, v. 28, Washington D.C., US Government Printing Office, p. 727-755.

Punkari, M., 1994, Function of the ice streams in the Scandinavian ice sheet: analyses of glacial geological data from southwestern Finland: Transactions of the Royal Society of Edinburgh: Earth Sciences, v. 85, p. 283-302.

Ronnert, L., 1992, Genesis of diamicton in the Oak Creek Formation of south-east Wisconsin, USA: Sedimentology, v. 39, p. 177-192.

Rooney, S.T., Blankenship, D.D., Alley, R.B., and Bentley, C.R., 1991, Seismic reflection profiling of a sediment-filled graben beneath Ice Stream B, West Antarctica: in Thomson, M.R., Crame, J.A., and Thomson, J.W., eds., Geological evolution of Antarctica, Cambridge, British Antarctic Survey, pp. 261-265.

Rosenqvist, I.T., 1962, What is the origin of the hydrous micas in Fennoscandia? Bulletin of the Geological Institutions of the University of Uppsala, v. 40, 265-268.

Rosenqvist, I.T., 1975, Origin and mineralogy of glacial and interglacial clays of southern Norway; Clays and Clay Minerals, v. 23, p. 153-159.

Ross, S.M., 1987, Introduction to probability and statistics for engineers and scientists: New York, John Wiley & Sons, p. 492.

Savage, M.L., and Ciesielski, P.F., 1983, A revised history of glacial sedimentation in the Ross Sea region: in Oliver, R.L., James, P.R., and Jago, J.B., eds., Antarctic Earth Science, Cambridge, Cambridge University Press, p. 555-559.

Savanick, G.A. and Johnson, D.I., 1974, Measurements of the strength of grain boundaries in rock: International Journal of Rock Mechanics, Mining Sciences and Geomechanical Abstracts, v. 11, p. 173-180.

Scherer, R.P., 1989, Microfossil assemblages in "deforming till" from Upstream B, West Antarctica: implications for ice-stream flow models: Antarctic Journal of the United States, v. 24, p. 54-55.

Scherer, R.P., 1991, Quaternary and Tertiary microfossils from beneath Ice Stream B: evidence for a dynamic West Antarctic Ice Sheet history: Palaeogeography, Palaeoclimatology, Palaeoceanography, v. 90, p. 395-412.

Scherer, R.P., 1994a, A speculative stratigraphic model for the central Ross embayment: Antarctic Journal of the United States., v. 29, p. 9-11.

Scherer, R.P., 1994b, A new method for the determination of absolute abundances of diatoms and other silt-sized sedimentary particles: Journal of Paleolimnology, v. 12, p. 171-180.

Sharp, M., and Gomez, B., 1986, Process of debris comminution in the glacial environment and implications for quartz sand-grain micromorphology:

Sedimentary Geology, v. 46, p. 33-47.

Sladen, J.A., and Wrigley, W., 1983, Geotechnical properties of lodgement till - a review: in Eyles, N., ed., Glacial geology, an indroduction for engineers and earth scientists: Oxford, Pergamon Press, p. 184-212.

Sugden, D.E., Knight, P.G., Livesey, N., Lorrain, R.D., Souchez, R.A., Tison, J.-L., and Jouzel, J., 1987, Evidence for two zones of debris entrainment beneath the Greenland ice sheet: Nature, v. 328, p. 238-241.

Turner, J.W., 1992, Dispersal and provenance of fine-grained sediments and the influence of marine transgression on the Ross Sea continental shelf, Antarctica [Ph.D. Thesis]: Columbus, Ohio State University, p. 284.

Webb, P.N., 1979, Initial report on geological materials collected at RISP Site J9: RISP Technical Report 79-1, Ross Ice Shelf Project Management Office, Lincoln, Nebraska, p. 126.

Whillans, I.M., and van der Veen, C.J., 1993, New and improved determinations of velocity of ice stream B and C, West Antarctica: Journal of Glaciology, v. 39, p. 483-490.

Zhang, J., Wong, T-F., and Davis, D.M., 1990, Micromechanics of pressure-induced grain crushing in porous rocks: Journal of Geophysical Research, v. 95, p. 341-352.

Table 1. Clast Lithology

Number frequency of different clast lithologies given in percent.

Sample	Clast Count	Schists %	Gneisses %	Plutonics %	Volcanics %	Sed. Rocks %	Quartz Frag. %
UpB	230	27	33	23	3	8	6
93-10	27	33	26	37	0	0	4
93-14	82	50	26	9	0	0	15

Table 2. Clay Mineralogy

Abundance of the different clay minerals in the clay-size fraction of selected samples.

Samples	Kaolinite %	Chlorite %	Illite %	Smectite %
89-4-20	9	13	61	18
89-6-30	11	10	51	29
89-7-20	7	16	58	19
89-8-0	11	14	53	22
92-1-60	9	12	60	19
Average UpB	9	13	57	21
93-10-20	8	12	55	25
93-14-20	3	21	73	3

Table 3. Diatom Abundances

Abundance of diatoms and diatom fragments in 10,000 counts per gram.

Diatoms	92-1-0	92-1-140	92-1-270	93-10	93-14
fragments <10μm	251	4	18	87	1
<¼ of a diatom	75	1	2	1	1
¼-½ of a diatom	5	0	0	0	0
>½ of a diatom	5	0	0	0	0
whole diatom	1	0	0	0	0

Figure 1. A. Location of the study area in West Antarctica. Letters A through E denote the individual Ross ice streams. Boundaries of the ice streams and ice elevation contour lines at 250 m spacing are from Whillans and van der Veen (1993, Figure 1), base map and position of mountain ranges and nunataks (in black) from Bentley (1982, Figure 1). Inset B shows the core sampling sites on Ice Stream B2 (89-4, 89-6, 89-7, 89-8, 92-1) and on Unicorn (93-10, 93-14). The shear margins between the slow moving Unicorn and the two branches of Ice Stream B (designated by B1 and B2) are shown as shaded bands. The "Fishhook," a faint linear feature seen in satellite images and probably marking a former shear margin, is shown with a dashed line (modified from Bentley *et al.* 1994, Figure 1).

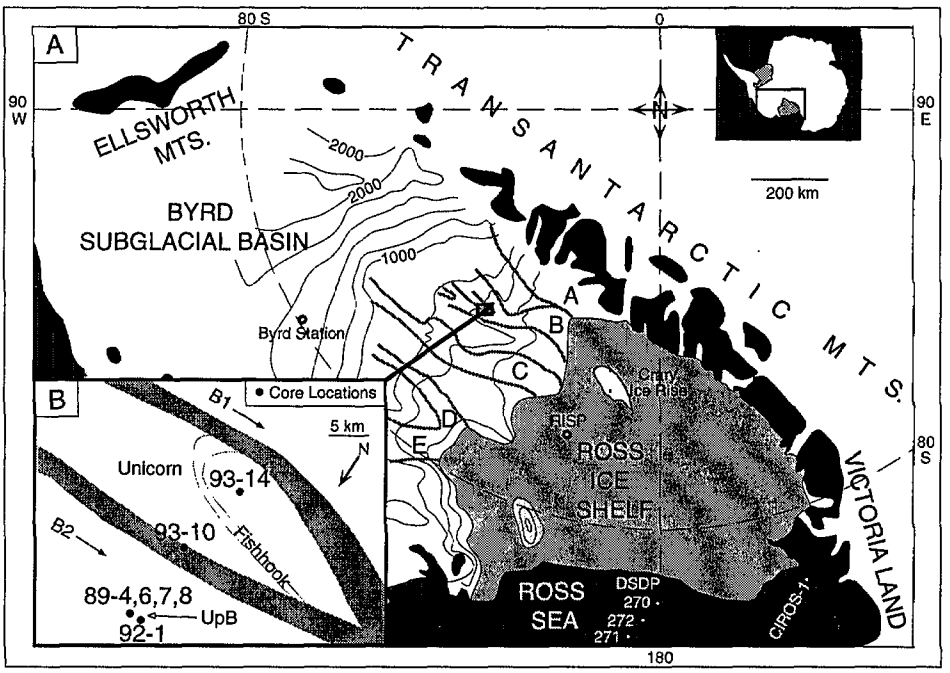
A
80 S
0
90 W
90 E
ELLSWORTH MTS.
TRANSANTARCTIC MTS.
2000
2000
1000
BYRD SUBGLACIAL BASIN
Byrd Station
200 km
A
B
C
D
E
Crary Ice Rise
RISP
ROSS ICE SHELF
VICTORIA LAND
80 S
B
B1
B2
• Core Locations
5 km
N
Unicorn
93-14
93-10
Fishhook
89-4,6,7,8
UpB
92-1
ROSS SEA
DSDP 270
272
271
CIROS-1
180

Figure 2. X-ray radiographs of the three upper sections of the core 92-1. The top of the core is in the lower left corner. The scale bar is 10 cm long.

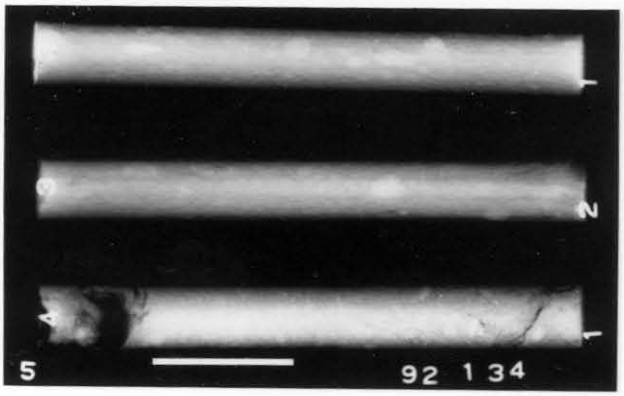
5
92 1 34

Figure 3. Photomicrograph of the UpB till (92-1-35) in plain light. Mineral grains (mainly quartz) appear light with fine matrix as a gray background. The dark particles are predominantly chlorite. A fragment of a schistose pebble is visible along the left boundary of the photograph. The scale bar has the length of 0.25 mm.

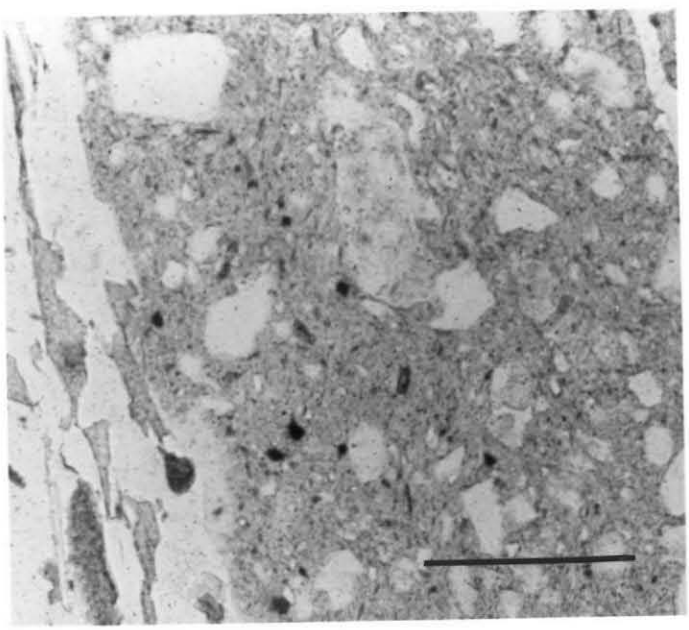

Figure 4. Lithology of the five UpB and two Unicorn cores, and variations in clast abundance within the cores.

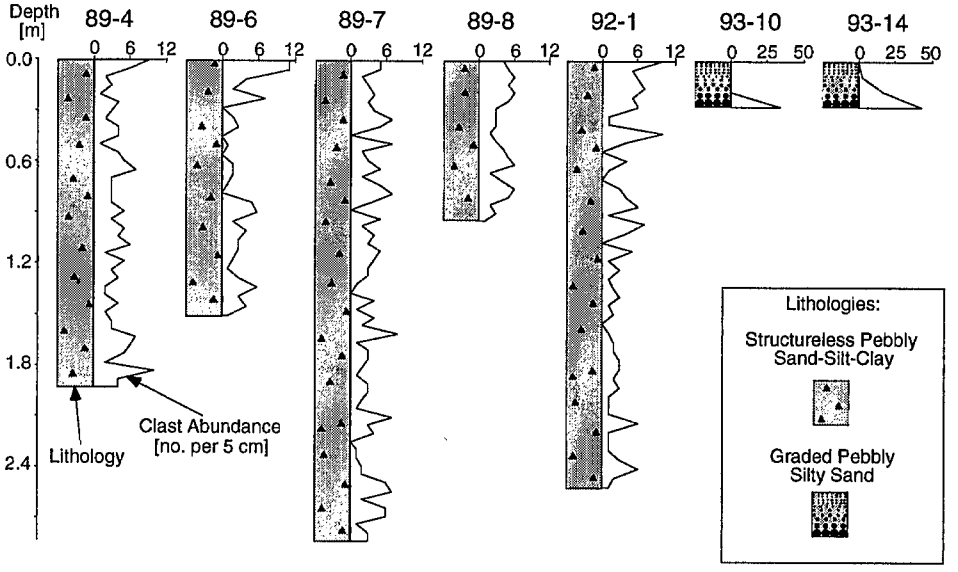
Depth [m]
89-4
89-6
89-7
89-8
92-1
93-10
93-14
0 6 12
0 25 50
0.0
0.6
1.2
1.8
2.4
Lithology
Clast Abundance [no. per 5 cm]
Lithologies:
Structureless Pebbly Sand-Silt-Clay
Graded Pebbly Silty Sand

Figure 5. A. Cumulative grain-size distribution for the 35 analyzed UpB samples (thin solid lines) and four Unicorn samples (thick solid and dashed lines). B. Mean grain-size distribution of 35 UpB samples and the grain-size distribution for the four individual Unicorn samples. C. Decomposition of the mean UpB distribution into two lognormal populations (light and dark gray shading).

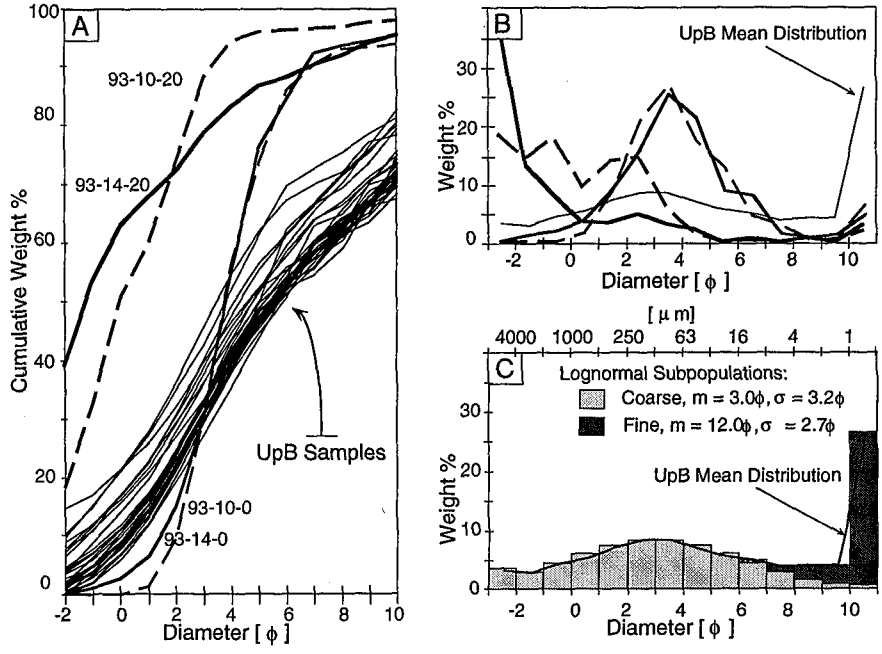
A
93-10-20
93-14-20
UpB Samples
93-10-0
93-14-0
Cumulative Weight %
Diameter [ϕ]
B
UpB Mean Distribution
Weight %
Diameter [ϕ]
[μ m]
4000 1000 250 63 16 4 1
C
Lognormal Subpopulations:
Coarse, m = 3.0ϕ, σ = 3.2ϕ
Fine, m = 12.0ϕ, σ = 2.7ϕ
UpB Mean Distribution
Weight %
Diameter [ϕ]

Figure 6. SEM microphotographs of sand grains (2ϕ to 3ϕ size) from the UpB till (A, B), the Unicorn sediments (C), and experimentally produced samples (D, E, F). The scale bars are 0.1 mm long in all of the photomicrographs. A quartz grain from the sample 89-4-20 (A) shows dull old fracture planes covered with etch pits (e) and separated by rounded edges. A feldspar grain from the same sample (B) has etch pits (e) and rounded edges. A feldspar grain from sample 93-14-20 (C) (left) has relatively smooth cleavage planes and no etch pits. Conchoidal fractures and arcuate steps (c) are visible on a quartz grain to the lower right of the feldspar grain whereas flat fracture surfaces dominate the quartz grain located near the top center of the photograph. Sharp edges are present on both quartz grains though some rounded edges can also be observed on the lower one. Grains produced by crushing with mortar and pestle (D) have very sharp edges combined with flat cleavage planes (p) on feldspar (upper left) and with flat (f) and conchoidal (c) fracture planes on quartz (center right). A quartz grain that was crushed and then treated with 10% HF (E) has the original fracture planes covered with etch pits and small crystals that precipitated during chemical treatment (the prominent striations in the background are on the top of the metal sample stub). In the same sample, a feldspar grain (F) shows abundant etch pits and crevasses following cleavage cracks.

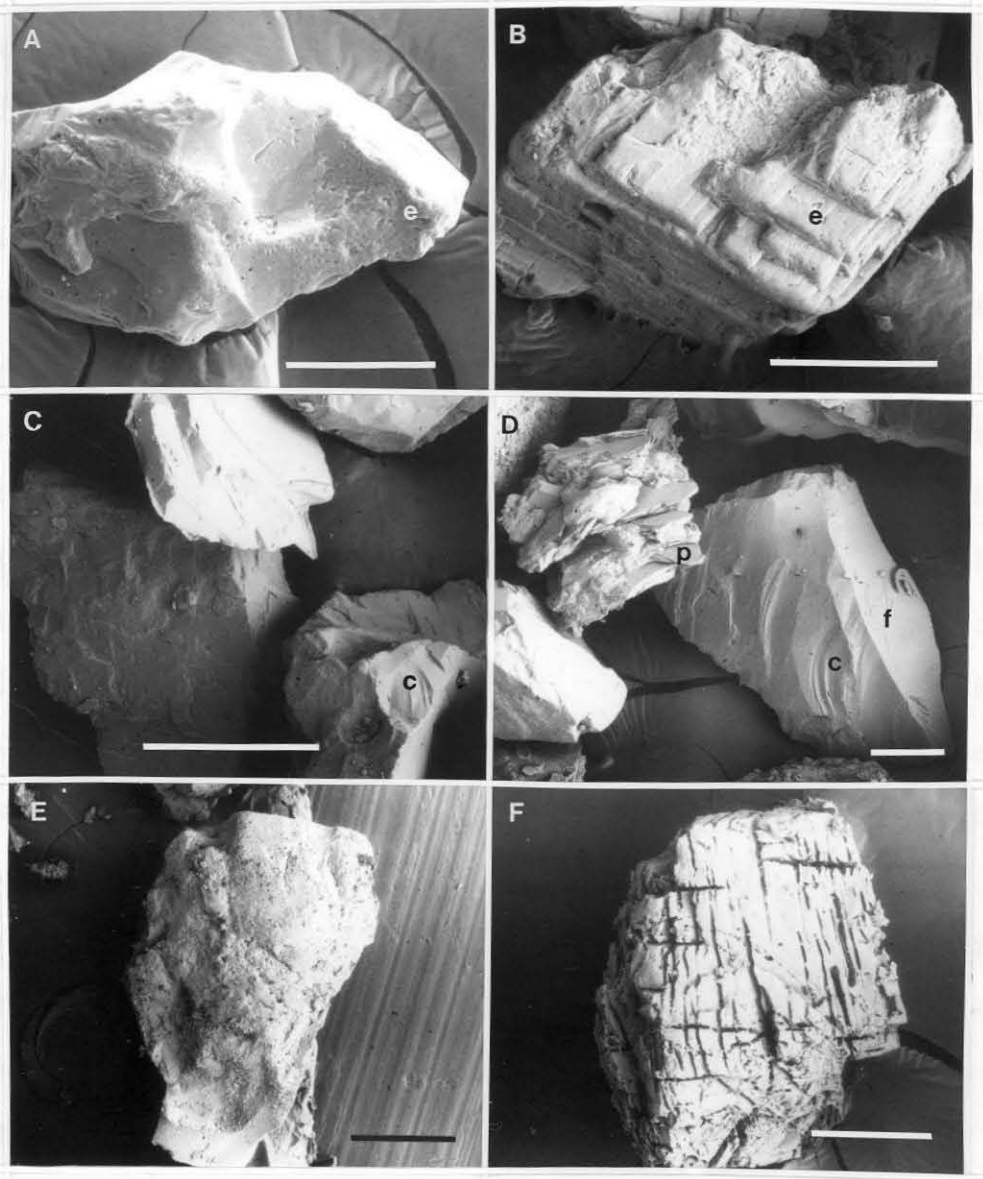
A
e
B
e
C
c
D
p
f
c
E
F

Figure 7. Comparison between the nine samples in which micromorphology of feldspar and quartz grains, 2ϕ-3ϕ in diameter, was analyzed. Sample interrelationships shown in (A) are revealed by a purely statistical procedure, the Q-mode (i.e., sample-oriented) factor analysis (Davis 1986, p. 563-573). This procedure makes no assumptions about the underlying cause of the observed interrelationships. Second factors reflect the most significant inter-sample relationships in Q-mode analysis (Davis 1986, p. 567-568). The magnitude of factor loadings reflects the contribution of an individual real sample to a given statistically generated factor. Based on the distribution of the artificially treated samples (crushed, tumbled, 1%HF, 10%HF, 5%NaOH) in the diagram, we interpret that positive factor loadings are characteristic for samples shaped predominantly by physical breakage whereas negative factor loadings indicate effects of chemical alteration. This interpretation is independently confirmed by the results of our weathering score assessment (B) following the method of Darmody (1985). This procedure reproduces closely the sample interrelationships revealed by the factor analysis. Negative weathering scores in (B) indicate predominance of chemical weathering microfeatures over physical breakage microfeatures. The opposite is true for the positive weathering scores. Bars are one standard error from the mean. The axes on the diagrams span the whole possible range of values for factor loadings (A) and weathering scores (B).

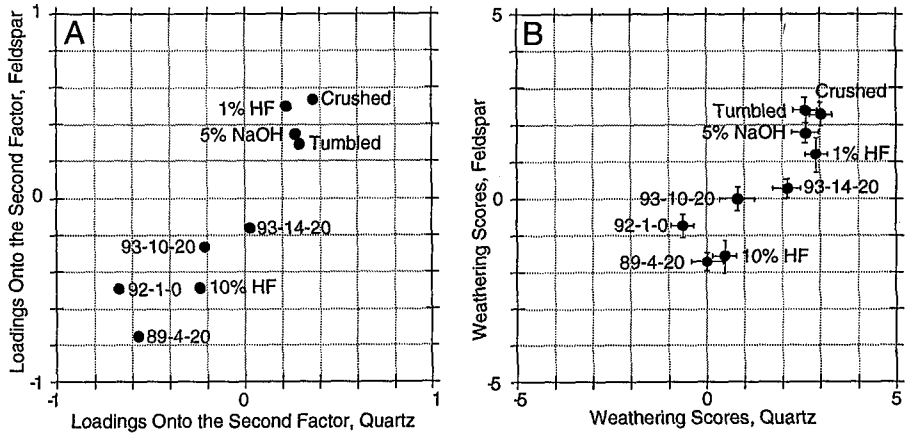
A
Loadings Onto the Second Factor, Feldspar
Loadings Onto the Second Factor, Quartz
1% HF
Crushed
5% NaOH
Tumbled
93-14-20
93-10-20
92-1-0
10% HF
89-4-20
1
0
-1
B
Weathering Scores, Feldspar
Weathering Scores, Quartz
5
0
-5
Crushed
Tumbled
5% NaOH
1% HF
93-14-20
93-10-20
92-1-0
89-4-20
10% HF

Figure 8. Krumbein roundness and sphericity plot for the UpB clasts, with contours at intervals of 2, 4, 6, 8% of data per 1% area. Solid symbols give average roundness and sphericity of the 230 clasts from UpB cores, 27 from 93-10 core, and 82 from 93-14 core. The size of the symbols is chosen to make them larger than ±1 standard error from the mean.

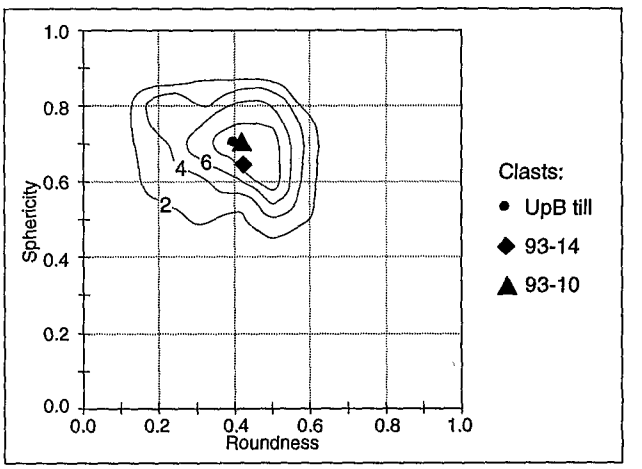
1.0
0.8
0.6
0.4
0.2
0.0
Sphericity
0.0
0.2
0.4
0.6
0.8
1.0
Roundness
2
4
6
Clasts:
UpB till
93-14
93-10

Figure 9. Quartz/plagioclase/potassium-feldspar composition of the matrix index fraction, 1ϕ-2ϕ, from all UpB and Unicorn samples and 100 clasts from the UpB cores.

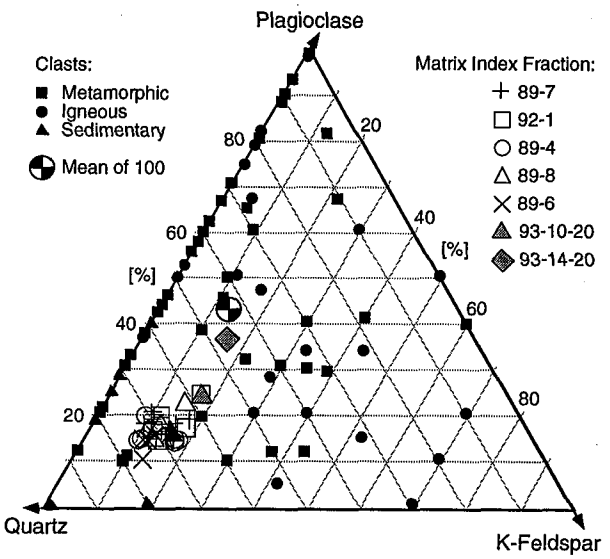
Plagioclase
Clasts:
Metamorphic
Igneous
Sedimentary
Mean of 100
Matrix Index Fraction:
89-7
92-1
89-4
89-8
89-6
93-10-20
93-14-20
[%]
20
40
60
80
Quartz
K-Feldspar

Figure 10. Changes in mineralogy with grain size in four selected samples. The category 'others' comprises muscovite, biotite, amphibole, pyroxene, chlorite and opaques. Vertical thick solid lines mark the 5ϕ size boundary. Composition of grains greater than 5ϕ was determined by optical mineralogy with relatively low standard error, 0-4%. The XRD determinations of mineralogy for the size fractions smaller than 5ϕ are only semiquantitative.

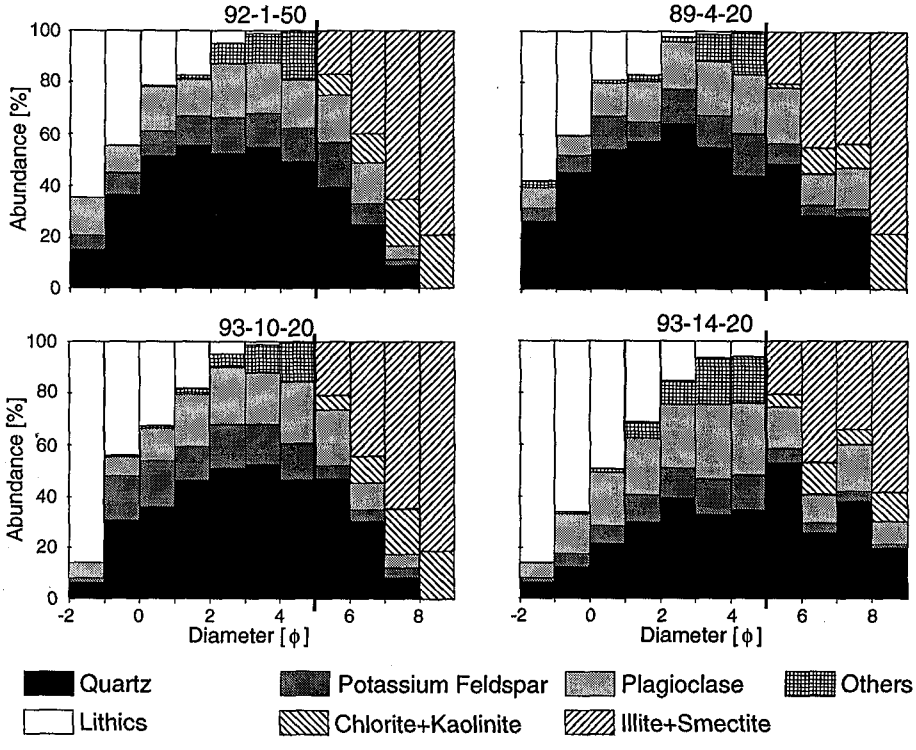
92-1-50
89-4-20
93-10-20
93-14-20
Abundance [%]
Diameter [ϕ]
Quartz
Lithics
Potassium Feldspar
Chlorite+Kaolinite
Plagioclase
Illite+Smectite
Others

Figure 11. Two pebbles from core 93-14 that show the best examples of striations (s) found on any of the UpB or Unicorn clasts. The scale bar is 5 mm long.


S
S
S
S

Figure 12. Comparison of the sand-silt-clay composition of the UpB till samples (solid diamonds) with an envelope for basal tills and selected individual till sheets from Ohio (Sladen and Wrigley 1983, Figure 8.1a).

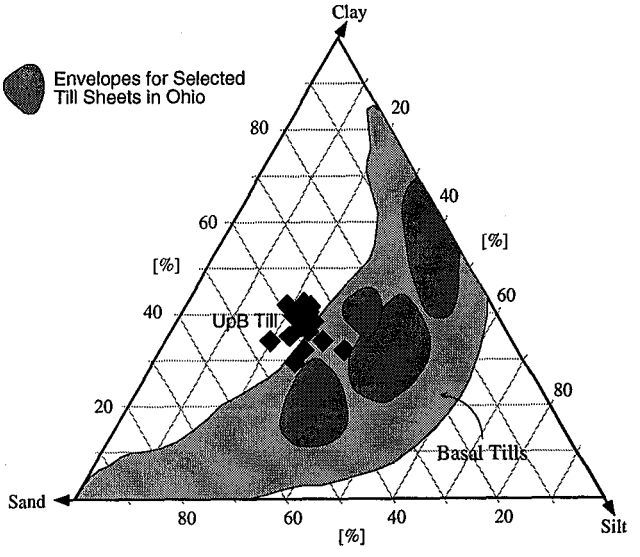
Clay
Envelopes for Selected
Till Sheets in Ohio
20
40
60
80
[%]
UpB Till
Basal Tills
Sand
Silt
80
60
40
20
[%]

Figure 13. Comparison of some textural properties and composition of the sediments from UpB and the Unicorn with the glacimarine and subglacial deposits from the Ross Sea sedimentary basin. A. Quartz-feldspar-lithics composition of sand fraction, 1ϕ to 4ϕ, from four selected samples (Figure 5). The feldspathic and basement petrofacies were defined by George (1989, Figure 4) for the same size fraction from Tertiary glacigenic sediments in the CIROS-1 core (location in our Figure 1A). B. Comparison of the sand-silt-clay size distribution for the UpB till matrix (Figure 12) with other basal tills and glacimarine deposits from the Ross Sea region. Data for the Ross Sea till (mean shown by shaded triangle, estimate of one standard deviation by large open circle) from Anderson and others (1980, Figure 3), for the RISP till from Webb (1979, Figure 15), for Mackay and Taylor Glacier till from Ross D. Powell (1995, personal communication), and for DSDP 272 facies from Hayes, Frakes *et al.* (1975, Figure 5, p. 219). C. Illite-smectite-kaolinite plot comparing selected UpB and Unicorn samples with glacigenic sediments from the Crary Ice Rise (CIR), Ross Ice Shelf Project (RISP), Byrd Station (Byrd), and the bottom of Ross Sea. Data for the four latter locations from Turner (1992).

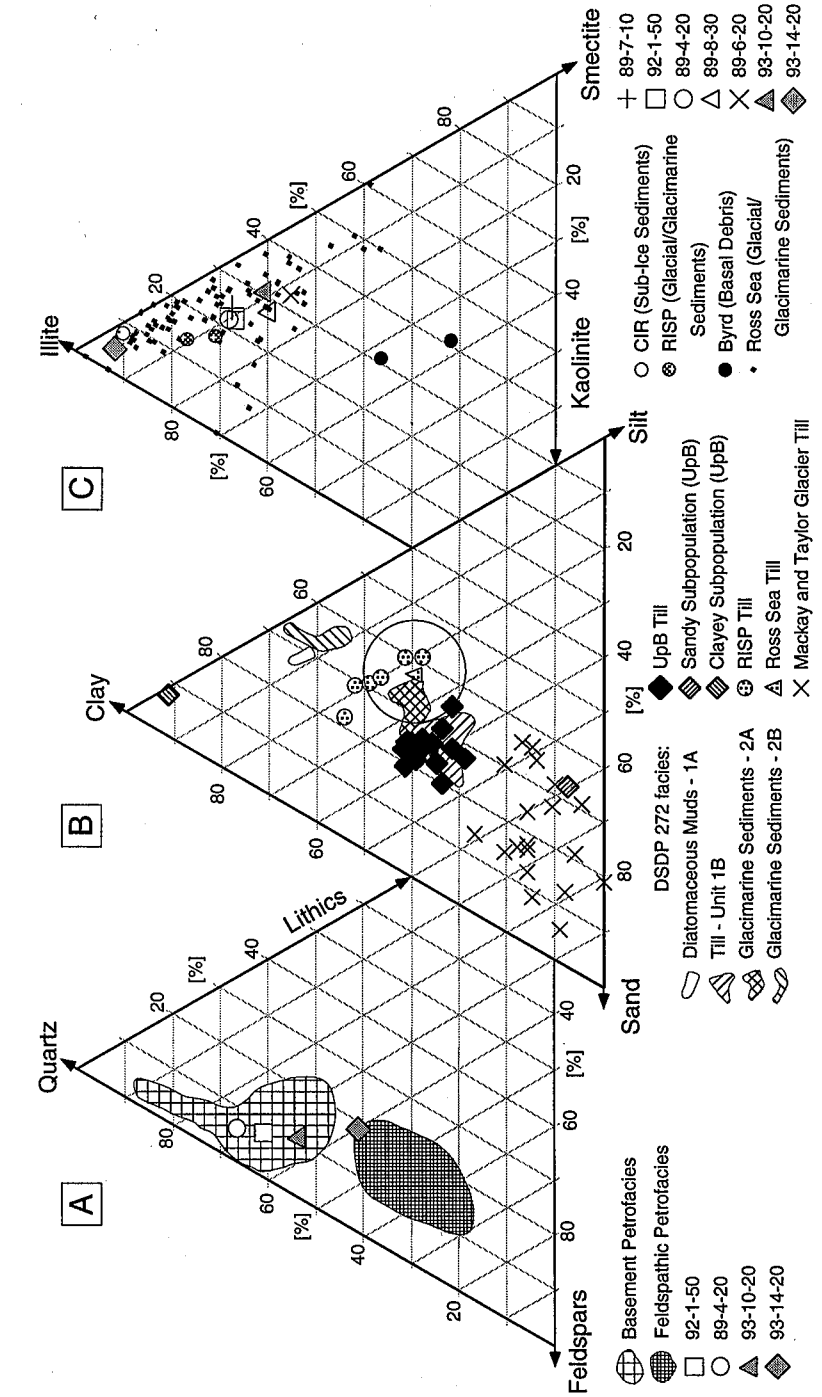
A
Quartz
Lithics
Feldspars
[%]
B
Clay
Sand
Silt
C
Illite
Kaolinite
Smectite
Basement Petrofacies
Feldspathic Petrofacies
92-1-50
89-4-20
93-10-20
93-14-20
DSDP 272 facies:
Diatomaceous Muds - 1A
Till - Unit 1B
Glacimarine Sediments - 2A
Glacimarine Sediments - 2B
UpB Till
Sandy Subpopulation (UpB)
Clayey Subpopulation (UpB)
RISP Till
Ross Sea Till
Mackay and Taylor Glacier Till
CIR (Sub-Ice Sediments)
RISP (Glacial/Glacimarine Sediments)
Byrd (Basal Debris)
Ross Sea (Glacial/ Glacimarine Sediments)
89-7-10
92-1-50
89-4-20
89-8-30
89-6-20
93-10-20
93-14-20

Figure 14. Abundance of the individual microfeatures on 30 quartz (A) and 30 feldspar (B) grains in six selected samples. The samples omitted to increase clarity of the graph (1%HF, 5%NaOH, tumbled) have a feature frequency spectrum almost identical to that of the sample of crushed grains. C and D show the loadings, in descending order, of the individual quartz and feldspar microfeatures onto the first R-mode factor. The microfeatures are identified by the same numbers as these used in the 'Laboratory Methods' section of this paper.

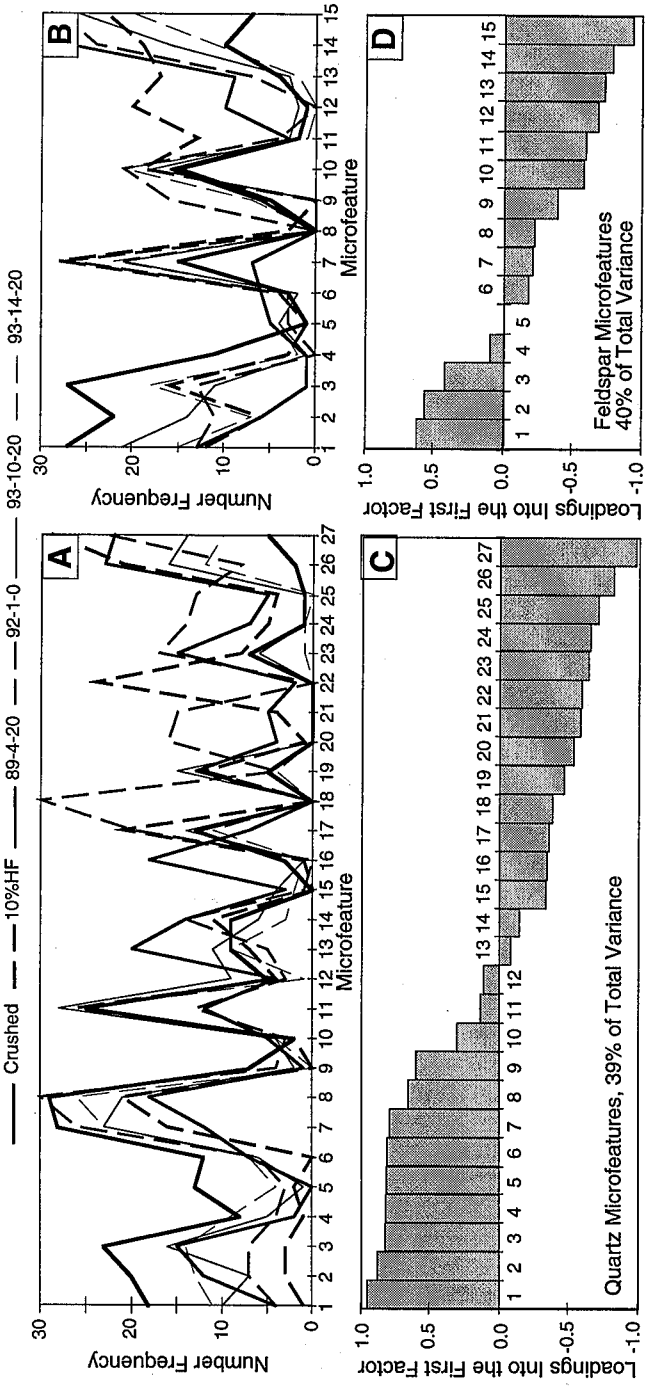
Crushed
10%HF
89-4-20
92-1-0
93-10-20
93-14-20
A
B
C
D
Number Frequency
Microfeature
Loadings Into the First Factor
Quartz Microfeatures, 39% of Total Variance
Feldspar Microfeatures
40% of Total Variance

Figure 15. Contact of two spherical grains in a perfectly plastic matrix. Grain to the upper left is pressed against the lower grain due to some arbitrary mechanism. Maximum load P on the second grain occurs when the perfectly plastic matrix starts to yield and the grain moves in the direction of loading. Mathematical symbols are explained in the text.

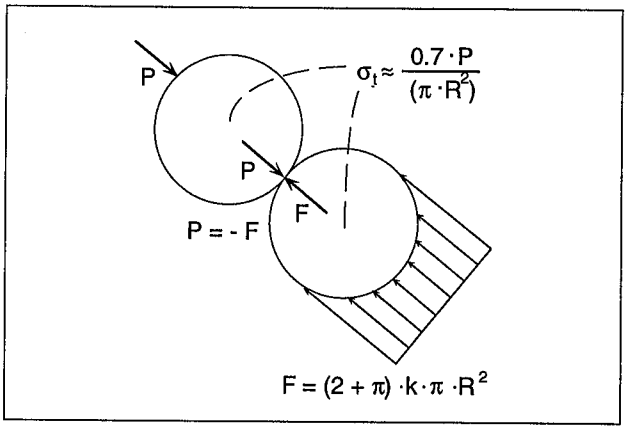
P
$\sigma_t \approx \frac{0.7 \cdot P}{(\pi \cdot R^2)}$
P
F
P = - F
$F = (2 + \pi) \cdot k \cdot \pi \cdot R^2$

APPENDIX 2.A.

Publication Resulting From CHAPTER 2

Chapter 2 was submitted for publication in *Journal of Sedimentary Research* in July 1996. Following the suggestions of two reviewers and the journal editor, this manuscript was subsequently revised and was published finally in the May 1998 issue of this journal (Tulaczyk, S., Kamb, B., Scherer, R.P., and Engelhardt, H.F., 1998, Sedimentary Processes at the Base of a West Antarctic Ice Stream: Constraints From Textural and Compositional Properties of Subglacial Debris: *J. Sed. Res.*, v. 68, p. 487-496). The revisions included three major changes: 1) removal of all data and discussion concerning the two sediment cores acquired at the 'Unicorn'; 2) further shortening of the manuscript by removal of several graphs which were judged to be secondary to the central theme of the manuscript, e.g., graphs showing mineralogical data; and 3) focusing the discussion part of the manuscript more on the origin of the UpB till itself rather than on the origin of deforming-bed tills in general.

CHAPTER 3

Ice Sliding Over Weak, Fine-Grained Tills: Dependence of Ice-Till Interactions on Till Granulometry

Slawek Tulaczyk

Division of Geological and Planetary Sciences, California Institute of Technology, Pasadena, CA 91125

Abstract

Two fundamental aspects of ice-till interactions, the strength of the ice-till coupling and the vertical distribution of deformation in till, may be strongly dependent on till granulometry. In particular, results of theoretical analysis of several physical processes involved in such interactions suggest the following hypotheses: 1) fine-grained tills facilitate ice sliding with ploughing and little distributed deformation; and 2) coarse-grained tills facilitate strong ice-till coupling and relatively deep till deformation (~0.1 m). The theoretical analysis is limited to Coulomb-plastic tills under low subglacial effective stresses (0-100 kPa). Fine-grained tills are represented in the analysis by a clay-rich till from beneath Ice Stream B (ISB), West Antarctica, and a silty Pleistocene till from Ohio. For comparison, two coarse-grained, clast-rich tills are also considered (from beneath the Trapridge Glacier, Yukon, and the Breidamerkurjökull Glacier, Iceland). The mechanical condition for ice sliding over till is defined as the situation in which the strength of the ice-till interface is lower than the strength of the till itself. Model calculations predict that this condition is more likely to be met in fine-grained rather than coarse-grained tills because of:

1) lower abundance of ploughing clasts (clast fraction ~0.01 vs. ~0.1); 2) widespread submergence of fine matrix particles even by a very thin basal water film (~10^{-6} m); and 3) greater susceptibility to interface smoothing due to ice-water surface tension. In addition, the theoretical analysis of ice-till interactions considers three potential mechanisms for distribution of deformation in tills of Coulomb-plastic rheology: 1) plastic deformation of till around a ploughing clast, which may affect till to depth of c. 2.7 to c. 4.5 times the clast diameter; 2) particle/clast bridging, which is typically observed to result in a shear-zone that is 10 times greater than the characteristic clast/particle diameter; and 3) vertical shear-zone migration due to water-pressure fluctuations. Combined, these three effects may result in distribution of a significant fraction of ice motion throughout ~0.1 m thickness of a coarse-grained, clast-rich till. However, lower clast abundance and smaller hydraulic diffusivity of a fine-grained till makes it a less favorable environment for significant strain distribution (predicted shear zone thickness ~0.01 m).

3.1. Introduction

The importance of ice-till interactions to glacier mechanics has been fully recognized only relatively recently (Alley *et al.*, 1986, 1987abc; Beget, 1986; Boulton, 1986; Boulton and Hindmarsh, 1987; Brown *et al.*, 1987; Clarke, 1987). Over the last decade, it has become apparent that ice motion over weak tills may play a major role in controlling dynamics of ice masses and in formation of the geologic record of glaciations (Alley, 1989ab, 1991; Boulton, 1996ab; Clark, 1992; Clark and Walder, 1994; Engelhardt *et al.*, 1990; Kamb, 1991; MacAyeal, 1992). In order to understand properly the function of till in evolution of ice masses and glacial geologic sequences, it is necessary to identify and quantify the physical processes that determine the nature of ice-till interactions.

Significant advancements in this direction have already been made by a number of research groups studying modern subglacial zones (Boulton and Hindmarsh, 1987; Blake, 1992; Blake *et al.*, 1994; Engelhardt *et al.*, 1978; Engelhardt and Kamb, 1997 and in press; Engelhardt *et al.*, 1990; Fisher and Clarke, 1994; Hooke *et al.*, 1997; Iverson *et al.*, 1994, 1995). Observations beneath mountain glaciers have shown mostly strong ice-till coupling and distribution of some till deformation down to 0.1-0.6 m depth (Boulton and Hindmarsh, 1987; Blake *et al.*, 1992; Engelhardt *et al.*, 1978; Hooke *et al.*, 1997). However, a recent borehole experiment of Engelhardt and Kamb (in press) suggests that the fast motion of a West Antarctic ice stream over a fine-grained till is accommodated predominantly by sliding. This apparent contrast in the character of ice interactions with tills beneath mountain glaciers and the till beneath Ice Stream B may be related to the contrasting granulometry of these distinctly different tills.

For logistical reasons, it is usually difficult to collect all the field data that are necessary to build a full physical description of the individual processes involved in ice-till interactions. Theoretical and laboratory research is needed to help supplement and generalize field observations (e.g., Iverson *et al.*, 1994; Kamb, 1991). In this work, I use theoretical constraints from mechanics of plastic granular media to show that two fundamental aspects of an ice-till system, the strength of ice-till coupling and the depth of till deformation, may significantly depend on till granulometry. The results suggest that sliding, with little distributed deformation, may be characteristic for ice motion over fine-grained tills. On the other hand, coarse, clast-rich tills may promote stronger ice-till coupling and relatively deeper distribution of till deformation. Throughout this work, the emphasis is on soft-bedded subglacial conditions in which tills are weak and deformable because they are under low subglacial effective stresses (<100 kPa, Brown *et al.*, 1987). The term 'till' will be used interchangeably with the terms 'granular medium' or 'soil' (in

the engineering sense).

3.2. Introductory Concepts

3.2.1. Till Rheology

The most important decision that must be made at the very beginning of a theoretical study of ice-till interactions is the choice of the rheologic models for both phases. It is widely accepted that deforming ice behaves as a power-law fluid with exponent of about 3 (e.g., Patterson, 1994, Chapter 5). However, the rheology of till, a complex mixture of solids, water, and sometimes gas, is less firmly established. Till is commonly treated as a material of either nearly linearly viscous or nearly Coulomb-plastic rheology (e.g., Boulton and Hindmarsh, 1987, vs. Kamb, 1991). There are fundamental differences between these two alternatives. For instance, ice motion over Coulomb-plastic till is more likely to be unstable than ice motion over viscous till (Kamb, 1991). The preponderance of observational evidence supports the Coulomb-plastic model for till rheology, and this model will be assumed in this paper [Hooke et al., 1997; Iverson et al., 1998; Kamb, 1991]. The only unequivocal support for a viscous or Bingham-type till rheology comes from the stress and strain-rate data presented for the subglacial zone of Breidamerkurjökull by Boulton and Hindmarsh (1987, Figure 7). However, the reliability of the Breidamerkurjökull dataset is unclear since the source of the highly variable shear-stresses estimates has never been explained (Hooke *et al.*, 1997, p. 173). Extensive studies on two other mountain glaciers overriding till, Trapridge glacier and Storglaciären, failed to confirm the viscous till model (Blake, 1992, p. 62; Hooke *et al.*, 1997). In addition, the data from Storglaciären support the Coulomb-plastic model. Two sets of extensive

laboratory shear box and ring shear tests on three different tills provide additional backing for the latter model (Iverson *et al.*, 1998; Kamb, 1991). Readers interested in the viscous representation of till rheology are encouraged to explore the extensive literature on this subject (Alley, 1989ab; Alley *et al.*, 1986; Alley *et al.*, 1987abc; Boulton, 1996ab; Boulton and Hindmarsh, 1987; Clark, 1991, 1992; Clark and Walder, 1994; Clark *et al.*, 1996; Jenson *et al.*, 1995, 1996; MacAyeal, 1992).

In the Coulomb-plastic model, till is idealized as a material with yield strength given by (Terzaghi *et al.*, 1996, equation 17.4):

$$\tau_f = c + p' \tan\phi \qquad (1a)$$

where c is the cohesion, ϕ is the angle of internal friction, and p' is the effective pressure typically expressed as:

$$p' = P - p_w \qquad (1b)$$

where P is the total stress, and p_w is the pore water pressure. If a shear stress lower than the yield strength is applied to such material, small deformation takes place (Figure 1). Thus, large-strain or continuous deformation is possible only when the yield strength of the till is reached. Unlike in the Bingham-model of Boulton and Hindmarsh (1987, equation 1), shear stresses in excess of the yield strength cannot be applied to the Coulomb-plastic till. In addition, strain-rates in this till are not explicitly determined by shear stresses but rather by other factors, e.g., rate of motion of the ice base which is applying the stresses to the till. Coulomb-plastic behavior of granular materials has long been accepted in soil mechanics because it has proven itself to adequately represent exhaustive field and laboratory data (reviews in Kamb, 1991, Mitchell, 1993; Scott, 1963; Terzaghi *et al.*, 1996). Application of the Coulomb-plastic model to tills makes it possible to utilize existing solutions from soil mechanics. However, this approximation of till rheology does neglect some second-order effects that occur during deformation of granular media (e.g.,

the slight strain-rate dependence of shear strength, Kamb 1991). The assumptions made here are justified by the goal of this work, which is focused on providing useful theoretical insights into first-order aspects of ice-till interactions.

3.2.2. Clast Ploughing and Breakdown of Hard-Bed Sliding Theory

In the case of ice sliding over bedrock, basal resistance to ice motion arises from ice regelation and plastic flow around obstacles of different sizes (Kamb, 1970; Lliboutry, 1979; Nye, 1969; Weertman, 1957). During this motion, relatively high stresses (~MPa) concentrate on bedrock obstacles but it is assumed that the obstacles are capable of withstanding these high stresses without being moved or destroyed. Such an assumption is reasonable for typical bedrock since strength of common rock lithologies is very high (~100 MPa, Jaeger and Cook, 1969, p. 146). When ice moves over unconsolidated sediments, ice velocity may be accommodated to some extent through deformation of the underlying sediments (e.g., Alley *et al.*, 1986; Boulton and Hindmarsh, 1987). To avoid terminological confusion, I would like to clarify that the term 'basal sliding' is used here to refer to this component of ice movement which is accommodated at the ice-till interface rather than within the deformable bed or the ice (Piotrowski and Tulaczyk, in press).

Brown *et al.* (1987, p. 8991) have recognized that when ice moves over till, the strength of the latter imposes a strict limit on how much stress can be applied by ice to any clast protruding from till into ice. This limit stems from the fact that when the force applied by ice to a clast exceeds the force necessary to produce a local sediment failure around the clast, the clast will start to plough through the till. To estimate the magnitude of this limiting force, Brown *et al.* (1987, p. 8991) assume that the local failure surface surrounding a clast has a hemiconical shape. In reality, a protrusion ploughing through a

till matrix must result in a more complex pattern of deformation because of the requirement of (near) incompressibility of till. To satisfy this requirement, the failing matrix must deform around the moving clast away from its stoss side and into its lee side (Figure 2). This deformation pattern increases significantly the force required to produce local failure around the clast.

Here, I estimate the stresses required to move a clast horizontally through a perfectly plastic till matrix (Figure 2). The matrix is assumed to be spatially homogeneous, incompressible, and deforming plastically under a yield stress equal to its undrained shear strength (i.e., strength at no volume change; Terzaghi *et al.*, 1996, p. 259). The two latter assumptions are reasonable as long as the rate of clast displacement through the matrix exceeds the rate of pore pressure dissipation around the clast. From dimensional analysis this condition is expressed by:

$$U_s > \frac{c_v}{d_c} \qquad (2)$$

where U_s is the sliding velocity, c_v is the hydraulic diffusion coefficient (coefficient of consolidation), and d_c is the clast diameter. The limited existing data suggest that the hydraulic diffusion coefficient is small for fine-grained tills and significantly greater for coarse tills, ~0.1 m^2y^{-1} for Ice Stream B till and the Two Rivers Till, Wisconsin, vs. ~10 m^2y^{-1} for Storglaciären till (Iverson *et al.*, in press; Engelhardt, unpublished data). The above condition holds easily for any clast with $d_c > 10^{-2}$ m and for sliding velocity > 10 m y^{-1} in the case of fine-grained tills but it breaks down for coarse tills when $d_c < 10^{-1}$ and U_p < 100 m y^{-1}. Upon breakdown of condition (2), strengthening of the till matrix should occur in the zone of compression in front of the clast and weakening in the zone of relative extension at the back. However, more detailed analysis shows that this strengthening is relatively small and may be neglected in the following order-of-magnitude estimates (Appendix 1). Use of the undrained till strength simplifies treatment of different aspects of

ice-till interactions and facilitates application of existing solutions from soil mechanics and the theory of plasticity.

Clasts at an ice-till interface are typically approximated in theoretical analysis as spheres submerged halfway in till and halfway in ice (Figure 3; Brown *et al.*, 1987; Alley, 1989b). Unfortunately, solutions for motion of rigid hemispheres through a plastic matrix do not seem to be available or easily derivable (Johnson, 1970, p. 481-482). However, soil resistance to indentation by a protrusion is not sensitive to the exact shape of the protrusion (Baligh, 1972, p. 67; Johnson, 1970, p. 481-482). By approximating the portion of a clast submerged in a till as a tilted cube (Figure 2), I can take advantage of the analytical solution of Baligh (1972, equation 5 & 8) for a rough wedge "skimming" the surface of a homogeneous plastic half space. The resulting equation shows that the ratio of the horizontal force necessary to move the clast to the horizontal area of the clast (critical stress, τ_c) is greater than the shear strength of the matrix (τ_f) by a constant factor k_c:

$$\tau_c = k_c \tau_f \approx 4.7 \tau_f \qquad (3)$$

Thus, ice needs to act on a ploughing clast with a stress that is roughly five times the yield strength of the matrix. Comparable values of k_c have been obtained for a similar problem of penetration of a flat punch into a plastic soil (4.83, 5.14, 5.2 to 5.7, Johnson, 1970, p. 481-482). The result given in (3) is also generally consistent with the treatments used previously by other workers in analysis of an indentor ploughing through till (Brown *et al.*, 1987; Fischer and Clarke, 1994; Humphrey *et al.*, 1993; Iverson *et al.*, 1994).

Calculations of shear stress exerted by sliding ice on a hemispherical particle (Lliboutry, 1979, equation 46; Brown *et al.*, 1987, equation 2) show that for any reasonable ice sliding speeds all particles larger than ~10^{-4} m should plough if the particles are embedded in a weak till matrix (Figure 4). Thus, in spite of the fact that clasts in a till do offer increased resistance as compared to the bulk till (3), they still cannot provide

nearly as significant retardation to ice motion as obstacles on a rigid bed. Therefore, the formulations used in the hard-bed sliding theory cannot be used for calculating the strength of the ice-till interface or the ice sliding velocities. New expressions must be developed for ice motion over till.

3.3. Strength of Ice-Till Coupling

3.3.1. Influence of Clasts

A model of an ice-till interface will be developed for the simplest case and then complicated by introduction of additional physical processes which should have important, first-order effects on the interface strength. Figure 4 suggests that a simple two-phase model for till (clasts+matrix) is a useful approximation of an ice-till interface. It is clear from previous arguments that clasts trapped at the ice-till interface will plough and contribute a stress τ_{ic} to the total interface strength:

$$\tau_{ic} = f_c \tau_c = f_c k_c \tau_f \qquad (4)$$

where f_c is the fraction of the total area of the interface covered by clasts. This equation is a simple generalization of (3) for the previously discussed case of a single ploughing clast.

The question that now arises is how to treat the direct contact between till matrix and ice. Formulation of such an expression is dependent on the choice of the predominant mechanism of ice motion over the till matrix. At first sight (Figure 4), regelation past small particles seems a logical choice since it can occur at relatively low stresses for particles of small diameter (~1-10 kPa for diameter $<10^{-5}$ m). However, both observations and theory suggest that surface-tension effects will retard formation of ice in small void spaces between small particles and, thus, hinder or prevent regelation past these particles (Alley *et*

al., in press; Everett, 1961; surface-tension effects will be later introduced into the interface-strength formulations in a slightly different context). If regelation is neglected, the problem may be simplified to the case of soil interaction with a rigid solid body. Data from soil mechanics suggest that the interface shearing stress (τ_{im}) between a rigid solid and a granular medium separated by a macroscopically flat boundary can be expressed as (Baligh 1972, p. 68-69):

$$\tau_{im} = (1\text{-}f_c)k_{im}\tau_f \qquad (5)$$

where $0 < k_{im} < 1.0$. From a physical standpoint, the value of this constant should tend towards 1.0 as the roughness of the solid-soil boundary approaches the roughness of intra-soil (till) failure planes. Thus, the interface shearing stress may be at most equal to the strength of the till. On the other hand, k_{im} should tend to zero when solid boundary becomes very smooth. In general, k_{im} is a function of the ratio of the coefficient of internal friction ($\mu_{(\phi)} = \tan\phi$ in (1a)) to the coefficient of interface friction (μ_{im}). However, lack of experimental data for ice-till interfaces prevents introduction of this more physically meaningful expression into (5). Soil mechanics investigations of soil-structure interactions suggest that value of k_{im} lies frequently in the range 0.5-1.0 (Scott and Schoustra, 1968, p. 205). For the time being, however, the usual assumption will be made that the roughness of the ice-till interface is governed at all scales by grain size (Figure 3, particles are half-submerged hemispheric bumps, Brown *et al.*, 1987; Alley, 1989ab). This postulate prompts the use of a conservative k_{im} value of 1.0. Towards the end of this chapter, surface-tension effects will be introduced to argue against universal applicability of this assumption to fine-grained tills.

Combination of (4) and (5) estimates the strength of an idealized ice-till interface as a simple function of one variable, the fractional area of clasts (f_c):

$$\tau_i = (1\text{-}f_c)k_{im}\,\tau_f + f_c\,k_c\,\tau_f \qquad (6)$$

Under this condition the strength of the interface is necessarily equal to ($\tau_i = \tau_f$ for $f_c = 0$) or greater than the intrinsic strength of the till. Thus, it can be expected that in this very simplified case there should be no tendency for the ice to slide along the interface because deformation on shear planes within the till is mechanically more favorable. However, even this very simple model does already suggest that interface strength should be greater for clast-rich and smaller for clast-poor tills.

3.3.2. Basal Water Film

The presence of a basal water film is likely to have an important influence on the interface shearing strength because such a film may separate the ice base from the underlying till over relatively large areas of the bed. Where such separation occurs, the interface strength goes practically to zero. Even if a channelized water system provides an important means of water drainage in a given ice-till system (e.g., Walder and Fowler, 1994), the presence of a relatively widespread water film can be expected because basal meltwater production has a distributed character and some form of a distributed drainage is needed to deliver the water to the channels/canals. Following Alley (1989ab), I assume that a water film of thickness d_w submerges all particles whose radii are equal to or smaller than d_w. Thus the fractional area of the bed submerged by the water film scales with the grain-size distribution of the till matrix. The assumption is made here that a basal water film is not thick enough to submerge clasts. This is a sound assumption because water films are expected to have thickness of the order of a mm or less (Weertman, 1972, Table 1).

Grain-size distribution is typically given for tills in the form of weight fractions of particles occurring in discrete size ranges. Therefore, it is useful to cast the mathematical

expressions of interface shearing strength in a way that accounts for this discretization of till granulometry. The fractional area of ice-clast contact can be calculated from the dry clast weight fraction (w_c) through (Brown *et al.*, 1987):

$$f_c = (1-n)\, w_c \tag{7a}$$

and the contribution of the j-th matrix size range to the ice-matrix contact area is obtained from the weight fraction of this size range (w_j):

$$f_j = w_j/(1-f_c) \tag{7b}$$

where: n is the till porosity. Note that (7b) assumes that pore spaces are part of the till matrix and that their contribution to the ice-matrix contact area scales in the same way as the contribution of the different particle size ranges. Since grain-size and pore-size distributions are related entities this assumption is reasonable.

The new formulation for the ice-till interface strength accounts for the influence of water film thickness in the following way:

$$\tau_i(d_w) = \tau_{ic} + \tau_{im}(d_w) = (k_c f_c + k_{im} f_{im}(d_w))\, \tau_f = (f_c\, k_c + k_{im}\, \Sigma f_j)\, \tau_f \tag{8}$$

where $f_{im}(d_w) = \Sigma f_j$ denotes summation of (7b) over the particle size ranges which are not submerged by the water film and are smaller than the minimum clast size (r_c) (i.e., $d_w < r_j < r_c$). In order to apply (8) to real tills, it is necessary to first specify the size-boundary between clasts and matrix particles (r_c). In sedimentology, the lower size boundary for pebbles is frequently taken to be 2×10^{-3} m (Pettijohn, 1975; p. 28). Figure 4 also supports a choice of r_c in the size range of the critical obstacles (10^{-3} to 10^{-2} m). In soil mechanics tests, which provide in practice the basis for estimation of till matrix strength (τ_f), particles greater than this are typically not included. Therefore, the sedimentological definition of clasts will be used here ($r_c > 2\times10^{-3}$ m). This value should be treated only as an approximate clast-matrix boundary. However, tills are typically poorly sorted with only several percent of weight fraction falling into each size interval. For this reason the main

features of my further analysis are not likely to be significantly affected by the uncertainties in r_c.

To examine the sensitivity of the interface shear strength to water-film thickness for tills of different granulometry, (8) is applied to two examples of fine-grained tills and two examples of coarse-grained tills (Figure 5). The fine-grained tills are represented by the clay-rich Ice Stream B till (henceforth the ISB till; Tulaczyk *et al.*, 1998, Figure 3) and an average of the silt-rich Tazewell and Cary tills from NE Ohio (henceforth the Ohio till; Shepps, 1953, table 1). The two coarse-grained tills are: the Breidamerkurjökull till (Boulton and Hindmarsh, 1987, Figure 3) and the Trapridge till (Clarke, 1987, Figure 4). The two latter have been selected for this analysis because in-situ measurements have documented that some deformation takes place in these two tills down to several decimeters of depth. The ISB till is the proposed deforming bed of Ice Stream B (Alley *et al.* 1986, 1987ab) and the Ohio till exemplifies the matrix-dominated southern Laurentide Pleistocene tills for which deforming-bed origin has been also advocated (Alley, 1991).

Figure 6 gives the results of application of (8) to these four tills. It plots the ratio of the interface shear strength to the matrix shear strength (τ/τ_f) versus the water film thickness (d_w). This ratio is used not only for the convenience arising from its dimensionless character, but also because of the special importance that is associated with the critical value of $\tau/\tau_f = 1.0$. When the interface is weaker than the till ($\tau/\tau_f < 1.0$), sliding along the interface is the mechanically favorable way to accommodate ice motion. For the opposite condition ($\tau/\tau_f > 1.0$), shear within the till should take place. When the two strengths are equal, either sliding or shear may accommodate the ice motion.

It is important to remember that this discussion concentrates on the simple case of a till whose strength does not change with depth. This is physically equivalent to assuming a lithostatic pore pressure distribution with depth. Another important case, that of a

hydrostatic pore pressure distribution, would tend to favor sliding or shear localized near the ice-till interface more than the lithostatic case does. This is because till strength increases with depth under a hydrostatic pore pressure distribution (Alley, 1989b, p. 123).

There is a significant difference in the impact of a water film of a given thickness on the interface strength for ice contact with coarse- and fine-grained tills (Figure 6). For the two fine-grained tills, the interface may be weaker than the till matrix even in the presence of an extremely thin water film ($< 10^{-6}$ m). This is especially true for the ISB till which has one-third of its material in particles smaller than 10^{-6} m. In addition, both of the fine-grained tills have a relatively low content of clasts (Figure 5) and the ice-till interface cannot be significantly strengthened by ploughing. On the other hand, the high abundance of clasts in the two coarse-grained tills more than makes up for the weakening caused by the presence of a water film. Thus, the interface strength for the coarse tills exceeds the bulk strength of the till matrix for almost any reasonable thickness of the basal water film (Figure 6).

3.3.3. Surface Tension Effect

Additional support for the previously proposed weakness of ice coupling with fine-grained tills is provided by another grain-size-dependent physical effect, the surface-tension effect. This phenomenon stems from the existence of ice-water capillary forces that hinder infiltration of ice into small pore spaces (Alley *et al.*, in press; Everett, 1961). The introduction of the surface-tension effect into the model of the ice-till interface is used here to argue against the previous assumption that the roughness of such interface is determined on all scales by particle size only. In this assumption, particles of all sizes form hemispherical bumps at the till surface and the ice surface conforms to them by invading the

pore spaces between the particles (Figure 3). However, capillary forces may prevent this invasion of ice into small pore spaces and, thus, may make the ice base much smoother than the till surface or any intra-till shear planes. This smoothing effect will act to decrease the strength of the interface by reducing the value of the coefficient of ice-matrix coupling, k_{im} in (5), (6), and (8), below its previously assumed maximum value of one.

Both theory and observations indicate that ice-water surface tension hinders growth of ice into small pore spaces (Alley *et al.*, in press; Everett, 1961; Hallet *et al.*, 1991). As a result, a high effective pressure may be necessary to make the geometry of an ice base comply perfectly with the roughness of a fine-grained till. Everett (1961) derived the mathematical expression that accounts for the surface-tension effect in growth of small ice crystals and protrusions. To better illustrate the physical basis of this phenomenon, parts of his derivation are reproduced here. The equation for Gibbs free energy of a small ice crystal/protrusion growing in contact with water under pressure of p_w is given by (Everett, 1961 equation 2):

$$\mu = \mu_i(p_w) + \nu_i \sigma_{iw} dA/dV \qquad (9)$$

where μ is the total Gibbs free-energy per mole of the small ice crystal/protrusion, μ_i is the Gibbs free energy of bulk ice (a function of pressure in the adjoining water, p_w), ν_i is the molar volume of ice, σ_{iw} is the ice-water surface energy (0.034 J m^{-2}, Ketcham and Hobbs, 1969), A is the area of the ice-water interface, and V is the volume of the ice crystal/protrusion. The second term in (9) represents the excess free energy that results from increasing the ice-water contact area when an ice crystal or protrusion experiences growth. Formally, the magnitude by which the energy of the small crystal/protrusion exceeds the free energy of bulk ice (i.e. $\mu - \mu_i(p_w)$) can be considered equivalent to the effect of increased pressure (p_i) within the crystal/protrusion:

$$\mu(p_i) - \mu_i(p_w) = \nu_i (p_i - p_w) \qquad (10a)$$

Comparison of (10a) and (9) shows that the pressure difference between the ice and water (i.e., the effective pressure, p') is uniquely related to the curvature of the ice-water interface:

$$p' = p_i - p_w = \sigma_{iw}\, dA/dV \qquad (10b).$$

In turn, if the effective pressure is treated as the independent variable, (10b) implies that the curvature of ice-water interface (dA/dV) changes in such a way as to always satisfy this relationship.

The implication of (10b) for ice base geometry is that it can no longer be assumed that the ice base simply conforms at all scales with the geometry of the top of the till. At the microscale, the geometry of the ice-till interface is now determined by a combination of till granulometry and the magnitude of the subglacial effective pressure (Figure 7). When the subglacial effective pressure is zero, the ice base remains absolutely flat ($dA/dV = 0$) and, thus, the roughness of the ice-till interface is vanishingly small. Only when a critical value of subglacial effective pressure (p_c') is reached will the ice perfectly comply with the curvature of the top of the till, and in this case the previously applied assumption will be valid. The measure of the curvature at the top of the till is provided by the specific surface area of the till (SSA) which is an intrinsic till property determined by grain size distribution (i.e., for critical p_c', $dA/dV = SSA$, both with units of area per volume) (Parks, 1990). Clearly, the subglacial effective pressure can take on a whole range of values between 0 and p_c' and for this range, the curvature of the ice base lies between 0 and SSA. When subglacial effective pressure exceeds the critical value, ice is free to regelate into the till following the physical law verified empirically by Iverson (1993) and Iverson and Semmens (1995) (also Alley *et al.*, in press).

For any given till, the magnitude of p_c' can be calculated from a modification of (10b):

$$p_c' = \sigma_{iw}\, SSA \qquad (11)$$

The specific surface area, *SSA*, can be estimated from grain-size distribution (e.g., Parks, 1990, p. 133-135) by applying the following summation over the discrete size ranges:

$$SSA = (1\text{-}n)\, \Sigma(w_j\, k_s/R_j) \qquad (12)$$

where: k_s is the particle shape factor (3 for a sphere, Parks, 1990, p. 133-134), and R_j is the characteristic particle radius in the *j*-th size class (chosen hereafter to be the mid-range for each class). Equations (11) and (12) are used to calculate p_c' and *SSA* for the four examples of coarse- and fine-grained tills. The results of these calculations are presented in Figures 8 and 5. These results illustrate well that the surface-tension effect is much less significant for the coarse tills than for the fine-grained tills. For instance, full conformity of the ice surface geometry to the till-surface geometry is possible at an effective pressure p' ($= p_c'$) of only a few kPa for the Breidamerkurjökull till but requires 104 kPa for the ISB till.

Explicit introduction of the surface-tension effect into the mathematical model of ice-till interface strength will require modification of the coefficient k_{im} which provides a parametric measure of ice base roughness and ice coupling with till matrix. From (10b) it follows that this coefficient should be dependent on the subglacial effective stress which controls the microscale ice-base roughness for $0 \le p' \le p_c'$. The exact form of this dependence is difficult to constrain because no relevant observational data are available. Nevertheless, it is reasonable to expect that the following two trends should hold in general: when $p' \rightarrow p_c'$ then $dA/dV \rightarrow SSA$ and $k_{im} \rightarrow 1.0$; and when $p' \rightarrow 0$ then $dA/dV \rightarrow 0$ and $k_{im} \rightarrow 0$. For the intermediate values, the simplest linear relationship is assumed here giving the following expressions:

$$k_{im}(p') = p'/p_c' = p'/(\sigma_{iw}\, SSA) \qquad \text{for } 0 \le p' \le p_c' \qquad (13a)$$

$$k_{im}(p') = 1.0 \qquad \text{for } p' > p_c' \qquad (13b)$$

$$k_{im}(p') = 0.0 \qquad \text{for } p' < 0 \qquad (13c)$$

where all of the terms have been explained previously.

Since the condition in (13b) is equivalent to the previous assumption of the maximum value of k_{im} and the condition (13c) simply implies no strength along the ice-till-matrix contact, the only case for which the equation for ice-till interface strength has to be modified is (13a). This new expression for the interface strength (with no water film) as a function of effective stress is derived by adding (5) to (6) and substituting (13a):

$$\tau_i = (f_c\, k_c + (1\text{-}f_c)\, p'/(\sigma_{iw}\, SSA))\; \tau_f = (f_c\, k_c + (1\text{-}f_c)\, p'/(\sigma_{iw}\, SSA))\; p' \tan\phi \qquad (14)$$

where the second part is cast in terms of subglacial effective pressure by substituting $\tau_f = p' \tan\phi$ (till shear strength without cohesion, (1a)).

Equation (14) indicates that, in absolute terms, strength of the interface is quite sensitive to the effective stress because it increases proportionally to the second power of p'. As before, it is most useful to treat the strength of the interface in relative terms as the non-dimensional ratio τ_i / τ_f. Application of (14) to the two fine-grained tills considered here shows clearly that the surface-tension effect incorporated into this mathematical model causes significant weakening of the ice-till interface. The non-dimensional strength ratio is below its critical value of 1.0 for almost the whole range of subglacial effective pressures relevant to the soft-bed conditions (0-100 kPa; Figure 8). Therefore, ice sliding with ploughing should be the mechanically preferred mode of ice motion associated with these fine-grained tills. In contrast, the influence of the surface-tension effect on the coupling of ice with the two coarse tills is not enough to make the interface weaker than the till, except for the Breidamerkurjökull till at effective pressures very near zero (Figure 8).

In general, the decreased geometric coupling of ice and till due to the ice-water surface-tension effect has a somewhat similar impact on the ice-till interface strength as the presence of a widespread basal water film (compare Figures 6 and 8). In nature, these two

effects are likely to act together and reinforce each other. To work through an example of such combined influence, it is assumed here that water-film thickness and subglacial effective pressure are mutually independent. A value of k_{im} calculated for each till from (13a) for a selected effective pressure (10 kPa) is plugged into expression (8). The calculated interface strengths (dashed lines in Figure 6) are extremely low for the fine-grained tills.

This section demonstrated relatively simple but insightful ways of calculating the ice-till interface strength with incorporation of three physical effects that have the potential of being the main controllers of ice-till interactions at and near the ice-till interface. The mathematical formulations chosen to represent these physical effects are not very well constrained by observational data. However, a consistent, robust feature displayed by the interface models examined here is the significant dependence of ice-till interface strength on till granulometry.

3.4. Distribution of Deformation

Distribution of till deformation with depth represents another extremely important aspect of ice-till interactions. Understanding of the individual processes that may distribute shear in tills is necessary to properly interpret field observations and to generate reliable models of coupled ice-till flow. In the viscous model of subglacial bed deformation it is assumed that distributed shear in tills results from the strain-rate dependence of till strength, typical for viscous materials (Alley, 1993). This simple effect is, however, no longer applicable if till is a material of Coulomb-plastic rheology which has no such dependence. The latter rheology is assumed here. In general, shear strain rates and strains are not uniquely determined by shear stresses in plastic materials (Salencon, 1977).

3.4.1. Influence of Clast Ploughing

As has been discussed in one of the previous sections, clast ploughing requires plastic flow of the till material from the stoss to the lee side of the clast (Figure 2). This flow distributes the deformation associated with the passing clast downwards to depths well below the ones that come directly in contact with the clast. Baligh (1972) conducted theoretical and experimental studies of plain-strain patterns of deformation around wedges of different shapes indenting homogeneous soil of plastic rheology. Figure 2 shows adaptation of Baligh's theoretical results to a ploughing clast. The patterns of deformation for an initially square grid are predicted from theory of perfect plasticity. This solution has a well-defined zone of distributed deformation, separated from the surrounding matrix by a sharp discontinuity and extending to the depth of:

$$Z = k_p\, a = (1+\sqrt{2})\, a \qquad (15)$$

where a is the maximum vertical dimension of the clast protruding into the till, and k_p is the constant indicated. After the ploughing clast passes, horizontal markers come back to their original position but vertical markers remain permanently deformed (Figure 2B). Experimental results are broadly consistent with the theory but differ in a few important details (Figure 9). The experimental zone of deformation has a much more diffused character and extends to significantly greater depth, $k_p \approx 4.5$. In addition, the ultimate shape of vertical markers is somewhat different because they indicate permanent strain only in the direction of ploughing. The differences between the theoretical and experimental results must result from the fact that the experimental clay matrix, like soils in general, does not behave as the perfectly rigid-plastic material assumed in the theory.

In nature, an ice-till interface can contain abundant ploughing clasts. Superposition

of numerous ploughing events like the one illustrated by Figures 2 and 9 will cause distributed deformation that corresponds to some fraction of the total relative ice-till motion. The thickness of the resulting shear zone should be several times greater than the depth to which ploughing clasts protrude from the ice base, a in (15). The transport distance at the top of the till due to one passage of a ploughing clast is equal to about a (Figures 2 and 9). If clast spacing is not much greater than two times a, then nearly all of the ice motion can be transferred to the underlying till via the deformation zones surrounding ploughing clasts. This mechanism may provide a very efficient way of distributing deformation in coarse tills in which clast spacing can easily be of the order of clast radius. On the other hand, fine-grained tills have typically small clasts and low clast abundance (Figure 5) and the ploughing-related deformation should be relatively insignificant in their case.

3.4.2. Grain Bridging

The mechanism of shear distribution discussed in the previous section concentrated on the case of a homogeneous, very fine-grained matrix being ploughed by clasts which are many times greater than the matrix grain-size (i.e., micron-size clays). Tills, however, typically contain a variety of different size particles which will interact with each other when ice motion is accommodated either at the ice-till interface or on shear zones within the till. It has been inferred from observational data that the thickness of a granular shear zone is controlled by the characteristic grain size of particles contained in the sheared material (Mulhaus and Vardoulakis, 1987; Roscoe, 1970). In geotechnical practice, it is commonly assumed that shear strain should distribute over a thickness Z given by a simple expression analogous to (15):

$$Z = k_r \, d_{ch} \approx 10 \, d_{ch} \qquad (16)$$

where: d_{ch} is the characteristic grain diameter, and k_r is a constant. The value of the constant is usually assumed to be c. 10 but some researchers put it as high as 15-50 (Maltman, 1992, p. 270). Tests performed as a part of this study on Ottawa sand (c. 0.25 mm in diameter) sheared in a ring shear device are consistent with $k_p \approx 10$ (Figure 10). At the basic level, the micromechanism of strain distribution in granular shear zones has probably to do with the formation and failure of grain bridges and grain networks (Hooke and Iverson, 1995; Iverson *et al.*, 1996).

The soil mechanics data that have led to formulation of the simple relationship expressed in (16) were collected for well-sorted materials containing similar-size particles. Application of the same rule to poorly-sorted materials, such as tills, is greatly complicated by the uncertainty in selection of the characteristic grain diameter. Intuitively, d_{ch} should represent the largest particles which during shear come frequently in contact with similar size particles. For matrix-dominated tills, these would be the matrix-size particles ($d_{ch} < 2$ mm). As the tills coarsen, the importance of clast interactions in distributing strain should increase. At the coarse extreme of clast-supported tills d_{ch} is of the order of the typical clast size (~0.01 to ~0.1 m). Thus, distribution of strain in tills due to particle interactions may vary from a zone whose thickness is of the order of several microns for clay-rich tills to a zone that is decimeters in thickness for clast-rich tills.

3.4.3. Fluctuations of Water Pressure

The two mechanisms of strain distribution discussed above have to do with the granular character of tills composed of rigid particles of different sizes. However, this inhomogeneous nature of tills is frequently neglected, leading to a theoretical approximation of a till as a fluid-like continuum (Boulton and Hindmarsh, 1987; Alley *et al.*, 1986,

1987abc). Under such an assumption, it has been argued that concentrated deformation should be characteristic for perfectly plastic tills and that distributed deformation observed beneath some glaciers provides an evidence for nearly linearly viscous rheology of tills (Alley, 1993, p. 205). This is a sound argument because strain-rate dependence of strength typical for viscous materials forces distribution of strain, but when strength is strain-rate independent deformation may collapse towards a single plane (Turcotte and Schubert, 1982, p. 318). However, for a Coulomb-plastic till changes in strength and distribution of strain may be caused by changes in effective pressure with depth and time. If these changes can force a vertical migration of the shear zone that accommodates the deformation, the time-integrated effect of this process will be to create a diffused, pseudo-viscous zone of deformation. This will happen even though at any instant in time the deformation will take place on a discrete zone in accordance with the intrinsic Coulomb-plastic rheology of a till. In other words, the effective-pressure dependence of strength in a Coulomb-plastic till may play a similar function with regard to strain distribution as the strain-rate dependence does for a viscous material. Therefore, even if the 'grainy', inhomogeneous nature of tills is neglected there is still a non-viscous mechanism that may lead to strain distribution.

To verify whether the conjecture of Coulomb-plastic strain distribution is plausible in the context of subglacial physical conditions, I solve a problem of time-dependent distribution of effective pressure driven by a periodic (daily) variation of water pressure in the basal water system. Diurnal fluctuations of basal water pressure are very common because of changes in meltwater supply (especially for mountain glaciers) and tidal forcing occurring on these timescales (Blake, 1992; Boulton and Hindmarsh, 1987; Engelhardt and Kamb, 1997; Hooke *et al.*, 1997; Iverson *et al.*, 1995). Assuming a constant total load (ice overburden pressure) and infinitesimal strains due to consolidation, the time-variable

distribution of excess pore water pressure in a one-dimensional vertical column of till can be described by the diffusion equation (Scott, 1963, equation 5-34):

$$c_v u_{zz} = u_t \tag{17}$$

where c_v is the hydraulic diffusion coefficient (coefficient of consolidation), $u(z,t)$ is the excess pore pressure (total water pressure less hydrostatic pressure), and u_{zz}, u_t denote the second derivative of $u(z,t)$ with respect to depth and the first derivative of $u(z,t)$ with respect to time. A commonly encountered analytical solution to (17) exists when the periodic boundary condition applied to the top of the till has the form:

$$u(0,t) = u_o + \Delta u \cos(\omega t) \tag{18}$$

where u_o is the time-averaged excess pore pressure at the top of the till, Δu is the magnitude of water pressure fluctuations, and $\omega = 2\pi/T$, where T is the period of the fluctuation. The solution is then given by (Turcotte and Schubert, 1982, 155-157):

$$u(z,t) = u_o + \Delta u \exp(-\psi z) \cos(\omega t - \psi z) \tag{19}$$

where $\psi = \sqrt{(\pi / (c_v T))}$. It follows from (19) that pore water pressure fluctuations decay quickly with depth and are very small already at the characteristic depth $2\delta = 2\sqrt{(c_v T)}$. Thus, the depth to which water-pressure fluctuations may influence strength properties of till is dependent on the hydraulic diffusivity of till, c_v. Hydraulic diffusivity depends sensitively on the content and mineralogy of clays in soil (Mitchell, 1993, p. 180). Data for tills are sparse but they suggest that clay-rich tills have $c_v \sim 10^{-8}$ m^2 s^{-1} and coarse tills $c_v \sim 10^{-6}$ m^2 s^{-1} (Engelhardt, unpublished data; Iverson *et al.*, in press, Table 1; Sauer *et al.*, 1993, Table 2). It is obvious already from this dimensional analysis that any effects of pore-pressure fluctuations on strain distribution will propagate significantly deeper (roughly ~10 times deeper) in coarse tills than in fine-grained tills.

To illustrate how pore water fluctuations may cause a time-dependent vertical migration of a shear zone, I work through an example. Changes in the subglacial effective

pressure can be calculated from (19) using:

$$p'(z,t) = \Delta p' z - u(z,t) \qquad (20)$$

where $\Delta p' = (\rho_t - \rho_w)g$ is the hydrostatic effective pressure gradient ($\Delta p' \approx$ 10 kPa m^{-1} for ρ_t the till density of c. 2,000 kg m^{-3}, ρ_w, the water density of c. 1,000 kg m^{-3}, and g, the acceleration of gravity of 9.81 m s^{-2}). The sign convention used here assumes that pore pressures below the overburden ice pressure (P in (1b)) are negative. This expression is used to calculate changes in effective pressure for a set of assumptions that is intended to emulate a 0.6 m thick layer of coarse till with hydraulic diffusivity of 10^{-6} m^2 s^{-1}. The system is subjected to a basal pore water fluctuation of amplitude Δu = +-10 kPa of period T = 24 hrs. = 86,400 s around an average basal excess pore water pressure of u_o = -50 kPa (Figure 12a). Figure 11A shows the effective pressure timelines at one hour intervals throughout the whole 24-hour cycle.

A model of till for which an assumption is made that till strength at any given depth is always a simple linear function of the current effective pressure (p' in (1a)), irrespective of previous effective pressures, can be called a 'perfectly remolded till model'. For this model, at any point in time the motion of overlying ice is accommodated on the weakest shear zone whose depth is determined by the depth of the minimum effective pressure, p_{min}'. One can use (20) to track the depth and record the magnitude of the minimum effective pressure through time (Figure 11B). For the considered example, the minimum effective pressure migrates downward to the depth of c. 0.3 m ($\approx \delta$) for half of the water-pressure cycle and remains at the ice-till interface (z = 0) for the other half of the cycle (Figure 11b). If the 'perfectly remolded till model' and a constant velocity of ice motion, U_i, are assumed and ice moves at a constant velocity throughout the cycle, till deformation will be distributed in a manner shown in Figure 11c.

The assumption of the 'perfectly remolded till' represents, however, an idealization.

In nature, it is observed that granular materials subjected first to a higher effective pressure and then sheared under a lower effective pressure (e.g., p_{min}') show a transient peak in strength (case d in Figure 1). This additional stress threshold will hinder the 'perfectly-remolded' strain distribution. Here, the other end-member assumption is considered: that the till behaves as a 'perfectly overconsolidated' material whose strength is always determined (following (1a)) by the maximum effective pressure that this material has ever experienced (p_{max}'). Under this assumption, all of the ice motion must be accommodated at the depth in till where the maximum effective pressure during the whole water-pressure cycle is smaller than the maximum effective pressure at all other depths (Figure 11B). For the considered example, this condition is met at the depth of c. 0.3 m ($\approx \delta$) resulting in a plug flow of till trapped between this shear zone and the ice base (Figure 11C).

Real granular materials show a behavior that is somewhere between the perfectly-remolded and perfectly-overconsolidated approximations (Scott, 1963). Thus, the shear stress threshold due to overconsolidation (Figure 1) may be at times small enough to be overcome implying that the strain in the till can be accommodated on planes characterized by the maximum ratio of shear stress to effective pressure at any given time. In addition, for till to remain overconsolidated, no physical remolding of the till structure acquired at higher effective pressures can take place. However, clasts dragged by the ice base may provide an efficient agent for remolding of till matrix and removing the effects of overconsolidation, making the material behave more like the 'perfectly remolded' end-member. Behavior of a 'real' till probably falls between the two end-members shown in Figure 11C.

The fluctuating subglacial effective stress (Figure 11A) also illustrates that the assumption of temporally and spatially constant till strength made in the preceding discussion of ice-till interface represents a relatively simple case. Ploughing clasts may

interact with a till whose strength changes with depth and time and these clasts are likely to influence the distribution of till strength through remolding. Future detailed and case-specific analyses of ice-till interactions should take these effects into account.

There is no simple way to verify whether water-pressure fluctuations are to any degree responsible for the distributed deformation occurring in <0.6 m thick shear zones beneath some mountain glaciers (Blake, 1992; Boulton and Hindmarsh, 1987; Hooke *et al.*, 1997; Iverson *et al.*, 1995). However, the physical conditions that have been observed beneath these glaciers (diurnal fluctuations of water pressure, relatively coarse tills) are consistent with the ones assumed here. The presented model suggests that strain distribution due to water-pressure fluctuations will occur over depths that should be roughly an order of magnitude greater for coarse tills ($Z \sim 0.1$ m) than for fine-grained tills ($Z \sim 0.01$ m).

3.5. Discussion

There is a dearth of physical models describing ice-till coupling and distribution of deformation in till (Hooke, 1997). The exception is the viscous-till model for which distributed till deformation is a result of the assumed and observed viscous till rheology (Alley, 1989b; Boulton and Hindmarsh, 1987). The question of whether there are significant differences in subglacial behavior of different types of till has not been explored enough, especially in the view of the fact that till has one of the broadest ranges of properties of sediment types. An initial step in this direction was made by Boulton (1974) who inferred that the strength of the ice-till coupling may be dependent on till granulometry, with coarser tills favoring strong coupling. The different physical mechanisms of ice-till interactions reviewed here support and refine this inference and, in

addition, suggest that the depth of till deformation may also be sensitive to till granulometry.

The great variability in till granulometry is well illustrated by a review of some of the published data on grain-size distribution in tills. The clast content reported from coarse, sand-rich tills can be relatively high (25-50%) and commonly clasts are of a diameter of ~0.1 m (Boulton and Hindmarsh, 1987, Figure 3; Clarke, 1987, Figure 4; Dreimanis and Vagners, 1972, Figure 8; Holmes, 1960, Figure 2; Jiao *et al.*, 1989). At the other end of the spectrum, fine-grained tills have typically 0-15% clasts and their matrix is dominated by silt- and clay-size material (Johnson, 1983; Kemmis, 1981, p. 148; Shepps, 1953, table 1; Tulaczyk *et al.*, 1998, Figure 3). The distribution of fine-grained and coarse till is mostly controlled by the character of source material and the distance of glacial transport (Dreimanis and Vagners, 1972). In general, coarse-grained till results from direct glacial erosion of lithified bedrock and fine-grained till is incorporated material from preexisting fine sediment, clay-rich sedimentary rocks and far-traveled, highly-comminuted bedrock (Mickelson *et al.*, 1983; Sladen and Wrigley, 1983).

Direct observations of ice-till interactions have been made mainly beneath mountain glaciers that are underlain by coarse till (Boulton and Hindmarsh, 1987; Blake, 1992; Blake *et al.*, 1994; Engelhardt *et al.*, 1978; Fischer and Clarke, 1994; Hooke *et al.*, 1997; Iverson *et al.*, 1995). Most of these studies reveal complex, spatially and temporally variable patterns of ice-till coupling and widely fluctuating, positive and negative strain rates. Despite the very rough nature of at least some of these tills (e.g., Blue Glacier till of Engelhardt *et al.*, 1978), complete decoupling of ice from till occurs when water pressures are near flotation level ($p' \approx 0$) (Engelhardt *et al.*, 1978; Hooke *et al.*, 1997; Iverson *et al.*, 1995). Engelhardt *et al.* (1978) have made a qualitative inference from their direct borehole observations that the ability of ice to intrude into till pore spaces is the main factor which

controls the strength of the ice-till coupling. This qualitative statement is reflected in a physical way by the surface-tension effect whose importance was inferred here from basic thermodynamic laws of ice interactions with granular media.

Beneath mountain glaciers where extensive studies of till deformation were conducted, the thickness of subglacial shear zones (Z) was observed/estimated to be: 0.1 m (Blue Glacier, Engelhardt *et al.*, 1978), 0.15-0.5 m (Trapridge, Blake *et al.*, 1994; Fischer and Clarke, 1994); 0.3 m (Storglaciären; Hooke *et al.*, 1997; Iverson *et al.*, 1995); 0.6 m (Breidamerkurjökull; Boulton and Hindmarsh, 1987). Grain-size distribution data available for Trapridge and Breidamerkurjökull (Figure 5) as well as the visual observations of Engelhardt *et al.* (1978) beneath Blue Glacier indicate that these coarse tills contain a significant fraction of clasts whose diameter is comparable to the thickness of the deforming zone in the sense of equation (16) (i.e., $0.1Z < d < 1.0Z$). Beneath the Blue Glacier, the only site where real-time borehole observations of till deformation were made, larger clasts were often found spanning the whole distance between the moving ice and the subtill bedrock. These clasts were accommodating ice motion by rolling in a ball-bearing fashion (Engelhardt *et al.*, 1978). It is difficult to assess from the published data just how important clasts are in distributing strain in coarse till, but there is the possibility that, in accordance with equations (15) and (16), they represent one of the main factors leading to creation of distributed shear zones in plastic tills.

However, not all of the features of the existing strain-rate records from tills of mountain glaciers can be attributed to the influence of clasts (Blake *et al.*, 1994). For instance, strain-rate fluctuations appear to be generally correlated with water-pressure fluctuations (Blake *et al.*, 1994; Hooke *et al.*, 1997; Iverson *et al.*, 1995). This suggests that changes in effective pressure may distribute till deformation. There are a number of potential mechanisms that can explain the linkage between strain-rates and effective

pressure. The shear-zone migration model described above represents one of them. Other possibilities that have been considered in the literature include till thinning/thickening and elastic response to cyclic loading (Blake, 1992; Hooke *et al.*, 1997, p. 177).

Data on ice interactions with fine-grained tills is very sparse. The only direct investigation of such modern subglacial system is the study of Ice Stream B, West Antarctica (Engelhardt *et al.*, 1990; Kamb, 1991; Engelhardt and Kamb, 1997, and in press). The presence of a weak, continuous layer of till beneath this ice stream was inferred first from seismic exploration data (Blankenship *et al.*, 1986, 1987; Rooney *et al.*, 1987, 1991) and then confirmed through drilling and sampling of the bed material (Engelhardt *et al.*, 1990). This material is composed of glacially recycled, Tertiary glacimarine sediments whose clay-rich, clast-poor character predetermines the very fine-grained nature of the ISB till (Tulaczyk *et al.*, 1998).

Borehole experiments suggest that bulk of the ice stream motion is accommodated by basal sliding, which may involve also till deformation in a thin shear zone (~cm) (Engelhardt and Kamb, in press). This concentration of sliding/shearing near the ice base is fully consistent with the results of the theoretical analysis presented here (e.g., Figures 6 and 8). These results predict that low clast content, susceptibility of the fine-till matrix to submergence by very thin water films, and strong surface-tension effects should combine beneath ISB to make the ice-till interface significantly weaker than the till itself. This situation favors a mechanical decoupling at the interface even though physically the till and the ice are separated only by a very thin water film (<0.1 mm, Engelhardt and Kamb, 1997). In the case of a perfectly flat ice base, pure sliding would be possible. However, the ice base is likely to contain some clasts and/or ice protrusions which will locally plough and deform the underlying till to depths scaling with their amplitude. The apparent variations in sliding velocity observed by Engelhardt and Kamb (in press) using a tethered

stake placed just beneath the ice base may be due to such irregularities interfering with the tethered stake. Water pressure beneath the ice stream fluctuates over about ±10 kPa with at times a predominantly diurnal period (Engelhardt and Kamb, 1997). These fluctuations cannot, however, cause significant distribution of deformation with depth because of the very low hydraulic diffusion coefficient of this clay-rich material ($c_v \sim 10^{-8}$ m^2 s^{-1}, Engelhardt, unpublished data).

Pleistocene fine-grained tills are quite common, but interpretation of their shear strain history from their sedimentological properties is very difficult (Alley, 1991 vs. Clayton *et al.*, 1989). Beget (1986, p. 238-239) hypothesized that sliding may have been a common mode of ice motion over the matrix-dominated tills of the Lake Michigan lobe. He proposed also that this sliding should be associated with localized deformation extending to a depth controlled by the size of ice and rocks protruding from the base. There is some sedimentological evidence that supports occurrence of ice sliding associated with clast ploughing and shallow deformation (Clark and Hansel, 1989; Ehlers and Stephan, 1979). Ice-till decoupling is very difficult to document for Pleistocene tills, unless it was associated with a water film thick enough to produce extensive stringers of sorted sediments (Alley, 1991, p. 72). In some localities, these stringers are common enough to provide strong evidence for widespread and long-lasting decoupling of ice from the underlying till (Brown *et al.*, 1987; Piotrowski and Tulaczyk, in press).

It has been previously proposed that only tills of viscous rheology are capable of deforming in a distributed manner and, thus, transporting debris subglacially (e.g., Alley, 1993). This proposition stems from the assumption that till is a fluid-like continuum in which shear strain distribution is caused by one and only one mechanism, the strain-rate dependence of strength. However, simple physical arguments presented here suggest that distributed deformation is not inherently inconsistent with Coulomb-plastic till. The

reasons that may make such distributed deformation possible in till include: 1) the fact that the till and the ice-till interface are not perfectly fluid-like or smooth at the scale of subglacial shear zones (i.e., the granular character of the till cannot be neglected); and 2) the presence of mechanisms other than strain-rate strengthening that may prevent concentration of shear strain on one failure plane (e.g., changing strength distribution due to changes in effective pressure). Unless it can be demonstrated that these influences are unimportant for a given till where distributed deformation is observed, the mere fact of distributed deformation cannot be used as conclusive proof of the viscous character of this till. Such unequivocal proof is provided only by data which show a viscous-type relationship between subglacial strain rates and stresses (e.g., Boulton and Hindmarsh, 1987).

Ice motion over till of plastic rheology can result in relatively low, but non-zero, subglacial transport and erosion rates. Taking the shear-zone-migration model as an example (Figure 11), one can estimate that the depth-averaged till velocity represents a significant fraction of ice velocity, 0.3 to 1.0. These values are broadly consistent with the ones calculated by Alley (0.1-0.5; 1989b, Figure 3) for viscously behaving tills, even though the assumed mechanism of strain distribution is greatly different. The depth over which the shear-zone migration distributes deformation is likely to be only of the order of a few centimeters for fine-grained tills and a few decimeters for coarse tills ($Z \approx \delta \equiv \sqrt{(c_v/T)}$ with $c_v = 10^{-8}$ m^2 s^{-1} for fine-grained tills and 10^{-6} m^2 s^{-1} for coarse tills). This is between one and two orders of magnitude less than the commonly postulated thickness of several meters for an actively deforming viscous till (Alley, 1991; Alley *et al.*, 1986; 1987abc; Boulton, 1996ab; Clark *et al.*, 1996; Jenson *et al.*, 1995, 1996). To remain in a steady-state, these thick viscous till beds are thought to require a relatively fast rate of debris delivery by subtill erosion and/or deposition from basal debris-laden ice (~0.1 mm/y,

Cuffey and Alley, 1996). Debris flux for a plastic, mobile till could be roughly one or more orders of magnitude smaller. Thus, such a mobile till bed needs to be resupplied with debris at a rate of only <~0.01 mm/y. These low till evacuation rates can be matched and exceeded by deposition of debris from basal ice melting at a rate ~1 mm/y and containing a reasonable volumetric concentration of debris, <~0.1 (Kirkbride, 1995, Figure 8.3).

3.6. Conclusions

This paper presents quantitative analysis of several physical mechanisms of potentially great importance to ice interactions with tills of Coulomb-plastic rheology. The nature of these mechanisms suggests that till granulometry has an important control over the strength of ice-till coupling and over the depth to which till deformation is distributed. With all other factors being equal, coarse, clast-rich tills should provide stronger ice-till coupling and thicker subglacial shear zones than fine-grained tills. The latter should favor ice decoupling and concentration of deformation in the vicinity of the ice base. A weak interface is predicted in the case of ice contact with fine-grained tills because: 1) support provided by the relatively scarce ploughing clasts is small; 2) large areas of the interface are submerged by a thin water film (~10^{-6} m); and 3) surface-tension effects hinder coupling of the ice base with the top of the till. Within the range of low subglacial effective pressures applicable to the soft-bed conditions (<100 kPa), fine-grained tills are likely to have interface strength significantly lower than the strength of the till itself ($\tau_i < \tau_f$). As long as the latter condition is met, sliding with ploughing is mechanically more advantageous than pervasive deformation in the underlying till. The strength of ice coupling with coarse tills is dominated by the effect of clast ploughing and is much less sensitive to the presence of a thin basal water film and to the surface-tension effect. As a

result, ice-till decoupling and sliding may occur only over a relatively narrow range of effective pressures that are very near zero.

I propose that there are at least three mechanisms that may cause greater depth distribution of strain in coarse, clast-rich tills than in fine-grained tills: 1) matrix deformation around ploughing clasts; 2) particle bridging; and 3) vertical shear-zone migration due to effective pressure fluctuations. For the first two, the thickness of a till shear zone should scale as a small multiple of the characteristic clast/particle diameter. These two mechanisms may result in relatively thick shear zones (~0.1 m) when large clasts (~0.01 m to ~0.1 m) are abundant. However, their influence should be negligible for clast-poor, fine-grained tills. In the case of the third mechanism, the thickness over which till deformation is distributed decreases with the square root of the hydraulic diffusivity of till. The existing measurements of the latter suggest that this thickness may, again, vary from ~0.1 m for coarse tills to ~0.01 m for fine-grained tills. The fact that there are physically viable mechanisms for distributing deformation in tills of Coulomb-plastic rheology indicates that, by themselves, observations of distributed deformation in modern subglacial zones do not provide an unequivocal evidence for viscous rheology of these tills.

The inference that behavior of a weak subglacial till in contact with moving ice may depend fundamentally on till granulometry is consistent with the existing set of observations from modern subglacial zones. Most of the previous interpretations of subglacial till deformation emphasized the controlling role of other physical conditions in determining till behavior. Moreover, till itself was largely treated within a framework of continuum mechanics and as a material whose basic properties do not differ significantly from one location to another. However, till is a very broad term, which encompasses a variety of sediments with widely differing characteristics. To formulate accurate physical laws that govern the mechanics of ice motion over till and the process of till generation by

subglacial shear, it is necessary to account for the variable properties of real till. The relative importance of the physical aspects of ice-till interactions discussed here can be further verified through direct field observations and laboratory experiments.

3.7. Appendix 1 - Clast Ploughing in Drained and Undrained Conditions

In the analysis of clast ploughing presented in the main body of this paper I have used undrained till strength to calculate ploughing resistance. However, the assumption of undrained conditions during ploughing will break down for relatively slow clast motion and for tills with high hydraulic diffusivity (2). It is important to verify whether the breakdown of this assumption may change in a fundamental way my conclusion regarding the high sensitivity of ice-till interactions to till granulometry. In this appendix I estimate the difference in till resistance to ploughing for drained and undrained conditions.

Relative motion of a clast through till produces a zone of compression in front of the clast and a zone of extension behind it (Figure 2). Under drained conditions, the strength of the till in both of these zones will be different, higher in compression (τ_c) and lower in extension (τ_e). The exact stress distribution and the geometry of slip lines accommodating till deformation around the clast are likely to be complex. However, the approximate symmetry of the shear zone surrounding the clast suggests that the drained till strength can be reasonably treated as an average of τ_c and τ_e (Figure 2, Tab. 2):

$$\tau_d = 0.5(\tau_c + \tau_e) \qquad (21)$$

To estimate the values of τ_c and τ_e, I consider a two-dimensional till experiencing ploughing by a single clast. Representative stress paths for the zones of compression and extension are illustrated in the Mohr diagram in Figure 12A. Since the considered system is perfectly drained, there is no build-up of pore water pressures and total stresses are equal

to effective stresses. Initially, the horizontal and vertical effective stresses are assumed to have the same magnitude ($\sigma_{ho}' = \sigma_{vo}' = p_o'$). During ploughing, the vertical stress remains constant at p_o' but the horizontal stress increases in front of the clast and decreases behind it. These changes continue until failure is reached. At failure, the two Mohr circles defined by the constant vertical stress and the two horizontal stresses (σ_{he}' and σ_{hc}') are tangential to the failure envelope (Figure 12A). The intersections of these circles with this envelope give τ_c and τ_e.

Analytical solutions for the stresses in extension and compression (Figure 12A) represent a classical problem in soil mechanics solved originally by Rankine (1857). It can be shown that the magnitudes of horizontal stresses are uniquely related to the constant vertical stress through the following expressions:

$$\sigma_{he}' = \frac{(1-\sin\phi)}{(1+\sin\phi)} p_o' \tag{22a}$$

$$\sigma_{he}' = \frac{(1+\sin\phi)}{(1-\sin\phi)} p_o' \tag{22b}$$

From the Mohr diagram, the failure shear strength can be expressed as:

$$\tau_f = 0.5\sigma_d \cos\phi \tag{23}$$

where: σ_d is the deviatoric stress, i.e., the principal stress difference (σ_1 - σ_2). In the considered simple case the horizontal and vertical stresses are the principal stresses, i.e., σ_d = σ_{hc} - σ_{vc} in compression and $\sigma_d = \sigma_{ve}$ - σ_{he} in extension (Figure 12A). Using this fact one can combine (22ab) and (23) to obtain the till shear strength in extension and compression:

$$\tau_e = \frac{\sin\phi\cos\phi}{(1+\sin\phi)} p_o' \tag{24a}$$

$$\tau_c = \frac{\sin\phi\cos\phi}{(1-\sin\phi)} p_o' \tag{24b}$$

Finally, equation (21) combined with (24ab) gives the overall drained till strength:

$$\tau_d = \frac{\sin\phi}{\cos\phi} p_o' = \tan\phi p_o' \tag{25}$$

Since I want to compare the drained and undrained till strength during ploughing, it is now necessary to express the undrained strength in terms of the same variables, p_o' and ϕ. To do so, let us start from the same initial isotropic stress state (Fig 12B, $\sigma_{ho}' = \sigma_{vo}' = p_o'$). At this initial state the total stresses are equal to the effective stresses (i.e., u = 0). However, this changes once the motion of the ploughing clasts induces a deviatoric stress which leads to a build-up in pore pressure which in plane strain and at failure will be given by (Scott, 1963, p. 272):

$$\Delta u = \Delta\sigma_m + A_f \sigma_d = \Delta[(\sigma_1 + \sigma_3)/2] + A_f(\sigma_1 - \sigma_2) \qquad (26)$$

where: $\Delta\sigma_m$ is the change in mean total stress, $(\sigma_1 + \sigma_3)/2$, and A_f is the value of the pore pressure parameter at failure. For a normally-consolidated soil a reasonable and a computationally convenient value of A_f is 1.0 (Scott, 1963, Figure 6-11). Having this constraint one can define the effective failure stresses for the zone of compression in front of the ploughing clast and the zone of extension behind it (Figure 12B). Both of these stress states are described by the same Mohr circle and the strength of the till in the undrained state is everywhere the same:

$$\tau_u = [\sin\phi \cos\phi /(1 + 2 \sin\phi)]\, p_o' \qquad (27)$$

Comparison of the expressions (25) and (27) shows that in the drained case till strength is greater than the undrained till strength by a factor whose exact value depends on the internal friction angle, $(1 + 2 \sin\phi)/(\cos\phi)^2$. The value of ϕ for tills lies typically within the range of 20-40° (Patterson, 1994, table 8.1). Therefore, in perfectly drained conditions a stress on a ploughing clast should be 2.1 - 3.9 times greater than the equivalent stress in perfectly undrained conditions. This is a moderate effect which does not change significantly the order-of-magnitude calculations shown in the main body of this paper. Moreover, the influence of this effect is generally consistent with my main proposition that ice coupling with coarse tills should be stronger than ice coupling with

fine-grained tills. Fine-grained tills are expected to have low hydraulic diffusivity and they should experience drained conditions less frequently than the coarse tills (see (2)). In addition, the coarse-grained tills have greater angle of internal friction than the fine-grained tills, e.g., for the ISB till $\phi = 24°$ and $\tau_d/\tau_u = 2.2$ whereas for the Breidamerkurjökull till $\phi = 32°$ and $\tau_d/\tau_u = 2.9$ (Boulton and Hindmarsh, 1987; Tulaczyk, unpublished data). With all other factors being equal, this will make the ice-till interface stronger for coarse tills.

The analysis of pore-pressure-dependence of ploughing stress presented in this appendix clearly shows that the assumption of undrained conditions made before does not limit significantly the generality of my conclusions.

3.8. Acknowledgments

This work was supported by the NSF grant OPP-9219279 to Barclay Kamb and Hermann Engelhardt as a part of research on the role of subglacial till in ice stream mechanics. Additional support to S.T. was provided by the Henry and Grazyna Bauer Fellowship. Sincere thanks go to Barclay Kamb, Ronald F. Scott, and Hermann Engelhardt of the California Institute of Technology for the many discussions that have continuously stimulated this research. However, the author bears sole responsibility for the content of this paper. Neal Iverson and Richard Alley have gratefully provided copies of their manuscripts in press. I thank Richard Alley and Jan Piotrowski for helpful criticisms, some of which are not answered here.

3.9. References

Alley, R.B., 1989a, Water-pressure coupling of sliding and bed deformation 1. Water system: Journal of Glaciology, v. 35, p. 108-118.

Alley, R.B., 1989b, Water-pressure coupling of sliding and bed deformation 2. Velocity-depth profiles: Journal of Glaciology, v. 35, p. 119-129.

Alley, R.B., 1991, Deforming-bed origin for southern Laurentide till sheets?: Journal of Glaciology, v. 37, p. 67-76.

Alley, R.B., 1993, How can low-pressure channels and deforming tills coexist subglacially: Journal of Glaciology, v. 38, p. 200-207.

Alley, R.B., Blankenship, D.D., Bentley, C.R., and Rooney, S.T., 1986, Deformation of till beneath Ice Stream B, West Antarctica: Nature, v. 322, p. 57-59.

Alley, R.B., Blankenship, D.D., Bentley, C.R., and Rooney, S.T., 1987a, Till beneath Ice Stream B, 3. Till deformation: evidence and implications: Journal of Geophysical Research, v. 92, p. 8921-8929.

Alley, R.B., Blankenship, D.D., Bentley, C.R., and Rooney, S.T., 1987b, Till beneath Ice Stream B, 4. A coupled ice-till flow model: Journal of Geophysical Research, v. 92, p. 8921-8929.

Alley, R.B., Blankenship, D.D., Rooney, S.T., and Bentley, C.R., 1987c, Continuous till deformation beneath ice sheets: Publication of the International Association of Hydrological Sciences, no. 170, p. 81-90.

Alley, R.B., Cuffey, K.M., Evenson, E.B., Strasser, J.C., Lawson, D.E., and Larson, G.J., 1998, How glaciers entrain and transport basal sediments: physical constraints: Quaternary Science Reviews, v. 16, p. 1017-1038.

Baligh, M.M., 1972, Applications of plasticity theory to selected problems in soil

mechanics [Ph.D. Thesis]: Pasadena, California Institute of Technology, p. 228.

Beget, J., 1986, Influence of till rheology on Pleistocene glacier flow in the southern Great Lakes area, U.S.A.: Journal of Glaciology, v. 32, p. 235-241.

Blake, E.W., 1992, The deforming bed beneath a surge-type glacier: Measurement of mechanical and electrical properties, Ph.D. Thesis: University of British Columbia, Vancouver, 179 p.

Blake, E.W., Fischer, U.H., and Clarke, G.K.C., 1994, Direct measurements of sliding at the glacier bed: Journal of Glaciology, v. 40, p. 595-599.

Blankenship, D.D., Bentley, C.R., Rooney, S.T., and Alley, R.B., 1986, Seismic measurements reveal a saturated porous layer beneath an active Antarctic ice stream: Nature, v. 322, p. 54-57.

Blankenship, D.D., Bentley, C.R., Rooney, S.T., and Alley, R.B., 1987, Till beneath Ice Stream B, 1. Properties derived from seismic travel times: Journal of Geophysical Research, v. 92, p. 8903-8911.

Boulton, G.S., 1974, Processes and patterns of glacial erosion, *in* Coates, D.R., ed., Glacial geomorphology: Binghamton, New York, State University of New York, p. 41-87.

Boulton, G.S., 1986, Geophysics - a paradigm shift in glaciology: Nature, v. 322, p. 18.

Boulton, G.S., 1996a, The origin of till sequences by subglacial sediment deformation beneath mid-latitude ice sheets: Annals of Glaciology, v. 22, p. 75-84.

Boulton, G.S., 1996b, Theory of glacial erosion, transport and deposition as a consequence of subglacial sediment deformation: Journal of Glaciology, v. 42, p. 43-62.

Boulton, G.S., and Hindmarsh, R.C.A., 1987, Sediment deformation beneath glaciers - rheology and geological consequences: Journal of Geophysical Research, v. 92, p.

9059-9082.

Brown, N.E., Hallet, B., and Booth, D.B., 1987, Rapid soft bed sliding of the Puget glacial lobe: Journal of Geophysical Research, v. 92, p. 8985-8997.

Clark, P.U., 1991, Striated clast pavements: Products of deforming bed? Geology, v. 19, p. 530-533.

Clark, P.U., 1992, Surface form of the southern Laurentide Ice Sheet and its implications to ice-sheet dynamics: Geological Society of America Bulletin, v. 104, p. 595-605.

Clark, P.U., and Hansel, A.K., 1989, Clast ploughing, lodgement, and glacier sliding over a soft glacier bed: Boreas, v. 18, p. 201-207.

Clark, P.U., and Walder, J.S., 1994, Subglacial drainage, eskers, and deforming beds beneath the Laurentide and Eurasian ice sheets: Geological Society of America Bulletin, v. 106, p. 304-314.

Clark, P.U., Licciardi, J.M., MacAyeal, D.R., and Jenson, J.W., 1996, Numerical reconstruction of a soft-bedded Laurentide ice-sheet during the last glacial maximum: Geology, v. 24, p. 679-682.

Clarke, G.K.C., 1987, Subglacial till: a physical framework for its properties and processes: Journal of Geophysical Research, v. 92, p. 9023-9036.

Clayton, L., Mickelson, D.M., and Attig, J.W., 1989, Evidence against pervasively deformed bed material beneath rapidly moving lobes of the southern Laurentide Ice Sheet: Sedimentary Geology, v. 62, p. 203-208.

Cuffey, K., and Alley, R.B., 1996, Is erosion by deforming subglacial sediments significant? (Toward till continuity): Annals of Glaciology, v. 22, p. 17-24.

Dreimanis, A., and Vagners, U.J., 1972, Bimodal distribution of rock and mineral fragments in basal tills, *in* Goldthwait, R.P., ed., Till; a symposium: Columbus, Ohio State University Press, p. 237-250.

Ehlers, J., and Stephan, H.-J., 1979, Forms at the base of till strata as indicators of ice movement: Journal of Glaciology, v. 22, p. 345-355.

Engelhardt, H.F., Harrison, W.D., and Kamb, B., 1978, Basal sliding and conditions at the glacier bed as revealed by borehole photography: Journal of Glaciology, v. 20, p. 469-508.

Engelhardt, H.F., Humphrey, N., Kamb, B., and Fahnestock, M., 1990, Physical conditions at the base of a fast moving Antarctic ice stream: Science, v. 248, p. 57-59.

Engelhardt, H.F., and Kamb, B., 1997, Basal hydraulic system of a West Antarctic ice stream: constraints from borehole observations: Journal of Glaciology, v. 43, p. 207-230.

Engelhardt, H.F., and Kamb, B., 1998, Sliding velocity of Ice Stream B: Journal of Glaciology, (in press).

Everett, D.H., 1961, The thermodynamics of frost damage to porous solids: Transactions of the Faraday Society, v. 57, p. 1541-1551.

Fischer, U.H., and Clarke, G.K.C., 1994, Plowing of subglacial sediment: Journal of Glaciology, v. 40, p. 97-106.

Hallet, B., Walder, J.S., and Stubbs, C.W., 1991, Weathering by segregation ice growth in microcracks at sustained sub-zero temperatures, verification from an experimental study using accoustic emisions: Permafrost and Periglacial Processes, v. 2, p. 283-300.

Holmes, C.D., 1960, Evolution of till-stone shapes, central New York: Geological Society of America, v. 71, p. 1645-1660.

Hooke, R.L., 1997, Principles of glacier mechanics: Prentice Hall, London, p. 248.

Hooke, R.L., and Iverson, N.R., 1995, Grain-size distribution in deforming subglacial

tills: role of grain fracture: Geology, v. 23, p. 57-60.

Hooke, R.L., Hanson, B., Iverson, N.R., Jansson, P., and Fischer, U.H., 1997, Rheology of till beneath Storglaciären, Sweden: Journal of Glaciology, v. 43, p. 172-179.

Humphrey, N., Kamb, B., Fahnestock, M., and Engelhardt, H., 1993, Characteristics of the bed of the lower Columbia Glacier, Alaska: Journal of Geophysical Research, v. 98, p. 837-846.

Iverson, N.R., 1993, Regelation of ice through debris at glacier beds: implications for sediment transport: Geology, v. 21, p. 559-562.

Iverson, N.R., Baker, R.W., and Hooyer, T.S., 1998, A ring shear device for the study of till deformation: Tests on tills with contrasting clay content: Quaternary Science Reviews, v. 16, p. 1057-1066.

Iverson, N.R., Hanson, B., Hooke, R.L., and Jansson, P., 1995, Flow mechanics of glaciers on soft beds: Science, v. 267, p. 80-81.

Iverson, N.R., Hooyer, T., and Hooke, R.L., 1996, A laboratory study of sediment deformation, stress heterogeneity and grain-size evolution: Annals of Glaciology, v. 22, p. 167-175.

Iverson, N.R., Jansson, P., and Hooke, R.L., 1994, In-situ measurements of the strength of deforming subglacial till: Journal of Glaciology, v. 40, p. 497-503.

Iverson, N.R., and Semmens, D.J., 1995, Intrusion of ice into porous media by regelation: a mechanism of sediment entrainment by glaciers: Journal of Geophysical Research, v. 100, p. 10,219-10,230.

Jaeger, J.C., and Cook, N.G.W., 1969, Fundamentals of rock mechanics: London, Metheuen, p. 513.

Jenson, J.W., Clark, P.U., MacAyeal, D.R., Ho, C., and Vela, J.C., 1995, Numerical

modeling of advective transport of saturated deforming sediment beneath the Lake Michigan lobe, Laurentide ice sheet: Geomorphology, v. 14, p. 157-166.

Jenson, J.W., MacAyeal, D.R., Clark, P.U., Ho, C.L., and Vela, J.C., 1996, Numerical modeling of subglacial sediment deformation - implications for the behavior of the Lake-Michigan lobe, Laurentide Ice-Sheet: Journal of Geophysical Research, v. 101, p. 8717-8728.

Jiao, K., Zheng, B., and Ma, Q., 1989, Paricle composition of glacial deposits in the West Kunlun Mts.: Bulletin of Glacier Research, v. 7, p. 153-159.

Johnson, A.M., 1970, Physical processes in geology: San Francisco, Freeman, Cooper, p. 577.

Johnson, M.D., 1983, The origin and microfabric of Lake Superior red clay: Journal of Sedimentary Petrology, v. 53, p. 859-873.

Kamb, B., 1970, Sliding motion of glaciers: theory and observations: Reviews of geophysics and Space Physics, v. 8, p. 673-728.

Kamb, B., 1991, Rheological nonlinearity and flow instability in the deforming-bed mechanism of ice stream motion: Journal of Geophysical Research, v. 96, p. 16,585-16,595.

Kemmis, T.J., 1981, Importance of the regelation process to certain properties of basal tills deposited by the Laurentide ice sheet in Iowa and Illinois, USA: Annals of Glaciology, v. 2, p. 147-152.

Ketcham, W.M., and Hobbs, P.V., 1969, An experimental determination of the surface energies of ice: Philosophical Magazine, v. 19, p. 1161-1173.

Kirkbride, M.P., 1995, Processes of transportation, *in* Menzies, ed., Modern glacial environments: Oxford, U.K., Butterworth Heinemann, p. 261-292.

Lliboutry, L., 1979, Local friction laws for glaciers: a critical review and new openings:

Journal of Glaciology, v. 23, p. 67-95.

MacAyeal, D.R., 1992, Irregular oscillations of the West Antarctic ice sheet: Nature, v. 359, p. 29-32.

Maltman, A., 1992, Deformation structures preserved in rocks, *in* Maltman, A., ed., The geologic deformation of sediments: London, Chapman and Hall, p. 261-308.

Mickelson, D.M., Clayton, L., Fullerton, D.S., Borns, H.W., 1983, The Late Wisconsin glacial record of the Laurentide ice sheet in the United States, *in* Wright, H.E., and Porter, S.C., eds., Late Quaternary environments of the United States: Minneapolis, University of Minnesota Press, p. 3-37.

Mitchell, J.K., 1993, Fundamentals of soil behavior: New York, John Wiley & Sons, p. 437.

Mulhaus, H.B., and Vardoulakis, I., 1987, The thickness of shear bands in granular materials: Geotechnique, v. 37, p. 271-283.

Nye, J.F., 1969, The calculation of sliding of ice over a wavy surface using a Newtonian viscous approximation: Proceedings of the Royal Society of London, v. 311, p. 445-467.

Parks, G.A., 1990, Surface energy and adsorption at mineral-water interfaces: an introduction, *in* Hochella, M.F., and White, A.F., eds., Mineral-water interface geochemistry, Reviews in Mineralogy, v. 23: Washington, D.C., Mineralogical Society of America, p. 133-175.

Patterson, W.S.B., 1994, The physics of glaciers: Oxford, U.K., Pergamon, p. 480.

Pettijohn, F.J., 1975, Sedimentary rocks: New York, Harper & Row, p. 628.

Piotrowski, J.A., and Tulaczyk, S.,1998, Subglacial conditions under the last ice sheet in northwest Germany: ice-bed separation and enhanced basal sliding: Quaternary Science Reviews (in press).

Rankine, W.J.M., 1957, On the stability of loose earth: Philosophical Transactions of the Royal Society of London, v. 147, p. 9-27.

Rooney, S.T., Blankenship, D.D., Alley, R.B., and Bentley, C.R., 1987, Till beneath Ice Stream B, 2. Structure and continuity: Journal of Geophysical Research, v. 92, p. 8913-8920.

Rooney, S.T., Blankenship, D.D., Alley, R.B., and Bentley, C.R., 1991, Seismic reflection profiling of a sediment-filled graben beneath Ice Stream B, West Antarctica, *in* Thomson, M.R., Crame, J.A., and Thomson, J.W., eds., Geological Evolution of Antarctica: Cambridge, U.K., British Antarctic Survey, p. 261-265.

Roscoe, K.H., 1970, The influence of strains in soil mechanics: Geotechnique, v. 20, p. 129-170.

Salencon, J., 1977, Applications of the theory of plasticity in soil mechanics: New York, John Wiley & Sons, 158 p.

Sauer, E.K., Egeland, A.K., and Christiansen, 1993, Compression characteristics and index properties of tills and intertill clays in southern Saskatchewan, Canada: Canadian Geotechnical Journal, v. 30, p. 257-275.

Scott, R.F., 1963, Principles of soil mechanics: Reading, Massachusetts, Addison-Wesley Publishing Company, p. 550.

Scott, R.F., and Schoustra, J.J., 1968, Soil: mechanics and engineering: New York, McGraw-Hill, p. 314.

Shepps, V.C., 1953, Correlation of the tills of northeastern Ohio by size analysis: Journal of Sedimentary Petrology, v. 23, p. 34-48.

Sladen, J.A., and Wrigley, W., 1983, Geotechnical properties of lodgement till - a review, *in* Eyles, N., ed., Glacial geology, an indroduction for engineers and earth

scientists: Oxford, U.K., Pergamon Press, p. 184-212.

Terzaghi, K., Peck, R.B., and Mesri, G., 1996, Soil mechanics in engineering practice: New York, John Wiley & Sons, p. 549.

Tulaczyk, S., Kamb, B., Scherer, R., and Engelhardt, H.F., 1998, Sedimentary processes at the base of a West Antarctic ice stream: constraints from textural and compositional properties of subglacial debris: Journal of Sedimentary Research, v. 68, p. 487-496.

Turcotte, D.L., and Schubert, G., 1982, Geodynamics; Applications of continuum physics to geological problems: John Wiley and Sons, New York, p. 450.

Walder, J.S., and Fowler, A., 1994, Channelized subglacial drainage over a deformable bed: Journal of Glaciology, v. 40, p. 3-15.

Weertman, J., 1957, On sliding of glaciers: Journal of Glaciology, v. 3, p. 33-38.

Weertman, J., 1972, General theory of water flow at the base of a glacier or ice sheet: Reviews of Geophysics and Space Physics, v. 10, p. 287-333.

Whillans, I.M., and van der Veen, C.J., 1993, New and improved determinations of velocity of Ice Stream B and C, West Antarctica: Journal of Glaciology, v. 39, p. 483-490.

Table 1. List of Symbols

Symbol	Meaning	Dimension*
A	Area of ice-water interface	L^2
P	Total load	FL^{-2}
R_i	Median particle radius in the j-th size class	L
SSA	Specific surface area	L^{-1}
T	Period of water-pressure fluctuations	T
U_i	Total ice velocity	LT^{-1}
U_s	Velocity component due to sliding	LT^{-1}
U_t	Velocity component due to till deformation	LT^{-1}
V	Volume of an ice crystal/protrusion	L^3
Z	Depth of till deformation	L
a	Depth to which a ploughing clast protrudes into till	L
c	Cohesion	FL^{-2}
c_v	Hydraulic diffusivity (coefficient of consolidation)	L^2T^{-1}
d_c	Clast diameter	L
d_{ch}	Characteristic particle diameter	L
d_w	Basal water film thickness	L
f_c	Fractional area covered by clasts	-
f_{im}	Unsubmerged fractional area of ice-matrix interface	-
f_i	Fractional area of ice contact with particles in the j-th size range	-
g	Acceleration of gravity	LT^{-2}
k_c	Till strength:critical stress proportionality factor	-
k_{im}	Ice-matrix coupling factor	-
k_D	Deformation depth:particle size proportionality factor	-
k_r	Shear zone thickness:particle size proportionality factor	-
k_s	Particle shape factor	-
n	Porosity	-
p'	Effective pressure	FL^{-2}
p_c'	Critical effective pressure	FL^{-2}
p_i	Ice pressure	FL^{-2}
p_w	Pore water pressure	FL^{-2}
r_c	Size boundary between clasts and matrix particles	L
r_i	Characteristic particle radius in the j-th size range	L
u	Excess pore pressure over hydrostatic pressure	FL^{-2}
u_o	Time-averaged excess pore pressure at the top of the till	FL^{-2}
t	Time	T
w_c	Dry clast weight fraction	-
w_i	Dry weight fraction of the j-th particle size range	-
z	Depth in till ($z = 0$ at the ice-till interface)	L
$\Delta p'$	Hydrostatic vertical effective pressure gradient	FL^{-3}
Δu	Magnitude of water-pressure fluctuations	FL^{-2}
δ	Characteristic depthscale	L^{-1}
ϕ	Internal friction angle	°
γ	Trailing angle of the cavity behind a ploughing clast	°
φ	Leading angle of a ploughing clas	°
μ	Total Gibbs free-energy	FL
μ_i	Gibbs free energy of bulk ice	FL
μ_{im}	Coefficient of ice-matrix friction	-
$\mu_{(\phi)}$	Coefficient of internal friction ($\equiv \tan\phi$)	-
v_i	Molar volume of ice	L^3
ρ_b	Buoyant till density	ML^{-3}
ρ_w	Water density	ML^{-3}
σ_{iw}	Specific surface energy of ice-water interface	FL^{-1}
τ_c	Critical stress for ploughing	FL^{-2}
τ_f	Till failure strength	FL^{-2}
τ_i	Ice-till interface strength	FL^{-2}
τ_{ic}	Ploughing component of interface strength	FL^{-2}
τ_{im}	Ice-matrix interface strength	FL^{-2}
ω	Frequency of water-pressure fluctuations	T^{-1}
ψ	Reciprocal of the depthscale for water-pressure fluctuations	L^{-1}
~	A number of the order of ...	N/A

*In addition to the usual dimensions of F, force (MLT^{-2}), L, length, M, mass, T, time, I use 'o' for degrees and '-' to denote a non-dimensional variable.

Table 2. List of Symbols Used in the Appendix 1

Symbol	Meaning	Dimension*
A_f	Pore pressure parameter at failure	-
p_o'	Initial effective pressure	FL^{-2}
Δu	Change in excess pore pressure	FL^{-2}
$\Delta u_{e,c}$	Δu in extension and compression	FL^{-2}
ϕ	Internal friction angle	°
σ , σ'	General total and effective stress	FL^{-2}
σ_1 , σ_2	Principal stresses	FL^{-2}
σ_D	Deviatoric stress (σ_1 - σ_2)	FL^{-2}
σ_{ho}'	Initial horizontal effective stress	FL^{-2}
σ_{hc}', σ_{he}'	Horizontal effective stress in compression and extension	FL^{-2}
σ_{hc} , σ_{he}	Horizontal total stress in compression and extension	FL^{-2}
$\Delta\sigma_m$	Change in mean total stress	FL^{-2}
σ_{vo}'	Initial vertical effective stress	FL^{-2}
σ_{vc}', σ_{ve}'	Vertical effective stress in compression and extension	FL^{-2}
σ_{vc} , σ_{ve}	Vertical total stress in compression and extension	FL^{-2}
τ_c	Till strength in drained compression	FL^{-2}
τ_d	Overall drained till strength	FL^{-2}
τ_e	Till strength in drained extension	FL^{-2}
τ_f	Till strength	FL^{-2}
τ_u	Undrained till strength	FL^{-2}

*In addition to the usual dimensions of F, force (MLT^{-2}), L, length, M, mass, T, time, I use 'o' for degrees and '-' for non-dimensional variables.

Figure 1. (a) Elastic-plastic and (b) rigid-plastic model for stress-strain behavior of granular materials compared to typical stress-strain curves from laboratory tests on normally consolidated (c) and overconsolidated (d) soils (modified from Scott, 1963, Figures 8-8 and 9-1).

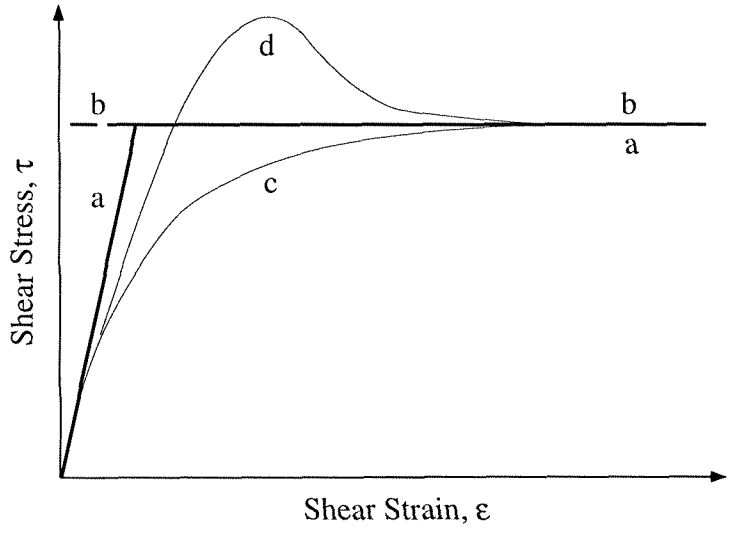
d
b
b
a
a
c
Shear Stress, τ
Shear Strain, ε

Figure 2. (A) Physical plane for the 2-D problem of a square clast ploughing perfectly rigid-plastic till. α and β denote the two families of slip-lines; φ is the leading angle of the ploughing clast and γ is the trailing angle of the cavity developed behind the clast ($\gamma = \arcsin(\sin\varphi/\sqrt{2})$). (B) Deformation of a square grid produced by migration of the ploughing clast as in (A). Both figures are adapted from Baligh (1972, Figures II-4 and II-11) who solved the plane-strain problem of a wedge indenting homogenous, perfectly rigid-plastic soil.

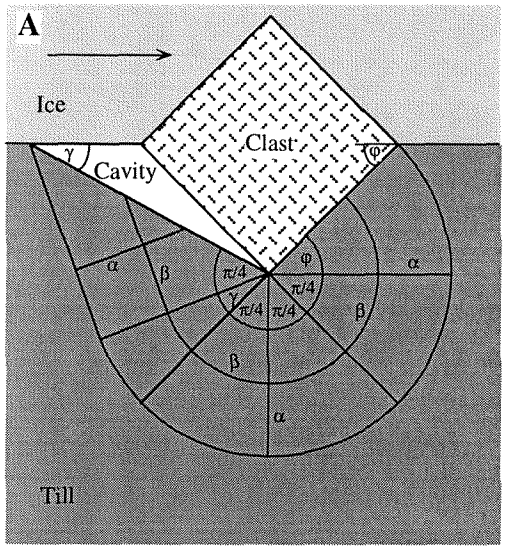
A
Ice
Clast
Cavity
γ
φ
α
β
π/4
φ
α
γ
π/4
π/4
π/4
β
β
α
Till

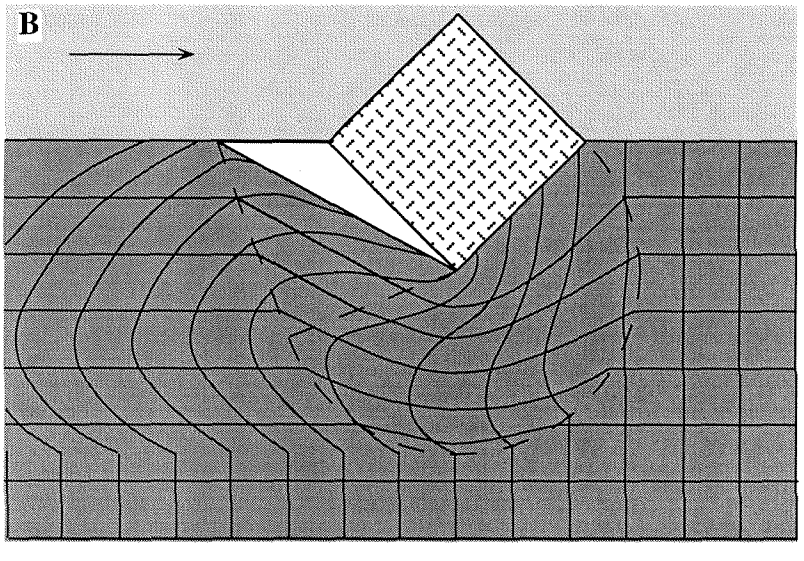
B

Figure 3. Illustration of the assumption that ice-till interface consists of spherical till particles half-way submerged in ice. Roughness of such interface is controlled at all scales by the grain size distribution of the till.

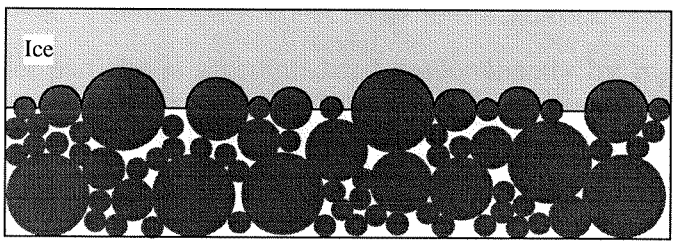
Ice

Figure 4. Local shear stress on a spherical particle (or obstacle) as a function of the particle radius and ice sliding velocity (Brown et al., 1987, equation 2; Lliboutry, 1979, equation 46). The critical obstacle size is in the range 0.001 to 0.01 m of particle radius. Ice motion over smaller particles is accommodated predominantly by regelation and over larger particles predominantly by plastic deformation. This fact gives a glaciological justification for treatment of till as a mixture of matrix and clasts. The cross-hatched rectangle indicates the selected size boundary between these two phases ($r_c = 2\times10^{-3}$ m). The thick lines show the stress-radius relationship for sliding velocity equal to the velocity of Ice Stream B at the camp UpB, West Antarctica (c. 440 m y^{-1}, Whillans and van der Veen, 1993) and the magnitude of the critical stress necessary for the particle to plough the weak till beneath Ice Stream B (this study, equation (3) with $\tau_f \approx 2$ kPa, Kamb, 1991).

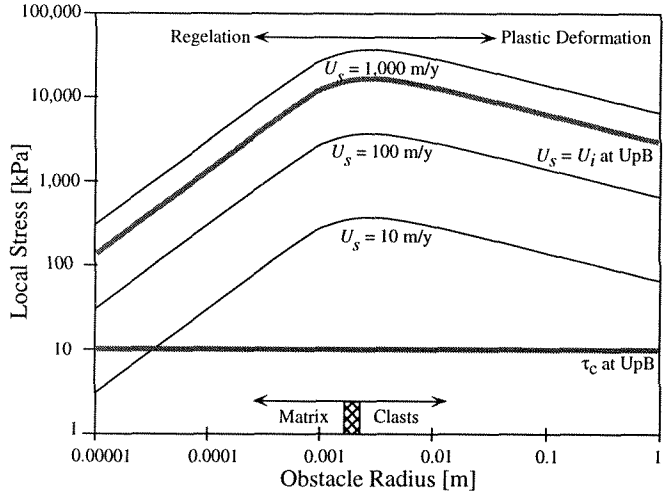
100,000
10,000
1,000
100
10
1
Local Stress [kPa]
Regelation
Plastic Deformation
U_s = 1,000 m/y
U_s = 100 m/y
U_s = 10 m/y
$U_s = U_i$ at UpB
τ_c at UpB
Matrix
Clasts
0.00001
0.0001
0.001
0.01
0.1
1
Obstacle Radius [m]

Figure 5. Cumulative weight fraction (solid lines, scale on the left) and cumulative specific surface area (SSA, dashed lines, scale on the right) of the four selected tills as a function of particle radius.

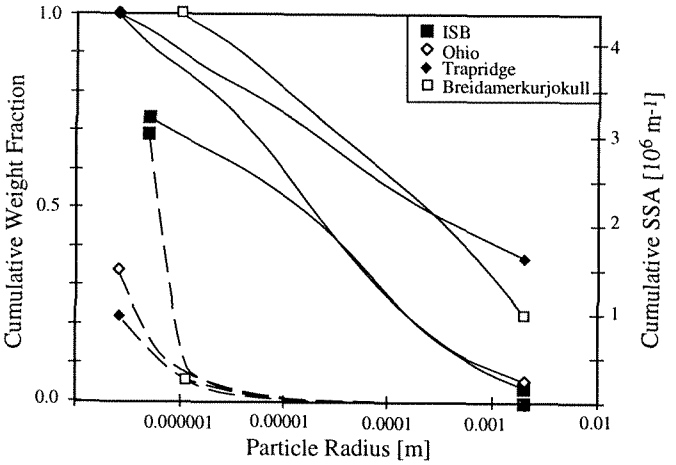
ISB
Ohio
Trapridge
Breidamerkurjokull
Cumulative Weight Fraction
Cumulative SSA [10^6 m^-1]
1.0
0.5
0.0
4
3
2
1
0.000001
0.00001
0.0001
0.001
0.01
Particle Radius [m]

Figure 6. Dependence of the non-dimensional interface strength on water film thickness for the four selected tills calculated using equation (8). The case of perfect ice-matrix coupling (k_{im} = 1.0) is given by the solid lines and the case of ice-matrix coupling determined by surface tension at 10 kPa subglacial effective pressure (k_{im} from equation (13)) is given by dashed lines. For the Breidamerkurjokull till these two cases are identical. The thick line marks the sliding criterion $\tau_f/\tau_f = 1$.

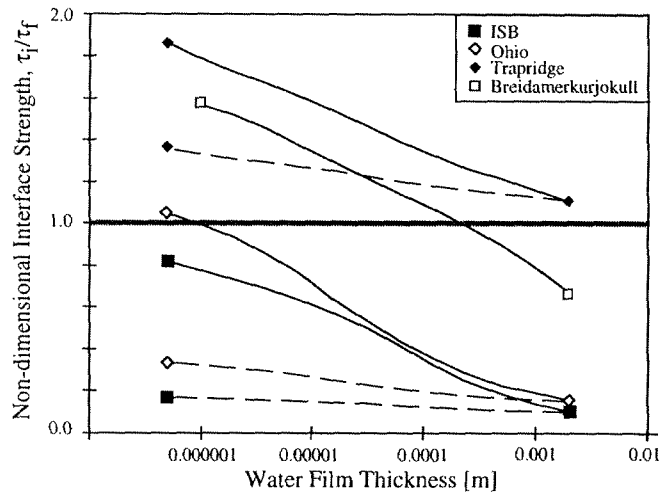
Non-dimensional Interface Strength, τ_i/τ_f
2.0
1.0
0.0
0.000001
0.00001
0.0001
0.001
0.01
Water Film Thickness [m]
ISB
Ohio
Trapridge
Breidamerkurjokull

Figure 7. Microscopic geometry of the ice-till interface as a function of subglacial effective pressure. Ice can intrude into all pore spaces as illustrated previously in Figure 3 only when effective pressure is at or above its critical value (p_c', given by equation (11)). At a smaller value of the subglacial effective pressure ($0 < p' < p_c'$) the maximum curvature of the ice base is limited by ice-water surface tension following equation (10b). Finally, at the effective pressure of zero, the ice base is constrained to be flat.

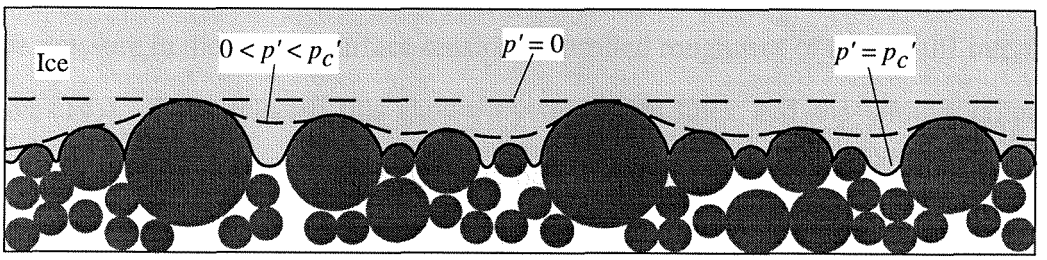
Ice
$0 < p' < p_c'$
$p' = 0$
$p' = p_c'$

Figure 8. Dependence of the non-dimensional interface strength on subglacial effective pressure in the case of surface-tension-controlled roughness of the ice-till interface (equation (14)). Four selected tills shown by thin solid lines and the sliding criterion shown by the thick gray line. Values of the critical subglacial effective pressure calculated from equation (12) are also given for each of the four tills.

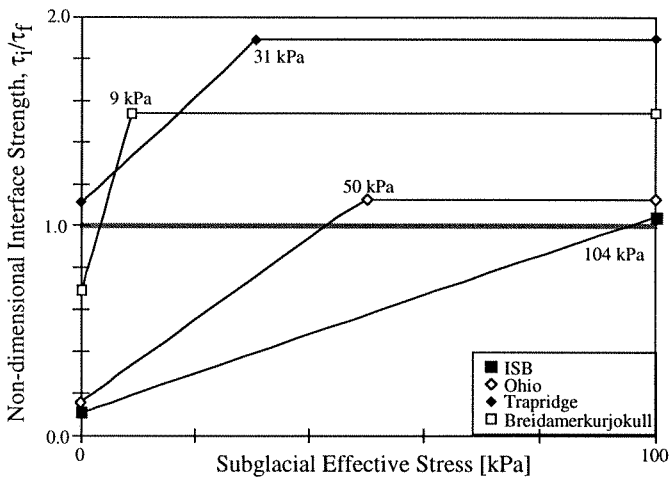
2.0
1.0
0.0
0
100
Non-dimensional Interface Strength, τ_i/τ_f
Subglacial Effective Stress [kPa]
31 kPa
9 kPa
50 kPa
104 kPa
ISB
Ohio
Trapridge
Breidamerkurjokull

Figure 9. Deformation of a square grid produced by a clast ploughing homogeneous till. The dashed line marks approximate extent of the zone of deformation around the clast. The marker lines near the top of the domain are locally too disturbed to recognize. Markers are traced from a photograph by Baligh (1972, Figure II-15) documenting an experiment in which a wedge with a 45° leading angle ploughed through a homogeneous layer of clay. I have added an ice base, drawn along the axis of symmetry of Baligh's experimental wedge. Figure 2 (this study) shows Baligh's theoretical solution to the same problem.

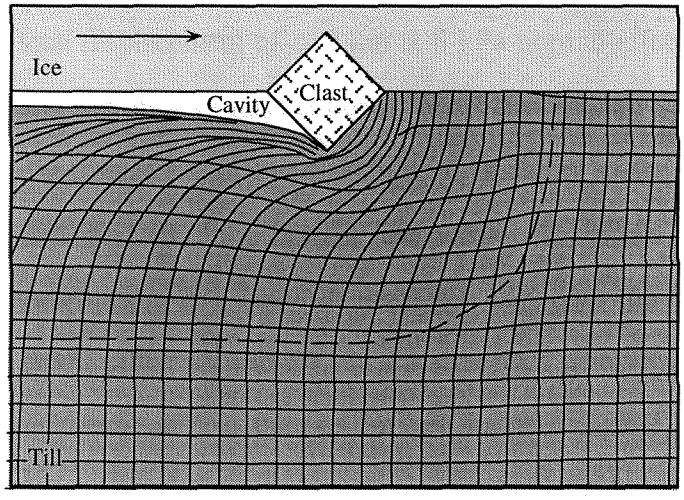
Ice
Cavity
Clast
Till

Figure 10. Strain distribution in Ottawa sand (c. 0.25 mm diameter) deformed in a ring shear device to a total displacement of c. 8 cm at 6 kPa normal effective stress. The figure shows post-shear distribution of marker beads (black dots) which were placed at the beginning of the shear experiment (A) in a vertical pile in the center of the sample chamber (short thick line at the left) and (B) in a straight line across the sample chamber (empty circles at the left). Dashed lines in (B) show an envelop e encircling the final positions of all 12 marker beads. Both results (A and B) illustrate the fact that some distribution of strain takes place in the Ottawa sand, in spite of the fact that the material has not shown a significant strain-rate dependence of strength in a series of strain-rate-controlled tests which were also performed as a part of this study (data not shown).

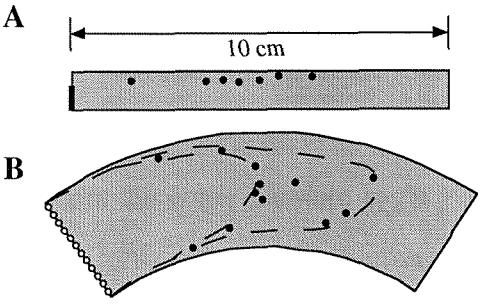
A
10 cm
B

Figure 11. (A) 1-hour timelines showing the distribution of effective pressure with depth during a 24-hours cycle of pore-water pressure fluctuations. A time-averaged hydrostatic pore pressure distribution is assumed (equation (20)). (B) (a) Migration of the minimum effective pressure with depth during 12 hours of the water-pressure cycle (line with solid circles). During the other half of the cycle, the minimum effective pressure is located at the top of the till (depth $z = 0$) and it is assumed that ice is then sliding over the top of the till. The second solid line (b) plots the values of the maximum effective pressure experienced at each depth throughout the water-pressure cycle. The square symbol marks the minimum of the latter function. (C) (a) Strain distribution in till for the case of an intra-till shear zone which follows the migration of the minimum water pressure in (B) ('perfectly-remolded till model'). (b) Plug-flow of till atop an intra-till shear zone which is fixed at the location of the least maximum effective pressure shown in (B) ('perfectly-overconsolidated till model'). In both cases the relative velocity of till, U_t, with depth is expressed as a fraction of the ice velocity, U_i, which is assumed to be constant throughout the water-pressure cycle. The position of the characteristic depthscale, $\delta = \sqrt{(c_v T)} \approx 0.3$ m, is shown in all three plots (A, B, and C).

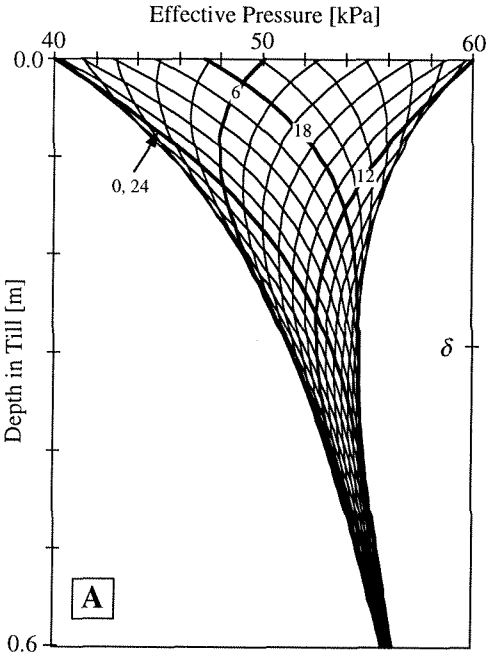
Effective Pressure [kPa]
40
50
60
0.0
0.6
Depth in Till [m]
6
18
12
0, 24
δ
A

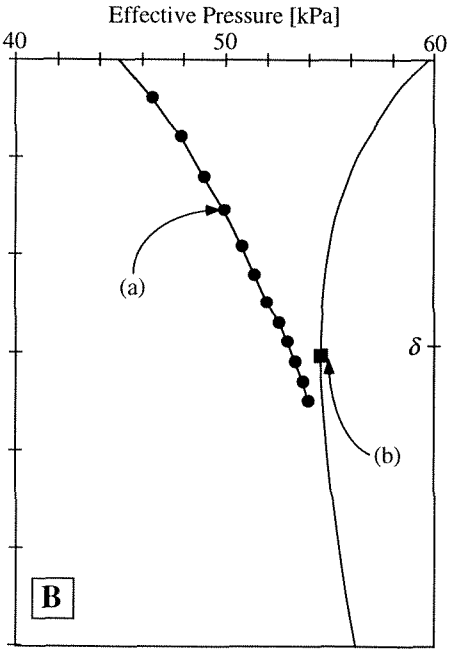
Effective Pressure [kPa]
40
50
60
(a)
δ
(b)
B

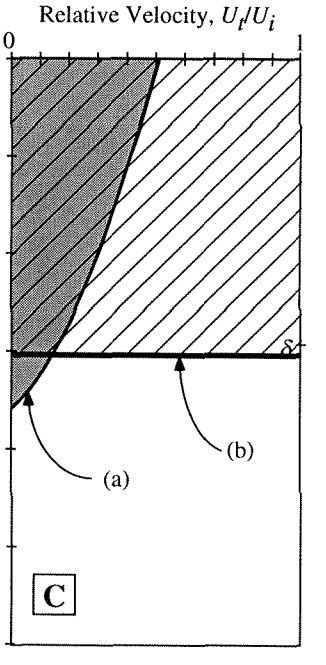
Relative Velocity, U_t/U_i
0
1
δ
(b)
(a)
C

Figure 12. Mohr diagrams showing two-dimensional effective stress states at failure in a pure horizontal extension and a pure horizontal compression under (A) drained and (B) undrained conditions. Horizontal and vertical stresses are the principal stresses. Stresses in the undrained case (B) are calculated assuming that at failure the excess pore pressure parameter, A_f, equals to one. In both examples, (A) and (B), the internal friction angle ϕ is 26.5°. Approximate orientation of slip lines is shown in the square boxes. In extension, slip lines make an angle of $45° + 0.5\phi$ with the horizontal and in compression this angle is $45° - 0.5\phi$.

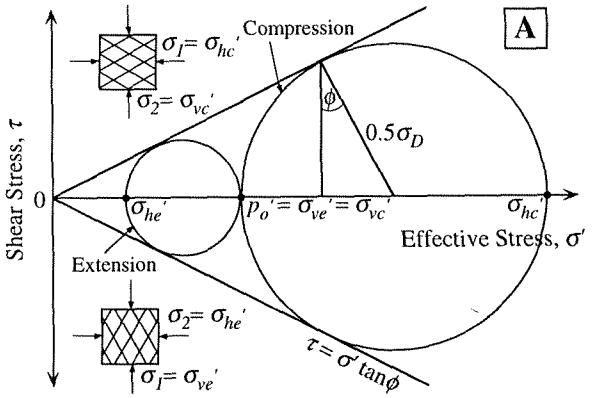
A
Compression
$\sigma_1 = \sigma_{hc}'$
$\sigma_2 = \sigma_{vc}'$
ϕ
$0.5\sigma_D$
Shear Stress, τ
0
σ_{he}'
$p_o' = \sigma_{ve}' = \sigma_{vc}'$
σ_{hc}'
Effective Stress, σ'
Extension
$\sigma_2 = \sigma_{he}'$
$\sigma_1 = \sigma_{ve}'$
$\tau = \sigma' \tan\phi$

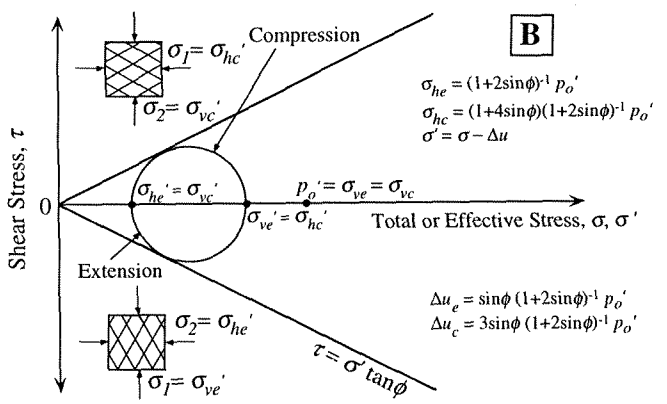
B
Compression
$\sigma_1 = \sigma_{hc}'$
$\sigma_2 = \sigma_{vc}'$
$\sigma_{he} = (1+2\sin\phi)^{-1} p_o'$
$\sigma_{hc} = (1+4\sin\phi)(1+2\sin\phi)^{-1} p_o'$
$\sigma' = \sigma - \Delta u$
Shear Stress, τ
0
$\sigma_{he}' = \sigma_{vc}'$
$p_o' = \sigma_{ve} = \sigma_{vc}$
$\sigma_{ve}' = \sigma_{hc}'$
Total or Effective Stress, σ, σ'
Extension
$\Delta u_e = \sin\phi\,(1+2\sin\phi)^{-1} p_o'$
$\Delta u_c = 3\sin\phi\,(1+2\sin\phi)^{-1} p_o'$
$\sigma_2 = \sigma_{he}'$
$\sigma_1 = \sigma_{ve}'$
$\tau = \sigma' \tan\phi$

CHAPTER 4

Basal Mechanics of Ice Stream B, West Antarctica. I. Till Mechanics.

Slawek Tulaczyk, Barclay Kamb, Hermann Engelhardt

Division of Geological and Planetary Sciences, California Institute of Technology,

Pasadena, CA 91125

Abstract

Data from laboratory geotechnical tests on the UpB till recovered from beneath Ice Stream B, West Antarctica, show that failure strength of this till is strongly dependent on effective stress but is practically independent of strain and strain rate. These data support use of Coulomb-plastic rheology in modeling of ice stream behavior and subglacial till deformation. Our geotechnical testing program combined triaxial, ring shear, and oedometer tests that were conducted to investigate till strength and compressibility. Experimental results show that the UpB till follows closely Coulomb's equation in which shear strength is a linear function of normal effective stress (apparent cohesion near zero and internal friction angle, ϕ, equal to 24°). Till compressibility is best described by a logarithmic function which relates void ratio to normal effective stress. In general, the UpB till behaves in laboratory geotechnical tests in ways consistent with the existing body of experimental evidence regarding mechanical behavior of granular materials. Based on our laboratory results we formulate the compressible-Coulomb-plastic till model in which there are three interrelated, primary state variables: shear strength, void ratio, and normal effective stress. This till model is used in the second part of our study to simulate response

of subglacial till to realistic effective stress forcings. These simulations demonstrate that the compressible-Coulomb-plastic till model is capable of reproducing fundamental features of the observed subglacial till kinematics: 1) occurrence of tilt rate oscillations and negative tilt rates in tiltmeter records, and 2) distribution of till deformation to depths of ~0.1 m beneath the ice base. Our laboratory and modeling results substantiate application of the compressible-Coulomb-plastic model in simulations of the motion of Ice Stream B over its weak till bed.

4.1. Introduction

Glaciological and geophysical studies indicate that fast motion of West Antarctic ice streams is possible because of an efficient basal lubrication provided by a layer of weak subglacial till (Figures 1 and 2) [Alley *et al.*, 1986, 1987ab; Blankenship *et al.*, 1986, 1987; Echelmeyer *et al.*, 1994; Engelhardt and Kamb, 1997, in press; Engelhardt *et al.*, 1990; Kamb, 1991; Smith, 1997]. Due to this lubrication, ice streams move roughly one hundred times faster than the rest of the ice sheet, ~100 m y^{-1} vs. ~1 m y^{-1}, and carry the majority of ice discharging from West Antarctica [Bentley, 1987; Bindschadler and Scambos, 1991; Bindschadler *et al.*, 1996; Shabtaie and Bentley, 1987; Whillans and van der Veen, 1993; Whillans *et al.*, 1987]. Construction of a well-constrained and self-consistent physical model of fast ice stream motion represents one of the most pressing tasks of modern glaciology [Alley, 1989ab; Alley *et al.*, 1989; Alley and Whillans, 1991; Clarke, 1987a; Fastook, 1987; Fowler and Johnson, 1995; MacAyeal, 1989; Marshall and Clarke, 1997; Payne and Dongelmans, 1997]. Without a model of this kind it is difficult to make reliable predictions regarding the future of the possibly unstable WAIS [Alley and Whillans, 1991; Bentley, 1997; Bindschadler, 1997, 1998; Bindschadler and Vornberger,

1998; MacAyeal, 1992]. Improved understanding of ice stream mechanics is also needed to reconstruct the behavior of Pleistocene ice masses [Alley and MacAyeal, 1994; Clark, 1992; Hughes, 1992, 1996; MacAyeal, 1993ab].

The fact that fast ice stream motion is accomplished under relatively low driving stresses prompted incorporation of some type of a basal or subglacial 'lubricant', e.g., a layer of unusually weak ice or a thick water film, into early models of ice streaming [Hughes, 1977; Weertman and Birchfield, 1982]. Subsequent seismic surveys suggested a presence of a several-meter-thick layer of weak till beneath Ice Stream B (thereafter referred to as ISB) [Blankenship *et al.*, 1986, 1987; Rooney *et al.*, 1987]. This finding led to the deforming-bed model of ice stream motion [Alley *et al.*, 1986, 1987ab]. Existence of this weak till layer beneath ISB has been consequently verified by drilling and sampling of the subglacial bed in the area of the seismic surveys (UpB area, Figure 1) [Engelhardt *et al.*, 1990; Scherer, 1991]. Acquisition of samples of this subglacial till (thereafter referred to as the UpB till) made it possible to study directly mechanical and sedimentological properties of the putative subglacial lubricant [Kamb, 1991; Tulaczyk *et al.*, 1998].

Although it is recognized that ice streams are lubricated by weak till, there are still two significantly different ways of incorporating the till into ice stream models. Initially, till was assumed to have a linear or mildly non-linear rheology similar to the rheology of ice [Alley, 1989b; Alley, *et al.* 1987b, 1989; MacAyeal, 1989]. However, results of subsequent stress- and strain-rate-controlled shear box tests on samples of the UpB till were consistent only with a highly non-linear or nearly-plastic rheology [Kamb, 1991]. This difference is significant from the point of view of ice-stream modeling because nearly-plastic till makes the ice-till system more prone to unstable behavior than linearly viscous till [Alley, 1990; Kamb, 1991]. Kamb's measurements of till strength have also shown that the UpB till is far too weak (ca. 2 kPa) to support the gravitational driving stress in its

entirety (ca. 13.5 kPa in the UpB area). A significant additional support of the driving stress appears to be provided by ice stream margins [Echelmeyer *et al.*, 1994; Jackson and Kamb, 1998; Raymond, 1996; van der Veen and Whillans, 1996; Whillans and van der Veen, 1997].

In addition to its pivotal function in ice streaming, subglacial till plays also an important role in the motion of mountain glaciers and in transport of glacial debris [Alley, 1991; Blake *et al.*, 1994; Boulton, 1979; Engelhardt *et al.*, 1978; Fischer and Clarke, 1994; Hooke and Elverhoi, 1996; Iverson *et al.*, 1994]. Intensive studies of several mountain glaciers have already yielded a wealth of data on behavior of till in subglacial environments [Boulton and Hindmarsh, 1987; Fischer and Clarke, 1997; Hooke *et al.*, 1997; Iverson *et al.*, 1995]. However, the dualism in treatment of till as a linear or highly non-linear/plastic material is present also in interpretations of these subglacial records. Clearly, further studies of till mechanics and till rheology are necessary to elucidate the exact nature of the individual processes involved in ice-till interactions. Laboratory testing of tills is in this respect an especially promising approach which supplements the difficult efforts aimed at investigating the *in situ* behavior of subglacial tills. The laboratory environment permits accurate measurement of till mechanical properties over a wide range of strains, strain rates, and stresses which can be selected to represent different subglacial conditions [Iverson and Semmens, 1995; Iverson *et al.*, 1997; Kamb, 1991].

In this manuscript we describe and discuss new results of soil mechanics tests performed on samples of the UpB till. The current work represents an extension of the earlier shear box tests on the UpB till [Kamb, 1991]. The current laboratory program entails triaxial, ring shear, and oedometer tests. Combination of these testing techniques makes it possible to investigate: 1) the influence of strain magnitude, strain rate, and effective stress on till strength, and 2) the compressibility of the UpB till. The results of

the laboratory tests are consistent with the findings of Kamb [1991] and with the general principles of soil mechanics. Motivated by these results, we formulate a Compressible-Coulomb-Plastic (CCP) till model which exhibits many features of the theoretical model of till mechanics proposed by Clarke [1987b]. Quantitative modeling shows that the CCP till responds to realistic stress forcings in ways which are consistent with the existing subglacial observations of till kinematics. Based on the results of our work we conclude that the experimentally-constrained CCP model of the UpB till can be used as an effective framework for modeling subglacial till deformation and ice stream motion. A model of ISB incorporating the principles of the CCP till mechanics is developed in a companion manuscript [Tulaczyk *et al.*, in preparation, III].

4.2. Till Sampling and Laboratory Procedures

As part of a drilling project focused on investigations of ice stream mechanics [Engelhardt and Kamb, 1997 and in press, Engelhardt *et al.*, 1990; Jackson and Kamb, 1998; Kamb, 1991], 12 till cores and a number of smaller till samples were acquired from beneath ISB in the UpB area between 1988 and 1995 (Figure 1). The spacing of till sampling sites varied from as little as several meters up to ca. 8 km (Figure 1B). The till cores were recovered using a 6-meter-long piston corer. Their lengths range between ca. 0.3 m and 3.0 m. Sedimentological analyses of the cores showed that the sampled subglacial material is granulometrically and mineralogically homogeneous [Tulaczyk *et al.*, 1998; this thesis Chapter 2]. The sedimentological properties of the core material are consistent with the conclusion that the piston corer has sampled the widespread till layer whose presence beneath ISB has been previously inferred from seismic data [Blankenship *et al.*, 1986, 1987; Rooney *et al.*, 1987, 1991].

After acquisition, the freshwater-saturated sediment cores were kept unfrozen. Upon arrival at our laboratory, they were cut into ca. 0.3-m-long sections, x-rayed, and stored at a temperature of approximately 1°C. To impede drying, the core sections are kept in the original core liner which is tightly capped and additionally sealed with a few layers of duct tape.

To reveal the mechanical behavior of the till we performed a sequence of laboratory tests guided by the standard procedures for soil testing [Bishop and Henkel, 1957; Bowles, 1992]. The main part of the mechanical testing program was based on triaxial, ring-shear and oedometer tests, as follows.

Six out of a total of seven triaxial compression tests were done under undrained conditions (U1, U2, U3, R1, R2, R3) and one under drained conditions (D1). We used undisturbed till samples in the first three tests (U1-3). The samples were 'undisturbed' in the sense that they were extracted from the core liner just before testing without any intentional remolding. However, microscopic examination of till thin sections suggests that the samples had experienced disturbance during acquisition from the sub-ice-stream environment via piston coring. The three 'undisturbed' samples were taken in 10-cm-long, 5-cm-diameter sections from the depth range of ca. 1.5-2.5 m in core 92-1 (Figure 1B). Independent measurements show that in this part of the core, till porosity is 0.369 to 0.392 (void ratio 0.585 to 0.645). Each sample was extracted from the core liner directly into rubber-membrane jacket and then placed in the triaxial apparatus. The triaxial compression tests of the type performed by us consist of three main stages [Bishop and Henkel, 1957; Bowles, 1992, p. 165-200]: 1) saturation stage, during which backpressure is applied to force dissolution of any gas bubbles in pore spaces; 2) preconsolidation stage, in which the sample is compressed under a chosen isotropic effective stress with drainage allowed; and 3) shearing stage during which the preconsolidated sample fails as it is shortened

axially by up to 25%. Pore pressure changes taking place during undrained shear were measured with a transducer attached to the base of the sample. Pore pressure, as well as axial load, axial piston displacement, and radial pressure, were digitally recorded at regular time intervals.

The next set of three triaxial tests (R1, R2, R3) was done by the same three-stage procedure but using the undisturbed samples which were thoroughly remolded and reconstituted to porosity of ca. 0.4. These tests were designed primarily to determine the influence of strain-rate on till failure strength. The axial displacement rate was varied over four orders of magnitude (axial velocity of $1.35\ 10^{-8}$ to $1.27\ 10^{-4}$ m s^{-1}).

Finally, for comparison with the six undrained tests, we performed one triaxial test for which drainage was allowed during shear (D1). The graphical and analytical methods described by Bishop and Henkel [1957, Figure 89 and the fourth equation in Table 7 with $c_v \cong 10^{-8}$ m^2 s^{-1}] enable estimation of the axial strain rate at which a triaxial sample of the UpB till should experience drained conditions (axial velocity of $2.5\ 10^{-7}$ m s^{-1}, strain rate of ca. $3\ 10^{-6}$ s^{-1}). The volume of water that had entered or exited the sample was read manually every five minutes using a burette (estimated reading error of $\pm$ 0.01 cm^3 with total drainage of a few cm^3).

In triaxial tests the total accumulated axial strain does not exceed typically 0.1 to 0.2. To verify whether the UpB till exhibits a significant strain-dependence of strength, we have constructed a small ring shear device in which the material was sheared to much greater strains. Our device is similar to the Bromhead apparatus used extensively for soil testing in the UK [Anayi *et al.*, 1989; Bromhead, 1979; Bromhead and Curtis, 1983; Stark and Eid, 1993; Stark and Vettel, 1992]. The lower plate of the device contains a sample chamber 2.9 cm wide, 1 cm deep, and with 17.4 cm centerline diameter, and is moved by a driving mechanism. In this ring shear device we can test only remolded samples. We

have used material that was previously tested in torvane measurements of till strength (cores 92-1 and 95-1). Prior to testing, all particles with diameter greater than 2 mm were removed by wet sieving. This coarse fraction constituted 7 weight% of the till solids. After the till sample is loaded into the chamber, the upper plate is placed on top, held with a square shaft so that it cannot rotate horizontally but can move up and down, and loaded with dead weight to achieve a desired normal stress. Thinning of the till sample caused by application of the normal load is monitored with displacement transducers. Once the sample stops consolidating, the driving mechanism is engaged and the lower plate with the sample is rotated at a constant rate with respect to the fixed upper plate. Shearing takes place in the till sample and the resulting torque is measured via calibrated strain gauges (arranged in a Wheatstone bridge) with a calibrated shear-stress precision of ± 0.01 kPa (over 0-100 kPa range) averaged over the horizontal cross section of the sample

An oedometer was used to investigate consolidation/swelling of UpB till samples in response to increase/decrease in normal effective stress [Bowles, 1992, p. 129-154]. The internal diameter of the cylindrical sample chamber in the oedometer is larger than the diameter of the till cores from the UpB area (6.1 cm vs. 5 cm). Therefore, only the central part of a sample consisted of 'undisturbed' material extracted from the cores without remolding. The remaining volume was filled by pressing additional till material in between the 'undisturbed' core and the chamber walls. This addition of remolded material should not influence the results substantially since a subsequent test on a completely remolded till sample did not differ significantly from the tests in which the central core of 'undisturbed' material was included. Sample thinning and thickening was monitored via a dial indicator with a precision of 0.025 mm in a total displacement range of 25.4 mm.

As a part of the laboratory analysis, we have measured the water content of the samples studied in the various geotechnical tests. The water content measurements

followed standard procedures [Bowles, 1992, p. 15-18]. Water content is recalculated into porosity and void ratio using the previously established density of till solids, ρ_s = 2,640 kg m^{-3} (Engelhardt, unpublished data), and assuming water density, ρ_w = 1,000 kg m^{-3}. We use both porosity, n_p, and void ratio, e, because the former is more familiar to geologists and glaciologists whereas the latter is more convenient and more commonly encountered in interpretations of soil mechanics tests. The two quantities are interrelated through the following equation [Scott, 1963, equation 1-13b]:

$$n_p = e/(1 + e) \qquad (1)$$

All mathematical symbols used by us are listed and explained in Table 1.

4.3. Laboratory Results

A set of laboratory tests was performed on samples of the UpB till to establish the physical controls on strength of the till and to ascertain whether its volume is sensitive to changes in effective stress. In this section, we discuss the results of these tests and compare them to the existing mechanical models of till and soil behavior [e.g., Boulton and Hindmarsh, 1987; Clarke, 1987b; Schofield and Wroth, 1968; Wood, 1992]. In our interpretation of laboratory tests we forego the use of the stress tensor in favor of a relatively simple two-dimensional stress state which consists of the shear stress, τ, and the effective normal stress, σ'_n, acting along the normal to the shear plane. This simple stress state which is very commonly used in soil mechanics relates also directly to the subglacial stress state which acts upon a till layer in nature (Figure 2). Casting the stress state in this way permits separate investigations of till response to the normal effective stress and the shear stress.

4.3.1 Strain-Strength Relationship

As observed previously by Kamb [1991] in shear box tests, a sheared sample of the ISB till experiences a transient period of strength mobilization before it reaches a more or less steady strength (Figure 3A). The triaxial tests show a similar transient in effective stress and also in pore pressure in the early stages of shearing. An example for test U2 is shown in Figure 3A. These transients are confined to relatively low shear strains (0.01 to 0.1). In triaxial tests performed on other tills failure occurs frequently at as little as 0.04 axial strain, which is equivalent to 0.055 shear strain [Bishop and Henkel, 1957, tables 2 and 8]. In our triaxial tests a relatively steady shear stress is reached at axial strain of ca. 0.04. The large-strain ring-shear tests (Figure 3BC) show that there is little change in till strength with strain; even for strains that greatly exceed the strains accumulated in triaxial tests. As expected from experience in soil mechanics [Bishop *et al.*, 1971; Skempton, 1985; Stark and Vettel, 1992, Figure 6], early in the test there is a small but perceptible peak in shear strength, which is followed by a drop-off to an 'ultimate' or 'residual' value (Figure 3B). The difference between the peak and the 'ultimate' coefficient of internal friction obtained from the ring shear test shown in Figure 3B is only 6%. The small magnitude of this drop-off is comparable to that in similar tests on other granular materials with index properties similar to that of the till (index of plasticity I_p = 15 to 16%, liquid limit LL = 34 to 35%, and plastic limit PL = 18%; see Mitchell [1993, Figure 14.51]).

The relatively constant value of failure strength observed in our tests as a function of strain is consistent with the prediction of critical-state soil mechanics stating that a continuously sheared granular medium achieves a critical state in which no further changes in shear stress and volume take place [Roscoe *et al.*, 1958; Schofield and Wroth, 1968, p. 19]. This observation encourages us to rely mainly on triaxial tests to reveal the mechanical

behavior of the UpB till. Subsequently, we will assume that the failure state achieved in the triaxial tests at relatively low strains (~0.04) provides a sufficient approximation to the critical or residual state. This allows us to take advantage of the fact that triaxial apparatus provides very reliable control of the effective stress state in soil samples undergoing shear, in contrast to shear-box or ring-shear tests which do not.

4.3.2. Influence of Strain Rate and Effective Stress on Strength

The fast motion of ISB seems to be facilitated by the very low strength of the underlying till [Kamb, 1991]. From the point of view of ice stream dynamics it is extremely important to determine whether strength of sub-ice-stream till is controlled by strain rate (viscous rheology) or effective stress (Coulomb-plastic rheology) or a combination of the two (Bingham rheology). Here, we use strain-rate variations in triaxial laboratory experiments to test the proposition that the UpB till exhibits viscous behavior. Data from triaxial tests are also used to the Coulomb-plastic model in which the strength of the UpB till should be simply determined by effective stress. This is achieved by shearing samples of the UpB till at different effective stresses.

Results of the tests (Table 2 and Figure 4) are consistent with the Coulomb-plastic model because they show that the strength of the UpB till is practically independent of strain rate and increases linearly with effective normal stress [Terzaghi *et al.*, 1996, equation 17.4]:

$$\tau_f = c_a + \sigma'_n \tan\phi = c_a + (\sigma_n - p_w) \tan\phi \qquad (2)$$

where c_a is the apparent cohesion, ϕ is the internal friction angle, σ_n is the total normal stress, $\sigma'_n = \sigma_n - p_w$ is the effective normal stress, and p_w is the pore pressure. Apparent cohesion and internal friction can be calculated from principal stresses measured in at least

two triaxial tests (Appendix 1, equation (11)). Table 2 gives the values of these parameters determined from three tests on undisturbed samples of the UpB till. The apparent cohesion is so small that we assume henceforth that it is equal to zero. This simplifies equation (2) and a number of subsequent calculations. For instance, we use this assumption to calculate shear stress and effective normal stress on the theoretical failure plane for each data reading in the six undrained triaxial tests (Figure 4A, Appendix 1, equation (13ab)). A small apparent cohesion would not change significantly these values, just as the value of ϕ is not very sensitive to the assumption of $c_a = 0$ (Table 2). The fact that the UpB till complies with the Coulomb-plastic law, equation (2), provides evidence for the frictional character of the shearing strength of this material [Terzaghi *et al.*, 1996, p. 132-136]. The evaluated internal friction angle, ϕ, is equal to ca. 24° and is consistent with the values characteristic of other granular materials having a plasticity index similar to that of the UpB till (I_p = 15 to 16%) [Kezdi, 1974, Table 28; Terzaghi *et al.*, 1996, Figure 19.7].

In Figure 4A, we plot the relationship between till strength and effective stress predicted for selected strain rates from the Bingham till model of Boulton and Hindmarsh [1987, Figure 7]. A modified version of this model has been used by Alley *et al.* [1987ab, 1989] and MacAyeal [1989] in modeling of ISB. The predictions of the Bingham till model contrast sharply with the results of our tests in which even large changes in shear strain rate, between ca. 1 y^{-1} to ca. 80,000 y^{-1}, cause no significant variation of the till shear strength away from the linear Coulomb law (Figure 4A). The range of shear strain rates applied in our tests (~1 y^{-1} to ~100 y^{-1}) was selected to cover the range of subglacial till deformation rates that would be expected if one assumes that a typical velocity of ice-stream or glacier motion, ~1 to ~100 m y^{-1}, is accommodated by a uniform shear over a till thickness of ~1 m.

Figure 4B shows that in accordance with the experience of soil and fault gouge mechanics [Berre and Bjerrum, 1973, p. 6-7; Bishop *et al.*, 1971, p. 302; Blanpied *et al.*, 1987, Figure 3; Marone *et al.*, 1990, table 2; Sheahan *et al.*, 1996, table 1; Skempton, 1985, p. 14], the strength of the UpB till increases by only a few percent per each decade of increase in strain rate (S is of the order of 0.01). Kamb [1991, equation 8] has shown that this rate of increase is equivalent to a highly non-linear, nearly-plastic rheology, $n \approx 50$ to 100 in a power flow law. Our measurements of pore pressure demonstrate that these slight till strength changes are caused by strain-rate-induced variations in pore pressure and effective stress (Figure 3A). Increasing strain rates cause increase in effective stress and strength; decreasing strain rates result in the opposite trend. The fact that this effect may account entirely for the observed changes in strength is illustrated by the strain-rate-independence of the ratio of shear strength and normal effective stress (Figure 4C). This result makes it evident that the observed small strain-rate dependence of till strength is not due to true viscous effects but rather due to the slight dependence of shear-induced pore pressure on strain rate. If till strength is interpreted in terms of the actual effective stress acting on the failure plane, the UpB till is a perfectly plastic material with failure strength determined by the frictional Coulomb relationship.

4.3.3. Compressibility

The complexity of behavior of granular materials is rooted to a great extent in their ability to change water content under different effective stress states [Wood, 1992, p. 4-5]. Significant volumetric changes may take place because the soil skeleton is much more compressible than soil water or soil particles [Mitchell, 1993, p. 170]. Soil compressibility is typically highly non-linear with the sensitivity of soil volume to changes in effective

stress decreasing with increasing magnitude of the stress [Scott, 1963, p. 168-177]. We use data from oedometer and triaxial tests to determine the volumetric behavior of the UpB till (Figure 5). Oedometer tests simulate the type of consolidation which is the most common in nature where a soil layer is typically subjected to a vertical normal stress that changes its thickness but is constrained in a horizontal direction in which the strain is equal to zero. This consolidation configuration is known in soil mechanics as the K_0-condition [Terzaghi *et al.*, 1996, p. 104]. Till samples consolidated in preparation for standard triaxial tests experiences an isotropic consolidation because the till is free to contract in all directions in response to an applied isotropic effective stress. Our results indicate that there is a slight difference in compressibility between the K_0 and isotropic consolidation (Figure 5A). An additional complication in treatment of soil compressibility arises from the fact that the latter depends on the effective stress history of a given soil sample. In this regard a soil may be in one of two states: 1) normally-consolidated or 'virgin' state in which the current effective stress is higher than any effective stresses to which the soil was subjected in the past, $\sigma'_n = \sigma'_{nmax}$, and 2) an overconsolidated state in which $\sigma'_n < \sigma'_{nmax}$).

We have determined the K_0-consolidation behavior of the UpB till for virgin and overconsolidated states as well as the virgin isotropic compressibility of this material (Figure 5A). The results of our tests are consistent with the formulation of till compressibility used in the till model of Clarke [1987b] which was based on the principles of critical-state soil mechanics [Roscoe *et al.*, 1958; Schofield and Wroth, 1968]. As proposed by Clarke [1987b, equation 35], test data show a logarithmic relationship between till void ratio and effective normal stress:

$$e = e_0 - C_\xi \log \sigma'_n \qquad (3)$$

where $e = V_w/V_s$ is the void ratio obtained by dividing the pore volume by the volume of solids, e_0 is the void ratio at the reference value of effective normal stress, chosen to be

equal to 1 kPa, C_ξ is the dimensionless coefficient of compressibility, and σ'_n is the effective normal stress expressed in kPa. The subscript ξ is replaced by c (for "consolidation) to denote the coefficient of compressibility in the virgin state and by s (for "swelling") to indicate the coefficient of compressibility in overconsolidated state. Following the convention adopted in soil mechanics and in Clarke's till model [1987b, p. 9,027], we designate a line approximating e - $\log\sigma'_n$ behavior of till in its virgin state as the Normal Consolidation Line (NCL). To differentiate between virgin consolidation under isotropic conditions, in triaxial tests, from that under the K_o-condition, in oedometer tests, we add appropriate subscripts (NCL_{iso}, NCL_{Ko}). The lines in the e - $\log\sigma'_n$ space defined by measurements on overconsolidated till samples are designated as the Unloading-Reloading Lines ($URL_{\#}$) with a number in the subscript giving the magnitude of the maximum effective normal stress to which this sample was ever subjected, σ'_{nmax} in kPa. We use the same line to approximate the expansion (swelling) of overconsolidated till on unloading and its compression on reloading. This is motivated by the fact that our data do not show a significant hysteresis during unloading and reloading (URL_{568}, URL_{71} in Figure 5A). This is an important observation because it indicates that consolidation and swelling of overconsolidated UpB till is dominated by elastic effects. That gives rise to the main difference between overconsolidated and virgin states; in the latter, most of the consolidation that occurs is non-recoverable. Consolidation is large in the virgin state because it involves permanent rearrangement of relative positions of soil particles ("plastic" volume change) in addition to an elastic compression of till skeleton: $C_c \cong 0.12$ and 0.15 vs. $C_s \cong 0.02$. These coefficients of compressibility fall within the lower part of the range of values measured on tills and other soils [Mitchell, 1993, p. 170; Sauer *et al.*, 1993].

The discussion of till compressibility was limited up to now to 'static' conditions in which till volume change is taking place while the sample is not undergoing significant

shear deformation. Observational evidence suggests that a granular material experiencing shear reaches a volume whose magnitude is controlled by the effective stress following the general form of equation (3) [Schofield and Wroth, 1968, p.19-21]. The e -logσ'_n relationship for a shearing soil is the so-called Critical State Line (CSL) [Clarke, 1987b; Wood, 1992, p. 141]. Typically, the CSL lies in the e -logσ'_n space parallel to, and slightly below the NCL [Clarke, 1987b, Figure 1; Jones, 1992, Figure 2.25; Karig and Morgan, 1992, Figure 6-13]. Results of our triaxial tests are consistent with this location of the CSL for the UpB till (Figure 5A). In the sample of the UpB till tested under drained conditions (D1), shearing has induced consolidation (Figure 5AB). In the six undrained tests, after an initial period of pore pressure drop positive excess pore pressures built up and normal effective stresses decrease as shear strains accumulate (Figure 5B). Therefore, shearing of the undrained test samples has moved their states in the e -logσ'_n space to the left of or down from their initial position on the NCL_{iso}. Because of the strain-rate effects discussed previously (section 3.3., Figure 3A), shear-induced excess pore pressures are larger when strain-rates are low and smaller when strain rates are high, e.g., 1,000 y^{-1} vs. 30,000-80,000 y^{-1} in Figure 5B). The e -σ'_n triaxial data collected at failure for the reference strain rate of ca. 1,000 y^{-1} is best fitted by a relationship of the form given by equation (3) (CSL in Figure 5A). The resulting CSL is indeed approximately parallel to the NCL_{iso} and is slightly offset from the latter to the left.

Our results suggest that the volume-change behavior of the UpB till is distinctly different from that of the Breidamerkurjokull till [Boulton and Hindmarsh, 1987, Figure 4]. These authors attributed a ca. 10% increase in porosity of Breidamerkurjokull till to the influence of shear upon initially normally consolidated till. In this situation, the CSL of the Breidamerkurjokull till should be placed far to the right or, equivalently, well above the NCL of this till (Figure 5A). Such behavior is abnormal in relation to the typical situation

in granular mechanics [e.g., Karig and Morgan, 1992]. This difference is important because previously it has been inferred that shear-induced porosity changes in the UpB till may have the same character and magnitude as the shear-induced porosity changes for the Breidamerkurjokull till [Alley *et al.*, 1986, 1987a].

4.4. Compressible-Coulomb-Plastic Till Model

Laboratory test data suggest a relatively simple mechanical model of the UpB till for which both void ratio and strength are dependent on the effective stress. This dependence is expressed by the equations (2) and (3) with numerical values of the appropriate coefficients given in Table 2 and Figure 5. In the case of till compressibility, there is a complication arising from the fact that a normally-consolidated till and overconsolidated till have different compressibility coefficients, C_c and C_s, respectively. The volume-effective-stress relation for shearing till is also somewhat different than in the normally-consolidated case. However, test results show that we can eliminate two potential state variables, strain magnitude and strain rate, which seem to have no significant influence on either till strength or compressibility. Such simplification neglects the transient strength-mobilization stage at the initial stages of shear. Thus, only three state variables are necessary to express the conditions of the UpB till: 1) void ratio, 2) effective stress, and 3) shear strength. We call the model of till mechanics obtained by combination of equations (2) and (3), the Compressible-Coulomb-Plastic (CCP) model. Its simplicity can be compared to the rigid-plastic rheological model commonly used for metals, with the additional provision for the effects of compressibility [Scott, 1963, p. 398-403; Wood, 1992, p. 2-6]. The CCP model fits into the physical framework of till mechanics proposed by Clarke [1987b] that itself was rooted in the critical-state soil mechanics [e.g., Schofield and Wroth, 1968].

Thanks to this we can take advantage of the large body of existing concepts and solutions that have been accumulated in the last several decades of soil mechanics research.

Perhaps the biggest challenge of modeling the response of Coulomb-plastic till to applied stress is posed by the fact that for plastic materials strain rates are in general not related uniquely to stresses. This represents a major departure from the viscous till model which is based on the very assumption that such a unique relationship does exist. Notwithstanding this complication, we demonstrate below that when our CCP till model is subjected to realistic subglacial stress forcings, it can reproduce essential aspects of *in situ* till kinematics observed beneath ISB and several mountain glaciers. This agreement between observed and modeled till behavior proves that the physics captured in the experimentally-constrained CCP till model may be also operating in modern subglacial zones.

4.4.1. Influence Of Till Compressibility On Tiltmeter Records

In recent years detailed tiltmeter records were collected over periods of several to a few dozens of days in tills underlying Trapridge Glacier, Yukon Territory, and Storglaciaren, Sweden [Blake, 1992; Blake *et al.*, 1992; Hooke *et al.*, 1997; Iverson *et al.*, 1995]. Tiltmeters are typically emplaced at depths of several decimeters below the ice base. They respond to strains in the surrounding till and provide an accurate record of tilt and tilt rates. One of the most persistent features of the different tiltmeter records is the presence of tilt-rate oscillations which span negative, i.e., upglacier, as well as positive, i.e., downglacier, values. These oscillations are temporally correlated with fluctuations in effective stress (Figure 6AB) [Hooke *et al.*, 1997, Figure 2; Iverson *et al.*, 1995, Figures 1 and 2]. The occurrence of negative tilt rates in subglacial tilt meter records is difficult to

explain. For instance, in the viscous or Bingham model changes from positive to negative tilt rates would require basal shear stress to reverse sometimes from its typical downglacier direction.

The close temporal correlation between fluctuations in subglacial effective stress and tilt rate oscillations suggests that the former drive the latter (Figure 6AB). Here we will show that the CCP till model provides a plausible causal link between fluctuations in normal effective stress and tilt-rate oscillations. In fact, one can neglect shear stresses altogether and the expected tilt rate oscillations will be obtained. This is because in the CCP model till rate oscillations may result solely from thickness changes experienced by a till layer when it is subjected to fluctuating normal effective stress. From equation (3) it is clear that a till layer subjected over some time Δt to a change in normal effective stress will experience a change in void ratio from an initial value $e_i = f(\sigma'_{n,i})$ to $e_{i+1} = f(\sigma'_{n,i+1})$. Geometric arguments can be used to show that these variations in till void ratio and till thickness result in a vertical strain (see Appendix 1, equation (15), for derivation):

$$\varepsilon_{n,\,i+1} = (e_i - e_{i+1})/(1 + e_i) \qquad (4).$$

where strains in compression (consolidation, $e_{i+1} < e_i$) are taken to be positive and strains in extension (swelling, $e_{i+1} > e_i$) negative. With a non-zero vertical strain and zero horizontal strain, i.e., the K_o-condition, all planes whose initial orientation does not coincide with the three principal strain directions will experience rotation. In the case of infinitesimal rotations and in the case when the principal axes of strain do not rotate, the rotation angle, $\Delta\Theta$, is equal to half the engineering shear strain, i.e., the tensor shear strain, and is given at a time t_{i+1} by (see Appendix 1, equation (16), for derivation):

$$\Delta\Theta_{i+1} = 0.5\ \gamma_{i+1} = 0.5\ \varepsilon_{n,\,i+1} \sin(2\Theta_i) \qquad (5)$$

where Θ_i is the initial angle of the plane measured from the vertical axis. A shear strain rate over a discrete time interval $\Delta t = t_{i+1} - t_i$ may be then obtained from:

$$\dot{\gamma}_{i+1} = (\gamma_{i+1} - \gamma_i)/\Delta t \qquad (6)$$

Because of the non-linearity introduced into this system of equations by the logarithmic form of (3), it is convenient to find rotations and tilt rates in response to changing effective normal stress, $\sigma'_n(t)$, by numerically integrating equations (3), (4), (5), and (6) through time. Since applicability of equation (5) is restricted to infinitesimal strains it is necessary to select time steps small enough so that for a specific forcing function, $\sigma'_n(t)$, the condition $\Delta\Theta_i <$ ca. 0.01 is fulfilled at all times [Means, 1979, p. 151].

Figures 6CD show rotation and tilt rate that would be recorded by three tiltmeters emplaced at different initial angles, Θ_o, into a layer of the UpB till which experiences virgin consolidation driven by a linear increase in normal effective stress over a period of five days (equation (3) with $C_c = 0.12$ and $e_o = 0.7$, Figure 5A). This forcing produces total rotations of several degrees and results in tilt rates that range between ca. 1 and 100 y^{-1}. These calculations demonstrate that tiltmeters may report net rotations even in a till that does not experience shear deformation caused by application of basal shear stress (τ_b in Figure 2). If influence of consolidation or swelling on tiltmeter records is neglected without verifying that this influence is indeed insignificant, the tiltmeter signal may be erroneously interpreted as being fully the result of shear deformation. This may be an especially acute problem in the cases when relatively small rotations, ca. 10°, are being used to calculate the effective viscosity of till. If the till has experienced a significant increase or decrease in the normal effective stress over the recording period, much of measured net rotation may be caused by change in till thickness. We have used in our calculations a conservative value of compressibility coefficient, $C_c = 0.12$ (Figure 5A). This number is within the lower range of C_c values measured by Sauer *et al.* [1993, Figure 20, C_c up to ca. 0.4] on different tills from Canada. Clearly, higher values of C_c would amplify the influence of effective stress changes on tiltmeter rotation.

Net tiltmeter rotations shown in Figure 7C result from virgin consolidation of the modeled CCP till. As long as till is not undergoing shear deformation, virgin consolidation is not fully reversible. However, once till is in its overconsolidated state it should react to changes in effective stress, $\sigma'_n(t) < \sigma'_{nmax}$, in a more or less elastic manner (URL's in Figure 5A). Here, we hypothesize that tiltmeters emplaced in an overconsolidated CCP till will record oscillations from negative to positive tilt rates if the till is subjected to a cyclically changing normal effective stress. To verify the plausibility of this hypothesis, we perform sample calculations for two cases which are designed to emulate: 1) response of a tiltmeter emplaced 0.1 m beneath ice base in a till of low hydraulic diffusivity ($c_v = 10^{-8}$ m^2 s^{-1}, value for the UpB till) [Tulaczyk *et al.*, in preparation II], and 2) response of a tiltmeter emplaced at 0.1 and 1.0 m beneath ice base in a high-diffusivity till ($c_v = 10^{-5}$ m^2 s^{-1}, upper limit estimated from data given by Bishop and Henkel [1957, table 10], Iverson *et al.* [1997, table 1], and Sauer *et al.* [1993, table 2]). Hydraulic diffusivity of soils depends mainly on clay mineralogy and clay abundance [Mitchell, 1993, p. 180]. The value of this coefficient for the UpB till appears to be close to the lower limit for tills, probably because of its clay-rich character [Tulaczyk *et al.*, 1998]. On the other hand, the selected upper limit is more representative for very coarse tills that do not contain a significant amount of clays. Such tills develop frequently beneath mountain glaciers where subglacial sediments come from crushing and abrasion of bedrock. Hydraulic diffusivity is a crucial parameter in modeling fluctuations in the subglacial effective stress when the latter are produced by oscillations in basal water pressure which propagate diffusively into the till layer below. Hydraulic diffusivity of till determines the rate of decay of the oscillatory signal and its time lag with depth [Tulaczyk, in press].

Following Tulaczyk [in press], we use in our modeling of effective stress changes a commonly encountered solution of the one-dimensional time-dependent diffusion equation, $c_v u_{zz} = u_t$, with a periodic boundary condition, $u(0,t) = u_o + \Delta u \cos(\omega t)$:

$$u(z,t) = u_o + \Delta u \exp(-\psi z) \cos(\omega t - \psi z) \quad (7)$$

where $u(z,t)$ is the excess pore pressure, t is the time variable, z is the vertical coordinate (Figure 2, $z = 0$ at the ice base), u_o is the time-averaged excess pore pressure at the top of the till, Δu is the amplitude of basal water pressure fluctuations, $\omega = 2\pi/T$, where T is the period of the fluctuations, and $\psi = \sqrt{[\pi / (c_v T)]}$. The above equation for time-dependent excess pore pressure can be superposed upon a time-averaged hydrostatic effective stress increase with depth to obtain:

$$\sigma'_n(z,t) = \Delta\sigma'_n z - u(z,t) \quad (8)$$

where we have assumed that the time-averaged effective stress changes linearly with depth, z, with $\Delta\sigma'_n = (\rho_t - \rho_w)g$ being the hydrostatic effective pressure gradient, wherein ρ_t is the till density, ρ_w is the water density, and g is the acceleration of gravity. The sign convention used in equations (7) and (8) assumes that pore pressures below the overburden ice pressure, σ_n (Figure 2), are negative. In addition to the hydrostatic case, we model also lithostatic conditions in which there is no time-averaged increase in effective stress with depth. To do so we simply modify equation (8) by assuming $\Delta\sigma'_n = 0$.

Figure 6E shows changes in effective stress calculated for the depth of 0.1 m in the low-diffusivity UpB till and for the depth of 0.1 and 1.0 m in the hypothetical high-diffusivity till. Both modeled systems are forced by diurnal fluctuations in basal water pressure, but we assume different values for the average basal water pressure and for the amplitude of water pressure oscillations (for the UpB till, u_o = -10 kPa, Δu = 10 kPa and for the high-diffusivity till, u_o = -100 kPa and Δu = 100 kPa). Selection of these values was guided by the observations made beneath ISB at the UpB camp [Engelhardt and

Kamb, 1997, Figures 12 and 13; Tulaczyk *et al.*, in preparation II] and by the record of effective stress from beneath Storglaciaren (Figure 6A) [Hooke *et al.*, 1997]. Our calculations show clearly that basal pore water pressure fluctuations are unable to propagate to the relatively shallow depth of 0.1 m in the low-diffusivity UpB till (Figure 7E). On the other hand, oscillations in basal water pressure have a strong influence on effective stresses at depths of 0.1 and 1.0 m in the high-diffusivity till (Figure 6E).

The time-dependent effective stresses shown in Figure 6E are used as forcing functions for the system of equations (3), (4), (5), and (6). Numerical time-integration of this system yields the simulated tilt rate records illustrated in Figure 6F. The tiltmeter emplaced at 0.1 m in the low-diffusivity UpB till remains practically motionless. However, large effective stress fluctuations in the high-diffusivity till produce significant oscillations in tilt rate. Since we assume in our model that thickness changes of overconsolidated till are elastic, i.e., reversible, no net rotation results from the cyclic effective stress forcing (Figure 6F). In terms of their periodicity and amplitude, the synthetic tiltmeter records are similar to the observed tiltmeter record from beneath Storglaciaren (Figure 6B) [Hooke *et al.*, 1997]. In our calculations we use a value of compressibility coefficient, $C_s = 0.02$, which is consistent with our tests on the UpB till in an overcondolidated state (Figure 5A). This is a relatively low value compared to these measured by Sauer *et al.* [1993] on a number of tills from Canada.

As illustrated in Figures 6GH, combination of a linear increase in subglacial effective stress through time with diurnal oscillations of effective stress may result in a quite complex simulated tiltmeter response. As before, the low hydraulic diffusivity of the UpB till does not permit any significant propagation of basal water pressure fluctuations to 0.1 m depth in till. Thus, the simulated tiltmeter rotates only slightly in response to the forced linear increase in subglacial effective stress (thick dashed line in Figure 6GH). In

the case of a tiltmeter emplaced at 0.1 m depth in the high-diffusivity till, the tilt rate shows a complicated behavior. This variability is due to the fact that the forcing function, $\sigma'_n(t)$ (thick solid line in Figure 6G), requires the till to consolidate as a virgin material (along the NCL) during a part of the cycle and to swell or consolidate as an overconsolidated material (along the URL) at remaining times. The simulated tiltmeter experiences net rotation caused by virgin consolidation and shows an oscillatory behavior which reflects the elastic till thickness changes in an overconsolidated state.

Our modeling demonstrates that till compressibility may have a significant effect on tiltmeters emplaced in subglacial till. Even without their response to basal shear stress, τ_b, tiltmeters may experience significant rotations and oscillations caused solely by till thickness changes triggered by variations in subglacial effective stress. Our experimentally-constrained CCP model of till mechanics is clearly capable of reproducing an important feature of *in situ* kinematics of subglacial tills. This provides support for the CCP model. Our calculations suggest also that in the case of the low-diffusivity UpB till, we should not expect the oscillatory tilt record that has been observed beneath mountain glaciers. This proposition may be tested in the future by instrumenting the bed of ISB with tiltmeters.

4.4.2. Vertical Distribution of Strain

In the previous section we have consciously limited ourselves to modeling the response of the CCP till to changes in effective normal stress only. In nature, however, there is typically a non-zero shear stress transmitted from the ice base to the top of the till (τ_b in Figure 2). In the classical theory of glacier mechanics, it is generally assumed that over a horizontal length scale of several ice thicknesses, basal shear stress balances the so-

called gravitational driving stress, i.e., the downglacier component of gravity acting on a given ice mass, τ_d [Patterson, 1994, p. 240]. However, the glacier bed may be composed partially or fully of weak till, i.e., a till whose strength is less than the driving stress, $\tau_f < \tau_d$. Under such conditions part of the support for the driving stress is shifted from the weak areas of the bed towards either localized basal sticky spots or the margins of a glacier or an ice stream [Echelmeyer *et al.*, 1994; Iverson *et al.*, 1995; Kamb, 1991; MacAyeal *et al.*, 1995; Raymond, 1996; Whillans and van der Veen, 1997].

The effective-stress dependence of till strength, equation (2), introduces an important complication into ice-till interactions because any vertical variations in effective stress state will cause changes in till strength distribution with depth. It is a mechanical requirement that the coupled ice-till motion should be accommodated by the weakest shear plane within a till layer. Therefore, vertical variations in till strength distribution may force a vertical migration of this weakest, active shear plane [Tulaczyk, in press]. The strength of this active shear plane determines the magnitude of basal resistance to ice motion. Over time, the net effect of vertical shear zone migration will be to distribute shear deformation over some thickness of the till layer. Distributed till deformation was expected to be characteristic only for tills of viscous rheology [Alley, 1993, p. 205]. However, shear-zone migration may produce a pseudo-viscous strain distribution in a Coulomb-plastic till [Tulaczyk, in press, Figure 11].

Using the concept of shear zone migration, we simulate the response of the CCP till to a forcing which combines oscillatory normal effective stress and basal shear stress such that $\tau_b = \tau_{fmin} < \tau_d$ at all times. We assume that, in a simulated one-dimensional column of till, ice motion is accommodated on a single shear plane which is located at the depth $z = Z_{sh}$ where the strength of the till is the least. Horizontal stress and strain gradients are assumed to be equal to zero in this till-column model. Till is treated as a homogeneous

continuum. This is a reasonable assumption for matrix-dominated tills like the UpB till in which clasts make up only a few percent of total volume [Tulaczyk *et al.*, 1998]. When the till is not overconsolidated, its strength is calculated from the Coulomb equation neglecting cohesion and using $\tan\phi = 0.44$ (Table 2; Figure 4). Overconsolidation has an important influence on shear zone migration and we explain in the next paragraph a new approach for its realistic treatment. An additional complication arises from the fact that the strength of the ice-till interface may be governed by different physics than the strength of intra-till shear zones. Theoretical analysis of ice-till interactions suggests that this is a distinct possibility in the case of the fine-grained UpB till which should favor ice base sliding over intra-till shear [Tulaczyk, in press]. Because at present there are not enough observational or theoretical constraints to reliably simulate physical processes at the ice-till interface, we neglect this complication and assume that the ice-till interface has its strength determined by the same physics as any other potential shear zone within the till.

Proper inclusion of the effect of overconsolidation on till strength is important because overconsolidation may localize strain and, thus, counteract the effects of variable effective stress which drives shear zone migration. An overconsolidated soil may exhibit a transient peak strength higher than the failure strength which would result from the current normal effective stress, $\sigma'_n < \sigma'_{nmax}$ [Scott, 1963, p. 364; Sheahan *et al.*, 1996]. Effectively, such soil retains a 'memory' of the peak effective stress, σ'_{nmax}, in a form of tighter particle packing than the one which would be produced by the current effective stress. Tighter soil structure requires higher shear stress to induce failure. Once this shear stress threshold is overcome, the sheared part of the overconsolidated soil increases its water content and decreases its strength to values consistent with the current σ'_n [Wood, 1992, p. 192-195]. This strain-weakening of overconsolidated till triggers strain localization.

In order to implement a realistic treatment of overconsolidation we use the Hvorslev failure criterion for overconsolidated soils [Wood, 1992, equation 7.40]:

$$\tau_{fov} = c_{ne}\,\sigma'_{ne} + \sigma'_{n}\tan\phi_{e} \qquad (9)$$

where τ_{fov} is the peak strength of overconsolidated soil, σ'_{ne} is the equivalent consolidation stress, c_{ne} is the effective cohesion, and ϕ_e is the effective internal friction angle. The two latter are frequently referred to as the Hvorslev strength parameters that are analogous to the Coulomb parameters in equation (2). The equivalent consolidation stress is obtained by horizontally projecting the void ratio of an overconsolidated soil sample, e_{ov}, onto the NCL and reading off the corresponding effective stress:

$$\sigma'_{ne} = 10^{(e_o - e_{ov})/C_c} \qquad (10)$$

where e_o and C_c are the parameters of the NCL (Figure 5A). Experiments indicate that light overconsolidation of soils does not produce a significant increase in soil strength [Wood, 1992, Figures 7.21 and 7.22]. We apply the regular Coulomb failure criterion, equation (2), when till is normally consolidated or lightly overconsolidated. The Hvorslev failure criterion, equation (9), is applied only for heavily overconsolidated till with overconsolidation ratio, OVR = $(\sigma'_{nmax}/\sigma'_{n}) > 2$ (Wood, 1993, p. 198-203). We use the Hvorslev strength parameters based on the original Hvorslev's measurements on Vienna clay, $c_{ne} = 0.1$ and $\tan\phi_e = 0.315$ [Wood, 1993, table 7.1], which fall within the midrange of values for the Hvorslev parameters derived for several other soils [Kezdi, 1979, table 8.2; Wood, 1993, table 7.1].

Effective stress functions are obtained as before by forcing the simulated column of till with diurnal fluctuations in basal water pressure (section 4.1., equations (7) and (8)). Because of the very low hydraulic diffusivity of the UpB till, the assumed basal water pressure fluctuations, u_o = 11 kPa and Δu = 10 kPa, affect only very shallow depths in this till, less than ca. 0.06 m (Figure 7A). In the lithostatic case, these oscillations alone

determine the distribution of σ'_n with depth whereas in the hydrostatic case we superpose them on a linear increase in effective stress with depth ($\Delta\sigma'_n$ = 10 kPa m^{-1}, equation (8), Figure 7A). Till strength timelines for a 24-hr cycle are given for the lithostatic and the hydrostatic case in Figures 7B and 7C, respectively. The influence of overconsolidation on till strength is manifested by the slight asymmetry of the 'tornado diagrams.' This occurs only at low effective stresses for which the threshold criterion, OVR = (σ'_{nmax}/σ'_n) > 2, is fulfilled and till is treated as a Hvorslev rather than a Coulomb material. This pattern of overconsolidation is, however, additionally complicated by our assumption that once motion on a given shear plane starts, the influence of overconsolidation is instanteneously erased and the material behaves as a Coulomb-plastic again. This is most apparent at the top of the simulated till, where till strength is always determined by the simple Coulomb relationship because shear concentrates along the ice-till interface for much of the water-pressure cycle (Figure 7D).

The complexity of conditions included in our modeled till system has prevented us from finding an explicit, analytical solution which would give us the position of the shear zone accommodating ice motion as a function of time. Instead, we have discretized the problem in space and time (Δt = 0.5 hr, Δz = 0.01 m), and manually traced the shear zone migration. The final and most important result of this procedure is presented in Figure 7D which shows the cumulative distribution of deformation in till after one diurnal cycle of effective stress changes. This viscous-like strain distribution results solely from a migration of a single shear zone whose position has been calculated by assuming plastic rheology of till with effective-stress dependence of till strength.

Our modeling of shear-zone migration suggests that fluctuations in basal water pressure may cause distributed deformation beneath ISB. However, due to the very low hydraulic diffusivity of the UpB till, distribution of deformation by this mechanism will be

limited to depths of less than 0.1 m beneath the ice base. Since dimensions of tiltmeters used in subglacial studies are typically ca. 0.1 m, it will be very difficult to verify this result with tiltmeter measurements. However, the result prompts the testable hypothesis that the UpB till is not experiencing a distributed shear deformation below the depths of several centimeters.

In Figure 8 we illustrate the fact that given a higher hydraulic diffusivity, shear zone migration may distribute till deformation over till thickness of up to one meter. This exceeds the depthscale of the thickest documented subglacial shear zone, 0.6 m [Boulton and Hindmarsh, 1987, Figure 2]. In addition, Figure 8 demonstrates the capability of the CCP till model to produce significant till sliding. This sliding occurs when the weakest shear plane develops at the base of the till. In our example, the till is assumed to terminate at depth of one meter where it is underlain by some hypothetical stronger geologic material. At present there is only one direct measurement of till sliding beneath Breidamerkurjokull, where local measurements of strain distribution suggest that ca. 10% of the ice motion was accommodated in this fashion over a period of several days [Boulton and Hindmarsh, 1987]. However, several authors considered the possibility that till sliding over bedrock represents an important means of glacial abrasion [Cuffey and Alley, 1996; Hindmarsh, 1996].

4.4.3. Sliding and Ploughing

Quantitative models of till behavior assume typically that at the scale of subglacial shear zones, ~0.1 or ~1 m, till is a perfect continuum [Alley, 1989b; Alley *et al.*, 1987ab; Boulton, 1996; Boulton and Hindmarsh, 1987; Tulaczyk, in press; this manuscript]. While this approach produces valuable insights into subglacial till behavior, the highly

inhomogeneous nature of many real tills may play a very important role in determining till response to subglacial stresses. For example, a majority of the tills whose *in situ* kinematics has been studied in the recent past contains a high fraction of clasts that are only few times smaller than the till thickness of ~0.1 m [Boulton and Hindmarsh, 1987, Figure 3; Clarke, 1987b, Figure 4; Hooke and Iverson, 1995, Figure 2]. Interactions amongst such clasts and between these clasts and till matrix may exert a dominant control over subglacial strain distribution and the strength of ice-till coupling [Tulaczyk, in press]. In addition, the ice sole itself may contain roughness elements, e.g., protruding clasts or ice protuberances, whose amplitude represents a significant fraction of till thickness. If till is deformable, such roughness elements will plough through the underlying till and will produce their own inhomogeneous strain field [Tulaczyk, in press, Figures 2 and 9].

Here, we show qualitatively that interaction of basal roughness elements with the UpB till provides a plausible explanation for the significant fluctuations of sliding velocity measured with a tethered stake emplaced beneath ISB (Figure 9A) [Engelhardt and Kamb, in press]. The motion of this ice stream may thus be accommodated by a combination of basal sliding with ploughing of the underlying plastic till. This motion mechanism has been previously proposed and discussed in detail by Brown *et al.* [1987].

During an observation period lasting ca. 26 days, the sliding velocity measured beneath ISB experienced several significant fluctuations (Figure 9A). Engelhardt and Kamb [in press] infer that at least during the initial stages of the measurement, the tethered stake was located within centimeters of the ice base. They also propose that the biggest and longest lasting dip in the measured sliding velocity occurred because the tethered stake was dragged by a clast or an ice bump protruding down from the ice base. Here we hypothesize that the other, smaller and shorter lasting velocity slow-downs may have occurred when the tethered stake found itself in a deformation zone surrounding ploughing

basal protuberances (Figure 9BC). In the zone around such protuberances, till is dragged in the direction of ice motion and a tethered stake imbedded in the till will record this as a slow-down. The recorded fluctuations in sliding velocity last typically one or two days and repeat at similar time intervals. Given an ice base velocity of ca. 1 m day^{-1}, the roughness elements generating the sliding fluctuations should have a wavelength of a few meters. According to our conceptual model (Figure 9BC), the magnitude of the apparent slow-downs is controlled by the relative amplitude of basal protuberances with respect to the depth at which the tethered stake is emplaced. If we accept the inference that this depth was only several centimeters [Engelhardt and Kamb, in press], the amplitude of most of the basal protrusions should have been smaller than this dimension because they have caused only moderate apparent slow-downs of ca. 20% of the total velocity. Each slow-down in sliding velocity is matched by a speed-up in distributed till deformation, the vertical integral of which equals the slow-down in sliding (Figure 9B).

Ice sliding over the UpB till accompanied by ploughing of the till by an undulating ice base provides a fitting qualitative explanation for the record of variable ice stream velocity relative to a tethered stake emplaced beneath ISB [Engelhardt and Kamb, in press]. Because the tethered stake may have been within only several centimeters of the ice base, one could alternatively explain the velocity fluctuations using vertical shear zone migration forced by fluctuations in basal water pressure (e.g., Figure 7). However, this explanation is not supported by the basal water pressure record obtained concurrently with the tethered stake measurement, because the two records are weakly correlated in time [Engelhardt and Kamb, in press, Figure 4].

4.5. Conclusions

As an extension of earlier work which involved shear box tests on the UpB till [Kamb, 1991], we have used triaxial and ring shear tests to study the dependence of the UpB till strength on: strain, strain rate, and effective stress. These tests demonstrate that after a transient stage of initial strength mobilization occurring at very low strains (~0.01) the strength of the UpB till changes only by several percent as further strain is accumulated. The failure strength of the UpB till reached at low strains is thus approximately equal to the steady-state (critical-state, residual, or ultimate) strength which is achieved at high strains. This shows that results of small and medium-strain tests, e.g., triaxial or shear box tests (maximum strains of ~0.1 and ~1), can be used as reliable approximations of high-strain behavior of the UpB till. Ring shear and triaxial tests in which we have varied shear strain rate by several orders of magnitude demonstrate an extremely low dependence of till strength on strain rate. In addition, the triaxial data reveal that the observed few-percent increase in till shear strength per decade of increase in strain rate is caused by strain-rate-induced variations in pore pressure. In general, the new laboratory test results corroborate the Coulomb-plastic rheology of the UpB till: the strength of this till is practically strain-rate-independent and is related to effective stress through the linear Coulomb relationship. Our test results show also that till void ratio depends sensitively on effective stress. In terms of its mechanical behavior, the UpB till is very similar to other soils whose strength is determined predominantly by the magnitude of frictional interparticle forces. Based on presented results we conclude that there are no inconsistencies between the existing body of observations constraining subglacial till behavior and the outcomes of our laboratory tests on the UpB till. The mechanical similarity of the UpB till to other soils encourages use of

concepts from soil mechanics in building qualitative understanding and quantitative models of subglacial till behavior.

Motivated by the results of our laboratory tests on the UpB till we formulate a Compressible-Coulomb-Plastic (CCP) till model which incorporates linear dependence of till strength on effective stress and logarithmic dependence of void ratio on effective stress but assumes no dependence of strength on strain rate or strain magnitude. By applying realistic stress forcings to a simulated column of the CCP till we are able to reproduce two fundamental aspects of the existing subglacial tiltmeter and strain marker records: 1) oscillations of tilt rates between negative and positive values, and 2) net rotation of tiltmeters and viscous-like vertical distribution of aggregate deformation in till. In the framework of the CCP model the oscillatory behavior of tiltmeters represents a byproduct of vertical thinning and thickening of overconsolidated till in response to a cyclic effective-stress forcing. In addition, consolidation of virgin till may produce net rotations of several degrees. These results indicate that till compressibility cannot be neglected in interpretations of subglacial tiltmeter records. Viscous-like vertical distribution of aggregate strain in till is produced in a column of the CCP till when the till is subjected to an oscillatory effective-stress forcing combined with a basal shear stress that equals the minimum strength of the till at all times. The only existing record of till behavior beneath ISB shows several significant slow-downs in the velocity of ice measured with respect to a tethered stake which was emplaced just beneath the ice base [Engelhardt and Kamb, in press]. The slow-downs can be reconciled with the plastic nature of the UpB till provided that the ice sole contains roughness elements which ploughed the top of the till and dragged the tethered stake along with the till. The foregoing examples of application of the CCP model to the interpretation of observations of till behavior illustrates the usefulness of the model in predicting the response of subglacial till to stress forcings. We hypothesize that

other tills can also be treated within the framework of the CCP model. This hypothesis is based on the fact that the UpB till is mechanically similar to other soils. Our hypothesis may be verified by future laboratory and field investigations of additional tills. Pending such verification, we propose the Compressible-Coulomb-Plastic model of the UpB till as the framework for understanding and modeling soft-bedded ice stream motion and ice-till interactions.

4.6. Appendix 1 - Derivations of Equations

In this appendix, we explain derivations of several important equations which are used in the manuscript and are not widely used in glaciological literature. The first part of this appendix relates to our evaluation of the effective normal stress, shear stress, and shear strain from the principal stresses and strains measured in the triaxial tests (equations (11) through (14)). In the second part, we devise a method for calculating tilt rates from changes in till thickness (equations (15) and (16)).

One can show from the Mohr-circle construction that apparent cohesion, c_a, and internal friction angle, ϕ, are related to the major and minor principal effective stresses at failure, σ'_{1f} and σ'_{3f} [Scott, 1963, equation 8-10b]:

$$(\sigma'_{1f} - \sigma'_{3f})/2 = c_a \cos\phi + [(\sigma'_{1f} + \sigma'_{3f})/2] \sin\phi \qquad (11)$$

Since this equation has two unknowns, at least two triaxial test results are needed to calculate c_a and ϕ. For materials with negligible apparent cohesion, equation (11) simplifies to a form that has only one unknown, ϕ, and requires only a single pair of σ'_{1f}, and σ'_{3f} to solve for it. To calculate the effective normal stress on any plane with its normal at Θ degrees to the direction of the major effective stress, we can use [Means, 1979, equation 9.4]:

$$\sigma'_n = 0.5(\sigma'_{1f} + \sigma'_{3f}) + 0.5(\sigma'_{1f} - \sigma'_{3f}) \cos(2\Theta) \qquad (12).$$

Failure planes in a Coulomb material with an angle of internal friction ϕ have orientation $\Theta = 45° + 0.5\phi$ and $-45° - 05\phi$, sign convention as in Means [1979, Figure 9.5]. Making use of equation (11), the expression for normal effective stress acting on failure planes in a cohesionless soil may be expressed purely in terms of principal stresses:

$$\sigma'_n = \sigma'_{3f}(1 + \sin\phi) = 2\,\sigma'_{1f}\,\sigma'_{3f}/(\sigma'_{1f} + \sigma'_{3f}) \qquad (13a)$$

Moreover, equations (2), (11), and (13a) can be combined to show that the shear stress on failure planes is related to principal stresses through:

$$\tau_f = \sqrt{(\sigma'_{1f}\,\sigma'_{3f})}\,(\sigma'_{1f} - \sigma'_{3f})\,(\sigma'_{1f} + \sigma'_{3f})^{-1} \qquad (13b)$$

The Mohr circle construction for infinitesimal strains shows that engineering shear strain accumulated on failure planes over some time interval Δt can be calculated from the major and minor principal strains, ε_1 and ε_3 [Means, 1979, Figure 16-3]:

$$\gamma = (\varepsilon_1 - \varepsilon_3)\sin(2\Theta) = (\varepsilon_1 - \varepsilon_3)\sin(0.5\pi + \phi) = (\varepsilon_1 - \varepsilon_3)\cos\phi \qquad (14a).$$

In the configuration of a triaxial test one can assume that the axial strain, $\Delta L/L_i = \varepsilon_1$, is the major principal strain and the radial strain, $\Delta R/R_i = \varepsilon_3$ is the minor principal strain. The symbols ΔL, ΔR, L_i, R_i represent, respectively, the changes in sample length and radius and the initial sample length and radius before the time Δt elapsed. Data from a standard triaxial test evaluate directly only the axial strain, ε_1 [Bishop and Henkel, 1957, p. 28]. The minor, radial strain can be related to the axial strain through the conservation of volume, $V_{i+1} = V_i + \Delta V$:

$$\varepsilon_3 = 1 - \sqrt{\{[(1 - \varepsilon_1)^{-1}]\,[1 + \Delta V\,(\pi\,R_i^2\,L_i)^{-1}]\}} \qquad (14b)$$

where ΔV is measured in drained triaxial tests and it is equal to zero in undrained tests. Substitution of equation (14b) into (14a) yields the expression that permits calculation of engineering shear strain on failure planes from triaxial test data, e.g., Figure 3A.

In order to derive an equation which gives vertical strain in a till layer with time-variable void ratio, i.e., equation (4), we assume the K_o-consolidation and swelling of a till layer. This assumption of no horizontal strain yields the following identity:

$$\varepsilon_{n,\,i+1} = \Delta Z/Z_i = (V_i - V_{i+1})/V_i \qquad (15)$$

where $\varepsilon_{n,i+1}$ is the vertical strain at time t_{i+1}, ΔZ is the till thickness change over the time step Δt, Z_i is the till thickness at $t_i = t_{i+1} - \Delta t$, and V_i, V_{i+1} are till volumes at the corresponding times, t_i and t_{i+1}. The expression for $\Delta Z = V_i - V_{i+1}$ was selected to obtain positive vertical strains when till experiences consolidation, i.e., its thickness and volume decrease from t_i to t_{i+1}. It can now be observed that for a saturated till with negligible compressibility of water and solid particles, the total volumes, $V_i = V_s + V_{w,i}$ and $V_{i+1} = V_s + V_{w,i}$, are a summation of a non-variable volume of till solids, $V_{s,i} = V_{s,i+1} = V_s$, with the variable volumes of pore water, $V_{w,i}$ and $V_{w,i+1}$. Using the definition of void ratio, $e = V_w/V_s$, we can substitute $V_i = (1 + e_i)V_s$ and $V_{i+1} = (1 + e_{i+1})V_s$ into equation (15) to obtain the desired equation (4). Furthermore, from Mohr circle one can note that when the minor principal strain is equal to zero, the following expression gives the infinitesmal engineering shear strain for a line inclined at Θ degrees to the major principal direction, i.e., the vertical direction in our problem [Means, 1979, equation 16.3]:

$$\gamma = \varepsilon_1 \sin(2\Theta) \qquad (16).$$

Geometrically, the engineering shear strain is the change in angle between two initially perpendicular lines, e.g., at Θ and $90° + \Theta$. For calculations of tilt magnitudes and tilt rates, equations (5) and (6), we want to have an expression for $\Delta\Theta$, i.e., the change in angle between the vertical direction and the line inclined initially at Θ.

4.7. Acknowledgments

This project was funded by grant OPP-9219279 from the National Science Foundation to B. Kamb and H. Engelhardt. Dr. Ronald F. Scott of the Division of Engineering and Applied Science at the California Institute of Technology has generously contributed equipment and expertise at many stages of this project. His help was especially vital during the design and construction of the ring shear device. We are thankful to Dr. Less Fruth and the management of Earth Technology Inc., Irvine, California, for making available their triaxial testing laboratory.

4.8. References

Alley, R.B., Water-pressure coupling of sliding and bed deformation. 1. Water system, *J. Glaciol.*, 35, 108-118, 1989a.

Alley, R.B., Water-pressure coupling of sliding and bed deformation. 2. Velocity-depth profiles, *J. Glaciol.*, 35, 119-129, 1989b.

Alley, R.B., Multiple steady states in ice-water-till systems, *Ann. Glaciol.*, 14, 1-5, 1990.

Alley, R.B., Deforming-bed origin for southern Laurentide till sheets, *J. Glaciol.*, 37, 67-76, 1991.

Alley, R.B., How can low-pressure channels and deforming tills coexist subglacially, *J. Glaciol.*, 38, 200-207, 1993.

Alley, R.B., D.D. Blankenship, C.R. Bentley, and S.T. Rooney, Deformation of till beneath Ice Stream B, West Antarctica, *Nature*, 322, 57-59, 1986.

Alley, R.B., D.D. Blankenship, S.T. Rooney, and C.R. Bentley, Till beneath Ice Stream B. 3. Till deformation - evidence and implications, *J. Geophys. Res.*, 92, 8,921-8,929, 1987a.

Alley, R.B., D.D. Blankenship, S.T. Rooney, and C.R. Bentley, Till beneath Ice Stream B. 4. A coupled ice-till flow model, *J. Geophys. Res.*, 92, 8,931-8,940, 1987b.

Alley, R.B., D.D. Blankenship, S.T. Rooney, and C.R. Bentley, Water-pressure coupling of sliding and bed deformation. 3. Application to Ice Stream B, Antarctica, *J. Glaciol.*, 35, 130-139, 1989.

Alley, R.B., and I.M. Whillans, Changes in the West Antarctic Ice Sheet, *Science*, 254, 959-963, 1991.

Alley, R.B., and D.R. MacAyeal, Ice-rafted debris associated with binge-purge oscillations of the Laurentide Ice Sheet, *Paleoceanography*, 9, 503-511, 1994.

Anayi, J.T., J.R. Boyce, C.D.F. Rogers, Modified Bromhead ring shear apparatus, *Geotech. Testing J.*, 12, 171-173, 1989.

Bentley, C.R., Antarctic ice streams - a review, *J. Geophys. Res.*, 92, 8,843-8,858, 1987.

Bentley, C.R., Rapid sea-level rise soon from West Antarctic Ice Sheet collapse, *Science*, 275, 1,077-1,078, 1997.

Berre, T., and L. Bjerrum, Shear strength of normally consolidated clays, *Proca. 8th Int. Conf. on Soil Mech. and Found. Engng.*, 1, 39-49, 1973.

Bindschadler, R., Monitoring ice sheet behavior from space, *Rev. Geophys.*, 36, 79-104, 1998.

Bindschadler, R., West Antarctic Ice Sheet collapse, *Science*, 276, 242-246, 1997.

Bindschadler, R., and T.A. Scambos, Satellite-image-derived velocity field of an Antarctic ice stream, *Science*, 252, 242-246, 1991.

Bindschadler, R., P. Vornberger, D.D. Blankenship, T. Scambos, and R. Jacobel, Surface velocity and mass-balance of Ice Stream D and Ice Stream E, West Antarctica, *J. Glaciol.*, 42, 461-475, 1996.

Bindschadler, R., and P. Vornberger, Changes in the West Antarctic Ice Sheet since 1963 from declassified satellite photography, *Science*, 279, 689-692, 1998.

Bishop, W., and D.J. Henkel, *The measurement of soil properties in the triaxial test*, E. Arnold, London, 1957.

Bishop, W., G.E. Green, V.K. Garga, A. Andresen, and J.D. Brown, A new ring shear apparatus and its application to the measurement of residual strength, *Geotechnique*, 12, 273-328, 1971.

Blake, E.W., *The deforming bed beneath a surge-type glacier: measurement of mechanical and electrical properties*, Ph.D. Thesis, The University of British Columbia, Vancouver, Canada, 1992.

Blake, E.W., Tools for examining subglacial bed deformation, *J. Glaciol.*, 38, 388-396, 1992.

Blake, E.W., U.H. Fischer, and G.K.C. Clarke, Direct measurement of sliding at the glacier bed, *J. Glaciol.*, 40, 595-599, 1994.

Blankenship, D.D., C.R. Bentley, S.T. Rooney, and R.B. Alley, Seismic measurements reveal a saturated porous layer beneath an active Antarctic ice stream, *Nature*, 322, 54-57, 1986.

Blankenship, D.D., C.R. Bentley, S.T. Rooney, and R.B., Alley, Till beneath Ice Stream B. 1. Properties derived from seismic travel times, *J. Geophys. Res.*, 92, 8,903-8,911, 1987.

Blanpied, M.L., T.E. Tullis, and J.D. Weeks, Frictional behavior of granite at low and high sliding velocity, *Geophys. Res. Lett.*, 14, 554-557, 1987.

Boulton, G.S., Processes of glacier erosion on different substrata, *J. Glaciol.*, 23, 15-37, 1979.

Boulton, G.S., Theory of glacial erosion, transport, and deposition as a consequence of subglacial sediment deformation, *J. Glaciol.*, 42, 43-62, 1996.

Boulton, G.S., and R.C.A. Hindmarsh, Sediment deformation beneath glaciers - rheology and geophysical consequences, *J. Geophys. Res.*, 92, 9,059-9,082, 1987.

Bowles, J.E., *Engineering properties of soils and their measurement*, McGraw-Hill, New York, 1992.

Bromhead, E.N., A simple ring shear apparatus, *Ground Engng.*, 12, 40-44, 1979.

Bromhead, E.N., and R.D. Curtis, A comparison of alternative methods of measuring the residual strength of London Clay, *Ground Engng.*, 16, 39-41, 1983.

Brown, N.E., B. Hallet, and D.B. Booth, Rapid soft bed sliding of the Puget glacial lobe, *J. Geophys. Res.*, 92, 8,985-8,997, 1987.

Clark, P.U., Surface form of the southern Laurentide Ice Sheet and its implications to ice sheet dynamics, *Geol. Soca. Am. Bull.*, 104, 595-605, 1992.

Clarke, G.K.C., Fast glacier flow - ice streams, surging, and tidewater glaciers, *J. Geophys. Res.*, 92, 8,835-8,841, 1987a.

Clarke, G.K.C., Subglacial till: a physical framework for its properties and processes, *J. Geophys. Res.*, 92, 9,023-9,037, 1987b.

Cuffey, K., and R.B. Alley, Is erosion by deforming subglacial sediments significant? (toward till continuity), *Ann. Glaciol.*, 22, 17-24, 1996.

Echelmeyer, K.A., W.D. Harrison, C. Larsen, and J.E. Mitchell, The role of the margins in the dynamics of an active ice stream, *J. Glaciol.*, 40, 527-538, 1994.

Engelhardt, H., W.D. Harrison, and B. Kamb, Basal sliding and conditions at the glacier bed as revealed by borehole photography, *J. Glaciol.*, 20, 469-508, 1978.

Engelhardt, H., N. Humphrey, B. Kamb, and M. Fahnestock, Physical conditions at the base of a fast moving Antarctic ice stream, *Science*, 248, 57-59, 1990.

Engelhardt, H., and B. Kamb, Basal hydraulic system of a West Antarctic ice stream - constrains from borehole observations, *J. Glaciol.*, 43, 207-230, 1997.

Engelhardt, H., and B. Kamb, Sliding velocity of Ice Stream B, *J. Glaciol.*, in press.

Fastook, J.L., Use of a new finite-element continuity model to study the transient behavior of Ice Stream C and causes of its present low velocity, *J. Geophys. Res.*, 92, 8,941-8,949, 1987.

Fischer, U.H., and G.K.C. Clarke, Plowing of subglacial sediment, *J. Glaciol.*, 40, 97-106, 1994.

Fischer, U.H., and G.K.C. Clarke, Clast collision frequency as an indicator of glacier sliding rate, *J. Glaciol.*, 43, 460-466, 1997.

Fowler, A.C., and C. Johnson, Hydraulic run-away - a mechanism for thermally-regulated surges of ice sheets, *J. Glaciol.*, 41, 554-561, 1995.

Hindmarsh, R.C.A., Sliding of till over bedrock: scratching, polishing, comminution, and kinematic-wave theory, *Ann. Glaciol.*, 22, p. 41-48, 1996.

Hooke, R.L., and A. Elverhoi, Sediment flux from a fjord during glacial periods, Isfjorden, Spitsbergen, *Global Planet. Change*, 12, 237-249, 1996.

Hooke, R.L., B. Hanson, N.R. Iverson, P. Jansson, and U.H. Fischer, Rheology of till beneath Storglaciaren, Sweden, *J. Glaciol.*, 43, 172-179, 1997.

Hooke, R.L., and N.R. Iverson, Grain-size distribution of deforming subglacial tills: role of grain fracture, *Geology*, v. 23, 57-60, 1995.

Hughes, T., West Antarctic ice streams, *Rev. Geophys. Space Phys.*, 15, 1-46, 1977.

Hughes, T., Abrupt climatic change related to unstable ice sheet dynamics - toward a new paradigm, *Global Planet. Change.*, 97, 203-234, 1992.

Hughes, T., Can ice sheets trigger abrupt climatic change? *Arctic Alpine Res.*, 28, 448-465, 1996.

Iverson, N.R., R.W. Baker, and T.S. Hooyer, A ring-shear device for the study of till deformation: tests on till with contrasting clay contents, *Quaternary Sci. Rev.*, 16, 1,057-1,066, 1997.

Iverson, N.R., B. Hanson, R.L. Hooke, and P. Jansson, Flow mechanism of glaciers on soft beds, *Science*, 267, 80-81, 1995.

Iverson, N.R., P. Jansson, R.L. Hooke, In-situ measurements of the strength of deforming subglacial till, *J. Glaciol.*, 40, 497-503, 1994.

Iverson, N.R., and D.J. Semmens, Intrusion of ice into porous-media by regelation - a mechanism of sediment entrainment by glaciers, *J. Geophys. Res.*, 100, 10,219-10,230, 1995.

Jackson, M., and B. Kamb, The marginal shear stress of Ice Stream B, West Antarctica, *J. Glaciol.*, 43, 415-426, 1997.

Jenson, J.W., D.R. MacAyeal, P.U. Clark, C.L. Ho, and J.C. Vela, Numerical modeling of subglacial sediment deformation - implications for the behavior of the Lake Michigan Lobe, Laurentide Ice Sheet, *J. Geophys. Res.*, 96, 16,585-16,595, 1996.

Jones, M., Mechanical principles of sediment deformation, in *The Geologic Deformation of Sediments*, edited by A. Maltman, Chapman & Hall, London, 37-72, 1992.

Kamb, B., Rheological nonlinearity and flow instability in the deforming-bed mechanism of ice stream motion, *J. Geophys. Res.*, 96, 16,585-16,595, 1991.

Karig, D., and J. Morgan, Tectonic deformation: stress paths and strain histories, in *The Geologic Deformation of Sediments*, edited by A. Maltman, Chapman & Hall, London, 167-204, 1992.

Kezdi, A., *Handbook of soil mechanics*, Elsevier, Amsterdam, 1974.

MacAyeal, D.R., Large-scale ice flow over a viscous basal sediment - theory and application to Ice Stream B, Antarctica, *J. Geophys. Res.*, 94, 4,071-4,087, 1989.

MacAyeal, D.R., Irregular oscillations of the West Antarctic Ice Sheet, *Nature*, 359, 29-32, 1992.

MacAyeal, D.R., A low-order model of the Heinrich event cycle, *Paleoceanography*, 8, 767-773, 1993a.

MacAyeal, D.R., Binge-purge oscillations of the Laurentide Ice Sheet as a cause of the North Atlantic Heinrich events, *Paleoceanography*, 8, 775-784, 1993b.

MacAyeal, D.R., R. Bindschadler, and T.A. Scambos, Basal friction of Ice Stream E, West Antarctic, *J. Glaciol.*, 41, 247-262, 1995.

Marone, C., C.B. Raleigh, and C.H. Scholz, 1990, Frictional behavior and constitutive modeling of simulated fault gouge, *J. Geophys. Res.*, 95, 7,007-7,025, 1990.

Marshall, S.J., and G.K.C. Clarke, A continuum mixture model of ice stream thermomechanics in the Laurentide Ice Sheet. 1. Theory, *J. Geophys. Res.*, 102, 20,599-20,613, 1997.

Means, W.D., Stress and strain: basic concepts of continuum mechanics for geologists, Springer-Verlag, New York, 1979.

Mitchell, J.K., *Fundamentals of soil behavior*, Wiley, New York, 1993.

Patterson, W.S.B., *The physics of glaciers*, 3rd ed., Pergamon/Elsevier, London, 1994.

Payne, A.J., and P.W. Dongelmans, Self-organization in the thermomechanical flow of ice sheets, *J. Geophys. Res.*, 102, 12,219-12,233, 1997.

Raymond, C., Shear margins in glaciers and ice sheets, *J. Glaciol.*, 42, 90-102, 1996.

Rooney, S.T., D.D. Blankenship, R.B. Alley, and C.R. Bentley, Till beneath Ice Stream B. 2. Structure and continuity, *J. Geophys. Res.*, 92, 8913-8920, 1987.

Rooney, S.T., D.D. Blankenship, R.B. Alley and C.R. Bentley, Seismic reflection profiling of a sediment-filled graben beneath Ice Stream B, West Antarctica, in *Geologic Evolution of Antarctica*, edited by M.R. Thomson, J.A. Crame, and J.W. Thomson, pp. 262-265, British Antarctic Survey, Cambridge, 1991.

Roscoe, K.H., A.N. Schofield, and C.P. Wroth, On the yielding of soils, *Geotechnique*, 8, 22-52, 1958.

Sauer, E.K., and A.K. Egeland, and E.A. Christiansen, Preconsolidation of tills and intertill clays by glacial loading in southern Saskatchewan, Canada, *Can. J. Earth Sci.*, 30, 420-430, 1993.

Scherer, R.P., Quaternary and Tertiary microfossils from beneath Ice Stream B - evidence for a dynamic West Antarctic Ice Sheet history, *Global Planet. Change*, 90, 395-412, 1991.

Schofield, A.N., and C.P. Wroth, *Critical state soil mechanics*, McGraw Hill, London, 1968.

Scott, R.F., *Principles of soil mechanics*, Addison-Wesley Publishing Company, Reading, Massachusets, 1963.

Shabtaie, S., and C.R. Bentley, West Antarctic ice streams draining into the Ross Ice Shelf - configuration and mass balance, *J. Geophys. Res.*, 92, 1,311-1,336, 1987.

Sheahan, T. C., C.C. Ladd, and J. T. Germaine, Rate-dependent undrained shear behavior of saturated clay, *J. Geotech. Engng.*, 122, 99-108, 1996.

Skempton, A.W., Residual strength of clays in landslides, folded strata and laboratory, *Geotechnique*, 35, 3-18, 1985.

Smith, A.M., Basal conditions on Rutford ice stream, West Antarctica, from seismic observations, *J. Geophys. Res.*, 102, 543-552, 1997.

Stark, T.D., and H.T. Eid, Modified Bromhead ring shear apparatus, *Geotech. Testing J.*, 16, 100-107, 1993.

Stark, T.D., and J.J. Vettel, Bromhead ring shear test procedure, *Geotech. Testing J.*, 15, 24-32, 1992.

Terzaghi, K., R.B. Peck, and G. Mesri, *Soil mechanics in engineering practice*, Wiley, New York, 1996.

Tulaczyk, S., Ice sliding over weak, fine-grained tills: dependence of ice-till interactions on till granulometry, in *Glacial Processes, Past and Modern*, edited by D.M. Mickelson and J. Attig, in press.

Tulaczyk, S., B. Kamb, H. Engelhardt, and R.P. Scherer, Sedimentary processes beneath a West Antarctic ice stream; constraints from textural and compositional properties of subglacial debris, *J. Sediment. Res.*, 68, 487-496, 1998.

Tulaczyk, S., B. Kamb, and H. Engelhardt, Basal mechanics of Ice Stream B, West Antarctica. II. Till hydrology, in preparation.

Tulaczyk, S., B. Kamb, and H. Engelhardt, Basal mechanics of Ice Stream B, West Antarctica. III. Undrained-plastic-bed model, in preparation.

van der Veen, C.J., and Whillans, I.M., Model experiments on the evolution and stability of ice streams, *Ann. Glaciol.*, 23, 129-137, 1996.

Weertman, J., and G.E. Birchfield, Subglacial water flow under ice streams and West Antarctic Ice Sheet stability, *Ann. Glaciol.*, 3, 316-320,1982.

Whillans, I.M., J. Bolzan, and S. Shabtaie, Velocity of ice streams B and C, Antarctica, *J. Geophys. Res.*, 92, 8,895-8,902, 1987.

Whillans, I.M., and C.J. van der Veen, New and improved determinations of velocity of Ice Stream B and Ice Stream C, *J. Glaciol.*, 39, 483-490, 1993.

Whillans, I.M., and C.J. van der Veen, The role of lateral drag in the dynamics of Ice Stream B, *J. Glaciol.*, 43, 231-237, 1997.

Wood, D.M., *Soil behaviour and critical state soil mechanics*, Cambridge University Press, Cambridge, UK, 1992.

Table 1. List of Notations

Symbol	Meaning	Dimension*
$\cdots_{i \text{ OR } i+1}$	Some quantity ... evaluated at time t_i or t_{i+1}	N/A
C_c, C_s	Compressibility coefficients for virgin and overconsolidated till	ND
H	Ice thickness	L
L, ΔL	Length and change in length of a triaxial sample	L
R, ΔR	Radius and change in radius of a triaxial sample	L
S	Slope of the τ_f - log($\dot{\gamma}$) line	ND
T	Period of water-pressure fluctuations	T
U_{ice}	Total ice velocity	LT^{-1}
U_s, U_t	Velocity components due to basal sliding and till deformation	LT^{-1}
V, ΔV	Till volume and till volume change	L^3
V_s, V_w	Volume of till solids and pore water	L^3
Z, ΔZ	Till thickness and till thickness change	L
c_a, c_e	Apparent and effective cohesion	FL^{-2}
c_v	Hydraulic diffusivity (coefficient of consolidation)	L^2T^{-1}
e, e_{ini}	Void ratio and initial void ratio	ND
e_o	Void ratio at the reference effective stress of 1 kPa	ND
e_{ov}	Void ratio of an overconsolidated till	ND
g	Acceleration of gravity	LT^{-2}
n	Stress exponent in the power law for till rheology	ND
n_w	Porosity	ND
p'_o	Initial preconsolidation stress in a triaxial sample	FL^{-2}
p_w	Pore pressure	FL^{-2}
u	Excess pore pressure over hydrostatic pressure	FL^{-2}
u_o	Time-averaged excess pore pressure at the top of the till	FL^{-2}
u_s	Shear-induced excess pore pressure	FL^{-2}
u_t	Derivative of u with respect to t	$FL^{-2}T^{-1}$
u_{zz}	Second derivative of u with respect to z	FL^{-4}
t, Δt	Time and a discrete time interval	T
x, Δx	Horizontal coordinate and a discrete horizontal interval	L
z, Δz	Depth in till (z = 0 at the ice-till interface) and a depth interval	L
Δu	Magnitude of basal water-pressure fluctuations	FL^{-2}
$\Delta\Theta$	Rotation angle	°
$\Delta\sigma'_n$	Hydrostatic vertical effective stress gradient	FL^{-3}
Θ	Orientation of a plane measured from the vertical direction	°
Θ_o	Initial tiltmeter orientation measured from the vertical direction	°
ε_n	Vertical strain	ND
ε_1, ε_3	Major and minor principal strain	ND
ϕ, ϕ_e	Internal friction angle and the effective internal friction angle	°
γ, $\dot{\gamma}$	Shear strain and shear strain rate	ND and T^{-1}
ρ_{ice}	Ice density	ML^{-3}
ρ_s, ρ_t	Density of till solids and bulk till density	ML^{-3}
ρ_w	Water density	ML^{-3}
σ'_1, σ'_{1f}	Major principal effective stress and its value at failure	FL^{-2}
σ'_3, σ'_{3f}	Minor principal effective stress and its value at failure	FL^{-2}
σ_n, σ'_n	Total normal load and normal effective stress	FL^{-2}
σ'_{ne}	Equivalent consolidation stress	FL^{-2}
σ'_{nmax}	Maximum past normal effective stress (preconsolidation stress)	FL^{-2}
τ	Shear stress	FL^{-2}
τ_b, τ_d	Basal shear stress and gravitational driving stress	FL^{-2}
τ_f, τ_{fmin}	Till failure strength and minimum till failure strength	FL^{-2}
τ_{fov}	Peak strength of overconsolidated till	FL^{-2}
ω	Frequency of water-pressure fluctuations	T^{-1}
ψ	Reciprocal of the depthscale for water-pressure fluctuations	L^{-1}
~ ...	A number of the order of ...	N/A

*In addition to the usual dimensions of F, force (MLT^{-2}), L, length, M, mass, T, time, I use '°' for degrees and 'ND' to denote a non-dimensional variable.

Table 2. Angle of Internal Friction and, Below the Diagonal, Apparent Cohesion Calculated From Combinations of Three Triaxial Test Data Sets Using Equation (11)[*]

Sample	U1	U2	U3
U1	24° [#]	24°	23°
U2	2 kPa	24° [#]	23°
U3	3 kPa	5 kPa	24° [#]

[*] The major and minor principal effective stresses at failure were calculated for each test by summing up all the values of these principal stresses measured after axial strain reached c. 0.04. At this point in the tests, the initial transient stage of strength mobilization has already ended.

[#] Assuming no apparent cohesion, i.e., $c_a = 0$ in equation (11).

Figure 1. (A) Letters A through E denote the individual ice streams flowing through the Ross Sea section of West Antarctica. Location map showing outlines of the ice streams, ice elevation contour lines (250 m interval), and major mountain ranges (after Tulaczyk *et al.* [1998, Figure 1]). (B) Locations of boreholes drilled on Ice Stream B in the UpB area during field seasons 1988-1995, shown in a stationary, geographic reference frame (the reference frame of the ice surface is moving 440 m y^{-1} at UpB [Whillans and van der Veen, 1993]). Individual boreholes are labeled with consecutive numbers indicating order of drilling during a given field season. The label numbers for these boreholes from which sediment cores were acquired are bold and underlined. In several other boreholes small amounts of subglacial sediments were recovered.

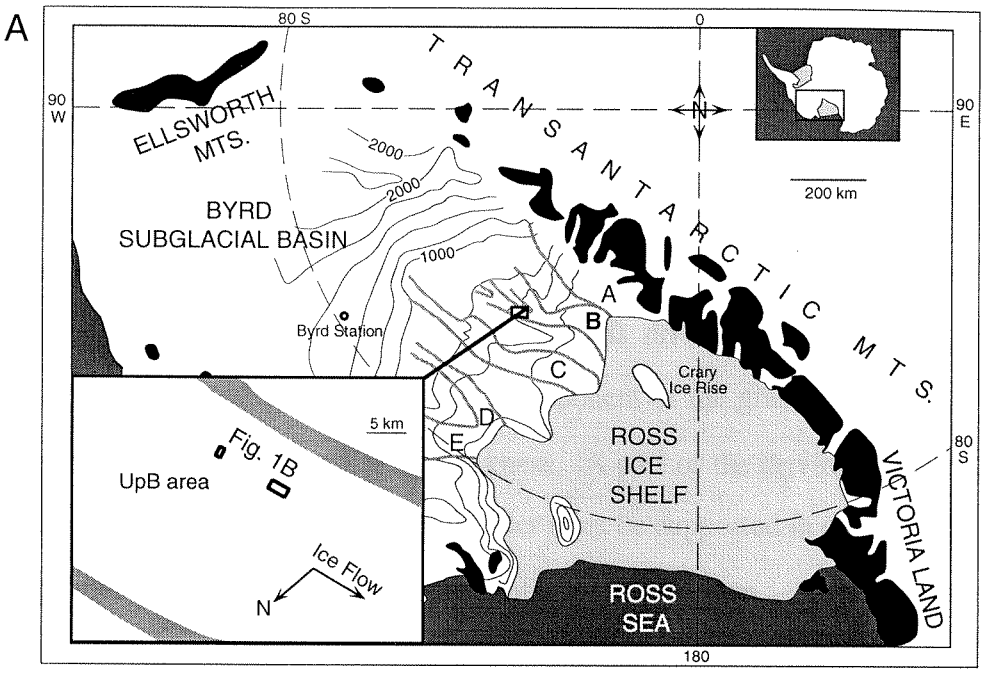
A
80 S
0
90 W
90 E
N
ELLSWORTH MTS.
TRANSANTARCTIC MTS.
2000
2000
1000
BYRD SUBGLACIAL BASIN
Byrd Station
200 km
A
B
C
D
E
Crary Ice Rise
ROSS ICE SHELF
VICTORIA LAND
80 S
5 km
Fig. 1B
UpB area
Ice Flow
N
ROSS SEA
180

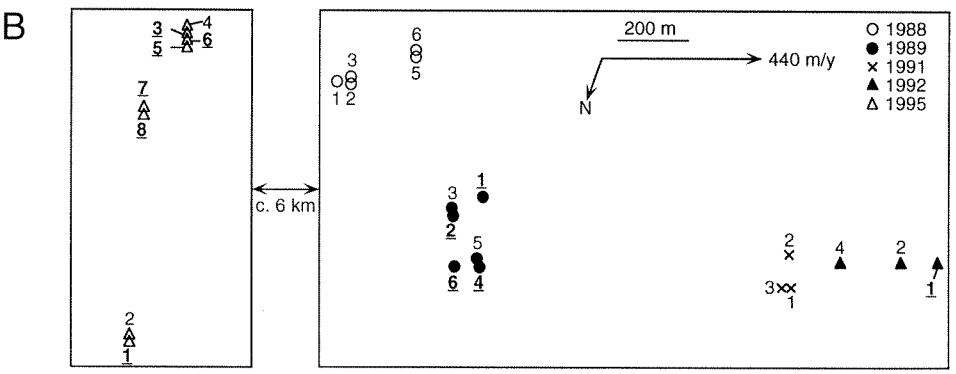
B
c. 6 km
200 m
440 m/y
N
1988
1989
1991
1992
1995

Figure 2. Schematic vertical cross-section through Ice Stream B, not to scale. In the lower left we show the two-dimensional, x-z coordinate system used in this manuscript. The slope of the ice surface (a) is in the x direction, which is the ice-stream flow direction (to the right). The large vertical arrow indicates the ice load, σ_n, acting on the top of the till. This ice load less the basal water pressure is the normal effective stress, σ'_n, at the ice-till interface. The ice-stream flow is driven by the gravitational driving stress, τ_d, which represents the downslope component of the gravitational force on the ice (per unit area), integrated over the ice thickness. A part of the driving stress is supported by the basal shear stress, τ_b, and the remainder must be supported in other ways such as by marginal shear stresses or outside the plane of the cross section. The basal shear stress is assumed to be equal to the till strength. The velocity of ice stream motion is assumed to be controlled predominantly by the ice stream margins [Echelmeyer et al., 1994; Jackson and Kamb, 1997; Raymond, 1996]. The ice-stream flow velocity U_{ice} is composed of a till-deformation component U_t and a basal sliding component U_s that occurs as a relative motion along the ice-till interface. We assume that internal ice shear deformation across horizontal planes does not contribute significantly to ice stream motion because the basal shear stress and hence the shear strain rate in the ice is very small.

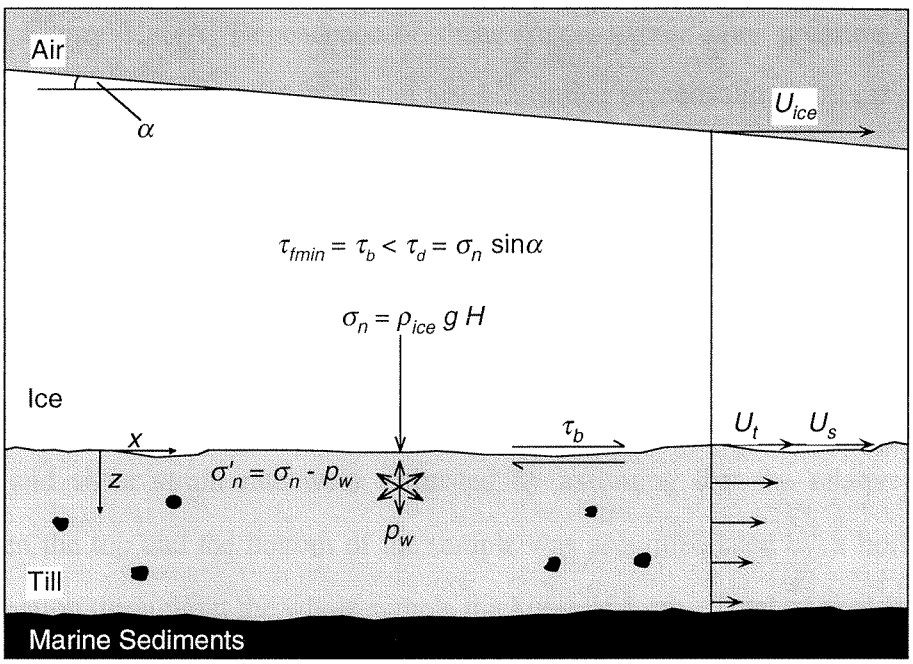
Air
α
U_{ice}
$\tau_{fmin} = \tau_b < \tau_d = \sigma_n \sin\alpha$
$\sigma_n = \rho_{ice}\, g\, H$
Ice
x
z
τ_b
U_t
U_s
$\sigma'_n = \sigma_n - p_w$
p_w
Till
Marine Sediments

Figure 3. (A) Dependence of shear stress, excess pore pressure, and effective normal stress on shear strain in triaxial test U2 (initial preconsolidation pressure p'_o = 205 kPa). Normal effective stress and shear stress on theoretical failure plane are calculated with equations (13ab). Shear strain on the failure plane is obtained from the measured axial strain through equations (14ab) with the assumption that the internal friction angle of the UpB till is equal to 24° (Table 2). (B) Plot of shear stress vs. estimated shear strain in a high-displacement and high-velocity ring shear test on a sample of the UpB till. The shear strain and shear strain rate were estimated by assuming that the relative displacement between the top and the bottom of the sample was accommodated by a homogeneous till deformation throughout the whole sample thickness of 1 cm. Total normal load was set to 20 kPa. (C) Results of a ring shear test in which the relative displacement rate was increased twice by a factor of 10 from an initial low value of 0.1 m d^{-1}. Shear strains and shear stresses estimated as in (B). The two distinct drop-offs in shear stress magnitude result from relaxation of the sheared till and the device itself that occurred when shearing was interrupted to increase the displacement rate.

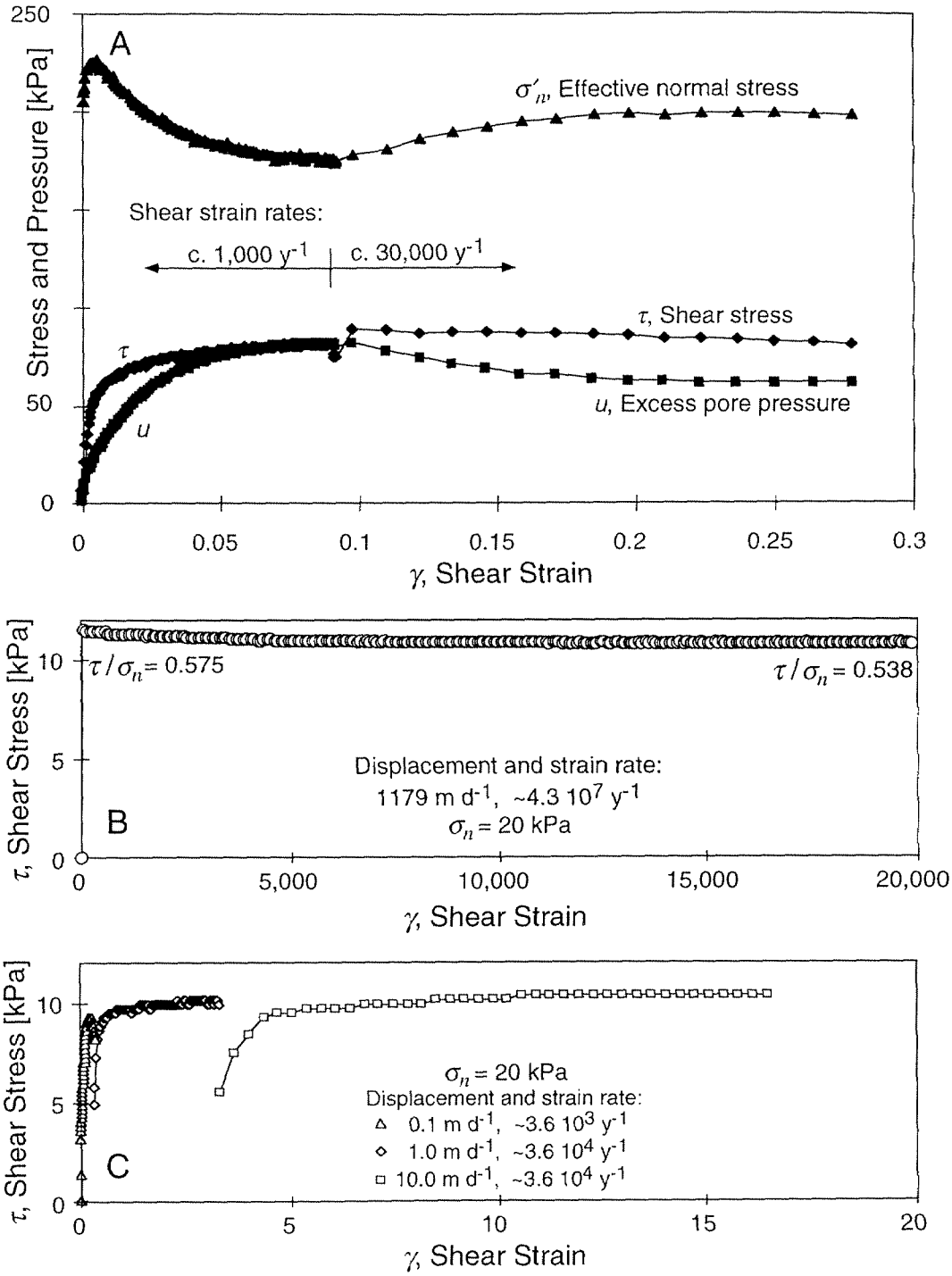
A
Stress and Pressure [kPa]
250
50
0
σ'_n, Effective normal stress
Shear strain rates:
c. 1,000 y^{-1}
c. 30,000 y^{-1}
τ, Shear stress
u, Excess pore pressure
τ
u
0
0.05
0.1
0.15
0.2
0.25
0.3
γ, Shear Strain
B
τ, Shear Stress [kPa]
10
5
0
τ / σ_n = 0.575
τ / σ_n = 0.538
Displacement and strain rate:
1179 m d^{-1}, ~4.3 10^7 y^{-1}
σ_n = 20 kPa
0
5,000
10,000
15,000
20,000
γ, Shear Strain
C
τ, Shear Stress [kPa]
10
5
0
σ_n = 20 kPa
Displacement and strain rate:
0.1 m d^{-1}, ~3.6 10^3 y^{-1}
1.0 m d^{-1}, ~3.6 10^4 y^{-1}
10.0 m d^{-1}, ~3.6 10^4 y^{-1}
0
5
10
15
20
γ, Shear Strain

Figure 4. (A) Relationship between shear stress and normal effective stress at failure in the six undrained triaxial tests on the UpB till (U1, U2, U3, R1, R2, R3) in which shear strain rate was varied from ca. 1 y^{-1} up to ca. 80,000 y^{-1}. Numbers in parenthesis give the count of data points plotted for each test. To exclude the pre-failure strength-mobilization stage we consider only observations made at axial strain greater than 0.04. Values of shear stress and normal effective stress are calculated from the measured principal effective stresses using equations (13ab). The solid line represents a least-squares fit to the data (R^2 is the correlation coefficient); the line has slope angle $\phi = 23.9°$ and axis intercept $c_a = 1.3$ kPa. For comparison, dashed lines show the relationship between shear stress and effective stress obtained for selected strain rates from the Bingham till rheology model of Boulton and Hindmarsh [1987]. (B) The shear stress data used in (A) are normalized by the initial preconsolidation stress and plotted against the logarithm of corresponding shear strain rate data. The solid line gives a best fit to the shear stress-strain rate data and the dashed line illustrates again the prediction of the Bingham till rheology model. Slope S of the best-fit curve in (B) is commonly used in soil mechanics as a measure of strain-rated-dependence of strength. The quantity S can be recalculated into the stress exponent in a power flow law of till, n [Kamb, 1991, eq. 8]. (C) Ratio of shear stress to effective normal stress plotted against shear strain rate for the same triaxial data as in (B). The solid, best-fit line indicates practically no dependence of this stress ratio on strain rate.

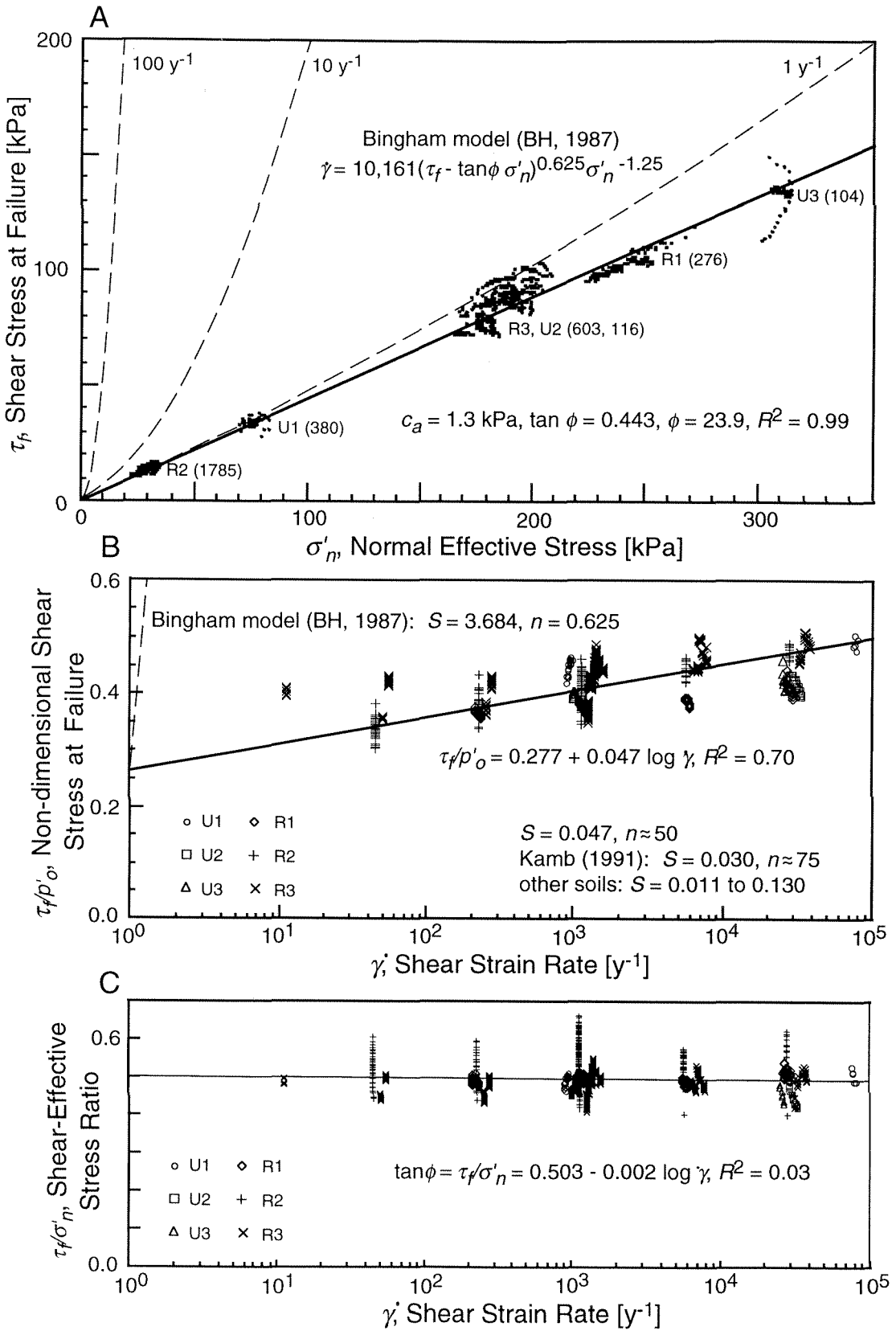
A
100 y-1
10 y-1
1 y-1
Bingham model (BH, 1987)
γ̇ = 10,161(τf - tanφ σ'n)0.625σ'n -1.25
U3 (104)
R1 (276)
R3, U2 (603, 116)
U1 (380)
R2 (1785)
ca = 1.3 kPa, tan φ = 0.443, φ = 23.9, R2 = 0.99
τf, Shear Stress at Failure [kPa]
σ'n, Normal Effective Stress [kPa]
B
Bingham model (BH, 1987): S = 3.684, n = 0.625
τf/p'o = 0.277 + 0.047 log γ̇, R2 = 0.70
S = 0.047, n≈50
Kamb (1991): S = 0.030, n≈75
other soils: S = 0.011 to 0.130
U1 R1
U2 R2
U3 R3
τf/p'o, Non-dimensional Shear Stress at Failure
γ̇, Shear Strain Rate [y-1]
C
tanφ = τf/σ'n = 0.503 - 0.002 log γ̇, R2 = 0.03
τf/σ'n, Shear-Effective Stress Ratio
γ̇, Shear Strain Rate [y-1]

Figure 5. (A) Compressibility of the UpB till in normally-consolidated (NCL), overconsolidated (URL), and sheared states (CSL). Triaxial test results (large circles, thick solid line) indicate that normally-consolidated till is somewhat less compressible under isotropic effective stress than in K_0-conditions in an oedometer test (solid squares, thick dashed line). Normal effective stress at failure is plotted for the six undrained triaxial tests in which void ratio was held constant during shear (small open circles drawn at every tenth observation). Much of the spread in these data is due to the strain-rate-dependence of effective stress. The critical state line (CSL, thin solid line) is obtained by least-squares fitting to these (e, σ'_n) data points which were collected at the selected reference strain rate of ca. 1,000 y^{-1}. Behavior of the UpB till in the overconsolidated state was determined in oedometer tests on two till samples preconsolidated to σ'_{nmax} = 71 kPa and σ'_{nmax} = 568 kPa, respectively (open triangles, URL_{71} and URL_{568}, thin dashed lines). In (B), triaxial data are used to illustrate the fact that shear has induced consolidation in the drained test, D1 - right-hand scale, which is consistent with the build-up of positive shear-induced pore pressures in undrained tests, U1, U2, and U3 - left-hand scale. In this respect, the UpB till is diametrically opposite in behavior to the Breidamerkurjokull till which has been reported to dilate by 10% upon shear, CSL (BH87) vs. NCL (BH87) [Boulton and Hindmarsh, 1987]. In undrained conditions such strong tendency to dilate would correspond to build-up of negative pore pressures. Shear-induced pore pressures are calculated from triaxial data with the following equation: $u_s = u - (\sigma_1 + 2\sigma_3)/3$ (notations in Table 1) [Sheahan *et al.*, 1996, p. 102].

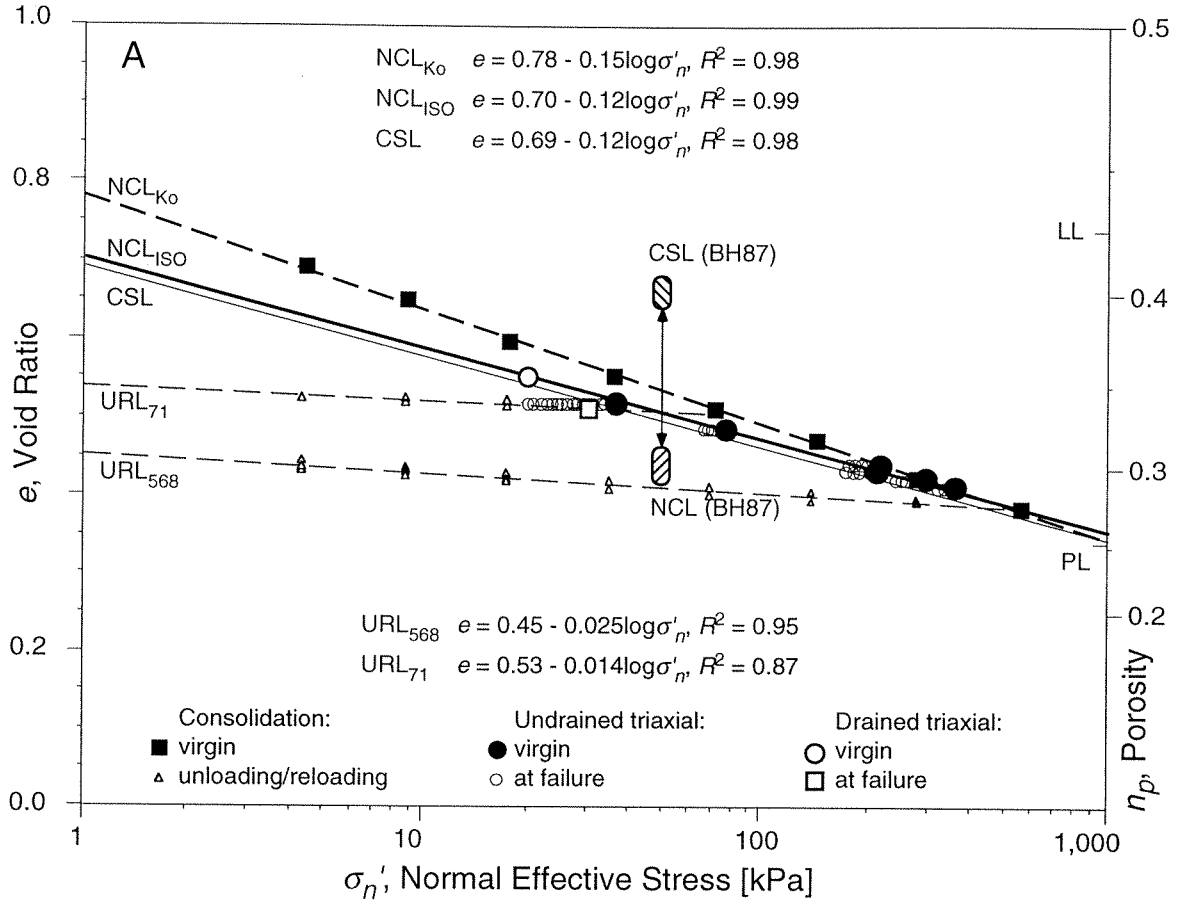
A
NCL_Ko e = 0.78 - 0.15logσ'n, R2 = 0.98
NCL_ISO e = 0.70 - 0.12logσ'n, R2 = 0.99
CSL e = 0.69 - 0.12logσ'n, R2 = 0.98
NCL_Ko
NCL_ISO
CSL
URL_71
URL_568
CSL (BH87)
NCL (BH87)
LL
PL
URL_568 e = 0.45 - 0.025logσ'n, R2 = 0.95
URL_71 e = 0.53 - 0.014logσ'n, R2 = 0.87
Consolidation:
virgin
unloading/reloading
Undrained triaxial:
virgin
at failure
Drained triaxial:
virgin
at failure
e, Void Ratio
np, Porosity
σn', Normal Effective Stress [kPa]

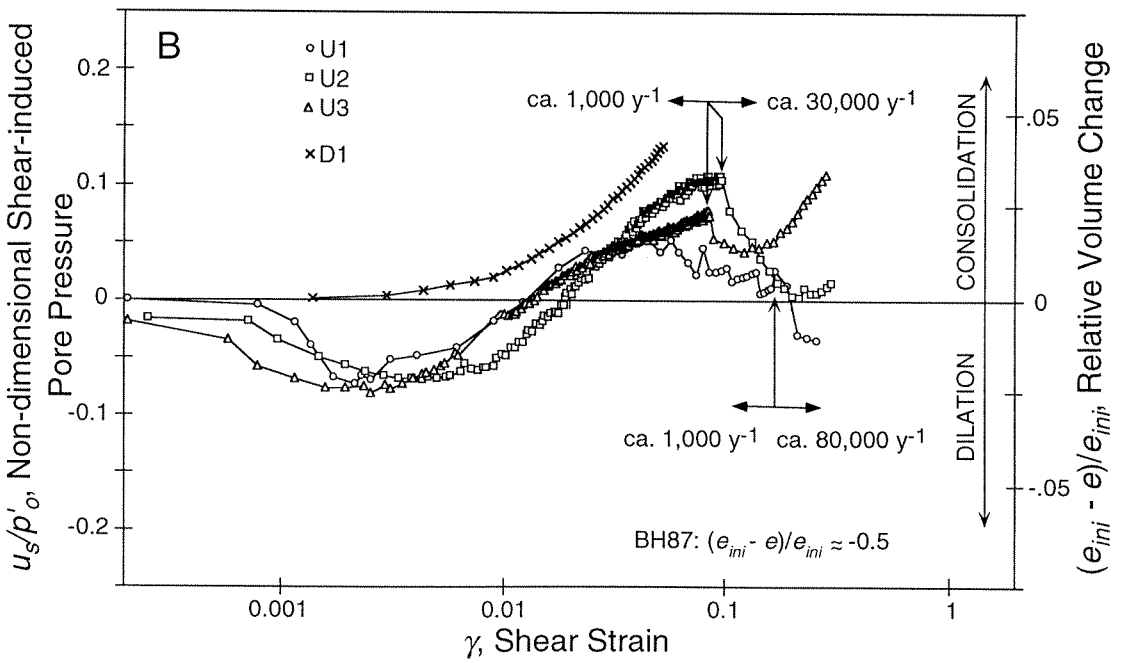
B
U1
U2
U3
D1
ca. 1,000 y-1
ca. 30,000 y-1
ca. 1,000 y-1
ca. 80,000 y-1
CONSOLIDATION
DILATION
BH87: (eini - e)/eini ≈ -0.5
us/p'o, Non-dimensional Shear-induced Pore Pressure
(eini - e)/eini, Relative Volume Change
γ, Shear Strain

Figure 6. Observed, (A) (B), and modeled, (C) through (H), fluctuations in subglacial effective stresses and subglacial strain rates. (A) and (B) show time series of effective normal stress and tilt rate reported by Hooke *et al.* [1997, Figure 2] from the subglacial zone of Storglaciaren, Sweden. The remaining diagrams display results of our modeling in which changes in effective stresses, (C), (E), (G), produce tiltmeter rotations, (D), (F), (H), following equations (5) and (6). In (C), a linear increase in effective stress (thick solid line, left-hand scale) is used to drive rotation of tiltmeters which have different initial orientations (three thin lines). Diagram (D) shows corresponding tilt rates for the same three tiltmeters. The second family of forcing functions considered, (E), represents diurnal fluctuations in subglacial effective stress. These forcing functions were calculated from equations (7) and (8) with input data selected to simulate conditions at 0.1 m depth in the UpB till (thick dashed line) and at 0.1 m and 1.0 m depth in a till beneath a mountain glacier (thick and thin solid lines) [Engelhardt and Kamb, 1997; Hooke *et al.*, 1997; Tulaczyk *et al.*, in preparation II]. Tilt rates resulting from these stress forcings are shown in (F). Diagrams (G) and (H) display the effective stress functions and tiltmeter strain rates which result from superposition of a linear increase in effective stress on an oscillatory effective stress signal.

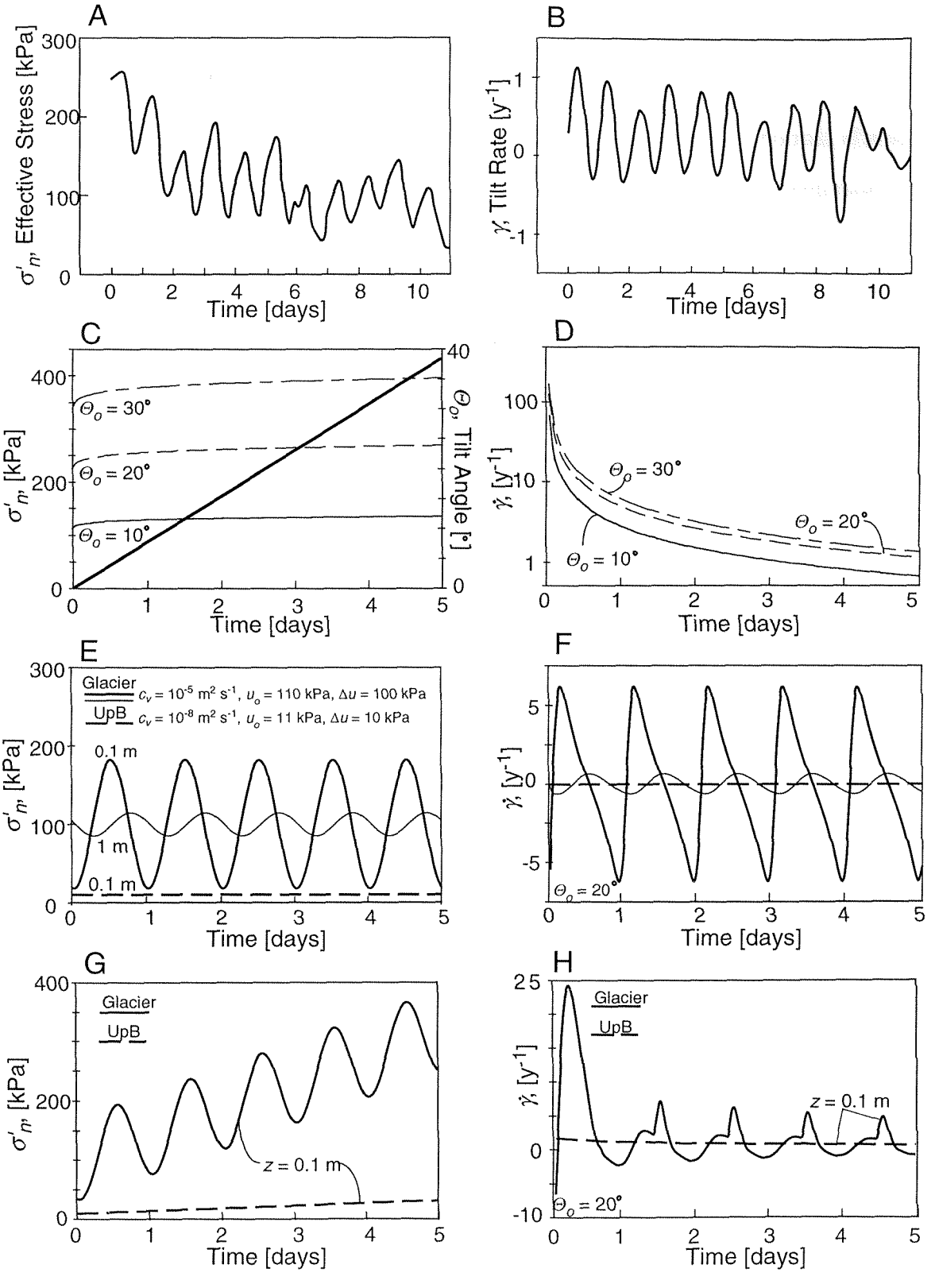
A
σ′n, Effective Stress [kPa]
Time [days]
B
γ̇, Tilt Rate [y-1]
Time [days]
C
σ′n, [kPa]
Θo, Tilt Angle [°]
Θo = 30°
Θo = 20°
Θo = 10°
Time [days]
D
γ̇, [y-1]
Θo = 30°
Θo = 20°
Θo = 10°
Time [days]
E
Glacier cv = 10-5 m2 s-1, uo = 110 kPa, Δu = 100 kPa
UpB cv = 10-8 m2 s-1, uo = 11 kPa, Δu = 10 kPa
σ′n, [kPa]
0.1 m
1 m
0.1 m
Time [days]
F
γ̇, [y-1]
Θo = 20°
Time [days]
G
Glacier
UpB
σ′n, [kPa]
z = 0.1 m
Time [days]
H
Glacier
UpB
γ̇, [y-1]
z = 0.1 m
Θo = 20°
Time [days]

Figure 7. (A) One-hour timelines illustrating the distribution of normal effective stress with depth during a diurnal cycle of basal water pressure fluctuations (equations (7) and (8); numbers 0, 6, 12, 18 denote hours elapsed since the beginning of the cycle). The selected parameters, c_v, u_o, and Δu, are representative of the subglacial zone of Ice Stream B in the UpB area. A linear increase in effective stress with depth, $\Delta\sigma'_n = 10$ kPa m^{-1}, may be superposed on these oscillations to simulate time-averaged hydrostatic conditions. Without this superposition the model simulates time-averaged lithostatic conditions. The diurnal oscillations in effective stress (A) trigger changes in till strength, (B) and (C). These strength changes follow the Coulomb equation, (2), for normal-consolidation and light overconsolidation and the Hvorslev equation, (9), for high overconsolidation. The results shown in (B) and (C) were used to track over time the position of the minimum till strength, τ_{fmin}. We assume that the shear zone which accommodates ice motion is at the depth level of τ_{fmin} and the two migrate up and down together. Spatial resolution of our supervised numerical tracking procedure was 0.01 m and temporal resolution 0.5 hr. Diagram (D) shows strain distribution in till after one water-pressure cycle assuming that the displacement rate across the migrating shear zone was always equal to ice velocity, U_{ice}. The relative velocity in till is given as a fraction of ice velocity which is taken to be constant throughout the cycle. Cumulatively, internal till deformation accounts for ca. 55% of U_{ice} while the remaining ca. 45% of U_{ice} is accommodated by basal sliding, which occurs when the weakest shear plane is at the top of the till.

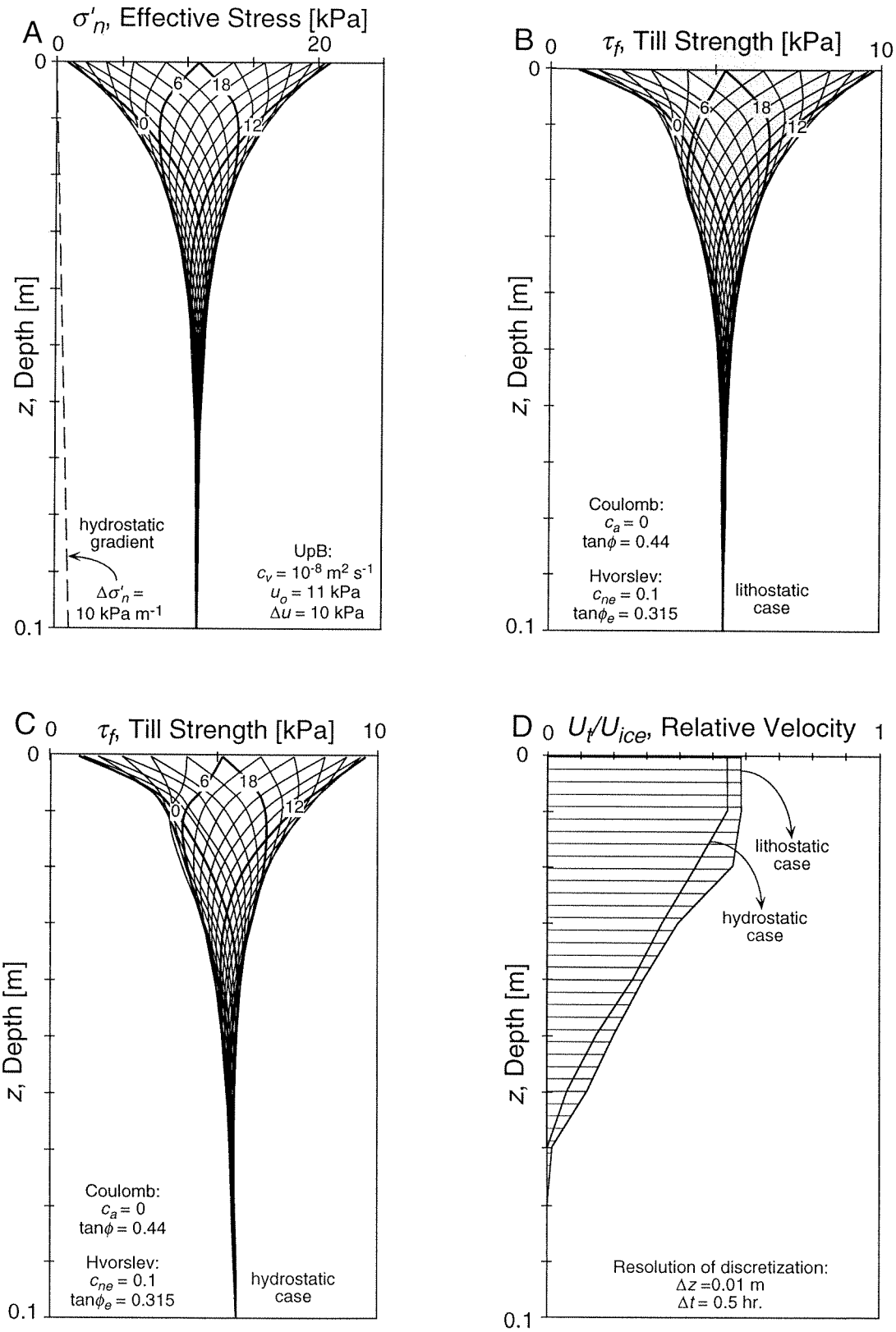
A
σ'_n, Effective Stress [kPa]
0
20
z, Depth [m]
0.1
6
18
10
12
hydrostatic gradient
$\Delta\sigma'_n$ = 10 kPa m^{-1}
UpB:
$c_v = 10^{-8}$ m^2 s^{-1}
u_o = 11 kPa
Δu = 10 kPa
B
τ_f, Till Strength [kPa]
10
0
18
12
Coulomb:
$c_a = 0$
tan$\phi = 0.44$
Hvorslev:
$c_{ne} = 0.1$
tan$\phi_e = 0.315$
lithostatic case
C
τ_f, Till Strength [kPa]
hydrostatic case
D
U_t/U_{ice}, Relative Velocity
1
lithostatic case
hydrostatic case
Resolution of discretization:
Δz =0.01 m
Δt = 0.5 hr.

Figure 8. This figure is very similar to Figure 7. However, here we are modeling changes in effective stress (A) and till strength distribution, (B) and (C), for a hypothetical high-diffusivity till experiencing at its top relatively large basal water pressure fluctuations characteristic for basal systems of mountain glaciers (Δu = 100 kPa). Because of the high hydraulic diffusivity of the modeled till, basal water pressure fluctuations propagate through its whole assumed thickness of 1.0 m. A significant portion of the total ice velocity, c. 35%, is accommodated during one cycle of water-pressure fluctuations by till sliding over its substratum (at z = 1.0 m). Till sliding takes place in our model when the weakest shear plane develops right at the bottom of the till. The remaining two-thirds of ice velocity is accommodated by a combination of internal till deformation and by basal sliding of ice.

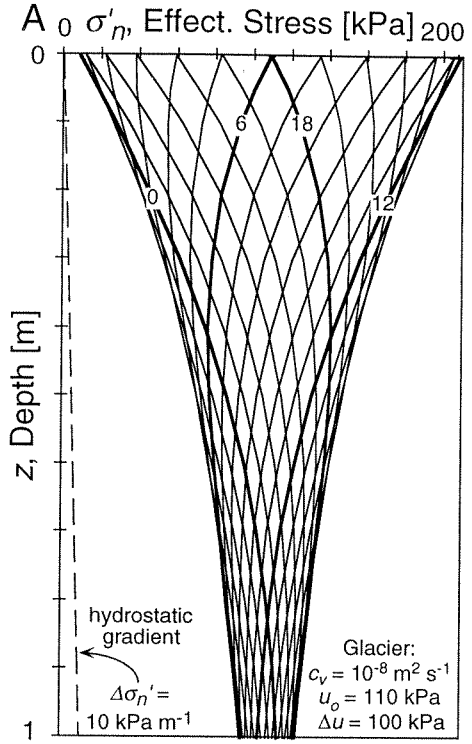
A
0
σ'_n, Effect. Stress [kPa]
200
0
1
z, Depth [m]
0
6
18
12
hydrostatic gradient
$\Delta\sigma_n'$ = 10 kPa m^{-1}
Glacier:
$c_v = 10^{-8}$ m^2 s^{-1}
u_o = 110 kPa
Δu = 100 kPa

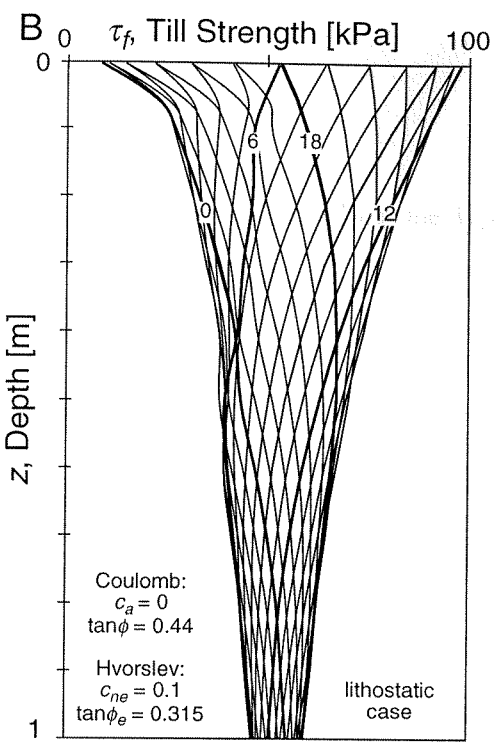
B
0
τ_f, Till Strength [kPa]
100
0
1
z, Depth [m]
0
6
18
12
Coulomb:
$c_a = 0$
$\tan\phi = 0.44$
Hvorslev:
$c_{ne} = 0.1$
$\tan\phi_e = 0.315$
lithostatic case

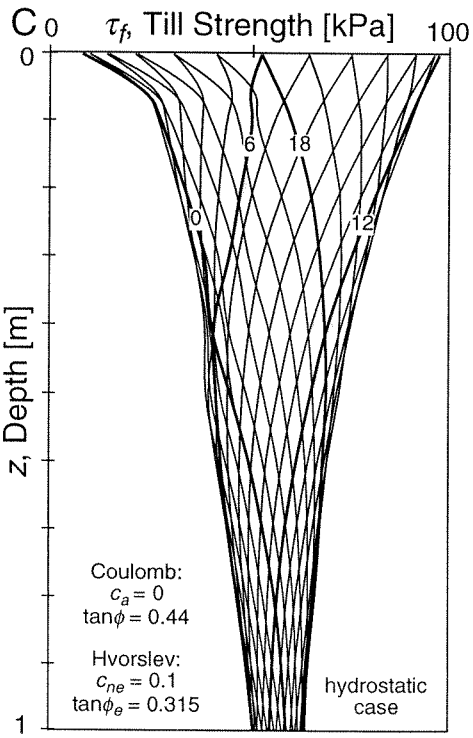
C
0
τ_f, Till Strength [kPa]
100
0
1
z, Depth [m]
0
6
18
12
Coulomb:
$c_a = 0$
$\tan\phi = 0.44$
Hvorslev:
$c_{ne} = 0.1$
$\tan\phi_e = 0.315$
hydrostatic case

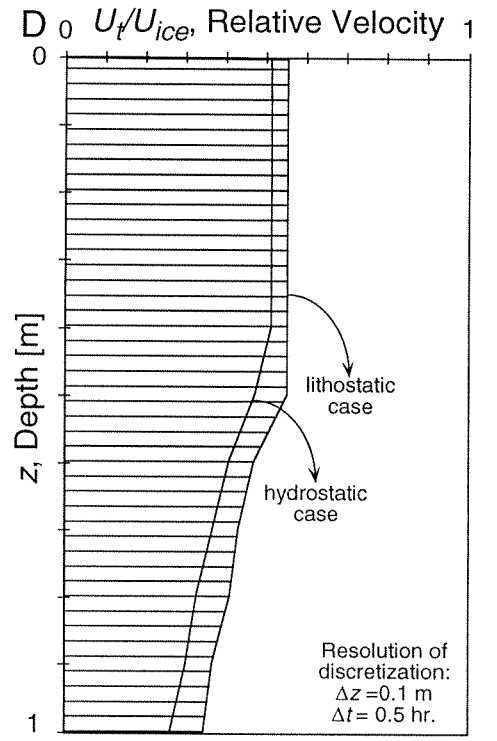
D
0
U_t/U_{ice}, Relative Velocity
1
0
1
z, Depth [m]
lithostatic case
hydrostatic case
Resolution of discretization:
Δz =0.1 m
Δt = 0.5 hr.

Figure 9. (A) Record of basal sliding obtained beneath Ice Stream B in the UpB area using a tethered stake; modified from Engelhardt and Kamb [in press, Figure 4]. The non-dimensional sliding velocity is obtained by dividing the measured sliding rate by the ice surface velocity U_{ice} = 440 m y^{-1} observed in the UpB area by Whillans and van der Veen [1993]. Vertical arrows point out major departures of the measured sliding velocity from the surface velocity. (B) and (C) illustrate how such departures may result from clasts or ice protrusions ploughing the underlying till. (B) shows an example of the pattern of deformation which may be caused by till ploughing (modified from Tulaczyk [in press, Figure 9]). Taking a reference frame moving with the ice (at speed U_{ice}), we can equivalently assume that the vertical grid markers in (B) represent progressive changes in the position and shape of one originally vertical marker which experiences progressive deformation due to passage of a ploughing clast or ice protuberance. Open symbols indicate consecutive positions of four simulated tethered stakes which were initially emplaced at different depths on the perfectly vertical grid marker (initial position $x = 0$). If these four simulated tethered stakes were to experience a passage of a ploughing protrusion as shown in (B), they would yield the sliding records shown in (C). We determined these synthetic sliding records by measuring off the horizontal distance of each symbol from x = 0 in (B) and dividing it by the distance at which this symbol would be located if the initially-vertical grid marker had not deformed.

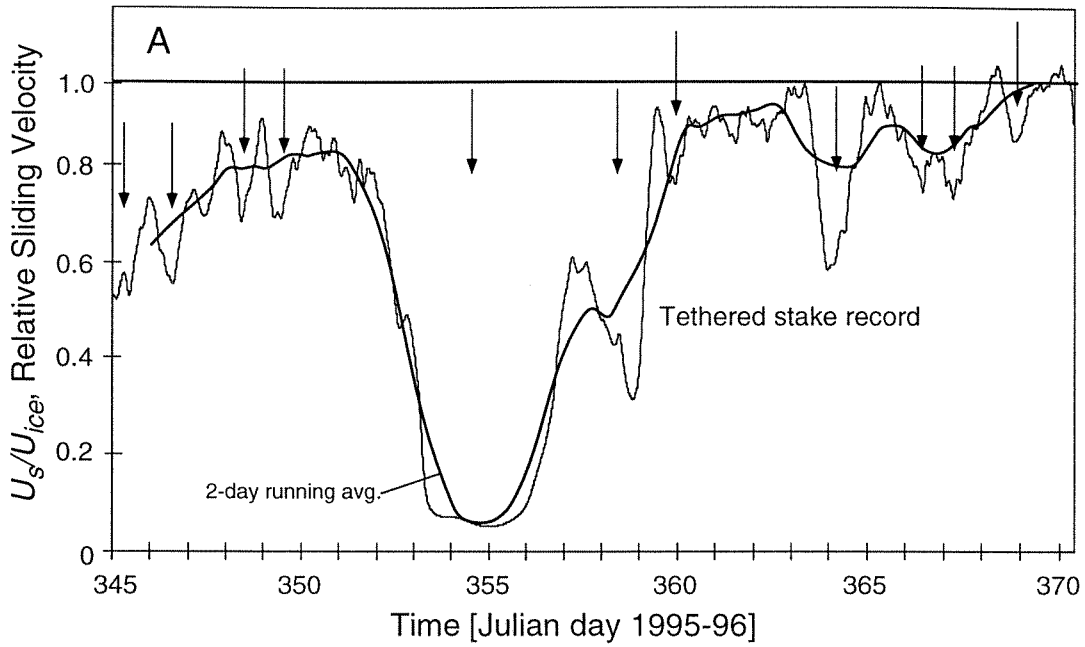
A
U_s/U_{ice}, Relative Sliding Velocity
1.0
0.8
0.6
0.4
0.2
0
Tethered stake record
2-day running avg.
345
350
355
360
365
370
Time [Julian day 1995-96]

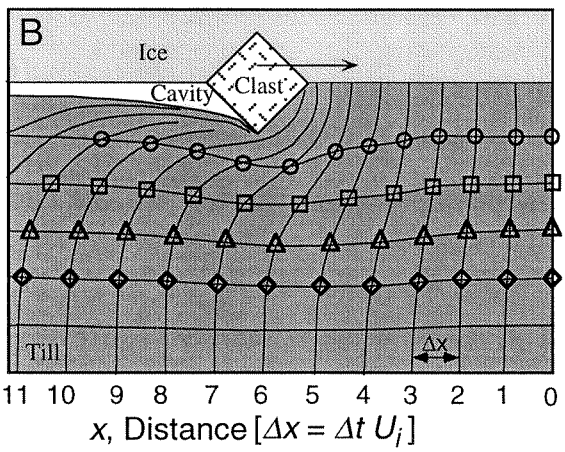
B
Ice
Cavity
Clast
Till
Δx
11 10 9 8 7 6 5 4 3 2 1 0
x, Distance [Δx = Δt U_i]

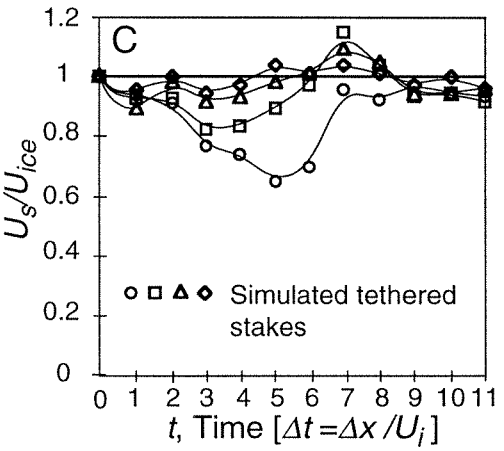
C
1.2
1
0.8
0.6
0.4
0.2
0
U_s/U_{ice}
Simulated tethered stakes
0 1 2 3 4 5 6 7 8 9 10 11
t, Time [Δt =Δx /U_i]

APPENDIX 4.A.

Data Tables for Chapter 4

4.A.1. Triaxial Data

The following seven tables contain the measurements made during six undrained triaxial compression tests, U1, U2, U3, R1, R2, and R3, and one drained triaxial compression test, D1. Other general information regarding sample characteristics is given in the heading at the top of each table. These headings include the date of the shearing stage of each triaxial test and the backpressure, i.e., the water pressure at which complete saturation of the triaxial sample was achieved. Sample saturation was verified using the B-value test described by Bowles [1992, p. 191]. Triaxial testing procedures are not discussed in this appendix in detail because they are sufficiently standard and can be easily obtained from the geotechnical literature [Bowles, 1992, p. 189-201; Bishop and Henkel, 1955].

Measured values shown in the seven tables represent raw data collected during the triaxial tests. The only pre-processing applied to the data was removal of initial instrument offsets and data conversion to the metric system. Each table for the six undrained triaxial tests gives: (1) the minor principal stress, σ_3, (2) axial force, F_a, (3) axial shortening, ΔL, and (4) pore pressure, p_w. All four quantities were digitally recorded at regular time intervals ranging between 10 and 20 s. The fifth quantity, axial velocity, u_a, was not measured directly but it was controlled using a system of gears which was built into the triaxial apparatus. In the drained test D1, the loss of water volume from the sheared sample was recorded manually at five-minute intervals. After the drained test, final water content

and final volumes of pore water and sample solids were estimated using the procedure described by Bowles [1992, p. 15-18].

The minor principal stress and the pore pressure were measured with two precalibrated pressure transducers. Due to signal digitalization, these measurements are accurate to ± 0.3 kPa. Axial force was monitored using a pre-calibrated proving ring whose accuracy was also limited to ± 2 N by the resolution of signal digitalization. Finally, sample shortening was measured with a linear displacement transducer, LVDT, with resolution of 0.001 mm.

All the stress, strain, and strain rate data used in Chapter 4 can be derived from these five quantities and from the sample lengths and radii given in table headers [Bowles, 1992; Bishop and Henkel, 1955].

Table A1. Data for the undrained triaxial compression test U1.

Date:	02/23/95
Sample material:	undisturbed UpB till, core 92-1
Initial weight:	245.8 gram
Pre-shear length:	8.36 cm
Pre-shear radius:	2.23 cm
Void ratio:	0.487
Saturation pressure:	625.4 kPa

#	σ_3 [kPa]	F_a [N]	ΔL [cm]	p_w [kPa]	u_a [µm/s]	#	σ_3 [kPa]	F_a [N]	ΔL [cm]	p_w [kPa]	u_a [µm/s]
1	692.9	0.0	0.0000	625.4	1.693	63	692.9	89.4	0.1110	634.3	1.693
2	692.9	0.0	0.0000	625.4	1.693	64	692.9	93.4	0.1133	634.3	1.693
3	694.3	3.2	0.0010	625.4	1.693	65	694.3	93.4	0.1158	634.3	1.693
4	694.3	8.5	0.0036	625.4	1.693	66	694.3	93.4	0.1171	634.3	1.693
5	694.3	16.9	0.0058	625.4	1.693	67	694.3	93.4	0.1181	635.0	1.693
6	694.3	29.8	0.0071	625.4	1.693	68	694.3	93.4	0.1207	634.3	1.693
7	694.3	42.7	0.0094	628.1	1.693	69	694.3	93.4	0.1229	634.3	1.693
8	694.3	51.2	0.0119	629.5	1.693	70	694.3	93.4	0.1242	634.3	1.693
9	694.3	55.2	0.0130	630.2	1.693	71	694.3	93.4	0.1242	634.3	1.693
10	694.3	59.6	0.0142	630.9	1.693	72	694.3	93.4	0.1265	634.3	1.693
11	694.3	63.6	0.0165	631.6	1.693	73	694.3	93.4	0.1290	634.3	1.693
12	694.3	63.6	0.0178	632.3	1.693	74	694.3	93.4	0.1300	634.3	1.693
13	694.3	68.1	0.0201	631.6	1.693	75	694.3	97.9	0.1313	635.0	1.693
14	694.3	72.1	0.0239	632.3	1.693	76	694.3	97.9	0.1326	635.0	1.693
15	694.3	72.1	0.0249	632.3	1.693	77	694.3	97.9	0.1349	635.0	1.693
16	694.3	72.1	0.0284	633.0	1.693	78	694.3	97.9	0.1374	635.0	1.693
17	694.3	72.1	0.0297	633.0	1.693	79	694.3	97.9	0.1397	635.0	1.693
18	694.3	72.1	0.0323	633.0	1.693	80	694.3	97.9	0.1410	635.0	1.693
19	694.3	76.5	0.0333	633.0	1.693	81	694.3	97.9	0.1420	635.0	1.693
20	694.3	76.5	0.0345	633.0	1.693	82	694.3	97.9	0.1445	635.0	1.693
21	694.3	76.5	0.0368	633.0	1.693	83	694.3	97.9	0.1458	635.0	1.693
22	694.3	76.5	0.0404	633.0	1.693	84	694.3	97.9	0.1481	635.0	1.693
23	694.3	76.5	0.0404	633.0	1.693	85	694.3	97.9	0.1481	634.3	1.693
24	694.3	81.0	0.0417	633.0	1.693	86	692.9	97.9	0.1504	635.0	1.693
25	694.3	81.0	0.0442	633.7	1.693	87	694.3	97.9	0.1529	635.0	1.693
26	694.3	81.0	0.0465	633.7	1.693	88	694.3	97.9	0.1552	635.0	1.693
27	694.3	81.0	0.0478	633.0	1.693	89	694.3	97.9	0.1565	635.0	1.693
28	694.3	81.0	0.0500	633.0	1.693	90	694.3	97.9	0.1577	635.0	1.693
29	694.3	81.0	0.0513	633.7	1.693	91	694.3	97.9	0.1588	635.0	1.693
30	694.3	81.0	0.0526	633.0	1.693	92	694.3	97.9	0.1613	635.0	1.693
31	694.3	85.0	0.0549	633.7	1.693	93	694.3	101.9	0.1636	635.0	1.693
32	694.3	85.0	0.0561	633.7	1.693	94	694.3	101.9	0.1648	635.0	1.693
33	694.3	85.0	0.0597	633.7	1.693	95	696.4	97.9	0.1671	635.0	1.693
34	694.3	85.0	0.0607	633.0	1.693	96	692.9	97.9	0.1684	635.7	1.693
35	692.9	85.0	0.0620	633.7	1.693	97	694.3	101.9	0.1707	635.0	1.693
36	694.3	85.0	0.0632	633.7	1.693	98	694.3	101.9	0.1720	635.0	1.693
37	694.3	85.0	0.0668	633.7	1.693	99	694.3	101.9	0.1742	635.7	1.693
38	692.9	85.0	0.0691	633.7	1.693	100	694.3	97.9	0.1755	635.7	1.693
39	694.3	85.0	0.0704	633.7	1.693	101	694.3	101.9	0.1768	635.7	1.693
40	694.3	85.0	0.0716	633.7	1.693	102	696.4	101.9	0.1791	635.7	1.693
41	694.3	89.4	0.0739	633.7	1.693	103	694.3	101.9	0.1803	635.7	1.693
42	694.3	89.4	0.0752	633.7	1.693	104	694.3	101.9	0.1826	635.7	1.693
43	694.3	85.0	0.0775	633.7	1.693	105	694.3	101.9	0.1814	635.7	1.693
44	694.3	89.4	0.0787	633.7	1.693	106	694.3	101.9	0.1852	635.7	1.693
45	694.3	89.4	0.0810	633.7	1.693	107	694.3	101.9	0.1875	635.7	1.693
46	694.3	89.4	0.0823	633.7	1.693	108	694.3	101.9	0.1900	636.4	1.693
47	694.3	89.4	0.0848	633.7	1.693	109	694.3	101.9	0.1910	636.4	1.693
48	694.3	89.4	0.0859	633.7	1.693	110	694.3	97.9	0.1923	635.7	1.693
49	694.3	89.4	0.0871	633.7	1.693	111	696.4	101.9	0.1935	635.7	1.693
50	694.3	89.4	0.0894	633.7	1.693	112	692.9	101.9	0.1958	635.7	1.693
51	694.3	89.4	0.0919	633.7	1.693	113	694.3	101.9	0.1984	635.7	1.693
52	694.3	89.4	0.0932	634.3	1.693	114	694.3	101.9	0.1994	635.7	1.693
53	694.3	89.4	0.0942	633.7	1.693	115	694.3	101.9	0.2007	635.7	1.693
54	694.3	89.4	0.0968	633.7	1.693	116	694.3	101.9	0.2019	635.7	1.693
55	694.3	89.4	0.0991	633.7	1.693	117	694.3	101.9	0.2042	635.7	1.693
56	694.3	89.4	0.1013	634.3	1.693	118	694.3	101.9	0.2065	636.4	1.693
57	694.3	93.4	0.1013	634.3	1.693	119	694.3	101.9	0.2078	636.4	1.693
58	694.3	93.4	0.1039	634.3	1.693	120	694.3	101.9	0.2103	635.7	1.693
59	694.3	89.4	0.1052	634.3	1.693	121	694.3	106.3	0.2113	635.7	1.693
60	694.3	89.4	0.1062	634.3	1.693	122	694.3	101.9	0.2126	635.7	1.693
61	694.3	89.4	0.1087	634.3	1.693	123	696.4	106.3	0.2149	636.4	1.693
62	694.3	93.4	0.1110	634.3	1.693	124	694.3	101.9	0.2162	636.4	1.693

Table A1. Continued.

#	σ_3 [kPa]	F_a [N]	ΔL [cm]	p_w [kPa]	u_a [μm/s]	#	σ_3 [kPa]	F_a [N]	ΔL [cm]	p_w [kPa]	u_a [μm/s]
125	694.3	101.9	0.2174	635.7	1.693	200	694.3	110.3	0.3477	637.1	1.693
126	694.3	106.3	0.2210	636.4	1.693	201	694.3	110.3	0.3487	637.1	1.693
127	694.3	101.9	0.2233	635.7	1.693	202	694.3	110.3	0.3487	637.1	1.693
128	694.3	101.9	0.2245	635.7	1.693	203	694.3	110.3	0.3513	637.1	1.693
129	694.3	106.3	0.2268	636.4	1.693	204	694.3	110.3	0.3536	637.1	1.693
130	694.3	101.9	0.2281	636.4	1.693	205	694.3	110.3	0.3561	637.8	1.693
131	694.3	106.3	0.2306	636.4	1.693	206	694.3	110.3	0.3571	637.1	1.693
132	694.3	106.3	0.2316	636.4	1.693	207	694.3	114.8	0.3584	637.1	1.693
133	694.3	106.3	0.2329	636.4	1.693	208	694.3	110.3	0.3607	637.1	1.693
134	694.3	106.3	0.2352	636.4	1.693	209	694.3	110.3	0.3620	636.4	1.693
135	694.3	106.3	0.2365	636.4	1.693	210	694.3	110.3	0.3645	637.1	1.693
136	694.3	106.3	0.2377	636.4	1.693	211	694.3	114.8	0.3655	637.1	1.693
137	694.3	106.3	0.2400	636.4	1.693	212	694.3	110.3	0.3680	637.1	1.693
138	694.3	106.3	0.2413	636.4	1.693	213	694.3	110.3	0.3691	637.1	1.693
139	694.3	106.3	0.2436	636.4	1.693	214	694.3	114.8	0.3716	637.1	1.693
140	694.3	106.3	0.2449	636.4	1.693	215	694.3	114.8	0.3716	637.1	1.693
141	694.3	106.3	0.2471	636.4	1.693	216	694.3	110.3	0.3739	637.1	1.693
142	694.3	106.3	0.2484	636.4	1.693	217	694.3	114.8	0.3752	637.1	1.693
143	694.3	106.3	0.2510	636.4	1.693	218	694.3	114.8	0.3774	637.1	1.693
144	694.3	106.3	0.2520	636.4	1.693	219	694.3	110.3	0.3787	637.1	1.693
145	694.3	106.3	0.2532	636.4	1.693	220	694.3	114.8	0.3810	637.1	1.693
146	694.3	101.9	0.2545	636.4	1.693	221	694.3	110.3	0.3835	637.1	1.693
147	694.3	106.3	0.2568	636.4	1.693	222	694.3	110.3	0.3848	636.4	1.693
148	694.3	106.3	0.2591	636.4	1.693	223	692.9	114.8	0.3858	637.1	1.693
149	694.3	110.3	0.2604	636.4	1.693	224	694.3	114.8	0.3884	637.1	1.693
150	694.3	106.3	0.2616	636.4	1.693	225	694.3	114.8	0.3894	637.1	1.693
151	694.3	106.3	0.2639	636.4	1.693	226	694.3	110.3	0.3907	637.1	1.693
152	694.3	106.3	0.2652	636.4	1.693	227	694.3	114.8	0.3929	637.1	1.693
153	694.3	106.3	0.2675	636.4	1.693	228	694.3	114.8	0.3942	637.1	1.693
154	694.3	106.3	0.2687	636.4	1.693	229	694.3	114.8	0.3967	637.1	1.693
155	694.3	106.3	0.2713	636.4	1.693	230	694.3	114.8	0.3978	637.1	1.693
156	694.3	106.3	0.2713	636.4	1.693	231	694.3	114.8	0.3990	637.1	1.693
157	694.3	106.3	0.2736	636.4	1.693	232	694.3	114.8	0.4013	637.1	1.693
158	694.3	106.3	0.2758	636.4	1.693	233	694.3	114.8	0.4039	637.1	1.693
159	694.3	106.3	0.2771	636.4	1.693	234	694.3	114.8	0.4051	636.4	1.693
160	694.3	106.3	0.2784	636.4	1.693	235	694.3	114.8	0.4074	637.1	1.693
161	694.3	110.3	0.2807	636.4	1.693	236	694.3	114.8	0.4074	637.1	1.693
162	694.3	106.3	0.2819	636.4	1.693	237	694.3	114.8	0.4097	637.1	1.693
163	694.3	110.3	0.2842	636.4	1.693	238	694.3	114.8	0.4122	637.1	1.693
164	694.3	106.3	0.2868	637.1	1.693	239	694.3	114.8	0.4133	637.1	1.693
165	694.3	110.3	0.2878	636.4	1.693	240	694.3	114.8	0.4145	637.1	1.693
166	694.3	106.3	0.2891	636.4	1.693	241	694.3	114.8	0.4171	637.1	1.693
167	694.3	110.3	0.2903	636.4	1.693	242	694.3	114.8	0.4194	636.4	1.693
168	692.9	110.3	0.2926	636.4	1.693	243	694.3	114.8	0.4206	637.1	1.693
169	694.3	110.3	0.2951	636.4	1.693	244	694.3	119.2	0.4216	637.1	1.693
170	694.3	106.3	0.2962	637.1	1.693	245	694.3	114.8	0.4229	637.1	1.693
171	694.3	110.3	0.2962	637.1	1.693	246	694.3	114.8	0.4252	637.1	1.693
172	694.3	110.3	0.2997	637.1	1.693	247	694.3	119.2	0.4265	637.1	1.693
173	694.3	110.3	0.3010	637.1	1.693	248	694.3	119.2	0.4290	637.1	1.693
174	694.3	106.3	0.3035	637.1	1.693	249	694.3	114.8	0.4300	637.1	1.693
175	694.3	110.3	0.3045	636.4	1.693	250	694.3	114.8	0.4313	637.1	1.693
176	694.3	110.3	0.3058	637.1	1.693	251	694.3	114.8	0.4336	637.1	1.693
177	694.3	110.3	0.3071	636.4	1.693	252	694.3	119.2	0.4361	637.1	1.693
178	694.3	110.3	0.3094	637.1	1.693	253	692.9	114.8	0.4374	636.4	1.693
179	694.3	110.3	0.3119	637.1	1.693	254	694.3	114.8	0.4384	637.1	1.693
180	694.3	110.3	0.3129	637.1	1.693	255	694.3	119.2	0.4409	637.1	1.693
181	694.3	110.3	0.3142	637.1	1.693	256	694.3	114.8	0.4420	637.1	1.693
182	694.3	110.3	0.3155	636.4	1.693	257	694.3	119.2	0.4432	636.4	1.693
183	694.3	110.3	0.3178	636.4	1.693	258	694.3	119.2	0.4455	637.1	1.693
184	694.3	110.3	0.3200	637.1	1.693	259	694.3	114.8	0.4468	637.1	1.693
185	694.3	110.3	0.3213	637.1	1.693	260	694.3	119.2	0.4493	637.1	1.693
186	694.3	110.3	0.3226	636.4	1.693	261	694.3	114.8	0.4503	637.1	1.693
187	694.3	110.3	0.3249	637.1	1.693	262	694.3	114.8	0.4516	637.1	1.693
188	694.3	110.3	0.3261	637.1	1.693	263	694.3	119.2	0.4539	637.8	1.693
189	694.3	110.3	0.3284	637.1	1.693	264	694.3	119.2	0.4552	637.1	1.693
190	694.3	110.3	0.3297	636.4	1.693	265	694.3	119.2	0.4577	637.1	1.693
191	694.3	110.3	0.3310	637.1	1.693	266	694.3	119.2	0.4587	637.1	1.693
192	694.3	110.3	0.3332	637.1	1.693	267	694.3	114.8	0.4613	637.1	1.693
193	694.3	114.8	0.3345	637.1	1.693	268	694.3	119.2	0.4636	637.1	1.693
194	694.3	110.3	0.3358	636.4	1.693	269	694.3	114.8	0.4648	637.1	1.693
195	694.3	110.3	0.3381	637.1	1.693	270	694.3	119.2	0.4658	637.1	1.693
196	694.3	110.3	0.3393	637.1	1.693	271	694.3	114.8	0.4671	636.4	1.693
197	694.3	110.3	0.3416	637.1	1.693	272	694.3	114.8	0.4707	637.1	1.693
198	694.3	110.3	0.3429	636.4	1.693	273	694.3	119.2	0.4707	637.1	1.693
199	694.3	110.3	0.3452	637.1	1.693	274	694.3	119.2	0.4732	637.1	1.693

Table A1. Continued.

#	σ_3 [kPa]	F_a [N]	ΔL [cm]	p_w [kPa]	u_a [μm/s]
275	694.3	119.2	0.4742	637.1	1.693
276	694.3	119.2	0.4768	637.1	1.693
277	694.3	119.2	0.4780	637.1	1.693
278	694.3	119.2	0.4790	637.1	1.693
279	694.3	114.8	0.4816	637.1	1.693
280	696.4	114.8	0.4826	637.1	1.693
281	694.3	119.2	0.4851	637.1	1.693
282	694.3	119.2	0.4862	637.1	1.693
283	694.3	119.2	0.4887	637.1	1.693
284	694.3	119.2	0.4900	637.1	1.693
285	694.3	114.8	0.4910	636.4	1.693
286	694.3	119.2	0.4935	637.1	1.693
287	694.3	119.2	0.4958	637.1	1.693
288	694.3	119.2	0.4958	637.1	1.693
289	694.3	114.8	0.4981	637.1	1.693
290	694.3	119.2	0.5006	637.1	1.693
291	696.4	119.2	0.5019	637.1	1.693
292	694.3	119.2	0.5029	637.1	1.693
293	694.3	119.2	0.5055	637.1	1.693
294	694.3	119.2	0.5065	637.1	1.693
295	694.3	119.2	0.5090	637.1	1.693
296	694.3	119.2	0.5090	637.1	1.693
297	694.3	119.2	0.5126	637.1	1.693
298	694.3	119.2	0.5138	636.4	1.693
299	694.3	119.2	0.5161	637.1	1.693
300	694.3	119.2	0.5174	637.1	1.693
301	694.3	114.8	0.5184	637.1	1.693
302	694.3	119.2	0.5210	637.1	1.693
303	694.3	119.2	0.5222	637.1	1.693
304	694.3	119.2	0.5245	637.1	1.693
305	694.3	123.2	0.5258	637.1	1.693
306	694.3	119.2	0.5281	637.1	1.693
307	694.3	119.2	0.5293	637.1	1.693
308	694.3	119.2	0.5306	637.1	1.693
309	694.3	119.2	0.5329	637.1	1.693
310	694.3	119.2	0.5342	637.1	1.693
311	694.3	119.2	0.5364	637.1	1.693
312	694.3	119.2	0.5377	637.1	1.693
313	694.3	119.2	0.5400	637.1	1.693
314	694.3	119.2	0.5413	637.1	1.693
315	694.3	123.2	0.5425	636.4	1.693
316	694.3	119.2	0.5448	637.1	1.693
317	694.3	119.2	0.5461	637.1	1.693
318	694.3	119.2	0.5484	637.1	1.693
319	694.3	123.2	0.5497	637.1	1.693
320	694.3	123.2	0.5509	637.1	1.693
321	694.3	119.2	0.5532	637.1	1.693
322	694.3	123.2	0.5545	637.1	1.693
323	694.3	119.2	0.5555	636.4	1.693
324	694.3	123.2	0.5580	637.1	1.693
325	694.3	123.2	0.5603	637.1	1.693
326	694.3	123.2	0.5616	637.1	1.693
327	694.3	123.2	0.5629	637.1	1.693
328	694.3	123.2	0.5639	637.1	1.693
329	694.3	119.2	0.5664	637.1	1.693
330	694.3	119.2	0.5687	637.1	1.693
331	694.3	123.2	0.5687	636.4	1.693
332	694.3	123.2	0.5712	637.1	1.693
333	694.3	123.2	0.5735	637.1	1.693
334	694.3	123.2	0.5758	637.1	1.693
335	694.3	123.2	0.5771	637.1	1.693
336	694.3	119.2	0.5784	637.1	1.693
337	692.9	123.2	0.5806	636.4	1.693
338	694.3	123.2	0.5819	637.1	1.693
339	694.3	119.2	0.5832	637.1	1.693
340	694.3	123.2	0.5855	637.1	1.693
341	694.3	119.2	0.5867	637.1	1.693
342	694.3	123.2	0.5890	637.1	1.693
343	694.3	119.2	0.5903	636.4	1.693
344	694.3	123.2	0.5926	637.1	1.693
345	692.9	123.2	0.5939	637.1	1.693
346	694.3	123.2	0.5961	636.4	1.693
347	694.3	123.2	0.5974	637.1	1.693
348	694.3	123.2	0.5987	637.1	1.693
349	694.3	123.2	0.6010	637.1	1.693
350	694.3	123.2	0.6035	637.1	1.693
351	694.3	123.2	0.6045	637.1	1.693
352	694.3	123.2	0.6058	637.1	1.693
353	694.3	123.2	0.6081	637.1	1.693
354	694.3	123.2	0.6093	637.1	1.693
355	694.3	123.2	0.6106	637.1	1.693
356	694.3	123.2	0.6142	637.1	1.693
357	694.3	123.2	0.6154	637.1	1.693
358	694.3	123.2	0.6177	637.1	1.693
359	694.3	123.2	0.6177	637.1	1.693
360	694.3	123.2	0.6200	637.1	1.693
361	694.3	123.2	0.6213	637.1	1.693
362	694.3	123.2	0.6238	637.1	1.693
363	694.3	123.2	0.6248	637.1	1.693
364	694.3	123.2	0.6274	637.1	1.693
365	694.3	123.2	0.6297	637.1	1.693
366	694.3	123.2	0.6309	637.1	1.693
367	694.3	123.2	0.6320	637.1	1.693
368	694.3	123.2	0.6332	637.1	1.693
369	694.3	123.2	0.6345	637.1	1.693
370	694.3	123.2	0.6368	637.1	1.693
371	694.3	123.2	0.6393	637.1	1.693
372	694.3	123.2	0.6403	637.1	1.693
373	694.3	123.2	0.6416	637.1	1.693
374	692.9	127.7	0.6441	637.1	1.693
375	694.3	127.7	0.6464	637.1	1.693
376	692.9	123.2	0.6464	637.1	1.693
377	692.9	123.2	0.6500	637.1	1.693
378	694.3	123.2	0.6513	637.1	1.693
379	694.3	123.2	0.6523	637.1	1.693
380	694.3	127.7	0.6535	637.1	1.693
381	694.3	123.2	0.6561	636.4	1.693
382	694.3	123.2	0.6584	636.4	1.693
383	694.3	123.2	0.6596	637.1	1.693
384	694.3	123.2	0.6619	637.1	1.693
385	694.3	123.2	0.6632	637.1	1.693
386	694.3	123.2	0.6642	637.1	1.693
387	694.3	123.2	0.6655	637.1	1.693
388	694.3	123.2	0.6690	636.4	1.693
389	694.3	127.7	0.6703	637.1	1.693
390	694.3	123.2	0.6716	636.4	1.693
391	694.3	127.7	0.6739	637.1	1.693
392	694.3	127.7	0.6764	637.1	1.693
393	694.3	123.2	0.6774	636.4	1.693
394	694.3	123.2	0.6800	637.1	1.693
395	694.3	123.2	0.6810	637.1	1.693
396	694.3	127.7	0.6810	637.1	1.693
397	694.3	127.7	0.6835	637.1	1.693
398	694.3	127.7	0.6858	637.1	1.693
399	694.3	123.2	0.6871	636.4	1.693
400	694.3	127.7	0.6894	637.1	1.693
401	694.3	123.2	0.6928	637.1	1.693
402	694.3	123.2	0.6929	637.1	1.693
403	694.3	123.2	0.6942	637.1	1.693
404	694.3	123.2	0.6967	637.1	1.693
405	692.9	127.7	0.6967	637.1	1.693
406	694.3	127.7	0.6990	637.1	1.693
407	694.3	123.2	0.7013	637.1	1.693
408	694.3	127.7	0.7026	636.4	1.693
409	694.3	123.2	0.7049	636.4	1.693
410	694.3	127.7	0.7061	636.4	1.693
411	694.3	127.7	0.7087	637.1	1.693
412	694.3	127.7	0.7097	636.4	1.693
413	694.3	127.7	0.7122	636.4	1.693
414	694.3	123.2	0.7132	637.1	1.693
415	694.3	127.7	0.7158	637.1	1.693
416	694.3	127.7	0.7170	637.1	1.693
417	694.3	127.7	0.7193	637.1	1.693
418	696.4	127.7	0.7193	636.4	1.693
419	694.3	123.2	0.7216	637.1	1.693
420	694.3	127.7	0.7229	637.1	1.693
421	694.3	127.7	0.7264	637.1	1.693
422	694.3	123.2	0.7264	636.4	1.693

Table A1. Continued.

#	σ_3 [kPa]	F_a [N]	ΔL [cm]	p_w [kPa]	u_a [µm/s]
423	694.3	127.7	0.7290	636.4	1.693
424	694.3	127.7	0.7313	637.1	1.693
425	694.3	127.7	0.7325	636.4	1.693
426	694.3	127.7	0.7348	636.4	1.693
427	694.3	127.7	0.7361	636.4	1.693
428	694.3	127.7	0.7371	637.1	1.693
429	694.3	123.2	0.7384	636.4	1.693
430	694.3	127.7	0.7409	636.4	1.693
431	694.3	127.7	0.7419	636.4	1.693
432	694.3	123.2	0.7445	637.1	1.693
433	694.3	123.2	0.7468	636.4	1.693
434	694.3	127.7	0.7480	636.4	1.693
435	694.3	127.7	0.7503	636.4	1.693
436	694.3	127.7	0.7516	637.1	1.693
437	694.3	127.7	0.7539	637.1	1.693
438	694.3	127.7	0.7539	637.1	1.693
439	692.9	127.7	0.7564	637.1	1.693
440	694.3	127.7	0.7587	636.4	1.693
441	694.3	123.2	0.7600	637.1	1.693
442	694.3	127.7	0.7612	636.4	1.693
443	694.3	127.7	0.7635	637.1	1.693
444	694.3	123.2	0.7648	636.4	1.693
445	694.3	127.7	0.7671	636.4	1.693
446	694.3	127.7	0.7684	637.1	1.693
447	692.9	127.7	0.7706	636.4	1.693
448	692.9	127.7	0.7719	637.1	1.693
449	694.3	127.7	0.7742	636.4	1.693
450	694.3	127.7	0.7742	637.1	1.693
451	694.3	127.7	0.7767	636.4	1.693
452	694.3	127.7	0.7790	637.1	1.693
453	694.3	123.2	0.7803	636.4	1.693
454	694.3	127.7	0.7826	636.4	1.693
455	694.3	127.7	0.7838	636.4	1.693
456	694.3	127.7	0.7851	636.4	1.693
457	694.3	127.7	0.7887	637.1	1.693
458	694.3	127.7	0.7899	637.1	1.693
459	694.3	127.7	0.7910	636.4	1.693
460	694.3	127.7	0.7935	636.4	1.693
461	694.3	127.7	0.7945	636.4	1.693
462	694.3	131.7	0.7971	636.4	1.693
463	694.3	127.7	0.7981	636.4	1.693
464	694.3	127.7	0.7993	637.1	1.693
465	694.3	127.7	0.8019	636.4	1.693
466	694.3	127.7	0.8029	637.1	1.693
467	694.3	127.7	0.8042	636.4	1.693
468	694.3	131.7	0.8065	636.4	1.693
469	694.3	127.7	0.8077	637.1	1.693
470	694.3	127.7	0.8103	636.4	1.693
471	694.3	127.7	0.8125	636.4	1.693
472	694.3	127.7	0.8138	636.4	1.693
473	692.9	131.7	0.8148	636.4	1.693
474	692.9	127.7	0.8174	636.4	1.693
475	694.3	127.7	0.8184	636.4	1.693
476	694.3	131.7	0.8209	636.4	1.693
477	694.3	131.7	0.8232	636.4	1.693
478	694.3	127.7	0.8245	636.4	1.693
479	694.3	131.7	0.8258	636.4	1.693
480	694.3	127.7	0.8280	637.1	1.693
481	694.3	127.7	0.8293	636.4	1.693
482	694.3	123.2	0.8303	636.4	1.693
483	694.3	131.7	0.8329	636.4	1.693
484	694.3	131.7	0.8352	637.1	1.693
485	694.3	127.7	0.8364	637.1	1.693
486	692.9	131.7	0.8377	636.4	1.693
487	694.3	123.2	0.8400	636.4	1.693
488	692.9	131.7	0.8412	636.4	1.693
489	694.3	127.7	0.8435	636.4	1.693
490	694.3	131.7	0.8448	636.4	1.693
491	694.3	127.7	0.8461	636.4	1.693
492	694.3	131.7	0.8484	637.1	1.693
493	694.3	131.7	0.8506	636.4	1.693
494	694.3	131.7	0.8532	636.4	1.693
495	694.3	131.7	0.8545	636.4	1.693
496	694.3	131.7	0.8555	636.4	1.693
497	692.9	127.7	0.8567	636.4	1.693
498	694.3	127.7	0.8590	636.4	1.693
499	694.3	127.7	0.8603	636.4	1.693
500	694.3	131.7	0.8616	636.4	1.693
501	694.3	131.7	0.8639	636.4	1.693
502	694.3	131.7	0.8664	636.4	1.693
503	694.3	131.7	0.8674	636.4	1.693
504	694.3	131.7	0.8687	637.1	1.693
505	694.3	131.7	0.8710	636.4	1.693
506	694.3	127.7	0.8722	637.1	1.693
507	694.3	131.7	0.8748	636.4	1.693
508	694.3	127.7	0.8758	636.4	1.693
509	692.9	127.7	0.8783	636.4	1.693
510	694.3	127.7	0.8793	636.4	1.693
511	694.3	127.7	0.8806	636.4	1.693
512	694.3	127.7	0.8832	636.4	1.693
513	694.3	127.7	0.8842	636.4	1.693
514	694.3	131.7	0.8867	636.4	1.693
515	694.3	131.7	0.8890	636.4	1.693
516	694.3	127.7	0.8903	636.4	1.693
517	694.3	131.7	0.8913	636.4	1.693
518	694.3	127.7	0.8938	636.4	1.693
519	694.3	131.7	0.8951	636.4	1.693
520	692.9	131.7	0.8974	636.4	1.693
521	694.3	131.7	0.8987	637.1	1.693
522	694.3	131.7	0.9009	636.4	1.693
523	694.3	127.7	0.9022	636.4	1.693
524	694.3	131.7	0.9045	636.4	1.693
525	694.3	131.7	0.9058	636.4	1.693
526	694.3	131.7	0.9081	636.4	1.693
527	694.3	131.7	0.9093	636.4	1.693
528	694.3	131.7	0.9116	636.4	1.693
529	694.3	131.7	0.9129	636.4	1.693
530	694.3	131.7	0.9141	636.4	1.693
531	692.9	127.7	0.9164	636.4	1.693
532	694.3	131.7	0.9177	636.4	1.693
533	694.3	131.7	0.9200	636.4	1.693
534	694.3	131.7	0.9213	636.4	1.693
535	694.3	131.7	0.9235	636.4	1.693
536	694.3	131.7	0.9261	636.4	1.693
537	694.3	131.7	0.9261	636.4	1.693
538	694.3	127.7	0.9284	637.1	1.693
539	694.3	131.7	0.9309	636.4	1.693
540	694.3	131.7	0.9319	636.4	1.693
541	692.9	131.7	0.9345	636.4	1.693
542	694.3	131.7	0.9357	636.4	1.693
543	694.3	131.7	0.9380	636.4	1.693
544	694.3	131.7	0.9393	636.4	1.693
545	694.3	127.7	0.9403	636.4	1.693
546	694.3	127.7	0.9428	636.4	1.693
547	694.3	131.7	0.9439	636.4	1.693
548	694.3	131.7	0.9464	637.1	1.693
549	692.9	131.7	0.9487	637.1	1.693
550	694.3	131.7	0.9500	636.4	1.693
551	694.3	131.7	0.9512	636.4	1.693
552	694.3	131.7	0.9522	636.4	1.693
553	694.3	131.7	0.9548	636.4	1.693
554	694.3	131.7	0.9561	636.4	1.693
555	694.3	131.7	0.9583	636.4	1.693
556	694.3	131.7	0.9596	636.4	1.693
557	694.3	131.7	0.9606	636.4	1.693
558	694.3	131.7	0.9632	637.1	1.693
559	694.3	131.7	0.9655	636.4	1.693
560	696.4	131.7	0.9667	636.4	1.693
561	694.3	131.7	0.9690	636.4	1.693
562	694.3	144.6	0.9942	639.9	42.333
563	694.3	144.6	1.1222	638.5	42.333
564	694.3	153.0	1.2499	636.4	42.333
565	694.3	148.6	1.3790	635.0	42.333
566	692.9	148.6	1.5070	634.3	42.333
567	694.3	157.5	1.6490	633.7	42.333
568	694.3	144.6	1.7280	630.9	42.333
569	692.9	127.7	1.7280	630.2	42.333
570	694.3	127.7	1.7280	629.5	42.333
571	694.3	127.7	2.4887	630.2	42.333

Table A2. Data for the undrained triaxial compression test U2.

Date:	02/23/95
Sample material:	undisturbed UpB till, core 92-1
Initial weight:	255.9 gram
Pre-shear length:	7.40 cm
Pre-shear radius:	2.12 cm
Void ratio:	0.437
Saturation pressure:	626.8 kPa

#	σ_3 [kPa]	F_a [N]	ΔL [cm]	p_w [kPa]	u_a [µm/s]	#	σ_3 [kPa]	F_a [N]	ΔL [cm]	p_w [kPa]	u_a [µm/s]
1	832.2	0.0	0.0000	626.8	1.693	61	832.2	221.1	0.1339	685.4	1.693
2	832.2	16.9	0.0013	627.4	1.693	62	832.2	225.1	0.1364	685.4	1.693
3	832.2	33.8	0.0036	630.9	1.693	63	832.2	225.1	0.1400	686.1	1.693
4	832.2	59.6	0.0048	633.7	1.693	64	832.2	225.1	0.1435	686.7	1.693
5	832.2	85.0	0.0074	636.4	1.693	65	832.2	225.1	0.1448	686.7	1.693
6	832.2	101.9	0.0097	639.2	1.693	66	832.2	225.1	0.1471	687.4	1.693
7	832.2	118.8	0.0119	641.9	1.693	67	832.2	229.5	0.1494	687.4	1.693
8	832.2	127.7	0.0145	643.3	1.693	68	834.3	225.1	0.1519	688.1	1.693
9	830.8	136.1	0.0168	644.7	1.693	69	832.2	229.5	0.1542	688.1	1.693
10	832.2	144.6	0.0193	646.8	1.693	70	832.2	229.5	0.1567	688.8	1.693
11	832.2	148.6	0.0216	647.4	1.693	71	834.3	229.5	0.1590	689.5	1.693
12	832.2	153.0	0.0229	648.8	1.693	72	832.2	229.5	0.1615	689.5	1.693
13	832.2	157.0	0.0251	649.5	1.693	73	832.2	229.5	0.1638	690.2	1.693
14	834.3	161.5	0.0277	650.9	1.693	74	832.2	229.5	0.1651	690.2	1.693
15	832.2	165.9	0.0287	652.3	1.693	75	832.2	233.5	0.1687	690.2	1.693
16	832.2	165.9	0.0323	653.0	1.693	76	830.8	233.5	0.1697	690.9	1.693
17	832.2	165.9	0.0335	654.3	1.693	77	832.2	233.5	0.1722	690.9	1.693
18	832.2	169.9	0.0361	654.3	1.693	78	832.2	233.5	0.1758	691.6	1.693
19	832.2	174.4	0.0384	655.0	1.693	79	832.2	233.5	0.1770	691.6	1.693
20	832.2	178.4	0.0406	656.4	1.693	80	832.2	233.5	0.1793	692.3	1.693
21	832.2	178.4	0.0419	656.4	1.693	81	832.2	229.5	0.1829	692.3	1.693
22	832.2	182.8	0.0455	657.8	1.693	82	832.2	233.5	0.1854	692.9	1.693
23	832.2	182.8	0.0467	659.2	1.693	83	832.2	233.5	0.1877	692.9	1.693
24	830.8	182.8	0.0490	659.9	1.693	84	832.2	233.5	0.1890	693.6	1.693
25	832.2	186.8	0.0516	660.5	1.693	85	832.2	238.0	0.1913	693.6	1.693
26	832.2	186.8	0.0538	661.9	1.693	86	832.2	233.5	0.1938	694.3	1.693
27	832.2	186.8	0.0564	661.9	1.693	87	832.2	238.0	0.1961	694.3	1.693
28	834.3	191.3	0.0587	664.0	1.693	88	832.2	238.0	0.1984	694.3	1.693
29	832.2	191.3	0.0610	664.0	1.693	89	832.2	238.0	0.2009	695.0	1.693
30	832.2	191.3	0.0635	665.4	1.693	90	832.2	238.0	0.2045	695.0	1.693
31	832.2	191.3	0.0645	666.1	1.693	91	832.2	238.0	0.2057	695.7	1.693
32	832.2	195.3	0.0671	666.7	1.693	92	832.2	238.0	0.2080	695.0	1.693
33	832.2	195.3	0.0706	668.1	1.693	93	832.2	238.0	0.2103	695.7	1.693
34	832.2	199.7	0.0729	668.8	1.693	94	830.8	238.0	0.2141	697.1	1.693
35	832.2	199.7	0.0754	669.5	1.693	95	832.2	238.0	0.2151	697.1	1.693
36	832.2	195.3	0.0765	669.5	1.693	96	832.2	238.0	0.2187	697.1	1.693
37	832.2	199.7	0.0790	670.2	1.693	97	832.2	242.4	0.2200	697.1	1.693
38	832.2	199.7	0.0813	670.9	1.693	98	832.2	242.4	0.2223	697.8	1.693
39	832.2	204.2	0.0848	672.3	1.693	99	832.2	242.4	0.2261	697.8	1.693
40	832.2	204.2	0.0861	672.3	1.693	100	832.2	242.4	0.2271	698.5	1.693
41	832.2	208.2	0.0886	673.0	1.693	101	832.2	242.4	0.2296	698.5	1.693
42	832.2	208.2	0.0909	674.3	1.693	102	832.2	246.4	0.2332	698.5	1.693
43	832.2	208.2	0.0932	674.3	1.693	103	832.2	246.4	0.2344	699.2	1.693
44	832.2	208.2	0.0945	675.7	1.693	104	832.2	242.4	0.2367	698.5	1.693
45	832.2	208.2	0.0968	676.4	1.693	105	832.2	246.4	0.2380	699.2	1.693
46	832.2	208.2	0.1006	677.1	1.693	106	832.2	246.4	0.2416	699.2	1.693
47	832.2	212.6	0.1016	677.1	1.693	107	832.2	246.4	0.2438	699.8	1.693
48	832.2	212.6	0.1041	678.5	1.693	108	832.2	246.4	0.2464	699.8	1.693
49	832.2	212.6	0.1064	678.5	1.693	109	832.2	246.4	0.2487	699.8	1.693
50	832.2	212.6	0.1090	679.2	1.693	110	832.2	246.4	0.2510	699.8	1.693
51	832.2	212.6	0.1113	679.8	1.693	111	832.2	246.4	0.2522	699.8	1.693
52	832.2	212.6	0.1135	680.5	1.693	112	832.2	246.4	0.2548	700.5	1.693
53	832.2	216.6	0.1161	680.5	1.693	113	832.2	246.4	0.2583	700.5	1.693
54	832.2	216.6	0.1184	681.9	1.693	114	832.2	250.9	0.2606	700.5	1.693
55	832.2	221.1	0.1209	681.9	1.693	115	832.2	250.9	0.2629	700.5	1.693
56	832.2	212.6	0.1232	682.6	1.693	116	832.2	250.9	0.2654	701.2	1.693
57	832.2	216.6	0.1255	683.3	1.693	117	832.2	250.9	0.2677	701.2	1.693
58	832.2	221.1	0.1293	684.0	1.693	118	832.2	250.9	0.2703	701.2	1.693
59	832.2	221.1	0.1303	684.0	1.693	119	832.2	250.9	0.2713	701.9	1.693
60	832.2	221.1	0.1328	684.7	1.693	120	832.2	250.9	0.2751	701.9	1.693

Table A2. Continued.

#	σ_3 [kPa]	F_a [N]	ΔL [cm]	p_w [kPa]	u_a [µm/s]
121	834.3	250.9	0.2774	701.9	1.693
122	832.2	250.9	0.2797	701.9	1.693
123	832.2	250.9	0.2822	702.6	1.693
124	832.2	250.9	0.2845	702.6	1.693
125	832.2	254.9	0.2870	702.6	1.693
126	832.2	250.9	0.2893	702.6	1.693
127	832.2	250.9	0.2916	702.6	1.693
128	832.2	254.9	0.2941	703.3	1.693
129	832.2	254.9	0.2964	703.3	1.693
130	832.2	254.9	0.2990	702.6	1.693
131	832.2	254.9	0.3012	703.3	1.693
132	832.2	254.9	0.3035	703.3	1.693
133	832.2	254.9	0.3061	704.0	1.693
134	832.2	250.9	0.3084	704.0	1.693
135	832.2	254.9	0.3109	704.0	1.693
136	832.2	259.3	0.3119	703.3	1.693
137	832.2	254.9	0.3155	704.0	1.693
138	832.2	254.9	0.3167	704.0	1.693
139	832.2	254.9	0.3203	704.0	1.693
140	832.2	254.9	0.3228	704.7	1.693
141	832.2	254.9	0.3251	704.7	1.693
142	832.2	259.3	0.3277	704.0	1.693
143	832.2	254.9	0.3299	704.7	1.693
144	832.2	259.3	0.3312	704.7	1.693
145	832.2	259.3	0.3335	704.7	1.693
146	830.8	259.3	0.3371	704.7	1.693
147	832.2	259.3	0.3396	705.4	1.693
148	832.2	254.9	0.3419	705.4	1.693
149	832.2	259.3	0.3442	705.4	1.693
150	832.2	259.3	0.3467	705.4	1.693
151	832.2	259.3	0.3490	706.0	1.693
152	832.2	259.3	0.3515	705.4	1.693
153	832.2	259.3	0.3538	705.4	1.693
154	832.2	259.3	0.3561	706.0	1.693
155	832.2	259.3	0.3574	706.0	1.693
156	832.2	259.3	0.3599	706.0	1.693
157	832.2	259.3	0.3622	706.0	1.693
158	832.2	259.3	0.3645	706.0	1.693
159	830.8	259.3	0.3683	706.7	1.693
160	832.2	263.3	0.3693	706.7	1.693
161	832.2	263.3	0.3729	706.7	1.693
162	832.2	263.3	0.3754	706.7	1.693
163	832.2	263.3	0.3777	706.7	1.693
164	832.2	259.3	0.3802	706.7	1.693
165	832.2	263.3	0.3813	706.7	1.693
166	830.8	263.3	0.3838	706.7	1.693
167	832.2	263.3	0.3861	706.7	1.693
168	832.2	267.8	0.3874	706.7	1.693
169	832.2	263.3	0.3909	706.7	1.693
170	832.2	263.3	0.3945	706.7	1.693
171	832.2	263.3	0.3957	706.7	1.693
172	832.2	267.8	0.3993	706.7	1.693
173	832.2	263.3	0.4016	706.7	1.693
174	832.2	263.3	0.4041	706.7	1.693
175	832.2	263.3	0.4051	706.7	1.693
176	832.2	263.3	0.4077	706.7	1.693
177	832.2	263.3	0.4112	707.4	1.693
178	834.3	263.3	0.4148	707.4	1.693
179	832.2	267.8	0.4161	707.4	1.693
180	832.2	263.3	0.4183	706.7	1.693
181	832.2	267.8	0.4196	706.7	1.693
182	832.2	267.8	0.4219	707.4	1.693
183	830.8	267.8	0.4255	707.4	1.693
184	832.2	267.8	0.4280	707.4	1.693
185	832.2	267.8	0.4290	707.4	1.693
186	832.2	267.8	0.4328	707.4	1.693
187	832.2	267.8	0.4338	707.4	1.693
188	832.2	267.8	0.4364	707.4	1.693
189	832.2	267.8	0.4387	707.4	1.693
190	832.2	267.8	0.4422	707.4	1.693
191	832.2	267.8	0.4448	707.4	1.693
192	832.2	267.8	0.4458	707.4	1.693
193	832.2	271.8	0.4493	707.4	1.693
194	830.8	267.8	0.4519	707.4	1.693
195	830.8	267.8	0.4542	708.1	1.693
196	832.2	267.8	0.4554	708.1	1.693
197	832.2	267.8	0.4590	708.1	1.693
198	832.2	267.8	0.4613	708.1	1.693
199	832.2	271.8	0.4638	707.4	1.693
200	832.2	267.8	0.4651	707.4	1.693
201	832.2	267.8	0.4674	708.1	1.693
202	832.2	271.8	0.4709	708.1	1.693
203	832.2	271.8	0.4735	708.1	1.693
204	830.8	271.8	0.4757	708.1	1.693
205	832.2	271.8	0.4780	708.1	1.693
206	832.2	250.9	0.4816	707.4	1.693
207	832.2	246.4	0.4816	707.4	1.693
208	832.2	246.4	0.4829	706.7	1.693
209	832.2	301.6	0.5164	708.8	42.333
210	830.8	301.6	0.5809	704.7	42.333
211	832.2	297.6	0.6431	701.2	42.333
212	832.2	301.6	0.7041	698.5	42.333
213	832.2	301.6	0.7673	695.7	42.333
214	832.2	301.6	0.8306	692.9	42.333
215	832.2	306.0	0.8941	692.3	42.333
216	832.2	306.0	0.9622	690.2	42.333
217	832.2	306.0	1.0267	689.5	42.333
218	832.2	301.6	1.0899	689.5	42.333
219	832.2	306.0	1.1544	688.8	42.333
220	832.2	306.0	1.2189	688.1	42.333
221	832.2	306.0	1.2837	688.1	42.333
222	832.2	306.0	1.3528	688.1	42.333
223	832.2	306.0	1.4186	688.1	42.333

Table A3. Data for the undrained triaxial compression test U3.

Date:	02/23/95
Sample material:	undisturbed UpB till, core 92-1
Initial weight:	255.6 gram
Pre-shear length:	8.30 cm
Pre-shear radius:	2.02 cm
Void ratio:	0.412
Saturation pressure:	627.4 kPa

#	σ_3 [kPa]	F_a [N]	ΔL [cm]	p_w [kPa]	u_a [µm/s]	#	σ_3 [kPa]	F_a [N]	ΔL [cm]	p_w [kPa]	u_a [µm/s]
1	972.2	0.0	0.0000	627.4	1.693	61	970.1	322.9	0.1471	723.4	1.693
2	970.1	25.4	0.0013	630.0	1.693	62	968.7	322.9	0.1494	724.5	1.693
3	970.1	63.6	0.0036	634.2	1.693	63	970.1	326.9	0.1506	724.0	1.693
4	970.1	101.9	0.0048	636.4	1.693	64	970.1	322.9	0.1529	725.3	1.693
5	970.1	131.7	0.0071	640.4	1.693	65	970.1	326.9	0.1565	726.0	1.693
6	970.1	157.0	0.0097	644.4	1.693	66	970.1	326.9	0.1590	725.8	1.693
7	972.2	173.9	0.0119	648.6	1.693	67	970.1	331.4	0.1603	726.8	1.693
8	970.1	182.8	0.0145	651.5	1.693	68	970.1	331.4	0.1638	726.8	1.693
9	970.1	195.3	0.0155	652.8	1.693	69	970.1	331.4	0.1648	727.6	1.693
10	970.1	199.7	0.0180	656.1	1.693	70	970.1	331.4	0.1684	727.7	1.693
11	970.1	208.2	0.0191	657.3	1.693	71	970.1	331.4	0.1697	727.9	1.693
12	970.1	216.6	0.0216	661.2	1.693	72	970.1	335.4	0.1722	728.4	1.693
13	970.1	221.1	0.0239	663.8	1.693	73	970.1	335.4	0.1745	729.5	1.693
14	970.1	225.1	0.0264	665.8	1.693	74	970.1	335.4	0.1768	729.2	1.693
15	970.1	229.5	0.0274	667.5	1.693	75	970.1	335.4	0.1806	729.7	1.693
16	970.1	233.5	0.0300	669.4	1.693	76	970.1	335.4	0.1816	729.8	1.693
17	972.2	238.0	0.0323	671.6	1.693	77	968.7	339.8	0.1829	729.9	1.693
18	970.1	242.0	0.0335	673.5	1.693	78	970.1	339.8	0.1864	731.2	1.693
19	970.1	242.0	0.0371	676.6	1.693	79	970.1	339.8	0.1887	731.5	1.693
20	972.2	246.4	0.0384	677.0	1.693	80	970.1	344.3	0.1913	731.9	1.693
21	970.1	246.4	0.0406	671.4	1.693	81	970.1	339.8	0.1935	732.1	1.693
22	970.1	225.1	0.0610	679.0	1.693	82	970.1	344.3	0.1961	731.8	1.693
23	970.1	203.7	0.0574	686.2	1.693	83	970.1	344.3	0.1996	733.0	1.693
24	970.1	254.9	0.0597	692.6	1.693	84	970.1	344.3	0.2009	732.5	1.693
25	970.1	267.8	0.0622	694.7	1.693	85	970.1	344.3	0.2032	733.5	1.693
26	968.7	271.8	0.0645	695.2	1.693	86	970.1	348.3	0.2055	733.1	1.693
27	970.1	276.2	0.0671	696.6	1.693	87	970.1	348.3	0.2080	734.1	1.693
28	970.1	280.2	0.0693	697.8	1.693	88	970.1	348.3	0.2103	734.4	1.693
29	970.1	280.2	0.0706	698.5	1.693	89	970.1	352.7	0.2129	734.8	1.693
30	968.7	284.7	0.0742	700.3	1.693	90	970.1	348.3	0.2151	735.0	1.693
31	970.1	284.7	0.0752	701.5	1.693	91	970.1	352.7	0.2174	735.2	1.693
32	970.1	284.7	0.0777	702.0	1.693	92	970.1	348.3	0.2200	734.9	1.693
33	970.1	288.7	0.0800	702.9	1.693	93	970.1	352.7	0.2210	735.1	1.693
34	970.1	288.7	0.0836	704.5	1.693	94	970.1	352.7	0.2248	736.2	1.693
35	970.1	293.1	0.0848	704.9	1.693	95	970.1	356.7	0.2248	736.2	1.693
36	970.1	293.1	0.0874	706.0	1.693	96	970.1	352.7	0.2283	736.7	1.693
37	968.7	293.1	0.0909	708.0	1.693	97	970.1	352.7	0.2319	736.3	1.693
38	970.1	293.1	0.0932	708.2	1.693	98	970.1	356.7	0.2342	737.2	1.693
39	970.1	293.1	0.0945	709.3	1.693	99	970.1	356.7	0.2367	737.0	1.693
40	970.1	297.6	0.0980	710.5	1.693	100	970.1	356.7	0.2377	737.0	1.693
41	970.1	297.6	0.0993	710.8	1.693	101	970.1	356.7	0.2413	736.9	1.693
42	970.1	297.6	0.1016	711.0	1.693	102	970.1	356.7	0.2438	738.2	1.693
43	970.1	301.6	0.1052	712.8	1.693	103	968.7	361.2	0.2461	738.3	1.693
44	970.1	306.0	0.1064	713.2	1.693	104	970.1	361.2	0.2474	738.6	1.693
45	970.1	306.0	0.1087	714.0	1.693	105	970.1	361.2	0.2510	740.0	1.693
46	970.1	306.0	0.1113	714.1	1.693	106	968.7	365.2	0.2535	740.9	1.693
47	970.1	306.0	0.1135	715.5	1.693	107	970.1	365.2	0.2545	741.3	1.693
48	968.7	310.0	0.1171	716.6	1.693	108	970.1	365.2	0.2581	741.1	1.693
49	970.1	310.0	0.1196	717.3	1.693	109	970.1	365.2	0.2593	740.7	1.693
50	970.1	310.0	0.1219	717.2	1.693	110	970.1	365.2	0.2616	740.8	1.693
51	970.1	314.5	0.1232	717.6	1.693	111	970.1	365.2	0.2642	740.7	1.693
52	970.1	314.5	0.1255	718.9	1.693	112	970.1	365.2	0.2664	740.7	1.693
53	970.1	314.5	0.1280	719.6	1.693	113	970.1	365.2	0.2677	740.9	1.693
54	970.1	314.5	0.1303	720.3	1.693	114	970.1	369.6	0.2713	741.5	1.693
55	970.1	318.5	0.1326	720.1	1.693	115	970.1	369.6	0.2738	740.8	1.693
56	970.1	318.5	0.1351	721.3	1.693	116	970.1	369.6	0.2761	741.5	1.693
57	970.1	318.5	0.1374	721.2	1.693	117	970.1	369.6	0.2784	741.7	1.693
58	970.1	322.9	0.1400	721.8	1.693	118	968.7	369.6	0.2809	742.0	1.693
59	970.1	322.9	0.1422	723.1	1.693	119	970.1	369.6	0.2819	741.6	1.693
60	970.1	322.9	0.1445	723.5	1.693	120	970.1	369.6	0.2858	742.1	1.693

Table A3. Continued.

#	σ_3 [kPa]	F_a [N]	ΔL [cm]	p_w [kPa]	u_a [μm/s]
121	970.1	369.6	0.2880	742.0	1.693
122	970.1	369.6	0.2893	742.6	1.693
123	970.1	378.1	0.2929	742.7	1.693
124	970.1	373.7	0.2939	742.6	1.693
125	970.1	373.7	0.2977	742.9	1.693
126	970.1	373.7	0.3000	743.1	1.693
127	970.1	373.7	0.3012	743.3	1.693
128	970.1	373.7	0.3048	743.8	1.693
129	970.1	373.7	0.3061	743.4	1.693
130	970.1	373.7	0.3084	743.9	1.693
131	970.1	373.7	0.3106	743.7	1.693
132	970.1	378.1	0.3142	743.6	1.693
133	970.1	378.1	0.3142	744.0	1.693
134	970.1	378.1	0.3180	744.0	1.693
135	968.7	378.1	0.3190	744.5	1.693
136	970.1	378.1	0.3226	744.4	1.693
137	970.1	378.1	0.3251	745.0	1.693
138	970.1	378.1	0.3274	744.9	1.693
139	970.1	378.1	0.3299	744.7	1.693
140	970.1	378.1	0.3322	745.4	1.693
141	970.1	378.1	0.3345	745.4	1.693
142	970.1	378.1	0.3371	745.4	1.693
143	970.1	378.1	0.3393	746.1	1.693
144	968.7	378.1	0.3419	745.5	1.693
145	970.1	382.5	0.3429	745.5	1.693
146	970.1	382.5	0.3467	746.3	1.693
147	970.1	382.5	0.3490	746.4	1.693
148	970.1	382.5	0.3503	745.8	1.693
149	970.1	382.5	0.3526	746.6	1.693
150	970.1	382.5	0.3548	746.6	1.693
151	970.1	382.5	0.3574	746.7	1.693
152	970.1	386.6	0.3609	746.3	1.693
153	970.1	386.6	0.3632	747.1	1.693
154	970.1	386.6	0.3645	747.1	1.693
155	970.1	386.6	0.3680	747.4	1.693
156	970.1	386.6	0.3706	746.9	1.693
157	970.1	386.6	0.3716	747.7	1.693
158	970.1	386.6	0.3752	747.9	1.693
159	970.1	386.6	0.3777	747.5	1.693
160	970.1	386.6	0.3790	747.7	1.693
161	970.1	386.6	0.3825	747.9	1.693
162	970.1	386.6	0.3835	748.1	1.693
163	970.1	386.6	0.3871	747.7	1.693
164	970.1	386.6	0.3896	748.6	1.693
165	970.1	386.6	0.3919	748.2	1.693
166	970.1	386.6	0.3945	748.5	1.693
167	968.7	386.6	0.3967	748.7	1.693
168	970.1	386.6	0.3993	749.0	1.693
169	970.1	391.0	0.4016	748.7	1.693
170	970.1	391.0	0.4039	748.9	1.693
171	970.1	391.0	0.4064	749.3	1.693
172	968.7	386.6	0.4087	748.9	1.693
173	970.1	386.6	0.4112	749.2	1.693
174	970.1	391.0	0.4122	749.5	1.693
175	970.1	391.0	0.4158	749.2	1.693
176	970.1	391.0	0.4196	749.7	1.693
177	970.1	391.0	0.4206	750.0	1.693
178	970.1	391.0	0.4242	749.6	1.693
179	970.1	391.0	0.4267	750.0	1.693
180	970.1	391.0	0.4290	749.5	1.693
181	968.7	391.0	0.4303	749.8	1.693
182	970.1	391.0	0.4338	750.2	1.693
183	970.1	391.0	0.4351	750.5	1.693
184	968.7	395.0	0.4374	750.9	1.693
185	970.1	395.0	0.4409	750.6	1.693
186	970.1	395.0	0.4435	751.0	1.693
187	970.1	391.0	0.4458	750.8	1.693
188	968.7	395.0	0.4481	750.6	1.693
189	970.1	395.0	0.4506	750.4	1.693
190	970.1	395.0	0.4529	750.8	1.693
191	970.1	395.0	0.4542	750.6	1.693
192	968.7	391.0	0.4577	751.1	1.693
193	970.1	395.0	0.4600	751.5	1.693
194	970.1	395.0	0.4625	751.1	1.693
195	970.1	395.0	0.4648	751.5	1.693
196	970.1	395.0	0.4674	751.1	1.693
197	970.1	395.0	0.4684	751.5	1.693
198	970.1	395.0	0.4722	752.0	1.693
199	970.1	395.0	0.4745	751.7	1.693
200	970.1	395.0	0.4768	752.1	1.693
201	970.1	395.0	0.4793	751.8	1.693
202	970.1	399.5	0.4816	751.5	1.693
203	970.1	395.0	0.4841	752.1	1.693
204	970.1	395.0	0.4864	752.5	1.693
205	970.1	399.5	0.4887	752.3	1.693
206	970.1	399.5	0.4912	752.1	1.693
207	970.1	395.0	0.4935	751.8	1.693
208	970.1	399.5	0.4961	752.2	1.693
209	970.1	395.0	0.4983	752.6	1.693
210	970.1	399.5	0.5006	752.5	1.693
211	970.1	395.0	0.5032	752.9	1.693
212	970.1	399.5	0.5055	753.5	1.693
213	970.1	395.0	0.5080	752.9	1.693
214	970.1	399.5	0.5103	752.1	1.693
215	970.1	403.5	0.5174	753.2	1.693
216	970.1	467.5	0.5174	752.4	1.693
217	970.1	441.7	0.5377	755.7	42.333
218	970.1	433.3	0.5977	751.6	42.333
219	970.1	433.3	0.6596	748.8	42.333
220	970.1	429.3	0.7267	746.0	42.333
221	970.1	420.8	0.7887	744.7	42.333
222	970.1	420.8	0.8522	743.3	42.333
223	970.1	411.9	0.9167	741.9	42.333
224	970.1	407.9	0.9787	740.5	42.333
225	970.1	399.5	1.0434	740.5	42.333
226	968.7	395.0	1.1151	739.8	42.333
227	970.1	395.0	1.1770	741.2	42.333
228	970.1	391.0	1.2418	741.9	42.333
229	970.1	382.5	1.3063	741.9	42.333
230	970.1	378.1	1.3708	741.9	42.333
231	970.1	378.1	1.4364	742.6	42.333
232	970.1	373.7	1.5022	742.6	42.333
233	970.1	373.7	1.5715	744.0	42.333
234	970.1	373.7	1.6360	744.7	42.333
235	970.1	331.4	1.6480	740.5	42.333

Table A4. Data for the undrained triaxial compression test R1.

Date:	05/23/95
Sample material:	remolded UpB till, core 92-1
Initial weight:	232.7 gram
Pre-shear length:	6.50 cm
Pre-shear radius:	2.16 cm
Void ratio:	0.425
Saturation pressure:	510.2 kPa

#	σ_3 [kPa]	F_a [N]	ΔL [cm]	p_w [kPa]	u_a [µm/s]	#	σ_3 [kPa]	F_a [N]	ΔL [cm]	p_w [kPa]	u_a [µm/s]
1	791.5	0.0	0.0000	510.2	1.693	61	791.5	341.2	0.0503	588.1	1.693
2	791.5	0.0	0.0000	510.2	1.693	62	791.5	341.2	0.0516	588.1	1.693
3	791.5	4.4	0.0013	510.9	1.693	63	791.5	341.2	0.0516	588.1	1.693
4	791.5	4.4	0.0025	510.9	1.693	64	791.5	345.6	0.0526	589.5	1.693
5	791.5	13.3	0.0036	513.0	1.693	65	791.5	345.6	0.0538	590.2	1.693
6	791.5	30.7	0.0036	515.1	1.693	66	791.5	345.6	0.0551	590.2	1.693
7	791.5	56.9	0.0048	517.1	1.693	67	791.5	345.6	0.0561	590.2	1.693
8	791.5	78.7	0.0048	519.2	1.693	68	792.9	345.6	0.0574	590.2	1.693
9	791.5	100.5	0.0061	521.3	1.693	69	791.5	349.6	0.0574	590.9	1.693
10	791.5	118.3	0.0071	524.0	1.693	70	791.5	349.6	0.0587	590.9	1.693
11	791.5	135.7	0.0071	526.1	1.693	71	791.5	349.6	0.0587	590.9	1.693
12	791.5	153.0	0.0071	528.8	1.693	72	791.5	354.1	0.0597	591.6	1.693
13	789.5	166.4	0.0084	530.9	1.693	73	791.5	349.6	0.0610	591.6	1.693
14	792.9	179.3	0.0097	532.3	1.693	74	791.5	354.1	0.0610	592.3	1.693
15	791.5	192.6	0.0109	535.1	1.693	75	791.5	354.1	0.0622	592.3	1.693
16	791.5	201.1	0.0109	537.8	1.693	76	791.5	354.1	0.0635	592.3	1.693
17	791.5	210.0	0.0119	539.9	1.693	77	791.5	354.1	0.0645	592.3	1.693
18	792.9	218.9	0.0132	542.6	1.693	78	791.5	354.1	0.0645	592.3	1.693
19	791.5	227.3	0.0145	545.4	1.693	79	791.5	358.5	0.0658	593.7	1.693
20	791.5	236.2	0.0145	548.2	1.693	80	791.5	354.1	0.0671	593.7	1.693
21	791.5	240.6	0.0155	550.2	1.693	81	791.5	354.1	0.0681	593.7	1.693
22	791.5	249.1	0.0168	553.0	1.693	82	791.5	354.1	0.0681	593.7	1.693
23	791.5	249.1	0.0180	555.0	1.693	83	791.5	358.5	0.0693	594.3	1.693
24	791.5	258.0	0.0180	557.8	1.693	84	791.5	358.5	0.0693	594.3	1.693
25	791.5	262.4	0.0193	559.2	1.693	85	791.5	358.5	0.0706	594.3	1.693
26	792.9	266.9	0.0203	561.3	1.693	86	791.5	358.5	0.0719	594.3	1.693
27	791.5	271.3	0.0203	563.3	1.693	87	791.5	363.0	0.0729	595.0	1.693
28	791.5	275.3	0.0216	565.4	1.693	88	791.5	363.0	0.0729	595.0	1.693
29	791.5	279.8	0.0216	567.5	1.693	89	791.5	358.5	0.0742	595.0	1.693
30	791.5	284.2	0.0229	568.8	1.693	90	789.5	363.0	0.0754	595.7	1.693
31	791.5	288.7	0.0239	570.9	1.693	91	791.5	363.0	0.0765	596.4	1.693
32	791.5	293.1	0.0251	572.3	1.693	92	791.5	367.4	0.0765	597.1	1.693
33	791.5	293.1	0.0264	573.0	1.693	93	791.5	363.0	0.0777	597.1	1.693
34	791.5	297.6	0.0274	574.4	1.693	94	791.5	363.0	0.0790	597.1	1.693
35	791.5	301.6	0.0274	575.0	1.693	95	791.5	363.0	0.0800	597.1	1.693
36	791.5	301.6	0.0287	575.7	1.693	96	789.5	367.4	0.0800	597.8	1.693
37	789.5	301.6	0.0300	575.7	1.693	97	791.5	367.4	0.0813	597.8	1.693
38	791.5	306.0	0.0300	576.4	1.693	98	791.5	363.0	0.0826	597.8	1.693
39	791.5	306.0	0.0323	577.1	1.693	99	791.5	363.0	0.0826	597.8	1.693
40	791.5	310.5	0.0323	577.8	1.693	100	791.5	363.0	0.0838	597.8	1.693
41	791.5	310.5	0.0335	577.8	1.693	101	791.5	363.0	0.0838	597.8	1.693
42	791.5	314.9	0.0335	578.5	1.693	102	791.5	367.4	0.0838	598.5	1.693
43	791.5	314.9	0.0348	579.2	1.693	103	791.5	349.6	0.0826	598.5	1.693
44	791.5	314.9	0.0358	579.9	1.693	104	791.5	393.7	0.0884	605.4	8.467
45	791.5	319.4	0.0358	580.6	1.693	105	791.5	393.7	0.0922	598.5	8.467
46	791.5	319.4	0.0371	581.2	1.693	106	791.5	398.1	0.0968	599.2	8.467
47	789.5	323.8	0.0384	581.9	1.693	107	791.5	398.1	0.1016	599.2	8.467
48	789.5	323.8	0.0396	581.9	1.693	108	791.5	398.1	0.1052	599.9	8.467
49	791.5	323.8	0.0396	581.9	1.693	109	791.5	398.1	0.1100	599.9	8.467
50	792.9	327.8	0.0406	582.6	1.693	110	791.5	398.1	0.1135	600.6	8.467
51	791.5	327.8	0.0419	582.6	1.693	111	791.5	398.1	0.1184	600.6	8.467
52	789.5	332.3	0.0432	584.0	1.693	112	791.5	402.1	0.1232	601.2	8.467
53	791.5	327.8	0.0432	584.0	1.693	113	791.5	402.1	0.1267	601.2	8.467
54	791.5	332.3	0.0442	584.7	1.693	114	791.5	402.1	0.1316	601.9	8.467
55	791.5	332.3	0.0442	584.7	1.693	115	791.5	402.1	0.1351	602.6	8.467
56	791.5	336.7	0.0455	586.1	1.693	116	791.5	406.6	0.1400	602.6	8.467
57	791.5	336.7	0.0467	586.1	1.693	117	791.5	406.6	0.1448	603.3	8.467
58	791.5	336.7	0.0467	586.1	1.693	118	791.5	406.6	0.1483	603.3	8.467
59	791.5	341.2	0.0478	586.8	1.693	119	791.5	406.6	0.1529	604.0	8.467
60	791.5	336.7	0.0490	586.8	1.693	120	791.5	406.6	0.1567	604.7	8.467

Table A4. Continued.

#	σ_3 [kPa]	F_a [N]	ΔL [cm]	p_w [kPa]	u_a [µm/s]
121	791.5	411.0	0.1613	604.7	8.467
122	791.5	411.0	0.1651	605.4	8.467
123	791.5	411.0	0.1697	605.4	8.467
124	791.5	411.0	0.1745	606.1	8.467
125	791.5	411.0	0.1781	606.1	8.467
126	789.5	411.0	0.1829	606.1	8.467
127	789.5	411.0	0.1877	606.8	8.467
128	789.5	411.0	0.1913	606.8	8.467
129	791.5	415.5	0.1948	606.8	8.467
130	791.5	415.5	0.1996	607.4	8.467
131	791.5	415.5	0.2032	607.4	8.467
132	791.5	411.0	0.2080	607.4	8.467
133	791.5	446.2	0.2200	613.0	42.333
134	791.5	446.2	0.2403	613.0	42.333
135	791.5	446.2	0.2629	612.3	42.333
136	791.5	446.2	0.2832	611.6	42.333
137	791.5	446.2	0.3061	609.5	42.333
138	791.5	446.2	0.3264	606.8	42.333
139	791.5	480.9	0.3454	604.0	42.333
140	791.5	454.6	0.3503	601.9	42.333
141	791.5	393.7	0.3538	603.3	1.693
142	789.5	393.7	0.3538	603.3	1.693
143	791.5	398.1	0.3551	604.7	1.693
144	791.5	398.1	0.3574	604.7	1.693
145	791.5	402.1	0.3574	605.4	1.693
146	791.5	402.1	0.3574	606.1	1.693
147	791.5	402.1	0.3586	606.8	1.693
148	789.5	402.1	0.3597	608.1	1.693
149	791.5	402.1	0.3609	608.8	1.693
150	791.5	406.6	0.3622	608.8	1.693
151	791.5	402.1	0.3635	609.5	1.693
152	791.5	406.6	0.3635	610.2	1.693
153	791.5	406.6	0.3645	610.9	1.693
154	789.5	406.6	0.3658	610.9	1.693
155	791.5	406.6	0.3658	611.6	1.693
156	791.5	406.6	0.3670	613.0	1.693
157	791.5	406.6	0.3680	613.0	1.693
158	791.5	411.0	0.3680	613.7	1.693
159	791.5	411.0	0.3693	613.7	1.693
160	791.5	411.0	0.3706	615.0	1.693
161	791.5	411.0	0.3716	615.0	1.693
162	791.5	411.0	0.3729	615.7	1.693
163	791.5	411.0	0.3741	615.7	1.693
164	791.5	411.0	0.3741	616.4	1.693
165	791.5	411.0	0.3754	616.4	1.693
166	791.5	411.0	0.3764	617.8	1.693
167	791.5	411.0	0.3764	617.8	1.693
168	791.5	411.0	0.3777	617.8	1.693
169	791.5	411.0	0.3790	617.8	1.693
170	791.5	411.0	0.3790	619.2	1.693
171	791.5	411.0	0.3800	619.2	1.693
172	791.5	411.0	0.3813	619.2	1.693
173	791.5	384.8	0.3813	621.2	0.339
174	791.5	389.2	0.3825	621.9	0.339
175	791.5	389.2	0.3825	621.9	0.339
176	789.5	389.2	0.3825	622.6	0.339
177	789.5	389.2	0.3825	622.6	0.339
178	791.5	389.2	0.3825	623.3	0.339
179	791.5	389.2	0.3838	623.3	0.339
180	791.5	389.2	0.3838	623.3	0.339
181	791.5	389.2	0.3825	624.0	0.339
182	791.5	389.2	0.3838	624.0	0.339
183	791.5	389.2	0.3838	624.0	0.339
184	791.5	389.2	0.3838	624.7	0.339
185	789.5	389.2	0.3825	624.7	0.339
186	789.5	389.2	0.3838	624.7	0.339
187	791.5	393.7	0.3838	624.7	0.339
188	791.5	393.7	0.3848	625.4	0.339
189	791.5	389.2	0.3838	625.4	0.339
190	791.5	393.7	0.3848	625.4	0.339
191	791.5	393.7	0.3848	626.1	0.339
192	791.5	393.7	0.3848	626.1	0.339
193	791.5	393.7	0.3848	626.1	0.339
194	791.5	393.7	0.3848	626.8	0.339
195	791.5	393.7	0.3861	626.8	0.339
196	791.5	393.7	0.3861	626.8	0.339
197	791.5	398.1	0.3848	627.4	0.339
198	791.5	406.6	0.3838	627.4	0.339
199	791.5	454.6	0.3993	625.4	42.333
200	789.5	459.1	0.4206	623.3	42.333
201	791.5	454.6	0.4422	619.9	42.333
202	791.5	450.2	0.4638	617.8	42.333
203	791.5	454.6	0.4851	616.4	42.333
204	791.5	454.6	0.5055	614.3	42.333
205	791.5	454.6	0.5271	612.3	42.333
206	791.5	428.4	0.5474	617.1	8.467
207	791.5	428.4	0.5509	616.4	8.467
208	791.5	432.8	0.5558	616.4	8.467
209	791.5	432.8	0.5593	616.4	8.467
210	789.5	432.8	0.5641	617.1	8.467
211	791.5	437.3	0.5677	617.1	8.467
212	791.5	432.8	0.5725	617.1	8.467
213	791.5	432.8	0.5773	617.8	8.467
214	791.5	437.3	0.5809	617.8	8.467
215	789.5	437.3	0.5857	617.8	8.467
216	792.9	432.8	0.5893	617.8	8.467
217	791.5	437.3	0.5941	617.8	8.467
218	791.5	437.3	0.5977	618.5	8.467
219	791.5	437.3	0.6012	617.8	8.467
220	791.5	437.3	0.6060	618.5	8.467
221	791.5	437.3	0.6106	618.5	8.467
222	791.5	411.0	0.6132	617.8	1.693
223	791.5	415.5	0.6144	617.8	1.693
224	791.5	415.5	0.6167	617.8	1.693
225	791.5	415.5	0.6167	618.5	1.693
226	789.5	415.5	0.6167	618.5	1.693
227	791.5	419.9	0.6180	618.5	1.693
228	791.5	419.9	0.6190	618.5	1.693
229	791.5	419.9	0.6190	618.5	1.693
230	791.5	419.9	0.6215	619.2	1.693
231	791.5	419.9	0.6215	619.2	1.693
232	789.5	423.9	0.6228	619.2	1.693
233	791.5	419.9	0.6228	619.2	1.693
234	791.5	419.9	0.6238	619.2	1.693
235	791.5	423.9	0.6251	619.2	1.693
236	791.5	423.9	0.6264	619.2	1.693
237	791.5	423.9	0.6264	619.9	1.693
238	791.5	423.9	0.6274	619.9	1.693
239	789.5	419.9	0.6287	619.9	1.693
240	789.5	423.9	0.6299	619.9	1.693
241	791.5	423.9	0.6287	619.9	1.693
242	791.5	423.9	0.6309	620.6	1.693
243	791.5	423.9	0.6322	620.6	1.693
244	791.5	423.9	0.6322	620.6	1.693
245	789.5	423.9	0.6335	620.6	1.693
246	791.5	423.9	0.6347	620.6	1.693
247	791.5	423.9	0.6347	620.6	1.693
248	791.5	423.9	0.6370	621.2	1.693
249	789.5	423.9	0.6370	621.2	1.693
250	791.5	428.4	0.6383	621.2	1.693
251	791.5	423.9	0.6383	621.2	1.693
252	791.5	423.9	0.6393	621.2	1.693
253	791.5	428.4	0.6406	621.2	1.693
254	789.5	423.9	0.6419	621.2	1.693
255	789.5	428.4	0.6419	621.2	1.693
256	791.5	423.9	0.6431	621.2	1.693
257	791.5	428.4	0.6441	621.2	1.693
258	791.5	428.4	0.6454	621.2	1.693
259	791.5	423.9	0.6454	621.9	1.693
260	791.5	423.9	0.6467	621.9	1.693
261	791.5	428.4	0.6467	621.9	1.693
262	791.5	428.4	0.6477	621.9	1.693
263	791.5	428.4	0.6490	621.9	1.693
264	791.5	428.4	0.6490	621.9	1.693
265	791.5	428.4	0.6502	621.9	1.693
266	789.5	428.4	0.6513	622.6	1.693

Table A4. Continued.

#	σ_3 [kPa]	F_a [N]	ΔL [cm]	p_w [kPa]	u_a [µm/s]
267	791.5	423.9	0.6525	622.6	1.693
268	791.5	428.4	0.6525	622.6	1.693
269	791.5	423.9	0.6538	622.6	1.693
270	791.5	428.4	0.6551	622.6	1.693
271	791.5	428.4	0.6561	622.6	1.693
272	791.5	428.4	0.6574	622.6	1.693
273	789.5	428.4	0.6574	622.6	1.693
274	789.5	428.4	0.6586	622.6	1.693
275	791.5	428.4	0.6586	622.6	1.693
276	789.5	428.4	0.6596	622.6	1.693
277	791.5	428.4	0.6609	622.6	1.693
278	791.5	423.9	0.6622	622.6	1.693
279	791.5	432.8	0.6622	622.6	1.693
280	791.5	428.4	0.6634	622.6	1.693
281	791.5	428.4	0.6657	623.3	1.693
282	789.5	428.4	0.6657	623.3	1.693
283	791.5	428.4	0.6657	623.3	1.693
284	791.5	428.4	0.6670	623.3	1.693
285	789.5	428.4	0.6680	623.3	1.693
286	791.5	432.8	0.6670	623.3	1.693
287	791.5	406.6	0.6693	623.3	0.339
288	791.5	406.6	0.6693	623.3	0.339
289	791.5	406.6	0.6706	623.3	0.339
290	791.5	406.6	0.6706	624.0	0.339
291	791.5	406.6	0.6706	624.0	0.339
292	791.5	411.0	0.6706	624.0	0.339
293	789.5	406.6	0.6706	624.7	0.339
294	791.5	402.1	0.6706	625.4	0.339
295	791.5	406.6	0.6716	625.4	0.339
296	789.5	411.0	0.6716	625.4	0.339
297	789.5	406.6	0.6716	626.1	0.339
298	791.5	411.0	0.6716	626.1	0.339
299	789.5	406.6	0.6716	626.8	0.339
300	789.5	406.6	0.6716	626.8	0.339
301	789.5	406.6	0.6716	626.8	0.339
302	791.5	406.6	0.6716	627.4	0.339
303	791.5	406.6	0.6728	627.4	0.339
304	791.5	406.6	0.6728	628.1	0.339
305	791.5	411.0	0.6728	628.1	0.339
306	791.5	411.0	0.6728	628.8	0.339
307	789.5	419.9	0.6716	628.1	0.339
308	791.5	476.4	0.6957	619.2	42.333
309	791.5	472.4	0.7160	615.7	42.333
310	791.5	468.0	0.7374	611.6	42.333
311	791.5	468.0	0.7577	606.8	42.333
312	791.5	446.2	0.7722	610.9	8.467
313	791.5	441.7	0.7780	610.9	8.467
314	791.5	446.2	0.7828	610.9	8.467
315	791.5	446.2	0.7864	610.9	8.467
316	791.5	446.2	0.7899	610.9	8.467
317	791.5	446.2	0.7948	610.9	8.467
318	791.5	450.2	0.7983	610.9	8.467
319	791.5	446.2	0.8031	610.9	8.467
320	791.5	446.2	0.8067	610.9	8.467
321	791.5	450.2	0.8115	610.9	8.467
322	791.5	446.2	0.8151	610.2	8.467
323	791.5	450.2	0.8186	610.9	8.467
324	791.5	450.2	0.8235	610.9	8.467
325	791.5	450.2	0.8283	610.9	8.467
326	791.5	450.2	0.8331	610.2	8.467
327	791.5	446.2	0.8367	610.2	8.467
328	789.5	450.2	0.8402	610.2	8.467
329	791.5	450.2	0.8438	610.2	8.467
330	789.5	450.2	0.8486	613.7	8.467
331	791.5	423.9	0.8509	616.4	1.693
332	789.5	423.9	0.8522	617.1	1.693
333	791.5	423.9	0.8522	617.8	1.693
334	791.5	423.9	0.8534	617.8	1.693
335	791.5	428.4	0.8545	619.2	1.693
336	789.5	428.4	0.8557	619.9	1.693
337	791.5	428.4	0.8545	619.9	1.693
338	791.5	428.4	0.8570	619.9	1.693
339	791.5	432.8	0.8570	620.6	1.693
340	789.5	428.4	0.8580	620.6	1.693
341	791.5	432.8	0.8593	621.2	1.693
342	791.5	432.8	0.8593	621.9	1.693
343	789.5	428.4	0.8606	621.9	1.693
344	789.5	432.8	0.8618	621.9	1.693
345	791.5	432.8	0.8628	623.3	1.693
346	791.5	432.8	0.8641	623.3	1.693
347	791.5	432.8	0.8641	623.3	1.693
348	791.5	411.0	0.8654	623.3	0.339
349	791.5	411.0	0.8654	624.0	0.339
350	791.5	411.0	0.8641	624.0	0.339
351	791.5	406.6	0.8654	624.0	0.339
352	791.5	411.0	0.8654	624.7	0.339
353	791.5	411.0	0.8654	624.7	0.339
354	789.5	411.0	0.8664	626.1	0.339
355	791.5	411.0	0.8664	626.8	0.339
356	791.5	411.0	0.8664	626.8	0.339
357	791.5	411.0	0.8664	627.4	0.339
358	791.5	411.0	0.8664	627.4	0.339
359	791.5	411.0	0.8664	628.1	0.339
360	791.5	411.0	0.8664	628.1	0.339
361	791.5	411.0	0.8677	628.1	0.339
362	791.5	411.0	0.8664	628.8	0.339
363	791.5	480.9	0.8738	620.6	42.333
364	791.5	476.4	0.8941	618.5	42.333
365	791.5	476.4	0.9131	615.0	42.333
366	791.5	472.4	0.9347	619.2	42.333
367	791.5	459.1	0.9502	615.0	42.333
368	791.5	437.3	0.9525	617.1	8.467
369	791.5	446.2	0.9573	621.2	8.467
370	791.5	450.2	0.9609	621.9	8.467
371	791.5	450.2	0.9657	621.2	8.467
372	791.5	450.2	0.9693	621.2	8.467
373	789.5	454.6	0.9728	621.2	8.467
374	791.5	454.6	0.9776	621.2	8.467
375	789.5	454.6	0.9812	621.2	8.467
376	791.5	454.6	0.9860	621.2	8.467
377	789.5	454.6	0.9896	621.2	8.467
378	791.5	454.6	0.9931	621.2	8.467
379	791.5	454.6	0.9980	621.2	8.467
380	791.5	454.6	1.0028	621.2	8.467
381	791.5	454.6	1.0063	621.2	8.467
382	791.5	454.6	1.0099	621.2	8.467
383	791.5	454.6	1.0157	621.2	8.467
384	791.5	454.6	1.0196	621.2	8.467
385	791.5	454.6	1.0241	621.2	8.467
386	791.5	428.4	1.0279	620.6	1.693
387	791.5	432.8	1.0290	620.6	1.693
388	791.5	432.8	1.0302	621.2	1.693
389	791.5	432.8	1.0302	621.2	1.693
390	789.5	437.3	1.0315	621.9	1.693
391	791.5	437.3	1.0315	622.6	1.693
392	791.5	437.3	1.0325	622.6	1.693
393	791.5	437.3	1.0325	623.3	1.693
394	791.5	437.3	1.0325	623.3	1.693
395	791.5	437.3	1.0338	623.3	1.693
396	791.5	437.3	1.0338	624.0	1.693
397	791.5	441.7	1.0351	624.7	1.693
398	789.5	441.7	1.0361	624.7	1.693
399	791.5	441.7	1.0373	625.4	1.693
400	791.5	441.7	1.0373	625.4	1.693
401	791.5	441.7	1.0386	625.4	1.693
402	789.5	441.7	1.0399	626.1	1.693
403	791.5	441.7	1.0399	626.1	1.693
404	791.5	441.7	1.0409	626.1	1.693
405	791.5	441.7	1.0422	626.1	1.693
406	791.5	441.7	1.0434	626.8	1.693
407	791.5	441.7	1.0434	626.8	1.693
408	791.5	441.7	1.0444	627.4	1.693
409	791.5	446.2	1.0457	627.4	1.693
410	791.5	446.2	1.0457	627.4	1.693

Table A5. Data for the undrained triaxial compression test R2.

Date:	05/23/95
Sample material:	remolded UpB till, core 92-1
Initial weight:	256.8 gram
Pre-shear length:	6.42 cm
Pre-shear radius:	2.48 cm
Void ratio:	0.518
Saturation pressure:	689.5 kPa

#	σ_3 [kPa]	F_a [N]	ΔL [cm]	p_w [kPa]	u_a [μm/s]	#	σ_3 [kPa]	F_a [N]	ΔL [cm]	p_w [kPa]	u_a [μm/s]
1	724.7	0.0	0.0074	689.5	1.693	61	724.7	56.5	0.0348	694.3	1.693
2	724.7	4.0	0.0084	688.8	1.693	62	723.3	52.5	0.0348	694.3	1.693
3	723.3	4.0	0.0097	688.8	1.693	63	724.7	52.5	0.0348	694.3	1.693
4	724.7	8.5	0.0097	688.8	1.693	64	723.3	52.5	0.0361	695.0	1.693
5	724.7	12.9	0.0097	689.5	1.693	65	723.3	52.5	0.0361	694.3	1.693
6	723.3	17.3	0.0109	690.2	1.693	66	723.3	52.5	0.0371	695.0	1.693
7	724.7	21.8	0.0109	690.2	1.693	67	724.7	52.5	0.0371	695.0	1.693
8	723.3	21.8	0.0109	690.2	1.693	68	724.7	52.5	0.0384	694.3	1.693
9	723.3	26.2	0.0119	690.9	1.693	69	723.3	52.5	0.0384	695.0	1.693
10	723.3	26.2	0.0119	690.9	1.693	70	723.3	56.5	0.0384	695.0	1.693
11	724.7	30.2	0.0119	690.9	1.693	71	723.3	56.5	0.0396	695.0	1.693
12	723.3	30.2	0.0132	691.6	1.693	72	723.3	52.5	0.0396	695.0	1.693
13	723.3	30.2	0.0132	691.6	1.693	73	724.7	52.5	0.0406	695.0	1.693
14	721.2	34.7	0.0132	691.6	1.693	74	723.3	56.5	0.0406	695.0	1.693
15	724.7	34.7	0.0145	691.6	1.693	75	723.3	56.5	0.0419	695.0	1.693
16	723.3	34.7	0.0132	691.6	1.693	76	723.3	56.5	0.0419	695.0	1.693
17	723.3	39.1	0.0145	692.3	1.693	77	723.3	52.5	0.0419	695.0	1.693
18	724.7	34.7	0.0145	691.6	1.693	78	723.3	56.5	0.0432	695.0	1.693
19	724.7	39.1	0.0145	692.3	1.693	79	724.7	56.5	0.0432	695.0	1.693
20	724.7	39.1	0.0157	692.3	1.693	80	724.7	56.5	0.0442	695.0	1.693
21	723.3	43.6	0.0157	692.3	1.693	81	724.7	56.5	0.0442	695.0	1.693
22	723.3	43.6	0.0168	692.3	1.693	82	723.3	56.5	0.0442	695.0	1.693
23	723.3	43.6	0.0157	692.3	1.693	83	723.3	56.5	0.0455	695.7	1.693
24	723.3	39.1	0.0168	692.9	1.693	84	724.7	56.5	0.0467	695.0	1.693
25	724.7	43.6	0.0168	692.3	1.693	85	724.7	56.5	0.0467	695.7	1.693
26	723.3	43.6	0.0180	692.9	1.693	86	723.3	56.5	0.0480	695.0	1.693
27	723.3	43.6	0.0168	692.3	1.693	87	723.3	56.5	0.0480	695.7	1.693
28	723.3	43.6	0.0180	692.9	1.693	88	723.3	56.5	0.0480	695.0	1.693
29	723.3	48.0	0.0193	692.9	1.693	89	723.3	56.5	0.0480	695.7	1.693
30	723.3	43.6	0.0193	692.9	1.693	90	724.7	56.5	0.0490	695.7	1.693
31	723.3	48.0	0.0193	693.6	1.693	91	723.3	56.5	0.0490	695.7	1.693
32	724.7	48.0	0.0203	692.9	1.693	92	723.3	56.5	0.0503	695.7	1.693
33	723.3	48.0	0.0203	692.9	1.693	93	723.3	56.5	0.0503	695.7	1.693
34	724.7	48.0	0.0216	693.6	1.693	94	724.7	56.5	0.0503	695.7	1.693
35	724.7	48.0	0.0203	693.6	1.693	95	723.3	56.5	0.0516	695.7	1.693
36	724.7	48.0	0.0229	693.6	1.693	96	723.3	56.5	0.0516	695.7	1.693
37	724.7	48.0	0.0229	692.9	1.693	97	723.3	56.5	0.0526	695.7	1.693
38	724.7	52.5	0.0229	693.6	1.693	98	723.3	56.5	0.0526	695.7	1.693
39	723.3	52.5	0.0239	693.6	1.693	99	723.3	56.5	0.0538	696.4	1.693
40	723.3	52.5	0.0239	693.6	1.693	100	724.7	56.5	0.0538	696.4	1.693
41	724.7	52.5	0.0239	693.6	1.693	101	723.3	56.5	0.0551	696.4	1.693
42	724.7	52.5	0.0251	693.6	1.693	102	724.7	56.5	0.0551	696.4	1.693
43	724.7	48.0	0.0251	692.9	1.693	103	724.7	56.5	0.0551	696.4	1.693
44	723.3	52.5	0.0251	693.6	1.693	104	724.7	56.5	0.0564	696.4	1.693
45	723.3	52.5	0.0277	693.6	1.693	105	723.3	56.5	0.0564	696.4	1.693
46	723.3	52.5	0.0277	693.6	1.693	106	724.7	56.5	0.0574	696.4	1.693
47	724.7	52.5	0.0277	693.6	1.693	107	723.3	56.5	0.0574	696.4	1.693
48	724.7	52.5	0.0277	693.6	1.693	108	724.7	56.5	0.0574	696.4	1.693
49	723.3	52.5	0.0287	693.6	1.693	109	723.3	52.5	0.0587	696.4	1.693
50	724.7	52.5	0.0300	693.6	1.693	110	724.7	56.5	0.0587	697.1	1.693
51	724.7	52.5	0.0300	694.3	1.693	111	723.3	56.5	0.0599	696.4	1.693
52	723.3	52.5	0.0300	693.6	1.693	112	723.3	56.5	0.0599	696.4	1.693
53	723.3	52.5	0.0300	693.6	1.693	113	723.3	60.9	0.0610	697.1	1.693
54	724.7	52.5	0.0312	693.6	1.693	114	723.3	56.5	0.0610	697.1	1.693
55	724.7	56.5	0.0300	693.6	1.693	115	723.3	56.5	0.0610	697.1	1.693
56	723.3	52.5	0.0312	694.3	1.693	116	723.3	56.5	0.0622	697.1	1.693
57	723.3	52.5	0.0323	694.3	1.693	117	724.7	60.9	0.0610	697.1	1.693
58	723.3	52.5	0.0323	694.3	1.693	118	723.3	60.9	0.0622	697.1	1.693
59	723.3	52.5	0.0335	694.3	1.693	119	723.3	56.5	0.0635	697.1	1.693
60	723.3	52.5	0.0335	694.3	1.693	120	723.3	56.5	0.0635	697.1	1.693

Table A5. Continued.

#	σ_3 [kPa]	F_a [N]	ΔL [cm]	p_w [kPa]	u_a [μm/s]
121	723.3	60.9	0.0645	697.1	1.693
122	723.3	60.9	0.0645	697.1	1.693
123	724.7	56.5	0.0658	697.1	1.693
124	723.3	60.9	0.0658	696.4	1.693
125	723.3	56.5	0.0658	697.8	1.693
126	723.3	56.5	0.0671	697.1	1.693
127	724.7	60.9	0.0683	697.1	1.693
128	723.3	56.5	0.0683	697.1	1.693
129	723.3	56.5	0.0683	697.1	1.693
130	724.7	56.5	0.0693	697.8	1.693
131	723.3	56.5	0.0693	697.8	1.693
132	723.3	60.9	0.0693	697.1	1.693
133	723.3	60.9	0.0706	697.1	1.693
134	724.7	60.9	0.0706	697.1	1.693
135	723.3	56.5	0.0706	697.1	1.693
136	723.3	60.9	0.0719	697.8	1.693
137	723.3	60.9	0.0719	697.1	1.693
138	724.7	60.9	0.0729	697.8	1.693
139	724.7	60.9	0.0742	697.8	1.693
140	723.3	60.9	0.0742	697.8	1.693
141	724.7	56.5	0.0742	697.8	1.693
142	724.7	56.5	0.0754	697.8	1.693
143	724.7	60.9	0.0754	697.8	1.693
144	724.7	56.5	0.0765	697.8	1.693
145	724.7	56.5	0.0765	697.8	1.693
146	724.7	56.5	0.0765	697.8	1.693
147	724.7	60.9	0.0765	698.5	1.693
148	724.7	60.9	0.0777	698.5	1.693
149	723.3	60.9	0.0790	697.8	1.693
150	723.3	43.6	0.0848	697.8	1.693
151	723.3	43.6	0.0861	697.8	1.693
152	723.3	43.6	0.0861	697.8	1.693
153	724.7	43.6	0.0861	697.8	1.693
154	724.7	43.6	0.0848	697.8	1.693
155	723.3	43.6	0.0861	697.8	1.693
156	724.7	39.1	0.0861	697.8	1.693
157	723.3	43.6	0.0861	697.8	1.693
158	723.3	43.6	0.0861	697.8	1.693
159	723.3	43.6	0.0861	697.8	1.693
160	723.3	43.6	0.0874	697.8	1.693
161	723.3	39.1	0.0874	697.8	1.693
162	723.3	34.7	0.0861	697.8	0.068
163	723.3	39.1	0.0861	697.8	0.068
164	724.7	39.1	0.0861	697.8	0.068
165	723.3	39.1	0.0861	697.8	0.068
166	723.3	34.7	0.0861	697.8	0.068
167	723.3	39.1	0.0861	697.8	0.068
168	723.3	34.7	0.0848	697.8	0.068
169	723.3	39.1	0.0861	698.5	0.068
170	723.3	39.1	0.0861	697.8	0.068
171	723.3	34.7	0.0861	697.8	0.068
172	723.3	39.1	0.0861	697.8	0.068
173	723.3	39.1	0.0861	698.5	0.068
174	723.3	34.7	0.0861	698.5	0.068
175	723.3	39.1	0.0861	697.8	0.068
176	723.3	34.7	0.0861	697.8	0.068
177	723.3	39.1	0.0861	698.5	0.068
178	723.3	34.7	0.0861	698.5	0.068
179	723.3	34.7	0.0861	698.5	0.068
180	721.2	39.1	0.0861	698.5	0.068
181	723.3	39.1	0.0861	698.5	0.068
182	724.7	39.1	0.0861	698.5	0.068
183	723.3	34.7	0.0848	698.5	0.068
184	723.3	34.7	0.0861	698.5	0.068
185	723.3	39.1	0.0861	698.5	0.068
186	723.3	39.1	0.0861	698.5	0.068
187	723.3	39.1	0.0861	698.5	0.068
188	723.3	34.7	0.0848	698.5	0.068
189	723.3	39.1	0.0861	698.5	0.068
190	723.3	34.7	0.0848	698.5	0.068
191	723.3	34.7	0.0861	698.5	0.068
192	723.3	34.7	0.0861	698.5	0.068
193	724.7	34.7	0.0861	698.5	0.068
194	724.7	34.7	0.0861	698.5	0.068
195	724.7	34.7	0.0861	698.5	0.068
196	723.3	39.1	0.0861	698.5	0.068
197	723.3	34.7	0.0848	698.5	0.068
198	723.3	34.7	0.0861	699.2	0.068
199	723.3	34.7	0.0848	698.5	0.068
200	723.3	34.7	0.0861	699.2	0.068
201	723.3	34.7	0.0861	699.2	0.068
202	724.7	34.7	0.0861	699.2	0.068
203	723.3	34.7	0.0861	698.5	0.068
204	724.7	39.1	0.0848	698.5	0.068
205	723.3	34.7	0.0848	699.2	0.068
206	723.3	34.7	0.0861	699.2	0.068
207	724.7	34.7	0.0861	699.2	0.068
208	724.7	34.7	0.0848	699.2	0.068
209	724.7	34.7	0.0848	699.2	0.068
210	724.7	34.7	0.0861	699.2	0.068
211	723.3	34.7	0.0848	699.2	0.068
212	724.7	34.7	0.0861	699.2	0.068
213	724.7	34.7	0.0861	699.2	0.068
214	724.7	34.7	0.0861	699.2	0.068
215	723.3	34.7	0.0848	699.2	0.068
216	724.7	34.7	0.0861	699.2	0.068
217	723.3	34.7	0.0861	699.2	0.068
218	723.3	34.7	0.0848	699.2	0.068
219	724.7	34.7	0.0848	699.2	0.068
220	723.3	34.7	0.0848	699.2	0.068
221	724.7	34.7	0.0848	699.2	0.068
222	723.3	34.7	0.0861	699.2	0.068
223	723.3	34.7	0.0861	699.2	0.068
224	723.3	34.7	0.0861	699.2	0.068
225	724.7	34.7	0.0861	699.2	0.068
226	723.3	34.7	0.0861	699.2	0.068
227	723.3	34.7	0.0848	699.2	0.068
228	723.3	34.7	0.0848	699.2	0.068
229	724.7	34.7	0.0861	699.2	0.068
230	723.3	34.7	0.0861	699.2	0.068
231	724.7	34.7	0.0848	699.8	0.068
232	723.3	34.7	0.0861	699.2	0.068
233	723.3	34.7	0.0861	699.8	0.068
234	723.3	30.2	0.0861	699.8	0.068
235	723.3	34.7	0.0848	699.2	0.068
236	723.3	34.7	0.0861	699.8	0.068
237	723.3	34.7	0.0848	699.8	0.068
238	723.3	34.7	0.0861	699.2	0.068
239	723.3	34.7	0.0861	699.8	0.068
240	723.3	34.7	0.0848	699.2	0.068
241	724.7	39.1	0.0861	699.8	0.068
242	723.3	34.7	0.0861	699.2	0.068
243	723.3	34.7	0.0861	699.2	0.068
244	724.7	34.7	0.0861	699.8	0.068
245	723.3	34.7	0.0848	699.8	0.068
246	723.3	34.7	0.0848	699.8	0.068
247	723.3	34.7	0.0848	699.8	0.068
248	723.3	34.7	0.0848	699.2	0.068
249	723.3	34.7	0.0861	699.8	0.068
250	724.7	34.7	0.0848	699.8	0.068
251	723.3	34.7	0.0848	699.8	0.068
252	723.3	34.7	0.0848	699.8	0.068
253	723.3	34.7	0.0932	700.5	0.068
254	724.7	30.2	0.0932	700.5	0.068
255	723.3	30.2	0.0922	700.5	0.068
256	724.7	34.7	0.0922	700.5	0.068
257	723.3	34.7	0.0932	700.5	0.068
258	723.3	34.7	0.0932	700.5	0.068
259	723.3	26.2	0.0922	700.5	0.068
260	724.7	34.7	0.0932	700.5	0.068
261	723.3	34.7	0.0932	700.5	0.068
262	723.3	30.2	0.0922	700.5	0.068
263	723.3	34.7	0.0922	700.5	0.068
264	723.3	30.2	0.0922	700.5	0.068
265	724.7	30.2	0.0932	700.5	0.068
266	724.7	30.2	0.0932	700.5	0.068

Table A5. Continued.

#	σ_3 [kPa]	F_a [N]	ΔL [cm]	p_w [kPa]	u_a [µm/s]
267	723.3	34.7	0.0932	700.5	0.068
268	723.3	30.2	0.0922	700.5	0.068
269	723.3	30.2	0.0922	700.5	0.068
270	723.3	34.7	0.0922	700.5	0.068
271	723.3	34.7	0.0922	700.5	0.068
272	723.3	34.7	0.0932	700.5	0.068
273	723.3	30.2	0.0922	700.5	0.068
274	723.3	34.7	0.0922	700.5	0.068
275	723.3	30.2	0.0922	700.5	0.068
276	723.3	34.7	0.0922	700.5	0.068
277	723.3	34.7	0.0932	700.5	0.068
278	723.3	30.2	0.0922	700.5	0.068
279	723.3	30.2	0.0922	700.5	0.068
280	723.3	30.2	0.0922	700.5	0.068
281	723.3	34.7	0.0922	700.5	0.068
282	723.3	34.7	0.0922	700.5	0.068
283	723.3	34.7	0.0922	700.5	0.068
284	723.3	30.2	0.0922	700.5	0.068
285	723.3	30.2	0.0922	700.5	0.068
286	723.3	34.7	0.0922	700.5	0.068
287	723.3	34.7	0.0922	700.5	0.068
288	724.7	34.7	0.0932	701.2	0.068
289	721.2	34.7	0.0932	700.5	0.068
290	723.3	39.1	0.0922	700.5	0.339
291	723.3	39.1	0.0932	701.2	0.339
292	723.3	39.1	0.0932	701.2	0.339
293	724.7	43.6	0.0932	700.5	0.339
294	723.3	43.6	0.0922	701.2	0.339
295	723.3	43.6	0.0922	701.2	0.339
296	723.3	43.6	0.0932	701.2	0.339
297	723.3	39.1	0.0932	701.9	0.339
298	723.3	43.6	0.0932	701.2	0.339
299	723.3	39.1	0.0932	700.5	0.339
300	723.3	43.6	0.0932	701.2	0.339
301	724.7	43.6	0.0932	701.2	0.339
302	723.3	43.6	0.0932	701.2	0.339
303	723.3	48.0	0.0932	701.2	0.339
304	724.7	48.0	0.0932	701.2	0.339
305	724.7	48.0	0.0932	701.2	0.339
306	723.3	48.0	0.0932	701.2	0.339
307	723.3	48.0	0.0932	701.2	0.339
308	723.3	48.0	0.0932	701.2	0.339
309	724.7	48.0	0.0932	701.2	0.339
310	723.3	48.0	0.0945	701.2	0.339
311	724.7	48.0	0.0932	701.9	0.339
312	724.7	48.0	0.0932	701.9	0.339
313	723.3	48.0	0.0945	701.9	0.339
314	723.3	48.0	0.0932	701.2	0.339
315	723.3	52.5	0.0945	701.2	0.339
316	723.3	52.5	0.0945	701.9	0.339
317	723.3	52.5	0.0945	701.2	0.339
318	723.3	52.5	0.0945	701.9	0.339
319	723.3	52.5	0.0945	701.9	0.339
320	724.7	48.0	0.0945	701.9	0.339
321	723.3	52.5	0.0945	701.9	0.339
322	723.3	52.5	0.0932	701.9	0.339
323	723.3	52.5	0.0945	701.2	0.339
324	723.3	52.5	0.0945	701.9	0.339
325	723.3	52.5	0.0945	701.2	0.339
326	723.3	52.5	0.0958	701.2	0.339
327	723.3	52.5	0.0958	701.9	0.339
328	724.7	52.5	0.0958	701.9	0.339
329	723.3	52.5	0.0945	701.9	0.339
330	723.3	52.5	0.0958	701.9	0.339
331	723.3	52.5	0.0945	701.2	0.339
332	723.3	52.5	0.0945	701.9	0.339
333	723.3	52.5	0.0958	701.9	0.339
334	723.3	52.5	0.0958	701.9	0.339
335	723.3	52.5	0.0958	701.2	0.339
336	723.3	52.5	0.0958	701.9	0.339
337	723.3	52.5	0.0958	701.9	0.339
338	724.7	52.5	0.0958	701.9	0.339
339	724.7	48.0	0.0958	701.9	0.339
340	723.3	52.5	0.0958	701.9	0.339
341	723.3	52.5	0.0958	701.9	0.339
342	723.3	52.5	0.0958	701.9	0.339
343	723.3	52.5	0.0958	701.9	0.339
344	724.7	52.5	0.0968	701.9	0.339
345	723.3	52.5	0.0968	701.9	0.339
346	724.7	52.5	0.0968	701.9	0.339
347	723.3	52.5	0.0968	701.2	0.339
348	723.3	52.5	0.0968	701.9	0.339
349	723.3	56.5	0.0968	701.9	0.339
350	723.3	52.5	0.0968	701.9	0.339
351	724.7	52.5	0.0968	701.9	0.339
352	723.3	52.5	0.0968	701.9	0.339
353	723.3	52.5	0.0968	701.9	0.339
354	724.7	56.5	0.0968	701.9	0.339
355	723.3	56.5	0.0968	701.9	0.339
356	723.3	56.5	0.0980	701.9	0.339
357	723.3	56.5	0.0968	701.9	0.339
358	723.3	52.5	0.0980	701.9	0.339
359	723.3	52.5	0.0968	702.6	0.339
360	723.3	56.5	0.0980	701.9	0.339
361	723.3	52.5	0.0980	701.9	0.339
362	723.3	52.5	0.0980	701.9	0.339
363	724.7	52.5	0.0980	701.9	0.339
364	723.3	56.5	0.0980	701.9	0.339
365	723.3	52.5	0.0980	701.9	0.339
366	723.3	56.5	0.0980	701.2	0.339
367	723.3	56.5	0.0980	701.9	0.339
368	723.3	56.5	0.0993	701.9	0.339
369	724.7	56.5	0.0980	701.9	0.339
370	723.3	52.5	0.0980	701.9	0.339
371	723.3	56.5	0.0993	701.9	0.339
372	723.3	52.5	0.0993	701.9	0.339
373	723.3	52.5	0.0993	701.9	0.339
374	724.7	56.5	0.0993	701.9	0.339
375	723.3	56.5	0.0993	701.9	0.339
376	723.3	56.5	0.0993	701.9	0.339
377	724.7	52.5	0.0993	701.9	0.339
378	723.3	52.5	0.0993	701.9	0.339
379	723.3	52.5	0.0993	701.9	0.339
380	723.3	52.5	0.0993	701.9	0.339
381	723.3	56.5	0.0993	701.9	0.339
382	723.3	52.5	0.1006	701.9	0.339
383	723.3	56.5	0.1006	701.9	0.339
384	723.3	52.5	0.1006	701.9	0.339
385	723.3	52.5	0.0993	701.9	0.339
386	724.7	56.5	0.1006	701.9	0.339
387	723.3	56.5	0.1006	702.6	0.339
388	723.3	56.5	0.1006	701.2	0.339
389	723.3	56.5	0.1006	701.9	0.339
390	724.7	56.5	0.1006	701.9	0.339
391	723.3	56.5	0.1016	701.9	0.339
392	723.3	56.5	0.1006	701.9	0.339
393	723.3	56.5	0.1006	701.9	0.339
394	723.3	52.5	0.1006	701.9	0.339
395	723.3	56.5	0.1006	701.9	0.339
396	723.3	56.5	0.1016	701.9	0.339
397	723.3	56.5	0.1006	701.9	0.339
398	723.3	56.5	0.1016	701.9	0.339
399	723.3	56.5	0.1016	701.9	0.339
400	723.3	56.5	0.1016	701.9	0.339
401	723.3	56.5	0.1016	701.9	0.339
402	723.3	56.5	0.1016	701.9	0.339
403	723.3	56.5	0.1016	701.9	0.339
404	724.7	52.5	0.1016	701.9	0.339
405	723.3	56.5	0.1016	701.9	0.339
406	723.3	56.5	0.1016	701.9	0.339
407	723.3	56.5	0.1029	701.9	0.339
408	723.3	56.5	0.1016	701.9	0.339
409	723.3	56.5	0.1029	701.9	0.339
410	723.3	52.5	0.1029	701.9	0.339

Table A5. Continued.

#	σ_3 [kPa]	F_a [N]	ΔL [cm]	p_w [kPa]	u_a [μm/s]
411	723.3	56.5	0.1029	702.6	0.339
412	723.3	56.5	0.1029	701.9	0.339
413	723.3	56.5	0.1029	701.9	0.339
414	723.3	56.5	0.1029	701.9	0.339
415	723.3	56.5	0.1029	701.9	0.339
416	723.3	56.5	0.1029	701.9	0.339
417	723.3	56.5	0.1029	701.9	0.339
418	723.3	56.5	0.1029	701.9	0.339
419	723.3	56.5	0.1029	701.9	0.339
420	723.3	52.5	0.1029	701.9	0.339
421	723.3	52.5	0.1041	701.9	0.339
422	723.3	56.5	0.1041	701.9	0.339
423	723.3	56.5	0.1029	701.9	0.339
424	723.3	56.5	0.1029	701.9	0.339
425	723.3	56.5	0.1041	701.9	0.339
426	723.3	52.5	0.1041	702.6	0.339
427	723.3	56.5	0.1041	701.9	0.339
428	723.3	43.6	0.1090	701.9	0.339
429	724.7	43.6	0.1077	701.9	0.068
430	723.3	43.6	0.1077	702.6	0.068
431	723.3	43.6	0.1077	701.9	0.068
432	723.3	48.0	0.1161	702.6	0.068
433	721.2	48.0	0.1161	701.9	0.068
434	723.3	48.0	0.1161	701.9	0.068
435	723.3	48.0	0.1161	702.6	0.068
436	723.3	48.0	0.1161	702.6	0.068
437	724.7	48.0	0.1161	701.9	0.068
438	724.7	48.0	0.1029	701.9	0.068
439	724.7	56.5	0.1041	702.6	0.068
440	723.3	60.9	0.1052	702.6	8.467
441	723.3	65.4	0.1064	702.6	8.467
442	724.7	65.4	0.1090	702.6	8.467
443	723.3	65.4	0.1113	702.6	8.467
444	723.3	65.4	0.1135	701.9	8.467
445	723.3	65.4	0.1161	701.2	8.467
446	723.3	65.4	0.1184	701.9	8.467
447	723.3	65.4	0.1209	701.2	8.467
448	723.3	65.4	0.1232	701.2	8.467
449	723.3	65.4	0.1255	701.2	8.467
450	723.3	65.4	0.1280	701.2	8.467
451	723.3	60 9	0.1303	700.5	8.467
452	723.3	65.4	0.1328	700.5	8.467
453	723.3	65.4	0.1351	700.5	8.467
454	723.3	65.4	0.1387	700.5	8.467
455	723.3	69 8	0.1400	700.5	8.467
456	723.3	65.4	0.1435	699.8	8.467
457	723.3	65.4	0.1458	699.8	8.467
458	723.3	65.4	0.1483	699.8	8.467
459	723.3	65.4	0.1506	699.8	8.467
460	723.3	65.4	0.1519	699.8	8.467
461	724.7	65.4	0.1554	699.2	8.467
462	723.3	52.5	0.1687	699.2	1.693
463	723.3	56.5	0.1687	699.2	1.693
464	723.3	56.5	0.1687	699.2	1.693
465	723.3	60.9	0.1687	699.8	1.693
466	723.3	60.9	0.1687	699.2	1.693
467	724.7	60.9	0.1697	699.2	1.693
468	723.3	60.9	0.1697	699.2	1.693
469	723.3	60.9	0.1697	699.2	1.693
470	723.3	56.5	0.1697	699.2	1.693
471	723.3	60.9	0.1709	699.8	1.693
472	723.3	60.9	0.1709	699.8	1.693
473	723.3	60.9	0.1722	699.8	1.693
474	723.3	60.9	0.1722	699.2	1.693
475	724.7	60.9	0.1735	699.8	1.693
476	723.3	60.9	0.1735	699.8	1.693
477	723.3	60.9	0.1735	699.8	1.693
478	723.3	60.9	0.1745	699.8	1.693
479	723.3	60.9	0.1745	699.2	1.693
480	723.3	60.9	0.1758	699.2	1.693
481	724.7	60.9	0.1758	699.8	1.693
482	723.3	60.9	0.1758	699.8	1.693
483	723.3	60.9	0.1770	699.8	1.693
484	723.3	60.9	0.1781	699.8	1.693
485	723.3	60.9	0.1781	699.8	1.693
486	723.3	60.9	0.1781	699.8	1.693
487	723.3	60.9	0.1781	699.8	1.693
488	724.7	60.9	0.1793	699.8	1.693
489	721.2	60.9	0.1806	699.8	1.693
490	723.3	60.9	0.1806	700.5	1.693
491	723.3	60.9	0.1806	699.8	1.693
492	723.3	60.9	0.1819	699.8	1.693
493	723.3	60.9	0.1819	699.8	1.693
494	723.3	60.9	0.1819	699.8	1.693
495	723.3	60.9	0.1829	699.8	1.693
496	723.3	60.9	0.1829	699.8	1.693
497	723.3	60.9	0.1842	699.8	1.693
498	723.3	48.0	0.1842	699.8	0.339
499	724.7	52.5	0.1842	699.8	0.339
500	723.3	48.0	0.1842	699.2	0.339
501	723.3	52.5	0.1842	699.8	0.339
502	723.3	52.5	0.1842	699.8	0.339
503	723.3	48.0	0.1842	699.8	0.339
504	723.3	52.5	0.1842	700.5	0.339
505	723.3	52.5	0.1842	700.5	0.339
506	723.3	52.5	0.1842	700.5	0.339
507	723.3	52.5	0.1842	700.5	0.339
508	723.3	52.5	0.1842	700.5	0.339
509	723.3	52.5	0.1842	699.8	0.339
510	723.3	52.5	0.1842	699.8	0.339
511	724.7	52.5	0.1842	700.5	0.339
512	724.7	56.5	0.1842	700.5	0.339
513	723.3	52.5	0.1842	700.5	0.339
514	723.3	52.5	0.1854	700.5	0.339
515	723.3	52.5	0.1854	700.5	0.339
516	723.3	56.5	0.1842	700.5	0.339
517	723.3	56.5	0.1842	700.5	0.339
518	724.7	56.5	0.1854	700.5	0.339
519	721.2	56.5	0.1854	700.5	0.339
520	723.3	52.5	0.1854	701.2	0.339
521	723.3	56.5	0.1854	701.2	0.339
522	723.3	56.5	0.1854	700.5	0.339
523	721.2	56.5	0.1842	700.5	0.339
524	723.3	56.5	0.1842	701.2	0.339
525	723.3	56.5	0.1854	701.2	0.339
526	724.7	56.5	0.1854	701.2	0.339
527	723.3	56.5	0.1854	701.2	0.339
528	723.3	56.5	0.1854	701.2	0.339
529	723.3	56.5	0.1864	701.2	0.339
530	723.3	56.5	0.1854	701.2	0.339
531	723.3	56.5	0.1854	700.5	0.339
532	723.3	56.5	0.1864	701.2	0.339
533	723.3	56.5	0.1864	701.2	0.339
534	724.7	56.5	0.1864	701.2	0.339
535	724.7	56.5	0.1854	701.2	0.339
536	723.3	56.5	0.1864	701.2	0.339
537	724.7	56.5	0.1864	701.2	0.339
538	723.3	56.5	0.1864	701.2	0.339
539	723.3	56.5	0.1864	701.2	0.339
540	723.3	56.5	0.1864	701.9	0.339
541	723.3	56.5	0.1864	701.9	0.339
542	723.3	56.5	0.1864	701.9	0.339
543	723.3	60.9	0.1864	701.2	0.339
544	723.3	56.5	0.1864	701.9	0.339
545	723.3	56.5	0.1864	701.9	0.339
546	723.3	56.5	0.1864	701.9	0.339
547	723.3	56.5	0.1864	701.9	0.339
548	724.7	56.5	0.1877	701.9	0.339
549	724.7	56.5	0.1877	701.9	0.339
550	723.3	56.5	0.1877	701.9	0.339
551	723.3	56.5	0.1877	701.9	0.339
552	723.3	56.5	0.1877	701.9	0.339
553	723.3	56.5	0.1877	701.9	0.339
554	723.3	56.5	0.1877	701.9	0.339
555	723.3	60.9	0.1877	702.6	0.339
556	723.3	56.5	0.1877	701.9	0.339
557	723.3	56.5	0.1877	701.9	0.339
558	723.3	56.5	0.1877	701 9	0.339
559	723.3	56.5	0.1890	701.9	0.339
560	723.3	56.5	0.1890	701.9	0.339

Table A5. Continued.

#	σ_3 [kPa]	F_a [N]	ΔL [cm]	p_w [kPa]	u_a [μm/s]
561	723.3	56.5	0.1890	701.9	0.339
562	723.3	56.5	0.1877	702.6	0.339
563	723.3	56.5	0.1877	701.9	0.339
564	723.3	56.5	0.1890	702.6	0.339
565	723.3	56.5	0.1890	701.9	0.339
566	723.3	60.9	0.1890	702.6	0.339
567	723.3	56.5	0.1890	701.9	0.339
568	723.3	56.5	0.1890	702.6	0.339
569	723.3	60.9	0.1890	701.9	0.339
570	723.3	60.9	0.1890	702.6	0.339
571	724.7	56.5	0.1890	702.6	0.339
572	723.3	56.5	0.1890	702.6	0.339
573	723.3	56.5	0.1900	702.6	0.339
574	723.3	56.5	0.1900	701.9	0.339
575	724.7	56.5	0.1900	702.6	0.339
576	724.7	56.5	0.1900	702.6	0.339
577	723.3	56.5	0.1900	702.6	0.339
578	723.3	56.5	0.1900	702.6	0.339
579	723.3	60.9	0.1900	702.6	0.339
580	723.3	56.5	0.1900	702.6	0.339
581	724.7	56.5	0.1900	702.6	0.339
582	723.3	56.5	0.1900	702.6	0.339
583	724.7	48.0	0.1913	702.6	0.068
584	724.7	48.0	0.1913	702.6	0.068
585	723.3	43.6	0.1913	702.6	0.068
586	723.3	43.6	0.1900	702.6	0.068
587	723.3	43.6	0.1900	702.6	0.068
588	723.3	48.0	0.1900	702.6	0.068
589	723.3	48.0	0.1900	702.6	0.068
590	723.3	43.6	0.1900	702.6	0.068
591	724.7	43.6	0.1900	702.6	0.068
592	723.3	48.0	0.1900	702.6	0.068
593	723.3	43.6	0.1900	702.6	0.068
594	723.3	48.0	0.1900	702.6	0.068
595	723.3	48.0	0.1900	702.6	0.068
596	723.3	48.0	0.1900	702.6	0.068
597	723.3	43.6	0.1913	703.3	0.068
598	723.3	43.6	0.1900	703.3	0.068
599	723.3	43.6	0.1900	702.6	0.068
600	723.3	43.6	0.1900	702.6	0.068
601	723.3	43.6	0.1900	702.6	0.068
602	724.7	43.6	0.1900	703.3	0.068
603	723.3	43.6	0.1900	703.3	0.068
604	723.3	43.6	0.1900	703.3	0.068
605	723.3	48.0	0.1900	703.3	0.068
606	724.7	48.0	0.1900	703.3	0.068
607	723.3	48.0	0.1900	703.3	0.068
608	723.3	48.0	0.1900	702.6	0.068
609	723.3	43.6	0.1913	703.3	0.068
610	723.3	43.6	0.1900	703.3	0.068
611	723.3	48.0	0.1900	702.6	0.068
612	723.3	48.0	0.1900	703.3	0.068
613	723.3	48.0	0.1900	703.3	0.068
614	723.3	48.0	0.1900	703.3	0.068
615	723.3	48.0	0.1900	703.3	0.068
616	724.7	48.0	0.1900	703.3	0.068
617	723.3	43.6	0.1900	703.3	0.068
618	723.3	48.0	0.1900	703.3	0.068
619	724.7	48.0	0.1900	704.0	0.068
620	723.3	48.0	0.1900	703.3	0.068
621	723.3	48.0	0.1890	703.3	0.068
622	723.3	48.0	0.1900	703.3	0.068
623	723.3	48.0	0.1900	703.3	0.068
624	723.3	48.0	0.1900	703.3	0.068
625	723.3	48.0	0.1913	703.3	0.068
626	723.3	48.0	0.1900	703.3	0.068
627	723.3	48.0	0.1900	703.3	0.068
628	723.3	48.0	0.1900	704.0	0.068
629	723.3	48.0	0.1900	703.3	0.068
630	723.3	52.5	0.1900	703.3	0.068
631	723.3	48.0	0.1900	703.3	0.068
632	723.3	48.0	0.1900	703.3	0.068
633	723.3	48.0	0.1900	703.3	0.068
634	723.3	48.0	0.1900	703.3	0.068
635	723.3	52.5	0.1900	703.3	0.068
636	723.3	48.0	0.1900	703.3	0.068
637	723.3	52.5	0.1913	704.0	0.068
638	723.3	48.0	0.1900	704.0	0.068
639	723.3	48.0	0.1913	703.3	0.068
640	724.7	52.5	0.1900	703.3	0.068
641	723.3	48.0	0.1900	704.0	0.068
642	723.3	52.5	0.1900	704.0	0.068
643	723.3	48.0	0.1900	704.0	0.068
644	723.3	52.5	0.1900	704.0	0.068
645	723.3	48.0	0.1900	704.0	0.068
646	723.3	48.0	0.1900	703.3	0.068
647	723.3	52.5	0.1900	704.0	0.068
648	723.3	52.5	0.1900	704.0	0.068
649	723.3	48.0	0.1913	704.0	0.068
650	723.3	52.5	0.1900	704.0	0.068
651	723.3	52.5	0.1900	704.0	0.068
652	723.3	52.5	0.1913	704.0	0.068
653	723.3	52.5	0.1900	704.0	0.068
654	723.3	52.5	0.1913	704.0	0.068
655	723.3	52.5	0.1913	704.0	0.068
656	723.3	52.5	0.1913	704.0	0.068
657	723.3	52.5	0.1913	704.0	0.068
658	723.3	52.5	0.1900	704.0	0.068
659	723.3	52.5	0.1913	704.0	0.068
660	723.3	52.5	0.1900	704.0	0.068
661	723.3	52.5	0.1913	704.0	0.068
662	723.3	52.5	0.1913	704.0	0.068
663	723.3	52.5	0.1900	704.0	0.068
664	723.3	52.5	0.1913	704.0	0.068
665	723.3	52.5	0.1900	704.0	0.068
666	723.3	52.5	0.1913	704.0	0.068
667	723.3	48.0	0.1900	704.7	0.068
668	723.3	52.5	0.1913	704.0	0.068
669	723.3	52.5	0.1900	704.7	0.068
670	723.3	52.5	0.1900	704.0	0.068
671	723.3	52.5	0.1900	704.7	0.068
672	723.3	52.5	0.1913	704.0	0.068
673	723.3	52.5	0.1913	704.0	0.068
674	723.3	52.5	0.1913	704.7	0.068
675	723.3	52.5	0.1913	704.7	0.068
676	723.3	52.5	0.1900	704.7	0.068
677	723.3	52.5	0.1913	704.7	0.068
678	723.3	48.0	0.1900	704.7	0.068
679	724.7	52.5	0.1913	704.0	0.068
680	723.3	52.5	0.1900	704.7	0.068
681	723.3	52.5	0.1913	704.7	0.068
682	723.3	52.5	0.1900	704.7	0.068
683	723.3	48.0	0.1913	704.7	0.068
684	723.3	52.5	0.1900	704.7	0.068
685	723.3	52.5	0.1900	704.7	0.068
686	723.3	52.5	0.1913	704.0	0.068
687	723.3	52.5	0.1913	704.7	0.068
688	723.3	52.5	0.1913	704.7	0.068
689	723.3	52.5	0.1913	704.7	0.068
690	723.3	52.5	0.1913	704.7	0.068
691	723.3	52.5	0.1913	704.7	0.068
692	723.3	52.5	0.1913	704.7	0.068
693	723.3	52.5	0.1913	704.7	0.068
694	723.3	52.5	0.1913	704.7	0.068
695	723.3	52.5	0.1913	704.7	0.068
696	723.3	52.5	0.1913	704.7	0.068
697	723.3	52.5	0.1913	704.7	0.068
698	723.3	52.5	0.1913	704.7	0.068
699	724.7	52.5	0.1913	704.7	0.068
700	721.2	52.5	0.1913	704.7	0.068
701	723.3	52.5	0.1913	704.7	0.068
702	723.3	52.5	0.1913	704.7	0.068
703	723.3	52.5	0.1913	704.7	0.068
704	723.3	48.0	0.1913	704.7	0.068
705	723.3	52.5	0.1913	704.7	0.068
706	723.3	52.5	0.1913	704.7	0.068
707	724.7	52.5	0.1913	704.7	0.068
708	723.3	52.5	0.1913	704.7	0.068
709	723.3	52.5	0.1913	704.7	0.068
710	723.3	52.5	0.1913	704.7	0.068

Table A5. Continued.

#	σ_3 [kPa]	F_a [N]	ΔL [cm]	p_w [kPa]	u_a [μm/s]
711	721.2	52.5	0.1913	704.7	0.068
712	723.3	52.5	0.1913	704.7	0.068
713	724.7	52.5	0.1900	704.7	0.068
714	724.7	52.5	0.1913	704.7	0.068
715	723.3	52.5	0.1913	704.7	0.068
716	723.3	52.5	0.1913	704.7	0.068
717	723.3	52.5	0.1913	704.7	0.068
718	723.3	52.5	0.1900	704.7	0.068
719	723.3	52.5	0.1913	704.7	0.068
720	723.3	52.5	0.1913	704.7	0.068
721	721.2	52.5	0.1913	704.7	0.068
722	723.3	52.5	0.1913	704.7	0.068
723	723.3	52.5	0.1913	704.7	0.068
724	723.3	52.5	0.1913	704.7	0.068
725	723.3	48.0	0.1913	704.7	0.068
726	723.3	52.5	0.1913	704.7	0.068
727	724.7	52.5	0.1913	704.7	0.068
728	724.7	52.5	0.1913	704.7	0.068
729	723.3	52.5	0.1913	704.7	0.068
730	723.3	56.5	0.1913	704.7	0.068
731	723.3	52.5	0.1913	704.7	0.068
732	721.2	52.5	0.1913	704.7	0.068
733	723.3	52.5	0.1913	704.7	0.068
734	723.3	52.5	0.1925	705.4	0.068
735	721.2	48.0	0.1913	704.7	0.068
736	723.3	52.5	0.1913	704.7	0.068
737	723.3	52.5	0.1913	705.4	0.068
738	723.3	52.5	0.1913	704.7	0.068
739	723.3	52.5	0.1913	704.7	0.068
740	723.3	52.5	0.1913	704.7	0.068
741	723.3	52.5	0.1925	704.7	0.068
742	724.7	52.5	0.1913	704.7	0.068
743	723.3	56.5	0.1974	705.4	1.693
744	723.3	56.5	0.1974	704.7	1.693
745	723.3	56.5	0.1984	704.7	1.693
746	723.3	60.9	0.1984	705.4	1.693
747	723.3	60.9	0.1984	704.7	1.693
748	723.3	56.5	0.1996	704.7	1.693
749	723.3	60.9	0.1996	704.7	1.693
750	723.3	60.9	0.1996	704.7	1.693
751	723.3	60.9	0.2009	704.7	1.693
752	724.7	60.9	0.2009	704.7	1.693
753	723.3	60.9	0.2009	705.4	1.693
754	723.3	60.9	0.2022	704.7	1.693
755	723.3	60.9	0.2032	704.7	1.693
756	723.3	60.9	0.2032	704.7	1.693
757	723.3	60.9	0.2032	704.7	1.693
758	723.3	60.9	0.2032	704.7	1.693
759	723.3	65.4	0.2045	704.7	1.693
760	723.3	60.9	0.2045	704.7	1.693
761	723.3	60.9	0.2057	704.7	1.693
762	723.3	60.9	0.2057	704.0	1.693
763	723.3	65.4	0.2057	704.0	1.693
764	723.3	65.4	0.2068	704.7	1.693
765	723.3	60.9	0.2068	704.0	1.693
766	723.3	60.9	0.2080	704.7	1.693
767	723.3	60.9	0.2080	704.7	1.693
768	723.3	60.9	0.2080	704.0	1.693
769	723.3	60.9	0.2093	704.7	1.693
770	723.3	60.9	0.2093	704.7	1.693
771	721.2	60.9	0.2103	704.0	1.693
772	723.3	60.9	0.2103	704.7	1.693
773	723.3	65.4	0.2103	704.0	1.693
774	723.3	60.9	0.2116	704.0	1.693
775	723.3	60.9	0.2116	704.7	1.693
776	723.3	60.9	0.2129	704.0	1.693
777	723.3	60.9	0.2129	704.0	1.693
778	723.3	60.9	0.2141	704.0	1.693
779	723.3	65.4	0.2141	704.0	1.693
780	723.3	60.9	0.2141	704.0	1.693
781	723.3	60.9	0.2151	704.0	1.693
782	723.3	65.4	0.2164	704.0	1.693
783	723.3	60.9	0.2164	704.0	1.693
784	723.3	65.4	0.2164	704.0	1.693
785	723.3	60.9	0.2177	704.0	1.693
786	723.3	69.8	0.2283	704.0	42.333
787	723.3	74.3	0.2403	703.3	42.333
788	723.3	69.8	0.2535	702.6	42.333
789	723.3	74.3	0.2667	701.9	42.333
790	723.3	74.3	0.2786	700.5	42.333
791	723.3	52.5	0.2977	700.5	1.693
792	723.3	56.5	0.2977	700.5	1.693
793	723.3	56.5	0.2977	700.5	1.693
794	723.3	56.5	0.2990	700.5	1.693
795	723.3	56.5	0.2990	700.5	1.693
796	723.3	56.5	0.2990	701.2	1.693
797	723.3	60.9	0.2990	701.2	1.693
798	723.3	60.9	0.3000	701.2	1.693
799	723.3	60.9	0.3000	701.2	1.693
800	723.3	60.9	0.3000	701.2	1.693
801	723.3	60.9	0.3012	700.5	1.693
802	723.3	60.9	0.3012	701.2	1.693
803	723.3	60.9	0.3025	701.2	1.693
804	723.3	60.9	0.3035	701.2	1.693
805	723.3	65.4	0.3025	701.2	1.693
806	723.3	60.9	0.3035	701.2	1.693
807	723.3	60.9	0.3035	701.2	1.693
808	723.3	60.9	0.3048	701.2	1.693
809	723.3	65.4	0.3048	701.9	1.693
810	723.3	60.9	0.3061	701.2	1.693
811	723.3	65.4	0.3061	701.2	1.693
812	723.3	60.9	0.3073	701.2	1.693
813	723.3	65.4	0.3061	701.9	1.693
814	724.7	60.9	0.3073	701.9	1.693
815	723.3	65.4	0.3073	701.9	1.693
816	723.3	65.4	0.3084	701.9	1.693
817	721.2	65.4	0.3084	701.9	1.693
818	723.3	65.4	0.3084	701.2	1.693
819	723.3	60.9	0.3096	701.2	1.693
820	723.3	65.4	0.3109	701.9	1.693
821	723.3	65.4	0.3109	701.9	1.693
822	723.3	65.4	0.3109	701.9	1.693
823	723.3	60.9	0.3119	701.9	1.693
824	723.3	65.4	0.3119	701.9	1.693
825	723.3	65.4	0.3119	701.9	1.693
826	723.3	65.4	0.3132	701.9	1.693
827	723.3	65.4	0.3145	701.9	1.693
828	723.3	60.9	0.3145	701.2	1.693
829	723.3	65.4	0.3132	701.2	1.693
830	723.3	65.4	0.3155	701.9	1.693
831	723.3	65.4	0.3155	701.9	1.693
832	723.3	60.9	0.3167	701.9	1.693
833	723.3	65.4	0.3167	701.9	1.693
834	723.3	65.4	0.3167	701.9	1.693
835	723.3	65.4	0.3180	701.9	1.693
836	723.3	60.9	0.3180	701.9	1.693
837	723.3	65.4	0.3180	701.9	1.693
838	723.3	65.4	0.3193	701.9	1.693
839	723.3	65.4	0.3193	701.9	1.693
840	724.7	65.4	0.3203	701.9	1.693
841	723.3	65.4	0.3203	701.9	1.693
842	723.3	60.9	0.3216	701.9	1.693
843	723.3	60.9	0.3216	701.9	1.693
844	723.3	65.4	0.3228	701.9	1.693
845	723.3	65.4	0.3228	701.9	1.693
846	723.3	65.4	0.3228	701.9	1.693
847	723.3	65.4	0.3239	701.9	1.693
848	723.3	60.9	0.3239	701.9	1.693
849	723.3	65.4	0.3239	702.6	1.693
850	723.3	65.4	0.3251	701.9	1.693
851	723.3	65.4	0.3264	702.6	1.693
852	723.3	65.4	0.3264	702.6	1.693
853	723.3	65.4	0.3277	701.9	1.693
854	723.3	60.9	0.3277	701.9	1.693
855	723.3	65.4	0.3277	701.9	1.693
856	723.3	60.9	0.3277	702.6	1.693
857	723.3	65.4	0.3287	701.9	1.693
858	723.3	65.4	0.3299	702.6	1.693
859	723.3	60.9	0.3299	702.6	1.693
860	723.3	65.4	0.3299	702.6	1.693

Table A5. Continued.

#	σ_3 [kPa]	F_a [N]	ΔL [cm]	p_w [kPa]	u_a [µm/s]
861	723.3	60.9	0.3312	701.9	1.693
862	723.3	65.4	0.3312	702.6	1.693
863	723.3	65.4	0.3312	701.9	1.693
864	723.3	60.9	0.3322	702.6	1.693
865	723.3	60.9	0.3299	703.3	1.693
866	723.3	65.4	0.3322	702.6	1.693
867	723.3	65.4	0.3335	702.6	1.693
868	723.3	69.8	0.3358	702.6	8.467
869	723.3	69.8	0.3383	702.6	8.467
870	723.3	69.8	0.3419	701.9	8.467
871	723.3	69.8	0.3432	701.9	8.467
872	723.3	69.8	0.3467	702.6	8.467
873	723.3	69.8	0.3480	701.9	8.467
874	723.3	69.8	0.3515	701.9	8.467
875	723.3	69.8	0.3538	701.9	8.467
876	723.3	69.8	0.3561	701.9	8.467
877	723.3	69.8	0.3586	701.9	8.467
878	723.3	69.8	0.3609	701.9	8.467
879	723.3	69.8	0.3645	701.9	8.467
880	723.3	69.8	0.3658	701.2	8.467
881	723.3	69.8	0.3693	701.2	8.467
882	723.3	65.4	0.3706	701.2	8.467
883	723.3	65.4	0.3741	701.2	8.467
884	723.3	69.8	0.3764	701.2	8.467
885	723.3	69.8	0.3790	701.2	8.467
886	723.3	69.8	0.3813	700.5	8.467
887	723.3	69.8	0.3838	700.5	8.467
888	723.3	52.5	0.3861	701.2	1.693
889	723.3	52.5	0.3874	701.2	1.693
890	723.3	52.5	0.3874	701.2	1.693
891	723.3	52.5	0.3874	701.2	1.693
892	723.3	56.5	0.3874	701.2	1.693
893	723.3	56.5	0.3874	701.9	1.693
894	723.3	60.9	0.3874	701.9	1.693
895	723.3	60.9	0.3884	701.9	1.693
896	723.3	60.9	0.3884	701.9	1.693
897	723.3	60.9	0.3884	701.9	1.693
898	723.3	60.9	0.3884	701.9	1.693
899	723.3	60.9	0.3896	701.9	1.693
900	723.3	65.4	0.3896	701.9	1.693
901	723.3	65.4	0.3909	701.9	1.693
902	723.3	65.4	0.3909	701.9	1.693
903	723.3	65.4	0.3909	701.9	1.693
904	723.3	65.4	0.3909	701.9	1.693
905	723.3	60.9	0.3922	701.9	1.693
906	723.3	65.4	0.3922	701.9	1.693
907	723.3	65.4	0.3922	702.6	1.693
908	724.7	65.4	0.3932	702.6	1.693
909	721.2	65.4	0.3932	702.6	1.693
910	723.3	65.4	0.3945	701.9	1.693
911	721.2	60.9	0.3945	702.6	1.693
912	723.3	65.4	0.3945	702.6	1.693
913	723.3	65.4	0.3957	701.9	1.693
914	723.3	65.4	0.3967	702.6	1.693
915	723.3	65.4	0.3967	702.6	1.693
916	723.3	65.4	0.3967	702.6	1.693
917	723.3	65.4	0.3980	702.6	1.693
918	723.3	65.4	0.3967	702.6	1.693
919	723.3	65.4	0.3980	702.6	1.693
920	724.7	65.4	0.3980	702.6	1.693
921	721.2	65.4	0.3993	702.6	1.693
922	723.3	65.4	0.3993	702.6	1.693
923	723.3	65.4	0.3993	702.6	1.693
924	723.3	65.4	0.4006	702.6	1.693
925	723.3	65.4	0.4006	702.6	1.693
926	724.7	65.4	0.4016	702.6	1.693
927	724.7	65.4	0.4028	702.6	1.693
928	721.2	65.4	0.4028	702.6	1.693
929	723.3	65.4	0.4028	702.6	1.693
930	723.3	65.4	0.4041	702.6	1.693
931	723.3	65.4	0.4041	702.6	1.693
932	723.3	60.9	0.4041	702.6	1.693
933	723.3	65.4	0.4051	702.6	1.693
934	723.3	65.4	0.4051	702.6	1.693
935	723.3	65.4	0.4051	702.6	1.693
936	723.3	65.4	0.4077	702.6	1.693
937	723.3	69.8	0.4077	702.6	1.693
938	723.3	69.8	0.4077	702.6	1.693
939	723.3	65.4	0.4077	702.6	1.693
940	723.3	65.4	0.4087	702.6	1.693
941	723.3	65.4	0.4087	702.6	1.693
942	723.3	69.8	0.4100	702.6	1.693
943	723.3	65.4	0.4100	703.3	1.693
944	723.3	65.4	0.4112	702.6	1.693
945	723.3	65.4	0.4112	702.6	1.693
946	723.3	65.4	0.4112	702.6	1.693
947	723.3	69.8	0.4125	702.6	1.693
948	723.3	65.4	0.4125	702.6	1.693
949	723.3	65.4	0.4125	703.3	1.693
950	723.3	69.8	0.4135	702.6	1.693
951	723.3	69.8	0.4148	702.6	1.693
952	723.3	65.4	0.4148	702.6	1.693
953	723.3	65.4	0.4148	702.6	1.693
954	723.3	69.8	0.4161	703.3	1.693
955	723.3	65.4	0.4161	703.3	1.693
956	723.3	65.4	0.4161	702.6	1.693
957	721.2	65.4	0.4161	703.3	1.693
958	723.3	65.4	0.4171	703.3	1.693
959	723.3	69.8	0.4171	702.6	1.693
960	723.3	65.4	0.4183	703.3	1.693
961	721.2	69.8	0.4183	703.3	1.693
962	723.3	69.8	0.4183	703.3	1.693
963	723.3	69.8	0.4196	703.3	1.693
964	723.3	69.8	0.4209	702.6	1.693
965	723.3	69.8	0.4209	703.3	1.693
966	723.3	69.8	0.4219	703.3	1.693
967	723.3	65.4	0.4219	703.3	1.693
968	723.3	69.8	0.4219	703.3	1.693
969	723.3	69.8	0.4232	703.3	1.693
970	723.3	69.8	0.4232	703.3	1.693
971	723.3	69.8	0.4244	703.3	1.693
972	723.3	65.4	0.4255	703.3	1.693
973	723.3	69.8	0.4255	703.3	1.693
974	723.3	65.4	0.4255	703.3	1.693
975	724.7	69.8	0.4255	702.6	1.693
976	723.3	69.8	0.4267	703.3	1.693
977	723.3	65.4	0.4280	703.3	1.693
978	723.3	65.4	0.4280	703.3	1.693
979	723.3	69.8	0.4280	703.3	1.693
980	723.3	69.8	0.4290	703.3	1.693
981	723.3	69.8	0.4303	703.3	1.693
982	723.3	69.8	0.4303	703.3	1.693
983	723.3	69.8	0.4303	703.3	1.693
984	723.3	69.8	0.4303	703.3	1.693
985	723.3	69.8	0.4315	703.3	1.693
986	723.3	65.4	0.4315	703.3	1.693
987	723.3	65.4	0.4328	703.3	1.693
988	723.3	65.4	0.4328	703.3	1.693
989	724.7	52.5	0.4387	703.3	0.339
990	723.3	52.5	0.4387	703.3	0.339
991	723.3	52.5	0.4387	703.3	0.339
992	723.3	52.5	0.4387	703.3	0.339
993	723.3	52.5	0.4387	703.3	0.339
994	723.3	52.5	0.4387	703.3	0.339
995	723.3	56.5	0.4387	703.3	0.339
996	723.3	56.5	0.4387	703.3	0.339
997	723.3	56.5	0.4387	703.3	0.339
998	723.3	56.5	0.4387	703.3	0.339
999	723.3	56.5	0.4387	703.3	0.339
1000	723.3	56.5	0.4387	703.3	0.339
1001	723.3	60.9	0.4387	703.3	0.339
1002	723.3	56.5	0.4387	703.3	0.339
1003	723.3	56.5	0.4387	703.3	0.339
1004	723.3	56.5	0.4387	704.0	0.339
1005	723.3	60.9	0.4387	704.0	0.339
1006	723.3	56.5	0.4387	704.0	0.339
1007	723.3	60.9	0.4387	703.3	0.339
1008	723.3	60.9	0.4399	703.3	0.339
1009	723.3	60.9	0.4387	704.0	0.339
1010	723.3	60.9	0.4399	704.0	0.339

Table A5. Continued.

#	σ_3 [kPa]	F_a [N]	ΔL [cm]	p_w [kPa]	u_a [μm/s]
1011	723.3	60.9	0.4399	704.0	0.339
1012	723.3	60.9	0.4399	704.0	0.339
1013	723.3	60.9	0.4399	704.0	0.339
1014	723.3	60.9	0.4399	703.3	0.339
1015	723.3	60.9	0.4399	704.7	0.339
1016	724.7	60.9	0.4399	704.0	0.339
1017	723.3	60.9	0.4399	704.0	0.339
1018	723.3	60.9	0.4399	704.0	0.339
1019	723.3	60.9	0.4399	704.0	0.339
1020	723.3	60.9	0.4412	704.7	0.339
1021	723.3	60.9	0.4387	704.0	0.339
1022	723.3	60.9	0.4399	704.0	0.339
1023	723.3	60.9	0.4399	704.7	0.339
1024	723.3	60.9	0.4412	704.7	0.339
1025	724.7	60.9	0.4399	704.0	0.339
1026	724.0	60.9	0.4399	704.0	0.339
1027	723.3	60.9	0.4412	704.7	0.339
1028	723.3	60.9	0.4412	704.0	0.339
1029	723.3	60.9	0.4412	704.7	0.339
1030	723.3	60.9	0.4412	704.7	0.339
1031	723.3	60.9	0.4412	704.7	0.339
1032	723.3	56.5	0.4412	704.7	0.339
1033	723.3	60.9	0.4412	704.7	0.339
1034	723.3	60.9	0.4412	704.7	0.339
1035	723.3	60.9	0.4422	704.7	0.339
1036	723.3	60.9	0.4412	704.7	0.339
1037	723.3	60.9	0.4412	704.7	0.339
1038	723.3	65.4	0.4412	704.7	0.339
1039	723.3	60.9	0.4422	704.7	0.339
1040	723.3	60.9	0.4412	704.7	0.339
1041	723.3	56.5	0.4412	704.7	0.339
1042	723.3	60.9	0.4422	704.7	0.339
1043	723.3	60.9	0.4422	704.7	0.339
1044	723.3	65.4	0.4422	705.4	0.339
1045	723.3	60.9	0.4422	704.7	0.339
1046	723.3	60.9	0.4422	704.7	0.339
1047	723.3	60.9	0.4422	705.4	0.339
1048	723.3	65.4	0.4422	704.7	0.339
1049	723.3	65.4	0.4422	704.7	0.339
1050	723.3	65.4	0.4422	705.4	0.339
1051	723.3	60.9	0.4422	704.7	0.339
1052	723.3	65.4	0.4435	705.4	0.339
1053	723.3	60.9	0.4435	705.4	0.339
1054	723.3	65.4	0.4435	705.4	0.339
1055	723.3	60.9	0.4422	705.4	0.339
1056	723.3	60.9	0.4435	705.4	0.339
1057	723.3	60.9	0.4435	704.7	0.339
1058	723.3	60.9	0.4435	705.4	0.339
1059	723.3	52.5	0.4448	704.7	0.068
1060	723.3	52.5	0.4448	704.7	0.068
1061	723.3	52.5	0.4435	704.7	0.068
1062	723.3	52.5	0.4448	705.4	0.068
1063	723.3	52.5	0.4435	705.4	0.068
1064	723.3	52.5	0.4435	705.4	0.068
1065	723.3	52.5	0.4448	705.4	0.068
1066	723.3	52.5	0.4435	704.7	0.068
1067	721.2	52.5	0.4435	705.4	0.068
1068	723.3	52.5	0.4435	704.7	0.068
1069	723.3	52.5	0.4435	705.4	0.068
1070	723.3	52.5	0.4435	705.4	0.068
1071	723.3	48.0	0.4435	705.4	0.068
1072	723.3	52.5	0.4435	704.7	0.068
1073	723.3	52.5	0.4435	705.4	0.068
1074	723.3	48.0	0.4435	705.4	0.068
1075	723.3	52.5	0.4435	705.4	0.068
1076	723.3	52.5	0.4435	704.7	0.068
1077	723.3	52.5	0.4435	705.4	0.068
1078	723.3	52.5	0.4435	705.4	0.068
1079	723.3	52.5	0.4435	705.4	0.068
1080	723.3	52.5	0.4435	705.4	0.068
1081	723.3	52.5	0.4435	705.4	0.068
1082	723.3	52.5	0.4435	705.4	0.068
1083	723.3	52.5	0.4435	705.4	0.068
1084	723.3	52.5	0.4448	705.4	0.068
1085	723.3	48.0	0.4435	706.0	0.068
1086	723.3	48.0	0.4435	705.4	0.068
1087	723.3	52.5	0.4435	705.4	0.068
1088	723.3	52.5	0.4435	706.0	0.068
1089	723.3	52.5	0.4448	705.4	0.068
1090	723.3	52.5	0.4435	705.4	0.068
1091	723.3	52.5	0.4435	705.4	0.068
1092	723.3	52.5	0.4435	706.0	0.068
1093	723.3	52.5	0.4435	706.0	0.068
1094	723.3	52.5	0.4435	705.4	0.068
1095	723.3	48.0	0.4435	705.4	0.068
1096	723.3	48.0	0.4435	706.0	0.068
1097	723.3	48.0	0.4435	705.4	0.068
1098	723.3	52.5	0.4435	705.4	0.068
1099	723.3	52.5	0.4435	706.0	0.068
1100	723.3	52.5	0.4435	705.4	0.068
1101	723.3	48.0	0.4435	706.0	0.068
1102	723.3	48.0	0.4435	705.4	0.068
1103	723.3	52.5	0.4435	706.0	0.068
1104	723.3	48.0	0.4435	706.0	0.068
1105	723.3	52.5	0.4435	706.0	0.068
1106	723.3	52.5	0.4435	706.0	0.068
1107	723.3	52.5	0.4435	706.0	0.068
1108	723.3	52.5	0.4435	706.0	0.068
1109	724.7	52.5	0.4435	706.0	0.068
1110	723.3	52.5	0.4435	706.0	0.068
1111	723.3	48.0	0.4435	706.0	0.068
1112	723.3	52.5	0.4435	706.0	0.068
1113	723.3	52.5	0.4435	706.0	0.068
1114	723.3	52.5	0.4435	706.0	0.068
1115	723.3	52.5	0.4435	706.0	0.068
1116	723.3	52.5	0.4435	706.0	0.068
1117	723.3	52.5	0.4435	706.0	0.068
1118	723.3	52.5	0.4435	706.0	0.068
1119	723.3	52.5	0.4435	706.0	0.068
1120	723.3	48.0	0.4435	706.0	0.068
1121	723.3	52.5	0.4435	706.0	0.068
1122	723.3	52.5	0.4435	706.0	0.068
1123	723.3	52.5	0.4435	706.0	0.068
1124	723.3	52.5	0.4435	706.0	0.068
1125	723.3	48.0	0.4435	706.0	0.068
1126	723.3	52.5	0.4435	706.0	0.068
1127	723.3	52.5	0.4435	706.0	0.068
1128	723.3	52.5	0.4435	706.0	0.068
1129	723.3	52.5	0.4435	706.0	0.068
1130	723.3	52.5	0.4435	706.0	0.068
1131	723.3	48.0	0.4435	706.7	0.068
1132	723.3	52.5	0.4435	706.0	0.068
1133	723.3	52.5	0.4435	705.4	0.068
1134	723.3	52.5	0.4435	706.0	0.068
1135	723.3	52.5	0.4435	706.7	0.068
1136	723.3	52.5	0.4435	706.0	0.068
1137	723.3	52.5	0.4435	706.0	0.068
1138	723.3	48.0	0.4435	706.0	0.068
1139	723.3	52.5	0.4435	706.0	0.068
1140	723.3	52.5	0.4435	706.0	0.068
1141	723.3	48.0	0.4435	706.0	0.068
1142	721.2	52.5	0.4422	706.0	0.068
1143	723.3	52.5	0.4435	706.0	0.068
1144	723.3	52.5	0.4435	706.0	0.068
1145	723.3	52.5	0.4435	706.0	0.068
1146	723.3	52.5	0.4435	706.0	0.068
1147	723.3	52.5	0.4435	706.0	0.068
1148	723.3	52.5	0.4435	706.0	0.068
1149	723.3	52.5	0.4435	706.0	0.068
1150	723.3	52.5	0.4435	706.7	0.068
1151	723.3	48.0	0.4435	706.0	0.068
1152	723.3	52.5	0.4435	706.7	0.068
1153	723.3	48.0	0.4435	706.0	0.068
1154	723.3	52.5	0.4435	706.0	0.068
1155	723.3	52.5	0.4435	706.7	0.068
1156	724.7	52.5	0.4435	706.0	0.068
1157	724.7	52.5	0.4435	706.7	0.068
1158	723.3	48.0	0.4435	706.0	0.068
1159	723.3	52.5	0.4435	706.0	0.068
1160	723.3	52.5	0.4435	706.0	0.068

Table A5. Continued.

#	σ_3 [kPa]	F_a [N]	ΔL [cm]	p_w [kPa]	u_a [µm/s]
1161	723.3	52.5	0.4435	706.7	0.068
1162	723.3	52.5	0.4448	706.7	0.068
1163	723.3	52.5	0.4435	706.7	0.068
1164	723.3	52.5	0.4435	706.0	0.068
1165	723.3	52.5	0.4435	706.7	0.068
1166	723.3	48.0	0.4435	706.7	0.068
1167	723.3	52.5	0.4435	706.7	0.068
1168	723.3	48.0	0.4435	706.7	0.068
1169	723.3	52.5	0.4435	706.7	0.068
1170	723.3	52.5	0.4435	706.0	0.068
1171	723.3	52.5	0.4435	706.0	0.068
1172	723.3	48.0	0.4448	706.7	0.068
1173	723.3	52.5	0.4435	706.0	0.068
1174	723.3	52.5	0.4435	706.7	0.068
1175	723.3	52.5	0.4435	706.7	0.068
1176	723.3	52.5	0.4435	706.7	0.068
1177	723.3	52.5	0.4435	706.7	0.068
1178	724.7	52.5	0.4435	706.7	0.068
1179	723.3	48.0	0.4435	706.7	0.068
1180	721.2	52.5	0.4435	706.7	0.068
1181	723.3	52.5	0.4435	706.7	0.068
1182	723.3	52.5	0.4435	706.7	0.068
1183	723.3	52.5	0.4448	706.7	0.068
1184	723.3	52.5	0.4435	706.7	0.068
1185	723.3	52.5	0.4435	706.7	0.068
1186	724.7	52.5	0.4435	706.7	0.068
1187	723.3	52.5	0.4435	706.7	0.068
1188	723.3	52.5	0.4435	706.7	0.068
1189	723.3	52.5	0.4435	706.7	0.068
1190	723.3	52.5	0.4435	706.7	0.068
1191	723.3	52.5	0.4435	706.7	0.068
1192	723.3	52.5	0.4435	706.7	0.068
1193	724.7	52.5	0.4435	706.7	0.068
1194	723.3	48.0	0.4435	706.7	0.068
1195	723.3	52.5	0.4435	706.7	0.068
1196	721.2	52.5	0.4435	706.7	0.068
1197	723.3	52.5	0.4435	706.7	0.068
1198	723.3	52.5	0.4435	706.7	0.068
1199	723.3	48.0	0.4448	707.4	0.068
1200	723.3	52.5	0.4435	706.7	0.068
1201	723.3	52.5	0.4435	706.7	0.068
1202	723.3	48.0	0.4435	706.7	0.068
1203	723.3	52.5	0.4422	706.7	0.068
1204	723.3	52.5	0.4435	706.7	0.068
1205	723.3	52.5	0.4435	706.7	0.068
1206	723.3	48.0	0.4435	706.7	0.068
1207	723.3	52.5	0.4435	707.4	0.068
1208	723.3	52.5	0.4435	707.4	0.068
1209	723.3	52.5	0.4435	706.7	0.068
1210	723.3	52.5	0.4435	707.4	0.068
1211	723.3	52.5	0.4448	707.4	0.068
1212	723.3	52.5	0.4435	706.7	0.068
1213	723.3	52.5	0.4448	707.4	0.068
1214	723.3	48.0	0.4422	706.7	0.068
1215	723.3	52.5	0.4435	707.4	0.068
1216	723.3	52.5	0.4435	707.4	0.068
1217	723.3	52.5	0.4435	707.4	0.068
1218	723.3	52.5	0.4435	707.4	0.068
1219	723.3	52.5	0.4435	706.7	0.068
1220	723.3	48.0	0.4435	707.4	0.068
1221	723.3	52.5	0.4435	707.4	0.068
1222	723.3	52.5	0.4435	707.4	0.068
1223	723.3	52.5	0.4435	707.4	0.068
1224	724.7	52.5	0.4435	707.4	0.068
1225	723.3	52.5	0.4435	706.7	0.068
1226	723.3	48.0	0.4435	706.7	0.068
1227	723.3	52.5	0.4435	706.7	0.068
1228	723.3	48.0	0.4435	707.4	0.068
1229	723.3	52.5	0.4435	707.4	0.068
1230	723.3	52.5	0.4435	707.4	0.068
1231	723.3	52.5	0.4435	707.4	0.068
1232	723.3	52.5	0.4435	706.7	0.068
1233	723.3	52.5	0.4435	707.4	0.068
1234	723.3	52.5	0.4435	707.4	0.068
1235	723.3	52.5	0.4435	707.4	0.068
1236	723.3	52.5	0.4448	707.4	0.068
1237	723.3	52.5	0.4435	707.4	0.068
1238	723.3	52.5	0.4435	707.4	0.068
1239	723.3	52.5	0.4448	707.4	0.068
1240	723.3	52.5	0.4435	707.4	0.068
1241	723.3	52.5	0.4435	706.7	0.068
1242	723.3	52.5	0.4435	707.4	0.068
1243	723.3	52.5	0.4435	707.4	0.068
1244	721.2	52.5	0.4435	707.4	0.068
1245	723.3	52.5	0.4435	707.4	0.068
1246	723.3	52.5	0.4435	707.4	0.068
1247	723.3	52.5	0.4435	707.4	0.068
1248	723.3	52.5	0.4448	707.4	0.068
1249	723.3	52.5	0.4435	707.4	0.068
1250	723.3	52.5	0.4435	706.7	0.068
1251	723.3	52.5	0.4435	707.4	0.068
1252	723.3	52.5	0.4435	707.4	0.068
1253	723.3	52.5	0.4435	707.4	0.068
1254	723.3	52.5	0.4435	707.4	0.068
1255	723.3	52.5	0.4435	707.4	0.068
1256	723.3	52.5	0.4435	707.4	0.068
1257	723.3	52.5	0.4435	707.4	0.068
1258	723.3	52.5	0.4448	707.4	0.068
1259	723.3	52.5	0.4448	706.7	0.068
1260	723.3	52.5	0.4448	707.4	0.068
1261	723.3	52.5	0.4448	707.4	0.068
1262	724.7	52.5	0.4435	707.4	0.068
1263	723.3	52.5	0.4435	707.4	0.068
1264	723.3	52.5	0.4435	707.4	0.068
1265	723.3	52.5	0.4435	707.4	0.068
1266	723.3	52.5	0.4448	707.4	0.068
1267	723.3	52.5	0.4448	707.4	0.068
1268	723.3	52.5	0.4435	707.4	0.068
1269	723.3	52.5	0.4435	707.4	0.068
1270	723.3	52.5	0.4448	707.4	0.068
1271	723.3	52.5	0.4448	707.4	0.068
1272	723.3	52.5	0.4435	707.4	0.068
1273	723.3	52.5	0.4435	707.4	0.068
1274	723.3	52.5	0.4435	707.4	0.068
1275	723.3	52.5	0.4435	707.4	0.068
1276	723.3	52.5	0.4435	707.4	0.068
1277	723.3	52.5	0.4435	707.4	0.068
1278	723.3	52.5	0.4435	707.4	0.068
1279	723.3	52.5	0.4448	707.4	0.068
1280	723.3	52.5	0.4435	707.4	0.068
1281	723.3	52.5	0.4435	707.4	0.068
1282	723.3	52.5	0.4435	707.4	0.068
1283	723.3	52.5	0.4435	707.4	0.068
1284	721.2	52.5	0.4435	707.4	0.068
1285	723.3	52.5	0.4435	707.4	0.068
1286	723.3	52.5	0.4448	707.4	0.068
1287	723.3	52.5	0.4435	707.4	0.068
1288	723.3	52.5	0.4448	707.4	0.068
1289	723.3	52.5	0.4435	707.4	0.068
1290	723.3	52.5	0.4448	707.4	0.068
1291	723.3	52.5	0.4435	707.4	0.068
1292	723.3	52.5	0.4435	707.4	0.068
1293	721.2	52.5	0.4435	707.4	0.068
1294	723.3	52.5	0.4448	707.4	0.068
1295	723.3	52.5	0.4435	707.4	0.068
1296	723.3	52.5	0.4435	707.4	0.068
1297	723.3	52.5	0.4435	707.4	0.068
1298	723.3	52.5	0.4448	707.4	0.068
1299	723.3	52.5	0.4435	707.4	0.068
1300	723.3	52.5	0.4435	707.4	0.068
1301	723.3	52.5	0.4448	707.4	0.068
1302	723.3	52.5	0.4448	707.4	0.068
1303	723.3	52.5	0.4448	707.4	0.068
1304	723.3	52.5	0.4435	707.4	0.068
1305	723.3	52.5	0.4448	707.4	0.068
1306	723.3	52.5	0.4435	707.4	0.068
1307	723.3	52.5	0.4435	707.4	0.068
1308	723.3	52.5	0.4435	707.4	0.068
1309	723.3	52.5	0.4422	707.4	0.068
1310	723.3	52.5	0.4435	707.4	0.068

Table A5. Continued.

#	σ_3 [kPa]	F_a [N]	ΔL [cm]	p_w [kPa]	u_a [μm/s]
1311	723.3	52.5	0.4435	707.4	0.068
1312	723.3	52.5	0.4448	707.4	0.068
1313	723.3	52.5	0.4448	707.4	0.068
1314	723.3	52.5	0.4448	707.4	0.068
1315	723.3	52.5	0.4435	707.4	0.068
1316	723.3	48.0	0.4435	707.4	0.068
1317	723.3	52.5	0.4435	707.4	0.068
1318	723.3	52.5	0.4435	707.4	0.068
1319	723.3	52.5	0.4435	707.4	0.068
1320	723.3	52.5	0.4435	707.4	0.068
1321	723.3	52.5	0.4448	707.4	0.068
1322	723.3	52.5	0.4448	707.4	0.068
1323	723.3	52.5	0.4448	707.4	0.068
1324	723.3	52.5	0.4435	707.4	0.068
1325	723.3	52.5	0.4448	707.4	0.068
1326	723.3	52.5	0.4435	707.4	0.068
1327	723.3	52.5	0.4448	707.4	0.068
1328	723.3	52.5	0.4435	707.4	0.068
1329	723.3	52.5	0.4435	707.4	0.068
1330	723.3	52.5	0.4448	707.4	0.068
1331	721.2	52.5	0.4435	707.4	0.068
1332	723.3	52.5	0.4435	707.4	0.068
1333	723.3	48.0	0.4448	707.4	0.068
1334	723.3	52.5	0.4448	707.4	0.068
1335	723.3	52.5	0.4448	707.4	0.068
1336	723.3	52.5	0.4448	707.4	0.068
1337	723.3	52.5	0.4448	707.4	0.068
1338	723.3	52.5	0.4435	707.4	0.068
1339	723.3	52.5	0.4448	707.4	0.068
1340	723.3	52.5	0.4448	707.4	0.068
1341	723.3	52.5	0.4435	707.4	0.068
1342	723.3	52.5	0.4448	707.4	0.068
1343	723.3	52.5	0.4448	707.4	0.068
1344	723.3	52.5	0.4448	707.4	0.068
1345	723.3	52.5	0.4448	707.4	0.068
1346	723.3	52.5	0.4435	707.4	0.068
1347	723.3	52.5	0.4435	707.4	0.068
1348	723.3	52.5	0.4435	707.4	0.068
1349	721.2	52.5	0.4435	707.4	0.068
1350	723.3	52.5	0.4448	707.4	0.068
1351	723.3	52.5	0.4435	707.4	0.068
1352	723.3	52.5	0.4435	707.4	0.068
1353	723.3	52.5	0.4435	707.4	0.068
1354	723.3	52.5	0.4448	707.4	0.068
1355	723.3	52.5	0.4435	707.4	0.068
1356	723.3	52.5	0.4435	707.4	0.068
1357	723.3	52.5	0.4448	707.4	0.068
1358	723.3	52.5	0.4448	707.4	0.068
1359	723.3	52.5	0.4435	707.4	0.068
1360	723.3	52.5	0.4448	707.4	0.068
1361	723.3	52.5	0.4448	707.4	0.068
1362	723.3	52.5	0.4435	707.4	0.068
1363	723.3	52.5	0.4448	707.4	0.068
1364	723.3	52.5	0.4448	707.4	0.068
1365	723.3	52.5	0.4448	707.4	0.068
1366	723.3	52.5	0.4448	707.4	0.068
1367	723.3	52.5	0.4448	707.4	0.068
1368	723.3	52.5	0.4448	707.4	0.068
1369	723.3	52.5	0.4448	707.4	0.068
1370	723.3	52.5	0.4448	707.4	0.068
1371	723.3	52.5	0.4448	707.4	0.068
1372	723.3	52.5	0.4448	707.4	0.068
1373	723.3	56.5	0.4435	707.4	0.068
1374	723.3	52.5	0.4448	707.4	0.068
1375	723.3	48.0	0.4435	707.4	0.068
1376	723.3	52.5	0.4448	707.4	0.068
1377	723.3	52.5	0.4448	707.4	0.068
1378	723.3	52.5	0.4448	707.4	0.068
1379	723.3	52.5	0.4448	707.4	0.068
1380	723.3	52.5	0.4448	707.4	0.068
1381	723.3	52.5	0.4448	707.4	0.068
1382	723.3	52.5	0.4435	707.4	0.068
1383	723.3	52.5	0.4448	707.4	0.068
1384	723.3	52.5	0.4435	707.4	0.068
1385	723.3	52.5	0.4435	707.4	0.068
1386	723.3	52.5	0.4448	707.4	0.068
1387	723.3	52.5	0.4448	707.4	0.068
1388	723.3	52.5	0.4435	707.4	0.068
1389	723.3	52.5	0.4448	707.4	0.068
1390	721.2	52.5	0.4435	707.4	0.068
1391	723.3	52.5	0.4448	707.4	0.068
1392	723.3	52.5	0.4448	707.4	0.068
1393	723.3	52.5	0.4448	707.4	0.068
1394	723.3	52.5	0.4448	707.4	0.068
1395	723.3	52.5	0.4435	707.4	0.068
1396	724.7	52.5	0.4448	707.4	0.068
1397	723.3	52.5	0.4448	707.4	0.068
1398	723.3	52.5	0.4448	707.4	0.068
1399	723.3	52.5	0.4448	707.4	0.068
1400	723.3	52.5	0.4448	707.4	0.068
1401	723.3	52.5	0.4448	707.4	0.068
1402	723.3	52.5	0.4435	707.4	0.068
1403	723.3	52.5	0.4448	707.4	0.068
1404	723.3	52.5	0.4448	707.4	0.068
1405	723.3	52.5	0.4448	707.4	0.068
1406	723.3	52.5	0.4448	707.4	0.068
1407	723.3	52.5	0.4448	707.4	0.068
1408	723.3	52.5	0.4448	707.4	0.068
1409	723.3	52.5	0.4448	707.4	0.068
1410	723.3	52.5	0.4448	707.4	0.068
1411	723.3	52.5	0.4448	707.4	0.068
1412	723.3	52.5	0.4448	707.4	0.068
1413	723.3	52.5	0.4448	707.4	0.068
1414	723.3	52.5	0.4448	707.4	0.068
1415	723.3	52.5	0.4448	707.4	0.068
1416	723.3	52.5	0.4448	707.4	0.068
1417	723.3	52.5	0.4448	707.4	0.068
1418	723.3	52.5	0.4448	707.4	0.068
1419	721.2	56.5	0.4448	707.4	0.068
1420	723.3	52.5	0.4448	707.4	0.068
1421	723.3	52.5	0.4448	707.4	0.068
1422	723.3	52.5	0.4448	707.4	0.068
1423	723.3	52.5	0.4448	707.4	0.068
1424	723.3	52.5	0.4435	707.4	0.068
1425	723.3	52.5	0.4448	707.4	0.068
1426	723.3	52.5	0.4448	707.4	0.068
1427	723.3	52.5	0.4448	707.4	0.068
1428	723.3	52.5	0.4448	707.4	0.068
1429	723.3	52.5	0.4448	707.4	0.068
1430	723.3	52.5	0.4435	707.4	0.068
1431	723.3	56.5	0.4448	707.4	0.068
1432	723.3	52.5	0.4448	707.4	0.068
1433	723.3	52.5	0.4448	707.4	0.068
1434	723.3	52.5	0.4448	707.4	0.068
1435	723.3	52.5	0.4435	707.4	0.068
1436	721.2	52.5	0.4448	707.4	0.068
1437	723.3	52.5	0.4448	707.4	0.068
1438	721.2	52.5	0.4448	707.4	0.068
1439	723.3	56.5	0.4448	707.4	0.068
1440	723.3	52.5	0.4448	707.4	0.068
1441	723.3	52.5	0.4448	707.4	0.068
1442	723.3	52.5	0.4448	707.4	0.068
1443	723.3	52.5	0.4448	708.1	0.068
1444	723.3	52.5	0.4448	707.4	0.068
1445	723.3	52.5	0.4448	707.4	0.068
1446	723.3	52.5	0.4448	707.4	0.068
1447	723.3	52.5	0.4448	707.4	0.068
1448	723.3	52.5	0.4448	707.4	0.068
1449	723.3	52.5	0.4448	707.4	0.068
1450	723.3	48.0	0.4448	707.4	0.068
1451	724.7	52.5	0.4448	707.4	0.068
1452	723.3	52.5	0.4448	707.4	0.068
1453	723.3	52.5	0.4448	707.4	0.068
1454	723.3	52.5	0.4448	707.4	0.068
1455	723.3	52.5	0.4448	708.1	0.068
1456	724.7	56.5	0.4448	707.4	0.068
1457	723.3	52.5	0.4448	707.4	0.068
1458	723.3	52.5	0.4448	707.4	0.068
1459	723.3	52.5	0.4448	707.4	0.068
1460	723.3	52.5	0.4448	707.4	0.068

Table A5. Continued.

#	σ_3 [kPa]	F_a [N]	ΔL [cm]	p_w [kPa]	u_a [μm/s]
1461	723.3	52.5	0.4448	707.4	0.068
1462	723.3	52.5	0.4448	708.1	0.068
1463	723.3	52.5	0.4448	707.4	0.068
1464	723.3	52.5	0.4448	707.4	0.068
1465	723.3	56.5	0.4448	707.4	0.068
1466	723.3	52.5	0.4448	707.4	0.068
1467	721.2	52.5	0.4435	708.1	0.068
1468	723.3	56.5	0.4448	707.4	0.068
1469	723.3	52.5	0.4435	707.4	0.068
1470	723.3	52.5	0.4448	707.4	0.068
1471	723.3	52.5	0.4448	707.4	0.068
1472	723.3	52.5	0.4435	707.4	0.068
1473	723.3	52.5	0.4448	707.4	0.068
1474	723.3	52.5	0.4448	707.4	0.068
1475	723.3	52.5	0.4448	708.1	0.068
1476	723.3	52.5	0.4448	708.1	0.068
1477	723.3	52.5	0.4435	707.4	0.068
1478	723.3	52.5	0.4448	707.4	0.068
1479	723.3	52.5	0.4448	708.1	0.068
1480	724.7	52.5	0.4448	708.1	0.068
1481	723.3	52.5	0.4435	707.4	0.068
1482	723.3	52.5	0.4448	708.1	0.068
1483	723.3	52.5	0.4435	708.1	0.068
1484	723.3	52.5	0.4448	708.1	0.068
1485	723.3	52.5	0.4435	707.4	0.068
1486	723.3	52.5	0.4448	707.4	0.068
1487	723.3	52.5	0.4448	708.1	0.068
1488	723.3	52.5	0.4448	708.1	0.068
1489	723.3	56.5	0.4448	707.4	0.068
1490	724.7	52.5	0.4448	707.4	0.068
1491	723.3	52.5	0.4448	708.1	0.068
1492	723.3	52.5	0.4448	708.1	0.068
1493	723.3	52.5	0.4448	707.4	0.068
1494	723.3	52.5	0.4448	708.1	0.068
1495	723.3	52.5	0.4448	707.4	0.068
1496	723.3	52.5	0.4435	708.1	0.068
1497	723.3	52.5	0.4435	708.1	0.068
1498	723.3	52.5	0.4448	707.4	0.068
1499	723.3	56.5	0.4448	707.4	0.068
1500	723.3	52.5	0.4448	708.1	0.068
1501	723.3	52.5	0.4448	707.4	0.068
1502	723.3	52.5	0.4448	708.1	0.068
1503	723.3	52.5	0.4448	707.4	0.068
1504	723.3	52.5	0.4448	707.4	0.068
1505	723.3	52.5	0.4448	707.4	0.068
1506	723.3	52.5	0.4448	708.1	0.068
1507	723.3	52.5	0.4448	708.1	0.068
1508	723.3	56.5	0.4435	707.4	0.068
1509	723.3	56.5	0.4448	707.4	0.068
1510	723.3	52.5	0.4448	708.1	0.068
1511	723.3	52.5	0.4448	708.1	0.068
1512	723.3	52.5	0.4448	708.1	0.068
1513	723.3	56.5	0.4448	707.4	0.068
1514	723.3	56.5	0.4448	707.4	0.068
1515	723.3	52.5	0.4435	708.1	0.068
1516	723.3	52.5	0.4448	707.4	0.068
1517	723.3	52.5	0.4448	708.1	0.068
1518	723.3	52.5	0.4448	708.1	0.068
1519	723.3	52.5	0.4448	708.1	0.068
1520	723.3	52.5	0.4448	708.1	0.068
1521	723.3	56.5	0.4448	708.1	0.068
1522	723.3	52.5	0.4448	708.1	0.068
1523	723.3	52.5	0.4448	707.4	0.068
1524	723.3	52.5	0.4435	708.1	0.068
1525	723.3	52.5	0.4448	707.4	0.068
1526	721.2	56.5	0.4448	707.4	0.068
1527	723.3	52.5	0.4448	707.4	0.068
1528	723.3	52.5	0.4448	708.1	0.068
1529	723.3	52.5	0.4448	708.1	0.068
1530	723.3	52.5	0.4448	708.1	0.068
1531	723.3	52.5	0.4448	707.4	0.068
1532	723.3	52.5	0.4448	708.1	0.068
1533	723.3	56.5	0.4448	708.1	0.068
1534	723.3	52.5	0.4448	708.1	0.068
1535	723.3	52.5	0.4448	708.1	0.068
1536	723.3	52.5	0.4448	708.1	0.068
1537	723.3	52.5	0.4448	708.1	0.068
1538	723.3	52.5	0.4448	707.4	0.068
1539	723.3	56.5	0.4448	708.1	0.068
1540	723.3	52.5	0.4448	708.1	0.068
1541	723.3	52.5	0.4435	708.1	0.068
1542	723.3	52.5	0.4448	708.1	0.068
1543	723.3	52.5	0.4448	707.4	0.068
1544	723.3	52.5	0.4448	707.4	0.068
1545	723.3	52.5	0.4448	708.1	0.068
1546	723.3	52.5	0.4448	708.1	0.068
1547	723.3	52.5	0.4448	708.1	0.068
1548	723.3	52.5	0.4448	707.4	0.068
1549	723.3	52.5	0.4448	708.1	0.068
1550	723.3	52.5	0.4448	708.1	0.068
1551	723.3	56.5	0.4448	708.1	0.068
1552	723.3	52.5	0.4448	707.4	0.068
1553	723.3	56.5	0.4448	708.1	0.068
1554	723.3	56.5	0.4448	708.1	0.068
1555	723.3	52.5	0.4448	708.1	0.068
1556	723.3	52.5	0.4448	708.1	0.068
1557	723.3	52.5	0.4448	707.4	0.068
1558	723.3	52.5	0.4448	707.4	0.068
1559	723.3	56.5	0.4448	707.4	0.068
1560	723.3	52.5	0.4448	708.1	0.068
1561	723.3	52.5	0.4448	707.4	0.068
1562	723.3	52.5	0.4448	708.1	0.068
1563	723.3	56.5	0.4448	708.1	0.068
1564	723.3	52.5	0.4448	708.1	0.068
1565	723.3	52.5	0.4448	708.1	0.068
1566	723.3	52.5	0.4448	708.1	0.068
1567	723.3	52.5	0.4448	708.1	0.068
1568	723.3	52.5	0.4448	708.1	0.068
1569	723.3	48.0	0.4448	708.1	0.068
1570	723.3	52.5	0.4448	708.1	0.068
1571	723.3	52.5	0.4448	708.1	0.068
1572	723.3	52.5	0.4448	708.1	0.068
1573	723.3	52.5	0.4448	708.1	0.068
1574	723.3	52.5	0.4448	708.1	0.068
1575	723.3	52.5	0.4448	708.1	0.068
1576	723.3	52.5	0.4448	708.1	0.068
1577	723.3	52.5	0.4448	708.1	0.068
1578	723.3	52.5	0.4448	708.1	0.068
1579	723.3	52.5	0.4448	708.1	0.068
1580	723.3	52.5	0.4435	708.1	0.068
1581	723.3	52.5	0.4448	708.1	0.068
1582	723.3	52.5	0.4448	708.1	0.068
1583	723.3	52.5	0.4448	708.1	0.068
1584	723.3	52.5	0.4448	708.1	0.068
1585	723.3	56.5	0.4448	707.4	0.068
1586	723.3	52.5	0.4448	707.4	0.068
1587	723.3	52.5	0.4448	708.1	0.068
1588	723.3	52.5	0.4448	707.4	0.068
1589	723.3	52.5	0.4435	708.1	0.068
1590	723.3	52.5	0.4448	707.4	0.068
1591	723.3	52.5	0.4448	707.4	0.068
1592	723.3	52.5	0.4448	708.1	0.068
1593	723.3	52.5	0.4448	708.1	0.068
1594	723.3	52.5	0.4448	708.1	0.068
1595	723.3	52.5	0.4448	708.1	0.068
1596	723.3	52.5	0.4448	708.1	0.068
1597	723.3	52.5	0.4448	707.4	0.068
1598	723.3	52.5	0.4448	708.1	0.068
1599	723.3	52.5	0.4448	708.1	0.068
1600	723.3	52.5	0.4448	708.1	0.068
1601	723.3	52.5	0.4448	708.1	0.068
1602	723.3	52.5	0.4448	708.1	0.068
1603	723.3	52.5	0.4448	708.1	0.068
1604	723.3	52.5	0.4448	708.1	0.068
1605	723.3	52.5	0.4448	708.1	0.068
1606	723.3	52.5	0.4435	708.1	0.068
1607	723.3	56.5	0.4448	708.1	0.068
1608	723.3	56.5	0.4448	708.1	0.068
1609	723.3	52.5	0.4448	708.1	0.068
1610	723.3	56.5	0.4448	708.1	0.068

Table A5. Continued.

#	σ_3 [kPa]	F_a [N]	ΔL [cm]	p_w [kPa]	u_a [µm/s]
1611	723.3	52.5	0.4448	708.1	0.068
1612	723.3	56.5	0.4448	708.1	0.068
1613	724.7	52.5	0.4448	708.1	0.068
1614	721.2	52.5	0.4448	708.1	0.068
1615	723.3	56.5	0.4448	708.1	0.068
1616	723.3	52.5	0.4448	708.1	0.068
1617	723.3	52.5	0.4448	708.1	0.068
1618	723.3	52.5	0.4448	707.4	0.068
1619	723.3	52.5	0.4448	708.1	0.068
1620	723.3	52.5	0.4448	708.1	0.068
1621	723.3	56.5	0.4448	708.1	0.068
1622	723.3	56.5	0.4448	708.1	0.068
1623	723.3	52.5	0.4448	708.1	0.068
1624	723.3	52.5	0.4448	708.1	0.068
1625	721.2	52.5	0.4435	708.1	0.068
1626	723.3	52.5	0.4448	708.1	0.068
1627	723.3	52.5	0.4448	708.1	0.068
1628	721.2	52.5	0.4458	708.1	0.068
1629	723.3	52.5	0.4448	708.1	0.068
1630	723.3	56.5	0.4458	708.1	0.068
1631	723.3	56.5	0.4448	708.1	0.068
1632	723.3	52.5	0.4448	708.1	0.068
1633	721.2	52.5	0.4448	708.1	0.068
1634	723.3	52.5	0.4448	708.1	0.068
1635	723.3	52.5	0.4448	708.1	0.068
1636	723.3	52.5	0.4458	708.1	0.068
1637	723.3	56.5	0.4448	708.1	0.068
1638	723.3	56.5	0.4458	708.1	0.068
1639	723.3	56.5	0.4448	708.1	0.068
1640	723.3	56.5	0.4448	708.1	0.068
1641	723.3	52.5	0.4448	707.4	0.068
1642	723.3	52.5	0.4448	708.1	0.068
1643	723.3	56.5	0.4448	708.1	0.068
1644	723.3	52.5	0.4435	708.1	0.068
1645	723.3	52.5	0.4448	708.1	0.068
1646	723.3	52.5	0.4448	708.1	0.068
1647	723.3	52.5	0.4448	707.4	0.068
1648	723.3	52.5	0.4448	708.1	0.068
1649	723.3	52.5	0.4448	708.1	0.068
1650	723.3	56.5	0.4448	708.1	0.068
1651	723.3	52.5	0.4448	708.1	0.068
1652	723.3	56.5	0.4448	708.1	0.068
1653	723.3	52.5	0.4448	708.1	0.068
1654	723.3	56.5	0.4448	708.1	0.068
1655	723.3	56.5	0.4448	708.1	0.068
1656	721.2	52.5	0.4448	708.1	0.068
1657	723.3	56.5	0.4448	708.1	0.068
1658	721.2	52.5	0.4448	708.1	0.068
1659	723.3	56.5	0.4448	708.1	0.068
1660	723.3	52.5	0.4448	708.1	0.068
1661	723.3	56.5	0.4448	708.1	0.068
1662	723.3	52.5	0.4448	708.1	0.068
1663	723.3	56.5	0.4448	708.1	0.068
1664	723.3	56.5	0.4448	707.4	0.068
1665	723.3	52.5	0.4448	708.1	0.068
1666	723.3	56.5	0.4448	708.1	0.068
1667	723.3	52.5	0.4448	708.1	0.068
1668	723.3	56.5	0.4448	708.1	0.068
1669	723.3	56.5	0.4448	708.1	0.068
1670	723.3	52.5	0.4448	708.1	0.068
1671	723.3	52.5	0.4448	708.1	0.068
1672	723.3	52.5	0.4448	708.1	0.068
1673	723.3	52.5	0.4458	708.1	0.068
1674	723.3	56.5	0.4448	708.1	0.068
1675	723.3	56.5	0.4448	708.1	0.068
1676	723.3	52.5	0.4448	708.1	0.068
1677	723.3	56.5	0.4448	708.1	0.068
1678	723.3	56.5	0.4448	708.1	0.068
1679	723.3	52.5	0.4448	708.1	0.068
1680	723.3	52.5	0.4448	708.1	0.068
1681	723.3	52.5	0.4448	708.1	0.068
1682	723.3	52.5	0.4448	708.1	0.068
1683	723.3	56.5	0.4448	708.1	0.068
1684	723.3	56.5	0.4448	708.1	0.068
1685	723.3	56.5	0.4448	708.1	0.068
1686	723.3	52.5	0.4448	708.1	0.068
1687	723.3	56.5	0.4448	708.1	0.068
1688	723.3	56.5	0.4448	708.1	0.068
1689	723.3	56.5	0.4458	708.1	0.068
1690	723.3	52.5	0.4448	708.1	0.068
1691	723.3	56.5	0.4448	708.1	0.068
1692	723.3	52.5	0.4448	708.1	0.068
1693	723.3	52.5	0.4448	708.1	0.068
1694	723.3	56.5	0.4458	708.1	0.068
1695	723.3	52.5	0.4458	708.1	0.068
1696	723.3	56.5	0.4448	708.1	0.068
1697	723.3	56.5	0.4458	708.1	0.068
1698	723.3	52.5	0.4448	708.1	0.068
1699	723.3	56.5	0.4458	708.1	0.068
1700	723.3	56.5	0.4448	708.1	0.068
1701	723.3	52.5	0.4448	708.1	0.068
1702	723.3	56.5	0.4448	708.1	0.068
1703	723.3	52.5	0.4448	708.1	0.068
1704	723.3	52.5	0.4458	708.1	0.068
1705	723.3	52.5	0.4448	708.1	0.068
1706	723.3	52.5	0.4458	708.1	0.068
1707	723.3	52.5	0.4448	708.1	0.068
1708	723.3	56.5	0.4458	708.1	0.068
1709	723.3	52.5	0.4458	708.1	0.068
1710	723.3	52.5	0.4448	708.1	0.068
1711	723.3	52.5	0.4458	708.1	0.068
1712	721.2	52.5	0.4448	708.1	0.068
1713	723.3	52.5	0.4448	708.1	0.068
1714	723.3	56.5	0.4448	708.1	0.068
1715	723.3	56.5	0.4448	708.1	0.068
1716	723.3	56.5	0.4448	708.1	0.068
1717	723.3	52.5	0.4448	708.1	0.068
1718	723.3	52.5	0.4448	708.1	0.068
1719	723.3	56.5	0.4448	708.1	0.068
1720	723.3	52.5	0.4448	708.1	0.068
1721	721.2	56.5	0.4448	708.1	0.068
1722	723.3	52.5	0.4448	708.1	0.068
1723	723.3	52.5	0.4448	708.1	0.068
1724	723.3	52.5	0.4448	708.1	0.068
1725	723.3	52.5	0.4448	708.1	0.068
1726	723.3	56.5	0.4448	708.1	0.068
1727	723.3	52.5	0.4448	708.1	0.068
1728	723.3	56.5	0.4448	708.1	0.068
1729	723.3	52.5	0.4458	708.1	0.068
1730	723.3	52.5	0.4448	708.1	0.068
1731	723.3	56.5	0.4448	708.1	0.068
1732	723.3	56.5	0.4448	707.4	0.068
1733	723.3	56.5	0.4458	708.1	0.068
1734	723.3	52.5	0.4448	708.1	0.068
1735	723.3	56.5	0.4448	708.1	0.068
1736	723.3	56.5	0.4448	708.1	0.068
1737	723.3	52.5	0.4458	708.1	0.068
1738	723.3	52.5	0.4458	708.1	0.068
1739	723.3	56.5	0.4448	708.8	0.068
1740	724.7	56.5	0.4448	708.1	0.068
1741	723.3	52.5	0.4448	708.1	0.068
1742	723.3	56.5	0.4458	708.1	0.068
1743	721.2	52.5	0.4448	708.1	0.068
1744	723.3	52.5	0.4458	708.1	0.068
1745	721.2	56.5	0.4448	708.1	0.068
1746	723.3	52.5	0.4448	708.1	0.068
1747	723.3	56.5	0.4458	708.1	0.068
1748	723.3	52.5	0.4448	708.1	0.068
1749	723.3	56.5	0.4458	708.1	0.068
1750	723.3	56.5	0.4448	708.1	0.068
1751	723.3	56.5	0.4448	708.1	0.068
1752	723.3	56.5	0.4448	708.1	0.068
1753	723.3	56.5	0.4448	708.1	0.068
1754	723.3	52.5	0.4448	708.1	0.068
1755	723.3	52.5	0.4458	708.1	0.068
1756	723.3	56.5	0.4448	708.1	0.068
1757	723.3	56.5	0.4448	708.1	0.068
1758	723.3	52.5	0.4448	708.1	0.068
1759	723.3	52.5	0.4458	708.1	0.068
1760	723.3	56.5	0.4448	708.1	0.068

Table A5. Continued.

#	σ_3 [kPa]	F_a [N]	ΔL [cm]	p_w [kPa]	u_a [μm/s]
1761	723.3	52.5	0.4458	708.1	0.068
1762	721.2	52.5	0.4458	708.1	0.068
1763	723.3	56.5	0.4458	708.1	0.068
1764	723.3	56.5	0.4458	708.1	0.068
1765	723.3	56.5	0.4458	708.1	0.068
1766	723.3	52.5	0.4458	708.1	0.068
1767	723.3	56.5	0.4448	708.1	0.068
1768	721.2	52.5	0.4458	708.1	0.068
1769	723.3	56.5	0.4458	708.1	0.068
1770	723.3	56.5	0.4458	708.1	0.068
1771	723.3	56.5	0.4448	708.1	0.068
1772	723.3	52.5	0.4458	708.1	0.068
1773	723.3	52.5	0.4458	708.1	0.068
1774	723.3	56.5	0.4448	708.1	0.068
1775	723.3	52.5	0.4458	708.1	0.068
1776	723.3	52.5	0.4448	708.1	0.068
1777	723.3	56.5	0.4448	707.4	0.068
1778	723.3	52.5	0.4458	708.1	0.068
1779	723.3	56.5	0.4448	708.1	0.068
1780	723.3	52.5	0.4448	708.1	0.068
1781	723.3	56.5	0.4458	708.1	0.068
1782	723.3	56.5	0.4458	708.1	0.068
1783	723.3	56.5	0.4448	708.1	0.068
1784	724.7	52.5	0.4448	708.1	0.068
1785	723.3	56.5	0.4448	708.1	0.068
1786	723.3	56.5	0.4458	708.1	0.068
1787	723.3	52.5	0.4448	708.1	0.068
1788	721.2	52.5	0.4448	708.1	0.068
1789	723.3	52.5	0.4448	708.1	0.068
1790	723.3	52.5	0.4448	708.1	0.068
1791	723.3	52.5	0.4448	708.1	0.068
1792	723.3	52.5	0.4448	708.1	0.068
1793	723.3	56.5	0.4458	708.1	0.068
1794	723.3	56.5	0.4458	708.1	0.068
1795	723.3	52.5	0.4448	708.1	0.068
1796	721.2	56.5	0.4458	708.1	0.068
1797	723.3	56.5	0.4458	708.1	0.068
1798	723.3	56.5	0.4458	708.1	0.068
1799	723.3	52.5	0.4448	708.1	0.068
1800	723.3	52.5	0.4458	708.1	0.068
1801	723.3	52.5	0.4448	708.1	0.068
1802	723.3	56.5	0.4458	708.1	0.068
1803	723.3	56.5	0.4458	708.1	0.068
1804	723.3	56.5	0.4458	708.1	0.068
1805	723.3	56.5	0.4448	708.1	0.068
1806	723.3	56.5	0.4458	708.1	0.068
1807	723.3	52.5	0.4448	708.1	0.068
1808	723.3	56.5	0.4458	708.1	0.068
1809	723.3	56.5	0.4448	708.1	0.068
1810	721.2	56.5	0.4458	708.1	0.068
1811	723.3	56.5	0.4448	708.1	0.068
1812	723.3	56.5	0.4448	708.1	0.068
1813	723.3	56.5	0.4448	708.1	0.068
1814	723.3	56.5	0.4448	708.1	0.068
1815	723.3	52.5	0.4448	708.1	0.068
1816	723.3	56.5	0.4458	708.1	0.068
1817	723.3	56.5	0.4458	708.1	0.068
1818	723.3	52.5	0.4458	708.1	0.068
1819	723.3	52.5	0.4458	708.1	0.068
1820	723.3	52.5	0.4458	708.1	0.068
1821	723.3	56.5	0.4458	708.1	0.068
1822	723.3	56.5	0.4448	708.1	0.068
1823	723.3	52.5	0.4458	708.1	0.068
1824	723.3	56.5	0.4458	708.1	0.068
1825	721.2	56.5	0.4458	708.1	0.068
1826	723.3	56.5	0.4458	708.1	0.068
1827	723.3	56.5	0.4458	708.1	0.068
1828	723.3	56.5	0.4458	708.1	0.068
1829	723.3	52.5	0.4458	707.4	0.068
1830	723.3	56.5	0.4458	708.1	0.068
1831	723.3	56.5	0.4458	708.1	0.068
1832	723.3	56.5	0.4458	708.1	0.068
1833	723.3	56.5	0.4458	708.1	0.068
1834	723.3	56.5	0.4458	708.1	0.068
1835	721.2	52.5	0.4458	707.4	0.068
1836	723.3	56.5	0.4448	708.1	0.068
1837	723.3	56.5	0.4448	708.1	0.068
1838	721.2	56.5	0.4448	708.1	0.068
1839	723.3	56.5	0.4458	708.1	0.068
1840	723.3	56.5	0.4458	708.1	0.068
1841	723.3	56.5	0.4458	708.1	0.068
1842	723.3	56.5	0.4458	708.1	0.068
1843	723.3	56.5	0.4448	708.1	0.068
1844	721.2	56.5	0.4458	708.1	0.068
1845	721.2	56.5	0.4458	708.1	0.068
1846	723.3	56.5	0.4458	708.1	0.068
1847	723.3	52.5	0.4448	708.1	0.068
1848	723.3	56.5	0.4458	708.1	0.068
1849	723.3	56.5	0.4458	708.1	0.068
1850	723.3	56.5	0.4458	708.1	0.068
1851	723.3	56.5	0.4458	708.1	0.068
1852	723.3	56.5	0.4458	708.1	0.068
1853	723.3	52.5	0.4448	708.1	0.068
1854	723.3	56.5	0.4458	708.1	0.068
1855	723.3	56.5	0.4448	708.1	0.068
1856	723.3	56.5	0.4458	708.1	0.068
1857	723.3	56.5	0.4458	708.1	0.068
1858	723.3	56.5	0.4458	708.1	0.068
1859	723.3	56.5	0.4458	708.1	0.068
1860	723.3	56.5	0.4458	708.1	0.068
1861	723.3	56.5	0.4458	708.1	0.068
1862	723.3	56.5	0.4458	708.1	0.068
1863	723.3	56.5	0.4458	708.1	0.068
1864	723.3	52.5	0.4458	708.1	0.068
1865	721.2	52.5	0.4458	708.1	0.068
1866	723.3	56.5	0.4458	708.1	0.068
1867	723.3	56.5	0.4458	708.1	0.068
1868	723.3	56.5	0.4458	708.1	0.068
1869	721.2	56.5	0.4458	708.1	0.068
1870	723.3	56.5	0.4458	708.1	0.068
1871	723.3	56.5	0.4458	708.1	0.068
1872	723.3	56.5	0.4458	708.1	0.068
1873	723.3	56.5	0.4458	708.1	0.068
1874	723.3	52.5	0.4458	708.1	0.068
1875	723.3	52.5	0.4458	708.1	0.068
1876	723.3	56.5	0.4458	708.1	0.068
1877	723.3	56.5	0.4458	708.8	0.068
1878	723.3	56.5	0.4458	708.1	0.068
1879	723.3	52.5	0.4458	708.8	0.068
1880	723.3	56.5	0.4448	708.1	0.068
1881	723.3	56.5	0.4458	708.1	0.068
1882	723.3	56.5	0.4458	708.1	0.068
1883	723.3	56.5	0.4458	708.8	0.068
1884	723.3	52.5	0.4458	708.8	0.068
1885	723.3	56.5	0.4458	708.1	0.068
1886	723.3	56.5	0.4458	708.1	0.068
1887	723.3	56.5	0.4458	708.8	0.068
1888	723.3	56.5	0.4458	708.1	0.068
1889	723.3	52.5	0.4458	708.1	0.068
1890	723.3	56.5	0.4458	708.8	0.068
1891	723.3	56.5	0.4458	708.1	0.068
1892	723.3	56.5	0.4448	708.1	0.068
1893	723.3	56.5	0.4458	708.8	0.068
1894	723.3	56.5	0.4458	708.8	0.068
1895	723.3	56.5	0.4448	708.1	0.068
1896	723.3	56.5	0.4458	708.1	0.068
1897	723.3	56.5	0.4458	708.1	0.068
1898	723.3	56.5	0.4448	708.1	0.068
1899	723.3	52.5	0.4448	708.8	0.068
1900	724.7	56.5	0.4458	708.1	0.068
1901	723.3	56.5	0.4458	708.8	0.068
1902	723.3	52.5	0.4458	708.1	0.068
1903	723.3	56.5	0.4458	708.1	0.068
1904	723.3	52.5	0.4458	708.1	0.068
1905	723.3	56.5	0.4448	708.1	0.068
1906	723.3	56.5	0.4458	708.8	0.068
1907	723.3	52.5	0.4458	708.8	0.068
1908	723.3	56.5	0.4458	708.1	0.068
1909	723.3	56.5	0.4458	708.1	0.068
1910	721.2	56.5	0.4458	708.1	0.068

Table A5. Continued.

#	σ_3 [kPa]	F_a [N]	ΔL [cm]	p_w [kPa]	u_a [μm/s]
1911	723.3	56.5	0.4458	708.1	0.068
1912	723.3	56.5	0.4458	708.1	0.068
1913	723.3	56.5	0.4458	708.8	0.068
1914	723.3	56.5	0.4458	708.1	0.068
1915	723.3	56.5	0.4458	708.1	0.068
1916	723.3	56.5	0.4470	708.8	0.068
1917	723.3	56.5	0.4458	708.8	0.068
1918	723.3	56.5	0.4458	708.8	0.068
1919	723.3	56.5	0.4458	708.1	0.068
1920	723.3	56.5	0.4458	708.8	0.068
1921	723.3	56.5	0.4458	708.1	0.068
1922	723.3	56.5	0.4458	708.8	0.068
1923	723.3	52.5	0.4458	708.1	0.068
1924	723.3	52.5	0.4458	708.8	0.068
1925	721.2	56.5	0.4458	708.8	0.068
1926	723.3	56.5	0.4458	708.1	0.068
1927	723.3	56.5	0.4458	708.8	0.068
1928	723.3	56.5	0.4470	708.1	0.068
1929	723.3	56.5	0.4458	708.1	0.068
1930	723.3	56.5	0.4458	708.8	0.068
1931	723.3	56.5	0.4458	708.1	0.068
1932	723.3	56.5	0.4458	708.1	0.068
1933	723.3	56.5	0.4458	708.8	0.068
1934	723.3	56.5	0.4458	708.8	0.068
1935	723.3	56.5	0.4458	708.8	0.068
1936	723.3	56.5	0.4458	708.8	0.068
1937	723.3	56.5	0.4458	708.1	0.068
1938	723.3	56.5	0.4458	708.1	0.068
1939	723.3	56.5	0.4458	708.8	0.068
1940	723.3	56.5	0.4458	708.1	0.068
1941	723.3	52.5	0.4506	708.1	0.068
1942	723.3	52.5	0.4506	708.1	0.068
1943	723.3	56.5	0.4506	708.1	0.068
1944	723.3	65.4	0.4506	708.1	1.693
1945	723.3	65.4	0.4519	708.1	1.693
1946	723.3	65.4	0.4519	708.1	1.693
1947	723.3	65.4	0.4519	708.1	1.693
1948	723.3	65.4	0.4519	708.8	1.693
1949	723.3	65.4	0.4531	708.1	1.693
1950	723.3	69.8	0.4531	708.1	1.693
1951	723.3	69.8	0.4531	708.8	1.693
1952	723.3	69.8	0.4531	708.1	1.693
1953	723.3	69.8	0.4542	708.1	1.693
1954	723.3	69.8	0.4554	708.1	1.693
1955	723.3	69.8	0.4554	708.1	1.693
1956	723.3	69.8	0.4554	708.1	1.693
1957	723.3	69.8	0.4554	707.4	1.693
1958	723.3	69.8	0.4567	708.1	1.693
1959	723.3	69.8	0.4567	708.1	1.693
1960	723.3	69.8	0.4577	707.4	1.693
1961	723.3	69.8	0.4577	708.1	1.693
1962	723.3	69.8	0.4590	708.1	1.693
1963	723.3	69.8	0.4590	708.1	1.693
1964	723.3	69.8	0.4577	707.4	1.693
1965	721.2	69.8	0.4602	707.4	1.693
1966	723.3	69.8	0.4602	707.4	1.693
1967	723.3	69.8	0.4615	707.4	1.693
1968	723.3	69.8	0.4615	707.4	1.693
1969	723.3	69.8	0.4615	707.4	1.693
1970	723.3	69.8	0.4625	707.4	1.693
1971	723.3	69.8	0.4625	707.4	1.693
1972	723.3	69.8	0.4625	707.4	1.693
1973	723.3	69.8	0.4638	707.4	1.693
1974	723.3	69.8	0.4638	707.4	1.693
1975	721.2	69.8	0.4651	707.4	1.693
1976	723.3	69.8	0.4651	707.4	1.693
1977	723.3	69.8	0.4661	707.4	1.693
1978	723.3	69.8	0.4661	707.4	1.693
1979	723.3	69.8	0.4674	707.4	1.693
1980	723.3	69.8	0.4674	707.4	1.693
1981	723.3	69.8	0.4674	707.4	1.693
1982	723.3	69.8	0.4686	707.4	1.693
1983	723.3	69.8	0.4686	707.4	1.693
1984	723.3	69.8	0.4696	707.4	1.693
1985	723.3	69.8	0.4696	707.4	1.693
1986	723.3	69.8	0.4696	707.4	1.693
1987	723.3	69.8	0.4709	707.4	1.693
1988	723.3	69.8	0.4722	707.4	1.693
1989	723.3	69.8	0.4722	707.4	1.693
1990	723.3	69.8	0.4722	707.4	1.693
1991	723.3	69.8	0.4735	707.4	1.693
1992	723.3	65.4	0.4735	707.4	1.693
1993	723.3	69.8	0.4745	707.4	1.693
1994	723.3	69.8	0.4745	707.4	1.693
1995	723.3	69.8	0.4745	707.4	1.693
1996	723.3	69.8	0.4757	707.4	1.693
1997	723.3	65.4	0.4770	707.4	1.693
1998	723.3	69.8	0.4770	707.4	1.693
1999	723.3	69.8	0.4770	707.4	1.693
2000	723.3	69.8	0.4770	707.4	1.693
2001	724.7	69.8	0.4780	706.7	1.693
2002	723.3	69.8	0.4780	707.4	1.693
2003	723.3	69.8	0.4793	707.4	1.693
2004	723.3	74.3	0.4780	707.4	1.693
2005	723.3	69.8	0.4806	707.4	1.693
2006	723.3	69.8	0.4793	707.4	1.693
2007	723.3	69.8	0.4816	707.4	1.693
2008	723.3	69.8	0.4816	707.4	1.693
2009	723.3	69.8	0.4829	707.4	1.693
2010	723.3	69.8	0.4829	707.4	1.693
2011	723.3	69.8	0.4829	707.4	1.693
2012	723.3	69.8	0.4841	707.4	1.693
2013	723.3	69.8	0.4854	707.4	1.693
2014	723.3	69.8	0.4854	706.7	1.693
2015	721.2	69.8	0.4854	707.4	1.693
2016	723.3	69.8	0.4854	706.0	1.693
2017	723.3	69.8	0.4864	706.7	1.693
2018	723.3	69.8	0.4864	707.4	1.693
2019	723.3	69.8	0.4877	706.7	1.693
2020	723.3	69.8	0.4877	707.4	1.693
2021	723.3	69.8	0.4890	706.7	1.693
2022	723.3	69.8	0.4890	706.7	1.693
2023	723.3	65.4	0.4900	706.7	1.693
2024	723.3	78.3	0.5057	706.7	42.333
2025	723.3	78.3	0.5177	706.7	42.333
2026	723.3	78.3	0.5306	706.0	42.333
2027	723.3	82.7	0.5438	705.4	42.333
2028	723.3	78.3	0.5570	704.7	42.333
2029	723.3	65.4	0.5738	704.0	1.693
2030	723.3	65.4	0.5738	704.0	1.693
2031	723.3	65.4	0.5748	704.0	1.693
2032	723.3	65.4	0.5738	704.0	1.693
2033	723.3	69.8	0.5738	704.0	1.693
2034	723.3	69.8	0.5748	704.7	1.693
2035	723.3	65.4	0.5748	704.0	1.693
2036	723.3	69.8	0.5761	704.0	1.693
2037	723.3	65.4	0.5773	704.0	1.693
2038	723.3	65.4	0.5773	704.7	1.693
2039	723.3	69.8	0.5773	704.7	1.693
2040	723.3	69.8	0.5786	704.7	1.693
2041	723.3	69.8	0.5796	704.7	1.693
2042	723.3	69.8	0.5796	704.7	1.693
2043	723.3	69.8	0.5796	704.0	1.693
2044	723.3	69.8	0.5796	704.7	1.693
2045	723.3	69.8	0.5809	704.7	1.693
2046	723.3	69.8	0.5809	704.7	1.693
2047	723.3	69.8	0.5822	704.7	1.693
2048	721.2	69.8	0.5822	704.7	1.693
2049	723.3	69.8	0.5822	704.7	1.693
2050	723.3	69.8	0.5822	704.7	1.693
2051	723.3	69.8	0.5832	704.7	1.693
2052	723.3	69.8	0.5832	704.7	1.693
2053	723.3	69.8	0.5845	704.7	1.693
2054	723.3	69.8	0.5845	704.7	1.693
2055	723.3	65.4	0.5857	704.7	1.693
2056	721.2	69.8	0.5857	704.0	1.693
2057	723.3	69.8	0.5870	704.7	1.693
2058	723.3	69.8	0.5870	704.7	1.693
2059	723.3	69.8	0.5870	704.7	1.693
2060	723.3	69.8	0.5880	704.7	1.693

Table A5. Continued.

#	σ_3 [kPa]	F_a [N]	ΔL [cm]	p_w [kPa]	u_a [µm/s]
2061	723.3	69.8	0.5880	704.7	1.693
2062	723.3	69.8	0.5880	704.7	1.693
2063	721.2	69.8	0.5893	704.7	1.693
2064	723.3	69.8	0.5906	705.4	1.693
2065	723.3	69.8	0.5906	704.7	1.693
2066	723.3	69.8	0.5906	705.4	1.693
2067	723.3	69.8	0.5916	704.7	1.693
2068	721.2	69.8	0.5916	705.4	1.693
2069	721.2	69.8	0.5928	704.7	1.693
2070	723.3	74.3	0.5928	704.7	1.693
2071	723.3	69.8	0.5928	705.4	1.693
2072	723.3	69.8	0.5941	704.7	1.693
2073	723.3	69.8	0.5951	704.7	1.693
2074	723.3	69.8	0.5941	704.7	1.693
2075	723.3	74.3	0.5951	704.7	1.693
2076	723.3	69.8	0.5951	704.7	1.693
2077	723.3	69.8	0.5964	705.4	1.693
2078	723.3	69.8	0.5977	705.4	1.693
2079	723.3	69.8	0.5977	704.7	1.693
2080	723.3	69.8	0.5977	704.7	1.693
2081	723.3	69.8	0.5989	704.7	1.693
2082	723.3	69.8	0.5989	704.7	1.693
2083	723.3	69.8	0.5999	704.7	1.693
2084	723.3	69.8	0.5989	705.4	1.693
2085	721.2	69.8	0.5999	705.4	1.693
2086	723.3	69.8	0.6012	705.4	1.693
2087	723.3	69.8	0.6012	705.4	1.693
2088	723.3	69.8	0.6012	705.4	1.693
2089	723.3	74.3	0.6025	705.4	1.693
2090	723.3	69.8	0.6025	705.4	1.693
2091	723.3	69.8	0.6035	705.4	1.693
2092	723.3	69.8	0.6035	705.4	1.693
2093	723.3	74.3	0.6048	705.4	1.693
2094	723.3	69.8	0.6048	704.7	1.693
2095	723.3	69.8	0.6060	705.4	1.693
2096	723.3	74.3	0.6060	705.4	1.693
2097	723.3	69.8	0.6060	705.4	1.693
2098	723.3	69.8	0.6073	705.4	1.693
2099	723.3	74.3	0.6073	705.4	1.693
2100	721.2	74.3	0.6083	705.4	1.693
2101	723.3	69.8	0.6083	705.4	1.693
2102	723.3	69.8	0.6083	705.4	1.693
2103	723.3	69.8	0.6083	705.4	1.693
2104	723.3	69.8	0.6096	705.4	1.693
2105	721.2	74.3	0.6109	705.4	8.467
2106	723.3	74.3	0.6132	705.4	8.467
2107	723.3	74.3	0.6154	704.7	8.467
2108	723.3	74.3	0.6180	705.4	8.467
2109	723.3	74.3	0.6203	704.7	8.467
2110	723.3	74.3	0.6238	705.4	8.467
2111	723.3	74.3	0.6251	704.7	8.467
2112	723.3	74.3	0.6287	704.7	8.467
2113	723.3	74.3	0.6312	704.7	8.467
2114	723.3	74.3	0.6335	704.7	8.467
2115	723.3	78.3	0.6358	704.7	8.467
2116	723.3	78.3	0.6383	704.0	8.467
2117	723.3	74.3	0.6406	704.7	8.467
2118	723.3	74.3	0.6431	704.7	8.467
2119	723.3	74.3	0.6454	704.7	8.467
2120	723.3	74.3	0.6490	704.7	8.467
2121	723.3	78.3	0.6515	704.7	8.467
2122	723.3	78.3	0.6538	704.7	8.467
2123	723.3	78.3	0.6574	704.7	8.467
2124	723.3	78.3	0.6599	704.0	8.467
2125	723.3	74.3	0.6622	704.0	8.467
2126	723.3	74.3	0.6645	704.0	8.467
2127	723.3	78.3	0.6670	704.0	8.467
2128	723.3	78.3	0.6693	704.0	8.467
2129	723.3	78.3	0.6718	704.0	8.467
2130	723.3	78.3	0.6741	703.3	8.467
2131	723.3	78.3	0.6764	703.3	8.467
2132	723.3	78.3	0.6802	704.0	8.467
2133	723.3	74.3	0.6825	704.0	8.467
2134	723.3	65.4	0.6896	704.0	1.693
2135	723.3	65.4	0.6909	704.0	1.693
2136	723.3	69.8	0.6909	704.0	1.693
2137	723.3	69.8	0.6909	704.7	1.693
2138	723.3	69.8	0.6922	704.7	1.693
2139	723.3	69.8	0.6922	704.0	1.693
2140	723.3	69.8	0.6922	704.0	1.693
2141	723.3	69.8	0.6922	704.0	1.693
2142	723.3	69.8	0.6932	704.7	1.693
2143	723.3	69.8	0.6944	704.7	1.693
2144	723.3	69.8	0.6944	704.0	1.693
2145	723.3	69.8	0.6944	704.0	1.693
2146	723.3	69.8	0.6957	704.7	1.693
2147	723.3	74.3	0.6957	704.7	1.693
2148	723.3	69.8	0.6957	704.7	1.693
2149	723.3	69.8	0.6967	704.7	1.693
2150	723.3	69.8	0.6967	704.0	1.693
2151	723.3	69.8	0.6967	704.7	1.693
2152	723.3	69.8	0.6980	704.0	1.693
2153	723.3	69.8	0.6980	704.7	1.693
2154	723.3	69.8	0.6993	704.7	1.693
2155	723.3	69.8	0.6993	704.7	1.693
2156	723.3	69.8	0.6993	704.7	1.693
2157	723.3	69.8	0.7003	704.7	1.693
2158	723.3	69.8	0.7003	704.0	1.693
2159	723.3	74.3	0.7015	704.7	1.693
2160	723.3	69.8	0.7015	704.7	1.693
2161	723.3	74.3	0.7028	704.7	1.693
2162	723.3	74.3	0.7028	704.7	1.693
2163	723.3	69.8	0.7028	704.7	1.693
2164	721.2	69.8	0.7041	704.7	1.693
2165	723.3	74.3	0.7041	704.7	1.693
2166	723.3	74.3	0.7051	705.4	1.693
2167	723.3	69.8	0.7051	704.7	1.693
2168	723.3	69.8	0.7064	704.7	1.693
2169	723.3	74.3	0.7064	704.7	1.693
2170	723.3	74.3	0.7076	704.7	1.693
2171	721.2	74.3	0.7076	704.7	1.693
2172	723.3	74.3	0.7076	704.7	1.693
2173	723.3	74.3	0.7076	704.7	1.693
2174	723.3	74.3	0.7087	704.7	1.693
2175	723.3	74.3	0.7087	704.7	1.693
2176	723.3	74.3	0.7099	705.4	1.693
2177	723.3	74.3	0.7112	704.7	1.693
2178	723.3	74.3	0.7099	704.7	1.693
2179	723.3	74.3	0.7112	705.4	1.693
2180	721.2	74.3	0.7125	705.4	1.693
2181	723.3	74.3	0.7125	705.4	1.693
2182	723.3	74.3	0.7135	704.7	1.693
2183	723.3	74.3	0.7135	704.7	1.693
2184	723.3	69.8	0.7135	704.7	1.693
2185	721.2	69.8	0.7135	705.4	1.693
2186	723.3	74.3	0.7148	704.7	1.693
2187	723.3	74.3	0.7148	704.7	1.693
2188	723.3	69.8	0.7160	705.4	1.693
2189	723.3	69.8	0.7170	705.4	1.693
2190	723.3	74.3	0.7170	705.4	1.693
2191	723.3	74.3	0.7170	705.4	1.693
2192	723.3	74.3	0.7170	705.4	1.693
2193	723.3	69.8	0.7196	704.7	1.693
2194	721.2	74.3	0.7196	704.7	1.693
2195	723.3	74.3	0.7196	705.4	1.693
2196	723.3	74.3	0.7196	704.7	1.693
2197	723.3	74.3	0.7206	705.4	1.693
2198	721.2	69.8	0.7206	705.4	1.693
2199	723.3	74.3	0.7219	705.4	1.693
2200	723.3	74.3	0.7219	705.4	1.693
2201	723.3	74.3	0.7231	704.7	1.693
2202	723.3	74.3	0.7231	705.4	1.693
2203	723.3	74.3	0.7231	705.4	1.693
2204	723.3	74.3	0.7244	704.7	1.693
2205	723.3	74.3	0.7244	705.4	0.339
2206	723.3	65.4	0.7267	705.4	0.339
2207	723.3	65.4	0.7267	705.4	0.339
2208	723.3	65.4	0.7267	705.4	0.339
2209	723.3	65.4	0.7267	705.4	0.339
2210	723.3	65.4	0.7267	705.4	0.339

Table A5. Continued.

#	σ_3 [kPa]	F_a [N]	ΔL [cm]	p_w [kPa]	u_a [µm/s]
2211	723.3	65.4	0.7267	705.4	0.339
2212	723.3	65.4	0.7267	705.4	0.339
2213	721.2	65.4	0.7267	705.4	0.339
2214	723.3	65.4	0.7280	705.4	0.339
2215	723.3	65.4	0.7267	705.4	0.339
2216	723.3	65.4	0.7280	706.0	0.339
2217	723.3	65.4	0.7267	705.4	0.339
2218	723.3	65.4	0.7267	705.4	0.339
2219	723.3	65.4	0.7267	705.4	0.339
2220	723.3	69.8	0.7267	705.4	0.339
2221	723.3	65.4	0.7280	706.0	0.339
2222	723.3	65.4	0.7267	706.0	0.339
2223	723.3	65.4	0.7254	706.0	0.339
2224	723.3	69.8	0.7280	706.0	0.339
2225	721.2	65.4	0.7280	706.0	0.339
2226	723.3	65.4	0.7280	706.0	0.339
2227	723.3	65.4	0.7280	706.0	0.339
2228	723.3	65.4	0.7280	706.0	0.339
2229	723.3	69.8	0.7280	706.0	0.339
2230	723.3	69.8	0.7280	706.0	0.339
2231	721.2	69.8	0.7280	706.0	0.339
2232	723.3	69.8	0.7280	706.0	0.339
2233	723.3	69.8	0.7280	706.0	0.339
2234	723.3	69.8	0.7290	706.7	0.339
2235	723.3	69.8	0.7280	706.0	0.339
2236	723.3	69.8	0.7290	706.0	0.339
2237	723.3	69.8	0.7290	706.0	0.339
2238	723.3	69.8	0.7290	706.7	0.339
2239	723.3	69.8	0.7290	706.0	0.339
2240	723.3	69.8	0.7290	706.7	0.339
2241	721.2	65.4	0.7290	706.0	0.339
2242	723.3	69.8	0.7290	706.0	0.339
2243	723.3	69.8	0.7290	706.7	0.339
2244	723.3	69.8	0.7290	706.7	0.339
2245	721.2	65.4	0.7290	706.7	0.339
2246	723.3	69.8	0.7303	706.0	0.339
2247	723.3	69.8	0.7303	706.0	0.339
2248	723.3	69.8	0.7290	706.0	0.339
2249	723.3	69.8	0.7290	706.7	0.339
2250	723.3	69.8	0.7303	706.0	0.339
2251	723.3	69.8	0.7303	706.0	0.339
2252	723.3	69.8	0.7303	706.0	0.339
2253	723.3	69.8	0.7303	706.7	0.339
2254	723.3	69.8	0.7303	706.7	0.339
2255	723.3	69.8	0.7290	706.7	0.339
2256	723.3	69.8	0.7303	706.0	0.339
2257	723.3	69.8	0.7303	706.0	0.339
2258	723.3	69.8	0.7303	706.7	0.339
2259	723.3	69.8	0.7315	706.7	0.339
2260	723.3	69.8	0.7303	706.0	0.339
2261	723.3	69.8	0.7315	706.7	0.339
2262	723.3	69.8	0.7315	706.7	0.339
2263	723.3	60.9	0.7338	706.7	0.339
2264	723.3	60.9	0.7338	706.7	0.339
2265	723.3	56.5	0.7338	706.7	0.068
2266	723.3	60.9	0.7328	706.7	0.068
2267	723.3	56.5	0.7338	706.7	0.068
2268	721.2	56.5	0.7338	706.7	0.068
2269	723.3	60.9	0.7338	706.7	0.068
2270	723.3	56.5	0.7338	706.7	0.068
2271	723.3	60.9	0.7338	706.7	0.068
2272	723.3	56.5	0.7328	706.7	0.068
2273	721.2	60.9	0.7338	706.7	0.068
2274	723.3	56.5	0.7328	706.7	0.068
2275	721.2	56.5	0.7338	707.4	0.068
2276	723.3	60.9	0.7328	706.7	0.068
2277	723.3	60.9	0.7338	706.7	0.068
2278	723.3	60.9	0.7338	706.7	0.068
2279	723.3	60.9	0.7338	706.7	0.068
2280	723.3	60.9	0.7338	706.7	0.068
2281	723.3	60.9	0.7328	707.4	0.068
2282	721.2	60.9	0.7338	706.7	0.068
2283	723.3	60.9	0.7338	706.7	0.068
2284	723.3	60.9	0.7338	706.7	0.068
2285	723.3	60.9	0.7338	706.7	0.068
2286	723.3	56.5	0.7328	707.4	0.068
2287	723.3	60.9	0.7328	707.4	0.068
2288	723.3	60.9	0.7338	707.4	0.068
2289	723.3	60.9	0.7338	707.4	0.068
2290	723.3	60.9	0.7338	707.4	0.068
2291	723.3	60.9	0.7338	707.4	0.068
2292	723.3	60.9	0.7338	707.4	0.068
2293	723.3	60.9	0.7338	707.4	0.068
2294	723.3	60.9	0.7338	707.4	0.068
2295	723.3	60.9	0.7338	707.4	0.068
2296	723.3	60.9	0.7338	707.4	0.068
2297	721.2	60.9	0.7338	707.4	0.068
2298	723.3	60.9	0.7338	707.4	0.068
2299	723.3	60.9	0.7328	707.4	0.068
2300	723.3	60.9	0.7338	707.4	0.068
2301	723.3	60.9	0.7338	707.4	0.068
2302	723.3	60.9	0.7338	707.4	0.068
2303	723.3	60.9	0.7338	707.4	0.068
2304	721.2	60.9	0.7338	707.4	0.068
2305	723.3	60.9	0.7338	707.4	0.068
2306	723.3	60.9	0.7328	706.7	0.068
2307	721.2	60.9	0.7338	707.4	0.068
2308	723.3	60.9	0.7338	707.4	0.068
2309	723.3	60.9	0.7338	707.4	0.068
2310	723.3	60.9	0.7338	707.4	0.068
2311	723.3	60.9	0.7338	707.4	0.068
2312	723.3	65.4	0.7338	707.4	0.068
2313	723.3	65.4	0.7338	707.4	0.068
2314	723.3	60.9	0.7338	707.4	0.068
2315	723.3	60.9	0.7338	707.4	0.068
2316	723.3	69.8	0.7351	707.4	1.693
2317	721.2	69.8	0.7351	707.4	1.693
2318	723.3	69.8	0.7351	707.4	1.693
2319	723.3	69.8	0.7351	707.4	1.693
2320	723.3	74.3	0.7351	707.4	1.693
2321	723.3	74.3	0.7363	707.4	1.693
2322	723.3	74.3	0.7363	707.4	1.693
2323	721.2	74.3	0.7374	707.4	1.693
2324	721.2	74.3	0.7374	707.4	1.693
2325	723.3	74.3	0.7386	707.4	1.693
2326	721.2	74.3	0.7386	707.4	1.693
2327	723.3	74.3	0.7399	707.4	1.693
2328	721.2	74.3	0.7399	707.4	1.693
2329	723.3	74.3	0.7399	707.4	1.693
2330	723.3	74.3	0.7409	707.4	1.693
2331	723.3	69.8	0.7409	707.4	1.693
2332	723.3	74.3	0.7409	707.4	1.693
2333	721.2	74.3	0.7422	707.4	1.693
2334	723.3	74.3	0.7422	707.4	1.693
2335	723.3	74.3	0.7435	707.4	1.693
2336	723.3	74.3	0.7435	707.4	1.693
2337	723.3	74.3	0.7447	707.4	1.693
2338	723.3	74.3	0.7447	707.4	1.693
2339	721.2	74.3	0.7447	707.4	1.693
2340	723.3	74.3	0.7457	706.7	1.693
2341	721.2	74.3	0.7457	707.4	1.693
2342	723.3	74.3	0.7470	707.4	1.693
2343	723.3	74.3	0.7470	707.4	1.693
2344	723.3	78.3	0.7483	707.4	1.693
2345	723.3	74.3	0.7483	707.4	1.693
2346	723.3	74.3	0.7493	707.4	1.693
2347	721.2	74.3	0.7493	707.4	1.693
2348	723.3	74.3	0.7493	707.4	1.693
2349	721.2	74.3	0.7506	707.4	1.693
2350	723.3	74.3	0.7506	707.4	1.693
2351	723.3	74.3	0.7518	707.4	1.693
2352	723.3	74.3	0.7518	707.4	1.693
2353	723.3	74.3	0.7531	707.4	1.693
2354	723.3	74.3	0.7531	707.4	1.693
2355	723.3	78.3	0.7531	707.4	1.693
2356	721.2	74.3	0.7541	706.7	1.693
2357	723.3	78.3	0.7541	706.7	1.693
2358	723.3	74.3	0.7554	706.7	1.693
2359	723.3	74.3	0.7554	706.7	1.693
2360	723.3	74.3	0.7554	707.4	1.693

Table A5. Continued.

#	σ_3 [kPa]	F_a [N]	ΔL [cm]	p_w [kPa]	u_a [μm/s]
2361	723.3	78.3	0.7567	707.4	1.693
2362	723.3	78.3	0.7567	706.0	1.693
2363	723.3	74.3	0.7577	706.7	1.693
2364	723.3	78.3	0.7577	707.4	1.693
2365	723.3	74.3	0.7590	707.4	1.693
2366	723.3	69.8	0.7590	707.4	1.693
2367	723.3	74.3	0.7602	706.7	1.693
2368	723.3	74.3	0.7602	707.4	1.693
2369	723.3	74.3	0.7602	706.7	1.693
2370	723.3	74.3	0.7612	706.7	1.693
2371	723.3	74.3	0.7602	706.7	1.693
2372	723.3	74.3	0.7625	706.7	1.693
2373	723.3	74.3	0.7625	707.4	1.693
2374	721.2	74.3	0.7625	706.7	1.693
2375	723.3	74.3	0.7638	706.7	1.693
2376	723.3	69.8	0.7650	706.7	1.693
2377	723.3	74.3	0.7650	706.7	1.693
2378	721.2	74.3	0.7650	707.4	1.693
2379	723.3	74.3	0.7661	706.7	1.693
2380	723.3	74.3	0.7661	706.7	1.693
2381	723.3	78.3	0.7673	706.7	1.693
2382	723.3	74.3	0.7673	706.7	1.693
2383	723.3	74.3	0.7673	707.4	1.693
2384	721.2	74.3	0.7686	706.7	1.693
2385	723.3	74.3	0.7686	706.7	1.693
2386	723.3	74.3	0.7686	706.7	1.693
2387	721.2	74.3	0.7696	706.7	1.693
2388	721.2	74.3	0.7709	706.7	1.693
2389	723.3	78.3	0.7696	706.7	1.693
2390	723.3	74.3	0.7709	706.7	1.693
2391	721.2	78.3	0.7722	706.7	1.693
2392	723.3	78.3	0.7722	706.7	1.693
2393	723.3	78.3	0.7722	706.7	1.693
2394	723.3	69.8	0.7722	706.7	1.693
2395	723.3	78.3	0.7734	706.7	1.693
2396	723.3	74.3	0.7744	706.7	1.693
2397	721.2	74.3	0.7744	706.7	1.693
2398	723.3	78.3	0.7757	706.7	1.693
2399	721.2	78.3	0.7757	706.7	1.693
2400	721.2	74.3	0.7757	706.7	1.693
2401	723.3	74.3	0.7770	706.7	1.693
2402	723.3	74.3	0.7770	706.7	1.693
2403	723.3	74.3	0.7780	706.7	1.693
2404	723.3	78.3	0.7780	706.7	1.693
2405	723.3	74.3	0.7793	706.7	1.693
2406	723.3	78.3	0.7793	706.7	1.693
2407	723.3	78.3	0.7805	706.7	1.693
2408	723.3	74.3	0.7805	706.0	1.693
2409	721.2	74.3	0.7816	706.7	1.693
2410	723.3	78.3	0.7816	706.7	1.693
2411	723.3	74.3	0.7816	706.7	1.693
2412	723.3	78.3	0.7828	706.0	1.693
2413	723.3	74.3	0.7841	706.7	1.693
2414	723.3	78.3	0.7816	706.7	1.693
2415	723.3	74.3	0.7841	706.7	1.693
2416	723.3	78.3	0.7889	706.0	1.693
2417	723.3	82.7	0.7973	706.7	1.693
2418	723.3	87.2	0.8092	706.0	42.333
2419	723.3	87.2	0.8212	705.4	42.333
2420	723.3	87.2	0.8341	705.4	42.333
2421	723.3	82.7	0.8473	704.7	42.333
2422	723.3	87.2	0.8593	704.7	42.333
2423	723.3	82.7	0.8725	704.7	42.333
2424	723.3	82.7	0.8857	704.0	42.333
2425	723.3	87.2	0.8976	704.0	42.333
2426	723.3	82.7	0.9108	704.0	42.333
2427	723.3	82.7	0.9228	703.3	42.333
2428	723.3	87.2	0.9370	703.3	42.333
2429	723.3	82.7	0.9489	703.3	42.333
2430	721.2	78.3	0.9550	703.3	42.333
2431	723.3	74.3	0.9634	704.0	8.467
2432	723.3	74.3	0.9657	704.0	8.467
2433	723.3	78.3	0.9680	703.3	8.467
2434	723.3	78.3	0.9705	704.0	8.467
2435	723.3	78.3	0.9728	703.3	8.467
2436	723.3	78.3	0.9754	704.0	8.467
2437	721.2	78.3	0.9776	704.0	8.467
2438	723.3	78.3	0.9799	704.0	8.467
2439	723.3	78.3	0.9825	703.3	8.467
2440	723.3	78.3	0.9848	703.3	8.467
2441	723.3	78.3	0.9883	703.3	8.467
2442	723.3	78.3	0.9909	703.3	8.467
2443	723.3	74.3	0.9931	704.0	8.467
2444	723.3	78.3	0.9957	703.3	8.467
2445	723.3	78.3	0.9980	703.3	8.467
2446	721.2	78.3	1.0003	703.3	8.467
2447	723.3	78.3	1.0041	703.3	8.467
2448	723.3	78.3	1.0063	703.3	8.467
2449	723.3	78.3	1.0086	703.3	8.467
2450	721.2	82.7	1.0112	703.3	8.467
2451	723.3	78.3	1.0135	704.0	8.467
2452	723.3	82.7	1.0160	704.0	8.467
2453	723.3	78.3	1.0183	703.3	8.467
2454	721.2	82.7	1.0206	703.3	8.467
2455	721.2	78.3	1.0231	703.3	8.467
2456	721.2	65.4	1.0244	703.3	1.693
2457	723.3	69.8	1.0244	703.3	1.693
2458	721.2	69.8	1.0244	703.3	1.693
2459	723.3	74.3	1.0244	704.0	1.693
2460	723.3	74.3	1.0254	704.0	1.693
2461	721.2	74.3	1.0254	704.0	1.693
2462	723.3	74.3	1.0254	704.0	1.693
2463	723.3	74.3	1.0267	704.0	1.693
2464	723.3	74.3	1.0267	704.0	1.693
2465	723.3	74.3	1.0279	704.0	1.693
2466	723.3	74.3	1.0279	704.0	1.693
2467	723.3	74.3	1.0279	704.7	1.693
2468	723.3	74.3	1.0290	704.7	1.693
2469	723.3	74.3	1.0290	704.7	1.693
2470	723.3	74.3	1.0302	704.7	1.693
2471	723.3	78.3	1.0302	704.7	1.693
2472	723.3	74.3	1.0315	704.7	1.693
2473	723.3	74.3	1.0315	704.7	1.693
2474	723.3	74.3	1.0325	704.7	1.693
2475	723.3	74.3	1.0325	704.7	1.693
2476	723.3	78.3	1.0325	704.7	1.693
2477	723.3	78.3	1.0338	704.7	1.693
2478	723.3	74.3	1.0338	704.7	1.693
2479	723.3	74.3	1.0351	704.7	1.693
2480	723.3	74.3	1.0351	704.7	1.693
2481	721.2	78.3	1.0363	704.7	1.693
2482	723.3	78.3	1.0363	704.7	1.693
2483	723.3	74.3	1.0363	704.7	1.693
2484	723.3	78.3	1.0363	704.7	1.693
2485	723.3	78.3	1.0373	704.7	1.693
2486	723.3	78.3	1.0373	704.7	1.693
2487	721.2	74.3	1.0386	704.7	1.693
2488	723.3	78.3	1.0386	704.7	1.693
2489	723.3	78.3	1.0399	704.7	1.693
2490	723.3	78.3	1.0399	704.7	1.693
2491	723.3	78.3	1.0399	704.7	1.693
2492	723.3	78.3	1.0409	704.7	1.693
2493	723.3	74.3	1.0409	705.4	1.693
2494	723.3	74.3	1.0422	705.4	1.693
2495	723.3	78.3	1.0422	704.7	1.693
2496	723.3	74.3	1.0434	704.7	1.693
2497	723.3	78.3	1.0434	705.4	1.693
2498	723.3	78.3	1.0434	704.7	1.693
2499	723.3	74.3	1.0447	704.7	1.693
2500	723.3	78.3	1.0447	704.7	1.693
2501	723.3	74.3	1.0457	704.7	1.693
2502	723.3	78.3	1.0457	705.4	1.693
2503	723.3	78.3	1.0470	705.4	1.693
2504	723.3	74.3	1.0470	704.7	1.693
2505	723.3	78.3	1.0483	705.4	1.693
2506	723.3	78.3	1.0483	705.4	1.693
2507	721.2	78.3	1.0483	704.7	1.693
2508	723.3	74.3	1.0493	705.4	1.693
2509	723.3	78.3	1.0493	705.4	1.693
2510	723.3	78.3	1.0505	705.4	1.693

Table A5. Continued.

#	σ_3 [kPa]	F_a [N]	ΔL [cm]	p_w [kPa]	u_a [μm/s]
2511	723.3	78.3	1.0505	705.4	1.693
2512	723.3	78.3	1.0518	705.4	1.693
2513	723.3	78.3	1.0518	704.7	1.693
2514	723.3	74.3	1.0518	705.4	1.693
2515	721.2	78.3	1.0528	705.4	1.693
2516	723.3	74.3	1.0528	705.4	1.693
2517	723.3	78.3	1.0528	705.4	1.693
2518	723.3	78.3	1.0541	705.4	1.693
2519	721.2	78.3	1.0541	705.4	1.693
2520	723.3	78.3	1.0554	705.4	1.693
2521	723.3	78.3	1.0566	705.4	1.693
2522	723.3	78.3	1.0566	705.4	1.693
2523	723.3	74.3	1.0566	704.7	1.693
2524	723.3	78.3	1.0566	705.4	1.693
2525	721.2	78.3	1.0577	705.4	1.693
2526	723.3	78.3	1.0577	705.4	1.693
2527	723.3	78.3	1.0589	705.4	1.693
2528	723.3	78.3	1.0589	705.4	1.693
2529	723.3	78.3	1.0602	705.4	1.693
2530	723.3	78.3	1.0602	705.4	1.693
2531	723.3	78.3	1.0602	705.4	1.693
2532	721.2	78.3	1.0602	705.4	1.693
2533	723.3	78.3	1.0612	705.4	1.693
2534	723.3	78.3	1.0612	705.4	1.693
2535	723.3	78.3	1.0625	705.4	1.693
2536	723.3	78.3	1.0638	704.7	1.693
2537	723.3	78.3	1.0638	705.4	1.693
2538	723.3	78.3	1.0638	705.4	1.693
2539	721.2	78.3	1.0650	705.4	1.693
2540	721.2	78.3	1.0650	705.4	1.693
2541	723.3	78.3	1.0660	705.4	1.693
2542	723.3	78.3	1.0673	705.4	1.693
2543	723.3	78.3	1.0673	705.4	1.693
2544	721.2	78.3	1.0673	705.4	1.693
2545	723.3	78.3	1.0686	704.7	1.693
2546	723.3	78.3	1.0686	705.4	1.693
2547	723.3	78.3	1.0686	705.4	1.693
2548	723.3	78.3	1.0686	705.4	1.693
2549	723.3	78.3	1.0709	705.4	1.693
2550	721.2	78.3	1.0696	705.4	1.693
2551	723.3	78.3	1.0709	705.4	1.693
2552	723.3	78.3	1.0721	706.0	1.693
2553	723.3	78.3	1.0721	705.4	1.693
2554	723.3	78.3	1.0721	705.4	1.693
2555	723.3	78.3	1.0732	705.4	1.693
2556	723.3	78.3	1.0732	705.4	1.693
2557	723.3	78.3	1.0744	705.4	1.693
2558	723.3	78.3	1.0744	705.4	1.693
2559	723.3	78.3	1.0744	705.4	1.693
2560	723.3	78.3	1.0757	705.4	1.693
2561	723.3	78.3	1.0757	705.4	1.693
2562	723.3	78.3	1.0757	705.4	1.693
2563	723.3	78.3	1.0770	705.4	1.693
2564	721.2	78.3	1.0770	705.4	1.693
2565	723.3	78.3	1.0780	705.4	1.693
2566	723.3	74.3	1.0792	705.4	1.693
2567	723.3	78.3	1.0792	706.0	1.693
2568	723.3	74.3	1.0792	705.4	1.693
2569	721.2	78.3	1.0792	706.0	1.693
2570	723.3	78.3	1.0805	705.4	1.693
2571	723.3	78.3	1.0805	705.4	1.693
2572	721.2	78.3	1.0805	705.4	1.693

Table A6. Data for the undrained triaxial compression test R3.

Date:	05/23/95
Sample material:	remolded UpB till, core 92-1
Initial weight:	254.9 gram
Pre-shear length:	6.10 cm
Pre-shear radius:	2.54 cm
Void ratio:	0.518
Saturation pressure:	379.9 kPa

#	σ_3 [kPa]	F_a [N]	ΔL [cm]	p_w [kPa]	u_a [µm/s]	#	σ_3 [kPa]	F_a [N]	ΔL [cm]	p_w [kPa]	u_a [µm/s]
1	584.7	0.0	0.0000	379.9	1.693	61	583.3	205.5	0.0406	416.9	1.693
2	584.7	4.4	0.0025	380.6	1.693	62	584.7	205.5	0.0406	417.7	1.693
3	584.7	8.9	0.0025	381.4	1.693	63	584.7	205.5	0.0419	417.2	1.693
4	584.7	13.3	0.0025	382.2	1.693	64	584.7	210.0	0.0432	418.0	1.693
5	584.7	17.8	0.0036	383.0	1.693	65	583.3	210.0	0.0432	418.1	1.693
6	584.7	26.2	0.0036	383.8	1.693	66	583.3	210.0	0.0442	418.9	1.693
7	584.7	30.7	0.0048	384.7	1.693	67	584.7	210.0	0.0455	419.7	1.693
8	584.7	39.6	0.0048	385.5	1.693	68	584.7	210.0	0.0455	419.9	1.693
9	584.7	48.5	0.0061	386.3	1.693	69	584.7	214.4	0.0467	420.7	1.693
10	584.7	56.9	0.0061	387.1	1.693	70	584.7	214.4	0.0478	420.8	1.693
11	584.7	65.8	0.0074	387.9	1.693	71	583.3	214.4	0.0478	420.2	1.693
12	584.7	74.3	0.0074	388.0	1.693	72	584.7	214.4	0.0478	421.0	1.693
13	584.7	83.2	0.0084	388.9	1.693	73	583.3	214.4	0.0490	421.9	1.693
14	584.7	92.1	0.0084	389.7	1.693	74	584.7	214.4	0.0490	422.0	1.693
15	584.7	96.5	0.0097	390.5	1.693	75	584.7	214.4	0.0503	422.8	1.693
16	584.7	105.0	0.0097	391.3	1.693	76	584.7	218.9	0.0516	422.2	1.693
17	583.3	109.4	0.0109	392.1	1.693	77	584.7	218.9	0.0516	423.1	1.693
18	584.7	113.9	0.0109	392.2	1.693	78	584.7	218.9	0.0526	423.9	1.693
19	584.7	122.8	0.0119	393.1	1.693	79	584.7	218.9	0.0526	424.0	1.693
20	584.7	126.8	0.0119	393.9	1.693	80	583.3	218.9	0.0538	424.8	1.693
21	584.7	126.8	0.0132	394.7	1.693	81	584.7	218.9	0.0551	424.9	1.693
22	584.7	131.2	0.0145	395.5	1.693	82	584.7	223.3	0.0551	425.1	1.693
23	584.7	135.7	0.0145	396.3	1.693	83	584.7	223.3	0.0561	425.9	1.693
24	584.7	140.1	0.0145	397.1	1.693	84	584.7	223.3	0.0574	426.7	1.693
25	584.7	144.6	0.0155	397.9	1.693	85	584.7	223.3	0.0574	426.8	1.693
26	584.7	149.0	0.0180	398.8	1.693	86	584.7	223.3	0.0587	426.9	1.693
27	583.3	149.0	0.0168	398.9	1.693	87	584.7	223.3	0.0587	426.4	1.693
28	584.7	153.0	0.0180	399.7	1.693	88	584.7	227.3	0.0599	427.9	1.693
29	584.7	157.5	0.0180	399.1	1.693	89	584.7	227.3	0.0599	428.0	1.693
30	584.7	157.5	0.0193	400.6	1.693	90	584.7	227.3	0.0610	427.4	1.693
31	584.7	161.9	0.0203	401.4	1.693	91	584.7	227.3	0.0622	428.9	1.693
32	584.7	161.9	0.0203	400.9	1.693	92	584.7	227.3	0.0622	429.1	1.693
33	584.7	161.9	0.0216	402.4	1.693	93	584.7	227.3	0.0635	429.9	1.693
34	584.7	166.4	0.0229	403.2	1.693	94	584.7	231.8	0.0645	430.7	1.693
35	584.7	170.8	0.0229	404.0	1.693	95	584.7	231.8	0.0645	430.8	1.693
36	583.3	170.8	0.0239	404.8	1.693	96	584.7	231.8	0.0658	430.3	1.693
37	584.7	174.8	0.0239	405.0	1.693	97	584.7	231.8	0.0658	431.1	1.693
38	583.3	174.8	0.0251	405.8	1.693	98	584.7	231.8	0.0671	431.2	1.693
39	584.7	174.8	0.0264	406.6	1.693	99	584.7	231.8	0.0681	432.0	1.693
40	584.7	179.3	0.0264	406.7	1.693	100	584.7	236.2	0.0681	432.1	1.693
41	584.7	179.3	0.0274	407.5	1.693	101	584.7	231.8	0.0693	432.9	1.693
42	584.7	179.3	0.0287	407.6	1.693	102	584.7	236.2	0.0693	432.4	1.693
43	584.7	183.7	0.0274	407.8	1.693	103	584.7	236.2	0.0706	433.2	1.693
44	584.7	183.7	0.0287	408.6	1.693	104	584.7	236.2	0.0719	433.3	1.693
45	584.7	188.2	0.0300	409.4	1.693	105	584.7	240.6	0.0719	433.4	1.693
46	584.7	188.2	0.0300	409.5	1.693	106	584.7	236.2	0.0719	433.6	1.693
47	584.7	188.2	0.0312	410.3	1.693	107	584.7	236.2	0.0742	434.4	1.693
48	583.3	192.6	0.0323	411.2	1.693	108	584.7	236.2	0.0742	434.4	1.693
49	584.7	192.6	0.0323	411.3	1.693	109	584.7	236.2	0.0742	435.1	1.693
50	584.7	192.6	0.0323	411.4	1.693	110	584.7	240.6	0.0754	435.1	1.693
51	583.3	197.1	0.0335	412.2	1.693	111	584.7	240.6	0.0765	435.0	1.693
52	584.7	197.1	0.0335	412.3	1.693	112	583.3	240.6	0.0765	435.7	1.693
53	584.7	197.1	0.0348	413.2	1.693	113	584.7	240.6	0.0777	435.7	1.693
54	584.7	192.6	0.0348	413.3	1.693	114	584.7	240.6	0.0777	435.7	1.693
55	584.7	201.1	0.0358	413.4	1.693	115	584.7	240.6	0.0803	436.3	1.693
56	584.7	201.1	0.0371	414.2	1.693	116	584.7	240.6	0.0790	436.3	1.693
57	584.7	201.1	0.0371	414.3	1.693	117	583.3	210.0	0.0803	437.7	0.339
58	584.7	201.1	0.0384	415.2	1.693	118	584.7	214.4	0.0803	438.3	0.339
59	584.7	201.1	0.0384	416.0	1.693	119	584.7	214.4	0.0803	438.3	0.339
60	584.7	201.1	0.0406	416.1	1.693	120	584.7	214.4	0.0813	438.3	0.339

Table A6. Continued.

#	σ_3 [kPa]	F_a [N]	ΔL [cm]	p_w [kPa]	u_a [μm/s]	#	σ_3 [kPa]	F_a [N]	ΔL [cm]	p_w [kPa]	u_a [μm/s]
121	584.7	218.9	0.0803	438.3	0.339	194	584.7	266.9	0.0968	439.6	1.693
122	583.3	218.9	0.0813	438.3	0.339	195	584.7	271.3	0.0980	439.6	1.693
123	584.7	218.9	0.0813	438.2	0.339	196	584.7	266.9	0.0980	439.6	1.693
124	584.7	223.3	0.0813	438.2	0.339	197	584.7	266.9	0.0993	439.6	1.693
125	584.7	218.9	0.0826	438.9	0.339	198	584.7	266.9	0.0993	439.5	1.693
126	584.7	218.9	0.0826	438.9	0.339	199	584.7	266.9	0.1006	439.5	1.693
127	584.7	218.9	0.0826	438.9	0.339	200	584.7	266.9	0.1016	440.2	1.693
128	584.7	218.9	0.0813	438.8	0.339	201	584.7	266.9	0.1029	439.5	1.693
129	584.7	223.3	0.0826	438.8	0.339	202	584.7	262.4	0.1029	439.5	1.693
130	584.7	223.3	0.0826	438.8	0.339	203	584.7	271.3	0.1041	439.4	1.693
131	584.7	223.3	0.0826	438.8	0.339	204	584.7	271.3	0.1052	439.4	1.693
132	584.7	223.3	0.0826	438.8	0.339	205	584.7	271.3	0.1052	439.4	1.693
133	584.7	223.3	0.0826	438.7	0.339	206	584.7	271.3	0.1064	439.4	1.693
134	584.7	223.3	0.0826	439.4	0.339	207	584.7	271.3	0.1077	439.4	1.693
135	584.7	223.3	0.0838	439.4	0.339	208	584.7	271.3	0.1077	439.3	1.693
136	584.7	223.3	0.0826	439.4	0.339	209	584.7	271.3	0.1148	440.0	1.693
137	583.3	223.3	0.0826	439.4	0.339	210	584.7	271.3	0.1184	439.3	1.693
138	584.7	227.3	0.0826	440.0	0.339	211	584.7	271.3	0.1125	440.0	1.693
139	584.7	227.3	0.0826	440.0	0.339	212	584.7	271.3	0.1125	440.0	1.693
140	584.7	227.3	0.0826	440.0	0.339	213	584.7	275.3	0.1135	439.9	1.693
141	584.7	227.3	0.0838	440.0	0.339	214	584.7	271.3	0.1148	440.6	1.693
142	584.7	227.3	0.0838	439.9	0.339	215	584.7	271.3	0.1148	440.6	1.693
143	584.7	223.3	0.0838	440.6	0.339	216	584.7	275.3	0.1161	441.3	1.693
144	584.7	227.3	0.0838	440.6	0.339	217	584.7	275.3	0.1161	441.2	1.693
145	584.7	227.3	0.0826	440.6	0.339	218	584.7	275.3	0.1184	441.9	1.693
146	584.7	227.3	0.0848	440.6	0.339	219	584.7	275.3	0.1184	441.9	1.693
147	584.7	227.3	0.0848	440.5	0.339	220	584.7	275.3	0.1184	441.9	1.693
148	584.7	227.3	0.0848	441.2	0.339	221	584.7	275.3	0.1196	442.5	1.693
149	584.7	227.3	0.0848	441.2	0.339	222	584.7	275.3	0.1207	442.5	1.693
150	584.7	231.8	0.0848	441.2	0.339	223	584.7	275.3	0.1207	442.5	1.693
151	584.7	227.3	0.0848	441.1	0.339	224	584.7	275.3	0.1219	442.5	1.693
152	584.7	231.8	0.0848	441.1	0.339	225	584.7	275.3	0.1232	443.1	1.693
153	584.7	231.8	0.0848	441.1	0.339	226	584.7	275.3	0.1232	443.1	1.693
154	584.7	231.8	0.0861	441.1	0.339	227	584.7	279.8	0.1255	443.1	1.693
155	584.7	231.8	0.0848	441.8	0.339	228	584.7	275.3	0.1255	443.8	1.693
156	584.7	231.8	0.0848	441.7	0.339	229	584.7	275.3	0.1255	443.8	1.693
157	584.7	231.8	0.0848	441.7	0.339	230	584.7	279.8	0.1267	443.7	1.693
158	584.7	227.3	0.0861	441.7	0.339	231	584.7	323.8	0.1267	443.7	42.333
159	583.3	231.8	0.0861	441.7	0.339	232	584.7	319.4	0.1267	438.2	42.333
160	584.7	231.8	0.0848	441.7	0.339	233	584.7	314.9	0.1410	434.7	42.333
161	584.7	231.8	0.0861	442.3	0.339	234	584.7	314.9	0.1590	432.6	42.333
162	584.7	231.8	0.0861	443.0	0.339	235	584.7	288.7	0.1877	433.3	1.693
163	583.3	231.8	0.0861	442.3	0.339	236	584.7	288.7	0.1890	435.3	1.693
164	584.7	231.8	0.0861	442.3	0.339	237	584.7	288.7	0.1890	437.4	1.693
165	584.7	231.8	0.0861	442.3	0.339	238	584.7	288.7	0.1900	438.8	1.693
166	584.7	231.8	0.0874	442.2	0.339	239	584.7	288.7	0.1900	440.1	1.693
167	584.7	231.8	0.0861	442.2	0.339	240	584.7	293.1	0.1913	439.4	1.693
168	583.3	231.8	0.0874	442.9	0.339	241	584.7	288.7	0.1925	439.4	1.693
169	584.7	231.8	0.0874	442.2	0.339	242	584.7	293.1	0.1935	440.1	1.693
170	584.7	231.8	0.0874	442.2	0.339	243	584.7	293.1	0.1935	440.7	1.693
171	583.3	231.8	0.0874	442.8	0.339	244	584.7	293.1	0.1948	440.7	1.693
172	584.7	231.8	0.0874	442.8	0.339	245	584.7	293.1	0.1948	440.7	1.693
173	584.7	236.2	0.0874	442.8	0.339	246	584.7	297.6	0.1961	441.4	1.693
174	584.7	236.2	0.0861	442.8	0.339	247	583.3	297.6	0.1974	441.3	1.693
175	583.3	236.2	0.0861	442.7	0.339	248	583.3	297.6	0.1974	442.0	1.693
176	584.7	236.2	0.0874	442.7	0.339	249	584.7	293.1	0.1984	442.0	1.693
177	584.7	236.2	0.0874	442.0	0.339	250	584.7	297.6	0.1996	442.7	1.693
178	584.7	236.2	0.0884	442.7	0.339	251	584.7	297.6	0.1996	443.3	1.693
179	584.7	236.2	0.0884	442.7	0.339	252	584.7	297.6	0.2009	443.3	1.693
180	584.7	236.2	0.0884	442.6	0.339	253	584.7	297.6	0.2009	444.0	1.693
181	584.7	236.2	0.0884	442.6	0.339	254	584.7	297.6	0.2019	444.0	1.693
182	584.7	236.2	0.0874	442.6	0.339	255	584.7	297.6	0.2032	443.9	1.693
183	584.7	236.2	0.0897	442.6	0.339	256	583.3	297.6	0.2045	444.6	1.693
184	584.7	231.8	0.0884	442.6	0.339	257	584.7	301.6	0.2045	444.6	1.693
185	584.7	253.5	0.0884	441.9	1.693	258	584.7	301.6	0.2057	445.3	1.693
186	584.7	258.0	0.0909	441.8	1.693	259	584.7	301.6	0.2068	445.2	1.693
187	584.7	258.0	0.0922	441.1	1.693	260	584.7	301.6	0.2068	445.9	1.693
188	584.7	262.4	0.0922	441.1	1.693	261	584.7	301.6	0.2080	445.9	1.693
189	584.7	262.4	0.0932	441.1	1.693	262	584.7	306.0	0.2080	445.9	1.693
190	584.7	262.4	0.0932	441.1	1.693	263	584.7	306.0	0.2093	446.5	1.693
191	584.7	262.4	0.0958	440.4	1.693	264	584.7	306.0	0.2103	446.5	1.693
192	584.7	262.4	0.0945	440.3	1.693	265	583.3	306.0	0.2103	447.2	1.693
193	584.7	266.9	0.0958	439.6	1.693	266	584.7	306.0	0.2116	447.2	1.693

Table A6. Continued.

#	σ_3 [kPa]	F_a [N]	ΔL [cm]	p_w [kPa]	u_a [μm/s]
267	584.7	301.6	0.2116	447.8	1.693
268	584.7	306.0	0.2129	447.8	1.693
269	583.3	310.5	0.2139	448.5	1.693
270	584.7	310.5	0.2139	449.2	1.693
271	584.7	306.0	0.2151	449.1	1.693
272	584.7	306.0	0.2151	449.1	1.693
273	584.7	306.0	0.2164	449.8	1.693
274	584.7	306.0	0.2164	449.8	1.693
275	584.7	310.5	0.2187	449.7	1.693
276	584.7	310.5	0.2187	450.4	1.693
277	584.7	310.5	0.2200	450.4	1.693
278	584.7	310.5	0.2212	451.1	1.693
279	584.7	310.5	0.2200	451.1	1.693
280	583.3	310.5	0.2223	451.7	1.693
281	584.7	314.9	0.2223	451.7	1.693
282	584.7	314.9	0.2235	451.7	1.693
283	584.7	314.9	0.2248	451.7	1.693
284	584.7	314.9	0.2261	452.3	1.693
285	584.7	314.9	0.2261	452.3	1.693
286	583.3	284.2	0.2261	453.0	0.339
287	584.7	288.7	0.2261	454.3	0.339
288	584.7	288.7	0.2271	454.3	0.339
289	584.7	288.7	0.2271	455.7	0.339
290	584.7	288.7	0.2271	456.4	0.339
291	584.7	293.1	0.2271	456.3	0.339
292	584.7	293.1	0.2271	457.0	0.339
293	583.3	293.1	0.2271	457.0	0.339
294	584.7	293.1	0.2271	457.0	0.339
295	584.7	297.6	0.2271	456.9	0.339
296	583.3	297.6	0.2283	457.6	0.339
297	584.7	293.1	0.2271	456.9	0.339
298	584.7	293.1	0.2283	457.6	0.339
299	583.3	297.6	0.2283	457.6	0.339
300	583.3	297.6	0.2283	457.5	0.339
301	584.7	297.6	0.2283	457.5	0.339
302	584.7	297.6	0.2296	458.2	0.339
303	584.7	297.6	0.2296	458.2	0.339
304	584.7	297.6	0.2296	458.1	0.339
305	584.7	297.6	0.2283	458.1	0.339
306	583.3	301.6	0.2283	458.1	0.339
307	584.7	297.6	0.2296	458.1	0.339
308	583.3	297.6	0.2296	458.1	0.339
309	584.7	297.6	0.2306	458.0	0.339
310	584.7	301.6	0.2296	458.0	0.339
311	584.7	301.6	0.2296	458.0	0.339
312	584.7	297.6	0.2296	458.0	0.339
313	584.7	301.6	0.2296	458.0	0.339
314	583.3	301.6	0.2306	457.9	0.339
315	583.3	301.6	0.2306	457.9	0.339
316	584.7	301.6	0.2306	457.9	0.339
317	584.7	301.6	0.2306	457.9	0.339
318	584.7	301.6	0.2306	457.9	0.339
319	584.7	297.6	0.2306	457.9	0.339
320	584.7	301.6	0.2319	457.8	0.339
321	584.7	301.6	0.2306	457.8	0.339
322	583.3	301.6	0.2319	457.8	0.339
323	584.7	301.6	0.2306	457.8	0.339
324	584.7	301.6	0.2319	457.8	0.339
325	584.7	306.0	0.2319	457.7	0.339
326	584.7	306.0	0.2319	457.7	0.339
327	584.7	306.0	0.2319	457.7	0.339
328	584.7	306.0	0.2332	457.7	0.339
329	584.7	301.6	0.2319	457.7	0.339
330	584.7	306.0	0.2319	457.6	0.339
331	583.3	306.0	0.2319	457.6	0.339
332	584.7	306.0	0.2332	457.6	0.339
333	584.7	306.0	0.2332	457.6	0.339
334	584.7	306.0	0.2332	457.6	0.339
335	584.7	310.5	0.2332	457.5	0.339
336	584.7	306.0	0.2332	457.5	0.339
337	584.7	306.0	0.2342	457.5	0.339
338	584.7	310.5	0.2342	457.5	0.339
339	584.7	310.5	0.2342	457.5	0.339
340	584.7	310.5	0.2342	457.4	0.339
341	584.7	310.5	0.2342	457.4	0.339
342	584.7	310.5	0.2342	457.4	0.339
343	584.7	310.5	0.2342	457.4	0.339
344	584.7	310.5	0.2342	457.4	0.339
345	584.7	310.5	0.2342	457.3	0.339
346	584.7	310.5	0.2355	457.3	0.339
347	584.7	310.5	0.2355	457.3	0.339
348	584.7	310.5	0.2355	457.3	0.339
349	584.7	310.5	0.2342	457.3	0.339
350	584.7	310.5	0.2355	457.2	0.339
351	584.7	310.5	0.2355	457.2	0.339
352	584.7	310.5	0.2355	457.2	0.339
353	584.7	314.9	0.2367	457.2	0.339
354	584.7	314.9	0.2367	457.9	0.339
355	584.7	314.9	0.2367	457.8	0.339
356	584.7	310.5	0.2367	457.8	0.339
357	584.7	314.9	0.2367	457.8	0.339
358	584.7	314.9	0.2367	457.8	0.339
359	584.7	314.9	0.2367	457.8	0.339
360	584.7	314.9	0.2380	457.7	0.339
361	584.7	310.5	0.2355	457.7	0.339
362	584.7	314.9	0.2367	457.7	0.339
363	584.7	314.9	0.2380	457.7	0.339
364	584.7	314.9	0.2380	457.7	0.339
365	584.7	314.9	0.2380	457.6	0.339
366	584.7	314.9	0.2380	457.6	0.339
367	584.7	314.9	0.2380	457.6	0.339
368	584.7	314.9	0.2380	457.6	0.339
369	583.3	314.9	0.2380	457.6	0.339
370	584.7	319.4	0.2390	457.5	0.339
371	583.3	314.9	0.2390	457.5	0.339
372	584.7	314.9	0.2380	457.5	0.339
373	584.7	319.4	0.2390	457.5	0.339
374	584.7	314.9	0.2390	457.5	0.339
375	584.7	319.4	0.2390	457.4	0.339
376	584.7	314.9	0.2390	457.4	0.339
377	584.7	314.9	0.2403	457.4	0.339
378	584.7	319.4	0.2403	457.4	0.339
379	584.7	319.4	0.2403	457.4	0.339
380	584.7	314.9	0.2403	457.3	0.339
381	584.7	375.9	0.2464	453.9	42.333
382	584.7	380.3	0.2654	449.7	42.333
383	584.7	375.9	0.2832	444.2	42.333
384	584.7	375.9	0.3035	440.0	42.333
385	584.7	327.8	0.3180	449.0	1.693
386	584.7	332.3	0.3180	449.6	1.693
387	584.7	332.3	0.3180	449.6	1.693
388	583.3	332.3	0.3193	450.3	1.693
389	584.7	336.7	0.3203	450.3	1.693
390	583.3	341.2	0.3203	450.3	1.693
391	583.3	336.7	0.3228	450.9	1.693
392	584.7	336.7	0.3228	450.9	1.693
393	584.7	341.2	0.3239	451.6	1.693
394	584.7	341.2	0.3239	451.6	1.693
395	584.7	341.2	0.3251	452.2	1.693
396	583.3	341.2	0.3264	452.2	1.693
397	584 7	345.6	0.3264	452.9	1.693
398	584 7	345.6	0.3274	452.9	1.693
399	584 7	345.6	0.3287	452.8	1.693
400	584.7	349.6	0.3287	452.8	1.693
401	583.3	345.6	0.3299	452.8	1.693
402	584.7	349.6	0.3312	452.8	1.693
403	584.7	349.6	0.3322	452.8	1.693
404	584.7	349.6	0.3322	452.7	1.693
405	584.7	349.6	0.3335	453.4	1.693
406	584.7	349.6	0.3335	453.4	1.693
407	584.7	349.6	0.3348	453.4	1.693
408	584.7	354.1	0.3348	453.4	1.693
409	584.7	354.1	0.3358	453.3	1.693
410	584.7	349.6	0.3371	453.3	1.693
411	584.7	354.1	0.3371	453.3	1.693
412	583.3	354.1	0.3383	453.3	1.693

Table A6. Continued.

#	σ_3 [kPa]	F_a [N]	ΔL [cm]	p_w [kPa]	u_a [μm/s]
486	583.3	358.5	0.3825	458.0	0.339
487	584.7	358.5	0.3825	458.0	0.339
488	583.3	358.5	0.3825	458.0	0.339
489	584.7	363.0	0.3825	458.0	0.339
490	584.7	363.0	0.3825	457.9	0.339
491	584.7	363.0	0.3813	457.9	0.339
492	584.7	363.0	0.3825	458.6	0.339
493	584.7	358.5	0.3838	458.6	0.339
494	583.3	363.0	0.3825	458.6	0.339
495	584.7	363.0	0.3838	458.5	0.339
496	584.7	363.0	0.3838	458.5	0.339
497	584.7	367.4	0.3838	458.5	0.339
498	584.7	367.4	0.3838	458.5	0.339
499	584.7	363.0	0.3838	458.5	0.339
500	584.7	367.4	0.3838	458.4	0.339
501	584.7	367.4	0.3838	459.1	0.339
502	584.7	367.4	0.3848	459.1	0.339
503	584.7	367.4	0.3848	459.1	0.339
504	584.7	367.4	0.3848	459.1	0.339
505	583.3	367.4	0.3848	459.0	0.339
506	584.7	367.4	0.3848	459.0	0.339
507	584.7	367.4	0.3848	459.0	0.339
508	583.3	367.4	0.3861	459.0	0.339
509	584.7	371.9	0.3848	459.0	0.339
510	584.7	367.4	0.3861	458.9	0.339
511	584.7	367.4	0.3861	459.6	0.339
512	584.7	371.9	0.3861	459.6	0.339
513	583.3	371.9	0.3861	459.6	0.339
514	583.3	371.9	0.3861	459.5	0.339
515	584.7	371.9	0.3861	459.5	0.339
516	584.7	371.9	0.3861	459.5	0.339
517	583.3	371.9	0.3874	459.5	0.339
518	583.3	371.9	0.3874	459.5	0.339
519	583.3	371.9	0.3874	459.4	0.339
520	584.7	371.9	0.3874	459.4	0.339
521	584.7	371.9	0.3884	459.4	0.339
522	584.7	371.9	0.3884	459.4	0.339
523	584.7	341.2	0.3884	460.1	0.068
524	584.7	341.2	0.3884	460.7	0.068
525	584.7	341.2	0.3884	461.4	0.068
526	584.7	341.2	0.3884	461.4	0.068
527	584.7	345.6	0.3884	462.1	0.068
528	584.7	345.6	0.3884	462.0	0.068
529	584.7	341.2	0.3874	462.7	0.068
530	584.7	345.6	0.3884	462.7	0.068
531	584.7	345.6	0.3884	462.7	0.068
532	584.7	341.2	0.3884	463.3	0.068
533	584.7	341.2	0.3884	463.3	0.068
534	584.7	345.6	0.3884	463.3	0.068
535	584.7	345.6	0.3874	463.3	0.068
536	584.7	345.6	0.3884	463.3	0.068
537	584.7	345.6	0.3874	463.9	0.068
538	584.7	341.2	0.3884	463.9	0.068
539	583.3	345.6	0.3884	463.9	0.068
540	584.7	345.6	0.3874	463.9	0.068
541	584.7	345.6	0.3874	463.8	0.068
542	584.7	341.2	0.3874	464.5	0.068
543	584.7	345.6	0.3884	464.5	0.068
544	584.7	341.2	0.3884	464.5	0.068
545	584.7	345.6	0.3884	464.5	0.068
546	584.7	345.6	0.3884	464.4	0.068
547	584.7	345.6	0.3874	464.4	0.068
548	584.7	341.2	0.3874	464.4	0.068
549	584.7	345.6	0.3884	465.1	0.068
550	583.3	341.2	0.3896	465.0	0.068
551	584.7	341.2	0.3884	465.0	0.068
552	584.7	345.6	0.3884	465.0	0.068
553	584.7	341.2	0.3884	465.0	0.068
554	584.7	345.6	0.3896	465.0	0.068
555	584.7	345.6	0.3884	465.6	0.068
556	584.7	341.2	0.3896	465.6	0.068
557	583.3	341.2	0.3884	465.6	0.068
558	583.3	341.2	0.3874	465.6	0.068
559	584.7	345.6	0.3896	465.6	0.068
560	584.7	341.2	0.3884	465.5	0.068
561	584.7	341.2	0.3884	465.5	0.068
562	584.7	345.6	0.3884	465.5	0.068
563	583.3	345.6	0.3896	465.5	0.068
564	583.3	345.6	0.3896	465.5	0.068
565	584.7	345.6	0.3884	465.4	0.068
566	584.7	341.2	0.3884	465.4	0.068
567	584.7	345.6	0.3896	465.4	0.068
568	584.7	402.1	0.3922	461.2	1.693
569	584.7	402.1	0.3922	461.2	1.693
570	584.7	402.1	0.3945	461.2	1.693
571	584.7	411.0	0.3945	460.5	1.693
572	583.3	411.0	0.3957	460.5	1.693
573	584.7	411.0	0.3957	460.5	1.693
574	584.7	411.0	0.3967	460.4	1.693
575	584.7	411.0	0.3980	459.7	1.693
576	583.3	411.0	0.3993	459.7	1.693
577	584.7	411.0	0.3993	459.7	1.693
578	583.3	411.0	0.4003	459.7	1.693
579	583.3	411.0	0.4003	459.7	1.693
580	584.7	411.0	0.4016	458.9	1.693
581	584.7	411.0	0.4028	458.9	1.693
582	584.7	415.5	0.4028	458.9	1.693
583	584.7	411.0	0.4041	458.9	1.693
584	583.3	415.5	0.4041	458.2	1.693
585	584.7	415.5	0.4064	458.2	1.693
586	583.3	415.5	0.4064	458.1	1.693
587	584.7	415.5	0.4087	458.1	1.693
588	584.7	415.5	0.4087	458.1	1.693
589	584.7	415.5	0.4087	457.4	1.693
590	584.7	415.5	0.4100	457.4	1.693
591	584.7	415.5	0.4100	457.4	1.693
592	584.7	415.5	0.4125	457.3	1.693
593	584.7	415.5	0.4125	457.3	1.693
594	584.7	415.5	0.4135	456.6	1.693
595	583.3	415.5	0.4148	456.6	1.693
596	584.7	415.5	0.4148	456.6	1.693
597	584.7	415.5	0.4148	456.5	1.693
598	583.3	415.5	0.4171	456.5	1.693
599	584.7	419.9	0.4171	456.5	1.693
600	584.7	419.9	0.4183	455.8	1.693
601	584.7	419.9	0.4196	455.8	1.693
602	584.7	419.9	0.4206	455.8	1.693
603	584.7	419.9	0.4219	455.7	1.693
604	583.3	419.9	0.4206	455.7	1.693
605	584.7	415.5	0.4219	455.0	1.693
606	583.3	419.9	0.4232	455.0	1.693
607	584.7	419.9	0.4244	455.0	1.693
608	584.7	419.9	0.4244	454.9	1.693
609	583.3	419.9	0.4255	454.2	1.693
610	583.3	419.9	0.4255	454.2	1.693
611	584.7	419.9	0.4267	454.2	1.693
612	583.3	423.9	0.4280	454.2	1.693
613	584.7	419.9	0.4280	454.2	1.693
614	584.7	419.9	0.4290	453.5	1.693
615	584.7	419.9	0.4303	452.7	1.693
616	583.3	423.9	0.4315	452.7	1.693
617	584.7	441.7	0.4364	452.0	8.467
618	584.7	441.7	0.4409	453.4	8.467
619	584.7	441.7	0.4448	454.0	8.467
620	584.7	441.7	0.4493	454.7	8.467
621	583.3	441.7	0.4529	454.0	8.467
622	584.7	441.7	0.4567	453.3	8.467
623	584.7	441.7	0.4613	452.6	8.467
624	584.7	441.7	0.4651	451.9	8.467
625	584.7	441.7	0.4686	451.2	8.467
626	584.7	441.7	0.4722	450.5	8.467
627	584.7	441.7	0.4770	449.7	8.467
628	583.3	441.7	0.4806	449.7	8.467
629	583.3	437.3	0.4854	449.0	8.467
630	584.7	437.3	0.4890	449.0	8.467
631	584.7	437.3	0.4925	448.3	8.467

Table A6. Continued.

#	σ_3 [kPa]	F_a [N]	ΔL [cm]	p_w [kPa]	u_a [μm/s]
632	583.3	441.7	0.4973	448.3	8.467
633	584.7	441.7	0.5009	448.3	8.467
634	584.7	441.7	0.5044	448.2	8.467
635	584.7	463.5	0.5138	447.5	42.333
636	583.3	463.5	0.5354	446.1	42.333
637	584.7	459.1	0.5558	444.7	42.333
638	583.3	459.1	0.5761	443.3	42.333
639	583.3	406.6	0.5928	444.7	1.693
640	584.7	411.0	0.5941	445.4	1.693
641	584.7	411.0	0.5941	446.0	1.693
642	583.3	415.5	0.5951	446.7	1.693
643	583.3	415.5	0.5964	447.4	1.693
644	583.3	415.5	0.5977	448.0	1.693
645	584.7	419.9	0.5987	448.0	1.693
646	583.3	419.9	0.5987	448.7	1.693
647	584.7	419.9	0.5999	448.7	1.693
648	584.7	419.9	0.6012	449.3	1.693
649	584.7	419.9	0.6025	449.3	1.693
650	584.7	423.9	0.6035	450.0	1.693
651	584.7	423.9	0.6025	450.0	1.693
652	584.7	423.9	0.6048	449.9	1.693
653	584.7	423.9	0.6060	450.6	1.693
654	584.7	423.9	0.6060	450.6	1.693
655	584.7	423.9	0.6071	450.6	1.693
656	583.3	423.9	0.6071	451.3	1.693
657	584.7	428.4	0.6083	451.2	1.693
658	584.7	428.4	0.6096	451.2	1.693
659	584.7	428.4	0.6109	451.2	1.693
660	584.7	428.4	0.6109	451.9	1.693
661	584.7	428.4	0.6119	451.8	1.693
662	584.7	428.4	0.6132	451.8	1.693
663	584.7	428.4	0.6132	451.8	1.693
664	584.7	432.8	0.6144	452.5	1.693
665	584.7	432.8	0.6144	452.5	1.693
666	584.7	432.8	0.6154	452.4	1.693
667	584.7	432.8	0.6167	452.4	1.693
668	583.3	432.8	0.6180	453.1	1.693
669	584.7	432.8	0.6190	453.1	1.693
670	584.7	432.8	0.6190	453.0	1.693
671	584.7	437.3	0.6203	453.0	1.693
672	583.3	437.3	0.6215	453.0	1.693
673	583.3	432.8	0.6215	453.0	1.693
674	584.7	437.3	0.6228	453.7	1.693
675	584.7	437.3	0.6238	453.6	1.693
676	584.7	437.3	0.6238	453.6	1.693
677	584.7	437.3	0.6251	453.6	1.693
678	583.3	437.3	0.6251	453.6	1.693
679	583.3	437.3	0.6264	453.6	1.693
680	584.7	441.7	0.6274	454.2	1.693
681	584.7	441.7	0.6287	454.2	1.693
682	584.7	441.7	0.6287	454.2	1.693
683	584.7	441.7	0.6299	454.2	1.693
684	583.3	441.7	0.6312	454.1	1.693
685	584.7	441.7	0.6322	454.1	1.693
686	584.7	441.7	0.6322	454.1	1.693
687	584.7	489.7	0.6551	449.3	42.333
688	584.7	485.3	0.6754	445.8	42.333
689	584.7	480.9	0.6980	443.7	42.333
690	584.7	476.4	0.7170	441.6	42.333
691	583.3	454.6	0.7280	442.3	8.467
692	583.3	459.1	0.7325	443.0	8.467
693	584.7	459.1	0.7374	443.6	8.467
694	583.3	463.5	0.7409	444.3	8.467
695	584.7	463.5	0.7457	444.3	8.467
696	584.7	463.5	0.7493	445.0	8.467
697	584.7	463.5	0.7529	445.6	8.467
698	583.3	463.5	0.7590	446.3	8.467
699	584.7	468.0	0.7625	446.3	8.467
700	583.3	463.5	0.7661	446.9	8.467
701	584.7	468.0	0.7709	446.9	8.467
702	583.3	468.0	0.7757	447.6	8.467
703	584.7	472.4	0.7793	447.6	8.467
704	584.7	472.4	0.7828	447.6	8.467
705	584.7	472.4	0.7877	448.2	8.467
706	583.3	472.4	0.7925	448.2	8.467
707	583.3	472.4	0.7960	448.2	8.467
708	584.7	472.4	0.8009	448.9	8.467
709	583.3	472.4	0.8054	448.8	8.467
710	584.7	472.4	0.8092	448.8	8.467
711	584.7	472.4	0.8128	449.5	8.467
712	584.7	472.4	0.8176	449.5	8.467
713	584.7	472.4	0.8222	449.4	8.467
714	583.3	472.4	0.8258	449.4	8.467
715	584.7	472.4	0.8306	449.4	8.467
716	584.7	446.2	0.8341	450.1	1.693
717	584.7	450.2	0.8354	450.1	1.693
718	584.7	450.2	0.8367	450.0	1.693
719	583.3	450.2	0.8367	450.0	1.693
720	584.7	454.6	0.8367	450.0	1.693
721	584.7	454.6	0.8390	450.7	1.693
722	584.7	454.6	0.8390	450.6	1.693
723	584.7	454.6	0.8402	450.6	1.693
724	584.7	459.1	0.8415	450.6	1.693
725	584.7	459.1	0.8415	450.6	1.693
726	583.3	459.1	0.8425	451.3	1.693
727	584.7	459.1	0.8438	451.2	1.693
728	584.7	463.5	0.8451	451.2	1.693
729	584.7	463.5	0.8451	451.2	1.693
730	584.7	463.5	0.8461	451.9	1.693
731	584.7	463.5	0.8473	451.8	1.693
732	584.7	463.5	0.8486	451.8	1.693
733	584.7	463.5	0.8486	451.8	1.693
734	584.7	463.5	0.8499	452.5	1.693
735	584.7	463.5	0.8509	452.5	1.693
736	584.7	463.5	0.8522	452.4	1.693
737	583.3	468.0	0.8522	452.4	1.693
738	584.7	468.0	0.8534	453.1	1.693
739	584.7	468.0	0.8545	453.1	1.693
740	583.3	468.0	0.8545	453.1	1.693
741	584.7	468.0	0.8557	453.0	1.693
742	584.7	468.0	0.8570	453.0	1.693
743	584.7	472.4	0.8570	453.7	1.693
744	584.7	468.0	0.8580	453.7	1.693
745	584.7	472.4	0.8593	453.6	1.693
746	584.7	472.4	0.8606	453.6	1.693
747	584.7	472.4	0.8606	453.6	1.693
748	583.3	472.4	0.8618	454.3	1.693
749	584.7	472.4	0.8628	454.3	1.693
750	583.3	472.4	0.8641	454.2	1.693
751	583.3	472.4	0.8641	454.2	1.693
752	584.7	476.4	0.8654	454.9	1.693
753	584.7	472.4	0.8664	454.9	1.693
754	583.3	476.4	0.8664	454.8	1.693
755	584.7	476.4	0.8677	454.8	1.693
756	583.3	476.4	0.8677	454.8	1.693
757	584.7	480.9	0.8689	454.8	1.693
758	584.7	480.9	0.8689	454.8	1.693
759	584.7	476.4	0.8702	454.7	1.693
760	584.7	472.4	0.8702	454.7	1.693
761	583.3	472.4	0.8702	454.7	1.693
762	584.7	437.3	0.8702	455.4	0.339
763	584.7	432.8	0.8702	455.4	0.339
764	584.7	432.8	0.8702	456.0	0.339
765	584.7	437.3	0.8702	456.0	0.339
766	584.7	441.7	0.8702	456.0	0.339
767	584.7	446.2	0.8689	456.0	0.339
768	584.7	446.2	0.8712	456.6	0.339
769	583.3	446.2	0.8702	456.6	0.339
770	583.3	450.2	0.8712	456.6	0.339
771	584.7	450.2	0.8702	456.6	0.339
772	584.7	450.2	0.8712	457.3	0.339
773	584.7	450.2	0.8712	457.2	0.339
774	584.7	450.2	0.8712	457.2	0.339
775	584.7	454.6	0.8712	457.2	0.339
776	584.7	454.6	0.8712	457.9	0.339
777	584.7	454.6	0.8712	457.8	0.339

Table A6. Continued.

#	σ_3 [kPa]	F_a [N]	ΔL [cm]	p_w [kPa]	u_a [μm/s]
778	584.7	454.6	0.8712	457.8	0.339
779	583.3	454.6	0.8712	457.8	0.339
780	584.7	454.6	0.8725	458.5	0.339
781	584.7	459.1	0.8725	458.5	0.339
782	583.3	459.1	0.8725	458.4	0.339
783	584.7	459.1	0.8725	458.4	0.339
784	584.7	454.6	0.8725	458.4	0.339
785	583.3	459.1	0.8738	458.4	0.339
786	583.3	459.1	0.8738	459.0	0.339
787	584.7	459.1	0.8738	459.0	0.339
788	584.7	459.1	0.8738	459.0	0.339
789	584.7	459.1	0.8738	459.0	0.339
790	584.7	463.5	0.8738	459.0	0.339
791	583.3	463.5	0.8738	458.9	0.339
792	584.7	459.1	0.8748	458.9	0.339
793	583.3	463.5	0.8748	459.6	0.339
794	584.7	459.1	0.8748	459.6	0.339
795	584.7	463.5	0.8748	459.6	0.339
796	584.7	463.5	0.8748	459.5	0.339
797	584.7	463.5	0.8760	459.5	0.339
798	584.7	463.5	0.8748	459.5	0.339
799	584.7	463.5	0.8760	459.5	0.339
800	584.7	472.4	0.8760	458.8	1.693
801	584.7	476.4	0.8760	458.8	1.693
802	584.7	476.4	0.8760	458.7	1.693
803	584.7	476.4	0.8760	458.0	1.693
804	584.7	485.3	0.8773	458.0	1.693
805	583.3	489.7	0.8783	457.3	1.693
806	583.3	494.2	0.8796	457.3	1.693
807	584.7	494.2	0.8796	456.6	1.693
808	584.7	494.2	0.8796	456.5	1.693
809	584.7	498.6	0.8809	456.5	1.693
810	584.7	498.6	0.8821	455.8	1.693
811	584.7	494.2	0.8821	455.8	1.693
812	584.7	498.6	0.8832	455.8	1.693
813	584.7	494.2	0.8844	455.8	1.693
814	583.3	498.6	0.8857	455.7	1.693
815	584.7	498.6	0.8857	455.0	1.693
816	584.7	498.6	0.8867	455.0	1.693
817	583.3	498.6	0.8893	455.0	1.693
818	583.3	498.6	0.8893	455.0	1.693
819	583.3	498.6	0.8905	454.3	1.693
820	583.3	498.6	0.8905	454.2	1.693
821	584.7	498.6	0.8915	454.2	1.693
822	583.3	498.6	0.8928	454.2	1.693
823	584.7	502.6	0.8928	454.2	1.693
824	584.7	463.5	0.8941	455.5	0.068
825	584.7	459.1	0.8941	456.2	0.068
826	584.7	459.1	0.8951	456.9	0.068
827	584.7	459.1	0.8951	457.6	0.068
828	584.7	454.6	0.8941	458.2	0.068
829	584.7	454.6	0.8951	458.9	0.068
830	583.3	454.6	0.8951	459.6	0.068
831	584.7	454.6	0.8951	460.2	0.068
832	584.7	454.6	0.8951	460.9	0.068
833	584.7	454.6	0.8951	461.6	0.068
834	584.7	450.2	0.8951	462.2	0.068
835	584.7	454.6	0.8951	462.2	0.068
836	583.3	454.6	0.8941	462.9	0.068
837	583.3	454.6	0.8951	462.9	0.068
838	584.7	450.2	0.8941	463.5	0.068
839	584.7	450.2	0.8951	463.5	0.068
840	584.7	450.2	0.8951	463.5	0.068
841	584.7	450.2	0.8951	464.2	0.068
842	584.7	446.2	0.8951	464.2	0.068
843	584.7	450.2	0.8951	464.1	0.068
844	584.7	446.2	0.8964	464.1	0.068
845	583.3	428.4	0.8951	464.8	0.014
846	584.7	423.9	0.8951	465.5	0.014
847	583.3	423.9	0.8951	466.1	0.014
848	584.7	423.9	0.8951	466.8	0.014
849	583.3	437.3	0.8964	467.5	0.014
850	584.7	441.7	0.8951	468.1	0.014
851	584.7	446.2	0.8964	468.1	0.014
852	584.7	476.4	0.8964	466.7	1.693
853	584.7	494.2	0.8964	465.3	1.693
854	584.7	502.6	0.8976	463.9	1.693
855	584.7	507.1	0.8976	463.2	1.693
856	584.7	507.1	0.8987	462.5	1.693
857	584.7	511.5	0.8999	461.8	1.693
858	584.7	511.5	0.9012	461.1	1.693
859	583.3	511.5	0.9012	461.1	1.693
860	583.3	516.0	0.9025	460.4	1.693
861	584.7	516.0	0.9035	460.3	1.693
862	584.7	516.0	0.9047	459.6	1.693
863	584.7	516.0	0.9047	459.6	1.693
864	584.7	520.4	0.9060	458.9	1.693
865	583.3	520.4	0.9060	458.9	1.693
866	584.7	520.4	0.9070	458.9	1.693
867	584.7	516.0	0.9083	458.1	1.693
868	584.7	520.4	0.9096	458.1	1.693
869	583.3	520.4	0.9096	457.4	1.693
870	583.3	520.4	0.9106	457.4	1.693
871	583.3	520.4	0.9119	456.7	1.693
872	584.7	520.4	0.9119	456.7	1.693
873	584.7	520.4	0.9131	456.7	1.693
874	584.7	520.4	0.9144	455.9	1.693
875	584.7	520.4	0.9154	455.9	1.693
876	584.7	520.4	0.9154	455.9	1.693
877	583.3	520.4	0.9167	455.9	1.693
878	584.7	520.4	0.9180	455.2	1.693
879	584.7	520.4	0.9190	455.2	1.693
880	584.7	520.4	0.9190	455.1	1.693
881	583.3	524.4	0.9202	455.1	1.693
882	583.3	524.4	0.9202	454.4	1.693
883	584.7	524.4	0.9215	454.4	1.693
884	584.7	520.4	0.9228	454.4	1.693
885	584.7	524.4	0.9238	454.3	1.693
886	584.7	524.4	0.9251	453.6	1.693
887	584.7	520.4	0.9251	453.6	1.693
888	584.7	524.4	0.9263	453.6	1.693
889	584.7	524.4	0.9274	453.6	1.693
890	583.3	524.4	0.9274	453.6	1.693
891	584.7	524.4	0.9286	452.9	1.693
892	583.3	524.4	0.9299	452.8	1.693
893	584.7	524.4	0.9309	452.8	1.693
894	584.7	524.4	0.9299	452.8	1.693
895	583.3	524.4	0.9322	452.8	1.693
896	584.7	524.4	0.9322	452.8	1.693
897	583.3	537.8	0.9347	452.7	1.693
898	583.3	550.7	0.9335	452.7	8.467
899	584.7	546.7	0.9370	451.3	8.467
900	584.7	550.7	0.9406	450.6	8.467
901	583.3	550.7	0.9441	449.9	8.467
902	584.7	546.7	0.9489	449.9	8.467
903	583.3	550.7	0.9538	449.2	8.467
904	583.3	546.7	0.9573	449.2	8.467
905	584.7	546.7	0.9609	448.4	8.467
906	583.3	546.7	0.9657	448.4	8.467
907	584.7	546.7	0.9693	447.7	8.467
908	584.7	546.7	0.9741	447.7	8.467
909	584.7	546.7	0.9789	447.7	8.467
910	584.7	546.7	0.9825	447.0	8.467
911	583.3	546.7	0.9873	446.9	8.467
912	583.3	546.7	0.9909	446.9	8.467
913	584.7	546.7	0.9944	446.2	8.467
914	583.3	546.7	1.0003	446.2	8.467
915	584.7	546.7	1.0038	446.2	8.467
916	583.3	546.7	1.0086	446.2	8.467
917	584.7	568.5	1.0183	444.8	42.333
918	583.3	568.5	1.0386	444.0	42.333
919	584.7	564.0	1.0602	443.3	42.333
920	584.7	559.6	1.0815	442.6	42.333
921	584.7	559.6	1.1019	441.9	42.333
922	583.3	537.8	1.1486	443.3	8.467
923	584.7	537.8	1.1521	444.0	8.467

Table A6. Continued.

#	σ_3 [kPa]	F_a [N]	ΔL [cm]	p_w [kPa]	u_a [µm/s]
924	583.3	537.8	1.1570	444.6	8.467
925	583.3	542.2	1.1605	445.3	8.467
926	584.7	542.2	1.1654	446.0	8.467
927	584.7	542.2	1.1699	446.6	8.467
928	584.7	542.2	1.1748	447.3	8.467
929	584.7	542.2	1.1783	448.0	8.467
930	583.3	537.8	1.1821	448.0	8.467
931	584.7	507.1	1.1857	443.3	1.693
932	583.3	516.0	1.1867	450.0	1.693
933	583.3	516.0	1.1880	450.7	1.693
934	584.7	516.0	1.1880	450.6	1.693
935	583.3	520.4	1.1892	451.3	1.693
936	584.7	520.4	1.1892	451.3	1.693
937	584.7	524.4	1.1902	452.0	1.693
938	584.7	524.4	1.1915	451.9	1.693
939	581.9	524.4	1.1928	451.9	1.693
940	584.7	524.4	1.1928	452.6	1.693
941	584.7	528.9	1.1941	452.6	1.693
942	584.7	528.9	1.1941	453.2	1.693
943	583.3	528.9	1.1951	453.2	1.693
944	584.7	528.9	1.1963	453.2	1.693
945	584.7	581.4	1.2070	449.7	42.333
946	583.3	576.9	1.2286	448.3	42.333
947	584.7	576.9	1.2502	446.9	42.333
948	584.7	572.9	1.2715	445.5	42.333
949	584.7	572.9	1.2931	444.1	42.333
950	584.7	568.5	1.3147	442.7	42.333
951	584.7	568.5	1.3360	441.3	42.333
952	584.7	568.5	1.3576	440.6	42.333
953	584.7	576.9	1.3780	439.9	42.333
954	584.7	576.9	1.4008	439.2	8.467
955	584.7	537.8	1.4221	440.6	8.467
956	583.3	542.2	1.4270	441.2	8.467
957	584.7	546.7	1.4305	441.9	8.467
958	583.3	546.7	1.4341	442.6	8.467
959	584.7	546.7	1.4389	443.2	8.467
960	584.7	550.7	1.4415	443.9	8.467
961	583.3	550.7	1.4460	443.9	8.467
962	584.7	555.1	1.4496	444.6	8.467
963	584.7	550.7	1.4544	445.2	8.467
964	583.3	550.7	1.4580	445.2	8.467
965	584.7	555.1	1.4628	445.9	8.467
966	583.3	555.1	1.4676	445.9	8.467
967	584.7	524.4	1.4724	447.9	1.693
968	584.7	524.4	1.4724	448.6	1.693
969	584.7	528.9	1.4737	449.3	1.693
970	584.7	524.4	1.4737	449.9	1.693
971	584.7	528.9	1.4747	449.9	1.693
972	584.7	528.9	1.4760	450.6	1.693
973	584.7	533.3	1.4773	450.6	1.693
974	584.7	533.3	1.4783	450.5	1.693
975	584.7	533.3	1.4783	451.2	1.693
976	584.7	537.8	1.4796	451.2	1.693
977	583.3	537.8	1.4808	451.2	1.693
978	584.7	537.8	1.4808	451.8	1.693
979	584.7	537.8	1.4818	451.8	1.693
980	584.7	537.8	1.4831	451.8	1.693
981	584.7	542.2	1.4844	452.5	1.693
982	584.7	542.2	1.4844	452.4	1.693
983	584.7	542.2	1.4856	452.4	1.693
984	584.7	542.2	1.4867	452.4	1.693
985	584.7	542.2	1.4879	453.1	1.693
986	584.7	542.2	1.4879	453.1	1.693
987	584.7	542.2	1.4892	453.0	1.693

Table A7. Data for the drained triaxial compression test D1.

Date:	10/28/97
Sample material:	remolded UpB till, core 92-1
Initial weight:	282.4 gram
Pre-shear length:	7.29 cm
Pre-shear radius:	2.41 cm
Post-shear volumes:	V_w = 45.2 cm^3 (water), V_s = 85.1 cm^3 (solids)
Saturation pressure:	691.6 kPa

#	σ_3 [kPa]	F_a [N]	ΔL [cm]	p_w [kPa]	u_a [µm/s]	ΔV [cm^3]	#	σ_3 [kPa]	F_a [N]	ΔL [cm]	p_w [kPa]	u_a [µm/s]	ΔV [cm^3]
1	711.6	0.0	0.0000	691.6	0.287	0	61	711.6	31.1	0.0328	690.9	0.287	0.12
2	711.6	0.0	0.0000	690.9	0.287		62	711.6	31.1	0.0343	690.9	0.287	
3	713.6	10.2	0.0000	691.6	0.287		63	711.6	31.1	0.0343	690.9	0.287	
4	711.6	15.6	0.0013	691.6	0.287		64	711.6	33.4	0.0356	690.9	0.287	
5	711.6	18.2	0.0013	690.9	0.287		65	711.6	33.4	0.0356	690.9	0.287	
6	711.6	18.2	0.0025	690.9	0.287		66	711.6	31.1	0.0356	690.9	0.287	
7	711.6	20.9	0.0038	691.6	0.287		67	711.6	31.1	0.0368	690.9	0.287	
8	711.6	23.1	0.0038	691.6	0.287		68	711.6	33.4	0.0368	690.9	0.287	
9	713.6	23.1	0.0038	690.9	0.287		69	711.6	33.4	0.0381	691.6	0.287	
10	711.6	23.1	0.0038	691.6	0.287		70	711.6	33.4	0.0381	690.9	0.287	
11	711.6	23.1	0.0053	691.6	0.287		71	711.6	33.4	0.0394	691.6	0.287	
12	711.6	23.1	0.0053	691.6	0.287		72	711.6	33.4	0.0409	691.6	0.287	
13	711.6	23.1	0.0066	690.9	0.287		73	711.6	31.1	0.0409	690.9	0.287	
14	711.6	23.1	0.0066	690.9	0.287		74	711.6	33.4	0.0409	690.9	0.287	
15	711.6	25.8	0.0079	690.9	0.287		75	711.6	31.1	0.0409	691.6	0.287	
16	711.6	25.8	0.0079	690.9	0.287	0.01	76	711.6	36.0	0.0422	690.9	0.287	0.17
17	711.6	25.8	0.0091	690.9	0.287		77	711.6	33.4	0.0422	690.9	0.287	
18	711.6	25.8	0.0091	690.9	0.287		78	711.6	33.4	0.0434	690.9	0.287	
19	711.6	25.8	0.0091	690.9	0.287		79	711.6	31.1	0.0434	690.9	0.287	
20	711.6	25.8	0.0091	690.9	0.287		80	711.6	33.4	0.0434	690.9	0.287	
21	713.6	25.8	0.0104	690.9	0.287		81	711.6	33.4	0.0434	690.9	0.287	
22	711.6	25.8	0.0104	691.6	0.287		82	713.6	36.0	0.0434	691.6	0.287	
23	711.6	25.8	0.0119	690.9	0.287		83	711.6	33.4	0.0460	690.9	0.287	
24	711.6	25.8	0.0132	691.6	0.287		84	711.6	33.4	0.0460	690.9	0.287	
25	711.6	28.5	0.0132	690.9	0.287		85	711.6	36.0	0.0472	690.9	0.287	
26	711.6	25.8	0.0132	690.9	0.287		86	711.6	31.1	0.0472	690.9	0.287	
27	711.6	25.8	0.0145	690.9	0.287		87	711.6	36.0	0.0472	690.9	0.287	
28	711.6	25.8	0.0157	691.6	0.287		88	711.6	36.0	0.0488	690.9	0.287	
29	711.6	25.8	0.0157	691.6	0.287		89	711.6	36.0	0.0488	690.9	0.287	
30	711.6	28.5	0.0157	690.9	0.287		90	711.6	36.0	0.0500	690.9	0.287	
31	711.6	28.5	0.0170	691.6	0.287	0.04	91	711.6	36.0	0.0513	690.9	0.287	0.23
32	711.6	25.8	0.0170	691.6	0.287		92	711.6	33.4	0.0500	690.9	0.287	
33	711.6	28.5	0.0170	691.6	0.287		93	711.6	36.0	0.0513	691.6	0.287	
34	711.6	28.5	0.0170	691.6	0.287		94	711.6	36.0	0.0513	690.9	0.287	
35	711.6	28.5	0.0170	690.9	0.287		95	711.6	36.0	0.0526	691.6	0.287	
36	711.6	28.5	0.0170	690.9	0.287		96	711.6	36.0	0.0538	690.9	0.287	
37	711.6	28.5	0.0198	690.9	0.287		97	711.6	36.0	0.0538	691.6	0.287	
38	711.6	31.1	0.0198	691.6	0.287		98	711.6	36.0	0.0551	690.9	0.287	
39	711.6	28.5	0.0211	690.9	0.287		99	711.6	36.0	0.0551	690.9	0.287	
40	711.6	31.1	0.0211	690.9	0.287		100	710.2	36.0	0.0538	690.9	0.287	
41	711.6	28.5	0.0224	691.6	0.287		101	711.6	36.0	0.0551	691.6	0.287	
42	711.6	31.1	0.0224	691.6	0.287		102	711.6	36.0	0.0566	690.9	0.287	
43	711.6	31.1	0.0224	691.6	0.287		103	711.6	36.0	0.0579	690.9	0.287	
44	711.6	31.1	0.0236	691.6	0.287		104	711.6	36.0	0.0579	690.9	0.287	
45	711.6	28.5	0.0236	690.9	0.287		105	711.6	36.0	0.0592	690.9	0.287	
46	711.6	31.1	0.0249	690.9	0.287	0.08	106	711.6	36.0	0.0592	690.9	0.287	0.28
47	711.6	31.1	0.0264	691.6	0.287		107	711.6	36.0	0.0592	690.9	0.287	
48	711.6	31.1	0.0249	690.9	0.287		108	711.6	36.0	0.0605	690.9	0.287	
49	711.6	31.1	0.0264	690.9	0.287		109	711.6	38.7	0.0592	691.6	0.287	
50	711.6	31.1	0.0264	690.9	0.287		110	711.6	36.0	0.0617	691.6	0.287	
51	711.6	31.1	0.0277	690.9	0.287		111	711.6	36.0	0.0617	690.9	0.287	
52	711.6	31.1	0.0290	690.9	0.287		112	711.6	38.7	0.0617	690.9	0.287	
53	711.6	31.1	0.0277	690.9	0.287		113	711.6	36.0	0.0632	690.9	0.287	
54	711.6	31.1	0.0302	690.9	0.287		114	711.6	38.7	0.0632	690.9	0.287	
55	711.6	31.1	0.0302	690.9	0.287		115	711.6	36.0	0.0632	690.9	0.287	
56	711.6	31.1	0.0302	691.6	0.287		116	711.6	38.7	0.0645	690.9	0.287	
57	711.6	31.1	0.0302	691.6	0.287		117	711.6	36.0	0.0645	690.9	0.287	
58	711.6	31.1	0.0315	690.9	0.287		118	711.6	36.0	0.0645	691.6	0.287	
59	711.6	31.1	0.0315	691.6	0.287		119	711.6	38.7	0.0658	690.9	0.287	
60	710.2	31.1	0.0328	691.6	0.287		120	710.2	38.7	0.0671	690.9	0.287	

Table A7. Continued.

#	σ_3 [kPa]	F_a [N]	ΔL [cm]	p_w [kPa]	u_a [μm/s]	ΔV [cm³]
121	711.6	36.0	0.0671	690.9	0.287	0.36
122	711.6	38.7	0.0671	690.9	0.287	
123	711.6	38.7	0.0671	691.6	0.287	
124	711.6	38.7	0.0696	690.9	0.287	
125	711.6	38.7	0.0696	690.9	0.287	
126	711.6	38.7	0.0696	690.9	0.287	
127	711.6	38.7	0.0696	690.9	0.287	
128	711.6	38.7	0.0711	691.6	0.287	
129	711.6	41.4	0.0724	691.6	0.287	
130	711.6	38.7	0.0724	690.9	0.287	
131	711.6	41.4	0.0724	690.9	0.287	
132	711.6	41.4	0.0737	691.6	0.287	
133	711.6	41.4	0.0737	690.9	0.287	
134	711.6	41.4	0.0749	690.9	0.287	
135	711.6	41.4	0.0737	690.9	0.287	
136	711.6	41.4	0.0762	690.9	0.287	0.42
137	711.6	41.4	0.0762	690.9	0.287	
138	711.6	41.4	0.0777	690.9	0.287	
139	711.6	38.7	0.0777	690.9	0.287	
140	711.6	41.4	0.0777	691.6	0.287	
141	711.6	41.4	0.0790	690.9	0.287	
142	710.2	41.4	0.0790	690.9	0.287	
143	711.6	41.4	0.0803	690.9	0.287	
144	711.6	41.4	0.0803	690.9	0.287	
145	710.2	41.4	0.0803	690.9	0.287	
146	711.6	41.4	0.0815	691.6	0.287	
147	711.6	41.4	0.0815	690.9	0.287	
148	711.6	41.4	0.0828	690.9	0.287	
149	711.6	44.0	0.0828	690.9	0.287	
150	711.6	38.7	0.0828	690.9	0.287	
151	711.6	41.4	0.0828	691.6	0.287	0.51
152	711.6	44.0	0.0856	691.6	0.287	
153	711.6	44.0	0.0856	690.9	0.287	
154	711.6	44.0	0.0856	690.9	0.287	
155	711.6	44.0	0.0869	690.9	0.287	
156	711.6	41.4	0.0869	691.6	0.287	
157	711.6	44.0	0.0869	691.6	0.287	
158	711.6	44.0	0.0881	691.6	0.287	
159	710.2	44.0	0.0894	690.9	0.287	
160	711.6	44.0	0.0894	690.9	0.287	
161	708.1	44.0	0.0894	690.9	0.287	
162	711.6	41.4	0.0907	690.9	0.287	
163	711.6	44.0	0.0907	690.9	0.287	
164	711.6	41.4	0.0922	691.6	0.287	
165	711.6	44.0	0.0922	691.6	0.287	
166	711.6	44.0	0.0922	691.6	0.287	0.57
167	711.6	44.0	0.0935	690.9	0.287	
168	711.6	41.4	0.0935	691.6	0.287	
169	711.6	44.0	0.0935	691.6	0.287	
170	711.6	44.0	0.0947	691.6	0.287	
171	711.6	41.4	0.0960	690.9	0.287	
172	711.6	44.0	0.0960	690.9	0.287	
173	711.6	44.0	0.0973	690.9	0.287	
174	711.6	41.4	0.0973	690.9	0.287	
175	711.6	41.4	0.0973	690.9	0.287	
176	711.6	41.4	0.0986	690.9	0.287	
177	711.6	44.0	0.1001	691.6	0.287	
178	711.6	46.3	0.1001	690.9	0.287	
179	711.6	44.0	0.1001	691.6	0.287	
180	710.2	44.0	0.1013	690.9	0.287	
181	710.2	44.0	0.1013	690.9	0.287	0.64
182	711.6	44.0	0.1013	690.9	0.287	
183	711.6	44.0	0.1026	690.9	0.287	
184	711.6	44.0	0.1026	690.9	0.287	
185	711.6	46.3	0.1039	691.6	0.287	
186	711.6	44.0	0.1039	690.9	0.287	
187	710.2	44.0	0.1052	690.9	0.287	
188	711.6	46.3	0.1052	690.9	0.287	
189	710.2	46.3	0.1067	691.6	0.287	
190	711.6	46.3	0.1067	690.9	0.287	
191	711.6	46.3	0.1080	690.9	0.287	
192	711.6	44.0	0.1080	690.9	0.287	
193	710.2	46.3	0.1080	691.6	0.287	
194	711.6	46.3	0.1092	690.9	0.287	
195	711.6	46.3	0.1092	690.9	0.287	
196	711.6	46.3	0.1092	690.9	0.287	0.72
197	711.6	46.3	0.1105	690.9	0.287	
198	710.2	46.3	0.1105	690.9	0.287	
199	711.6	46.3	0.1118	691.6	0.287	
200	711.6	46.3	0.1118	690.9	0.287	
201	711.6	46.3	0.1130	691.6	0.287	
202	711.6	46.3	0.1130	690.9	0.287	
203	710.2	46.3	0.1146	690.9	0.287	
204	711.6	46.3	0.1146	691.6	0.287	
205	711.6	46.3	0.1146	690.9	0.287	
206	711.6	46.3	0.1146	690.9	0.287	
207	710.2	46.3	0.1158	690.9	0.287	
208	711.6	46.3	0.1171	690.9	0.287	
209	711.6	46.3	0.1171	691.6	0.287	
210	710.2	46.3	0.1184	691.6	0.287	
211	711.6	46.3	0.1184	690.9	0.287	0.76
212	711.6	46.3	0.1196	691.6	0.287	
213	711.6	46.3	0.1196	691.6	0.287	
214	711.6	46.3	0.1196	690.9	0.287	
215	710.2	46.3	0.1209	690.9	0.287	
216	710.2	46.3	0.1209	691.6	0.287	
217	711.6	48.9	0.1224	690.9	0.287	
218	711.6	46.3	0.1224	690.9	0.287	
219	710.2	46.3	0.1224	690.9	0.287	
220	711.6	46.3	0.1237	690.9	0.287	
221	711.6	46.3	0.1224	690.9	0.287	
222	711.6	46.3	0.1250	690.9	0.287	
223	711.6	46.3	0.1250	690.9	0.287	
224	711.6	46.3	0.1262	691.6	0.287	
225	711.6	46.3	0.1262	690.9	0.287	
226	711.6	46.3	0.1262	690.9	0.287	0.83
227	711.6	46.3	0.1275	690.9	0.287	
228	711.6	46.3	0.1275	690.9	0.287	
229	711.6	44.0	0.1290	690.9	0.287	
230	711.6	46.3	0.1290	690.9	0.287	
231	711.6	48.9	0.1290	690.9	0.287	
232	711.6	48.9	0.1303	690.9	0.287	
233	710.2	46.3	0.1303	690.9	0.287	
234	711.6	46.3	0.1303	690.9	0.287	
235	711.6	48.9	0.1316	690.9	0.287	
236	710.2	48.9	0.1328	690.9	0.287	
237	710.2	48.9	0.1328	690.9	0.287	
238	710.2	46.3	0.1328	690.9	0.287	
239	711.6	48.9	0.1354	690.9	0.287	
240	710.2	46.3	0.1354	690.9	0.287	
241	711.6	48.9	0.1354	690.9	0.287	0.90
242	711.6	48.9	0.1354	690.9	0.287	
243	710.2	46.3	0.1369	690.9	0.287	
244	711.6	48.9	0.1369	690.9	0.287	
245	711.6	48.9	0.1382	690.9	0.287	
246	711.6	48.9	0.1382	691.6	0.287	
247	711.6	48.9	0.1394	690.9	0.287	
248	710.2	46.3	0.1394	690.9	0.287	
249	711.6	46.3	0.1407	690.9	0.287	
250	711.6	48.9	0.1407	690.9	0.287	
251	711.6	48.9	0.1407	690.9	0.287	
252	711.6	48.9	0.1420	690.9	0.287	
253	711.6	48.9	0.1435	691.6	0.287	
254	711.6	48.9	0.1435	690.9	0.287	
255	711.6	48.9	0.1435	690.9	0.287	
256	711.6	48.9	0.1435	690.9	0.287	0.95
257	710.2	48.9	0.1448	690.9	0.287	
258	711.6	48.9	0.1461	690.9	0.287	
259	711.6	48.9	0.1461	690.9	0.287	
260	711.6	48.9	0.1473	690.9	0.287	
261	711.6	46.3	0.1461	690.9	0.287	
262	711.6	48.9	0.1473	690.9	0.287	
263	711.6	48.9	0.1486	690.9	0.287	
264	711.6	48.9	0.1486	690.9	0.287	
265	711.6	48.9	0.1486	691.6	0.287	
266	711.6	48.9	0.1499	691.6	0.287	

Table A7. Continued.

#	σ_3 [kPa]	F_a [N]	ΔL [cm]	p_w [kPa]	u_a [μm/s]	ΔV [cm³]
267	711.6	51.6	0.1499	690.9	0.287	
268	711.6	48.9	0.1514	690.9	0.287	
269	710.2	51.6	0.1514	691.6	0.287	
270	711.6	48.9	0.1527	691.6	0.287	
271	711.6	51.6	0.1527	690.9	0.287	1.00
272	710.2	51.6	0.1539	691.6	0.287	
273	711.6	51.6	0.1539	690.9	0.287	
274	710.2	51.6	0.1552	690.9	0.287	
275	711.6	48.9	0.1539	691.6	0.287	
276	711.6	51.6	0.1539	691.6	0.287	
277	711.6	51.6	0.1565	690.9	0.287	
278	711.6	51.6	0.1565	690.9	0.287	
279	711.6	51.6	0.1565	690.9	0.287	
280	711.6	51.6	0.1580	691.6	0.287	
281	711.6	51.6	0.1593	690.9	0.287	
282	711.6	48.9	0.1593	690.9	0.287	
283	711.6	51.6	0.1605	690.9	0.287	
284	711.6	51.6	0.1593	690.9	0.287	
285	711.6	51.6	0.1605	690.9	0.287	
286	710.2	51.6	0.1618	690.9	0.287	1.06
287	711.6	51.6	0.1618	691.6	0.287	
288	711.6	51.6	0.1631	690.9	0.287	
289	711.6	51.6	0.1631	690.9	0.287	
290	711.6	51.6	0.1643	690.9	0.287	
291	711.6	51.6	0.1643	690.9	0.287	
292	711.6	51.6	0.1659	691.6	0.287	
293	710.2	51.6	0.1659	691.6	0.287	
294	711.6	51.6	0.1659	690.9	0.287	
295	710.2	51.6	0.1671	691.6	0.287	
296	711.6	54.3	0.1671	690.9	0.287	
297	711.6	51.6	0.1684	691.6	0.287	
298	711.6	54.3	0.1684	691.6	0.287	
299	711.6	54.3	0.1697	690.9	0.287	
300	711.6	51.6	0.1697	691.6	0.287	
301	711.6	51.6	0.1697	690.9	0.287	1.13
302	711.6	51.6	0.1709	691.6	0.287	
303	711.6	51.6	0.1709	690.9	0.287	
304	711.6	51.6	0.1725	690.2	0.287	
305	711.6	54.3	0.1737	690.9	0.287	
306	711.6	51.6	0.1725	690.9	0.287	
307	711.6	54.3	0.1725	690.9	0.287	
308	711.6	51.6	0.1737	690.9	0.287	
309	711.6	51.6	0.1763	690.9	0.287	
310	710.2	54.3	0.1750	690.9	0.287	
311	710.2	54.3	0.1763	690.9	0.287	
312	710.2	51.6	0.1763	691.6	0.287	
313	711.6	51.6	0.1763	690.9	0.287	
314	710.2	54.3	0.1775	690.9	0.287	
315	711.6	54.3	0.1775	690.9	0.287	
316	710.2	54.3	0.1788	690.9	0.287	1.18
317	711.6	54.3	0.1788	690.9	0.287	
318	711.6	54.3	0.1803	691.6	0.287	
319	711.6	54.3	0.1803	690.9	0.287	
320	711.6	54.3	0.1816	691.6	0.287	
321	711.6	54.3	0.1816	690.9	0.287	
322	711.6	54.3	0.1829	690.9	0.287	
323	711.6	51.6	0.1829	691.6	0.287	
324	711.6	54.3	0.1842	690.9	0.287	
325	711.6	51.6	0.1842	690.9	0.287	
326	711.6	54.3	0.1842	690.9	0.287	
327	710.2	54.3	0.1854	691.6	0.287	
328	711.6	54.3	0.1854	690.9	0.287	
329	710.2	54.3	0.1854	690.9	0.287	
330	711.6	56.9	0.1869	690.9	0.287	
331	710.2	54.3	0.1869	691.6	0.287	1.25
332	711.6	56.9	0.1869	690.9	0.287	
333	711.6	54.3	0.1895	690.9	0.287	
334	710.2	54.3	0.1895	690.9	0.287	
335	711.6	54.3	0.1895	691.6	0.287	
336	711.6	56.9	0.1908	690.9	0.287	
337	711.6	54.3	0.1920	690.9	0.287	
338	711.6	56.9	0.1920	690.9	0.287	
339	711.6	56.9	0.1920	691.6	0.287	
340	710.2	54.3	0.1920	690.9	0.287	
341	711.6	54.3	0.1933	690.9	0.287	
342	711.6	56.9	0.1933	691.6	0.287	
343	711.6	54.3	0.1948	691.6	0.287	
344	711.6	56.9	0.1948	691.6	0.287	
345	711.6	56.9	0.1961	690.9	0.287	
346	711.6	56.9	0.1961	691.6	0.287	1.29
347	711.6	56.9	0.1961	690.9	0.287	
348	710.2	56.9	0.1974	690.9	0.287	
349	711.6	56.9	0.1974	690.9	0.287	
350	711.6	56.9	0.1986	690.9	0.287	
351	711.6	56.9	0.1986	690.9	0.287	
352	710.2	59.2	0.1999	691.6	0.287	
353	711.6	56.9	0.1999	690.9	0.287	
354	710.2	56.9	0.2012	690.9	0.287	
355	711.6	56.9	0.2012	690.9	0.287	
356	710.2	56.9	0.2027	691.6	0.287	
357	711.6	56.9	0.2027	690.9	0.287	
358	710.2	56.9	0.2027	690.9	0.287	
359	710.2	56.9	0.2040	690.9	0.287	
360	710.2	56.9	0.2052	690.9	0.287	
361	711.6	59.2	0.2052	690.9	0.287	1.35
362	710.2	56.9	0.2052	691.6	0.287	
363	711.6	56.9	0.2052	691.6	0.287	
364	711.6	56.9	0.2065	690.9	0.287	
365	711.6	59.2	0.2065	690.9	0.287	
366	711.6	56.9	0.2078	691.6	0.287	
367	711.6	56.9	0.2078	690.9	0.287	
368	711.6	59.2	0.2093	690.9	0.287	
369	711.6	59.2	0.2093	690.9	0.287	
370	710.2	56.9	0.2106	690.9	0.287	
371	711.6	56.9	0.2106	690.9	0.287	
372	710.2	59.2	0.2106	690.9	0.287	
373	711.6	59.2	0.2118	690.9	0.287	
374	711.6	59.2	0.2118	690.9	0.287	
375	711.6	59.2	0.2131	690.9	0.287	
376	710.2	59.2	0.2131	690.9	0.287	1.46
377	711.6	56.9	0.2144	690.9	0.287	
378	711.6	59.2	0.2144	690.9	0.287	
379	711.6	59.2	0.2144	690.9	0.287	
380	710.2	59.2	0.2156	690.9	0.287	
381	711.6	56.9	0.2156	691.6	0.287	
382	711.6	59.2	0.2172	690.9	0.287	
383	711.6	61.8	0.2172	690.9	0.287	
384	711.6	61.8	0.2172	691.6	0.287	
385	710.2	59.2	0.2184	690.9	0.287	
386	711.6	59.2	0.2184	690.9	0.287	
387	711.6	59.2	0.2197	690.9	0.287	
388	711.6	59.2	0.2197	690.9	0.287	
389	710.2	59.2	0.2210	690.9	0.287	
390	711.6	61.8	0.2197	690.9	0.287	
391	711.6	61.8	0.2223	690.9	0.287	1.50
392	710.2	59.2	0.2223	690.9	0.287	
393	711.6	59.2	0.2238	690.9	0.287	
394	710.2	61.8	0.2238	690.9	0.287	
395	710.2	61.8	0.2238	690.9	0.287	
396	711.6	61.8	0.2250	690.9	0.287	
397	710.2	61.8	0.2250	690.9	0.287	
398	710.2	61.8	0.2250	690.2	0.287	
399	711.6	61.8	0.2276	690.9	0.287	
400	711.6	61.8	0.2263	690.9	0.287	
401	711.6	61.8	0.2276	690.9	0.287	
402	711.6	61.8	0.2289	690.9	0.287	
403	710.2	61.8	0.2289	690.9	0.287	
404	710.2	61.8	0.2301	690.9	0.287	
405	710.2	61.8	0.2289	691.6	0.287	
406	711.6	61.8	0.2301	691.6	0.287	1.55
407	711.6	59.2	0.2316	690.9	0.287	
408	711.6	61.8	0.2316	690.9	0.287	
409	711.6	64.5	0.2329	690.9	0.287	
410	710.2	61.8	0.2342	690.9	0.287	

Table A7. Continued.

#	σ_3 [kPa]	F_a [N]	ΔL [cm]	p_w [kPa]	u_a [μm/s]	ΔV [cm^3]
411	711.6	61.8	0.2329	690.9	0.287	
412	711.6	64.5	0.2342	690.9	0.287	
413	711.6	61.8	0.2355	690.9	0.287	
414	710.2	64.5	0.2355	690.9	0.287	
415	710.2	61.8	0.2355	691.6	0.287	
416	711.6	59.2	0.2355	690.9	0.287	
417	711.6	64.5	0.2355	690.9	0.287	
418	711.6	64.5	0.2383	690.9	0.287	
419	710.2	64.5	0.2383	690.9	0.287	
420	710.2	64.5	0.2383	691.6	0.287	
421	710.2	64.5	0.2383	690.9	0.287	1.60
422	711.6	61.8	0.2395	690.9	0.287	
423	711.6	64.5	0.2395	690.9	0.287	
424	711.6	64.5	0.2408	691.6	0.287	
425	710.2	64.5	0.2408	690.9	0.287	
426	711.6	64.5	0.2421	690.9	0.287	
427	711.6	64.5	0.2421	691.6	0.287	
428	710.2	64.5	0.2433	691.6	0.287	
429	711.6	64.5	0.2433	690.9	0.287	
430	711.6	61.8	0.2433	690.9	0.287	
431	710.2	61.8	0.2446	690.9	0.287	
432	711.6	64.5	0.2461	690.9	0.287	
433	710.2	64.5	0.2461	690.9	0.287	
434	710.2	64.5	0.2461	691.6	0.287	
435	710.2	64.5	0.2474	690.9	0.287	
436	710.2	64.5	0.2474	690.9	0.287	1.65
437	711.6	64.5	0.2487	690.9	0.287	
438	711.6	64.5	0.2487	690.9	0.287	
439	711.6	64.5	0.2487	690.9	0.287	
440	711.6	61.8	0.2499	690.9	0.287	
441	711.6	61.8	0.2499	691.6	0.287	
442	710.2	64.5	0.2499	690.9	0.287	
443	711.6	64.5	0.2525	690.9	0.287	
444	710.2	64.5	0.2525	690.9	0.287	
445	711.6	64.5	0.2525	691.6	0.287	
446	711.6	64.5	0.2525	690.9	0.287	
447	711.6	61.8	0.2540	690.9	0.287	
448	711.6	64.5	0.2540	690.9	0.287	
449	711.6	64.5	0.2553	690.9	0.287	
450	711.6	67.2	0.2553	690.9	0.287	
451	711.6	67.2	0.2565	690.9	0.287	1.70
452	711.6	67.2	0.2565	690.9	0.287	
453	710.2	67.2	0.2565	691.6	0.287	
454	710.2	67.2	0.2565	690.9	0.287	
455	710.2	67.2	0.2578	690.9	0.287	
456	710.2	67.2	0.2591	690.9	0.287	
457	710.2	64.5	0.2591	690.9	0.287	
458	711.6	67.2	0.2591	690.9	0.287	
459	710.2	67.2	0.2606	690.9	0.287	
460	711.6	67.2	0.2591	690.9	0.287	
461	710.2	64.5	0.2619	690.9	0.287	
462	710.2	67.2	0.2619	690.9	0.287	
463	711.6	67.2	0.2631	690.9	0.287	
464	711.6	67.2	0.2631	690.9	0.287	
465	710.2	64.5	0.2644	690.9	0.287	
466	710.2	67.2	0.2657	690.9	0.287	1.73
467	711.6	67.2	0.2657	691.6	0.287	
468	711.6	67.2	0.2657	690.9	0.287	
469	710.2	67.2	0.2670	690.9	0.287	
470	711.6	67.2	0.2670	690.9	0.287	
471	710.2	67.2	0.2670	690.9	0.287	
472	711.6	69.4	0.2670	690.9	0.287	
473	711.6	67.2	0.2697	691.6	0.287	
474	710.2	64.5	0.2697	690.9	0.287	
475	711.6	67.2	0.2697	691.6	0.287	
476	711.6	67.2	0.2697	690.9	0.287	
477	710.2	67.2	0.2710	690.9	0.287	
478	710.2	67.2	0.2710	690.9	0.287	
479	710.2	67.2	0.2723	691.6	0.287	
480	711.6	67.2	0.2723	690.9	0.287	
481	710.2	67.2	0.2736	691.6	0.287	1.78
482	711.6	67.2	0.2736	690.9	0.287	
483	710.2	67.2	0.2751	690.9	0.287	
484	711.6	67.2	0.2751	691.6	0.287	
485	710.2	67.2	0.2764	690.9	0.287	
486	710.2	67.2	0.2764	690.9	0.287	
487	710.2	69.4	0.2776	691.6	0.287	
488	710.2	67.2	0.2776	690.9	0.287	
489	710.2	67.2	0.2789	690.9	0.287	
490	711.6	67.2	0.2789	691.6	0.287	
491	710.2	67.2	0.2789	690.9	0.287	
492	710.2	67.2	0.2802	690.9	0.287	
493	710.2	69.4	0.2802	690.9	0.287	
494	710.2	69.4	0.2802	690.9	0.287	
495	710.2	69.4	0.2814	690.9	0.287	
496	710.2	69.4	0.2814	691.6	0.287	1.82
497	711.6	69.4	0.2830	690.9	0.287	
498	710.2	69.4	0.2830	690.9	0.287	
499	711.6	69.4	0.2842	690.9	0.287	
500	710.2	67.2	0.2842	690.9	0.287	
501	710.2	67.2	0.2855	691.6	0.287	
502	710.2	69.4	0.2855	690.9	0.287	
503	710.2	69.4	0.2868	690.9	0.287	
504	710.2	69.4	0.2868	691.6	0.287	
505	710.2	69.4	0.2868	691.6	0.287	
506	710.2	69.4	0.2880	690.9	0.287	
507	710.2	69.4	0.2880	690.9	0.287	
508	710.2	69.4	0.2880	690.9	0.287	
509	710.2	69.4	0.2896	690.9	0.287	
510	708.1	69.4	0.2908	690.2	0.287	
511	710.2	69.4	0.2908	690.9	0.287	1.87
512	711.6	69.4	0.2908	690.9	0.287	
513	710.2	69.4	0.2921	690.9	0.287	
514	711.6	69.4	0.2921	690.9	0.287	
515	710.2	69.4	0.2921	690.9	0.287	
516	711.6	69.4	0.2934	690.9	0.287	
517	711.6	69.4	0.2934	691.6	0.287	
518	711.6	69.4	0.2946	691.6	0.287	
519	710.2	69.4	0.2946	690.9	0.287	
520	711.6	69.4	0.2959	691.6	0.287	
521	710.2	69.4	0.2959	690.9	0.287	
522	711.6	69.4	0.2974	690.9	0.287	
523	711.6	72.1	0.2974	690.9	0.287	
524	711.6	69.4	0.2974	691.6	0.287	
525	711.6	69.4	0.2987	691.6	0.287	
526	711.6	72.1	0.2987	690.9	0.287	1.91
527	710.2	69.4	0.3000	690.9	0.287	
528	710.2	72.1	0.2987	690.9	0.287	
529	711.6	69.4	0.3012	690.9	0.287	
530	710.2	69.4	0.3012	690.9	0.287	
531	710.2	72.1	0.3012	690.9	0.287	
532	711.6	72.1	0.3025	691.6	0.287	
533	710.2	69.4	0.3025	690.9	0.287	
534	711.6	72.1	0.3040	691.6	0.287	
535	710.2	72.1	0.3040	690.9	0.287	
536	711.6	72.1	0.3040	690.9	0.287	
537	710.2	72.1	0.3053	690.9	0.287	
538	711.6	72.1	0.3066	690.9	0.287	
539	710.2	72.1	0.3066	691.6	0.287	
540	710.2	72.1	0.3066	690.9	0.287	

4.A.2. Ring Shear Device, Procedures, and Data

Ring shear tests are less widely used than triaxial tests in the engineering practice and ring shear devices are not readily available. Therefore, a small ring shear device was built specifically for this study to verify the influence of strain magnitude on shear strength of the UpB till (Figure A1). Brief description of the device and the experimental procedures is provided below.

4.A.2.1. Device and Experimental Procedures

Figure A1 shows a schematic diagram of the ring shear device used in this study. Design of the device is similar to that of the Bromhead ring shear device used in soil mechanics investigations in the U.K. [Anayi et al., 1989; Stak and Eid, 1993; Stak and Vettel, 1992]. The apparatus is connected to a data logger (CR-10 Campbell Scientific) that collects, stores, and transfers to a computer data from sensors mounted on the ring shear device. The existing sensors measure torque on the upper (immobile) shaft and vertical settlement of the upper platen due to sample consolidation before the shearing stage of the test (Figure A1). The driving mechanism is equipped in a speed-control box and two gear boxes which can be rearranged to permit shearing at displacement velocities between ~0.1 and ~1000 m day^{-1}. Total rotation of the device during a given test is not directly measured but it is estimated from the elapsed time since the beginning of the experiment and the imposed constant rotation rate. Normal load can range between 6 and 100 kPa and is applied by dead weights placed on the upper platen (Figure A1). The lower platen, which holds an annular till specimen is rotated by an electrical engine.

During test, the till specimen shears on top against an immobile lid. Bishop et al. [1971] pointed out that in such situation there is a danger that the sample will slip along the

contact with the lid surface. This problem is circumvented here by covering this lid surface with a plastic mesh of 2 mm spacing. This modification forces the shear to take place in soil below the lid. Experiments with strain markers show that the thickness of the resulting shear zone is a few millimeters for relatively fine grained materials (e.g., Ottawa sand with ca. 0.25 mm particle diameter) but reaches the whole thickness of the sample chamber for coarse tills with millimeter-size particles (Black Rapids Glacier till). Knowing the thickness of the shear zones and assuming linear strain distribution, one can estimate shear strains and strain rates from the known horizontal shear displacements and displacement rates. The ring shear device has been successfully used to shear Ottawa sand and the clay-rich UpB till under the full design range of effective normal stresses and to a maximum relative displacement of 1,350 m, which corresponds to ca. 400,000 strains.

To prepare the ring shear device for a shear run, a till specimen is packed into the sample chamber of the ring shear device (Figure A1) and covered with c. 3 mm of water. A small amount of the till is pressed into the supporting mesh covering the sample lid. The prepared loading platen is then put on the top of the specimen. The till matrix is left to consolidate under a desired total load. Specimen thinning during the consolidation stage is monitored with three vertical displacement transducers. Sample drainage during the consolidation stage and the subsequent shearing stage is possible at the top of the sample via an annular ring of 3-mm thick porous plastic material which is located between the plastic mesh and the metal body of the upper platen (Figure A1). After consolidation, the sample is sheared by engaging an electrical engine which drives the lower platen of the ring shear device. The shear continues until the desired relative shear displacement is achieved.

Ring shear tests on the UpB till and the Ottawa sand show that sample extrusion may occur at low effective normal loads for the former, finer, material. However, even in the worst case (the UpB till sheared under 6 kPa of effective load), extrusion of ~15% of the sample took rapidly place on the beginning of the test only to cease later. Therefore,

sample extrusion does not prevent achieving large magnitude strains in the ring shear tests. Sinking of the sample lid into the specimen may produce a side friction on the lid and change somewhat the stress distribution. However, this effect should be small because the area of side friction on the lid is small (~6 cm^2 for 1 mm sinkage) compared to the area of the main shear zone beneath the lid surface (158 cm^2).

4.A.2.2. Data

The two tables enclosed below show the results of two ring shear experiments. In both of the experiments samples of the UpB till were prepared from material used previously in torvane tests in which sections from cores 92-1 and 95-1 were utilized. Water content of the mixed till sample was increased to the point of liquefying the material and the resulting slurry was sieved through a 2-mm sieve to remove the coarse particles. Subsequently, the till material was allowed to lose its liquid-like character by air drying.

The first experiment, Table A8, was designed to achieve high total displacement of ca. 200 m. This was done by imposing a relatively high rotation rate of 1.5 rpm, i.e., 1179 m day^{-1}. In the second experiment, Table A9, a sample of the till was sheared at three different displacement rates which were increased twice by a factor of ten.

Both tables list the estimated horizontal displacement, D, and the measured shear stress, τ. Table A9 shows also the horizontal displacement rate, u_τ. In the latter table, measurements made when the ring shear device was stopped for several minutes to change the displacement rate are not given.

Figure A1. (A) A cross-section through the ring shear device and (B) an enlarged cross-section (2.5×) through the sample chamber. The dotted parts rotate during shear.

A

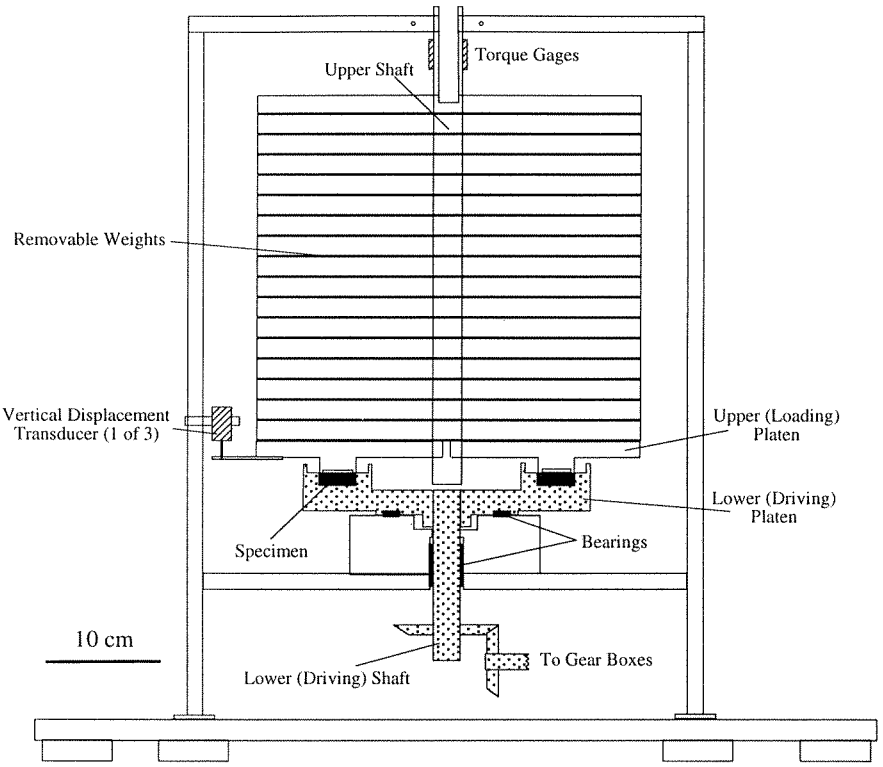

Sensors:

Torque Gages - 4 x Omega SG-6/120-LY41 in Wheatstone bridge, calibrated sensitivity: 0.0458 mV/N-m

Vertical Displacement Transducers - 3 x Omega LD400-5, pre-calibrated sensitivity: 672 mV/mm

B

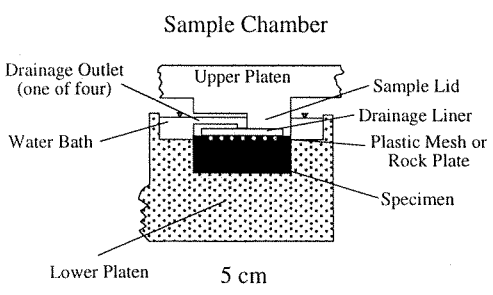

Table A8. Large displacement ring shear test shown in Figure 3B.

#	*D* [m]	τ [kPa]	#	*D* [m]	τ [kPa]	#	*D* [m]	τ [kPa]	#	*D* [m]	τ [kPa]
1	0.0	0.0	63	50.8	11.0	125	101.6	10.9	187	152.3	10.9
2	0.8	11.5	64	51.6	11.0	126	102.4	10.9	188	153.2	10.8
3	1.6	11.4	65	52.4	11.0	127	103.2	10.9	189	154.0	10.8
4	2.5	11.4	66	53.2	11.0	128	104.0	10.9	190	154.8	10.8
5	3.3	11.4	67	54.1	11.0	129	104.8	10.9	191	155.6	10.8
6	4.1	11.4	68	54.9	11.0	130	105.7	10.9	192	156.4	10.8
7	4.9	11.4	69	55.7	11.0	131	106.5	10.9	193	157.2	10.8
8	5.7	11.4	70	56.5	11.0	132	107.3	10.9	194	158.1	10.8
9	6.6	11.3	71	57.3	11.0	133	108.1	10.9	195	158.9	10.8
10	7.4	11.3	72	58.1	11.0	134	108.9	10.9	196	159.7	10.8
11	8.2	11.3	73	59.0	11.0	135	109.7	10.9	197	160.5	10.8
12	9.0	11.3	74	59.8	11.0	136	110.6	10.9	198	161.3	10.8
13	9.8	11.3	75	60.6	11.0	137	111.4	10.8	199	162.2	10.8
14	10.6	11.3	76	61.4	11.0	138	112.2	10.9	200	163.0	10.8
15	11.5	11.3	77	62.2	11.0	139	113.0	10.9	201	163.8	10.8
16	12.3	11.3	78	63.1	11.0	140	113.8	10.9	202	164.6	10.8
17	13.1	11.3	79	63.9	11.0	141	114.7	10.8	203	165.4	10.9
18	13.9	11.3	80	64.7	11.0	142	115.5	10.9	204	166.3	10.8
19	14.7	11.3	81	65.5	10.9	143	116.3	10.8	205	167.1	10.8
20	15.6	11.2	82	66.3	11.0	144	117.1	10.8	206	167.9	10.8
21	16.4	11.3	83	67.2	10.9	145	117.9	10.8	207	168.7	10.8
22	17.2	11.2	84	68.0	11.0	146	118.8	10.9	208	169.5	10.8
23	18.0	11.2	85	68.8	10.9	147	119.6	10.8	209	170.4	10.8
24	18.8	11.2	86	69.6	11.0	148	120.4	10.8	210	171.2	10.8
25	19.7	11.2	87	70.4	10.9	149	121.2	10.8	211	172.0	10.9
26	20.5	11.2	88	71.3	10.9	150	122.0	10.8	212	172.8	10.8
27	21.3	11.2	89	72.1	11.0	151	122.9	10.8	213	173.6	10.8
28	22.1	11.2	90	72.9	10.9	152	123.7	10.9	214	174.4	10.8
29	22.9	11.2	91	73.7	10.9	153	124.5	10.9	215	175.3	10.8
30	23.8	11.2	92	74.5	10.9	154	125.3	10.8	216	176.1	10.8
31	24.6	11.2	93	75.3	10.9	155	126.1	10.8	217	176.9	10.8
32	25.4	11.1	94	76.2	10.9	156	126.9	10.9	218	177.7	10.8
33	26.2	11.1	95	77.0	10.9	157	127.8	10.9	219	178.5	10.8
34	27.0	11.1	96	77.8	10.9	158	128.6	10.8	220	179.4	10.8
35	27.8	11.1	97	78.6	10.9	159	129.4	10.8	221	180.2	10.8
36	28.7	11.1	98	79.4	10.9	160	130.2	10.8	222	181.0	10.8
37	29.5	11.1	99	80.3	10.9	161	131.0	10.8	223	181.8	10.8
38	30.3	11.1	100	81.1	10.9	162	131.9	10.8	224	182.6	10.8
39	31.1	11.1	101	81.9	10.9	163	132.7	10.9	225	183.5	10.8
40	31.9	11.1	102	82.7	10.9	164	133.5	10.8	226	184.3	10.8
41	32.8	11.1	103	83.5	10.9	165	134.3	10.9	227	185.1	10.8
42	33.6	11.1	104	84.4	10.9	166	135.1	10.8	228	185.9	10.8
43	34.4	11.1	105	85.2	10.9	167	136.0	10.9	229	186.7	10.8
44	35.2	11.0	106	86.0	10.9	168	136.8	10.8	230	187.6	10.8
45	36.0	11.0	107	86.8	10.9	169	137.6	10.8	231	188.4	10.8
46	36.9	11.0	108	87.6	10.9	170	138.4	10.8	232	189.2	10.8
47	37.7	11.0	109	88.5	10.9	171	139.2	10.8	233	190.0	10.8
48	38.5	11.0	110	89.3	10.9	172	140.0	10.8	234	190.8	10.8
49	39.3	11.0	111	90.1	10.9	173	140.9	10.8	235	191.6	10.8
50	40.1	11.0	112	90.9	10.9	174	141.7	10.8	236	192.5	10.8
51	41.0	11.0	113	91.7	10.9	175	142.5	10.9	237	193.3	10.9
52	41.8	11.0	114	92.5	10.9	176	143.3	10.8	238	194.1	10.9
53	42.6	11.0	115	93.4	10.9	177	144.1	10.9	239	194.9	10.8
54	43.4	11.0	116	94.2	10.9	178	145.0	10.8	240	195.7	10.8
55	44.2	11.0	117	95.0	10.9	179	145.8	10.8	241	196.6	10.8
56	45.0	11.0	118	95.8	10.9	180	146.6	10.8	242	197.4	10.8
57	45.9	11.0	119	96.6	10.9	181	147.4	10.9	243	198.2	10.8
58	46.7	11.0	120	97.5	10.9	182	148.2	10.8	244	199.0	10.8
59	47.5	11.0	121	98.3	10.9	183	149.1	10.8	245	199.8	10.8
60	48.3	11.0	122	99.1	10.9	184	149.9	10.8	246	200.7	10.8
61	49.1	11.0	123	99.9	10.9	185	150.7	10.9			
62	50.0	11.0	124	100.7	10.9	186	151.5	10.8			

Table A9. Variable displacement ring shear test shown in Figure 3C.

#	D [cm]	τ [kPa]	u_τ [m/d]	#	D [cm]	τ [kPa]	u_τ [m/d]	#	D [cm]	τ [kPa]	u_τ [m/d]
1	0.000	0.0	0.1	77	0.264	10.9	0.1	153	2.118	11.6	1.0
2	0.003	1.7	0.1	78	0.267	10.9	0.1	154	2.153	11.6	1.0
3	0.007	3.7	0.1	79	0.271	10.7	0.1	155	2.188	11.6	1.0
4	0.010	4.4	0.1	80	0.274	10.7	0.1	156	2.222	11.6	1.0
5	0.014	4.8	0.1	81	0.278	10.7	0.1	157	2.257	11.6	1.0
6	0.017	5.0	0.1	82	0.281	10.7	0.1	158	2.292	11.6	1.0
7	0.021	5.0	0.1	83	0.285	10.7	0.1	159	2.326	11.6	1.0
8	0.024	5.2	0.1	84	0.288	10.7	0.1	160	2.361	11.8	1.0
9	0.028	5.5	0.1	85	0.292	10.7	0.1	161	2.396	11.6	1.0
10	0.031	5.5	0.1	86	0.295	10.5	0.1	162	2.431	11.6	1.0
11	0.035	5.7	0.1	87	0.299	10.5	0.1	163	2.465	11.6	1.0
12	0.038	5.7	0.1	88	0.302	10.5	0.1	164	2.500	11.6	1.0
13	0.042	5.9	0.1	89	0.306	10.5	0.1	165	2.535	11.8	1.0
14	0.045	5.9	0.1	90	0.309	10.5	0.1	166	2.569	11.8	1.0
15	0.049	6.1	0.1	91	0.312	10.3	0.1	167	2.604	11.6	1.0
16	0.052	6.3	0.1	92	0.316	10.3	0.1	168	2.639	11.6	1.0
17	0.056	6.6	0.1	93	0.319	10.3	0.1	169	2.674	11.8	1.0
18	0.059	6.8	0.1	94	0.323	10.3	0.1	170	2.708	11.8	1.0
19	0.063	7.0	0.1	95	0.326	10.0	0.1	171	2.743	11.8	1.0
20	0.066	7.2	0.1	96	0.330	10.0	0.1	172	2.778	11.8	1.0
21	0.069	7.2	0.1	97	0.333	10.0	0.1	173	2.813	11.8	1.0
22	0.073	7.4	0.1	98	0.337	9.8	0.1	174	2.847	11.8	1.0
23	0.076	7.4	0.1	99	0.340	9.8	0.1	175	2.882	11.8	1.0
24	0.080	7.6	0.1	100	0.344	9.8	0.1	176	2.917	11.8	1.0
25	0.083	7.6	0.1	101	0.347	9.8	0.1	177	2.951	11.8	1.0
26	0.087	7.9	0.1	102	0.347	4.4	1.0	178	2.986	11.8	1.0
27	0.090	8.1	0.1	103	0.382	7.4	1.0	179	3.021	11.8	1.0
28	0.094	8.1	0.1	104	0.417	9.0	1.0	180	3.056	11.8	1.0
29	0.097	8.3	0.1	105	0.451	9.8	1.0	181	3.090	11.6	1.0
30	0.101	8.5	0.1	106	0.486	10.3	1.0	182	3.125	11.6	1.0
31	0.104	8.7	0.1	107	0.521	10.5	1.0	183	3.160	11.8	1.0
32	0.108	8.7	0.1	108	0.556	10.7	1.0	184	3.194	11.8	1.0
33	0.111	9.0	0.1	109	0.590	10.7	1.0	185	3.229	11.8	1.0
34	0.115	9.2	0.1	110	0.625	10.9	1.0	186	3.264	11.6	1.0
35	0.118	9.4	0.1	111	0.660	10.9	1.0	187	3.299	11.8	1.0
36	0.122	9.6	0.1	112	0.694	10.9	1.0	188	3.333	11.8	1.0
37	0.125	9.8	0.1	113	0.729	10.9	1.0	189	3.368	11.6	1.0
38	0.128	10.0	0.1	114	0.764	10.9	1.0	190	3.368	7.9	10.0
39	0.132	10.0	0.1	115	0.799	10.9	1.0	191	3.715	9.8	10.0
40	0.135	10.3	0.1	116	0.833	10.9	1.0	192	4.063	10.7	10.0
41	0.139	10.3	0.1	117	0.868	11.1	1.0	193	4.410	11.4	10.0
42	0.142	10.3	0.1	118	0.903	11.1	1.0	194	4.757	11.6	10.0
43	0.146	10.3	0.1	119	0.937	11.1	1.0	195	5.104	11.6	10.0
44	0.149	10.5	0.1	120	0.972	11.1	1.0	196	5.451	11.8	10.0
45	0.153	10.5	0.1	121	1.007	11.1	1.0	197	5.799	11.8	10.0
46	0.156	10.5	0.1	122	1.042	11.1	1.0	198	6.146	11.8	10.0
47	0.160	10.5	0.1	123	1.076	11.1	1.0	199	6.493	11.8	10.0
48	0.163	10.5	0.1	124	1.111	11.1	1.0	200	6.840	12.0	10.0
49	0.167	10.7	0.1	125	1.146	11.1	1.0	201	7.188	12.0	10.0
50	0.170	10.7	0.1	126	1.181	11.1	1.0	202	7.535	12.0	10.0
51	0.174	10.7	0.1	127	1.215	11.4	1.0	203	7.882	12.0	10.0
52	0.177	10.7	0.1	128	1.250	11.4	1.0	204	8.229	12.0	10.0
53	0.181	10.7	0.1	129	1.285	11.1	1.0	205	8.576	12.2	10.0
54	0.184	10.9	0.1	130	1.319	11.4	1.0	206	8.924	12.2	10.0
55	0.188	10.9	0.1	131	1.354	11.4	1.0	207	9.271	12.2	10.0
56	0.191	10.7	0.1	132	1.389	11.4	1.0	208	9.618	12.2	10.0
57	0.194	10.7	0.1	133	1.424	11.4	1.0	209	9.965	12.2	10.0
58	0.198	10.9	0.1	134	1.458	11.4	1.0	210	10.313	12.2	10.0
59	0.201	10.9	0.1	135	1.493	11.4	1.0	211	10.660	12.4	10.0
60	0.205	10.7	0.1	136	1.528	11.4	1.0	212	11.007	12.4	10.0
61	0.208	10.7	0.1	137	1.563	11.4	1.0	213	11.354	12.4	10.0
62	0.212	10.7	0.1	138	1.597	11.4	1.0	214	11.701	12.4	10.0
63	0.215	10.7	0.1	139	1.632	11.4	1.0	215	12.049	12.7	10.0
64	0.219	10.7	0.1	140	1.667	11.4	1.0	216	12.396	12.7	10.0
65	0.222	10.7	0.1	141	1.701	11.6	1.0	217	12.743	12.7	10.0
66	0.226	10.7	0.1	142	1.736	11.4	1.0	218	13.090	12.7	10.0
67	0.229	10.7	0.1	143	1.771	11.6	1.0	219	13.438	12.7	10.0
68	0.233	10.7	0.1	144	1.806	11.6	1.0	220	13.785	12.7	10.0
69	0.236	10.9	0.1	145	1.840	11.6	1.0	221	14.132	12.7	10.0
70	0.240	10.9	0.1	146	1.875	11.6	1.0	222	14.479	12.7	10.0
71	0.243	10.9	0.1	147	1.910	11.6	1.0	223	14.826	12.7	10.0
72	0.247	10.9	0.1	148	1.944	11.6	1.0	224	15.174	12.7	10.0
73	0.250	10.9	0.1	149	1.979	11.6	1.0	225	15.521	12.7	10.0
74	0.253	10.7	0.1	150	2.014	11.6	1.0	226	15.868	12.7	10.0
75	0.257	10.9	0.1	151	2.049	11.6	1.0	227	16.215	12.7	10.0
76	0.260	10.9	0.1	152	2.083	11.6	1.0	228	16.562	12.7	10.0

CHAPTER 5

Basal Mechanics of Ice Stream B, West Antarctica. II. Bed Hydrology

Slawek Tulaczyk, Barclay Kamb, Hermann Engelhardt

Division of Geological and Planetary Sciences, California Institute of Technology,
Pasadena, CA 91125

Abstract

High water contents measured in the till recovered from beneath Ice Stream B, near camp UpB, indicate that the effective stresses in the sub-ice-stream environment are very low, *ca.* 0.1-30 kPa. These new effective stress estimates are consistent with the small till strength measured in shear box tests, *ca.* 2 kPa [Kamb, 1991]. Theoretical analysis of the efficiency and stability of sub-ice-stream water flow in: 1) the subglacial groundwater system, 2) a basal water film, and 3) a system of basal canals, shows that long-distance transport of meltwater from beneath Ice Stream B towards its grounding line may be negligible. A new model of sub-ice-stream hydrology is proposed to explain the very high till water content, and very low till strength and subglacial effective stress. In this 'undrained-bed' model, the magnitudes of these quantities are determined by a negative feedback mechanism between the basal melting rate and the till strength. Due to this negative feedback, basal conditions migrate towards the condition of basal melting rate equal to zero. This condition in turn, is fulfilled when the till is weak, water-rich, and subjected to low subglacial effective stress.

5.1. Introduction

Fast ice motion through basal sliding or bed deformation is possible when basal resistive stresses are decreased by build-up of subglacial water pressures to near flotation level [Alley *et al.*, 1986; Bentley, 1987; Bindschadler, 1983; Boulton and Hindmarsh, 1987; Engelhardt *et al.*, 1978; Hooke, 1989; Iken and Bindschadler, 1986; Kamb, 1970, 1987; Kamb *et al.*, 1985; Lliboutry, 1987]. Geophysical and borehole studies have shown that this is also the case for the fast-moving West Antarctic ice streams beneath which water pressure is almost equal to the overburden ice pressure [Blankenship *et al.*, 1986, 1987; Engelhardt *et al.*, 1990; Engelhardt and Kamb, 1997].

The association of fast ice motion with low subglacial effective stresses shows that there are some fundamental links between the mechanical and hydrological processes which govern basal motion. Since generation of reliable and self-consistent models of ice stream behavior represents one of the most important tasks facing modern glaciology, there is a clear need for improved understanding of these mechanical and hydrological sub-ice-stream processes. A number of previous theoretical works addressed these issues [e.g., Alley 1989ab; Alley *et al.*, 1989; Boulton and Caban, 1995; Boulton *et al.*, 1995; Fowler and Johnson, 1995; Kamb, 1991; Lingle and Brown, 1987; Schoemaker, 1986; Walder and Fowler, 1994] but their decisive resolution is still hampered by the scarcity of direct observational constraints and the complexity of subglacial processes.

Recent borehole experiments and laboratory tests on samples of the subglacial till recovered from beneath the UpB area of Ice Stream B provide new constraints on *in situ* subglacial water pressure and on mechanical and hydrological properties of the sub-ice-stream sediments [Engelhardt *et al.*, 1990; Kamb, 1991; Engelhardt and Kamb, 1997; Tulaczyk *et al.*, in preparation I]. We present new estimates of subglacial effective stresses

based on till water content data and results of laboratory consolidation tests. These new estimates are consistent with the low strength of the sub-ice-stream till measured previously in shear-box tests [Kamb, 1991]. The origin of the small effective stresses and low bed strength beneath Ice Stream B is subsequently explained by a new model of sub-ice-stream hydrology.

5.2. Laboratory Methods

The laboratory methods employed in this study include mainly measurements of till water content and oedometer tests of till compressibility. Water content is measured using the standard soil mechanics method in which sample weight loss is determined after drying in an oven [Bowles, 1992, p. 15-18]. Initial weight of till samples used in this procedure varied between *ca.* 30 and 90 grams. Water content, w, is obtained from [Bowles, 1992, eq. 1-1]:

$$w = M_w M_s^{-1} \qquad (1)$$

where M_w is the mass of water evaporated from the sample and M_s is the mass of sample solids. We express w, as well as the other two measures of soil water content, i.e., void ratio and porosity, as decimal fractions rather than a percentage, e.g., 0.250 instead of 25.0%. Measurements of water content on three subsamples from three prepared homogeneous batches of till yielded standard deviations of w between 0.0004 and 0.0009. Most till samples used for water content determination were also used subsequently in analyses of grain-size distribution [Tulaczyk *et al.*, 1998]. These analyses revealed that the till samples had highly variable content of clasts, i.e., particles with diameter greater than 4 mm, which made up between 0 and 15% of till solids. Variability of clast content results from combination of relatively small sample volume and overall scarcity of clasts which

make up on average only *ca.* 3% of the UpB till [Tulaczyk *et al.*, 1998]. To eliminate this variability from our water content calculations we use the measured mass of till matrix solids, i.e., particles smaller than 4 mm, as M_s in equation (1). Such adjustment could not have been made only for the four samples from the core 89-4.

Once till water content is established, till void ratio and porosity can be calculated from:

$$n \equiv V_w \, (V_w + V_s)^{-1} = (1 + w \, \rho_s \, \rho_w^{-1})^{-1} \qquad (2a)$$

$$e \equiv V_w \, V_s^{-1} = w \, \rho_s \, \rho_w^{-1} \qquad (2b)$$

where $\rho_s \cong 2{,}640$ kg m^{-3} is the density of till solids and $\rho_w \cong 1{,}000$ kg m^{-3} is the water density. Density of the UpB till solids was measured by Engelhardt using the standard method described by Bowles [1992, p. 71-78]. Because of low pressure- and temperature-dependence of density of common minerals and water, e.g., compressibility of *ca.* 2×10^{-8} kPa^{-1} and 5×10^{-7} kPa^{-1}, respectively [Mitchell, 1993, p. 170], the density of these materials in the laboratory is not significantly different from their *in situ* density [Weast, 1987, p. F4-F5], at pressure of *ca.* 9.2 MPa and temperature of -1°C.

An oedometer was used to study the compressibility of the UpB till. In this apparatus [Bowles, 1992, p. 129-154], a cylindrical sample of till is subjected to a succession of different vertical effective stress levels. In response to the stress changes, water is expelled and the sample experiences thinning and thickening without strain in the horizontal direction. The thickness changes have typically a magnitude of several millimeters and were monitored with a dial indicator with a precision of 0.025 mm. Elastic response of the apparatus is subtracted from dial readings. After an oedometer test is terminated, the water content of the whole till sample is determined. Given the final water content, the known thickness changes, and assuming full sample saturation, till water content at all stages of the test can be calculated. If a few volume percent of air is present

in a sample, as may be the case with the samples of the UpB till (section 5.3), all but the final till water contents will be overestimated by a few percent.

5.3. Sediment Disturbance During Sampling and Storage

Interpretation of present-day subglacial physical conditions from till water content and till preconsolidation data is not a routine procedure in glaciology. Therefore, it is especially important to consider the influence of till sampling and storage on these two till properties.

Till cores were acquired from beneath Ice Stream B using access through boreholes drilled with a hot-water drill [Engelhardt and Kamb, 1997]. Once the ice sole is penetrated, the hot-water jet which emanates from the drill tip under high pressure will cause disturbance in the sediments underlying the ice sole. Because of its hydrodynamic character, this type of disturbance, if present, is clearly evident in the recovered sediment samples. The evidence for the water-jet disturbance consists of selective winnowing of fine particles and clear grading of coarser particles with depth in the affected sediment core. Such sorted or graded sediments have been found in boreholes located in: 1) slow-moving ice south of the UpB area of Ice Stream B (so-called 'Unicorn'), and 2) the slow-moving section of Ice Stream C (Tulaczyk, unpublished data). Within the UpB area, only one sediment core, 95-3 - drilled at the 'sticky spot' of Rooney *et al.* [1987], has been disturbed by the hot-water jet. This core is excluded from further consideration here because its water content no longer reflects the *in situ* water content of the UpB till.

The lack of winnowed material in most of the till cores acquired in the UpB area is attributed to the fact that the ice slides over the till there at 3-4 cm hr^{-1} [Engelhardt and Kamb, in press]: during the few hours between completion of a borehole and piston

coring, the bottom of each borehole moves away, by basal sliding, from the disturbed area and onto the adjacent bed, from which the core sample is then obtained [Tulaczyk *et al.*, 1998, p. 488].

The UpB till cores have apparently experienced pervasive disturbance of their microfabric caused by degassing of pore water during depressurization occurring when sediments are withdrawn from their subglacial environment to the surface, i.e., a pressure drop from *ca.* 9.2 MPa to *ca.* 0.1 MPa. This disturbance of till microfabric has been made evident by measurements on till thin sections which show that the long axes of elongated sand grains are aligned preferentially parallel to the core axis. Since the *in situ* microfabric of till is expected to be horizontal or sub-horizontal [Johnson, 1983], the measured vertical orientation of sand grains is very likely an artifact of the sampling process. We attribute this microfabric disturbance to degassing of pore water because the UpB till cores contain also abundant millimeter-size, gas-filled voids which are also aligned along the core axis. It is again unlikely that such voids occur in the till *in situ* because gas solubility is very high at the high subglacial pressure of 9.2 MPa. For example *ca.* 2 cm^3 of air can dissolve in one gram of water at 9.2 MPa and 0°C [Weast, 1987, p. B332]. As cores get depressurized during withdrawal to the surface, gas solubility drops and gas-filled voids may form. Addition of volume due to void formation leads to pervasive axial expansion of the core, which causes rotation of elongated sand grains into their observed, axis-parallel orientation. Three laboratory measurements with a gas-content indicator (Soiltest ELE Inc., Concrete air indicator kit, model CT 157) on samples from the core 95-7 yielded an average of 2.4 volume % of gas.

The original arrangement of particles is not preserved in the UpB cores due to the degassing-induced disturbance. As we will demonstrate later, this may lower the preconsolidation pressure estimated from till compressibility using data from oedometer

tests. However, formation of gas-filled voids has no influence on till water content, which we will also use to estimate the subglacial effective stress.

Water content could theoretically be changed during withdrawal of the UpB till cores by: (1) dissipation of the water pressure difference between the inside of the sediment core and the water in the borehole, and (2) drainage due to self-weight of water once the core is pulled above the water level in a given borehole, *ca.* 100 m below ice surface [Engelhardt and Kamb, 1997]. However, for the UpB till these two processes should be negligible because this material has very low hydraulic diffusivity and conductivity (c_v of *ca.* 10^{-8} m^2 s^{-1} and k_h of *ca.* 10^{-10} m s^{-1}). The timescale over which the processes (1) and (2) act during core recovery is $t_c = 10^3$ to 10^4 seconds. This means that for the diffusive process (1) the length of a core affected by pore-water dissipation is equal to only several millimeters (given by $\sqrt{(t_c / c_v)}$). In the case of drainage driven by self-weight of water, i.e., hydraulic gradient of one, the displacement distance of pore water will be also negligible, i.e., of the order of a micron (given by $k_h t_c$).

Analysis of the different possible modes of till disturbance during sampling suggests that *in situ* till water content is being preserved in the sampled cores up to the point of their recovery at the ice surface. The biggest uncertainty associated with our subsequent laboratory measurements of till water content is related to water loss that takes place in storage. To impede water loss, the till cores were stored in: 1) zip-lock bags (89-4 and 89-6), 2) capped sections of the metal core tube (89-7 and 89-8), 3) capped sections of plastic core liner (all cores obtained after 1990). To test how fast the water loss of till proceeds in storage, we have made repeated measurements of till water content on nine sections of the UpB till cores. Five of these repeated measurements were done on the core 89-4 five years after original water content measurements and the four remaining measurements were performed on the core 92-1 one and a half years after the

corresponding original water content measurement. In both cases the drying rate ranged between one and two percent of water content loss per year.

The best solution to the problem of till drying is to make water content measurements as quickly as possible after core acquisition. It takes one to three months before the till cores come to our laboratory from the field site in Antarctica. All water content measurements on till cores recovered during the season 1995-96 were made with this minimum time delay. In the case of the cores 89-4 and 92-1, water content was measured within up to six months from core acquisition. However, systematic measurement of water content in cores 89-6, 89-7, and 89-8 was done four years after these cores were brought out from beneath Ice Stream B. During these four years core 89-6 was stored in plastic zip-lock bags and some of the stored sections have shown clear signs of drying, e.g., cracking, at the time of sampling for water content measurements. The water content measured in these samples was consistently lower than in all the other cores, 0.179 to 0.205, vs. average of 0.25. The results for the core 89-6 are discarded as unreliable as are two other low water content measurements from parts of cores 92-1 and 95-1 which had not been sealed well and showed macroscopic evidence of drying (Table 1). We do use the results of water content measurements made on the two cores which were stored for four years in capped sections of the original metal core tubes. When unsealed the air in these sections had a distinct stale stench suggesting that the core was well isolated from its environment. In addition, the measured water contents are comparable to the most reliable values obtained in the 1995-96 till cores.

Water loss in fine-grained materials such as the UpB till changes not only the water content of the sediment but may also increase its apparent preconsolidation pressure. This occurs because desiccation increases the all-around capillary pressure at the air-water interface on the outside surface of a sediment sample [Terzaghi *et al.*, 1996, p. 94-96]. As

a result, a drying fine-grained sediment is subjected to an isotropic compression which contracts the sediment structure as the pore water is lost. If this pressure exceeds the past maximum pressure that a given till sample was subjected to, the preconsolidation stress recorded in the sample will be reset to this higher value.

In summary, due to the influence of water loss by evaporation, the water content measured on the UpB till samples in laboratory represents a lower bound on the *in situ* till water content. Disturbance of the preconsolidation pressure recorded in the till cores is, however, more complex because of the competing effects of degassing-induced microstructure disturbance which tends to lower the preconsolidation pressure and drying-induced increase in preconsolidation pressure.

5.4. Till Water Content and Subglacial Effective Stresses

The current study in which we use the properties of the UpB till cores to estimate subglacial effective stress was prompted by our observation that the previous best estimates of the *in situ* effective stress, *ca.* 50-60 kPa, may be too high to explain the low strength of the till and its high water content. Previous best estimate of subglacial effective stress equal to 50 kPa was based on low shear wave velocities inferred for the till layer beneath the UpB area of Ice Stream B [Blankenship *et al.*, 1986, 1987]. They inferred also that the range of uncertainty for this estimate is from 10 to 90 kPa. Subsequently, Engelhardt and Kamb [1997] used measurements of borehole water level and estimates of the ice overburden pressure to calculate basal effective stresses in 24 boreholes drilled within the same area on Ice Stream B. The mean average of these measurements is 63 kPa with two standard errors of the mean yielding a 95%-confidence interval between 39 and 87 kPa.

Since the internal friction coefficient of the UpB till is equal to *ca.* 0.45 (Tulaczyk *et*

al., in preparation I), the shear strength of this till *in situ* should be 22.5 or 28.4 kPa for subglacial effective stress of 50 and 63 kPa, respectively. However, laboratory measurements of till strength have yielded values that are an order of magnitude lower than this, *ca.* 2 kPa [Kamb, 1991]. *In situ* measurements with a borehole torvane also indicate till strength of only several kPa [Kamb, unpublished data] as does modeling of the ice-stream velocity profile [Echelmeyer *et al.*, 1994]. Moreover, till strength of 22.5-28.4 kPa would be significantly greater than the low gravitational driving stress acting on the ice stream in the UpB area, $\tau_d \approx 13.5$ kPa. Such strong till could not provide the efficient basal lubrication which is considered to be necessary for the fast motion of Ice Stream B to occur [Alley *et al.*, 1987ab; Kamb, 1991; MacAyeal, 1989].

In the following discussion, we show that the high till water content and the preconsolidation pressures recorded in the UpB till indicate that the *in situ* effective stress beneath the UpB area of Ice Stream B is indeed appropriately low to explain the measured low strength of the till [Kamb, 1991].

5.4.1. Till Water Content

Table 1 and Figure 1 give the void ratio and porosity measured in till cores recovered from beneath Ice Stream B during three field seasons 1989-90, 1992-93, and 1995-96; for borehole locations see Tulaczyk *et al.* [in preparation I, Figure 1]. Mean average void ratio and porosity of all the 51 measurements is 0.665 and 0.399, respectively. This is in an excellent agreement with the estimate of till porosity, $n \approx 0.4$, $e \approx 0.667$, derived previously from compressional wave velocities by Blankenship *et al.* [1986, 1987]. In general, the till sampled in the different bed locations shows consistently high water content. For instance, the cores 92-1 and 95-1 which were sampled in

boreholes located *ca.* 8 kilometers apart have remarkably similar water content along most of their length (Figure 1). Variability of till water content within individual cores appears to be as large as water content variability between cores. Especially noticeable are high water contents occurring in core 92-1 from depth *ca.* 0.6 m upward, and in core 89-7 from depth *ca.* 1.8 m upward (Figure 1).

5.4.2. Preconsolidation Stress

Application of effective stress to soils induces changes in soil water content and microstructure. If the applied effective stress is higher than any effective stress experienced previously by a given soil sample, so-called normal consolidation takes place. During normal consolidation most of the changes in soil volume and microstructure are non-recoverable. We have already previously shown that this is also true for the UpB till [Tulaczyk *et al.*, in preparation I, Figure 5]. Thanks to these non-recoverable changes, a soil sample preserves a 'memory' of the highest past effective stress called the preconsolidation stress, to which the given sample was subjected. This 'memory' of past overconsolidation can be effectively retained only under static condition. If shear deformation occurs the preconsolidation stress is reset to a lower value, equal to the effective stress which have acted on a given till volume during its deformation.

Casagrande [1936] developed a method which is widely used to estimate the preconsolidation stress [Terzaghi *et al.*, 1996, p. 101-106]. In his method, a soil sample is placed in an oedometer and consolidated at increasingly higher levels of normal effective stress. Once the preconsolidation stress is exceeded, soil compressibility increases markedly because the sample is again in its normally-consolidated rather than preconsolidated state. The data obtained in the oedometer test are then plotted on a void-

ratio vs. effective-stress diagram. The point of highest curvature on a curve fitted to the test data is found and a graphical construction proposed by Casagrande [1936] is used to estimate the value of preconsolidation stress (Figure 2). Casagrande's method has been used in a number of previous investigations of subglacial effective stresses [Boulton and Dobbie, 1993; Harrison, 1958; Sauer and Christiansen, 1988, 1991].

The first four consolidation tests on samples of the UpB till were performed by Engelhardt in 1990 using the material from the core 89-4 (Figure 2A). These tests indicated that over the whole range of applied effective stresses, from 25 kPa to 400 kPa, the till samples are in the normally-consolidated state. Thus, the tests did not provide evidence to support the proposition that subglacial effective stress is approximately 50-60 kPa. To verify that the till is capable of recording preconsolidation stress of *ca.* 50-60 kPa, we have run an oedometer test in which a remolded till sample from core 95-1 was first consolidated to 53 kPa, then completely unloaded and again reconsolidated (Figure 2B). Application of the Casagrande's method to the results of this test yields an estimate of preconsolidation stress, 60 kPa, which is close to the real preconsolidation stress, 60 kPa vs. 53 kPa. Another sample which had also been preconsolidated to 53 kPa but then completely remolded by hand with no addition of water still yields a relatively high preconsolidation stress of 32 kPa [Figure 2C]. The latter result demonstrates that the degassing-induced disturbance of till microstructure alone could not have completely obliterated the 'memory' of a subglacial preconsolidation stress experienced by the UpB till. As discussed above, core drying should cause an increase in the preconsolidation stress, as demonstrated in test C3 (Figure 2D).

Given the results of our experimental tests (Figure 2), we conclude that the first four consolidation tests on material from core 89-4 (Figure 2A) did not detect the preconsolidation stress because this stress is smaller than the lowest effective stress applied

in the tests, 25 kPa. Subsequently, two new consolidation tests on samples from cores 95-1 and 95-5-1 were run starting at effective stress of 4.5 and 2.2 kPa (Figure EF). These tests show the characteristic bend associated with transition from preconsolidated to normally-consolidated state. Application of Casagrande's construction to these data yields low preconsolidation stresses of 4.4 kPa and 13 kPa.

5.4.3. Estimates of Subglacial Effective Stress From Till Water Content

The existing water content data can be combined with the information on till compressibility to obtain additional estimates of subglacial effective stress. The simplest estimate can be derived by assuming that *in situ* all till samples were in a normally-consolidated state. The equivalent consolidation stress can then be obtained by projecting the measured till void ratio, e, onto the experimentally-determined normal-consolidation line of the form $e = e_o - C_c \log \sigma'_n$ (Table 2):

$$\sigma'_{NC} = 10^{(e_o - e)/C_c} \qquad (3)$$

where σ'_{NC} denotes the equivalent consolidation stress under the assumption of normal consolidation, e_o is the till void ratio at the reference effective stress of 1 kPa, and C_c is the till compressibility in the normally-consolidated state. Since the states to the right of the normal-consolidation line are considered to be inadmissible [Mitchell, 1993], σ'_{NC} represents the lower bound on the subglacial preconsolidation stress estimated from till water content.

The corresponding upper bound can be calculated by assuming that the till was in an overconsolidated state when it was sampled from its sub-ice-stream environment. Then, till water content was determined by a two-stage process: 1) consolidation along the normal-consolidation line to some maximum past preconsolidation stress, σ'_p, and 2)

swelling along an unloading-reloading line ($e = e_{ur} - C_s \log\sigma'_n$) to some effective stress $\sigma'_n < \sigma'_p$ (where e_{ur} and C_s are empirically-constrained quantities analogous to e_o and C_c). Clearly, we cannot constrain both σ'_n and σ'_p at the same time. However, in accordance with our intention to get the upper limit on σ'_p, it is best to assume a low value for the subglacial effective stress σ'_n to which the sample was unloaded. We choose a low value of 1 kPa which permits us to express the upper bound on the subglacial preconsolidation stress as:

$$\sigma'_{OC} = 10^{(e_o - e)/(C_c - C_s)} \qquad (4).$$

Because C_s is much smaller than C_c (Table 2), σ'_{OC} is not very sensitive to the choice of the effective stress σ'_n. For instance, by lowering the choice of σ'_n by an order of magnitude, i.e., to 0.1 kPa, preconsolidation stress for the average void ratio of the UpB till $e = 0.665$ would change from 10.4 kPa to 15.1 kPa given the mean values of e_o, C_c, and C_s from Table 2. Equation (4) may be modified to allow for σ'_n other than one kPa by multiplying the right-hand side of this equation by the term: $\sigma'^{\,C_s/(C_s - C_c)}_n$. Figure 2 illustrates the fact that there is a reasonably close agreement between the preconsolidation stress calculated from till water content using equations (3) and (4) and the preconsolidation stress that is known or estimated with Casagrande's method.

All subglacial preconsolidation pressures calculated from the till water content data (Table 1) are plotted in Figure 3. Almost all of these pressures are lower than the two previous best estimates of the average effective stress beneath Ice Stream B, 50 and 63 kPa [Blankenship *et al.*, 1987; Engelhardt and Kamb, 1997]. The mean average ± two standard errors of the lower bound, σ'_{NC}, is 11.7 ± 2.6 kPa and of the upper bound, σ'_{OC}, 18.3 ± 4.4 kPa. These low subglacial effective stresses suggest low *in situ* till strength, 5.2 ± 1.1 kPa and 8.1 ± 1.9 kPa. The confidence intervals of the two previous evaluations of subglacial effective stress in UpB till largely overlap with the range of preconsolidation

stresses calculated from till water content (Figure 3). This suggests that there is no fundamental disagreement between the three different methods of calculating the effective stress from: 1) seismic data, 2) borehole water levels, and 3) water content [Blankenship *et al.*, 1987; Engelhardt and Kamb, 1997; this study]. However, the third method, which is proposed here, does yield the smallest range of uncertainty in the estimate of the average subglacial effective stress (Figure 3). The preconsolidation stresses calculated using this method are also in good agreement with the low *in situ* till strength inferred from laboratory measurements and from the ice-stream velocity profile [Echelmeyer *et al.*, 1994; Kamb, 1991].

5.5. Subglacial Water System

The existing data make it evident that, at least in the UpB area, water pressure beneath Ice Stream B is just barely smaller than the overburden ice pressure of *ca.* 9.2 MPa. This very high water pressure must be controlled by the hydrologic system beneath the ice stream. In this section of our manuscript, we analyze three main processes that determine the nature of the sub-ice-stream hydrologic system: 1) groundwater flow, 2) water flow in a basal water system, and 3) local water storage in till. Based on these analyses, we hypothesize that the high sub-ice-stream water pressure is controlled mainly by the third process with little or no long-distance drainage of subglacial water occurring through the groundwater and basal flow.

5.5.1. Groundwater Flow

Evacuation of glacial meltwater from beneath Ice Stream B via groundwater flow in

a layer of subglacial till was modeled previously by Lingle and Brown [1987]. These authors considered a two-dimensional centerline model of groundwater flow in a meters-thick layer of till of adjustable hydraulic conductivity. From a coupled ice-flow/heat-flow model, they have inferred that an average melting rate beneath the drainage basin of Ice Stream B should be of the order of 10^{-3} to 10^{-2} m y^{-1}. In order to accommodate this relatively large melting rate, their groundwater flow model required the till to have an extremely high hydraulic conductivity of 10^{-2} m s^{-1}, a value that is characteristic of gravel but not of glacial till [Lingle and Brown, 1987].

New data elucidating important aspects of the groundwater system beneath Ice Stream B became available thanks to geophysical and borehole investigations in the UpB area [Engelhardt *et al.*, 1990; Engelhardt and Kamb, 1997; Rooney *et al.*, 1991]. We take these new constraints into consideration in our effort to re-evaluate the role of the subglacial groundwater system in draining the base of Ice Stream B.

Geophysical and sedimentological data indicate that the till beneath Ice Stream B is underlain by a several-hundred-meter-thick sequence of clay-rich glacimarine sediments which are inferred to be similar in their textural characteristics to the till itself [Rooney *et al.*, 1991; Tulaczyk *et al.*, 1998]. The glacimarine sequence rests on crystalline bedrock. This justifies allowing the groundwater flow to take place in a much thicker hydrogeologic unit than just within the several-meter-thick subglacial till. In our modeling, we combine the till and the glacimarine sediments into one hydrogeologic unit with hydraulic conductivity equal to that measured in the laboratory on samples of the UpB till, $k_h \sim 10^{-10}$ m s^{-1} (Figure 4A).

The finding that sub-ice-stream water pressures are almost equal to the ice overburden pressure has also an important implication for models of subglacial groundwater flow [Blankenship *et al.*, 1987; Engelhardt and Kamb, 1997]. Thanks to this

fact, we have a well-constrained upper boundary condition for the simulated groundwater system. The distribution of water pressure or hydraulic head at the top of this system can be simply derived from the known ice surface elevation:

$$P_p(x, 0) = H_i(x)\, g\, \rho_i \tag{5a}$$

$$H_f(x, 0) = P_p\, (\rho_w\, g)^{-1} = H_i(x)\, \rho_i\, \rho_w^{-1} \tag{5b}$$

where: $P_p(x, 0)$ and $H_f(x, 0)$ are the pore pressure and the hydraulic head at the ice base, x is the horizontal space variable running along the ice flow direction, z is the vertical space variable, $H_i(x)$ is the ice thickness, g is the acceleration of gravity, ρ_i is the ice density ($\approx$ 900 kg m^{-3}), and ρ_w is the water density ($\cong$ 1,000 kg m^{-3}). Knowing the distribution of the hydraulic head, the approximate geometry of the groundwater system and its hydraulic conductivity, we can estimate the infiltration rate at the base of the ice stream. The guiding question of our modeling was whether or not this infiltration rate is comparable to the glaciologically-reasonable rate of basal melting of the order of 10^{-3} m y^{-1}. If such were the case, then the subglacial groundwater system could provide sufficient means for draining away basal meltwater.

First, we consider a simple analytical groundwater flow model which is similar to the models used previously by Boulton and Jones [1979] and Boulton and Paul [1976]. In this model, we solve for infiltration rate in a rectangular domain which extends along the whole length of the centerline of Ice Stream B, i.e., over an interval 310 km long ending at grounding line. The sedimentary aquifer is assumed to be 1,000 m thick and to be underlain by impermeable bedrock. Combination of Darcian flow and mass conservation yields the following expression for the infiltration rate, q_v:

$$q_v = k_h\, b\, \mathrm{d}^2h/\mathrm{d}x^2 \tag{6}$$

where b is the aquifer thickness, k_h is the hydraulic conductivity and $h(x)$ is the hydraulic head at the top of the aquifer. It is important to note that the infiltration rate, q_v, represents

downward motion of water away from the ice base on the top of the aquifer, only if q_v is negative. If this quantity is positive it represents seepage of groundwater out of the aquifer into a hypothetical basal water system. Having equation (6) we can now digitize the ice-surface profile along the centerline of the ice stream [Lingle and Brown, 1987, figure 2] and convert it to hydraulic head with equation (5b). Subsequently we use a least-square fit polynomial to obtain a continuous, differentiable function $h(x)$ (Figure 4B).

This modeling effort yielded a result which was somewhat unexpected. Because the ice stream profile is for the most part concave upward, the second derivative of the hydraulic head distribution is positive over most of the modeled length of the ice stream. This means that q_v is positive as well (equation 6) and that the subglacial groundwater system should discharge water at the top delivering water to the ice base, rather than downward, away from the ice base (Figure 4B). Because of the very low hydraulic conductivity of the sedimentary aquifer, $k_h = 10^{-10}$ m s^{-1}, the velocity of water inflow/outflow at the top of the aquifer is extremely small, i.e., a fraction of a micron per year. The results of this simple groundwater flow model are thus inconsistent with our intuitive idea that basal meltwater may be evacuated via the groundwater system at a rate comparable to the common basal melting rate of ~10^{-3} m s^{-1}.

To check whether this inconsistency may be an artifact of the simplicity of our model, we have run a more complicated two-dimensional finite-element simulation of steady-state groundwater flow beneath Ice Stream B. A FORTRAN code written by Dr. J. Hall (Division of Engineering and Applied Science, Caltech) and modified by S. Tulaczyk was used to solve Laplace's equation with hydraulic head as the variable and with the appropriate boundary conditions [Freeze and Cherry, 1979, p. 64]:

$$\partial^2 h/\partial x^2 + \partial^2 h/\partial z^2 = 0 \qquad (7).$$

The geometry of the modeled domain is shown in Figure 4C. We consider a domain which

extends from the crest of the ice divide to the grounding line (630 km) and down to a depth of 4,000 m below sea level. The hydraulic head distribution and the geometry of the ice base are derived from data given in figure 2 of Lingle and Brown [1987]. As compared to the previous, simpler model, we increase the transmissivity of the groundwater system by assuming that the crystalline bedrock underlying the sedimentary unit is highly fractured and has a high hydraulic conductivity of 10^{-4} m s^{-1} [Freeze and Cherry, 1979, table 2.2]. The boundary between the sedimentary sequence and the bedrock is arbitrarily selected to be always halfway between the ice base and the depth of 4,000 m.b.s.l. As before, we prescribe the hydraulic head equal to the ice overburden pressure at the top of the modeled domain. The other three boundaries, bottom, left, and right, have been assigned a no-flow condition, i.e., impermeable barriers. Flow of water out of the system takes place beyond the grounding line because the right-hand no-flow boundary is assigned at x = 650 km, i.e., 20 km beyond the grounding line. Between x = 630 and 650 the prescribed hydraulic head at the top of the system is constant and equal to zero, i.e., at sea level. As shown in Figure 4D, the result of the computational model is in fundamental agreement with the simple analytical model; both predict that water should be flowing upward out of the groundwater system beneath Ice Stream B (from x = 320 to 630 km). Again, we attribute this fact to the concave-upward nature of the hydraulic head distribution over the length of the ice stream. With such geometry, the horizontal hydraulic gradient decreases towards the grounding line, thus, diminishing the horizontal flux of water in the system. Because of mass conservation, this decreasing capacity of the system to transport water horizontally must be accommodated by vertical water seepage out of the modeled domain. Introduction of the high-conductivity layer did increase the velocity of water influx/outflow to ~ 10^{-4} m s^{-1}, compared to ~ 10^{-7} m s^{-1} in the simple model. Infiltration of water into the subglacial groundwater system takes place only beneath the first *ca.* 150 km away from the ice divide

at $x = 0$. In this section, the ice-surface profile and the hydraulic gradient derived from it are convex-upward, and their second derivatives are positive. It should be noted here that we have assumed that the hydraulic gradient beneath the slow-moving part of the ice, $x = 0$ to 320 km, is also given by equation (5a), i.e., basal water pressure is equal to the ice overburden pressure. Whereas this assumption is well justified by the existing observations beneath Ice Stream B [e.g., Engelhardt and Kamb, 1997], it is uncertain how close to reality it is beneath the ice sheet. Water pressure in the only borehole drilled to the bottom of the central part of the West Antarctic ice sheet, at Byrd Station, was only 140 kPa below the overburden ice pressure [Alley *et al.*, 1987c]. Qualitatively, hydraulic head smaller than its assumed maximum value, i.e., the one given by equation (5a), would have simply the effect of decreasing the horizontal hydraulic gradient and decreasing the magnitude of the infiltration rate. Such modification, however, could not change the fact that water beneath the ice stream part of the model, i.e., beyond $x = 320$ km, seeps upward at the top of the domain.

Given the close general agreement between the results of our two models, we conclude that the groundwater system beneath Ice Stream B does not provide an efficient means of evacuation of basal meltwater. The two physical controls that appear to be responsible for this lack of drainage capacity of the groundwater system are: 1) the concave-upward distribution of hydraulic head imposed by the downstream flattening of ice-surface profile, and 2) the very low hydraulic conductivity of the sediment sequence inferred to underlie the ice stream [Rooney *et al.*, 1991; Tulaczyk *et al.*, 1998].

5.5.2. Basal Water System

Basal meltwater could also be evacuated from beneath Ice Stream B by means of a

distributed or a channelized basal system in which long-distance water transport would be confined to pathways or conduits along the ice-till interface. However, our quantitative and qualitative analysis of such basal systems shows that they too may be incapable of draining a significant amount of water from beneath Ice Stream B.

A basal water film represents the most commonly used model of a distributed basal drainage system for ice streams resting on rigid and deformable substrata [Weertman and Birchfield, 1982; Alley, 1989a]. The quantity of water which may be transported by a laminar flow in such a water film is highly dependent on its thickness, d_w [Alley, 1989a; Engelhardt and Kamb, 1997; Weertman, 1972]:

$$q = \phi_w \, d_w^{\,3} \, P_g \, (12 \, \mu)^{-1} \tag{8}$$

where q is the water flux in the direction of the pressure gradient P_g (units of q are m^3 per meter width per second), and ϕ_w is the fraction of the bed area covered by the water film. If basal water pressure is at the ice overburden pressure (equation (5)), then the water pressure gradient in a horizontal water film is given by [Alley, 1989a, equation 26]:

$$P_g = \rho_i \, g \, \alpha_s \tag{9}$$

For Ice Stream B, the ice surface slope, α_s, is *ca.* 10^{-3} and P_g is of the order of 10 Pa m^{-1}.

Typically, the basal water film assumed in modeling of meltwater transport is relatively thick ~ 10^{-3} to ~ 10^{-2} m [Alley, 1989a; Weertman, 1972; Weertman and Birchfield, 1982]. However, borehole experiments performed by Engelhardt and Kamb [1997] in the UpB area of Ice Stream B indicate that the water film, if it exists at all, is less than *ca.* 10^{-4} m thick. Because of the sensitive dependence of water flux in the film on film thickness, this constraint shows that a long-distance water transport in a distributed basal system is inefficient at UpB. This can be illustrated with an order of magnitude calculation of q using equation (8) and the following approximate values for the relevant coefficients and independent variables: $\phi_w \sim 10^{-1}$, $d_w \sim 10^{-4}$ m, $P_g \sim 10$ Pa m^{-1}, $\mu \sim 10^{-3}$ Pa s. Given

these values the downstream water flux at UpB should be $q \sim 10^{-10}$ m^2 s^{-1} or $\sim 10^{-3}$ m^2 y^{-1}. Dividing q by the approximate length of the ice stream upglacier of the UpB area, *ca.* 10^5 m, we can get an estimate of the average basal melting rate that can be drained in the thin basal water film. This basal melting rate is of the order of a hundredth of a micron per year, i.e., 10^{-8} m y^{-1}, which is five to six orders of magnitude less than the basal melting rate that has been frequently assumed or calculated from ice-flow models for Ice Stream B, i.e., $\sim 10^{-4}$ to 10^{-2} m y^{-1} [Alley, 1989a; Alley *et al.*, 1987a; Engelhardt and Kamb, 1997; Lingle and Brown, 1987; Weertman and Birchfield, 1982].

If one assumes that meltwater is indeed being produced at the base of Ice Stream B at high rates, the only remaining means of evacuating this mass of water is a channelized basal water system. Engelhardt and Kamb [1997] proposed that this system is composed of a network of 'canals' - features that were introduced into modeling of basal water flow over a deformable bed through the theoretical analysis of Walder and Fowler [1994]. These authors proposed that canals are flat, low conduits incised into the till, with ~0.1 m depth and ~1 m width. In Walder and Fowler's model a canal is kept open primarily by the ability of sediment erosion to keep up with the assumed viscous creep of till into the canal. The creep itself is driven by the effective stress difference between the canal and the surrounding till.

Laboratory results show that the UpB till has a plastic rather than viscous rheology [Kamb, 1991; Tulaczyk *et al.*, in preparation I]. This fact complicates direct application of the theoretical canal model which uses the assumption of linearly viscous till [Walder and Fowler, 1994]. Our analysis of the problem suggests that incorporation of plastic till rheology introduces an instability into the hypothetical canal system. This instability should be most pronounced when subglacial pore pressure is very close to the ice overburden pressure and till is weak, as it is the case in the UpB area of Ice Stream B

[Engelhardt and Kamb, 1997; Kamb, 1991].

Unlike in the case of viscous till for which a stable balance between sediment erosion and till creep may exist, canal incised into a till of plastic rheology will have two possible states: 1) one in which the canal has a steady-state geometry or is being deepened by erosion, and 2) a second one in which the canal collapses, i.e., total filling takes place by till deforming into the canal. The first state occurs when the effective stress differential between the canal and its surroundings is below a critical value, σ'_c, and the second one, when this critical value is exceeded. The critical effective stress depends on the failure strength of the till, τ_f. An approximate value of the critical effective stress may be obtained by assuming that canal collapse due to infilling by till of plastic rheology represents a reverse of the well-known engineering problem of soil penetration by a flat punch or a strip load [Johnson, 1970, p. 481; Scott, 1963, p. 425-426]:

$$\sigma'_c = (2 + \pi)\tau_f \qquad (10).$$

The choice of an appropriate value for τ_f is difficult because of dependence of till strength on effective stress which will be spatially variable near a channel. However, the most relevant failure strength is that of the till beneath the channel bottom where the vertical effective stress is zero. In this location, the strength of the till is determined mainly by past preconsolidation of the material and is mostly given by the so-called 'true cohesion' [Kezdi, 1974, p. 224]. The strength of the UpB till, *ca.* 2 kPa, measured by Kamb [1991] in unconfined shear box tests can be used for τ_f in this context. Under these conditions, canal collapse will not occur only if the vertical effective stress acting on the till in the vicinity of the canal is less than $\sigma'_c \approx 10$ kPa.

Figure 5 illustrates the fact that canal collapse is plausible given reasonable assumptions about the nature of the canal drainage system. From water level measurements in boreholes, Engelhardt and Kamb [1997] inferred that if canals do exist

beneath Ice Stream B, then they may have a spacing of *ca.* 50 - 300 m. Thus, in our simple model, we assume that the simulated canal drains water from a distance of 100 m away from the canal banks. We have verified that this drainage cannot take place, to any significant extent, via Darcian water flow in the till. Therefore, we model the water collection system as a thin, i.e., $d_w = 10^{-4}$ m, basal water film. If we require that the water film drains towards the canal all the meltwater produced at a constant rate m_r, the hydraulic head distribution transverse to the canal axis, $h_{(y)}$, can be obtained from equation (8) by substituting $m_r y$ for q and $\rho_w\, g\, dh/dy$ for P_g, and then integrating:

$$h = H_f - [6\, \mu\, m_r\, (\phi_w\, d_w^{\,3}\, \rho_w\, g)^{-1}]\, y^2 \qquad (11)$$

where the constant of integration was evaluated by setting the hydraulic head at the drainage divide, i.e., $y = 0$, to the maximum physically-admissible value of $h = H_f$, i.e., the flotation level given by equation (5b). Order-of-magnitude values of the coefficients and independent variables used in equation (11) are as follows: $\phi_w \sim 10^{-1}$, $6\mu \sim 10^{-2}$ Pa s, $d_w \sim 10^{-4}$ m, $\rho_w \sim 10^3$ kg m^{-3}, $g \sim 10$ m s^{-2}.

Figure 5 plots three examples of hydraulic head distributions for the melting rate of $\sim 10^{-3}$, 10^{-4}, and 10^{-5} m y^{-1}. Very small hydraulic gradients are sufficient to drain water produced at the lowest melting rate but for the melting rate of 10^{-4} m y^{-1}, the hydraulic head near the canal reaches critical value, $H_c \approx 1$ m, for which the vertical effective stress is *ca.* 10 kPa, i.e., the threshold value for canal collapse (equation (10) with $\tau_f = 2$ kPa). Canal collapse is thus a clear possibility under reasonable assumptions made about the basal melting rate and water-film thickness.

Our simple analysis demonstrates that incorporation of the experimentally-established plastic rheology of the UpB till into a model of basal drainage via canals introduces a significant element of instability. Given the very low strength of the UpB till, canals are stable only within a fairly narrow window of subglacial water pressures that are

between *ca.* 0 and 10 kPa below the ice overburden pressure. If water pressure in the canals, and thus in their vicinity, drops below *ca.* 10 kPa, canals will be filled by intruding till. A basal drainage system made up of canals may be strongly affected by local collapses because it must drain meltwater all the way to the grounding line, which requires continuity of the canal network over distances of ~10^5 m.

Based on our theoretical analysis, we infer that beneath Ice Stream B there is no organized, long-distance basal drainage system which could be draining a significant amount of basal meltwater.

5.5.3. Feedback Between Water Storage in Till and Basal Melting

Our proposition that beneath Ice Stream B there may be no efficient drainage of meltwater towards the grounding line is quite unorthodox from the point of view of the traditional models of subglacial water systems. In such models it is frequently assumed that basal meltwater is generated at relatively high rates of ~ 10^{-3} to 10^{-2} m y^{-1} beneath fast moving ice. An assumption of this type automatically requires the existence of some type of an efficient subglacial or basal drainage system. Therefore, the question that is being posed in the glaciological literature is mainly what is the nature of the sub-ice-stream drainage system rather than the question whether or not such a system exists. In this section of our manuscript we show that a physically-admissible model of sub-ice-stream bed hydrology may be created without assuming that basal meltwater is being drained at high rates from beneath the ice stream to the grounding line. In this 'undrained' bed model any basal meltwater that is being generated is assumed to go entirely into local storage as pore water in till. Furthermore, a negative feedback effect arises from the interdependence between the basal melting rate, till water content, and till strength. This negative feedback

mechanism should maintain basal melting rate at or near zero, thus eliminating the need for significant long-distance transport of meltwater.

First, let us look at the physical variables which control the magnitude of the basal melting rate, m_r. This rate is determined by balance of thermal energy at the base of an ice mass where we have two sources of thermal energy, geothermal flux and shear heating, and one sink of thermal energy, conductive heat loss [Lingle and Brown, 1987, equation 10]:

$$m_r = (\tau_b U_b + G - k_i \Theta_b) (L_i \rho_i)^{-1} \qquad (12)$$

where τ_b is the basal shear stress, U_b is the velocity of basal sliding, G is the geothermal flux, k_i = 2.1 W m^{-1} °C^{-1} is the thermal conductivity of ice, Θ_b is the basal temperature gradient, L_i = 333.5 kJ kg^{-1} is the latent heat of ice fusion and ρ_i is the ice density. m_r denotes melting, i.e., generation of meltwater at the ice base, only if it is greater than zero. If m_r is less than zero, then it gives the rate of basal freeze-on. However, for simplicity we will keep referring to m_r as the basal melting rate, keeping in mind its broader meaning.

If we can establish the appropriate values for the variables in equation (12), we will be able to estimate what is the sign and the magnitude of basal melting beneath Ice Stream B. Borehole measurements in the UpB area show that the basal temperature gradient there is equal to *ca.* 0.041 °C m^{-1} [Engelhardt and Kamb, 1993]. For an ice stream whose motion is accommodated at the base by deformation of till of plastic rheology, the magnitude of the basal shear stress is equal to the plastic strength of the till, i.e., $\tau_b = \tau_f$. From laboratory measurements we know that τ_f is equal to *ca.* 2 kPa [Kamb, 1991]. Given the low basal stress, internal deformation of ice does not contribute significantly to ice stream velocity, and the observed ice stream velocity of 440 m y^{-1} [Whillans and van der Veen, 1993] can be multiplied by τ_f to obtain the shear heating term in equation (12). Unfortunately, the geothermal flux has not been constrained by direct observations in the

area of interest. Rose [1979] used temperature measurements in the Byrd station borehole located several hundred kilometers to the east and north of the UpB area to infer that the geothermal flux is equal to *ca.* 0.06 W m^{-2}.

Figure 6A illustrates a range of values of the basal melting rate given reasonable bounds on the geothermal flux, between 0.05 and 0.08 W m^{-2} [Turcotte and Schubert, 1982, Table 4-1]. The first-order observation that can be made is that both basal melting and freezing are possible beneath Ice Stream B, depending on the exact value of the geothermal flux and the shear heating. Let us first consider the case that there is generation of basal meltwater at the base of Ice Stream B and ask the question: what happens to basal meltwater if one disallows a long-distance transport towards the grounding line? Since the water is being generated at the ice base, there is a possibility that the meltwater will pond along the ice-till interface. However, our experience with remolding till in the laboratory in the presence of free water indicates that deformation of till permits free water to be incorporated into till pore spaces. As a result of such remolding, till increases its water content. Since there are theoretical and observational reasons to believe that the till beneath Ice Stream B experiences some deformation at least near its top [Engelhardt and Kamb, in press; Tulaczyk *et al.* in preparation I], we hypothesize that any meltwater generated at the base of this ice stream is eventually incorporated into the underlying till. Thus, the rate of change of till void ratio in undrained conditions, i.e., no long-distance transport of meltwater, can be expressed as a function of the basal melting rate:

$$de/dt = m_f/Z_s \qquad (13)$$

where t is the time variable and Z_s is the thickness of till solids contained in the 'active' till layer. Use of Z_s instead of the overall thickness of the 'active' till is more convenient when void ratio is the dependent variable. By the 'active' till layer we understand that part of the subglacial till which undergoes deformation continuously or frequently. The physical

controls on the depth of till deformation in the case of till of plastic rheology were discussed in Tulaczyk [in press] and Tulaczyk *et al.* [in preparation I].

Inspection of equation (13) shows that in undrained conditions the till void ratio will increase as long as the melting rate is positive. However, the melting rate itself depends in an indirect way on till void ratio because the latter controls the undrained till strength (Figure 6B). Typically, strength of tills or other soils is expressed as a function of effective stress rather than till void ratio. However, in shearing soils the three variables: strength, effective stress, and void ratio are interrelated [Schofield and Wroth, 1968, p. 19]. This is because the effective stress controls both soil volume and strength. In the effective stress-void ratio space, the state of a till whose water content is being increased by remolding, i.e., shearing, in the presence of free water will migrate along the critical-state line towards lower effective stresses (e.g., CSL in Clarke [1987] and Tulaczyk *et al.* [in preparation I, Figure 5A]).

The idea that till strength should decrease with increasing water content and increase with decreasing water content is qualitatively reasonable. The quantitative relationship between τ_f and e based on the data shown in Figure 6B represents a specific expression of this qualitative idea:

$$\tau_f = \exp(13.8 - 21.7e) \qquad (14)$$

where τ_f is in kPa and e is expressed as a decimal fraction. To see how sensitive the basal melting rate, m_r, is to changes in till void ratio and strength we substitute equation (14) for τ_b in equation (12) and evaluate the new expression using the same values of independent variables as in Figure 6A and assuming the geothermal flux inferred by Rose [1979], G = 0.06 W m^{-2}. Figure 7A shows that the melting rate is very sensitive to till void ratio. For instance, at e equal to 0.58 and till strength of *ca.* 3.5 kPa, the melting rate is *ca.* 2×10^{-3} m y^{-1}, but an increase in till void ratio by only 3% brings the till strength down to *ca.* 2.0 kPa

and the melting rate to near zero. Thus, an initial positive basal melting rate, m_r, will tend to decrease with time towards zero due to the negative feedback described by equations (12), (13), and (14). The characteristic timescale, T, for this process can be estimated from an integral of equation (13):

$$T \sim \Delta e \, Z_s / m_{rav} \qquad (15)$$

where Δe is the required change in void ratio and m_{rav} is the average melting rate over the time T. Given reasonable values of $\Delta e \sim 10^{-2}$, $Z_s \sim 1$ m, and $m_{rav} \sim 10^{-3}$ m y^{-1}, the characteristic timescale is of the order of 10 years.

If we consider a hypothetical case in which the initial basal melting rate is negative rather than positive, i.e., water freeze-on is taking place at the ice sole, a similar negative feedback effect forcing the m_r to migrate towards a steady-state value of zero may still operate. This is because in the considered closed and undrained system of till and ice, accretion of new ice at the base has to take place at the cost of withdrawal of water from till. This freeze-on driven consolidation of till will decrease till void ratio and increase till strength leading to a negative feedback similar to the one described above, i.e., stronger till causes increased shear heating and increased shear heating diminishes the magnitude of basal freeze-on. One could argue that such freeze-on consolidation must not take place when ice sole experiences freeze-on. Instead, the ice could simply form in till pore spaces without inducing water loss in the still unfrozen till. However, in the case of the fine-grained UpB till such basal accretion of till will be hindered by surface-tension effects which prevent ice from forming or infiltrating into small pore spaces. As calculated in Tulaczyk [in press], effective stress beneath Ice Stream B must reach *ca.* 100 kPa before these surface-tension effect will be overcome. At this high effective stress the strength of the UpB till would be roughly an order of magnitude greater, *ca.* 45 kPa [Tulaczyk *et al.*, in preparation I] than the observed strength of *ca.* 2 kPa [Kamb, 1991]. Since in here we

are interested only in till strength variations of a few kPa away from this value [Figure 7A], we may safely assume that freeze-on driven consolidation rather than basal accretion of till is the correct process to consider.

To verify that freeze-on driven consolidation may strengthen a several-meter-thick layer of till with low hydraulic diffusivity, e.g., $c_v \sim 10^{-8}$ m^2 s for the UpB till (Figure 4A), we have run finite-difference models of one-dimensional consolidation forced by freeze-on occurring at a constant rate of 10^{-3} m y^{-1} (Figure 7B). The modeling results demonstrate that freeze-on driven consolidation propagates relatively uniformly throughout a several-meters-thick till layer. This type of consolidation may increase the strength of a till layer by a few kilopascals within several years (Figure 7B). Such a small increase in till strength is sufficient to significantly increase the basal melting rate (Figure 7A). From the point of view of the physical processes considered here (equations (12), (13), and (14)), the initial state of basal freezing appears to be as unsustainable as an initial state of basal melting.

The above analyses of the negative feedback between till strength and basal melting rate are based on an assumption that the changes in till strength considered here, $\Delta\tau_f$ of *ca.* 1 kPa (Figure 7A), are small enough not to influence the sliding velocity of the ice stream, V_b in equation (12). In a separate manuscript [Tulaczyk *et al.*, in preparation III] we relax this assumption and show that a similar negative feedback between meltwater production and till strength may still exist. This is possible because the relative influence of small till strength changes on the rate of basal melting is much greater than their influence on ice stream velocity.

The undrained ice-stream bed model discussed in this section represents a physically viable alternative to the traditional models of sub-ice-stream hydrology in which a relatively high basal melting rate and an efficient water drainage system are assumed. The undrained-bed model is also consistent with the existing observations of low till strength

and low subglacial effective stresses (Figure 2 and 3) [Engelhardt and Kamb, 1997; Kamb, 1991]. According to the physics embedded in our model, low till strength of a few kilopascals is necessary to produce the steady-state value of basal melting rate, $m_r = 0$. At the same time, such low *in situ* till strength is possible only if the subglacial effective stress is low, *ca.* 1-10 kPa, and the till is water-rich.

5.6. Conclusions

We have combined measurements of water content in till cores recovered from beneath Ice Stream B with laboratory constraints on the compressibility of this till to obtain new estimates of *in situ* subglacial effective stress. The mean average of these estimates is several times lower than the previous best estimates of the subglacial effective stress from seismic data and borehole water level measurements, *ca.* 11.3 to 18.7 kPa vs. 50 kPa and 63 kPa, respectively (Figures 2 and 3) [Blankenship *et al.*, 1987; Engelhardt and Kamb, 1997]. A significant portion of the till cores recovered from beneath the UpB area of Ice Stream B has high water content consistent with preconsolidation pressures of the order of ~1 kPa only. These new, lower estimates of *in situ* subglacial pressure are significant because they are consistent with the low till strength, *ca.* 2 kPa, measured in shear box tests [Kamb, 1991].

The effective stresses beneath Ice Stream B are controlled by the processes taking place in the subglacial water system. From the results of our modeling of possible sub-ice-stream water drainage systems, we infer that there is no significant long-distance transport of meltwater from beneath Ice Stream B to its grounding line. Instead, we propose a new undrained-bed model of sub-ice-stream hydrology. In this model any water produced at the base of Ice Stream B must be disposed of locally, through an increase in the local water

storage as pore water in the underlying till. Incorporation of any basal meltwater into the till structure is possible as long as the till is being deformed, i.e., remolded, continuously or intermittently. On the other hand, if the ice sole experiences basal freeze-on, water may be extracted from till through freeze-on driven consolidation which will trigger an increase in till strength. Thus, the basal melting rate influences the water content in till, which in turn changes the subglacial effective stress and till strength. We show that a negative feedback effect between basal melting rate and till strength may exist. Due to this negative feedback, till water content, till strength, and shear heating adjust in steady-state to such values at which the basal melting rate is at zero. Our calculations indicate that, for the latter condition to be fulfilled, the shear heating term in the basal thermal energy balance must be low. This requires a low steady-state value of till strength because the ice stream velocity is high. Appropriately low till strength, i.e., τ_f of a few kPa, is consistent with the results of shear-box measurements of strength and with the very low subglacial effective stresses inferred from the high till water content (Figure 3) [Kamb, 1991].

The undrained-bed model of the hydrologic system beneath Ice Stream B shows that there may be a close coupling between the thermal, mechanical, and hydrological processes which determine the physical conditions at the bed of this ice stream. Proper incorporation of this coupling into models of ice stream motion may be necessary to explain ice stream stability and evolution.

5.7. References

Alley, R.B., Water-pressure coupling of sliding and bed deformation. 1. Water system, *J. Glaciol.*, 35, 108-118, 1989a.

Alley, R.B., Water-pressure coupling of sliding and bed deformation. 2. Velocity-depth

profiles, *J. Glaciol.*, 35, 119-129, 1989b.

Alley, R.B., D.D. Blankenship, C.R. Bentley, and S.T. Rooney, Deformation of till beneath Ice Stream B, West Antarctica, *Nature*, 322, 57-59, 1986.

Alley, R.B., D.D. Blankenship, S.T. Rooney, and C.R. Bentley, Till beneath Ice Stream B. 3. Till deformation - evidence and implications, *J. Geophys. Res.*, 92, 8,921-8,929, 1987a.

Alley, R.B., D.D. Blankenship, S.T. Rooney, and C.R. Bentley, Till beneath Ice Stream B. 4. A coupled ice-till flow model, *J. Geophys. Res.*, 92, 8,931-8,940, 1987b.

Alley, R.B., D.D. Blankenship, S.T. Rooney, and C.R. Bentley, Continuous till deformation beneath ice sheets: *IAHS*, 170, 81-91, 1987c.

Alley, R.B., D.D. Blankenship, S.T. Rooney, and C.R. Bentley, Water-pressure coupling of sliding and bed deformation. 3. Application to Ice Stream B, Antarctica, *J. Glaciol.*, 35, 130-139, 1989.

Bentley, C.R., Antarctic ice streams - a review, *J. Geophys. Res.*, 92, 8,843-8,858, 1987.

Bindschadler, R., The importance of pressurized subglacial water in separation and sliding at the glacier bed, *J. Glaciol.*, 29, 3-19, 1983.

Blankenship, D.D., C.R. Bentley, S.T. Rooney, and R.B. Alley, Seismic measurements reveal a saturated porous layer beneath an active Antarctic ice stream, *Nature*, 322, 54-57, 1986.

Blankenship, D.D., C.R. Bentley, S.T. Rooney, and R.B., Alley, Till beneath Ice Stream B. 1. Properties derived from seismic travel times, *J. Geophys. Res.*, 92, 8,903-8,911, 1987.

Boulton, G.S., and P.E. Caban, Groundwater flow beneath ice sheets: Part II - its impact on glacier tectonic structures and moraine formation, *Quat. Sci. Rev.*, 14, 563-587,

1995.

Boulton, G.S., P.E. Caban, and K. van Gussel, Groundwater flow beneath ice sheets: Part I - large scale patterns, *Quat. Sci. Rev.*, 14, 545-562, 1995.

Boulton, G.S., and K.E. Dobbie, Consolidation of sediments by glaciers: relationship between sediment geotechnics, soft-bed glacier dynamics and subglacial groundwater flow, *J. Glaciol.*, 39, 26-44, 1993.

Boulton, G.S., and R.C.A. Hindmarsh, Sediment deformation beneath glaciers - rheology and geophysical consequences, *J. Geophys. Res.*, 92, 9,059-9,082, 1987.

Boulton, G.S., and A.S. Jones, Stability of temperate ice caps and ice sheets resting on beds of deformable sediment, *J. Glaciol.*, v. 24, p. 29-43, 1979.

Boulton, G.S., and M.A. Paul, The influence of genetic processes on some geotechnical properties of subglacial tills, *Q. J. Engng. Geol.*, 9, 159-194, 1976.

Bowles, J.E., *Engineering properties of soils and their measurement*, McGraw-Hill, New York, 1992.

Casagrande, A., The determination of the preconsolidation load and its practical significance, *Proc. 1st. Int. Conf. Soil Mech. and Found. Engng.*, 3, 60-64, 1936.

Echelmeyer, K.A., W.D. Harrison, C. Larsen, and J.E. Mitchell, The role of the margins in the dynamics of an active ice stream, *J. Glaciol.*, 40, 527-538, 1994.

Engelhardt, H., W.D. Harrison, and B. Kamb, Basal sliding and conditions at the glacier bed as revealed by borehole photography, *J. Glaciol.*, 20, 469-508, 1978.

Engelhardt, H., N. Humphrey, B. Kamb, and M. Fahnestock, Physical conditions at the base of a fast moving Antarctic ice stream, *Science*, 248, 57-59, 1990.

Engelhardt, H.F., and Kamb, B., Vertical temperature profile of ice stream B: *Antarctic J. U.S.*, 28, 63-66, 1993.

Engelhardt, H., and B. Kamb, Basal hydraulic system of a West Antarctic ice stream - constrains from borehole observations, *J. Glaciol.*, 43, 207-230, 1997.

Engelhardt, H., and B. Kamb, Sliding velocity of Ice Stream B, *J. Glaciol.*, in press.

Fowler, A.C., and C. Johnson, Hydraulic run-away - a mechanism for thermally-regulated surges of ice sheets, *J. Glaciol.*, 41, 554-561, 1995.

Freeze, R.A., and J.A. Cherry, *Groundwater*, Prentice-Hall, Englewood Cliffs, New Jersey, 1979.

Harrison, W., Marginal zones of vanished glaciers reconstructed from the preconsolidation pressure values of overriden silts, J. *Geol.*, 66, 72-95, 1958.

Hooke, R.L., Englacial and subglacial hydrology: a qualitative review, *Arct. Alp. Res.*, 21, 221-233, 1989.

Iken, A., and R.A. Bindschadler, Combined measurements of subglacial water pressure and surface velocity of Findelengletscher, Switzerland: conclusions about drainage system and sliding mechanism, *J. Glaciol.*, 32, 101-119, 1986.

Johnson, A.M., *Physical processes in geology*, Freeman, Cooper & Company, San Francisco, 1970.

Johnson, M.D., The origin and microfabric of Lake Superior red clay, *J. Sed. Petrology*, 53, 859-873, 1983.

Kamb, B., Sliding motion of glaciers: theory and observations: *Rev. Geophys. Space Phys.*, 8, 673-728, 1970.

Kamb, B., Glacier surge mechanism based on linked cavity configuration of the basal water conduit system, *J. Geophy. Res.*, 92, 9,083-9,100, 1987.

Kamb, B., Rheological nonlinearity and flow instability in the deforming-bed mechanism of ice stream motion: *J. Geophys. Res.*, 96, 16,585-16,595, 1991.

Kamb, B., Raymond, C.F., Harrison, W.D., Engelhardt, H., Echelmeyer, K.A.,

Humphrey, N., Brugman, M.M., Pfeffer, T., 1985, Glacier surge mechanism - 1982-1983 surge of Variegated Glacier, Alaska: *Science*, 227, 469-479.

Kezdi, A., *Handbook of soil mechanics*, Elsevier, Amsterdam, 1974.

Lingle C.S., and T.J. Brown, A subglacial aquifer bed model and water pressure dependent basal sliding relationship for a West Antarctic ice stream, *in Dynamics of the West Antarctic Ice Shet*, edited by C.J. van der Veen and J. Oerlemans, D. Reidel Publishing Co., Dordrecht, 249-285, 1987.

Lliboutry, L., Realistic, yet simple bottom boundary conditions for glaciers and ice sheets, *J. Geophys. Res.*, 92, 9101-9109, 1987.

MacAyeal, D.R., Large-scale ice flow over a viscous basal sediment - theory and application to Ice Stream B, Antarctica, *J. Geophys. Res.*, 94, 4,071-4,087, 1989.

Mitchell, J.K., *Fundamentals of soil behavior*, Wiley, New York, 1993.

Rooney, S.T., D.D. Blankenship, R.B. Alley, and C.R. Bentley, Till beneath Ice Stream B. 2. Structure and continuity, *J. Geophys. Res.*, 92, 8913-8920, 1987.

Rooney, S.T., Blankenship, D.D., Alley, R.B., and Bentley, C.R., 1991, Seismic reflection profiling of a sediment-filled graben beneath Ice Stream B, West Antarctica: in *Geological Evolution of Antarctica*, edited by M.R. Thomson, J.A. Crame, and J.W. Thomson, British Antarctic Survey, Cambridge, 261-265, 1991.

Rose, K.E., Characteristics of ice flow in Marie Byrd Land, Antarctica, *J. Glaciol.*, 24, 63-75, 1979.

Sauer, E.K., and E.A. Christiansen, Preconsolidation pressures in intertill glacilacustrine clay near Blaine Lake, Saskatchewan, *Can. Geotech. J.*, 25, 831-839, 1988.

Sauer, E.K., and E.A. Christiansen, Preconsolidation pressures in the Battleford Formation, southern Saskatchewan, Canada, *Can. J. Earth. Sci.*, 28, 1613-1623, 1991.

Schoemaker, E.M., Subglacial hydrology for an ice sheet resting on a deformable aquifer, *J. Glaciol.*, 32, 20-30, 1986.

Schofield, A.N., and C.P. Wroth, *Critical state soil mechanics*, McGraw Hill, London, 1968.

Scott, R.F., *Principles of soil mechanics*, Addison-Wesley Publishing Company, Reading, Massachusets, 1963.

Terzaghi, K., B.P. Peck, and G. Mesri, *Soil mechanics in engineering practice*, Wiley, New York, 1996.

Tulaczyk, S., Ice sliding over weak, fine-grained tills: dependence of ice-till interactions on till granulometry, in *Glacial Processes, Past and Modern*, edited by D.M. Mickelson and J. Attig, in press.

Tulaczyk, S., B. Kamb, and H. Engelhardt, Basal mechanics of Ice Stream B, West Antarctic*a.* II. Till mechanics, in preparation I.

Tulaczyk, S., B. Kamb, and H. Engelhardt, Basal mechanics of Ice Stream B, West Antarctic*a.* III. Undrained-plastic-bed model, in preparation III.

Tulaczyk, S., B. Kamb, H. Engelhardt, and R.P. Scherer, Sedimentary processes beneath a West Antarctic ice stream; constraints from textural and compositional properties of subglacial debris, *J. Sediment. Res.*, 68, 487-496, 1998.

Turcotte, D.L., and Schubert, G., *Geodynamics; Applications of continuum physics to geological problems*, Wiley, New York, 1982.

Walder, J.S., and A. Fowler, Channelized subglacial drainage over a deformable bed, *J. Glaciol.*, 40, 3-15, 1994.

Weast, R.C., *CRC Handbook of chemistry and physics*, CRC Press, Boca Raton, Florida, 1987.

Weertman, J., General theory of water flow at the base of a glacier or ice sheet: *Rev.*

Geophys. Space Phys., 10, 287-333, 1972.

Weertman, J., and Birchfield, G.E., Subglacial water flow under ice streams and West Antarctic ice-sheet stability: *Ann. Glaciol.*, 3, 316-320, 1982.

Whillans, I.M., and C.J. van der Veen, New and improved determinations of velocity of Ice Streams B and C, West Antarctica, *J. Glaciol.*, 39, 483-490, 1993.

Table 1. Void Ratio/Porosity of the UpB Sediment Cores.

Depth[1] [m]	89-4[2] e/n_p	89-7 e/n_p	89-8 e/n_p	92-1 e/n_p	95-1 e/n_p	95-4[3] e/n_p	95-5-1[4] e/n_p	95-5-2[4] e/n_p	95-5-3[4] e/n_p	95-6 e/n_p	95-7 e/n_p	95-8 e/n_p
0	.672/.402	.678/.404	.565/.361	.472/.32[5]	.610/.379		.721/.419	.848/.459	.701/.412	.684/.406	.637/.389	.715/.417
0.05						.623/.384						
0.10						x[6]						
0.15				.845/.458		x					.626/.385	
0.20						x						
0.25						x		.661/.398		.675/.403		
0.30			.582/.368			x		x[6]		x[6]		
0.35		.684/.406			.647/.393	x		x		x		
0.40						x	.757/.431	x	.626/.385	x		.631/.387
0.45				.938/.484		x		x		x		x[5]
0.50						x		x	x[6]	x	.597/.374	x
0.55						x		x	x	x		x
0.60	.582/.368					x		x	x	x		x
0.65			.578/.366			x	.783/.439	x	x	x		x
0.70		.733/.423			.656/.396	x		x	x	x		x
0.75						x	.802/.445	x	x	x		x
0.80				.621/.383		x	x[6]	x	x	x		x
0.85						x	x	x	x	x	.634/.388	x
0.90						x	x	x	x	x	x[6]	x
0.95			.563/.360			x	x	x	x	x	x	x
1.00			x[6]			x	x	x	x	x	x	x
1.05		.608/.378[7]	x		.621/.383	x	x	x	x	x	x	x
1.10	.603/.376		x	.608/.378		x	x	x	x	x	x	x
1.15			x			x	x	x	x	x	x	x
1.20			x			x	x	x	x	x	x	x
1.25			x			x	x	x	x	x	x	x
1.30			x			x	x	x	x	x	x	x
1.35			x			x	x	x	x	x	x	x
1.40		.764/.433	x		.634/.388	x	x	x	x	x	x	x
1.45			x	.621/.383		x	x	x	x	x	x	x
1.50			x			x	x	x	x	x	x	x
1.55			x			x	x	x	x	x	x	x
1.60			x			x	x	x	x	x	x	x
1.65			x			x	x	x	x	x	x	x
1.70	.692/.409		x			x	x	x	x	x	x	x
1.75		.704/.413	x	.658/.397	.610/.379	x	x	x	x	x	x	x
1.80			x			x	x	x	x	x	x	x
1.85			x			x	x	x	x	x	x	x
1.90	x[6]		x			x	x	x	x	x	x	x
1.95	x		x			x	x	x	x	x	x	x
2.00	x		x			x	x	x	x	x	x	x
2.05	x		x			x	x	x	x	x	x	x
2.10	x	.590/.371	x	.585/.369	.658/.397	x	x	x	x	x	x	x
2.15	x		x			x	x	x	x	x	x	x
2.20	x		x			x	x	x	x	x	x	x
2.25	x		x			x	x	x	x	x	x	x
2.30	x		x			x	x	x	x	x	x	x
2.35	x		x			x	x	x	x	x	x	x
2.40	x		x	.626/.385		x	x	x	x	x	x	x
2.45	x	.656/.396	x	x[6]	.715/.417	x	x	x	x	x	x	x
2.50	x		x	x		x	x	x	x	x	x	x
2.55	x		x	x		x	x	x	x	x	x	x
2.60	x		x	x		x	x	x	x	x	x	x
2.65	x		x	x		x	x	x	x	x	x	x
2.70	x		x	x		x	x	x	x	x	x	x
2.75	x		x	x		x	x	x	x	x	x	x
2.80	x	.634/.388	x	x	.506/.336[5]	x	x	x	x	x	x	x
2.85	x	x[6]	x	x		x	x	x	x	x	x	x
2.90	x	x	x	x		x	x	x	x	x	x	x
2.95	x	x	x	x	.639/.390	x	x	x	x	x	x	x
3.00	x	x	x	x	x[6]	x	x	x	x	x	x	x

[1] Depth below the core top rounded off to the nearest 0.05 m.

[2] Measured by H. Engelhardt (personal communication).

[3] This till sample was found stuck to the borehole torvane after the latter was retrieved from the borehole 95-4. The sample was stored in a closed glass jar for two months before the water content was measured.

[4] Three short cores were recovered from the borehole 95-5.

[5] These values are considered unreliable and are not used in the subsequent data analysis. They were measured on samples which were exposed to air and have shown signs of drying.

[6] Core bottom.

Table 2. Reference Void Ratio (at σ'_n of 1 kPa) and Till Compressibility in Normally-Consolidated and Overconsolidated State, C_c and C_s Respectively

Consolidation Tests	e_o	C_c	C_s
C1	0.800	0.155	-
C2	0.854	0.178	-
C3	0.743	0.130	0.025
C4	0.787	0.147	0.023
C5	0.741	0.123	-
C6	0.861	0.174	0.014
Mean	0.797	0.151	0.021
Standard Error	0.023	0.009	0.004

Figure 1. Void ratio and porosity in the UpB till cores plotted against the depth below the core top (Table 1). Data points for the three longest cores, 89-7, 92-1, and 95-1, are connected with solid lines.

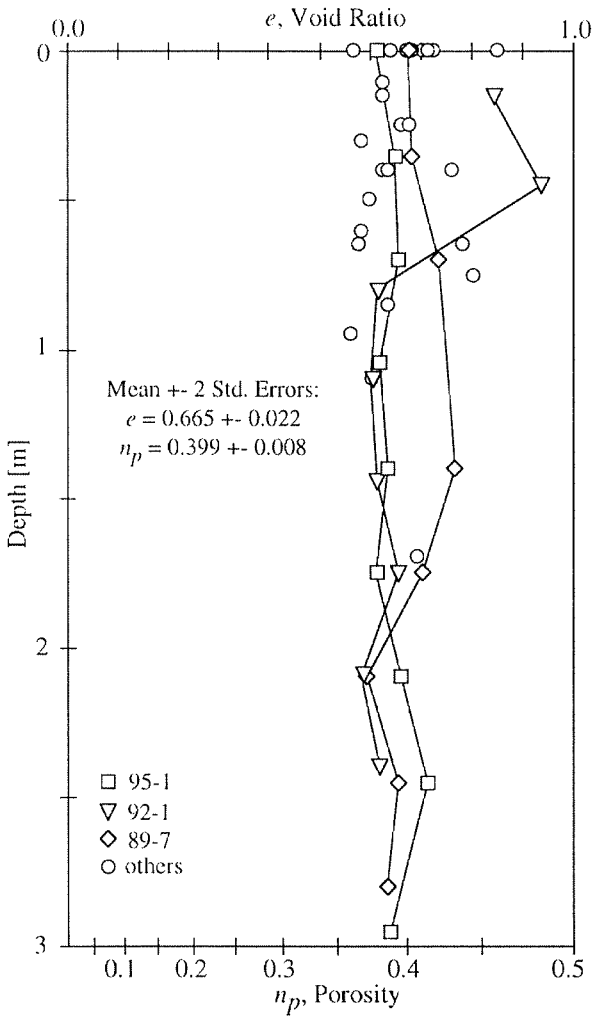
e, Void Ratio
0.0
1.0
0
1
2
3
Depth [m]
Mean +- 2 Std. Errors:
e = 0.665 +- 0.022
n_p = 0.399 +- 0.008
95-1
92-1
89-7
others
0.1
0.2
0.3
0.4
0.5
n_p, Porosity

Figure 2. (A) Four oedometer tests on samples from core 89-4 which were subjected to affective stresses between 25 and 400 kPa. The symbol e_{ini} designates initial till void ratio (all data collected by Engelhardt). The best-fit line whose equation is given at the top of the diagram represents the normal-consolidation line. (B) Control test, C1, in which a remolded sample of the UpB till was first preconsolidated to 53 kPa, then completely unloaded, and again reloaded starting at initial stress level of 4.5 kPa. Open circles denote the data collected when the sample was in its preconsolidated state and solid circles show sample's behavior in normal consolidation. Actual preconsolidation pressure, and the preconsolidation pressure estimates made using the graphical method of Casagrande [1936] and equations (3) and (4) are denoted by: σ'_p, σ'_{pC}, σ'_{NC}, σ'_{OC}, respectively. (C) In this test, C2, a remolded sample of the till was also preconsolidated to 53 kPa and then completely unloaded. However, before reloading, this sample was thoroughly remolded by hand without adding any extra water. (D) In the test C3 an unremolded till sample from core 95-1 was allowed to dry for four hours at room temperature (*ca.* 22°C) before being loaded to stresses between 4.5 kPa and 568 kPa in an oedometer. Open triangles illustrate the behavior of till samples in unloading and reloading. Diagrams (E) and (F) show the results of oedometer tests C4 and C5 which were performed on unremolded and untreated till samples from cores 95-5-1 and 95-1, starting at low effective stresses, 2.25 kPa and 4.5 kPa respectively.

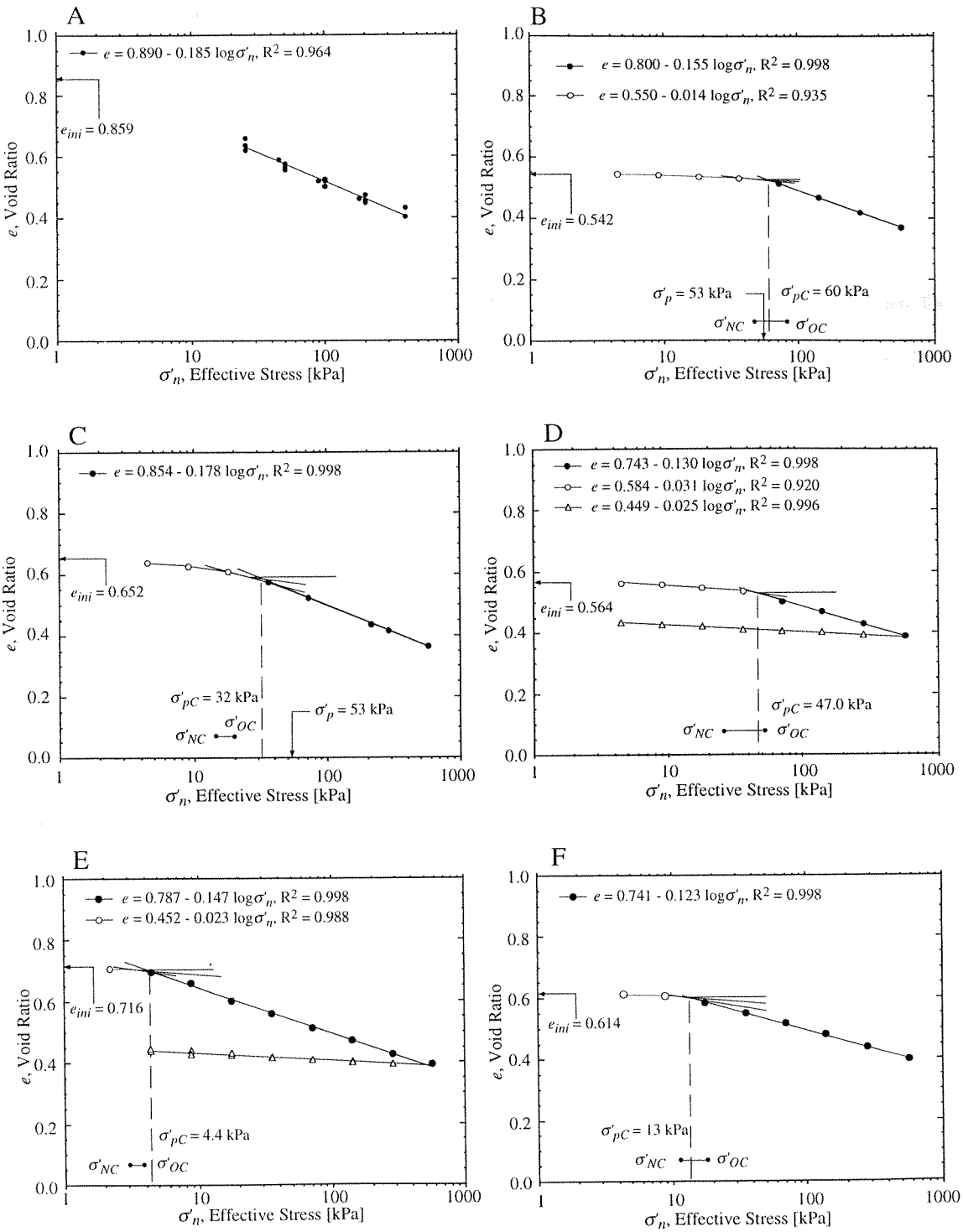
A
e = 0.890 - 0.185 log σ'n, R2 = 0.964
eini = 0.859
e, Void Ratio
σ'n, Effective Stress [kPa]
B
e = 0.800 - 0.155 log σ'n, R2 = 0.998
e = 0.550 - 0.014 log σ'n, R2 = 0.935
eini = 0.542
σ'p = 53 kPa
σ'pC = 60 kPa
σ'NC
σ'OC
C
e = 0.854 - 0.178 log σ'n, R2 = 0.998
eini = 0.652
σ'pC = 32 kPa
σ'OC
σ'NC
σ'p = 53 kPa
D
e = 0.743 - 0.130 log σ'n, R2 = 0.998
e = 0.584 - 0.031 log σ'n, R2 = 0.920
e = 0.449 - 0.025 log σ'n, R2 = 0.996
eini = 0.564
σ'pC = 47.0 kPa
σ'NC
σ'OC
E
e = 0.787 - 0.147 log σ'n, R2 = 0.998
e = 0.452 - 0.023 log σ'n, R2 = 0.988
eini = 0.716
σ'pC = 4.4 kPa
σ'NC
σ'OC
F
e = 0.741 - 0.123 log σ'n, R2 = 0.998
eini = 0.614
σ'pC = 13 kPa
σ'NC
σ'OC

Figure 3. Preconsolidation stresses estimated using equations (3) and (4) from the till water content data given in Table 1 and Figure 1. For comparison, we show also two estimates of the average subglacial effective stress made from seismic data and borehole measurements of water level [Blankenship *et al.*, 1987; Engelhardt and Kamb, 1997]. The confidence interval for the mean average effective stress calculated from till water content is given as ± two standard errors of the mean. In the case of the average effective stress derived from borehole water level measurements we add to the two standard errors of the mean a range of ± 30 kPa of uncertainty estimated by Kamb and Engelhardt [1997, p. 213]. The confidence interval given by Blankenship *et al.* [1987], 10 to 90 kPa, is based on their evaluation of the uncertainties arising from the use of different empirical equations to calculate effective stress from shear-wave velocities.

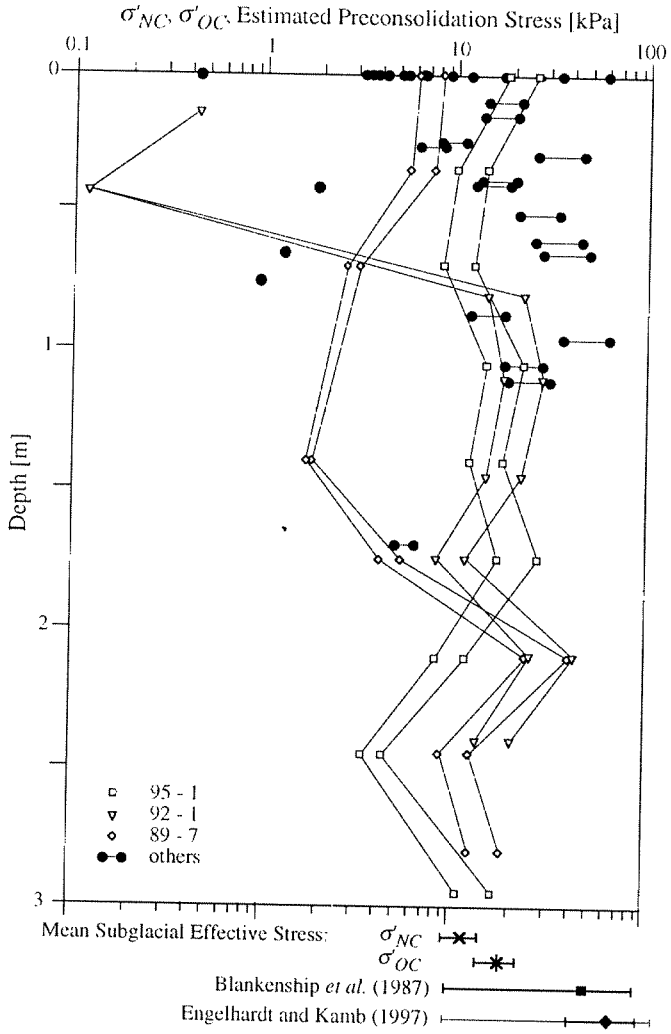
σ'_{NC}, σ'_{OC}, Estimated Preconsolidation Stress [kPa]
0.1
1
10
100
0
1
2
3
Depth [m]
95 - 1
92 - 1
89 - 7
others
Mean Subglacial Effective Stress:
σ'_{NC}
σ'_{OC}
Blankenship *et al.* (1987)
Engelhardt and Kamb (1997)

Figure 4. (A) Hydraulic conductivity, k_h, and hydraulic diffusivity, c_v, of the UpB till as a function of effective stress. These values were calculated with the method described by Bowles [1992, p. 129-154] using the consolidation data obtained during the initial loading sequence of test C4 (Figure 2E). (B) Vertical infiltration or seepage rates (thick solid line) calculated from the simple, centerline model of the groundwater system beneath Ice Stream B, equation (6). The origin of the horizontal axis (x = 0) is located in the approximate area of the onset of Ice Stream B. The thin solid line (calculated from the polynomial given in the upper right corner) represents the best-fit approximation of the hydraulic head distribution derived from ice-surface elevation data [Lingle and Brown, 1987, Figure 2]. (C) Geometry of the subglacial groundwater system simulated using a two-dimensional finite-element model. The system domain has its origin (x = 0) at the ice divide and follows the centerline of Ice Stream B between x = 320 and 630 km and the centerline of the ice stream's drainage area between x = 0 and 320 km [Lingle and Brown, 1987, Figure 2]. The groundwater system consists of an upper unit with low hydraulic conductivity, the aquitard, and a lower unit with high hydraulic conductivity, the aquifer. The thin solid line shows the hydraulic head distribution estimated from ice-surface elevation data [Lingle and Brown, 1987, Figure 2] for the top of the groundwater system. Diagram (D) gives the basal infiltration and seepage rates obtained from the finite-element model whose domain is depicted in (C).

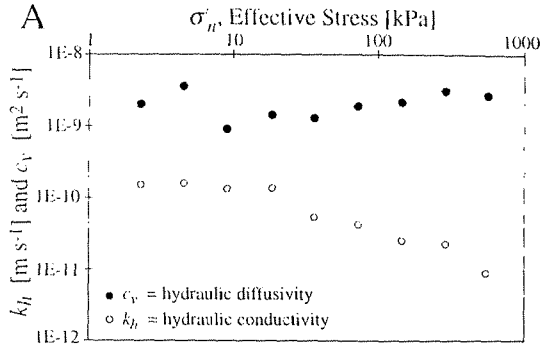
A
σ'_n, Effective Stress [kPa]
1
10
100
1000
1E-8
1E-9
1E-10
1E-11
1E-12
k_h [m s^{-1}] and c_v [m^2 s^{-1}]
c_v = hydraulic diffusivity
k_h = hydraulic conductivity

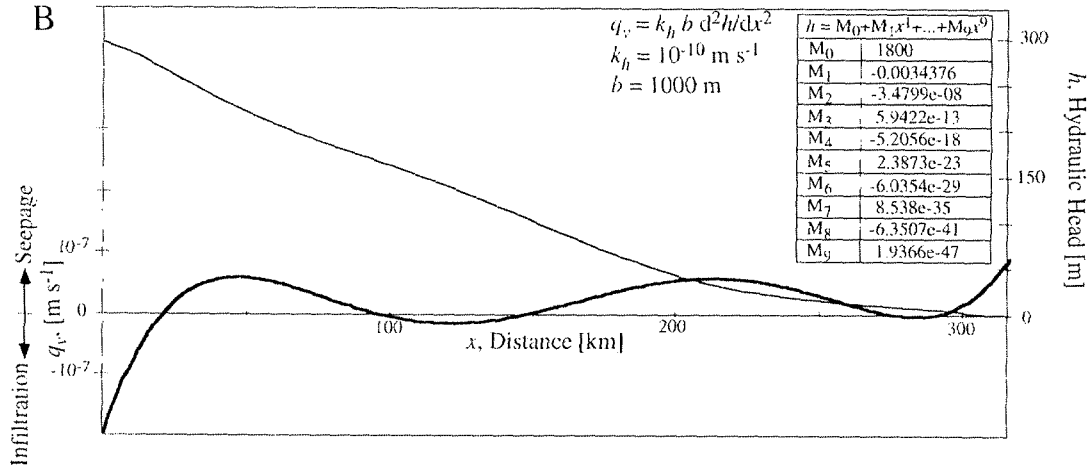
B
$q_v = k_h\, b\, d^2h/dx^2$
$k_h = 10^{-10}$ m s^{-1}
b = 1000 m
$h = M_0+M_1x^1+...+M_9x^9$
M0 1800
M1 -0.0034376
M2 -3.4799e-08
M3 5.9422e-13
M4 -5.2056e-18
M5 2.3873e-23
M6 -6.0354e-29
M7 8.538e-35
M8 -6.3507e-41
M9 1.9366e-47
300
150
0
h, Hydraulic Head [m]
Infiltration
Seepage
q_v, [m s^{-1}]
10^{-7}
0
-10^{-7}
100
200
300
x, Distance [km]

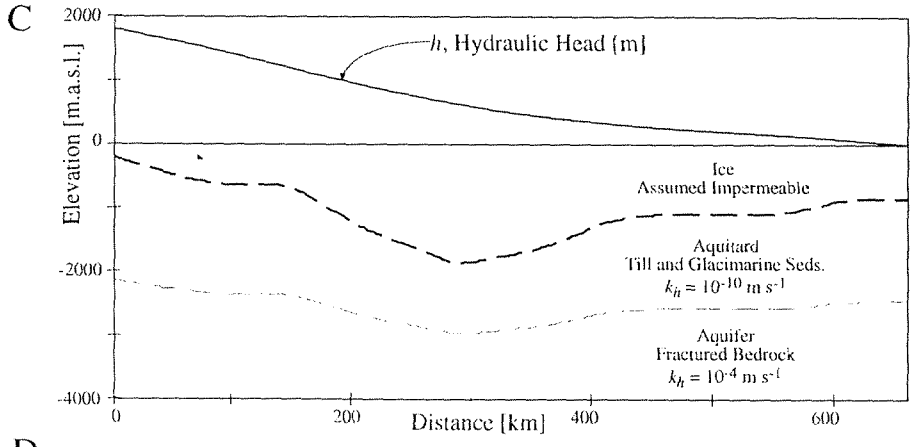
C
2000
0
-2000
-4000
Elevation [m.a.s.l.]
h, Hydraulic Head [m]
Ice
Assumed Impermeable
Aquitard
Till and Glacimarine Seds.
$k_h = 10^{-10}$ m s^{-1}
Aquifer
Fractured Bedrock
$k_h = 10^{-4}$ m s^{-1}
0
200
400
600
Distance [km]

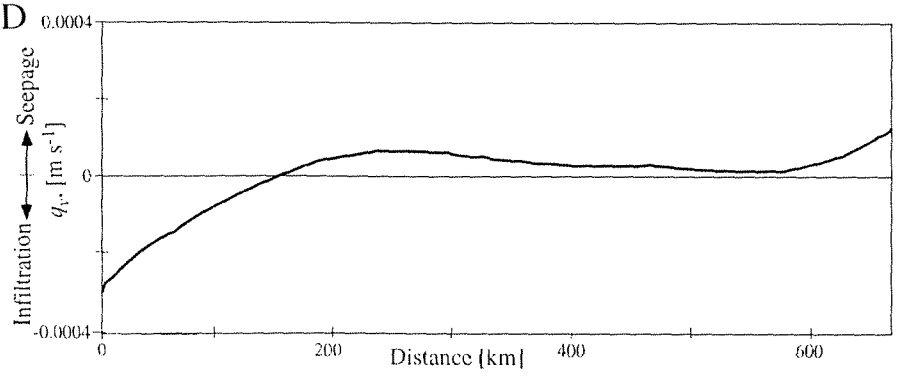
D
0.0004
0
-0.0004
Infiltration
Seepage
q_v, [m s^{-1}]
0
200
400
600
Distance [km]

Figure 5. A schematic cross section through a canal and one half of its drainage area perpendicular to the canal axis. The sketch is not to scale except for the basal hydraulic head distribution (solid curves) calculated with equation (11) for three different values of basal melting rate, m_r. The two dashed horizontal lines denote the hydraulic head levels under condition of flotation, H_f, and under the critical condition which may lead to canal collapse, H_c.

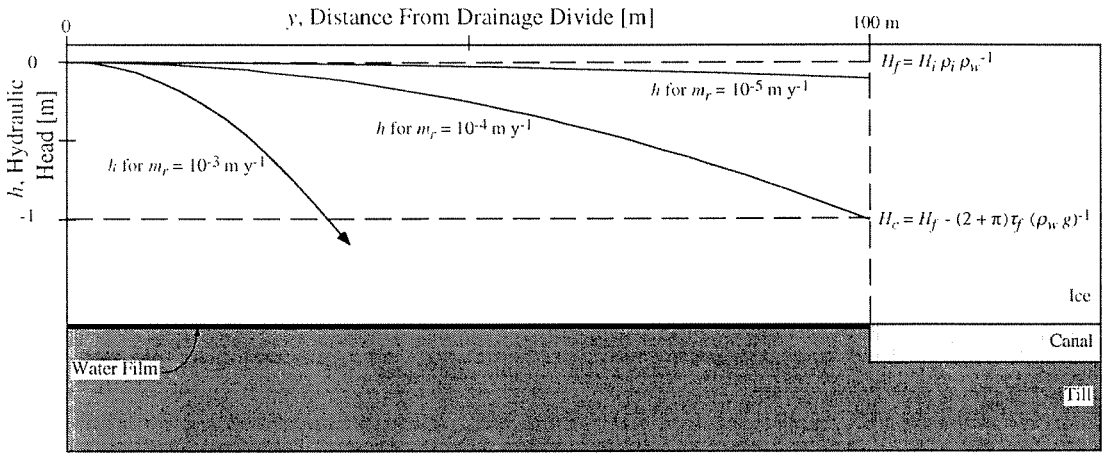
y, Distance From Drainage Divide [m]
0
100 m
0
-1
h, Hydraulic Head [m]
$H_f = H_i \rho_i \rho_w^{-1}$
h for $m_r = 10^{-5}$ m y^{-1}
h for $m_r = 10^{-4}$ m y^{-1}
h for $m_r = 10^{-3}$ m y^{-1}
$H_c = H_f - (2 + \pi)\tau_f (\rho_w g)^{-1}$
Ice
Canal
Water Film
Till

Figure 6. (A) Dependence of the basal melting rate at UpB on the geothermal flux (equation (12)). (B) Empirical relationship between the undrained strength of the UpB till, τ_f, and the till void ratio, e. The thick solid line and the equation give the best-fit τ_f - e relationship derived from results of six undrained triaxial tests, R1, R2, R3, U1, U2, U3 [Tulaczyk *et al.*, in preparation I]. The data from four torvane strength tests on undisturbed samples of the UpB till, solid squares, and from 16 shear box tests, open square [Kamb, 1991], are used as an independent check on the best-fit relationship.

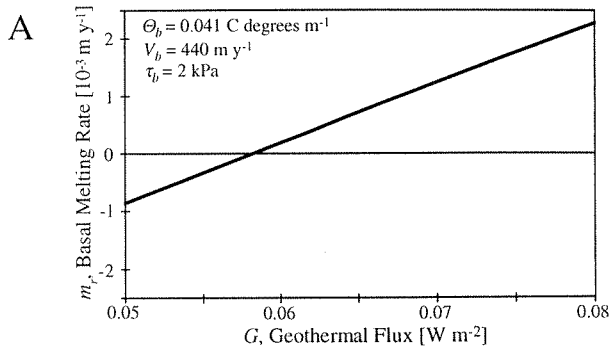
A
Θ_b = 0.041 C degrees m^{-1}
V_b = 440 m y^{-1}
τ_b = 2 kPa
m_r, Basal Melting Rate [10^{-3} m y^{-1}]
2
1
0
-1
-2
0.05
0.06
0.07
0.08
G, Geothermal Flux [W m^{-2}]

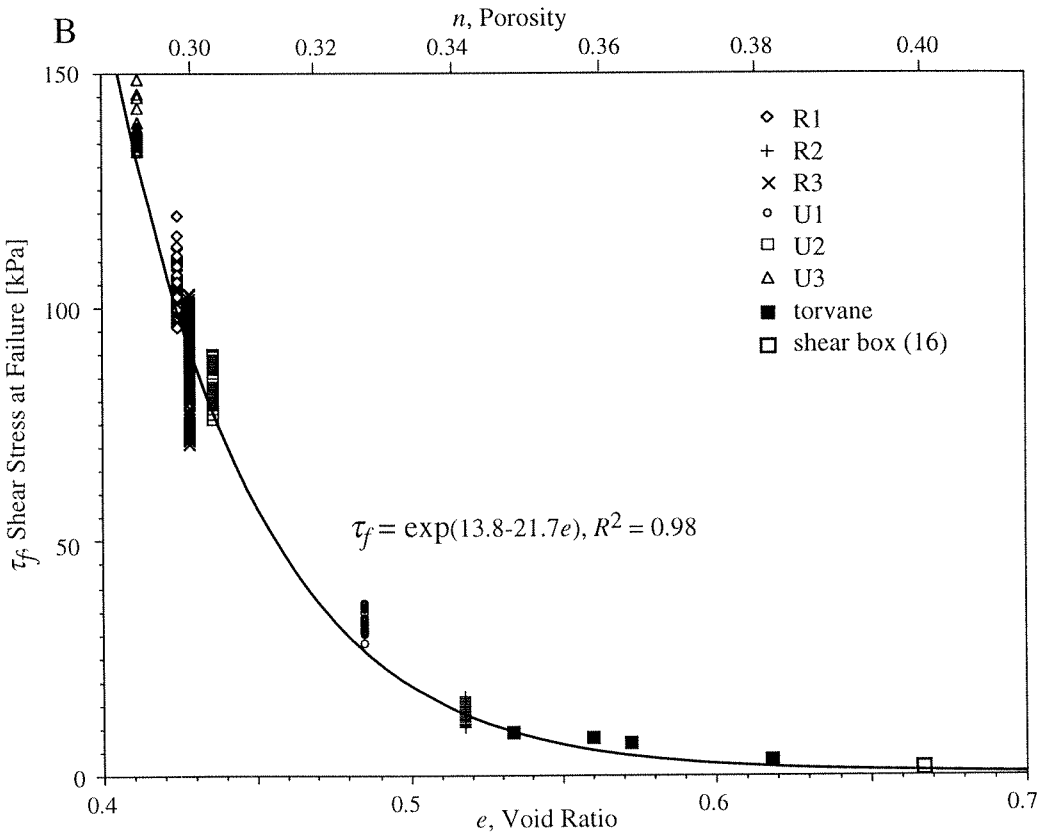
B
n, Porosity
0.30
0.32
0.34
0.36
0.38
0.40
150
100
50
0
τ_f, Shear Stress at Failure [kPa]
R1
R2
R3
U1
U2
U3
torvane
shear box (16)
τ_f = exp(13.8-21.7e), R^2 = 0.98
0.4
0.5
0.6
0.7
e, Void Ratio

Figure 7. (A) Sensitivity of the basal melting rate at UpB to void ratio and till strength (equations (12) and (14)). (B) Consolidation of a five-meter-thick till layer driven by a constant basal ice freeze-on rate of 10^{-3} m y^{-1}. This result is obtained by solving a one-dimensional version of the diffusion equation used to describe the process of consolidation [Scott, 1963, equation 5-43]. The till is assumed to have a constant hydraulic diffusivity of the order of that characteristic for the UpB till, i.e., c_v of 10^{-8} m^2 s^{-1} (Figure 4A). Lower boundary condition is a no-flow condition at z = 5 m, and the initial distribution of the effective stress is assumed to be hydrostatic with the hydrostatic stress gradient equal to 10 kPa m^{-1}.

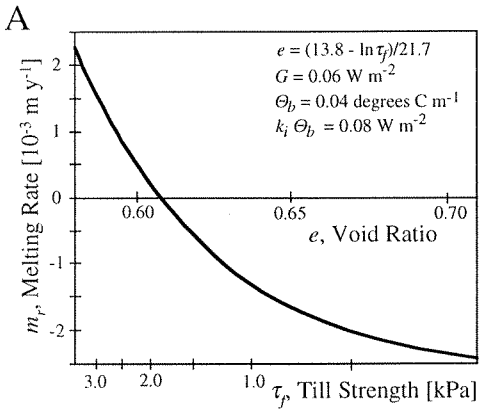
A
$e = (13.8 - \ln\tau_f)/21.7$
$G = 0.06$ W m^{-2}
$\Theta_b = 0.04$ degrees C m^{-1}
$k_i\,\Theta_b = 0.08$ W m^{-2}
m_r, Melting Rate [10^{-3} m y^{-1}]
2
1
0
-1
-2
0.60
0.65
0.70
e, Void Ratio
3.0
2.0
1.0
τ_f, Till Strength [kPa]

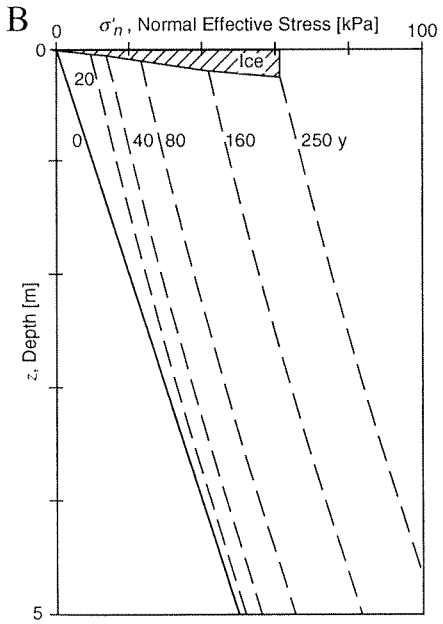
B
0
σ'_n, Normal Effective Stress [kPa]
100
0
Ice
20
0
40
80
160
250 y
z, Depth [m]
5

CHAPTER 6

Basal Mechanics of Ice Stream B, West Antarctica. III. Undrained-Plastic-Bed Model

Slawek Tulaczyk, Barclay Kamb, Hermann Engelhardt

Division of Geological and Planetary Sciences, California Institute of Technology, Pasadena, CA 91125

Abstract

Based on the results of our studies of the physical conditions beneath Ice Stream B, we formulate a new analytical ice-stream model, the undrained-plastic-bed model (henceforth the UPB model). Mathematically, the UPB model is represented by a non-linear system of four coupled equations which express the interrelationships among ice sliding velocity, till strength, water storage in till, and basal melting rate. The salient feature of the UPB model is its ability to produce two thermo-mechanically-controlled equilibrium states, one with a strong bed and slow ice velocities ('ice-sheet' mode) and one with a weak bed and fast ice velocities ('ice-stream' mode). This bimodality of basal conditions predicted by our model is consistent with the available observations of subglacial conditions beneath slow and fast moving ice in West Antarctica. Basal conditions that do not correspond to these two steady-states may occur transiently during switches between the two stable modes. The UPB model demonstrates that ice streams may be prone to thermally-triggered instabilities, during which small perturbations in the basal thermal energy balance grow, leading to generation or elimination of the basal

conditions which cause ice streaming. Use of the UPB model to verify the hypothesis that the West Antarctic Ice Sheet may become unstable in the near future will be possible if the present-day thermal state of these ice masses is observationally constrained.

6.1. Introduction

Studies of modern West Antarctic ice streams show that fast ice streaming is caused by an efficient basal lubricant, a weak basal till [Alley *et al.*, 1986, 1987ab; Blankenship *et al.*, 1986, 1987; Engelhardt and Kamb, 1997; Engelhardt *et al.*, 1990; Kamb, 1991]. Because of this weakness of the bed a significant part of the gravitational driving stress appears to be borne by ice stream margins [Echelmeyer *et al.*, 1994; Jackson and Kamb, 1997; Raymond, 1996; van der Veen and Whillans, 1996; Whillans and van der Veen, 1997]. The Pleistocene geologic record also suggests that ice streaming took place predominantly where lubrication by weak till was available [Alley and MacAyeal, 1994; Clark, 1992; Marshall *et al.*, 1996]. Thus, the temporal and spatial patterns of slow (sheet-like) and fast (stream-like) ice motion are governed by the subglacial ice-till-water system, which couples geological, glaciological, and hydrological factors and processes. Recent advances have contributed significantly to our understanding of this complex system [Alley *et al.*, 1986; 1987ab, 1989; Anandakrishnan and Bentley, 1993; Blankenship *et al.*, 1986, 1987; Boulton, 1996; Clark and Walder, 1994; Clarke, 1987; Echelmeyer *et al.*, 1994; Jackson and Kamb, 1997; Kamb, 1991; MacAyeal, 1992; Raymond, 1996; Walder and Fowler, 1994]. Despite these exciting developments several fundamental questions of modern glaciology remain: 1) what factors decide where and when basal lubrication and associated ice streaming appear? 2) once active, how fast and in what fashion do ice streams evolve? 3) what processes bring an end to ice stream activity? The physics which govern this complex ice stream system needs to be resolved and included in a realistic ice-

stream model which can be used for reliable predictions of ice-stream and ice-sheet behavior. The need for such reliable predictions is quite clear. Fast-moving ice streams have a primary control over the mass balance of the West Antarctic Ice Sheet whose stability needs to be investigated because of the existing concerns that this ice sheet could increase the near-future global sea-level rise [Bentley, 1987, 1997; Bindschadler, 1997]. Ice streams are also presumed to have caused significant fluctuations in volume and extent of the Pleistocene ice sheets [Alley, 1991; Clark, 1992: MacAyeal, 1993ab]. Moreover, ice sheets affected by large ice streams may have provided a pacemaker for regional/global climatic changes [Hughes, 1996; MacAyeal, 1993ab].

In this manuscript we propose a new ice-stream model. The model is based on the results of borehole and laboratory investigations of the physical conditions beneath Ice Stream B near the UpB camp [Engelhardt *et al.*, 1990; Engelhardt and Kamb, 1993, 1997, in press; Kamb, 1991; Kamb and Engelhardt, 1991; Tulaczyk *et al.*, 1998; Tulaczyk *et al.*, in preparation, I and II]. This new model encapsulates relatively complex interactions between subglacial processes in a small number of equations and reveals the conditions for ice stream stability and evolution.

6.2. Undrained-Plastic-Bed Model

Our choice of the equations describing the most important subglacial processes which need to be included in a model of a sub-ice-stream bed is largely based on the data and physical arguments developed previously in Tulaczyk *et al.* [in preparation, I and II]. In fact, the model discussed here represents simply a generalization of the undrained-bed model developed in Tulaczyk *et al.* [in preparation, II]. There, feedbacks between the basal melting rate, till void ratio, and till strength were expressed with the following three equations:

$$m_r = (\tau_b U_b + G - k_i \Theta_b) (L_i \rho_i)^{-1} \quad (1a)$$

where m_r is the basal melting rate, τ_b is the basal shear stress, U_b is the basal sliding velocity, G is the geothermal flux, $k_i = 2.1$ W m^{-1} °C^{-1} is the thermal conductivity of ice, Θ_b is the basal temperature gradient, $L_i = 333.5$ kJ kg^{-1} is the latent heat of ice fusion and $\rho_i \cong$ 900 kg m^{-3} is the ice density;

$$de/dt = m_r/Z_s \quad (1b)$$

where e is the till void ratio, t is the time variable and Z_s is the thickness of subglacial till expressed as the thickness of pure till solids, i.e., thickness of the till layer assuming zero void ratio;

$$\tau_f = \exp(a - be) \quad (1c)$$

where τ_f is the failure strength of till in kPa, e is the void ratio expressed with a decimal fraction, and $a \cong 13.8$ and $b \cong 21.7$ are experimentally-constrained coefficients [Tulaczyk *et al.*, in preparation II, Figure 6B].

The only element that is now needed to make the whole ice-stream model physically self-contained is the relationship between ice stream velocity and till strength. Here, we make the assumption that till strength determines basal resistance to ice stream motion, i.e., till strength equals the basal shear stress, $\tau_f = \tau_b$. Because laboratory tests on samples of the UpB till show that the rheology of this material is plastic [Kamb, 1991; Tulaczyk *et al.*, in preparation I], we have to forego use of any ice sliding law which is based on the assumption that there is a direct, linear or mildly non-linear relationship between sliding velocity and basal stress. Thus, any form of the commonly used 'sliding law' $U_b = k\ \tau_b^m\ \sigma'^{-p}_n$ relating sliding velocity, U_b, to basal stress, τ_b, and effective stress, σ'_n, is not suitable (k, m, p are empirical constants) [Bentley, 1987, table 1]. Raymond [1996, p. 100] has derived an equation giving the velocity of an ice stream moving in a rectangular channel with a homogenous till bed having everywhere velocity-independent strength $\tau_f = \tau_b$:

$$U_b = (1 - \tau_b/\tau_d)^n\ W^{n+1}\ U_d \quad (1d)$$

where $\tau_d = \rho_i\, g\, H_i \sin \alpha_s$ is the driving stress (g = 9.8 m s^{-2} is the acceleration of gravity, H_i is the ice thickness and α_s is the ice surface slope), W is the ice stream half-width given in multiples of ice thickness, and $U_d = 2^{1-n}\, \tau_d^n\, H_i\, (n+1)^{-1}\, B^{-n}$ is the calculated surface velocity for ice moving purely by internal ice deformation with basal shear stress $\tau_b = \tau_d$ (n, B, are the ice flow-law constants [Raymond, 1996, equation (7)]). For simplicity we have assumed that the whole ice stream moves with the centerline velocity [see Echelmeyer *et al.*, 1994].

Figure 1A shows an example of the dependence of ice stream velocity on the bed strength, τ_b, and the ice stream half-width, W, assuming driving stress of 13 kPa, ice stream thickness of 1,000 meters, and standard parameters for the ice flow law: n equal to 3 and $2^{1-n}\,(n+1)^{-1}B^{-n}$ equal to 1.45×10^{-16} (s kPa)$^{-3}$ for ice temperature of -15°C [Engelhardt and Kamb, 1993; Patterson, 1994, p. 97]. This diagram illustrates the major features of equation (1d) in which ice stream velocity is determined by partitioning the support of the gravitational driving stress into two components: 1) the basal shear stress, and 2) the marginal shear stress which is incorporated into equation (1d) as $(\tau_d - \tau_b)$. In this approach, the weaker the bed gets the more of the gravitational stress has to be supported by ice deformation in the ice stream shear margins. This requires higher marginal shear strain rates and higher ice stream velocities [Echelmeyer *et al.*, 1994; Jackson and Kamb, 1997; Raymond, 1996; Whillans and van der Veen, 1997]. The maximum ice stream velocity for a given half-width and gravitational driving stress occurs when the bed strength is equal to zero (Figure 1A). On the other hand, when bed strength is equal to the driving stress, the sliding component of ice stream velocity, U_b, is equal to zero. Qualitatively, this is an expected behavior because when bed strength is larger than the driving stress, the ice bed becomes rigid and the mechanism of enhanced basal sliding due to till deformation cannot operate. Instead, ice moves only by internal deformation which under the low

gravitational driving stress typical for ice streams results in very slow ice surface motion, of the order of 1.0 m y^{-1}, much smaller than ice streaming velocities of order 100 m y^{-1}.

To verify whether the mechanical ice-stream model represented by equation (1d) is capable of reproducing the observed velocities of Ice Stream B, we have calculated velocity vs. bed-strength curves for four selected cross sections of this ice stream and compared them with observed velocities (Figure 1B) [Bindschadler *et al.*, 1987; Shabtaie *et al.*, 1987; Whillans and van der Veen, 1993]. The predicted and observed velocities agree quite well provided that the bed beneath all of the four considered cross sections is as weak as the bed beneath the UpB area of Ice Stream B, i.e., τ_b of a few kPa [Echelmeyer *et al.*, 1994; Kamb, 1991; Tulaczyk *et al.*, in preparation II]. This general agreement is especially remarkable if one considers the simplicity of equation (1d), with no adjustable parameters such as an enhancement factor in the ice-flow law [Echelmeyer *et al.*, 1994; Jackson and Kamb, 1997]. Given this general agreement, we conclude that the plastic-bed model of ice stream motion expressed by equation (1d) captures the first-order aspects of the dependence of ice stream velocity on the bed strength. In subsequent sections, we couple this plastic-bed model of ice stream mechanics to the undrained-bed model formulated by Tulaczyk *et al.* [in preparation II] and analyze the properties of this coupled system (equations (1a), (1b), (1c) and (1d)).

6.3. Conditions for Ice Stream Stability

Previously [Tulaczyk *et al.*, in preparation II], we have shown that under undrained conditions a sub-ice-stream till bed will adjust into a steady-state in which the till is weak enough so that the shear-heating term in equation (1a) is small and the steady-state melting rate, m_r, is equal to zero. However, a major limitation of the previous model was the fact that it did not include an expression for ice stream velocity as a function of till strength.

Rather, we had to rely on an assumption that the adjustments in till strength are small enough so that ice stream velocity may be considered unperturbed by them. Inclusion of equation (1d) in the current model removes the need for such an assumption and permits analysis of the dependence of the basal melting rate on bed strength over the whole range of bed strengths possible beneath an active ice stream, i.e., $0 \leq \tau_b \leq \tau_d$. This is done by substituting equation (1d) for U_b in equation (1a). Clearly, the new equation has only one independent variable and two adjustable parameters, the geothermal flux, G, and the basal ice temperature gradient, Θ_b.

Figure 2A illustrates the nature of the dependence of the basal melting rate on till strength, calculated using equations (1a) and (1d) with the basal gradient measured at UpB, *ca.* 0.04°C m^{-1} [Engelhardt and Kamb, 1993] and three assumed values of the geothermal flux, 0.04, 0.06, 0.08 W m^{-2}. The shape of the m_r - τ_b curves is always the same because it is always determined by the shear heating term $\tau_b\ U_b$ in equation (1a). The difference between the two other thermal energy terms in equation (1a), i.e., G - $k_i\Theta_b$, determines the vertical offset of these curves. Analysis of the shear heating function $\tau_b\ U_b$ shows that it reaches a maximum at the bed strength $\tau_b = (n+1)^{-1}\ \tau_d$, i.e., $\tau_b = 0.25\ \tau_d$ for n =3. To the left of this maximum, shear heating drops off because the bed strength falls towards zero and the corresponding increase in ice stream velocity is not fast enough to counteract this fall. To the right of the maximum, shear heating also drops off because the velocity decreases faster than the bed strength increases.

By substituting the term $\tau_b = (n+1)^{-1}\tau_d$ into equation (1a) we can show that the magnitude of the maximum shear heating is given by:

$$(\tau_b\ U_b)_{\max} = n\ (n+1)^{-1}\ W^{n+1}\ U_d\ \tau_d \qquad (2).$$

The fact that there is an upper bound on shear heating has an important implication because it means that the proposed condition for ice stream stability, i.e., melting rate equal to zero [Tulaczyk *et al.*, in preparation II], may be met only if the following is true:

$$G - k_i\Theta_b \geq -(\tau_b U_b)_{\max} \qquad (3).$$

In addition, shear heating cannot be a negative quantity. Inspection of equation (1a) shows that for the melting rate to be zero for at least one value of bed strength, τ_b, the following must hold:

$$G - k_i\Theta_b \leq 0 \qquad (4).$$

In polar ice masses the latter condition is likely to be generally met because prolonged shear heating and horizontal and vertical advection of cold ice during ice motion will tend to make the basal heat loss greater than the geothermal flux. The influence of ice flow on ice temperature gradient can be visualized if we first imagine a steady-state column of ice which does not experience any deformation. In this ice column the basal thermal gradient will have a constant value throughout and this value will adjust to make the conductive heat loss equal to the geothermal flux. Introduction of vertical thinning of ice into this hypothetical steady-state ice column is equivalent to compressing the temperature profile, i.e., to increasing the conductive heat flow away from the bed. Similarly, if horizontal ice flow brings colder ice from upstream, as it usually does, the basal thermal gradient will increase again.

Let us now concentrate on the case in which the two thermal conditions, equations (3) and (4), are fulfilled. With the exception of the case $(\tau_b U_b)_{\max} + G - k_i\Theta_b = 0$, there will always be two values of the bed strength for which the basal melting rate is zero (Figure 2A). This is a result which could not have been predicted with the simpler analysis of stability of the basal system performed in Tulaczyk *et al.* [in preparation II]. The result raises the question whether there are two stable equilibrium states in our undrained-plastic-bed model (henceforth the UPB model). This can be verified by performing a linear stability analysis on the system of the four coupled equations which constitute the UPB model, i.e., equations (1a), (1b), (1c), and (1d). Let us consider values of till void ratio, $e = e_o$, till strength, $\tau_b = \tau_o$, and ice stream velocity, $U_b = U_o$, for which the basal melting rate

is zero, $m_r = 0$. The problem then is to verify whether a small initial perturbation, for instance in till void ratio, Δe_{ini}, will grow or decay with time. If perturbations decay with time, then the system is in a stable equilibrium at $m_r = 0$; if they grow with time, then the equilibrium at $m_r = 0$ is only meta-stable.

We assume that over relatively short timescales of dozens of years, the magnitudes of the geothermal flux and the basal heat loss do not change with time. Therefore, time-dependence is introduced into the UPB model only through equation (1b). To apply a perturbation in till void ratio $\Delta e = e - e_o$ with an initial value Δe_{ini}, we rewrite equation (1b):

$$d\Delta e/dt = m_r/Z_s \qquad (5).$$

Our goal is now to express the basal melting rate m_r as a function of Δe and to find a time-dependent solution to this differential equation, $\Delta e(t)$. Since the perturbation in till void ratio is assumed to be small, we can find the resulting small changes in till strength, $\Delta\tau_b$, and ice stream velocity, ΔU_b, by linearizing equations (1c) and (1d):

$$\Delta\tau_b = \Delta e\, [d\tau_b/de]_{e_o} = - b\, \tau_o\, \Delta e \qquad (6a)$$

$$\Delta U_b = \Delta\tau_b\, [dU_b/d\tau_b]_{\tau_o} = - n\, U_o\, (\tau_d - \tau_o)^{-1} \Delta\tau_b = n\, b\, U_o\, \tau_o\, (\tau_d - \tau_o)^{-1}\, \Delta e \qquad (6b)$$

where the terms $[d\tau_b/de]_{e_o}$ and $[dU_b/d\tau_b]_{\tau_o}$ are used to denote derivatives of equations (1c) and (1d) evaluated at $e = e_o$ and $\tau_b = \tau_o$, respectively. These new expressions for $\Delta\tau_b$ and ΔU_b can be introduced into equation (5) through a modified version of equation (1a):

$$m_r = [(\tau_o + \Delta\tau_b)\, (U_o + \Delta U_b) + G - k_i\Theta_b\,]\, (L\, \rho_i)^{-1} \qquad (7).$$

After we eliminate one small term ($\Delta\tau_b\, \Delta U_b$) and take advantage of the fact that the term ($\tau_o\, U_o + G - k_i\Theta_b$) is, by assumption, equal to zero, the desired form of equation (5) emerges:

$$d\Delta e/dt = b\, (G - k_i\Theta_b)\, (\tau_d - (n+1)\tau_o)\, (\tau_d - \tau_o)^{-1}\, (L\, \rho_i\, Z_s)^{-1}\, \Delta e = C_1\, \Delta e \qquad (8)$$

where the constant C_1 is defined by (8). The time-dependent solution to this differential equation is:

$$\Delta e_{(t)} = \Delta e_{ini} \exp(C_1\, t) \qquad (9)$$

where the initial condition $\Delta e = \Delta e_{ini}$ at time $t = 0$ has been already imposed.

From the exponential form of equation (9), we can conclude that the equilibrium state at $m_r = 0$ is stable if and only if $C_l < 0$, so that perturbation decays with time. The system is metastable for $C_l > 0$ because in this case perturbations grow with time. Inspection of equation (8) reveals that the sign of C_l is opposite to the sign of the factor (τ_d - $(n + 1)\tau_o$). This is because $(G - k_i\Theta_b)$ is negative by inequality (4), (τ_d - τ_o) is positive if ice-stream-type motion occurs (equation (1d)), and all other constants are positive. We conclude that stable equilibrium in the UPB model occurs at $m_r = 0$ if and only if the till strength at which the basal melt is equal to zero is constrained in relation to the gravitational driving stress by:

$$\tau_o < (n + 1)^{-1} \tau_d \qquad (10).$$

For the commonly assumed value of the flow-law exponent $n = 3$ [Patterson, 1994, p. 94], this condition becomes: $\tau_o < 0.25\tau_d$.

Along with the sign of the constant C_l in equation (9), we are also interested in calculating the value of C_l because the magnitude of this constant determines the characteristic response time of the UPB model to perturbations. The e-folding time during which the initial perturbion Δe_{ini} will decay by the inverse of the base of natural logarithm, i.e., by 0.369, is given for equation (9) by C_l^{-1}. We calculate from (8) that this e-folding time is of the order of 10 years; assuming that the difference between the geothermal flux and the conductive heat loss $(G - k_i\Theta_b)$ is ~0.01 W m^{-2} [Tulaczyk *et al.*, in preparation II, Figure 7A], $b = 21.7$, $L = 333{,}500$ J kg^{-1}, $\rho_i \approx 900$ kg m^{-3}, $Z_s \approx 1$ m, and $\tau_o \approx 0.1\tau_d$ (which fulfills the stability condition (10)). Thus, if Ice Stream B is governed by the physics embedded in the UPB model, ice velocity transients caused by hypothetical perturbations in basal physical conditions should last less than several decades. Repeated observations within the main trunk of Ice Stream B indicate that its surface velocities are relatively constant over the period of several years [Whillans and van der Veen, 1993].

Using the condition (10) we show in Figure 2B the location of the stable and the metastable equilibrium along the ice stream velocity vs. bed-strength curve for the example of Ice Stream B at the UpB camp, considered above and in Figure 2A. Around the stable equilibrium, i.e., $m_r = 0$ and $\tau_o < 0.25\tau_d$, the UPB system exhibits a negative feedback which brings the bed conditions back to the steady-state. However, around the metastable equilibrium, $m_r = 0$ and $\tau_o > 0.25\tau_d$, there is positive feedback which will reinforce small perturbations, pushing the UPB system either towards the stable equilibrium or completely out of the range of the weak-bed state ($\tau_b < \tau_d$.) for which ice streaming occurs (equation (1d)).

The physical significance of the stability condition (equation (10)) is quite striking because this condition shows that a steady-state ice stream should have a weak till bed. Observations from drilling at the UpB camp on Ice Stream B are consistent with this stability condition. In addition, we have shown (Figure 1B) that ice stream velocities predicted with equation (1d) correspond to the high velocities observed on Ice Stream B only if the bed beneath other parts of this ice stream is also weak, i.e., a few kPa. Thus, the physics of the UPB model of ice stream motion agrees very well with the observational constraints available for Ice Stream B. In the near future, boreholes will be drilled by the Caltech glaciological group to the bed of Ice Stream D. This drilling program will offer the opportunity to verify the generality of the UPB model's prediction that till beds beneath ice streams have strength which is small compared to the driving stress.

Inspection of the UPB model (equations (1a), (1b), (1c), and (1d)) shows that in addition to the active, ice-stream mode, this model has a second stable mode, in which the ice base is undergoing freeze-on ($m_r < 0$), the strength of the till bed is greater than the driving stress, and ice moves slowly by internal deformation alone. We call this the 'ice-sheet' mode. Strictly speaking, both of these modes can be included explicitely into the

UPB model by modifying the ice-flow equation (1d) to include the basal sliding velocity component (U_b) and the velocity component due to internal ice deformation (U_{def}):

$$U_{ice} = U_b + U_{def} = [(1 - \tau_b/\tau_d)^n W^{n+1} U_d + 2^{1-n} \tau_b^n H_i (n+1)^{-1} B^{-n} \quad (11)$$

where U_{ice} is the ice surface velocity and all the other symbols have been previously explained (see equation (1d)). However, the sliding component U_b (where W is typically ~10) is significantly greater than the deformational component U_{def} for all values of τ_b but the ones very near τ_d ($\tau_b \approx 0.99\ \tau_d$). Thus, the modification shown in (11) does not change significantly the physics of the UPB model. Basal states between the ice-stream and ice-sheet modes can be achieved only transiently when the system migrates from one of the two steady-states to the other. Within the physical framework of the UPB model such switches between the two modes may be achieved by changing the basal conductive heat loss ($k_i \Theta_b$). This may force the m_r - τ_b curve (e.g., Figure 2A) to move completely below or above the line $m_r = 0$. If the m_r - τ_b curve for an active ice stream migrates completely below this line, i.e., basal freeze-on occurs for all admissible combinations of τ_b and U_b, then the ice-stream mode will be replaced by the ice sheet mode. If the sytem is in the ice-sheet mode and the m_r - τ_b curve will migrate above the $m_r = 0$ line, i.e., basal melting will turn on, then the system will gradually switch to the ice stream mode.

The two modes inferred from the physics of the UPB model correspond well to the previous glaciological inferences made in West Antarctica where fast ice-stream motion (~ 100 m y^{-1}) over a presumably weak till bed occurs adjacent to slow ice-sheet motion (~ 1 m y^{-1}) over a presumably strong bed. Our model offers a physical explanation for why such a pattern of contrasting basal conditions and contrasting ice velocities may develop.

A third stable mode can be inferred from the UPB model. This mode arises when the condition specified by inequality (4), i.e., $G - k_i\Theta_b \leq 0$, is relaxed. As mentioned before, if the geothermal flux is greater than the conductive heat loss, then the basal thermal energy balance is always positive because shear heating is a positive quantity. Therefore,

only a basal melting rate greater than zero is possible under these conditions. When the basal melting rate is always positive, till weakening driven by $m_r > 0$ will inevitably move the UPB system towards an extremely water-rich till whose strength will be zero (equations (1b) and (1c)). Such till is possible only when the subglacial effective stress is zero, i.e., when the ice weight is borne entirely by the pore pressure. With bed strength equal to zero, the ice-stream velocity will take on the maximum value given by equation (1d) for $\tau_b = 0$. This stable mode can be called an 'ice-shelf-like' mode because of the condition $\tau_b = 0$ and because of the inference that the ice in this mode would be practically afloat, i.e., subglacial pore pressure would equal the ice overburden pressure [Patterson, 1994, p. 290-301]. As we have suggested in the statement following inequality (4), the condition necessary for occurrence of the ice-shelf-like mode, i.e., $G - k_i\Theta_b > 0$, is not likely to be fulfilled. However, special circumstances, e.g., rapid enough increase in geothermal flux along an ice-stream flow path, under which this condition could be true, cannot be excluded. From an ice-stream dynamics point of view, there is a relatively small difference between this ice-shelf-like mode, $\tau_b = 0$, and the 'ice-stream' mode, $0 < \tau_b = \tau_o < 0.25\ \tau_d$, because in both cases the velocities of ice motion predicted with equation (1d) are similarly high, e.g., for $n = 3$ the steady-state velocity in the 'ice-stream' mode is between 42% and 100% of the velocity in the 'ice-shelf-like' mode. Pending new data which could verify whether the condition $G - k_i\Theta_b > 0$ is realistic for the West Antarctic ice streams, we propose that the steady-state of these ice streams corresponds to the 'ice-stream' mode of the UPB model.

6.4. Near-Future Evolution of the West Antarctic Ice Streams

In the previous section of this manuscript (6.3.) we have discussed the physical conditions for ice stream stability that follow from the physics embedded in the UPB

model. Here, we analyze what types of physical perturbations are necessary to cause significant near-future changes in ice discharge through an ice stream that obeys the UPB physics. This analysis is directly relevant to the current discussion regarding the potential instability of the West Antarctic Ice Sheet, which could contribute to future global sea level rise [Bindschadler, 1997, 1998; Bentley, 1997].

Figure 1B shows that surface velocities observed on Ice Stream B are close to the maximum ice stream velocities that can be predicted using the UPB model (equation (1d) with $\tau_b = 0$). This is consistent with Ice Stream B being at present in the stable ice-stream mode of the UPB model, in which the bed strength is low and the ice velocity is correspondingly high. If this interpretation is correct, the UPB model implies that Ice Stream B is not predisposed to increase its ice discharge in the near future and therby contribute to an increase in the global sea level rise. Moreover, since for Ice Stream B there are no conclusive constraints on the magnitude of the geothermal flux and only one constraint on the magnitude of the conductive heat loss, that of Engelhardt and Kamb [1993], we cannot preclude the possibility that this ice stream may experience stoppage in the near future. As discussed before, in the UPB model ice stream stoppage is initiated when the basal thermal regimen changes to freezing for all admissible values of shear heating, i.e., when $G + (\tau_b\ U_b)_{\max} < k_i \Theta_b$. This may occur, for instance, if ice-stream thinning or the horizontal advection of cold ice from upstream increases the basal temperature gradient Θ_b beyond some threshold value for which the above inequality is satisfied. As illustrated by the thick solid line in Figure 2A whose peak just barely protrudes into the melting field of the diagram ($m_r > 0$), the current thermal state of the ice base in the UpB area may be close to this thermal threshold. An increase in basal temperature gradient by only a few percent of its present value, e.g., by 0.002 °C m^{-1}, would be sufficient to shift the basal melting curve below $m_r = 0$ and to force this part of the ice stream out of the stable ice-stream mode with weak bed and high velocities. Once

this happens, a positive feedback effect forces the system into the ice-sheet mode, with strong bed and slow velocities. The positive feedback occurs because a small initial basal freezing rate strengthens the till, which in turn slows down the ice stream velocity, which decreases shear heating and, thus, increases the basal freezing rate. Modeling of freeze-on driven till consolidation [Tulaczyk *et al.*, in preparation II, figure 7B] shows that significant strengthening of till by this mechanism may take place over relatively short timescales of dozens of years. Therefore, if an appropriate cooling of the ice base takes place in the near future, Ice Stream B may start to shut down and decrease rather than increase discharge of ice from the West Antarctic Ice Sheet into the ocean.

It is necessary to point out one major assumption whose removal opens the possibility for a near-future increase in the velocity and discharge of Ice Stream B. For the sake of simplicity, we have up to now considered the ice stream geometry, expressed in equation (1d) by the non-dimensional half-width, W, as fixed. However, recent observational and theoretical studies have pointed out the possibility that ice stream margins may migrate outward [Jacobel *et al.*, 1996; van der Veen and Whillans, 1996; Whillans and van der Veen, 1997]. Because of the non-linear dependence of ice stream velocity on ice stream geometry, i.e., $U_b \propto W^{n+1}$ (equation (1d)) (Figure 1A), a few percent increase in W would cause a significant increase in ice discharge.

Geophysical and geological investigations suggest that the part of the West Antarctic ice sheet which is affected by ice streaming is underlain by an extension of the Ross Sea sedimentary basin which contains poorly indurated and fine-grained glacimarine deposits [Rooney *et al.*, 1991; Tulaczyk *et al.*, 1998]. If basal meltwater starts being generated beneath slow-moving ice resting on such sediments, these sediments could develop a layer of weak till similar to that found beneath the UpB part of Ice Stream B [Tulaczyk *et al.*, 1998]. This is most likely to happen along the ice stream shear margins where a significant part of the gravitational energy of an active ice stream is dissipated

[Echelmeyer *et al.*, 1994; Harrison and Echelmeyer, 1994; Jackson and Kamb, 1997]. An increased basal melting due to this localized shear heating could lead to an outward migration of ice stream margins which would increase W and U_b. Even though the UPB model in its present form is not suitable to assess quantitatively the feedbacks that may occur locally in the basal system near shear margins, it provides a guidance in qualitative evaluation of such feedbacks. On the basis of this model we predict that there is a positive feedback which forces a migration of the basal system from the ice-sheet mode to the ice-stream mode as soon as the threshold conditions, $\tau_b < \tau_d$ and $m_r > 0$, are fulfilled. At this point, the reinforcing interactions among basal melting, bed strength, and ice stream velocity, start to push the system towards the 'ice-stream' mode even without any additional external supply of thermal energy.

At the most basic level, the UPB ice-stream model is consistent with the previous suggestions that ice stream evolution is controlled by the changes in the basal thermal regimen [MacAyeal, 1993ab]. It is plausible that the near-future evolution of the West Antarctic ice streams will be determined by an interplay between two competing tendencies: 1) the tendency of the basal thermal regimen in an active ice stream to switch to freezing due to ice stream thinning and/or horizontal advection of cold ice [MacAyeal, 1993ab], and 2) the tendency of the basal thermal regimen beneath slow-moving ice adjacent to an ice stream to switch to melting because of an increased shear heating in ice stream marginal shear zones. Given the scarcity of data constraining the current thermal state of the West Antarctic ice streams and their surroundings, it is impossible to use the UPB model to make conclusive predictions regarding the near-future evolution of the West Antarctic Ice Sheet. However, the UPB model does show that the ice streams may be prone to relatively fast stoppages or to significant increases in their velocity in response to relatively small changes in the basal thermal energy balance. As we have calculated previously, the characteristic time constant for changes in the UPB system is of the order of only 10 years (C_1^{-1} in the

equation (9)). To this extent, the model substantiates the concern that the West Antarctic ice streams may play an important role in changing the contribution of the West Antarctic Ice Sheet to the ongoing global sea-level rise.

The version of the UPB model presented in this manuscript is relatively simple but the same physical principles and feedbacks can be easily incorporated into numerical models of ice stream and ice sheet motion. Such numerical UPB models will have the advantage of being able to account explicitly for the evolution of the basal temperature gradient, removing the disadvantage that we faced here of treating the gradient as an adjustable parameter. Combination of a numerical UPB model with well-constrained data on the distribution of the present-day geothermal flux and basal heat loss has the potential to provide a conclusive resolution to the dilemma concerning the potential near-future instability of the West Antarctic Ice Sheet.

6.5. Conclusions

The undrained-bed model formulated previously in Tulaczyk *et al.* [in preparation II] can be coupled with an expression for the velocity of an ice stream moving over a till bed of plastic rheology to obtain a physically self-consistent ice-stream model, the Undrained-Plastic-Bed (UPB) model. In the UPB model, ice stream velocity is controlled directly by ice deformation in the shear margins and the bed strength enters only as an indirect control, i.e., it determines the partitioning of the driving stress between the bed and the margins. The observed high velocities of Ice Stream B (~400 m y-1) can be reproduced by our ice-stream model, provided that the low strength of subglacial till observed in the UpB area of this ice stream is also representative for other locations.

Stability analysis performed on the UPB model reveals two stable modes: 1) an 'ice-stream' mode in which the basal melting rate is equal to zero, the bed strength is much

smaller than the driving stress, and ice velocities are high; and 2) an 'ice-sheet' mode in which the melting rate is less than zero, bed strength is greater than the driving stress, and basal sliding velocity is zero. The UPB model suggests also that evolution of an ice stream may be controlled by the evolution of the basal thermal regimen. For instance, ice stream stoppage is possible when the basal conductive heat loss exceeds the heat supplied by a combination of the geothermal flux and the maximum shear heating, i.e., $k_i \Theta_b > G + (\tau_b U_b)_{max}$. In this situation, the stability condition $m_r = 0$ cannot be fulfilled for any bed strength and the positive feedback between basal freezing and bed strength will force the ice stream system to migrate towards the second stable mode, the 'ice-sheet' mode. The transition in the opposite direction, i.e., from the 'ice-sheet' mode to the 'ice-stream' mode, is also a run-away process which takes over as soon as the following two threshold conditions are met: 1) bed strength equal to the driving stress, $\tau_b = \tau_d$, and 2) melting rate greater than zero, $m_r > 0$. This result demonstrates that small perturbation in the basal thermal energy balance may trigger major rearrangements in an ice stream system. With improved constraints on the present-day thermal state of the West Antarctic Ice Sheet, a numerical version of the UPB model can be used to test the hypothesis that this ice sheet may experience a significant internally-triggered instability in the near future.

6.6. References

Alley, R.B., Deforming-bed origin for southern Laurentide till sheets: *J. Glaciol.*, 37, 67-76, 1991.

Alley, R.B., D.D. Blankenship, C.R. Bentley, and S.T. Rooney, Deformation of till beneath Ice Stream B, West Antarctica, *Nature*, 322, 57-59, 1986.

Alley, R.B., D.D. Blankenship, S.T. Rooney, and C.R. Bentley, Till beneath Ice Stream B. 3. Till deformation - evidence and implications, *J. Geophys. Res.*, 92, 8,921-8,929, 1987a.

Alley, R.B., D.D. Blankenship, S.T. Rooney, and C.R. Bentley, Till beneath Ice Stream B. 4. A coupled ice-till flow model, *J. Geophys. Res.*, 92, 8,931-8,940, 1987b.

Alley, R.B., D.D. Blankenship, S.T. Rooney, and C.R. Bentley, Water-pressure coupling of sliding and bed deformation. 3. Application to Ice Stream B, Antarctica, *J. Glaciol.*, 35, 130-139, 1989.

Alley, R.B., and D.R. MacAyeal, Ice-rafted debris associated with binge/purge oscillations of the Laurentide Ice Sheet: *Paleoceanog.*, 9, 503-511, 1994.

Anandakrishnan, S., and C.R. Bentley, Micro-earthquakes beneath Ice Stream B and Ice Stream C, West Antarctica: *J. Glaciol.*, 39, 455-462, 1993.

Bentley, C.R., Antarctic ice streams - a review, *J. Geophys. Res.*, 92, 8,843-8,858, 1987.

Bentley, C.R., Rapid sea-level rise soon from West Antarctic Ice Sheet collapse, *Science*, 275, 1077-1078, 1997.

Bindschadler, R., West Antarctic Ice-Sheet collapse, *Science*, 276, 662-663, 1997.

Bindschadler, R., Monitoring ice sheet behavior from space, *Rev. Geophys.*, 36, 79-104, 1998.

Bindschadler, R., S.N. Stephenson, D.R. MacAyeal, and S. Shabtaie, Ice dynamics at the mouth of Ice Stream B, Antarctica, J. Geophys. Res., 92, 8,885-8,894, 1987.

Blankenship, D.D., C.R. Bentley, S.T. Rooney, and R.B. Alley, Seismic measurements reveal a saturated porous layer beneath an active Antarctic ice stream, *Nature*, 322, 54-57, 1986.

Blankenship, D.D., C.R. Bentley, S.T. Rooney, and R.B., Alley, Till beneath Ice Stream B. 1. Properties derived from seismic travel times, *J. Geophys. Res.*, 92, 8,903-8,911, 1987.

Boulton, G.S., Theory of glacial erosion, transport and deposition as a consequence of subglacial sediment deformation, *J. Glaciol.*, 42, 43-62, 1996.

Clark, P.U., Surface form of the southern Laurentide Ice Sheet and its implications to ice-sheet dynamics: *Geol. Soc. Am. Bull.*, 104, 595-605, 1992.

Clark, P.U., and J.S. Walder, Subglacial drainage, eskers, and deforming beds beneath the Laurentide and Eurasian ice sheets, *Geol. Soc. Am. Bull.*, 106, 304-314, 1994.

Clarke, G.K.C., Subglacial till: a physical framework for its properties and processes, *J. Geophys. Res.*, 92, 9023-9037, 1987.

Echelmeyer, K.A., W.D. Harrison, C. Larsen, and J.E. Mitchell, The role of the margins in the dynamics of an active ice stream, *J. Glaciol.*, 40, 527-538, 1994.

Engelhardt, H., N. Humphrey, B. Kamb, and M. Fahnestock, Physical conditions at the base of a fast moving Antarctic ice stream, *Science*, 248, 57-59, 1990.

Engelhardt, H.F., and B. Kamb, Vertical temperature profile of ice stream B: *Ant. J. U.S.*, 28, 63-66, 1993.

Engelhardt, H., and B. Kamb, Basal hydraulic system of a West Antarctic ice stream - constrains from borehole observations, *J. Glaciol.*, 43, 207-230, 1997.

Engelhardt, H., and B. Kamb, Sliding velocity of Ice Stream B, *J. Glaciol.*, in press.

Harrison, W., and K. Echelmeyer, Temperature measurements in the margin of Ice Stream B, *Ant. J. U.S.*, 29, 60-61, 1993.

Hughes, T.J., Can ice sheets trigger abrupt climatic change? *Arct. Alp. Res.*, 28, 448-465, 1996.

Jackson, M., and Kamb, B., The marginal shear stress of Ice Stream B, *J. Glaciol.*, 43, 415-426, 1997.

Jacobel, R.W., T.A. Scambos, C.F. Raymond, and A.M. Gades, Changes in the configuration of ice stream flow in the West Antarctic Ice Sheet, *J. Geophys. Res.*, 101, 5499-5504, 1996.

Kamb, B., Rheological nonlinearity and flow instability in the deforming-bed mechanism of ice stream motion: *J. Geophys. Res.*, 96, 16,585-16,595, 1991.

Kamb, B., and H.F. Engelhardt, Antarctic ice stream B: conditions controlling its motion and interactions with the climate system, *IAHS*, 208, 145-154, 1991.

MacAyeal, D.R., Irregular oscillations of the West Antarctic ice sheet, *Nature*, 359, 29-32, 1992.

MacAyeal, D.R., A low-order model of the Heinrich event cycle, *Paleoceanog.*, 8, 767-773, 1993a.

MacAyeal, D.R., Binge/purge oscillations of the Laurentide ice sheet as a cause of the North-Atlantic Heinrich events: *Paleoceanog.*, 8, 775-784, 1993b.

Marshall, S.J., Clarke, G.K.C., Dyke, A.S., and Fisher, D.A., 1996, Geologic and topographic controls on fast-flow in the Laurentide and Cordilleran ice sheets: *J. Geophys. Res.*, 101, 17,827-17,839.

Patterson, W.S.B., *The physics of glaciers*, Pergamon, Oxford, 1994.

Raymond, C., Shear margins in glaciers and ice sheets, *J. Glaciol.*, 42, 90-102, 1996.

Rooney, S.T., Blankenship, D.D., Alley, R.B., and Bentley, C.R., 1991, Seismic reflection profiling of a sediment-filled graben beneath Ice Stream B, West Antarctica: in *Geological Evolution of Antarctica*, edited by M.R. Thomson, J.A. Crame, and J.W. Thomson, British Antarctic Survey, Cambridge, 261-265, 1991.

Shabtaie, S., Whillans, I.M., and C.R. Bentley, The morphology of ice streams A, B, and C, West Antarctica, and their environs, *J. Geophys. Res.*, 92, 8,865-8,883, 1987.

Tulaczyk, S., B. Kamb, and H. Engelhardt, Basal mechanics of Ice Stream B, West Antarctica. I. Till mechanics, in preparation I.

Tulaczyk, S., B. Kamb, and H. Engelhardt, Basal mechanics of Ice Stream B, West Antarctica. II. Bed hydrology, in preparation II.

Tulaczyk, S., B. Kamb, H. Engelhardt, and R.P. Scherer, Sedimentary processes beneath a West Antarctic ice stream; constraints from textural and compositional properties of subglacial debris, *J. Sediment. Res.*, 68, 487-496, 1998.

van der Veen, C.J., and I.M. Whillans, Model experiments on the evolution and stability of ice streams: *Ann. Glaciol.*, 23, 129-137, 1996.

Walder, J.S., and A. Fowler, Channelized subglacial drainage over a deformable bed, *J. Glaciol.*, 40, 3-15, 1994.

Whillans, I.M., and C.J. van der Veen, New and improved determinations of velocity of Ice Streams B and C, West Antarctica, *J. Glaciol.*, 39, 483-490, 1993.

Whillans, I.M., and C.J. van der Veen, The role of lateral drag in the dynamics of Ice Stream B, Antarctica: *J. Glaciol.*, 43, 231-237, 1997.

Figure 1. (A) Two examples of velocity-bed strength curves calculated using equation (1d). The non-dimensional half-widths, W, of 20 and 40 ice thicknesses are representative of the range of typical values for the trunk stream of Ice Stream B. In these and all subsequent calculations, standard flow-law parameters for ice at the temperature of -15°C are assumed [Patterson, 1994, table 5.2]. (B) Application of the plastic-till model (equation (1d)) to four selected cross sections, (a), (b), (c), and (d), of Ice Stream B for which accurate data on ice stream geometry and velocity are available [Bindschadler *et al.*, 1987; Shabtaie *et al.*, 1987]. Cross section (b) is located in the UpB area of Ice Stream B (a situation sketch (C) with outlines of the ice stream, ISB, is in the upper right of the diagram). Approximate width and thickness of ice in these cross sections is given by the cross-hatched rectangles in the center right. Concave-upward curves show the velocities predicted from the model and the horizontal lines show the observed velocities. Intersections of the corresponding pairs of curves and lines are marked with solid squares.

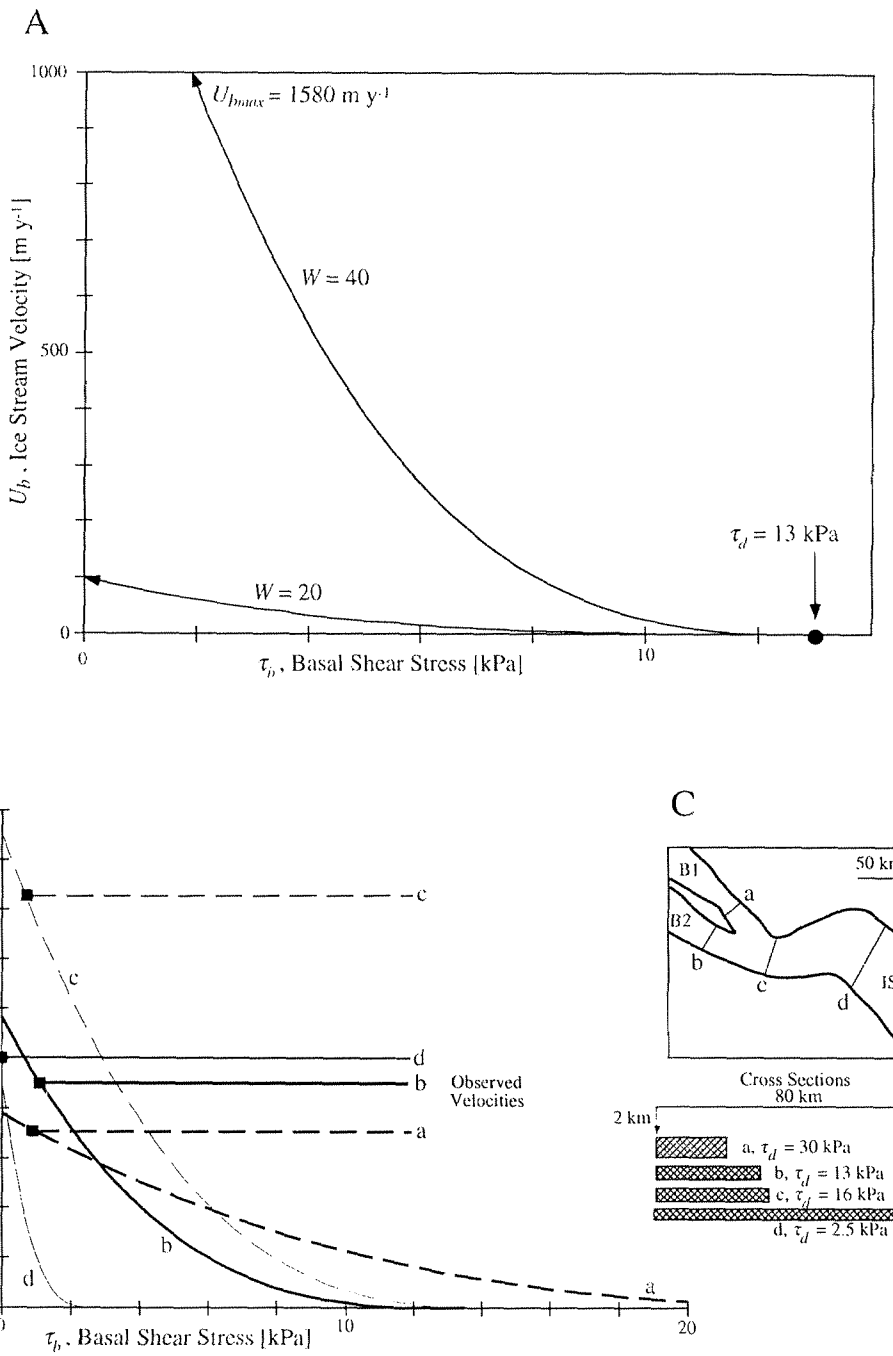
A
1000
500
0
U_{bmax} = 1580 m y^{-1}
W = 40
W = 20
τ_d = 13 kPa
U_b , Ice Stream Velocity [m y^{-1}]
0
10
τ_b , Basal Shear Stress [kPa]
B
1000
500
0
c
d
b
a
Observed Velocities
U_b , Ice Stream Velocity [m y^{-1}]
0
10
20
τ_b , Basal Shear Stress [kPa]
C
B1
B2
a
b
c
d
ISB
50 km
Cross Sections
80 km
2 km
a, τ_d = 30 kPa
b, τ_d = 13 kPa
c, τ_d = 16 kPa
d, τ_d = 2.5 kPa

Figure 2. (A) The basal melting rate, m_r, as a function of the basal strength calculated for the cross section of Ice Stream B in the UpB area ((b) in Figure 1B) using a combination of equations (1a) and (1d). Positive m_r denotes melting of basal ice and negative m_r denotes basal freezing. The assumed basal temperature gradient, Θ_b = 0.04°C m^{-1}, corresponds to that measured by Engelhardt and Kamb [1993] in the UpB area. The geothermal flux, G, is not known. The thick solid line is plotted assuming G of 0.06 W m^{-2} and the two dashed thin lines assuming 0.04 and 0.08 W m^{-2}. The open and the solid circle are plotted where the condition of basal melting rate equal to zero is met. (B) Ice stream velocity-bed strength curve calculated from equation (1a) for the same cross-section of Ice Stream B ((b) in Figure 1B). The open and the solid circles are drawn for the same values of the bed strength, τ_b, as in Figure 2A. They indicate the stable equilibrium and the metastable equilibrium inferred from the linear stability analysis of the UPB ice-stream model. The arrows show the directions in which the UPB system migrates when perturbations take it out of either of the two equilibrium states.

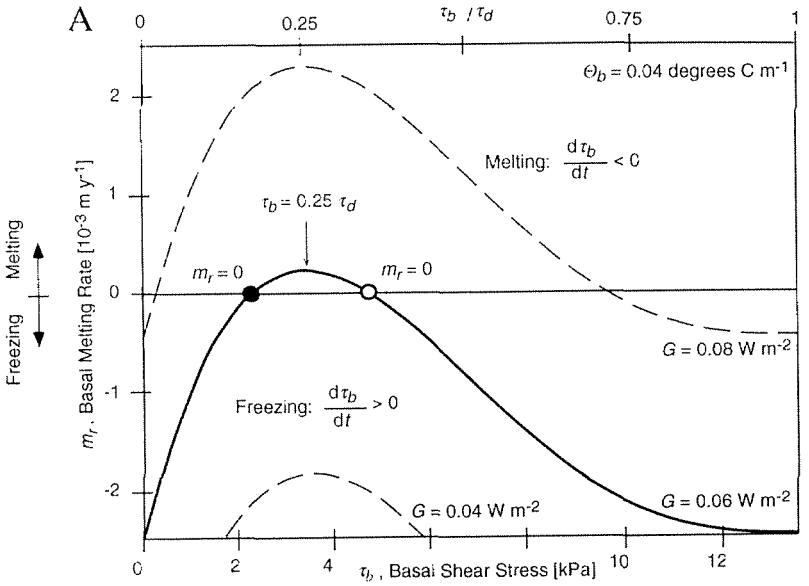
A
0
0.25
τ_b / τ_d
0.75
1
Θ_b = 0.04 degrees C m^{-1}
Melting: $\frac{d\tau_b}{dt} < 0$
τ_b = 0.25 τ_d
m_r = 0
m_r = 0
Freezing
Melting
m_r, Basal Melting Rate [10^{-3} m y^{-1}]
2
1
0
-1
-2
G = 0.08 W m^{-2}
Freezing: $\frac{d\tau_b}{dt} > 0$
G = 0.04 W m^{-2}
G = 0.06 W m^{-2}
0
2
4
τ_b, Basal Shear Stress [kPa]
10
12

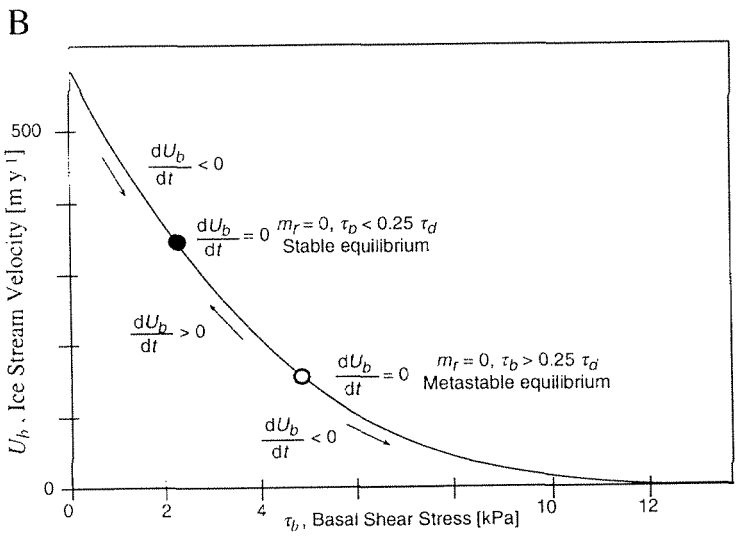
B
500
0
U_b, Ice Stream Velocity [m y^{-1}]
$\frac{dU_b}{dt} < 0$
$\frac{dU_b}{dt} = 0$
m_r = 0, τ_b < 0.25 τ_d
Stable equilibrium
$\frac{dU_b}{dt} > 0$
$\frac{dU_b}{dt} = 0$
m_r = 0, τ_b > 0.25 τ_d
Metastable equilibrium
$\frac{dU_b}{dt} < 0$
0
2
4
τ_b, Basal Shear Stress [kPa]
10
12

CHAPTER 7

General Summary

Samples of till from beneath Ice Stream B (at camp UpB), West Antarctica, provide the first opportunity to study the origin and mechanical properties of the weak sedimentary material which facilitates the fast motion of this ice stream. In this study, results of sedimentological and geotechnical laboratory tests are combined with the physical principles of ice, water, and soil physics to provide new constraints on the role of weak subglacial tills in ice stream mechanics and to develop a new, self-consistent model of ice streaming. This model demonstrates that ice streaming may represent one of two thermo-mechanically-controlled stable modes admissible for a part of an ice mass; the other mode being the classical ice-sheet-type flow through internal ice deformation. Because of the largely non-parametric nature of this new ice-stream model, its numerical version can be used in the future to test the hypothesis that the West Antarctic Ice Sheet may soon experience a significant internally-triggered instability which could amplify the ongoing global sea-level rise.

Sedimentological properties of the UpB till recovered from beneath Ice Stream B are consistent with generation of this material through glacial recycling of the (inferred) sub-till Tertiary glacimarine sediments from the Ross Sea sedimentary basin which extends beneath this part of the West Antarctic Ice Sheet. Sedimentary particles from the UpB till bear no evidence of the recent crushing and abrasion that is common in other subglacial environments. This lack of significant comminution in the subglacial environment of Ice Stream B may be due to its setting over the easily erodible, clay-rich Tertiary sediments. The resulting fine-grained till matrix inhibits glacial comminution, because it facilitates buildup of high pore water pressures and hinders interparticle stress concentrations. These sedimentological observations are consistent with the conjecture that subglacial deformation

of weak, fine-grained tills does not produce significant comminution of till debris. Extensive layers of weak till may develop preferentially where ice overrides preexisting, poorly indurated, fine-grained sediments. Since such weak till layers create a permissive condition for ice streaming, subglacial geology may have a first-order control over the location, extent, and basal mechanics of ice streams.

In the past, much of the modeling of ice-till interactions was based on the simplifying assumption that subglacial till behaves like a perfectly smooth continuum with linearly, or mildly non-linearly, viscous rheology and no compressibility. However, results of laboratory tests on the samples of the UpB till have consistently shown that this material has a Coulomb-plastic rheology, i.e., its strength depends linearly on the effective stress but is practically independent of strain-rate. In addition, laboratory tests have also demonstrated that the UpB till has a significant compressibility, a feature that may not be neglected in modeling of subglacial till kinematics and in interpretations of in situ measurements of strain and tilt beneath ice masses. In the course of this project, simulations of till deformation have shown that a Coulomb-plastic till model is capable of reproducing many fundamental features of subglacial till behavior: 1) a viscous-like distribution of strain with depth, 2) oscillations of tilt rates measured by tiltmeters, 3) till sliding over its substratum, and 4) ice sliding with ploughing over weak till. Analysis of the basic physical processes involved in ice-till interactions suggests also that the nature of these interactions may be strongly dependent on till granulometry. For instance, fine-grained tills may facilitate ice sliding and only limited distributed deformation of till (depth of ~ 0.01 m) whereas coarse-grained tills may favor strong ice-till coupling and relatively deep till deformation (depth of ~ 0.1 m). All these simulations of subglacial till behavior demonstrate clearly that the compressible, Coulomb-plastic till model derived from laboratory geotechnical tests on the UpB till is consistent with the existing observations of subglacial till behavior, and that, thus, this experimentally-constrained model can be used in modeling of ice stream motion.

Modeling of subglacial groundwater flow and water drainage in a basal water system beneath Ice Stream B suggests that the low sub-ice-stream effective stresses estimated from the high water content of the UpB till may be due to a lack of long-distance transport of meltwater from beneath the ice stream towards its grounding line. This inference motivated development of a new model of sub-ice-stream hydrology: the undrained-bed model. In this model, water storage in the till is the only term that is needed to describe the subglacial hydrologic system. If melting occurs at the bed of the ice stream then till water content is increased and if freezing occurs, the till water content is decreased. However, the rates of basal melting and freezing are not independent of till water content because the latter controls the strength of the till, and the strength of the till influences shear heating, which, in turn, has a major influence on basal melting and freezing. As a result of these interactions between till water storage, till strength, and shear heating, there is a negative feedback effect which forces the till bed to attain such steady-state water content and strength in which basal melting rate is equal to zero. This requires the till to become very weak, which is consistent with laboratory measurements of the strength of the UpB till of only a few kPa.

The undrained-bed model is further generalized by adding an equation which gives the dependence of ice stream velocity on till strength. The whole mathematical construction, called the undrained-plastic-bed or UPB model, is made up of a non-linear system of four coupled equations which combine four fundamental physical aspects of ice streaming: 1) ice mechanics, 2) till mechanics, 3) bed hydrology, and 4) basal thermal energy balance. The non-linear dynamics embedded in the UPB model produces two thermo-mechanically-controlled equilibrium states, one with a strong bed and slow ice velocities ('ice-stream' mode) and one with a weak bed and fast ice velocities ('ice-sheet' mode). This bimodality of basal conditions predicted by our model is consistent with the available observations of subglacial conditions beneath slow and fast moving ice in West Antarctica. Basal conditions that do not correspond to these two steady-states may occur

transiently during switches between the strong and weak basal modes. These transitional states are unstable due to positive feedback effects which force bifurcation of basal conditions. Switches between the two stable modes are forced by changes in basal conductive heat loss. The UPB model predicts, for instance, that stoppage of an active ice stream occurs when conductive heat loss becomes high enough to cause basal freezing for all admissible combinations of basal shear stress and ice stream velocity. On the other hand, commencement of ice streaming occurs when conductive heat loss is low enough to permit basal melting when the till bed is initially strong and ice moves slowly by internal deformation.